The Use of Intracoronary Optical Coherence Tomography in Interventional Cardiology: Safety, Feasibility and Clinical Applications

Peter Barlis

ISBN: 978-90-8559-544-1

Front cover illustration: Vulnerable plaque rupture of the thin fibrous cap with thrombus

Printed by Optima Grafische Communicatie, Rotterdam, The Netherlands

The Use of Intracoronary Optical Coherence Tomography in Interventional Cardiology: Safety, Feasibility and Clinical Applications

Het gebruik van intracoronairen optisch coherentie tomografie in interventie cardiologie: Veiligheid, haalbaarheid en klinische toepassingen

Thesis

to obtain the degree of Doctor from the
Erasmus University Rotterdam
by command of the
rector magnificus

Prof.dr. S.W.J. Lamberts

and in accordance with the decision of the Doctorate Board

The public defence shall be held on

Wednesday May 27, 2009 at 13.45 o'clock

by

Peter Barlis
born at Melbourne, Australia

Doctoral Committee

Promoters

Prof.dr. P.WJ.C. Serruys
Prof.dr. C. Di Mario

Other members

Prof.dr. W.J. van der Giessen
Prof.dr. P.J. de Feijter
Prof.dr. E. Boersma

Co-promoter

Dr. E. Regar

For Kathy, Anthony & Zoe

Table of Contents

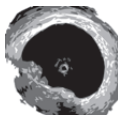

Chapter 1

Introduction & Overview

Peter Barlis

Interventional cardiology has witnessed tremendous change since 1977 when Andreas Gruentzig successfully performed the first balloon angioplasty. Whereas initial concerns revolved around maintaining vessel patency with issues of recoil and restenosis, the introduction of stents changed the landscape forever. Inherent with their use, stents, and, more specifically, drug-eluting stents (DES), have become central to improved patient outcomes but, at some cost. Catastrophic, yet fortunately still rare complications such as stent thrombosis have re-ignited an intense need for greater scrutiny when developing and, subsequently implanting DES into our patients.

The demand for detailed information regarding coronary artery disease has seen intravascular imaging become pivotal at delineating atherosclerosis and tissue responses following stent implantation. In fact, the strategy that relied on angiography alone is evolving to include better confirmation of disease severity and stenting technique. With this, optical coherence tomography (OCT) has grown exponentially with a broad diffusion amongst catheterisation laboratories worldwide.

Optical coherence tomography is a procedurally demanding technique. Individual experience is often frustrated initially with disappointing images as a result of inadequate blood clearance. With perseverance and adequate proctorship however, one cannot help but be impressed by the clarity and resolution afforded by this imaging modality. It is these images that have attracted considerable attention at cardiology conferences internationally and have helped instil OCT as the most sensitive intravascular imaging technique available today.

The aim of this thesis was to evaluate the role of OCT in contemporary coronary intervention. Part 1 embraces the principles of the technique and the physical properties of OCT (chapter 2) and gives an insight into where OCT is placed compared to other intravascular imaging modalities (chapter 3). Despite the adoption of OCT in more and more catheterisation laboratories, little has been documented as to its safety, so, in chapter 4, we review the procedural safety of intracoronary OCT in a large group of patients across six leading European centres.

In part 2, we focus on the means of achieving adequate visualisation of the vessel and we provide evidence for the validity of quantitative OCT data. Chapter 5 is a landmark piece of work and draws upon our initial experience at the Royal Brompton Hospital, London, UK while introducing OCT to our lab. For the first time, we also reported on a classification system to assess stent strut apposition, namely by incorporating the precise strut width (inclusive of metal and polymer) when categorising a strut as apposed or not. The validity of data is robustly depicted in chapters 6 & 7 with a comparison to a novel quantitative analysis system and the proprietary system, respectively.

In an attempt to do away with the cumbersome occlusion balloon whilst imaging with OCT, a simplified technique of using contrast flush through the guiding catheter has been developed. Chapter 8 focuses on the significant advantages of this method, namely the ability to visualise ostial and proximal coronary segments and improved patient tolerability. This technique has now become established and is also incorporated in the next generation OCT consoles using Fourier domain imaging.

Part 3 of the thesis explores the exciting area of coronary stent imaging. This is emerging as a key indication for OCT given the increased scrutiny placed on DES as a result of the risk of thrombosis. Tissue coverage or the lack thereof has been linked to stent thrombosis in post-mortem studies, hence, a technique that can detect microscopic amounts of tissue in-vivo is

appealing. The LEADERS trial OCT sub-study (chapter 11) looked at tissue coverage of biolimus and sirolimus-eluting stents 9 months following implantation in an 'all-comer' patient population. The novel biolimus stent incorporates a biodegradable polymer and may offer several advantages over and above permanent polymer-based platforms. Chapter 12 goes further and uses OCT to explore the advantages of a bare metal stent sprayed with rapamycin compared to the first generation sirolimus stent.

Apart from its unique ability to detect tissue coverage, its high resolution makes OCT applicable in assessing strut apposition. Chapters 13 explores the use of OCT in overlapping DES. We identified that this region was associated with a significantly higher rate of malapposed struts despite high pressure dilatation. Chapter 15 gives insights into the role of different stent platforms and the influence of cell design and strut thickness on the incidence of incomplete stent apposition. Other applications afforded to be the high resolution of OCT are in examining suspected cases of stent fracture (chapter 16) and stent thrombosis (chapter 20) where we identify incomplete strut apposition on OCT and the presence of eosinophils histologically, raising the possibility of a hypersensitivity reaction to polymer in this multi-faceted disease entity.

Part 4 of the thesis focuses on the application of OCT in assessing atherosclerotic plaque. The modality can accurately differentiate between different plaque types, namely fibrous, lipid-rich and calcific. Chapter 22 describes a unique pilot study using the first generation OCT system to examine culprit and non-culprit coronary lesions in patients presenting with acute coronary syndromes or stable angina pectoris. Chapter 23 also incorporates intravascular ultrasound, virtual histology and intravascular magnetic resonance imaging to compare a multi-modality strategy and detecting and characterising atherosclerotic plaque in-vivo.

The final section of the main body of the thesis (Part 5) deals with new developments in OCT technology. Fourier-domain OCT (FD-OCT) systems employ a novel wavelength-swept laser as a light source and acquire images at line rates at least 10 times faster than time-domain systems without loss of image quality (pullback speed of 20mm/sec compared to 3.0mm/sec). This speed advantage results from the elimination of mechanical scanning of the reference mirror and the signal-to-noise advantages of Fourier-domain signal processing. Such advances with faster pullback speeds will see OCT become simpler and will help minimise the need for large volumes of contrast during image acquisition.

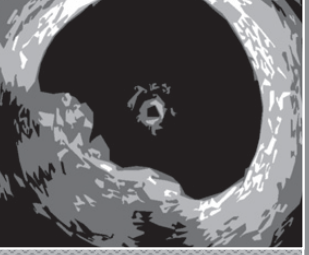

Part 1

Principles & Safety of OCT

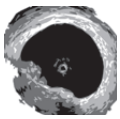

Chapter 2

Principles of intra-coronary optical coherence tomography

Peter Barlis, Jun Tanigawa, Patrick W. Serruys, Evelyn Regar

Intravascular imaging techniques remain complimentary to assessing vascular structures or results following stent implantation. The recent introduction of optical coherence tomography (OCT) to the coronary circulation has given unique insights into vessel microstructures and responses following stenting. Compared to intravascular ultrasound (IVUS), OCT has a ten-fold higher resolution with fewer artefacts, primarily as a result of the near infra-red light used as opposed to sound to generate the image. This advantage has seen OCT successfully applied to the assessment of atherosclerotic plaque (including thin cap fibroatheroma and macrophage distribution within a culprit lesion), stent apposition and tissue coverage, introducing a new era in intravascular coronary imaging. (1-11) This chapter will introduce the principles of OCT and how this novel technology has been implemented into both the clinical and research arenas.

Technical considerations

Whereas ultrasound produces images from backscattered sound "echoes," OCT uses infrared light waves that reflect off the internal microstructure within the biological tissues. Table 1 illustrates the characteristics of OCT compared to other imaging modalities.

	OCT	IVUS	Fluoroscopy	Angioscopy	MRI
Resolution (μm)	10-15	80-120	100-200	<200	80-300
Probe size (μm)	140	700	NA	800	NA
Ionizing radiation	No (near infra-red light)	No (ultrasound)	Yes	No	No

Table 1: Overview of image resolution of different coronary imaging modalities

Since the speed of light is much faster than that of sound, an interferometer is required to measure the backscattered light. The interferometer splits the light source into two "arms" – a reference arm and a sample arm, which is directed into the tissue. The frequencies and bandwidths of infrared light (1310nm broadband super luminescent) are orders of magnitude higher than medical ultrasound. The imaging depth of current OCT systems is approximately 1.5-2.0mm with an axial and lateral resolution of 15μm and 25μm, respectively. The mobile OCT System cart (LightLab Imaging Inc., Westford, MA, USA) contains the optical imaging engine and the computer. The mouse, keyboard, two monitors, two storage drawers, and the patient interface unit (PIU) are all mounted on top of the cart (Figure 1).

The ImageWire

The imaging probe (ImageWire™ LightLab Imaging Inc., Westford, MA, USA) has a maximum outer diameter of 0.019″ (with a standard 0.014" radiolucent coiled tip) and contains a single-mode fiber optic core within a translucent sheath (Figure 2).

see colour section

Figure 1: the mobile OCT cart incorporating the system console, monitor, and patient interface unit

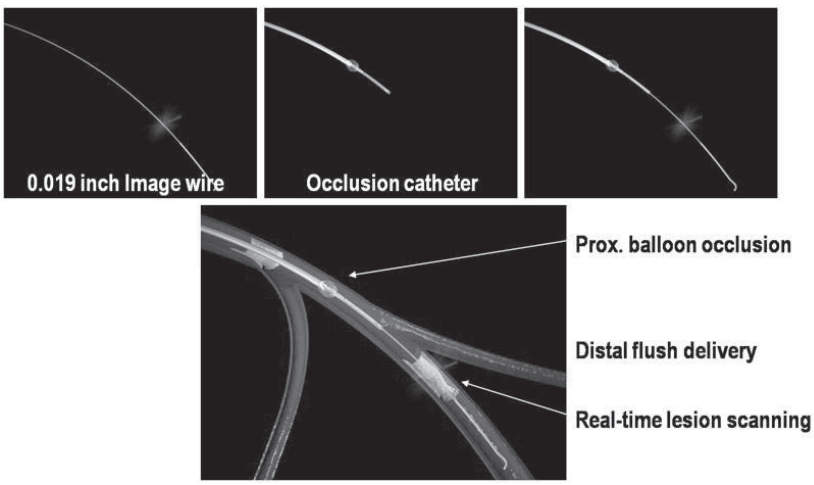

Figure 2: The OCT catheter and dedicated optical imaging wire (LightLab Imaging Inc., Westford, MA, USA) in current commercial use. The occlusion balloon is positioned proximal to the region of interest and the imaging wire is then inserted with real-time image acquisition performed at a rate up to 3 mm/sec

The image wire is connected at its proximal end to the imaging console that permitted real-time data processing and two-dimensional representation of the backscattered light in a cross-sectional plane. Since the imaging wire is not torquable, it can be advanced distal to the region of interest using the over-the-wire occlusion balloon (for the occlusive technique, see below) or a

simple micro-catheter for the non-occlusive technique (see below, e.g. Transit, Cordis Johnson &Johnson, USA or ProGreat, Terumo Japan, with inner lumens >0.020″). Unlike an IVUS transducer, the optical sensor of the image wire is invisible under fluoroscopy and therefore one must estimate the correct position, using the distal 15mm radiopaque tip of the ImageWire. As there are no direct radiopaque markers for the infrared sensor, it is possible to inadvertently miss imaging an area of interest resulting in incomplete distal lesion edge assessment. Imaging after stent implantation facilitates positioning because it is sufficient to advance the proximal end of the radiopaque wire tip at least 1cm distal to the stent struts to image the entire stented segment. For imaging prior to treatment, it is important to note that the occlusion balloon is too bulky to cross severe stenoses before pre-dilatation and that the imaging wire should be advanced distal to the lesion to ensure that the segment of interest is fully visualised. In such circumstances, the non-occlusive technique is advantageous.

Techniques for blood removal

As the light used is unable to penetrate red blood cells, OCT requires temporary blood evacuation prior to image acquisition. This remains one of the major limitations precluding the routine use of OCT and warrants further consideration.

Proximal balloon occlusion and flush

The proximal occlusion balloon catheter (Helios, Goodman Co, Japan) is an over-the-wire 4.4Fr catheter (inner diameter 0.025”), compatible with 6Fr guiding catheters (inner lumen diameter ≥0.071”), which is advanced distal to region of interest using a conventional angioplasty guide wire (0.014”). The guide wire is then replaced by the OCT ImageWire™ (0.019” maximum diameter), and the occlusion balloon catheter is withdrawn proximal to the segment to be assessed leaving the imaging wire in distal position.

During imaging acquisition, coronary blood flow is removed by continuous flush of Ringer’s lactate solution via the end-hole of the occlusion balloon catheter at a flow rate of 0.5-0.7ml/sec during simultaneous balloon inflation (0.5-0.7atm). The vessel occlusion time is limited to a maximum of 30sec to avoid haemodynamic instability or arrhythmias. A 1.0 mm/sec pullback permits the assessment of an up to 30mm long coronary segment with a frame rate of 15.6 frames/sec.

This technique permits OCT image acquisition without the use of additional contrast for flushing however, as the balloon needs to be positioned in the proximal segment of the vessel, visualisation of such regions of the artery is limited. Further, occlusion balloon use is frequently associated with chest discomfort for the patient with associated electrocardiographic ischemia changes.

Non-occlusive technique

With improvements in the acquisition speeds of OCT data (currently peaking at 3.0mm/sec however, up to 20mm/sec will be available with optical frequency domain OCT), blood can be evacuated by continuous flush through the guiding catheter, thus doing away with the cumbersome proximal balloon occlusion and thereby simplifying the acquisition process. Here,

the OCT imaging wre is advanced carefully distal to the region of interest. As the fragile wire does not have the properties of a guidewire, it needs to be directed distally using an over the wire catheter (e.g.Transit, Cordis, Johnson & Johnson or ProGreat, Terumo, Japan). With the wire in position, viscous iso-osmolar contrast (Iodixanol, Visipaque™, GE Health Care, Cork, Ireland) at 37° Celsius is used to clear the artery from blood and connected to the standard Y-piece of the guiding catheter. The contrast is either injected manually through the Y-piece or automatically using a pump injector. During continuous contrast injection, the automated OCT pullback is performed at 3.0mm/sec. The pullback is stopped after visualisation of the region of interest or in case of significant signs of ischaemia, arrhythmia or patient intolerance. Cross sectional images are acquired at 20 frames/sec.

After completion of the OCT study, the image wire is removed, and intra-coronary nitrates are usually administered according to local standards and an angiogram should be taken. The procedure should be terminated if there is any haemodynamic compromise during the infusion and OCT acquisition.

OCT Applications

Although OCT has a number of varied clinical and research uses, the main applications at this present time are the assessment of:

1. Stent apposition
2. Stent strut neointimal coverage at follow-up
3. Atherosclerotic plaques (including the characterisation of vulnerable plaques)

1. Stent Apposition

OCT is more accurate in assessing strut apposition compared with IVUS because of higher resolution but its poor penetration (approximately 1.5mm) makes it inferior to IVUS in assessing stent expansion. Stent struts appear as highly reflective surfaces and cast shadows on the vessel wall behind. Even if the stent struts are well apposed to the vessel wall with OCT, the stent may not be optimally expanded given that it is more difficult to identify the external elastic membrane compared with IVUS. Since OCT can show only the endo-luminal surface of the strut due to limited penetration through the metal with resulting shadowing (Figure 3, arrows), strut and polymer thickness should be considered in assessing apposition for each type of DES design. Table 2 lists the thickness of commercially available.

In an evaluation of OCT findings following stent implantation to complex coronary lesions, Tanigawa et al (12) examined a total of 6,402 struts from 23 patients (25 lesions) and found 9.1±7.4% of all struts in each lesion treated were malapposed. Univariate predictors of malapposition on multilevel logistic regression analysis where: implantation of a sirolimus-eluting stent (SES), presence of overlapping stents, longer stent length and type C lesions. Likely mechanical explanations for malapposition of stent struts include increased strut thickness, closed cell design or acute stent recoil. The latter has been demonstrated in SES to be in the range of 15%, despite the use of high pressure balloon dilatation. (13)

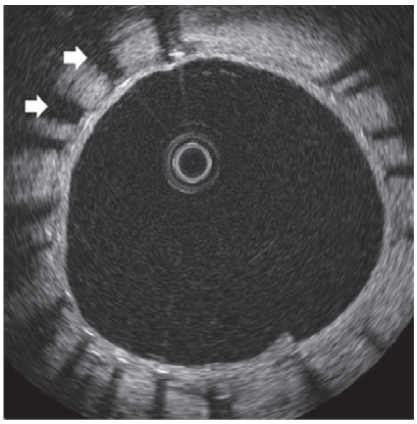

Figure 3 – This OCT cross-section shows a thin layer of tissue covering the stent struts. As infrared light is unable to penetrate the metal struts, shadowing results (arrows)

see colour section

Manufacturer	Name	Drug	Metal Strut	Polymer	Total Thickness
Cordis, J&J	Cypher Select	Sirolimus	0.0055" (140μm)	0.0003" (7μm)	0.0061" (154μm)
Boston Scientific	Taxus Liberte	Paclitaxel	0.0038" (97μm)	0.0006" (15μm)	0.0050" (127μm)
Medtronic	Endeavor	Zotarolimus	0.0036" (91μm)	0.0003" (8μm)	0.0042" (107μm)
Abbott	Xience V	Everolimus	0.0032" (81μm)	0.0003" (8μm)	0.0035" (89μm)
Translumina	Yukon	Rapamycin	0.0034" (87 μm)	NA	0.0034" (87 μm)
Orbus Neich	Genous	EPC capture	0.0040" (100μm)	NA	0.0040" (100μm)
Medtronic	Driver	NA	0.0036" (91μm)	NA	0.0036" (91μm)

Table 2: Thickness of stent struts (NA - not applicable)

2. Stent strut tissue coverage

One of the 'hotly' debated topics currently in the interventional cardiology literature remains stent thrombosis. It appears that this condition is multi-factorial with premature discontinuation of dual anti-platelet therapy, stent under-expansion, hypersensitivity and lack of endothelial tissue coverage all being implicated.(14-18) Unlike conventional stents which developed circumferential coverage with an average thickness of 500μm or more, well visualised with IVUS and angiography (corresponding to 1mm late loss),(6) DES delay and prevent the hyperplastic response so that the average late lumen loss for sirolimus- or paclitaxel- eluting stents can be as

low as 0.1 or 0.2mm,(19,20) which means the amount of intimal thickening will not be detectable with IVUS. OCT offers a potential alternative to detect and measure these tiny layers of intimal coverage and to assess late strut malapposition that can be distinguished, if images immediately after implantation are also available, into persistent (present already at the time of stent implantation) and acquired (negative remodeling or disappearance of superficial components behind struts such as thrombus).(6)

Small-scale studies have successfully used OCT to evaluate neointimal stent strut coverage at follow-up. Matsumoto et al studied 34 patients following sirolimus-eluting stent (SES) implantation. The mean neointima thickness was 52.5 microns, and the prevalence of struts covered by thin neointima undetectable by IVUS was 64%. The average rate of neointima-covered struts in an individual SES was 89%. Nine SES (16%) showed full coverage by neointima, whereas the remaining stents had no visible strut coverage.(5) Similarly, Takano et al (10) studied 21 patients (4,516 struts) 3 months following SES implantation. Rates of exposed struts and exposed struts with malapposition were 15% and 6%, respectively. These were more frequent in patients with acute coronary syndrome (ACS) than in those with non-ACS (18% vs 13%, $p < 0.0001$; 8% vs 5%, $p < 0.005$, respectively). The same group have recently reported 2 year follow-up OCT findings with the thickness of neointimal tissue at 2-years being greater than that at 3-months (71 ± 93 μm vs. 29 ± 41 μm, respectively; $p<0.001$). Frequency of uncovered struts was found to be lower in the 2-year group compared to the 3-month group (5% vs. 15%, respectively; $p<0.001$) and, in contrast, prevalence of patients with uncovered struts did not differ between the 3-month and the 2-year group (95% vs. 81%, respectively) highlighting that exposed struts continued to persist at long-term follow-up. (21)

3. Atherosclerotic plaque assessment

Several imaging modalities have been used to assess and identify VP including coronary angioscopy, intravascular ultrasound (IVUS) and magnetic resonance imaging. Recently, there has been significant interest in the field of VP detection using OCT,(1-4,22-26) with the technique able to detect and quantify thin cap fibroatheroma (TCFA) and macrophage distribution.(2-4,25) Several morphologic features described in autopsy series are of particular interest in such vulnerable plaques. These include the presence of a thin fibrous cap, a necrotic lipid core and the accumulation of macrophages.(2,3,25) Nevertheless, the assessment of plaque by OCT remains largely qualitative with the notable exception of the measurement of the thickness of the fibrous cap covering necrotic areas. The other limitation of OCT for plaque quantification is the inability to provide a full thickness analysis of large plaques because of its limited penetration. OCT however, offers obvious advantages when dealing with superficial structures such as the fibrous cap.(6)

Optical coherence tomography is highly sensitive and specific for the characterization of plaques when compared to histological examination. Yabushita et al (27) performed an in-vitro study of more than 300 human atherosclerotic artery segments. When compared to histological examination, OCT had a sensitivity and specificity of 71-79% and 97-98% for fibrous plaques, 95-96% and 97% for fibrocalcific plaques, and 90-94.5% and 90-92% for lipid-rich plaques, respectively. Further, the inter-observer and intra-observer variability of OCT measurements were high (κ values of 0.88 and 0.91 respectively). Table 3 highlights the OCT features of

fibrous, lipid and calcific plaques. Figure 4 demonstrates the OCT appearance of lipid-rich plaque with TCFA.

Recently, Kubo et al (22) used OCT, together with IVUS and angioscopy to assess plaque characteristics in 30 patients presenting with AMI. The imaging devices were consecutively used following initial mechanical thrombectomy and found the incidence of plaque rupture by OCT to be 73%, significantly higher than that detected by both angioscopy (47%, p= 0.035) and IVUS (40%, p =0.009). The incidence of TCFA was 83% in this patient population and only OCT was able to estimate the fibrous cap thickness (mean 49±21μm). Further, intracoronary thrombus was observed in all cases by OCT and angioscopy but was identified only in 33% of patients by IVUS (p< 0.001). The potential for OCT in such circumstances is clearly evident with intense research currently ongoing to detect vulnerable lesions early on in their natural history, thereby limiting morbidity and mortality.

Fibrous	Lipid-rich	Calcified
High reflectivity Homogenous Finely textured	Low reflectivity Homogenous Diffuse margins	Low reflectivity Inhomogeneous Sharp margins or Isolated, strong reflections in dark background

Table 3: OCT appearance of different atherosclerotic plaques

OCT Precautions and Limitations

OCT remains a specialised technique that should not be performed unless a thorough proctorship has been undertaken. As the procedure demands temporary blood removal and flush (either lactated ringers or contrast), it should not be performed in patients with poor left ventricular function or those presenting with haemodynamic compromise. Further, it is contra-indicated in patients with single remaining vessel or those with impaired renal function. Lesions that are ostial or proximally located cannot be adequately imaged using proximal balloon occlusion and thus a non-occlusive technique may be preferred in these circumstances. Large calibre vessels often preclude complete circumferential imaging and this remains a technological limitation that is currently being refined.

The next generation image wires will offer improved durability and trackability. Future systems will offer smoother L-mode acquisition and edge-detection software with faster acquisition speeds such as optical frequency-domain imaging (OFDI). Eventually, automated plaque morphology detection will also be included.(6) All these advances will build on an already unique imaging technology that will play a pivotal role in better understanding coronary artery disease well into the future.

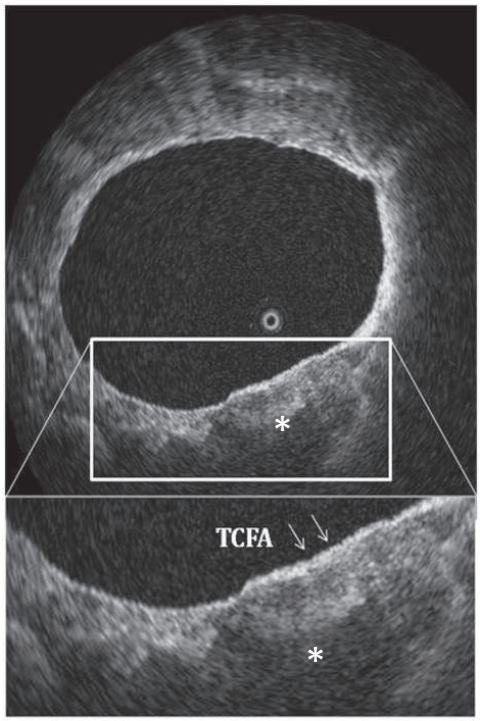

Figure 4: The OCT appearance of lipid-rich plaque and TCFA. This plaque has the typical characteristics of being poorly reflective with diffuse borders (*). The overlying thin fibrous cap is bright and highly reflective. The mean cap thickness was 44 microns.

see colour section

References

1. Regar E, Schaar JA, Mont E, Virmani R, Serruys PW. Optical coherence tomography. Cardiovasc Radiat Med 2003;4:198-204.
2. Tearney GJ, Yabushita H, Houser SL, et al. Quantification of macrophage content in atherosclerotic plaques by optical coherence tomography. Circulation 2003;107:113-9.
3. Jang IK, Tearney GJ, MacNeill B, et al. In vivo characterization of coronary atherosclerotic plaque by use of optical coherence tomography. Circulation 2005;111:1551-5.
4. Tearney GJ, Jang IK, Bouma BE. Optical coherence tomography for imaging the vulnerable plaque. J Biomed Opt 2006;11:021002.
5. Shite J, Matsumoto D, Yokoyama M. Sirolimus-eluting stent fracture with thrombus, visualization by optical coherence tomography. Eur Heart J 2006;27:1389.
6. Tanigawa J, Barlis P, Di Mario C. Intravascular Optical Coherence Tomography: Optimisation of image acquisition and quantitative assessment of stent strut apposition. EuroIntervention 2007;3:128-136.
7. Tanigawa J, Barlis P, Di Mario C. Do unapposed stent struts endothelialise? In vivo demonstration with optical coherence tomography. Heart 2007;93:378.
8. Prati F, Zimarino M, Stabile E, et al. Does optical coherence tomography identify arterial healing after stenting? An in vivo comparison with histology, on a rabbit carotid model. Heart 2007.
9. Tanigawa J, Barlis P, Dimopoulos K, Di Mario C. Optical coherence tomography to assess malapposition in overlapping drug-eluting stents. EuroIntervention 2008;3:580-83.
10. Takano M, Inami S, Jang IK, et al. Evaluation by optical coherence tomography of neointimal coverage of sirolimus-eluting stent three months after implantation. Am J Cardiol 2007;99:1033-8.
11. Barlis P, Serruys PW, DeVries A, Regar E. Optical coherence tomography assessment of vulnerable plaque rupture: predilection for the plaque 'shoulder'. Eur Heart J 2008:ehn085.

12. Tanigawa J, Barlis P, Kaplan S, Goktekin O, Di Mario C. Stent strut apposition in complex lesions using optical coherence tomography. Am J Cardiol 2006;98:Suppl 1: 97M.
13. Regar E, Schaar J, Serruys PW. Images in cardiology. Acute recoil in sirolimus eluting stent: real time, in vivo assessment with optical coherence tomography. Heart 2006;92:123.
14. Barlis P, Virmani R, Sheppard MN, Tanigawa J, Di Mario C. Angiographic and histological assessment of successfully treated late acute stent thrombosis secondary to a sirolimus-eluting stent. Eur Heart J 2007;28:1675.
15. Joner M, Finn AV, Farb A, et al. Pathology of drug-eluting stents in humans: delayed healing and late thrombotic risk. J Am Coll Cardiol 2006;48:193-202.
16. Virmani R, Guagliumi G, Farb A, et al. Localized hypersensitivity and late coronary thrombosis secondary to a sirolimus-eluting stent: should we be cautious? Circulation 2004;109:701-5.
17. Park DW, Park SW, Park KH, et al. Frequency of and risk factors for stent thrombosis after drug-eluting stent implantation during long-term follow-up. Am J Cardiol 2006;98:352-6.
18. Fujii K, Carlier SG, Mintz GS, et al. Stent underexpansion and residual reference segment stenosis are related to stent thrombosis after sirolimus-eluting stent implantation: an intravascular ultrasound study. J Am Coll Cardiol 2005;45:995-8.
19. Morice MC, Serruys PW, Sousa JE, et al. A randomized comparison of a sirolimus-eluting stent with a standard stent for coronary revascularization. N Engl J Med 2002;346:1773-80.
20. Fujii K, Mintz GS, Kobayashi Y, et al. Contribution of stent underexpansion to recurrence after sirolimus-eluting stent implantation for in-stent restenosis. Circulation 2004;109:1085-8.
21. Takano M, Yamamoto M, Inami S, et al. Long-term follow-up evaluation after sirolimus-eluting stent implantation by optical coherence tomography: do uncovered struts persist? J Am Coll Cardiol 2008;51:968-9.
22. Kubo T, Imanishi T, Takarada S, et al. Assessment of culprit lesion morphology in acute myocardial infarction: ability of optical coherence tomography compared with intravascular ultrasound and coronary angioscopy. J Am Coll Cardiol 2007;50:933-9.
23. Chia S, Christopher Raffel O, Takano M, Tearney GJ, Bouma BE, Jang IK. In-vivo comparison of coronary plaque characteristics using optical coherence tomography in women vs. men with acute coronary syndrome. Coron Artery Dis 2007;18:423-7.
24. Giattina SD, Courtney BK, Herz PR, et al. Assessment of coronary plaque collagen with polarization sensitive optical coherence tomography (PS-OCT). Int J Cardiol 2006;107:400-9.
25. Jang IK, Bouma BE, Kang DH, et al. Visualization of coronary atherosclerotic plaques in patients using optical coherence tomography: comparison with intravascular ultrasound. J Am Coll Cardiol 2002;39:604-9.
26. Barlis P, Serruys PW, DeVries A, Regar E. Optical coherence tomography assessment of vulnerable plaque rupture: predilection for the plaque 'shoulder'. Eur Heart J 2008; 29:2023
27. Yabushita H, Bouma BE, Houser SL, et al. Characterization of human atherosclerosis by optical coherence tomography. Circulation 2002;106:1640-5.

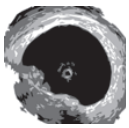

Chapter 3

Novel intravascular imaging technologies

Hector Garcia-Garcia, Nieves Gonzalo, Peter Barlis, Patrick W. Serruys

The ability to detect vulnerable plaques *in vivo* is essential to study their natural history and to evaluate potential therapeutic interventions that may ultimately favorably impact on acute coronary syndrome (ACS) and death. Coronary angiography offers valuable information on the long-term behavior of complex coronary lesions but does have several limitations. Goldstein et al (1) reported that patients with ST-segment elevation myocardial infarction (STEMI) and multiple complex lesions had an increased incidence of recurrent ACS during the year following STEMI compared to patients with a single complex lesion (19.0% vs 2.6%, p <0.001, respectively). Taking this into consideration however, angiography only permits a 2-dimensional view of the arteries and is unable to give precise detail about the vessel wall. As a result, a number of invasive imaging modalities are being tested or used, specifically geared toward the evaluation of vulnerable plaque (2). These techniques are capable of giving unique detail on the vessel wall, lumen, plaque tissue composition and the status of inflammation and therefore circumvent many of the limitations of coronary angiography. This chapter will provide a contemporary review of these technologies with particular reference to their use in the assessment of vulnerable plaque and coronary stents.

1. Histopathological vulnerable plaque definitions

The "classical", most described phenotype of vulnerable plaque is a thin capped fibroatheroma (TCFA) (3), characterized by a large necrotic core with an overlying thin cap infiltrated by macrophages. Smooth muscle cells within the cap are absent or few. The thickness of the fibrous cap near the rupture site measures 23 ± 19 μm, with 95% of caps measuring <65 μm(4,5). Rupture of a TCFA with exposure of the thrombogenic necrotic core to circulating platelets is thought to be responsible for 60% of all acute coronary syndromes (ACS) (5). Macrophage infiltration of the thin cap with release of matrix metalloproteinases and local inflammation can cause extracellular matrix degradation and subsequent plaque rupture (6,7). Excessive mechanical strain, particularly at the junction of the TCFA and the normal vessel wall is another factor predisposing to rupture (8,9).

Chevuru et al. (10) reported new pathological evidence on TCFA characterization. The prevalence of TCFA and rupture is *low* (0.46±0.95 and 0.38±0.70 per heart, respectively), *focal* in nature and located in the *proximal segments* of coronary arteries. In earlier studies, up to 3 TCFA were found per heart(11). Necrotic core size was relatively *small* for both, TCFA (1.6±1.8mm$^{2;}$ length 2.7±2.0mm) and ruptured plaques (2.2±1.9mm^2; length 1.9±3.6mm). In previous studies, the size of necrotic core in TCFAs was 1.7±1.1mm^2 with a length of 8mm (range 2-17mm), and in ruptured plaques 3.8±5.5mm^2, with a length of 9mm (range 2.5-22mm)(12).

The second recognized phenotype of vulnerable plaque, accounting for approximately 40% of coronary thromboses in pathology series is plaque erosion in lesions consisting of either pathological intimal thickening or thick-capped fibroatheroma (13). These lesions typically have a high smooth muscle cell content and are rich in proteoglycans and are more common in young women and smokers, but are not associated with other conventional risk factors such as hypercholesterolemia (14,15).

Thirdly, there are calcified nodules, which may protrude into the vessel lumen and comprise up to 5% of lesions in pathological series. These lesions are characterized by an absence of endothelial and inflammatory cells (15). In addition, intra-plaque hemorrhage secondary to leakage from the vasa vasorum may also play a pathological role (16).

2. Imaging of vulnerable plaques

Angioscopy

Coronary angioscopy (CAS) is a well-established technique that allows direct visualization of the plaque surface and intra-luminal structures. It enables assessment of the plaque color (white, red, yellow), and can illuminate plaque complications such as rupture, intimal tears and thrombosis with a higher sensitivity compared to angiography (17-20). On angioscopy, normal artery segments appear as glistening white, whereas atherosclerotic plaques can be categorized based on their angioscopic color as yellow. Platelet-rich thrombus at the site of plaque rupture is characterized as white granular material, and fibrin/erythrocyte-rich thrombus as an irregular, red structure protruding into the lumen. Yellow plaques are associated with ACS (21) and thrombosis (22). They have also been correlated with other features of vulnerability such as positive remodeling and increased distensibility (23).
The major limitation of angioscopy is that it is a rather specialized technique that requires a blood-free field during image acquisition, which can be obtained either by complete vessel occlusion or by continuous saline flushing distal to the angioscope. Presently, coronary angioscopy (Vecmova®, Clinical Supply Co., Gifu, Japan) can be performed while blood is cleared from the field of view by injection of 5-10 ml normal saline. Nevertheless, angioscopy only allows limited assessment of the coronary tree (i.e. vessels > 2 mm diameter) and assessment of stenotic lesions may prove technically difficult. Furthermore, imaging is only of the luminal surface and, although changes in the vessel wall are reflected on the surface, this might not be sufficiently sensitive to detect subtle alterations in plaque composition or plaque burden in the presence of positive remodeling (24).
Kubo et al (20) recently used CAS, optical coherence tomography (OCT) and IVUS to assess culprit lesion morphology in acute myocardial infarction (AMI). The incidence of plaque rupture observed by OCT was 73%, 47% by CAS ($p=0.035$) and by IVUS 40%, ($p=0.009$). Furthermore, OCT (23%) was superior to CAS (3%, $p=0.022$) and IVUS (0%, $p=0.005$) in the detection of fibrous cap erosion. The intra-coronary thrombus was observed in all cases by OCT and CAS, but was identified in 33% by IVUS (vs. OCT, $p<0.001$).

Intravascular ultrasound radiofrequency analysis: Virtual histology

Description of the technique

Grey-scale IVUS imaging is formed by the envelope (amplitude) of the radiofrequency signal, discarding a considerable amount of information lying beneath and between the peaks of the signal. The frequency and power of the signal commonly differ between tissues, regardless of similarities in the amplitude. IVUS-Virtual Histology (IVUS-VH, Volcano Corp., Rancho Cordoba, USA) involves spectral analysis of the data and evaluates different spectral parameters (Y-intercept, minimum power, maximum power, mid-band power, frequency at minimum power, frequency at maximum power, slope, etc.) to construct tissue maps that classify plaque into four major components (fibrous, fibrolipidic, necrotic core and calcium). Different plaque components are assigned different color codes: calcified (white), fibrous (green), fibrolipidic (greenish-yellow) and necrotic core (red) (25). Although this classification was initially evaluated *in vitro*, more recently IVUS-VH pre- and post-procedure have also been correlated with pathological atherectomy specimens showing good correlation for all 4 tissue types (26). As assessed by IVUS-VH, the sensitivity and specificity for fibrous tissue was 86% and 90.5%, fibrofatty 79.3% and 100%, necrotic core 67.3% and 92.9% and dense calcium 50% and 98.9% respectively.

IVUS-VH data is currently acquired using a commercially available 64-element phased-array catheter (Eagle Eye™ 20 MHz catheter, Volcano Corporation, Rancho Cordova, USA). Using an automated pullback device, the transducer is withdrawn at a continuous speed of 0.5 mm/s up to the ostium. IVUS-VH acquisition is ECG-gated at the R-wave peaks using a dedicated console.
IVUS B-mode images are reconstructed by customized software and contour detection is performed using cross-sectional views with semi-automatic contour detection software to provide quantitative geometrical and compositional measurements. Due to the limitations of manual calibration (27), the radiofrequency data is normalized using a technique known as "Blind Deconvolution", an iterative algorithm that deconvolves the catheter transfer function from the backscatter, thus accounting for catheter-to-catheter variability (28,29).
It has been our observation that in the near field, an excessive amount of necrotic core is present. The developers have accounted for this with a corrected version introduced in the latest release of the classification tree.

Virtual histology and plaque characterization

Lesion classification is based on static images obtained from autopsy specimens. In brief, some believe that atherosclerotic lesion progression starts with pathologic intimal thickening in which lipid accumulates in areas rich in proteoglycans (lipid pools), but no trace of necrotic core. Others believe that the earliest change of atherosclerosis is the fatty streak, also called as intimal xanthoma. The earliest lesion with a necrotic core is the fibroatheroma (FA), and this is the precursor lesion that may give rise to symptomatic heart disease**.** Thin-capped fibroatheroma (TCFA) is a lesion characterized by a large necrotic core containing numerous cholesterol clefts. The overlying cap is thin and rich in inflammatory cells, macrophages and T lymphocytes with few smooth muscle cells. Plaques prone to rupture are those with decrease cap thickness, large lipid-necrotic core and severe inflammatory infiltrate A study done by Burke et al(4). identified a cut-off value for cap thickness of <65 microns for vulnerable coronary plaque definition.
Virtual Histology can potentially identify detect thin-cap fibroatheromas (TCFAs). In addition, the progression of the disease can also be followed-up. Table 1 outlines the virtual histology plaque and lesion types that are proposed based on the above pathologic data. (figure 1).

Lesion Type	Brief Description
Adaptive Intimal Thickening (AIT)	<600 μm of intima thickness
Pathological Intimal Thickening (PIT)	≥600 μm thickness for >20% of the circumference with FF >15%, and no confluent NC or DC
Fibrotic Plaque (FT)	Dominant FT and no confluent NC or DC
Fibrocalcific Plaque (FC)	Confluent DC with no confluent NC
Fibroatheroma (FA)	Confluent NC not at the lumen on three consecutive frames
Thin Cap Fibroatheroma (TCFA)	Confluent NC at the lumen on three consecutive frames

FT – fibrous tissue; FF – fibro-fatty tissue; NC – necrotic core; and DC – dense calcium.

Table 1: VH-IVUS Proposed Lesion Types

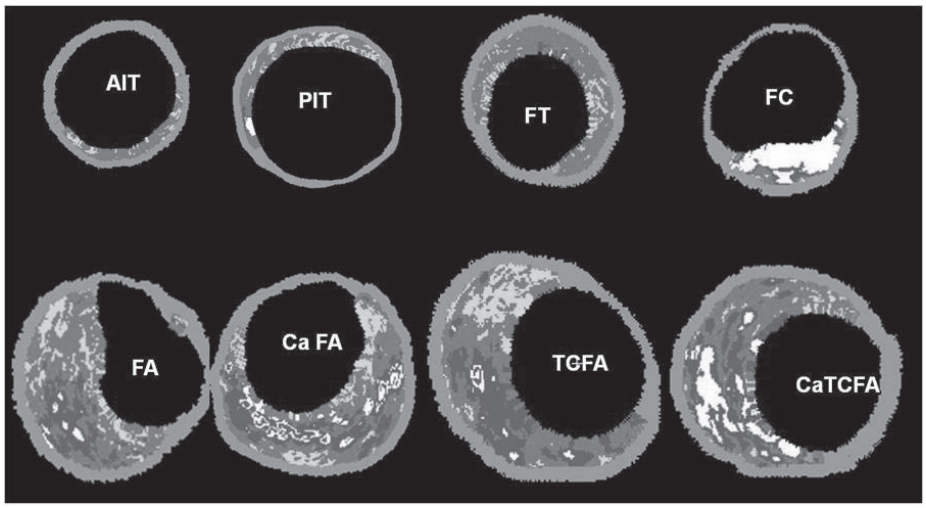

Figure 1. IVUS-Virtual histology proposed lesion types. AIT, adaptative intimal thickening; PIT, pathological intimal thickening; FT, fibrotic plaque; FC, fibrocalcific; FA, fibroatheroma;CaFA, calcified fibroatheroma; TCFA, thin-capped fibroatheroma.

see colour section

Our group recently evaluated the incidence of IVUS-derived thin-cap fibroatheroma (IDTCFA) using IVUS-VH (30). Two independent IVUS analysts defined IDTCFA as a lesion fulfilling the following criteria in at least 3 consecutive cross-sectional areas: 1) necrotic core ≥10% without evident overlying fibrous tissue, 2) lumen obstruction ≥ 40%. In this study, 62% of patients had at least one IDTCFA in the interrogated vessels. ACS patients had a significantly higher incidence of IDTCFA than stable patients [3.0 (interquartile range 0.0, 5.0) IDTCFA/coronary vs. 1.0 (interquartile range 0.0, 2.8) IDTCFA/coronary, p= 0.018]. Finally, a clear clustering pattern was seen along the coronaries, with 66.7 % of all IDTCFAs located in the first 20 mm whereas further along the vessels the incidence was significantly lower (33.3%, p=0.008). This distribution of IDTCFAs is consistent with previous *ex vivo* and clinical studies, with a clear clustering pattern from the ostium demonstrating a non-uniform distribution of vulnerable plaques along the coronary tree (31). Patients presenting with ACS had a significantly higher prevalence of IDTCFA even in non-culprit vessels, supporting the concept of a multi-focal process (32). Of note, the lesion percent area stenosis and the mean necrotic core areas of the IDTCFAs detected by IVUS-VH were also similar to previously reported histopathological data (55.9 % vs. 59.6 % and 19 % vs. 23 % respectively) (12).

It is worth mentioning that, although the most accepted threshold to define a cap as "thin" has previously been set at <65 μm, this was based on post mortem studies that studied ruptured plaques (33). Extrapolation of such criteria to *in vivo* studies therefore requires caution. It is well established that tissue shrinkage occurs during tissue fixation (34). Shrinkage (particularly of collagen, the main component of fibrous caps) of up to 60 %, 15 % and 80% can occur during critical-point-drying, free-drying, and air-drying respectively (35). Furthermore, post-mortem contraction of arteries is an additional confounding factor (36,37). Since the axial resolution of IVUS-VH is 246 μm, we assumed that the absence of visible fibrous tissue overlying a necrotic core suggested a cap thickness of below 246 μm and used the absence of such tissue to define a thin fibrous cap (38).

We have recently developed software to quantify the amount of necrotic core in contact with the lumen, enabling refinement of our analysis. Our current definition of an IVUS-derived TCFA

(IDTCFA) is a lesion fulfilling the following criteria in at least 3 consecutive cross-sectional areas (CSAs): 1) plaque burden ≥ 40%; 2) confluent necrotic core ≥ 10% in direct contact with the lumen (i.e. no visible overlying tissue) in the investigated CSA; all consecutive CSAs having the same morphologic characteristics are considered as part of the same IDTCFA lesion (39). In a recent study, using this refined definition of TCFA as assessed by IVUS-VH, in patients with ACS underwent IVUS of all three epicardial coronaries, on average, there were 2 IVUS-derived thin cap fibroatheroma (IDTCFA) per patient with half of them showing outward remodeling(39).
The potential value of IVUS-VH in the prediction of adverse coronary events is currently under evaluation in two international multicentre prospective studies (PROSPECT and IBIS 2 trials).

Virtual histology and coronary embolization

Recently, two studies evaluated the usefulness of IVUS-VH plaque composition to predict the risk of embolization during stenting (40,41). In one of them, 71 patients with STEMI that underwent primary PCI within 12 hours of the beginning of the symptoms were included. After crossing the lesion with a guidewire and performing thrombectomy with an aspiration catheter, VH-IVUS of the infarct-related vessel was performed. The stent was then deployed without embolic protection. ST segment re-elevation was used as a marker of distal embolization during stenting. Eleven patients presented with ST segment re-elevation after stenting. Total plaque volume was similar in both groups, but the NC volume was significantly higher in the group of patients with ST segment re-elevation (32.9 ± 14.1 mm^3 vs. 20.4 ± 19.1 mm^3, $p < 0.05$). On receiver-operating characteristic curves, NC volume was the best predictor of ST re-elevation after stent deployment as compared with fibrous, fibro-lipid, dense calcium, and total plaque volumes. The cut-off point for NC volume that was best predictive for ST re-elevation was 33.4 mm^3, with a sensitivity of 81.7% and a specificity of 63.6%. The second study included 44 patients who underwent elective coronary stenting. Plaque composition was assessed with VH-IVUS, and small embolic particles liberated during stenting were detected as high-intensity transient signals (HITS) with a Doppler guidewire. Patients were divided into the tertiles according to the HITS counts. Dense calcium and NC area were significantly larger in the highest tertile. In the multivariate logistic regression analysis, only necrotic core area was an independent predictor of high HITS counts (odds ratio 4.41, $p = 0.045$).

Intravascular Ultrasound Radiofrequency analysis: Palpography

This technique allows the assessment of local mechanical tissue properties. For a defined pressure difference, soft tissue (e.g. lipid-rich) components will deform more than hard tissue components (e.g. fibrous, calcified) (42,43). Radiofrequency data obtained at different pressure levels are compared to determine the local tissue deformation.
Each palpogram represents the strain information for a certain cross section over the full cardiac cycle. The longitudinal resolution of the acquisitions depend on heart rate and pullback speed. With a heart rate of 60 bpm and a pullback speed of 1.0 mm/s, the longitudinal resolution is 1.0 mm. Palpograms are acquired using a 20-MHz phased array IVUS catheter (Eagle Eye™ 20 MHz catheter, Volcano Therapeutics, Rancho Cordova, USA). Digital radiofrequency data are acquired using a custom-designed workstation.
The local strain is calculated from the gated radiofrequency traces using cross-correlation analysis and displayed, color-coded, from blue (for 0% strain) to red to yellow (for 2% strain) (44). Plaque strain values are assigned a Rotterdam Classification (ROC) score ranging from 1 to 4 (ROC I= 0-<0.6 %; ROC II= 0.6- <0.9 %; ROC III= 0.9-<1.2 %; ROC IV= >1.2 %) (45) (figure 2).

see colour section

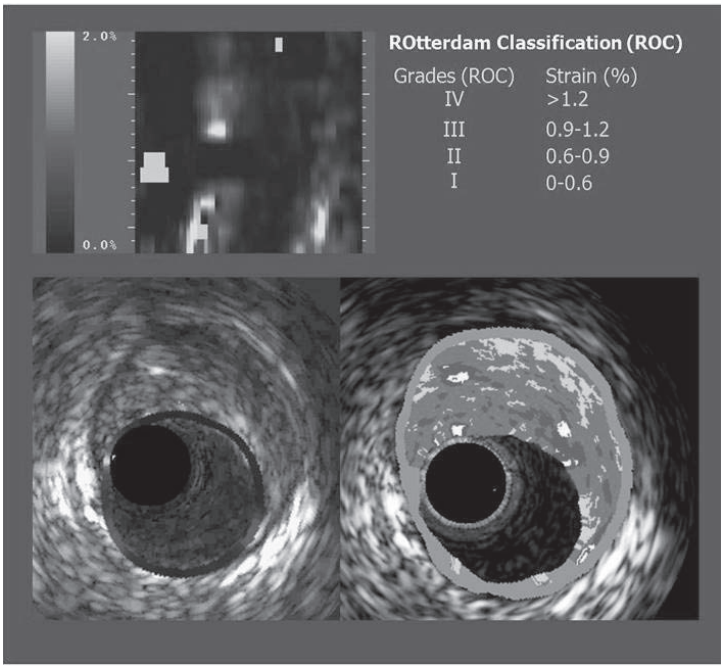

Figure 2. IVUS-palpography. In the upper left side the palpography strain map is opened up. The local strain is calculated from the gated radiofrequency traces using cross-correlation analysis and displayed, color-coded, from blue (for 0% strain) to red to yellow (for 2% strain). Plaque strain values are assigned a Rotterdam Classification (ROC) score ranging from 1 to 4 (ROC I= 0-<0.6 %; ROC II= 0.6- <0.9 %; ROC III= 0.9-<1.2 %; ROC IV= >1.2 %). At the bottom, in the same cross-sectional area a high-strain spot (ROC III) is shown (left); in the virtual histology (VH) image (right) a confluent necrotic core area in contact with the lumen is seen, suggesting an IVUS-derived thin capped fibroatheroma. The IVUS-VH color-code is fibrous tissue (green), fibro-fatty tissue (light green), necrotic core (red) and dense calcium (white).

Our group has demonstrated that palpography has a high sensitivity (88%) and specificity (89%) to detect vulnerable plaques *in vitro* (42). Postmortem coronary arteries were investigated with intravascular elastography and subsequently processed for histology. There was a positive correlation between the presence of high strain and the degree of macrophage infiltration ($P<0.006$) and an inverse relation between the amount of smooth muscle cells and strain ($P<0.0001$). Vulnerable plaques identified by palpography had a thinner cap than non-vulnerable plaques ($P<0.0001$). In a subsequent study, 55 patients with either stable or unstable angina, or acute MI were analyzed. Among patients with stable angina, the prevalence of deformable plaques was significantly lower per vessel (0.6+/-0.6) than in patients presenting with unstable angina (1.6+/-0.7, p=0.0019) or with acute MI (2.0+/-0.7, p<0.0001). In the IBIS I study, on palpography, both the absolute number of high-strain spots (grade 3/4) in the ROI (p=0.009) and their density per cm (p=0.012) decreased significantly between baseline and follow-up. This decrease in the overall population was largely driven by changes in the subgroup of patients with STEMI; this group had both the highest number of high-strain spots at baseline and the most marked relative decrease during follow-up compared to patients with other clinical presentations. At 6-month follow-up, the density of high-strain spots (1.2±1.4/cm) was comparable among clinical subgroups (46).

The potential value of IVUS-palpography is currently under evaluation in two international multicentre prospective studies, PROSPECT and IBIS 2 trials. These two studies have also

obtained IVUS-virtual histology during the same IVUS pullback, allowing for the assessment of both morphological and biomechanical properties of a particular plaque. Assessing several characteristics of a given plaque could potentially enhance invasive risk stratification by identifying very high-risk plaques, thereby lowering the number of vulnerable plaques that deserve to be serially followed and, ultimately treated (figure 2).

Optical coherence tomography

Optical coherence tomography OCT) is an optical analogue of ultrasound, however it uses light instead of sound to create an image (47,48). For OCT imaging, low coherence, near infrared light with a wavelength around 1300 nm is used since it minimizes the energy absorption in the light beam caused by protein, water, hemoglobin, and lipid. The light waves are reflected by the internal microstructures within biological tissues as a result of their differing optical indices.
This technique provides a resolution of 10-20μm *in vivo* (49); this level of detail is well beyond the level of resolution of IVUS (100-150μm) (50). OCT has been demonstrated to be highly sensitive and specific for characterizing atherosclerotic plaques *in vitro* when compared with histological analysis (51-53) with a sensitivity and specificity of 71-79% and 97-98% for fibrous plaques, 95-96% and 97% for fibrocalcific plaques, and 90-94% and 90%-92% for lipid-rich plaques, respectively. In addition, the inter- and intra-observer reliabilities of OCT assessment were high (kappa values of 0.88 and 0.91, respectively) (53). *In vitro* comparison of OCT with IVUS have demonstrated superior delineation by OCT of structural details such as thin caps, lipid pools or tissue proliferation (54). An *in vitro* comparison of OCT, integrated backscatter IVUS (similar methodology to IVUS-VH) and conventional IVUS found that OCT had the best potential for tissue characterization of coronary plaques, with higher sensitivity and specificity compared to the other imaging modalities (55). However, a recent study comparing OCT to histopathology reported a lower sensitivity for plaque components. Misclassification occurred in 41% of lesions, predominantly due to a combination of incomplete penetration depth into the vessel wall and the inability to distinguish calcium deposits from lipid pools (56).
In a pilot clinical study, our group performed *in vivo* OCT analysis of the coronary arterial wall in patients who were undergoing percutaneous coronary intervention. Imaging was possible in all patients and the entire vessel circumference was visualized at all times. A wide spectrum of different plaque morphologies was observed. OCT allowed for differentiation of the normal artery wall and inhomogeneous, mixed plaques, as well as thin cap fibroatheromas with inhomogeneous, low-reflecting necrotic cores, covered by highly-reflecting thin fibrous caps (50).
As a result of its high axial resolution, there is no doubt that OCT is the *in vivo* gold standard for identifying and measuring the thickness of the fibrous cap (figure 3); an *in vivo* study found a significant difference in minimal cap thickness between acute MI and stable angina patients, with median (interquartile range) values of 47.0 (25.3-184.3) μm and 102.6 (22.0-291.1) μm respectively ($p= 0.02$) (57). On top of its reliability as a tool to measure the thickness of the cap *in vivo*, recent post-mortem and *in vivo* studies have shown that OCT is capable of evaluating the macrophage content of infiltrated fibrous caps (58,59).
Kubo et al. (20) evaluated the ability of intracoronary OCT to assess culprit lesions during primary PCI in patients with acute MI. The thickness of the remnants of the fibrous cap after symptomatic rupture measured was 49±21μm. The main limitation of OCT is the shallow tissue penetration depth (1.5-2mm) which hampers imaging of the entire vessel wall in large vessels and light absorbance by blood that currently needs to be overcome by saline infusion and balloon occlusion, thereby precluding interrogation of long and proximal segments of the coronary tree.

see colour section

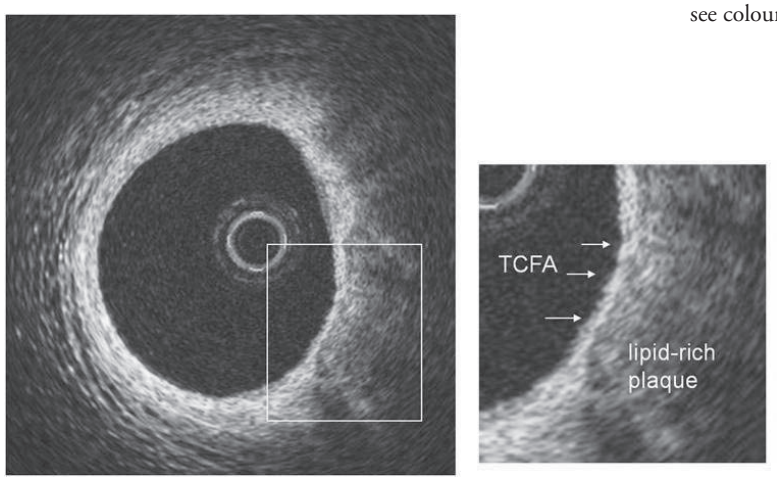

Figure 3: thin cap fibroatheroma visualised with OCT as a highly reflective thin band (arrows)

This has recently been partly overcome with the use of non-occlusive techniques whereby contrast is flushed through the guiding catheter during simultaneous image acquisition at 3.0mm/seconds (M3, LightLab Imaging Inc., Westford, MA, USA). Furthermore, even more encouraging is the use of optical frequency domain imaging (OFDI) that enables even faster pullback speeds without compromise of image quality and resolution.

Thermography

Atherosclerosis is accompanied by inflammation, and vulnerable plaques have been associated with increased macrophage activity, metabolism and inflammation (60). Activated macrophages produce thermal energy, which might be detected on the surface of these atherosclerotic lesions using specially-designed catheters equipped with thermistor sensors at the distal tip (61). A rise in temperature can be found in atherosclerotic plaques as compared to disease-free coronary segments. Temperature differences between an atherosclerotic plaque and normal vessel wall increase progressively from patients with stable angina to patients with acute MI with a maximum temperature difference to the background temperature of 1.5±0.7°C (62). In a prospective study, Stefanadis et al reported an association between temperature heterogeneity and the incidence of adverse events at follow-up in patients with coronary artery disease undergoing successful PCI (63). In addition, treatment with statins seemed to affect the thermographic results: in non-culprit lesions the temperature difference was lower in the group treated with statins compared with the untreated group (0.06 ± 0.05°C vs. 0.11 ± 0.10°C; p = 0.05) (64).

However, there are several different aspects that deserve further investigation. The prevalence and distribution of inflammatory cells in stable and unstable atherosclerotic plaque is unclear, and the predictive value of 'warm' lesions remains elusive. Furthermore, the impact of different coronary flow conditions on plaque temperature ('cooling effect') is still not completely understood (65,66). Simulations have revealed that the correct interpretation of intravascular thermographic measurements requires data on the flow and on the morphologic characteristics of the atherosclerotic plaque (67).

There are a few limitations to the routine use of thermography in the catheterization laboratory: (i) most of the catheters used still comprise over-the-wire systems; (ii) accurate temperature

assessment requires direct contact of the thermistors with the vessel wall, with the associated potential risk of endothelial damage (68) and (iii) as the temperature within the vessel changes rapidly with fluid application, any intracoronary injection of contrast, flush or medication has to be avoided before and during measurements.

Intravascular Magnetic Resonance

Magnetic resonance (MR) is a non-ionizing diagnostic tool exploiting the spins of the nuclear protons in a strong magnetic field. For intravascular diagnosis, two different approaches have been introduced.
The first, conventional approach visualizes the anatomical structure by using a coil placed in a catheter or wire in combination with an external magnet (MR imaging). While this approach has previously been shown to be able to provide detailed information on structure and composition of the arterial wall and plaque, (69) the procedure has to be performed in a MR magnet, not in a cardiac catheterization laboratory. The accuracy for MRI differentiation of plaque components has been validated in vitro and feasibility demonstrated in vivo (70). The 0.030-inch IVMRI coil had a sensitivity and specificity of 73% and 85% respectively for lipid, 83% and 81% respectively for fibrous tissue and 100% and 97% respectively for calcification. Subsequently, the same system was applied in human iliac arteries *in vivo* using a 1.5T magnet with a resolution of 312µm. Complete vessel wall analysis was possible in all 25 patients and required 20 minutes for an arterial segment of 20mm length. Compared to IVUS, mean lumen diameters were similar, but the outer wall area was overestimated by IVMRI (mean $116.4\pm4.7mm^2$ vs. $86.6\pm5.8mm^2$, p=0.0001). However, inter-observer agreements for IVMRI were much higher (kappa 0.68-0.79) than for IVUS (kappa 0.21).

The other, novel approach analyses the chemical composition by placing both, the coils and miniaturized magnets on the tip of a catheter, without the need of external magnets (MR spectroscopy) and can be performed in the cardiac catheterization laboratory(71). MR spectroscopy can identify fibrous and lipid-rich tissue by measuring differential water diffusion in a field of view. Acquired data is displayed as color-code sectors based on the lipid fraction index (LFI) for each zone of the FOV. Blue indicates no lipid, gray correspond to intermediate lipid content and yellow indicates high-lipid content (figure 4). Clinical feasibility of catheter-based, self-contained IV MR spectroscopy has been recently demonstrated in patients scheduled for coronary catheterization(72).

Preclinical trials employing this technology demonstrated its capacity to differentiate plaque components of human aortas, coronary and carotid arteries in vitro: IVMR spectroscopy was able to accurately detect different components (fibrous cap, smooth muscle cells, organizing thrombus, fresh thrombus, edema, lipid and calcium) with sensitivities and specificities ranging from 84-100%. Agreement with histology for grading the extent of intra-plaque lipid accumulation was 74% and 80% for grading intimal thickness. Further analysis revealed high correlation to histological analysis of a wide spectrum of plaque types in 15 of 16 (94%) aortic lesions and 16 of 18 (89%) coronary lesions (sensitivity 100%, specificity 89%), including one plaque rupture, three TFCAs, seven thick-cap fibrous atheroma, four fibrocalcific plaques, two intimal xanthomas, and one adaptive intimal thickening (73).
Current limitations include the limited field of view, the size of the catheter, the need for direct vessel wall contact and the time required for acquisition. In the past, the use of an auto-perfusion balloon during data acquisition has been proposed to limit ischemia(74).

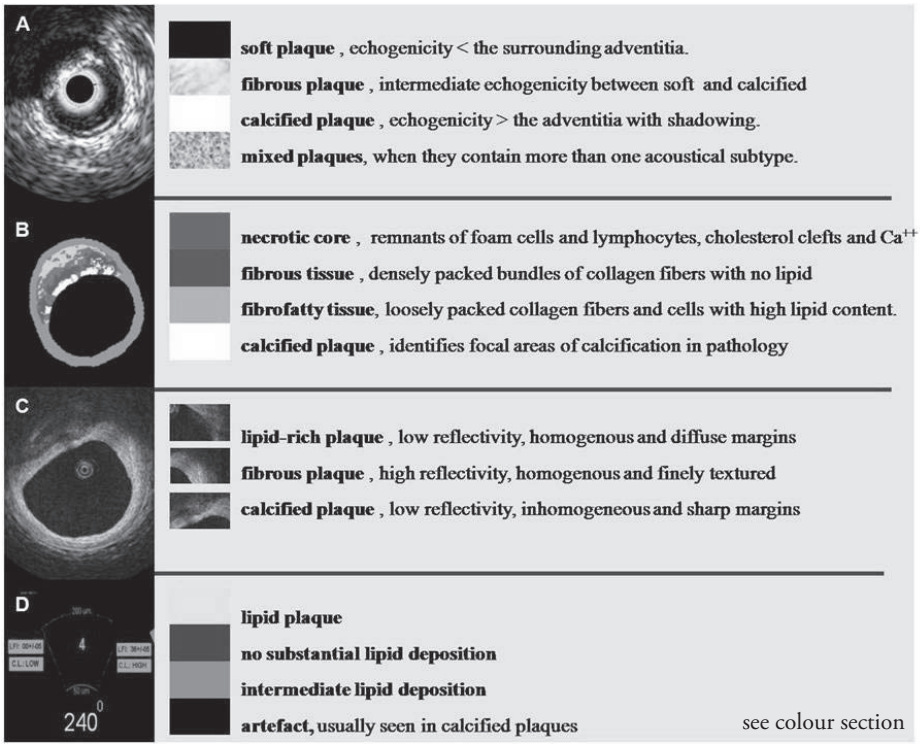

Figure 4. Multi-modality imaging in the coronary arteries. The same coronary segment (represented by one frame) has been imaged by 4 different imaging techniques. In the grey-scale IVUS (panel A), IVUS-virtual histology (panel B), optical coherence tomography (panel C) and intravascular magnetic resonance spectroscopy (IVMR) the results of the same frame across different techniques are shown. Of note, in the upper left quadrant of the plaque a calcified area is seen in three imaging modalities, but in IVMR where an artifact is observed. On the right hand side, the different plaque and tissues types across the coronary imaging techniques is shown.

Clearly IVMR diagnostics remain an exciting area still under development. Catheter-based system will further increase the user friendliness, their sample volume and allow for scanning of longer arterial segments. Upcoming developments include the improvement MR plaque differentiation by the use of contrast agents, such as paramagnetic gadolinium-based contrast(75) or supra-paramagnetic contrast agents (iron oxide nanoparticles), that can accumulate in macrophages (76). There are still a few unanswered questions, including the effect of the thermal energy generated on small arteries and on coronary artery stents, although conventional MRI appears safe in this setting(77).

Recently in our center, a study has been started to explore a multi-modality imaging approach of atherosclerotic plaque in-vivo. The same coronary segment is assessed by greyscale IVUS, IVUS-VH and OCT and IVMR (figure 4). This has been a challenging process, since we are dealing with the different imaging resolutions and the lack of common nomenclature and classification across these imaging techniques.

Raman and near infrared spectroscopy

A number of spectroscopic intravascular imaging techniques have been developed recently and are still under investigation (78). Spectroscopy can provide qualitative and quantitative information about chemical plaque composition. The Raman effect is created when incident laser light (typically 750-850nm wavelength) excites molecules in a tissue sample, which scatter light at a different wavelength. This change in wavelength, called the "Raman effect" is dependent on the chemical components of the tissue sample (79,80) and can therefore provide quantitative information about molecular composition (81-83). Raman spectroscopy has shown acceptable correlation compared with histology ($r = 0.68$ for cholesterol and $r = 0.71$ calcification) (83) and with IVUS *in vitro* (82).
Raman spectroscopy technology collect scattered light with optical fibers and route the collected signal to spectrometer systems for analysis. Previously optical fiber probes utilized a region of the Raman spectrum called the "fingerprint" (FP) region (< ~1800 cm^{-1} shifted light) to conduct remote assays, but due to techinical problems with this approach, it has been recently replaced by using another region of the Raman spectrum, called high wavenumber (HW) Raman shifted light (> ~2500 cm^{-1} shifted light). This
allows us to collect Raman spectra via a single optical fiber, simplifying the size and complexity of the catheter and making it clinically feasible. Thus, the optical catheter system (OCS) (vPredict™) has been introduced as a tool for measuring the chemical composition of coronary vessels *in-vivo* using Raman spectroscopy and the subsequent mapping and quantification of the vessel and plaque components for evaluating plaque progression. In a xenograft model, lipid-laden plaque were identified with the collected Raman spectra by utilizing the overall cholesterol content, i.e. the sum of the free cholesterol and cholesterol esters contents, and setting a decision threshold at 12 %, as determined in previous studies. As expected, the lipid laden plaques exhibit an increased content of free cholesterol and cholesterol esters, while the non-atherosclerotic samples are mainly protein and triglycerides. **Table 2.**

Demonstrated:	Collagen, Elastin, Myosin, Triglycerides, Beta-carotene, Foam cells, Cholesterol/esters, Hemoglobin, Fibrin
Possible:	Metalloproteinases, Low density lipoprotein (LDL), Oxidized LDL, Proteoglycans, Glycosaminoglycans, Plasmin, Nucleic acids, Nitrotyrosine

Table 2. Plaque/vessel components detectable by Raman spectroscopy.

The vPredict OCS delivers infrared light to the vessel wall through optical fibers contained within a small flexible catheter and captures a portion of the reflected light for spectral analysis. This analysis provides information about the composition of the underlying tissue.
Alternatively, near infrared (NIR) molecular vibrational transitions can be measured in the NIR region (750–2500 nm) (84) and laser spectroscopy using wavelengths of 360-510 nm has been evaluated *in vitro* (85).

Near-infrared spectroscopy observes how different substances absorb and scatter NIR light to different degrees at various wavelengths. A NIR spectrometer emits light into a sample and measures the proportion of light that is returned over a wide range of optical wavelengths. The return signal is then plotted as a graph of absorbance (y-axis) at different wavelengths (x-axis) called a spectrum.
In aortic and coronary artery autopsy specimens, the ability of the technique to identify lipid-rich TCFA through blood has been confirmed (86). A catheter-based system has been developed to address the challenges of access to the coronary artery, blood, motion, and the need to scan that must be overcome for use in patients. Initial clinical experience in six patients with stable angina demonstrates that high-quality NIR spectra can be safely obtained (87). Additional studies are planned to validate the ability of the technique to identify lipid-rich coronary artery plaques and ultimately link chemical characterization with subsequent occurrence of an ACS (88,89).

3. Imaging of coronary stents

Intravascular Ultrasound radiofrequency analysis: Virtual Histology

Intravascular ultrasound– virtual histology classifies stent struts as "dense calcium" (DC) and "necrotic core" (NC). We applied this property to follow-up the degradation of a bioabsorbable stent by measuring the temporal changes in IVUS-VH characteristics. 27 consecutive patients treated with a single bioabsorbable everolimus-eluting stent (BVS, Abbott Laboratories, IL USA) in simple lesions were imaged with IVUS-VH after predilation (pre-stenting cohort of 13 pts), post-stenting and again following 6 months. There was an increase in absolute "dense calcium" and "necrotic core" by 297% and 256% respectively from pre- to post-stenting. Overall, patients (n=27) with post-stenting and follow-up VH showed a significant decrease in "dense calcium" (28.3% vs. 20.9, $p<0.001$). Individually, in 21 out of 27 patients, there was a regression in the "calcified" pattern**.** Although not significantly, "necrotic core" content also decreased (22.4% vs. 20.3, $p=0.227$). In turn, both fibrofatty and fibrous tissue increased (5.0% vs. 7.4, $p=0.024$ and 44.3% vs. 51.4%, $p=0.006$ respectively). In conclusion, the quantitative assessment of the IVUS-VH changes at 6 months suggests a reduction of the DC compatible with early struts alteration of the BVS. (figure 5).

Optical coherence tomography

OCT permits the detailed assessment of stents and their relation to the vessel wall, both immediately following implantation and, at follow-up. Furthermore, OCT also allows the quantification of neointimal tissue surrounding each individual stent strut. Unlike bare metal stents (BMS), which develop circumferential coverage with an average thickness of 500μm or more, well visualized with IVUS and angiography, (90) drug-eluting stents (DES) delay and prevent this hyperplastic response so that the average late lumen loss can be as low as 0.1 or 0.2mm, (91,92) which means the amount of intimal tissue will not be detectable with IVUS. (90)
Several small studies have recently been published highlighting the application of OCT in the detection of stent tissue coverage at follow-up. Matsumoto et al (93) studied 34 patients following sirolimus-eluting stent (SES) implantation. The mean neointima thickness was 52.5 microns, and the prevalence of struts covered by thin neointima undetectable by IVUS was 64%. The average rate of neointima-covered struts in an individual SES was 89%. Nine SES (16%) showed full coverage by neointima, whereas the remaining stents had partially uncovered struts.(93) Similarly, Takano et al (94) studied 21 patients (4,516 struts) 3 months following SES implantation. Rates of exposed struts and exposed struts with malapposition were 15% and 6%, respectively. These were more frequent in patients with ACS than in those with non-ACS (18%

vs 13%, p <0.0001; 8% vs 5%, p <0.005, respectively). The ability of OCT to image at high resolution is the major advantage over IVUS and it also affords the potential to quantify the amount of neointimal tissue formed over struts, an application which remains elusive for a technique like angioscopy. OCT is now also being incorporated in more and more clinical stent trials with the goal of assessing neointimal tissue coverage, an important potential surrogate marker for late thrombosis. (95,96) (figure 6)

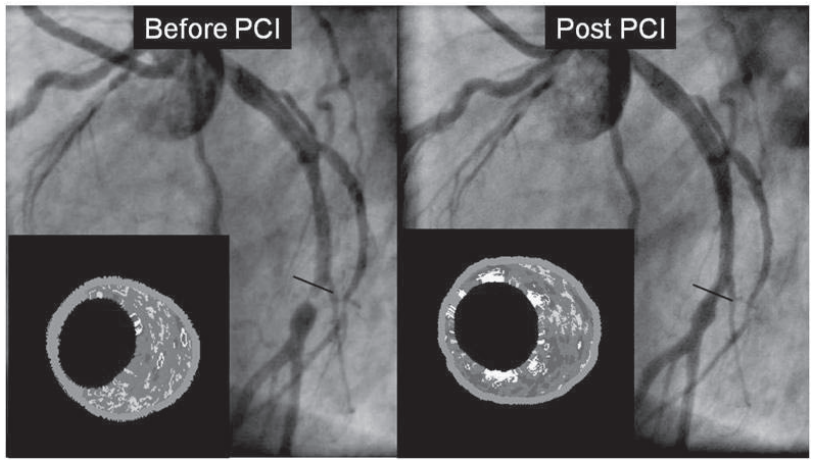

Figure 5. IVUS-virtual histology in stented segments. In the left hand side, a coronary angiogram of the left coronary system shows on the distal segment of the left circumflex artery an eccentric lesion. A pre-stenting virtual histology (VH) frame showed a fibrotic type of plaque (location of VH frame is indicated by a black line). On the right hand side, the post-stenting VH frame is depicted. Of note, at the lumen and surrounding areas an increase in the amount of "dense calcium" and "necrotic core" is observed. This is due to the presence of stent struts that are misclassified by VH. (percutaneous coronary intervention – PCI).

see colour section

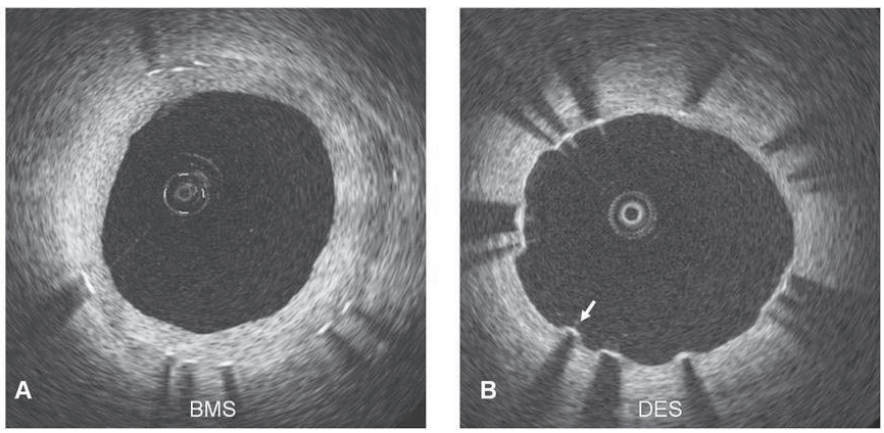

Figure 6: A: Demonstrates the optical coherence tomography (OCT) imaging of a bare metal stent 4 months following implantation. The circumferential tissue struts are visible with shadowing induced by the metal. The neointimal tissue measured between 140 and 220 microns in thickness
B: OCT imaging of a drug-eluting stent (DES) at 4 months follow-up showing the circumferential struts with a very thin neointimal layer (10-40 microns thick). The arrow indicates a strut with no visible tissue coverage

Conclusions

Several invasive imaging techniques are currently under development to detect vulnerable coronary plaques in human coronary arteries *in vivo*. To date however, none of the techniques described above have been sufficiently validated and, more importantly, they have not demonstrated a sound and reproducible ability to predict future adverse cardiac events. Intravascular palpography and virtual histology, based on conventional IVUS catheters, appear to be very promising and their predictive role is presently under investigation in a large international trial.

Very rigorous and well-designed studies are compelling for defining the role of each imaging modality. Non-invasive techniques and the assessment of humoral and genetic factors comprise complementary and important tools in this direction.

At present, the main purpose of all these evolving techniques is to improve our understanding of atherosclerotic disease and to define its natural history. Ultimately, the aim is to identify patients at high risk for future cardiovascular events and to evaluate the benefits from either local or systemic therapeutic interventions.

References

1. Goldstein JA, Demetriou D, Grines CL, Pica M, Shoukfeh M, O'Neill WW. Multiple complex coronary plaques in patients with acute myocardial infarction. N Engl J Med 2000;343:915-22.
2. Waxman S, Ishibashi F, Muller JE. Detection and treatment of vulnerable plaques and vulnerable patients: novel approaches to prevention of coronary events. Circulation 2006;114:2390-411.
3. Kolodgie FD, Burke AP, Farb A, et al. The thin-cap fibroatheroma: a type of vulnerable plaque: the major precursor lesion to acute coronary syndromes. Curr Opin Cardiol. 2001;16:285-92.
4. Burke AP, Farb A, Malcom GT, Liang YH, Smialek J, Virmani R. Coronary risk factors and plaque morphology in men with coronary disease who died suddenly. N Engl J Med 1997;336:1276-82.
5. Virmani R, Kolodgie FD, Burke AP, Farb A, Schwartz SM. Lessons from sudden coronary death: a comprehensive morphological classification scheme for atherosclerotic lesions. Arterioscler Thromb Vasc Biol 2000;20:1262-75.
6. Moreno PR, Falk E, Palacios IF, Newell JB, Fuster V, JT. F. Macrophage infiltration in acute coronary syndromes. Implications for plaque rupture. Circulation 1994;90:775-8.
7. Ross R. Atherosclerosis -- An Inflammatory Disease. N Engl J Med 1999;340:115-126.
8. Loree HM, Kamm RD, Stringfellow RG, RT. L. Effects of fibrous cap thickness on peak circumferential stress in model atherosclerotic vessels. Circ Res 1992;71:850-8.
9. Richardson PD, Davies MJ, GV. B. Influence of plaque configuration and stress distribution on fissuring of coronary atherosclerotic plaques. Lancet 1989;2:941-4.
10. Cheruvu PK, Finn AV, Gardner C, et al. Frequency and distribution of thin-cap fibroatheroma and ruptured plaques in human coronary arteries: a pathologic study. J Am Coll Cardiol 2007;50:940-9.
11. Kolodgie FD, Virmani R, Burke AP, et al. Pathologic assessment of the vulnerable human coronary plaque. Heart 2004;90:1385-91.
12. Virmani R, Burke AP, Kolodgie FD, Farb A. Vulnerable plaque: the pathology of unstable coronary lesions. J Interv Cardiol 2002;15:439-46.
13. Farb A, Burke AP, Tang AL, et al. Coronary Plaque Erosion Without Rupture Into a Lipid Core : A Frequent Cause of Coronary Thrombosis in Sudden Coronary Death. Circulation 1996;93:1354-1363.
14. Arbustini E, Dal Bello B, Morbini P, et al. Plaque erosion is a major substrate for coronary thrombosis in acute myocardial infarction. Heart 1999;82:269-272.
15. Virmani R, Kolodgie FD, Burke AP, Farb A, Schwartz SM. Lessons From Sudden Coronary Death : A Comprehensive Morphological Classification Scheme for Atherosclerotic Lesions. Arterioscler Thromb Vasc Biol 2000;20:1262-1275.
16. Kolodgie FD, Gold HK, Burke AP, et al. Intraplaque Hemorrhage and Progression of Coronary Atheroma. N Engl J Med 2003;349:2316-2325.
17. Mizuno K, Satomura K, Miyamoto A, et al. Angioscopic evaluation of coronary-artery thrombi in acute coronary syndromes. N Engl J Med 1992;326:287-291.

18. Sherman CT, Litvack F, Grundfest W, et al. Coronary angioscopy in patients with unstable angina pectoris. N Engl J Med 1986;315:913-919.
19. de Feyter PJ, Ozaki Y, Baptista J, et al. Ischemia-Related Lesion Characteristics in Patients With Stable or Unstable Angina : A Study With Intracoronary Angioscopy and Ultrasound. Circulation 1995;92:1408-1413.
20. Kubo T, Imanishi T, Takarada S, et al. Assessment of culprit lesion morphology in acute myocardial infarction: ability of optical coherence tomography compared with intravascular ultrasound and coronary angioscopy. J Am Coll Cardiol 2007;50:933-9.
21. Thieme T, Wernecke KD, Meyer R, et al. Angioscopic evaluation of atherosclerotic plaques: validation by histomorphologic analysis and association with stable and unstable coronary syndromes. J Am Coll Cardiol 1996;28:1-6.
22. Ueda Y, Ohtani T, Shimizu M, Hirayama A, Kodama K. Assessment of plaque vulnerability by angioscopic classification of plaque color. Am Heart J 2004;148:333-5.
23. Takano M, Mizuno K, Okamatsu K, Yokoyama S, Ohba T, Sakai S. Mechanical and structural characteristics of vulnerable plaques: analysis by coronary angioscopy and intravascular ultrasound. J Am Coll Cardiol 2001;38:99-104.
24. Smits PC, Pasterkamp G, de Jaegere PP, de Feyter PJ, Borst C. Angioscopic complex lesions are predominantly compensatory enlarged: an angioscopy and intracoronary ultrasound study. Cardiovasc Res 1999;41:458-64.
25. Nair A, Kuban BD, Tuzcu EM, Schoenhagen P, Nissen SE, Vince DG. Coronary Plaque Classification With Intravascular Ultrasound Radiofrequency Data Analysis. Circulation 2002;106:2200-2206.
26. Nasu K, Tsuchikane E, Katoh O, et al. Accuracy of In Vivo Coronary Plaque Morphology Assessment: A Validation Study of In Vivo Virtual Histology Compared With In Vitro Histopathology. Journal of the American College of Cardiology 2006;47:2405-2412.
27. Rodriguez-Granillo GA, Aoki J, Ong AT, et al. Methodological considerations and approach to cross-technique comparisons using in vivo coronary plaque characterization based on intravascular ultrasound radiofrequency data analysis: insights from the Integrated Biomarker and Imaging Study (IBIS). Int J Cardiovasc Intervent 2005;7:52-8.
28. Kaaresen K. Deconvolution of sparse spike trains by iterated window maximization. IEEE Trans Signal Process 1997;45:1173-1183.
29. Kaaresen K, Bolviken E. Blind deconvolution of ultrasonic traces accounting for pulse variance. IEEE Trans Ultrason Ferroelectr Freq Control 1999;46:564-573.
30. Rodriguez-Granillo GA, Garcia-Garcia HM, Mc Fadden EP, et al. In Vivo Intravascular Ultrasound-Derived Thin-Cap Fibroatheroma Detection Using Ultrasound Radiofrequency Data Analysis. Journal of the American College of Cardiology 2005;46:2038-2042.
31. Wang JC, Normand SL, Mauri L, Kuntz RE. Coronary artery spatial distribution of acute myocardial infarction occlusions. Circulation 2004;110:278-84.
32. Rioufol G, Finet G, Ginon I, et al. Multiple Atherosclerotic Plaque Rupture in Acute Coronary Syndrome: A Three-Vessel Intravascular Ultrasound Study 10.1161/01.CIR.0000025609.13806.31. Circulation 2002;106:804-808.
33. Burke AP, Farb A, Malcom GT, Liang Y, Smialek J, R V. Coronary Risk Factors and Plaque Morphology in Men with Coronary Disease Who Died Suddenly. N Engl J Med 1997;336:1276-1282.
34. Lowder ML, Li S, Carnell PH, RP. V. Correction of distortion of histologic sections of arteries. Journal of Biomechanics;In Press, Corrected Proof.
35. Boyde A, Jones SJ, Tamarin A. Dimensional changes during specimen preparation for scanning electron microscopy. Scanning Electron Microsc 1977;1:507-18.
36. Fishbein MC, Siegel RJ. How big are coronary atherosclerotic plaques that rupture? Circulation 1996;94:2662-6.
37. Siegel RJ, Swan K, Edwalds G, Fishbein MC. Limitations of postmortem assessment of human coronary artery size and luminal narrowing: differential effects of tissue fixation and processing on vessels with different degrees of atherosclerosis. J Am Coll Cardiol 1985;5:342-6.
38. Nair A , Calvetti D, DG V. Regularized Autoregressive Analysis of Intravascular Ultrasound Data: Improvement in Spatial Accuracy of Plaque Tissue Maps. IEEE Trans Ultrason Ferroelectr Freq Control 2004;51:420-431.

39. Garcia-Garcia HM, Goedhart D, Schuurbiers JC, et al. Virtual histology and remodeling index allow in vivo identification of allegedly high risk coronary plaques in patients with acute coronary syndromes: a three vessel intravascular ultrasound radiofrequency data analysis. Eurointervention 2006;2:338-344.
40. Kawaguchi R, Oshima S, Jingu M, et al. Usefulness of virtual histology intravascular ultrasound to predict distal embolization for ST-segment elevation myocardial infarction. J Am Coll Cardiol 2007;50:1641-6.
41. Kawamoto T, Okura H, Koyama Y, et al. The relationship between coronary plaque characteristics and small embolic particles during coronary stent implantation. J Am Coll Cardiol 2007;50:1635-40.
42. Schaar JA, de Korte CL, Mastik F, et al. Characterizing Vulnerable Plaque Features With Intravascular Elastography. Circulation 2003;108:2636-2641.
43. Schaar JA, Regar E, Mastik F, et al. Incidence of High-Strain Patterns in Human Coronary Arteries: Assessment With Three-Dimensional Intravascular Palpography and Correlation With Clinical Presentation. Circulation 2004;109:2716-2719.
44. de Korte CL, Carlier SG, Mastik F, et al. Morphological and mechanical information of coronary arteries obtained with intravascular elastography; feasibility study in vivo. Eur Heart J 2002;23:405-13.
45. van Mieghem CAG, Bruining N, Schaar JA, et al. Rationale and methods of the integrated biomarker and imaging study (IBIS): combining invasive and non-invasive imaging with biomarkers to detect subclinical atherosclerosis and assess coronary lesion biology. The International Journal of Cardiovascular Imaging (formerly Cardiac Imaging) 2005;21:425-441.
46. Van Mieghem CA, McFadden EP, de Feyter PJ, et al. Noninvasive detection of subclinical coronary atherosclerosis coupled with assessment of changes in plaque characteristics using novel invasive imaging modalities: the Integrated Biomarker and Imaging Study (IBIS). J Am Coll Cardiol 2006;47:1134-42.
47. Regar E vLA, Serruys PW. Optical coherence tomography in cardiovascular research. London: Informa Healthcare 2007;ISBN 1841846112.
48. Huang D, Swanson EA, Lin CP, et al. Optical coherence tomography. Science 1991;254:1178-81.
49. Brezinski ME, Tearney GJ, Bouma BE, et al. Imaging of coronary artery microstructure (in vitro) with optical coherence tomography. Am J Cardiol 1996;77:92-3.
50. Regar E, Schaar JA, Mont E, Virmani R, Serruys PW. Optical coherence tomography. Cardiovascular Radiation Medicine 2003;4:198-204.
51. Jang IK, Bouma BE, Kang DH, et al. Visualization of coronary atherosclerotic plaques in patients using optical coherence tomography: comparison with intravascular ultrasound. J Am Coll Cardiol 2002;39:604-9.
52. Patwari P, Weissman NJ, Boppart SA, et al. Assessment of coronary plaque with optical coherence tomography and high-frequency ultrasound. Am J Cardiol 2000;85:641-4.
53. Yabushita H, Bouma BE, Houser SL, et al. Characterization of Human Atherosclerosis by Optical Coherence Tomography. Circulation 2002;106:1640-1645.
54. Brezinski ME, Tearney GJ, Weissman NJ, et al. Assessing atherosclerotic plaque morphology: comparison of optical coherence tomography and high frequency intravascular ultrasound. Heart 1997;77:397-403.
55. Kawasaki M, Bouma BE, Bressner J, et al. Diagnostic Accuracy of Optical Coherence Tomography and Integrated Backscatter Intravascular Ultrasound Images for Tissue Characterization of Human Coronary Plaques. Journal of the American College of Cardiology 2006;48:81-88.
56. Manfrini O, Mont E, Leone O, et al. Sources of Error and Interpretation of Plaque Morphology by Optical Coherence Tomography. The American Journal of Cardiology 2006;98:156-159.
57. Jang IK, Tearney GJ, MacNeill B, et al. In Vivo Characterization of Coronary Atherosclerotic Plaque by Use of Optical Coherence Tomography. Circulation 2005;111:1551-1555.
58. Tearney GJ, Yabushita H, Houser SL, et al. Quantification of Macrophage Content in Atherosclerotic Plaques by Optical Coherence Tomography. Circulation 2003;107:113-119.
59. MacNeill BD, Jang IK, Bouma BE, et al. Focal and multi-focal plaque macrophage distributions in patients with acute and stable presentations of coronary artery disease. Journal of the American College of Cardiology 2004;44:972-979.
60. Fuster V. Human lesion studies. Ann N Y Acad Sci 1997;811:207-24; discussion 224-5.

61. Casscells W, Hathorn B, David M, et al. Thermal detection of cellular infiltrates in living atherosclerotic plaques: possible implications for plaque rupture and thrombosis. Lancet 1996;347:1447-51.
62. Stefanadis C, Diamantopoulos L, Vlachopoulos C, et al. Thermal heterogeneity within human atherosclerotic coronary arteries detected in vivo: A new method of detection by application of a special thermography catheter. Circulation 1999;99:1965-71.
63. Stefanadis C, Toutouzas K, Tsiamis E, et al. Increased local temperature in human coronary atherosclerotic plaques: an independent predictor of clinical outcome in patients undergoing a percutaneous coronary intervention. J Am Coll Cardiol 2001;37:1277-83.
64. Toutouzas K, Drakopoulou M, Mitropoulos J, et al. Elevated plaque temperature in non-culprit de novo atheromatous lesions of patients with acute coronary syndromes. J Am Coll Cardiol 2006;47:301-6.
65. Stefanadis C, Toutouzas K, Tsiamis E, et al. Thermal heterogeneity in stable human coronary atherosclerotic plaques is underestimated in vivo: the "cooling effect" of blood flow. J Am Coll Cardiol 2003;41:403-8.
66. Diamantopoulos L, Liu X, De Scheerder I, et al. The effect of reduced blood-flow on the coronary wall temperature: Are significant lesions suitable for intravascular thermography? 10.1016/S0195-668X(03)00440-8. Eur Heart J 2003;24:1788-1795.
67. ten Have AG, Gijsen FJ, Wentzel JJ, Slager CJ, van der Steen AF. Temperature distribution in atherosclerotic coronary arteries: influence of plaque geometry and flow (a numerical study). Phys Med Biol 2004;49:4447-62.
68. Verheye S, De Meyer GRY, Krams R, et al. Intravascular thermography: Immediate functional and morphological vascular findings. Eur Heart J 2004;25:158-165.
69. Correia LC, Atalar E, Kelemen MD, et al. Intravascular magnetic resonance imaging of aortic atherosclerotic plaque composition. Arterioscler Thromb Vasc Biol 1997;17:3626-32.
70. Larose E, Yeghiazarians Y, Libby P, et al. Characterization of human atherosclerotic plaques by intravascular magnetic resonance imaging. Circulation 2005;112:2324-31.
71. Blank A, Alexandrowicz G, Muchnik L, et al. Miniature self-contained intravascular magnetic resonance (IVMI) probe for clinical applications. Magn Reson Med 2005;54:105-12.
72. Regar E HB, Grube E, Halon D, Wilensky R.L, Virmani R, Schneiderman J, Sax S, Friedmann H, Serruys PW, Wijns W. First-In-Man application of a miniature self-contained intracoronary magnetic resonance probe. A multi-centre safety and feasibility trial. Eurointervention 2006;2:77-83.
73. Schneiderman J, Wilensky RL, Weiss A, et al. Diagnosis of thin-cap fibroatheromas by a self-contained intravascular magnetic resonance imaging probe in ex vivo human aortas and in situ coronary arteries. J Am Coll Cardiol 2005;45:1961-9.
74. Quick HH, Ladd ME, Hilfiker PR, Paul GG, Ha SW, Debatin JF. Autoperfused balloon catheter for intravascular MR imaging. J Magn Reson Imaging 1999;9:428-34.
75. Barkhausen J, Ebert W, Heyer C, Debatin JF, Weinmann HJ. Detection of atherosclerotic plaque with Gadofluorine-enhanced magnetic resonance imaging. Circulation 2003;108:605-9.
76. Kooi ME, Cappendijk VC, Cleutjens KB, et al. Accumulation of ultrasmall superparamagnetic particles of iron oxide in human atherosclerotic plaques can be detected by in vivo magnetic resonance imaging. Circulation 2003;107:2453-8.
77. Porto I, Selvanayagam J, Ashar V, Neubauer S, Banning AP. Safety of magnetic resonance imaging one to three days after bare metal and drug-eluting stent implantation. Am J Cardiol 2005;96:366-8.
78. Moreno PR, Muller JE. Identification of high-risk atherosclerotic plaques: a survey of spectroscopic methods. Current Opinion in Cardiology 2002;17:638-647.
79. Brennan JF, 3rd, Romer TJ, Lees RS, Tercyak AM, Kramer JR, Jr., Feld MS. Determination of human coronary artery composition by Raman spectroscopy. Circulation 1997;96:99-105.
80. Baraga JJ, Feld MS, Rava RP. In situ Optical Histochemistry of Human Artery Using Near Infrared Fourier Transform Raman Spectroscopy. PNAS 1992;89:3473-3477.
81. Romer TJ, Brennan JF, Fitzmaurice M, et al. Histopathology of Human Coronary Atherosclerosis by Quantifying Its Chemical Composition With Raman Spectroscopy. Circulation 1998;97:878-885.

82. Romer TJ, Brennan JF, Puppels GJ, et al. Intravascular Ultrasound Combined With Raman Spectroscopy to Localize and Quantify Cholesterol and Calcium Salts in Atherosclerotic Coronary Arteries. Arterioscler Thromb Vasc Biol 2000;20:478-483.
83. van de Poll SWE, Kastelijn K, Schut TCB, et al. On-line detection of cholesterol and calcification by catheter based Raman spectroscopy in human atherosclerotic plaque ex vivo. Heart 2003;89:1078-1082.
84. Wang J, Geng YJ, Guo B, et al. Near-infrared spectroscopic characterization of human advanced atherosclerotic plaques. J Am Coll Cardiol 2002;39:1305-13.
85. Marcu L, Fishbein MC, Maarek JM, Grundfest WS. Discrimination of Human Coronary Artery Atherosclerotic Lipid-Rich Lesions by Time-Resolved Laser-Induced Fluorescence Spectroscopy. Arterioscler Thromb Vasc Biol 2001;21:1244-1250.
86. Moreno PR, Lodder RA, Purushothaman KR, Charash WE, O'Connor WN, Muller JE. Detection of lipid pool, thin fibrous cap, and inflammatory cells in human aortic atherosclerotic plaques by near-infrared spectroscopy. Circulation 2002;105:923-7.
87. Moreno PR, Muller JE. Identification of high-risk atherosclerotic plaques: a survey of spectroscopic methods. Curr Opin Cardiol 2002;17:638-47.
88. Caplan JD, Waxman S, Nesto RW, Muller JE. Near-infrared spectroscopy for the detection of vulnerable coronary artery plaques. J Am Coll Cardiol 2006;47:C92-6.
89. Waxman S, Ishibashi F, Caplan JD. Rationale and use of near-infrared spectroscopy for detection of lipid-rich and vulnerable plaques. J Nucl Cardiol 2007;14:719-28.
90. Tanigawa J, Barlis P, Di Mario C. Intravascular Optical Coherence Tomography: Optimisation of image acquisition and quantitative assessment of stent strut apposition. EuroIntervention 2007;3:128-136.
91. Morice MC, Serruys PW, Sousa JE, et al. A randomized comparison of a sirolimus-eluting stent with a standard stent for coronary revascularization. N Engl J Med 2002;346:1773-80.
92. Fujii K, Mintz GS, Kobayashi Y, et al. Contribution of stent underexpansion to recurrence after sirolimus-eluting stent implantation for in-stent restenosis. Circulation 2004;109:1085-8.
93. Matsumoto D, Shite J, Shinke T, et al. Neointimal coverage of sirolimus-eluting stents at 6-month follow-up: evaluated by optical coherence tomography. Eur Heart J 2006.
94. Takano M, Inami S, Jang IK, et al. Evaluation by optical coherence tomography of neointimal coverage of sirolimus-eluting stent three months after implantation. Am J Cardiol 2007;99:1033-8.
95. Finn AV, Joner M, Nakazawa G, et al. Pathological correlates of late drug-eluting stent thrombosis: strut coverage as a marker of endothelialization. Circulation 2007;115:2435-41.
96. Finn AV, Nakazawa G, Joner M, et al. Vascular responses to drug eluting stents: importance of delayed healing. Arterioscler Thromb Vasc Biol 2007;27:1500-10.

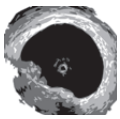

Chapter 4

A Multi-Centre Evaluation of the Safety of Intra-Coronary Optical Coherence Tomography

Peter Barlis, Nieves Gonzalo, Carlo Di Mario, Francesco Prati, Lutz Buellesfeld, Johannes Rieber, Miles C. Dalby, Giuseppe Ferrante, Maria Cera, Eberhard Grube, Patrick W. Serruys, Evelyn Regar

Aims: *Optical coherence tomography (OCT) is increasingly being applied to the coronary arteries. However, the risks associated with the imaging procedure are not yet well defined. The purpose of the present multi-centre registry was, for the first time, to assess the acute complications associated with the clinical use of intra-coronary OCT in a large number of patients.*

Methods & Results: *Consecutive patients from 6 centres who had OCT examination were retrospectively included. All adverse events and complications, even if transient, were noted. Risks were categorised into: 1) self-limiting 2) major complications including major adverse cardiac events (MACE) and 3) mechanical device failure. A total of 468 patients underwent OCT examination for evaluation of: plaque (40.0%), percutaneous coronary intervention (28.2%) or follow-up stent tissue coverage (31.8%). OCT was performed using a non-occlusive flush technique in 45.3% with a mean contrast volume of 36.6±9.4ml. Transient chest pain and QRS widening/ST-depression/elevation were observed in 47.6% and 45.5% respectively. Major complications included 5 (1.1%) cases of ventricular fibrillation due to balloon occlusion and/or deep guide catheter intubation, 3 (0.6%) cases of air embolism and 1 case of vessel dissection (0.2%). There were no cases of coronary spasm or MACE during or within the 24 hour period following OCT examination.*

Conclusions: *OCT is a specialised technique with a relatively steep learning curve. Major complications are uncommon and can be minimised with careful procedural planning and having an awareness of the potential contributory risks, especially deep guide catheter intubation during contrast flushing. Upcoming developments will make OCT more practical and less procedurally demanding, also potentially conserving contrast volume considerably.*

Optical coherence tomography (OCT) is an intracoronary imaging technique using near infrared light with a much higher spatial resolution than intravascular ultrasound (IVUS). The 15 micron resolution permits detailed characterisation of the vessel wall giving new insights into the in-vivo characterisation of atherosclerotic plaque and tissue responses following stent implantation. Unlike IVUS however, the technique requires flushing of the coronary artery to allow light transmission with the first generation OCT system also mandating proximal vessel balloon occlusion. Whilst the imaging resolution benefits of OCT are clear, the need for a flush system increases the complexity of the technique, and the risks associated with this have not been evaluated. The purpose of the present multi-centre registry was, for the first time, to assess the acute complications associated with the clinical use of intracoronary OCT in a large number of patients.

Methods

Study population and OCT procedure

We conducted a multicentre registry to evaluate the safety of OCT. Data from patients undergoing OCT examination in 6 centres were reviewed. Consecutive patients who had OCT examination performed before January 31, 2008 were retrospectively included. Weight adjusted heparin was administered as standard prior to OCT imaging. All OCT examinations were carried out using a dedicated optical wire (ImageWire, LightLab Imaging Inc., Westford, MA, USA) connected to either the M2 or M3 OCT console (LightLab Imaging Inc., Westford, MA, USA). All participating centres completed the demographic, clinical and procedural case information using a uniform datasheet that was centrally analysed. The indications to perform OCT were categorised into evaluation of (A) lesion/plaque, (B) percutaneous coronary intervention (PCI) or (C) stent tissue coverage at follow-up. The number of vessels imaged, together with the OCT flushing strategy (with or without proximal vessel balloon occlusion, see below) were recorded. OCT exclusion criteria applied by operators/centres included impaired left ventricular ejection fraction (<30%), renal impairment (serum creatinine >1.5mg/dL), single remaining or tortuous

vessel. When the non-occlusive technique was used, the additional contrast load required to permit imaging in a blood-free environment was documented.

Flush strategy

Infrared light is unable to penetrate blood, thus imaging must be accompanied by transient clearance of the field of view from blood. In clinical intracoronary OCT, two methods have been established: 1) using a proximal occlusion balloon with flushing of crystalloid solution through the end hole of the balloon catheter using a power injector or 2) A non-occlusive approach with contrast flush injection via the guiding catheter.(1)

Balloon occlusion method

A low-pressure, short over-the-wire balloon (Helios, Goodman Inc, Nagoya, Japan) with large inner lumen is advanced over a conventional guidewire distal to the region of interest. The guidewire is then replaced with the dedicated OCT imaging wire and the balloon catheter is positioned in the proximal part of the vessel. Inflation of the balloon is performed using a dedicated indeflator to 0.5-0.7atm during which coronary blood flow is replaced by continuous infusion of Ringer's lactate or physiological saline at a rate of 0.5-1.2ml/sec using a power injector (e.g. Mark-V ProVis, Medrad, Inc. Indianola, PA, US).(1-3) A motorised pullback of the image wire is then commenced at a rate of 1.0mm/sec to acquire images.

Non-occlusive technique

As the handling of the OCT image wire is limited by the fact that it contains an optical fibre and is not comparable to a standard guidewire with respect to steerability, pushability and torqueability, its safe passage distal to the region of interest can be facilitated by use of an over-the-wire catheter (e.g. single lumen Transit, Cordis, Johnson & Johnson, Miami, FL, US or double lumen 0.023" TwinPass, Vascular Solutions Inc, Minneapolis, Minnesota, US). The automated pullback (at 3.0mm/sec) is then commenced during simultaneous flushing of viscous iso-osmolar contrast (e.g. Iodixanol 320, Visipaque™, GE Health Care, Cork, Ireland) through the guiding catheter. This can be achieved either manually or by use of an automated power injector (e.g. Mark-V ProVis, Medrad, Inc. Indianola, PA, US).(1-3)

OCT risks

Any complication judged by the operators to have occurred during or within the immediate 24-hour period following OCT examination was included. All events and complications were included, even if transient with no clinical sequeale
Risks were categorised into:

1) Self-limiting events
2) Major complications (arrhythmia, embolisation, coronary dissection or spasm) including major adverse cardiac events (defined as MI, emergency revascularisation including percutaneous or surgical, and death).
3) Mechanical device failure

Furthermore, all risks were classified based on their eventual outcome as: A) Immediate correction with no specific action required B) transient but requiring specific treatment with resolution before the patient left the catheterisation laboratory or C) required

treatment/surveillance following discharge from the catheterisation laboratory (including lengthening patient's hospitalisation).

Study centres

The 6 participating centres were located in the Netherlands (1 centre), United Kingdom (2 centres), Italy (1 centre), Germany (2 centres). The number of OCT studies contributed by each centre was: Thoraxcenter (Rotterdam, the Netherlands n= 162, 34.6%), Royal Brompton Hospital (London, UK, n=91 19.4%), St Giovanni Hospital (Italy, n=85, 18.2%), Helios Heart Centre (Siegburg, Germany, n=64, 13.7%). Medizinische Poliklinik, University of Munich (Munich, Germany, n=36, 7.7%) and Harefield Hospital (Middlesex, UK, n=30, 6.4%).

Statistical analysis

Descriptive analyses were used. Results are quoted as percentages for categorical data or as mean ± standard deviation for continuous variables. Continuous and categorical variables were compared with the t-test and the chi-square/Fisher's exact test as appropriate. A p value of <0.05 was considered significant.

Results

Baseline clinical and procedural characteristics

A total number of 468 OCT examinations were recorded. Table 1 shows the baseline clinical and procedural characteristics. OCT was performed for plaque/lesion evaluation in 187 (40.0%), PCI evaluation in 132 (28.2%) and for the assessment of stent tissue coverage at follow-up in 149 (31.8%) of patients. A total of 510 vessels were imaged (1.1±0.3/patient). The LAD and RCA were the most frequently imaged vessels. A small proportion of patients had OCT imaging of the left main coronary artery (1.2%) and a bypass graft (1.0%).

Of the 468 patients, 256 (54.7%) had images acquired during proximal balloon occlusion while the remaining 212 (45.3%) had OCT using a non-occlusive technique. In these patients, the additional mean contrast load used for flushing during OCT imaging was 36.6±9.4ml.

Risks of OCT

All observed complications are summarised in Table 2. The eventual outcome of the adverse events and complications encountered is depicted in Table 3.

1) Self-limiting events

As expected, the most frequent observation was transient chest pain during OCT image acquisition (47.6%). In all cases this settled following cessation of imaging and was significantly more frequent in patients imaged using the occlusive compared to non-occlusive technique (69.9% vs. 20.8%, $p<0.001$). In association, transient electrocardiographic changes were also observed with widening of the QRS complex or ST-segment depression in 41.0% and ST-elevation in 4.5%, almost exclusively in those imaged using proximal vessel balloon occlusion. Sinus brady and tachycardia was infrequently observed and settled promptly following cessation of imaging. There were 2 (0.4%) cases of transient atrio-ventricular block that spontaneously resolved following deflation of the proximal occlusion balloon and withdrawal of the catheter.

	n=468
Age (yrs)	63.7±9.1
Males	367 (78.4)
Hypertension	264 (56.4)
Diabetes Mellitus	94 (20.1)
Dyslipidaemia	279 (59.6)
Baseline LVEF (%)	61.5±11.2
Prior myocardial infarction	138 (29.5)
Prior coronary artery bypass grafting	23 (4.9)
Prior PCI	247 (52.7)
Clinical Presentation	
Stable angina	248(53.0)
Unstable angina	121 (25.9)
ACS/STEMI	99 (21.1)
Indication for OCT	
Plaque/lesion assessment	187 (40.0)
PCI assessment	132 (28.2)
Follow-up stent tissue coverage	149 (31.8)
Target vessel	n=510
Number of vessels imaged/patient	1.1±0.3
Left Main	6 (1.2)
Left anterior descending	222 (43.5)
Diagonal	14 (2.7)
Right	163 (32.0)
Left circumflex	83 (16.3)
Obtuse marginal	17 (3.3)
Graft	5 (1.0)
OCT System used	
M2	323 (69.0)
M3	145 (31.0)
OCT flushing technique	
Proximal balloon occlusion technique	256 (54.7)
Non-occlusive technique	212 (45.3)
Mean contrast volume (non-occlusive technique, ml)	36.6±9.4

Table 1: Baseline clinical and procedural characteristics

LVEF-left ventricular ejection fraction; PCI-percutaneous coronary intervention; ACS-acute coronary syndrome; STEMI-ST elevation myocardial infarction; OCT-optical coherence tomography;

	All (n=468)	Occlusive technique (n=256)	Non-occlusive technique (n=212)	p-value
Self-limiting events				
Chest pain	223 (47.6)	179 (69.9)	44 (20.8)	<0.001
Widening QRS/ST depression	192 (41.0)	139 (54.3)	53 (25)	<0.001
ST elevation	21 (4.5)	17 (6.6)	4 (1.9)	0.01
Sinus bradycardia	14 (3.0)	11 (4.3)	3 (1.4)	0.07
Sinus tachycardia	10 (2.1)	7 (2.7)	3 (1.4)	0.33
Atrio-ventricular block	2 (0.4)	2 (0.8)	0	0.19
Major Complications				
Arrhythmias				
Atrial fibrillation	0	0	0	-
Ventricular tachycardia	0	0	0	-
Ventricular fibrillation	5 (1.1)	3 (1.2)	2 (0.9)	0.81
Coronary spasm	0	0	0	-
Dissection	1 (0.2)	1 (0.4)	0	0.36
Perforation	0	0	0	-
Thrombus	0	0	0	-
Air embolism	3 (0.6)	2 (0.8)	1 (0.5)	0.68
Mechanical device failure				
Wire tip fracture	1 (0.2)	0	1 (0.5)	0.45
Major adverse cardiac events during the procedure or in the 24 hour period post.	0	0	0	-

Table 2: Risks of OCT

Immediate resolution	96.7%
Required specific treatment but resolved before leaving the catheterisation laboratory	3.1%
Persisting beyond discharge from catheterisation laboratory (including requiring ongoing clinical surveillance)	0.2%

Table 3: Outcome of adverse events/complications

2) Major complications

Ventricular fibrillation

Ventricular fibrillation (VF) occurred in 5 (1.1%) patients. In all cases, sinus rhythm was promptly restored following cessation of OCT imaging and external defibrillation. Three of the 5 cases occurred during proximal balloon occlusion. The 2 cases seen with the non-occlusive technique were in the context of deep guide catheter intubation of the left coronary artery during simultaneous contrast injection.

Air embolism

There were 3 (0.6%) cases of air embolisation. In 1 case, this occurred early on in the procedure, when introducing the guiding catheter specifically with the intention to perform OCT. Two other cases occurred during flushing of the crystalloid solution with air inadvertently introduced during connection of the flush lines. All cases responded promptly to air aspiration, treatment with nitrates and in 1 case, nitroprusside administration.

Coronary dissection

A minor type-A coronary dissection was observed in 1 (0.4%) patient as a result of the imaging wire. Coronary blood flow was not impaired and further treatment was not indicated.

Coronary spasm

There were no cases of coronary spasm observed during OCT imaging.

MACE

There were no MACEs observed during or in the 24 hour period following OCT imaging. In one patient, stenosis was observed at the site of previous balloon occlusion 4 months following OCT evaluation of the LCx. Due to the presence of multi-vessel coronary disease with angina, the patient was referred for CABG.

3) Mechanical device failure

Although there was no adverse clinical outcome observed, in 1 (0.2%) patient having OCT 9 months following stent implantation, the imaging wire became entrapped amongst stent struts in the LAD with subsequent fracture at the distal tip. Four month follow-up was uneventful with control angiography showing patent vessel without flow abnormalities.

Discussion

This is the first systematic registry to demonstrate the acute risks related to OCT imaging in a large number of patients. The high-resolution, together with advantages over other imaging modalities such as IVUS, have made OCT very popular for the detailed assessment of atherosclerotic plaque and coronary stents. As a result, this study provides essential safety information that will see OCT performed in a more informed manner, both for operators and patients alike.

Several groups have reported their clinical experience with OCT over the last few years.(2-11) Nevertheless, only limited information about acute complications of this procedure is available. Recently, Yamaguchi et al (12) examined the feasibility of OCT and IVUS imaging in 76 patients. Although transient chest pain and electrocardiographic changes caused by imaging were not considered as part of their study, there were no adverse events reported following both IVUS and OCT, with the latter being performed exclusively using the occlusive method. In contrast, the present study included a large number of consecutive patients undergoing OCT examination, and recorded all potential adverse events, even if transient and benign. We believe this permits a more informed assessment and is therefore representative of the 'real world' application and safety of OCT imaging.

The present study also assessed patients having OCT imaging using the non-occlusive technique that will, because of its simpler procedural requirements, become the mainstay method for OCT image acquisition, eliminating the cumbersome proximal balloon occlusion requirements. Such developments will be realised in the not too distant future with the introduction into clinical practice of faster image acquisition speeds thanks to optical frequency-domain technologies. Therefore, the expected rise in OCT use is another reason why comprehensively reporting the safety profile of the technique remains of paramount clinical importance.

The spectrum of adverse events observed in relation to OCT imaging in our study was broad. The majority of events recorded were minor and transient, with chest pain being the most frequent. This is not surprising as, in a significant proportion of patients (54.7%), images were obtained during proximal balloon vessel occlusion. In all cases, the chest pain resolved following cessation of imaging or deflation of the occlusion balloon. The mechanisms purporting to link balloon coronary occlusion and chest pain are complex and include the triggering of several neural responses stimulating coronary mechanoceptors and vagal/sympathetic cardiac afferent fibres.(13,14)

Electrocardiographic changes were observed in almost half the patients. Such changes are also frequently observed during angioplasty and stent implantation and are likely reflective of underlying ischaemia. In addition to ST-segment changes, transient prolongation of the QRS interval was seen. Although this study was not designed to measure the QRS interval, prolongation was judged visually during OCT imaging. This remains a highly sensitive marker of ischaemia during percutaneous coronary intervention (PCI), even more so than ST-segment changes and chest pain which is highly subjective.(15) Furthermore, coronary occlusion, particularly of proximal or middle artery segments is directly linked to observations of QRS prolongation.(15) The knowledge that almost half of all patients are likely to experience some level of chest discomfort and/or electrocardiographic changes of ischaemia during OCT imaging should serve to inform patients prior to the procedure and, where indicated, encourage the use of pre-medication, such as short acting analgesics.

The frequency of arrhythmias observed, particularly life-threatening VF that occurred in 5 (1.1%) of patients, warrants further analysis. Several studies have shown the incidence of VF during coronary angioplasty is about 1.5%,(16,17) with the rate dropping down to around 0.6% for diagnostic procedures.(18,19) In addition to ischaemia, other mechanisms have also been identified including reperfusion, electrolyte imbalances, coronary instrumentation, osmolarity and electrolyte composition of contrast agents and intra-coronary thrombus. (20-26)

Iodixanol (Visipaque™, GE Health Care, Cork, Ireland) is the contrast agent that is preferentially used for flushing during the non-occlusive method. The advantage lies in its higher viscosity relative to other agents, which permits optimal blood clearance for OCT imaging at the

given flush volumes through the guiding catheter. This agent has also been shown to have a lower propensity to cause VF given its lower osmolality, higher viscosity and higher concentration of sodium and calcium chloride molecules compared to other non-ionic media. (27-30)

In the 2 cases in which VF occurred during contrast flush, the operators reported deeply intubating the guide into the left coronary artery in an attempt to optimally deliver the contrast flush. Such a move, in hindsight is thought to potentiate the risk of VF with prior reports showing that the combination of a wedged catheter and contrast flush is a high-risk situation for inducing VF.(24,31,32) Given that VF was more frequent in the patients during the occlusive technique with flush of crystalloid solution and, therefore no contrast, it is obvious that other mechanisms are at play, with ischemia still a major contributor. Nevertheless, reporting of such events encourages further work in developing alternative, non-contrast based flushing solutions that are bio-compatible while eliminating the potential unwanted effects of contrast agents.

Other complications, such as dissection and air embolisation are not specific to OCT and can be observed at any stage of an invasive procedure. Recently Kim et al (33) reported a single case of thrombus formation during elective OCT interrogation of LAD stents at 7 months follow-up. Although this is a potential complication with any arterial instrumentation, we did not observe any such cases in our cohort of patients, all treated with weight adjusted heparin prior to OCT assessment.

Compared to IVUS, the present study did not identify cases of vessel spasm with dissection seen in 1 patient and device related failure in a further 1 patient. Prior IVUS studies found an incidence of 3% of coronary spasm, in some, also resulting in abrupt vessel occlusion.(34) This was irrespective of the size of the IVUS catheter used.(34) Technical failure of the IVUS system was observed in 0.4% including guide wire winding or breakage of the catheter.(34) Such complications are fortunately uncommon but are inherent with invasive procedures requiring intra-coronary catheter manipulation and instrumentation.

The incidence of complications encountered in relation to the OCT procedure is consistent with safety data from coronary angioscopy. Similarly, angioscopy requires balloon occlusion during image acquisition although balloon-related vessel injury has not been shown to be a problem 6 months following angioscopic examination.(35) The general trend for OCT image acquisition is to eliminate this aspect thereby simplifying the procedure considerably.

Angioscopic technology has also remained rather stagnant over the years causing it to be used only by a select few specialised centres world-wide. In contrast, OCT has rapidly evolved from the initial use of angioplasty balloons and catheters to dedicated, low profile materials, all contributing to a safer procedure. Further, OCT permits the accurate quantification of both plaque and tissue strut coverage and is also compatible with 6 French guiding catheters. With rapid technology progression in the field, we expect OCT to being widely applied in the near future

Limitations

This study was a retrospective analysis, however included a large number of consecutive patients undergoing OCT at different centres. Also, as OCT is a relative 'new comer' to the field of intravascular imaging, cases from the early phase of OCT technology development were included in this study meaning that complication rates were also inclusive of this early experience and might reflect to a certain degree the learning curve of the technique. Nevertheless, to allow an

informed assessment about the safety profile, all potential adverse events were included, even if transient and benign.

Conclusions

OCT technology has moved at a rapid pace with greater refinements in materials and technique already contributing to increased clinical uptake. Future developments such as optical frequency domain imaging will see OCT use simplified and therefore become conducive to more centres and operators world-wide. Nevertheless, OCT is a specialized technique with a relatively steep learning curve and therefore, requires adequate proctorship. Major complications are uncommon and can be minimised with careful procedural planning and being aware of the potential contributory risks, especially deep guide catheter intubation during contrast flushing and minimising the duration of image acquisition in preference for more frequent but shorter imaging runs. Developments will also make OCT more practical and less procedurally demanding, also potentially conserving contrast volume considerably. The benefits in relation to a greater understanding of coronary artery disease and responses following stent implantation are enormous, meaning that light-based imaging will continue to develop well beyond the current, predominantly research based applications. Knowledge of the procedural safety profile is therefore essential to help inform patients and operators.

References

1. Prati F, Cera M, Ramazzotti V, et al. From bench to bedside. Circ J 2008;72:839-43.
2. Prati F, Cera M, Ramazzotti V, Imola F, Giudice R, Albertucci M. Safety and feasibility of a new non-occlusive technique for facilitated intracoronary optical coherence tomography (OCT) acquisition in various clinical and anatomical scenarios. EuroIntervention 2007;3:365-70.
3. Tanigawa J, Barlis P, Di Mario C. Intravascular Optical Coherence Tomography: Optimisation of image acquisition and quantitative assessment of stent strut apposition. EuroIntervention 2007;3:128-136.
4. Tanigawa J, Barlis P, Kaplan S, Goktekin O, Di Mario C. Stent strut apposition in complex lesions using optical coherence tomography. Am J Cardiol 2006;98:Suppl 1: 97M.
5. Tanigawa J, Barlis P, Dimopoulos K, Di Mario C. Optical coherence tomography to assess malapposition in overlapping drug-eluting stents. EuroIntervention 2008;3:580-83.
6. Takano M, Yamamoto M, Inami S, et al. Long-term follow-up evaluation after sirolimus-eluting stent implantation by optical coherence tomography: do uncovered struts persist? J Am Coll Cardiol 2008;51:968-9.
7. Takano M, Inami S, Jang IK, et al. Evaluation by optical coherence tomography of neointimal coverage of sirolimus-eluting stent three months after implantation. Am J Cardiol 2007;99:1033-8.
8. Matsumoto D, Shite J, Shinke T, et al. Neointimal coverage of sirolimus-eluting stents at 6-month follow-up: evaluated by optical coherence tomography. Eur Heart J 2007;28:961-7.
9. Chen BX, Ma FY, Wei L, et al. Neointimal Coverage of Bare Metal and Sirolimus-Eluting Stents Evaluated with Optical Coherence Tomography. Heart 2007:hrt.2007.118679.
10. Kubo T, Imanishi T, Takarada S, et al. Assessment of culprit lesion morphology in acute myocardial infarction: ability of optical coherence tomography compared with intravascular ultrasound and coronary angioscopy. J Am Coll Cardiol 2007;50:933-9.
11. Tanigawa J, Barlis P, Di Mario C. Heavily calcified coronary lesions preclude strut apposition despite high pressure balloon dilatation and rotational atherectomy: in-vivo demonstration with optical coherence tomography. Circ J 2008;72:157-60.
12. Yamaguchi T, Terashima M, Akasaka T, et al. Safety and feasibility of an intravascular optical coherence tomography image wire system in the clinical setting. Am J Cardiol 2008;101:562-7.
13. Malliani A, Pagani M, Lombardi F, Cerutti S. Cardiovascular neural regulation explored in the frequency domain. Circulation 1991;84:482-92.
14. Manfrini O, Morgagni G, Pizzi C, Fontana F, Bugiardini R. Changes in autonomic nervous system activity: spontaneous versus balloon-induced myocardial ischaemia. Eur Heart J 2004;25:1502-8.

15. Cantor AA, Goldfarb B, Ilia R. QRS prolongation: a sensitive marker of ischemia during percutaneous transluminal coronary angioplasty. Catheter Cardiovasc Interv 2000;50:177-83.
16. Bredlau CE, Roubin GS, Leimgruber PP, Douglas JS, Jr., King SB, 3rd, Gruentzig AR. In-hospital morbidity and mortality in patients undergoing elective coronary angioplasty. Circulation 1985;72:1044-52.
17. Dorros G, Cowley MJ, Simpson J, et al. Percutaneous transluminal coronary angioplasty: report of complications from the National Heart, Lung, and Blood Institute PTCA Registry. Circulation 1983;67:723-30.
18. Davis K, Kennedy JW, Kemp HG, Jr., Judkins MP, Gosselin AJ, Killip T. Complications of coronary arteriography from the Collaborative Study of Coronary Artery Surgery (CASS). Circulation 1979;59:1105-12.
19. Nishimura RA, Holmes DR, Jr., McFarland TM, Smith HC, Bove AA. Ventricular arrhythmias during coronary angiography in patients with angina pectoris or chest pain syndromes. Am J Cardiol 1984;53:1496-9.
20. Goldstein JA, Butterfield MC, Ohnishi Y, Shelton TJ, Corr PB. Arrhythmogenic influence of intracoronary thrombosis during acute myocardial ischemia. Circulation 1994;90:139-47.
21. Gorenek B. Tachyarrhythmias in percutaneous coronary interventions. J Electrocardiol 2006;39:412 e1-5.
22. Huang JL, Ting CT, Chen YT, Chen SA. Mechanisms of ventricular fibrillation during coronary angioplasty: increased incidence for the small orifice caliber of the right coronary artery. Int J Cardiol 2002;82:221-8.
23. Missri J, Jeresaty RM. Ventricular fibrillation during coronary angiography: reduced incidence with nonionic contrast media. Cathet Cardiovasc Diagn 1990;19:4-7.
24. Pedersen HK, Jacobsen EA, Mortensen E, Refsum H. Contrast-medium-induced ventricular fibrillation: arrhythmogenic mechanisms and the role of antiarrhythmic drugs in dogs. Acad Radiol 1995;2:1082-8.
25. Quigley PJ, Maurer BJ. Ventricular fibrillation during coronary angiography: association with potassium-containing glyceryl trinitrate. Am J Cardiol 1985;56:191.
26. Rudoff J, Phillips L. High-osmolality and low-osmolality contrast agents. N Engl J Med 1992;327:203-4.
27. Baath L, Almen T. Reducing the risk of ventricular fibrillation by adding sodium to ionic and non-ionic contrast media with low iodine concentration. Coronary perfusion of the isolated rabbit heart with meglumine diatrizoate or iopentol at 140 mg I/ml and 0-154 mmol Na+/l. Acta Radiol 1989;30:207-12.
28. Hayakawa K, Yamashita K. Low-osmolality contrast media-induced ventricular fibrillation. Invest Radiol 1989;24:298-301.
29. Morris TW, Ventura J. Incidence of fibrillation with dilute contrast media for intra-arterial coronary digital subtraction angiography. Invest Radiol 1986;21:416-8.
30. Chai CM, Karlsson JO, Almen T. Incidence of ventricular fibrillation during left coronary arteriography in pigs: comparison of a solution of the nonionic dimer iodixanol with solutions of five different nonionic monomers. Acta Radiol 2008;49:150-6.
31. Pedersen HK. Electrolyte addition to nonionic contrast media. Cardiac effects during experimental coronary arteriography. Acta Radiol Suppl 1996;405:1-31.
32. Pedersen HK, Jacobsen EA, Refsum H. Contrast media-induced ventricular fibrillation: an experimental study of the effects of dimeric contrast media during wedged catheter injection in dogs. Acad Radiol 1994;1:136-44.
33. Kim JS, Choi EY, Choi D, Jang Y. Images in cardiovascular medicine. Catastrophic thrombus formation during optical coherence tomography. Circulation 2008;118:e101-2.
34. Hausmann D, Erbel R, Alibelli-Chemarin MJ, et al. The safety of intracoronary ultrasound. A multicenter survey of 2207 examinations. Circulation 1995;91:623-30.
35. Hamon M, Lablanche JM, Bauters C, McFadden EP, Quandalle P, Bertrand ME. Effect of balloon inflation in angiographically normal coronary segments during coronary angioscopy: a quantitative angiographic study. Cathet Cardiovasc Diagn 1994;31:116-21.

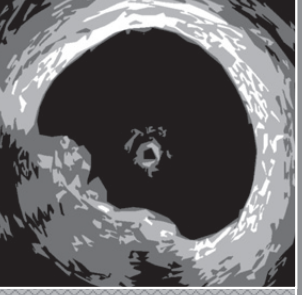

Part 2

OCT technique and methodology

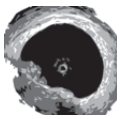

Chapter 5

Intravascular optical coherence tomography: Optimisation of image acquisition and quantitative assessment of stent strut apposition

Jun Tanigawa, Peter Barlis, Carlo Di Mario

Stent expansion, apposition and symmetry were the three criteria of intravascular ultrasound (IVUS) guided optimal stent deployment in the bare metal stent era (1), with at least the criterion of stent expansion maintaining its clinical relevance in the drug-eluting stent (DES) era (2). Two prospective studies showed that stent malapposition immediately following DES implantation was not associated with increased adverse clinical events (3,4). Thus, initial concerns that immediate stent malapposition would affect drug delivery to the vessel wall and lead to DES failure appeared to be unfounded. Coronary IVUS, however, formerly the gold standard for assessing stent strut apposition, is imprecise in the detection of stent malapposition observed in around 7% of lesions (3,4), a figure which is probably grossly underestimated. This is due to the limited axial and lateral resolution of the ultrasound waves (100-150 μm) and the constant presence of artefacts around stent struts (side-lobes, shadowing). Optical coherence tomography (OCT) uses infrared light with the advantage of greater resolution (10-15 μm) and less strut induced artefacts compared with IVUS (5,6). Unlike the first OCT prototypes used by Jang et al (5,6), new commercial systems (LightLab Imaging Inc., Westford, MA, USA) can acquire contiguous images with a motorised pullback system as used with IVUS7. Still, OCT has some disadvantages including a more complex process of image acquisition that requires transient proximal flow occlusion with a balloon. Since there is definite learning curve to achieve optimal image quality, this article will focus on methods and techniques to attain optimal assessment of stent strut apposition, using the current OCT system.

Proximal balloon occlusion and blood removal

The new OCT system consists of the Helios™ proximal occlusion balloon catheter and ImageWire™. Because of the length and maximal diameter of the currently available occlusion balloon, the luminal diameter proximal to the culprit lesion must be between 2.5 mm and 4.0 mm, and ostial or very proximal lesions (< 15 mm from ostium) are not suitable for imaging. Other contraindications are listed in Table 1.

Table 1. Exclusion criteria for optical coherence tomography.
Poor left ventricular function
Haemodynamic instability
Single remaining vessel
Lumen proximal to the culprit lesion < 2.5mm or > 4.0mm
Ostial/very proximal (< 15mm from ostium) lesion
Highly tortuous proximal vessel

The Helios™ proximal occlusion balloon catheter is an over-the-wire 4.4 Fr catheter (inner diameter 0.025”), compatible with 6Fr guiding catheters (inner lumen diameter > 0.071”), which is advanced distal to the stented lesion using a conventional angioplasty guidewire (0.014”). The guide wire is then replaced by the OCT ImageWire™ (0.019” maximum diameter), and the

occlusion balloon catheter is withdrawn proximal to the segment to be assessed leaving the imaging wire in position (Figure 1).

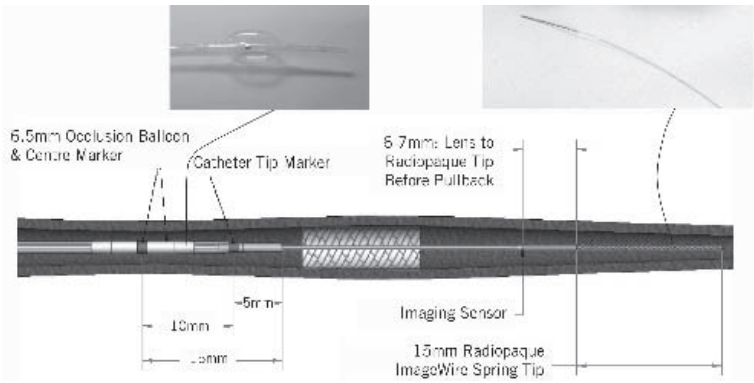

Figure 1. Helios™ proximal occlusion balloon catheter and ImageWire™. Intra-coronary flush is continuously performed via the end-hole of the (over-the-wire) occlusion balloon catheter and the occlusion balloon dilated proximal to the target segment during observation

During imaging acquisition, coronary blood flow must be removed and we adopted a continuous flush of Ringer's lactate solution via the end hole of the occlusion balloon catheter at a flow rate of 0.5- 1.5 ml/sec. Two Y-connectors are needed and attached to both a guiding and an occlusion balloon catheter respectively as shown in Figure 2. We use a power injector (Mark V ProVis, Medrad, Inc., Indianola, PA, USA) for this slow injection with a setting of rise/fall: 0 sec, pressure limit: 100 psi, delay: 0 sec under inflation of the highly compliant occlusion balloon proximal to the lesion (0.5- 0.7 Atm). The vessel occlusion time is limited to a maximum of 30 sec to avoid haemodynamic instability or arrhythmias. The stented segments are imaged using an automated pull-back (1.0 mm/sec) from distal to proximal. The cross sectional images are acquired at 15.4 frames/sec. In case the segment of interest is not completely studied because its length is > 30 mm or the continuous pull-back has to be interrupted due to patient instability, chest pain or arrhythmias, a second pull-back is performed again to accomplish complete lesion assessment.

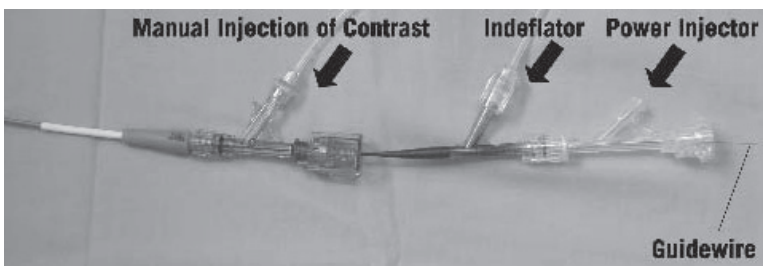

Figure 2. Proximal end of guiding catheter and proximal occlusion balloon catheter showing the connections for the indeflator, power injector and guidewire.

How to optimise image quality

With increasing experience, we are generally able to acquire optimal images in around 90% of each lesion or stented segment studied. The main cause of failure remains inadequate blood removal. We believe optimal positioning of the balloon and selection of the infusion rate can overcome this problem in most cases. In the last 20 cases studied, images inadequate for assessment were taken in 1/20 (5%) and the cause of failure was inability to cross a very calcified and tortuous vessel with a stiff and bulky delivery balloon. There are however, some limitations that may preclude complete lesion and stent assessment and these will be discussed in detail below. In brief, the major limitations have to do with incomplete lesion assessment during placement of the imaging wire, inadequate blood removal and finally the limited scan range (5 mm) of the current OCT system. It has also been challenging to remove coronary blood flow completely in lesions involving large side branches and immediately following recanalisation of chronic total occlusions due to the flow from collaterals. The two crucial points therefore required to obtain optimal cross sectional images using the current OCT system are correct placement of the imaging optic sensor and optimisation of blood removal using the proximal occlusion balloon with continuous intra-coronary flush. We provide some tips and tricks that may be useful.

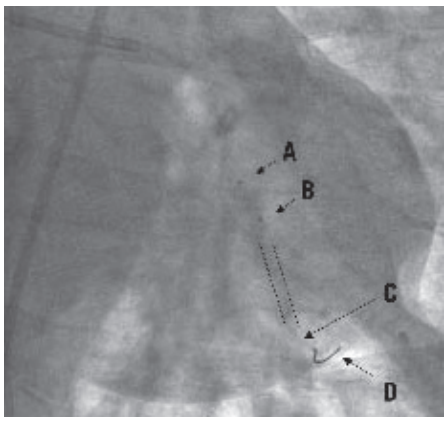

Figure 3. ImageWireTM placement. The infrared sensor (C), located 6-7 mm proximal to the distal 15 mm radiopaque wire tip (D) when fully advanced is invisible under fluoroscopy. It is correctly positioned distal to the stent (indicated by dotted lines). The occlusion balloon catheter tip marker (B; 5 mm proximal to the distal end) is above the proximal end of the stented segment. (A) indicates the centre marker of the occlusion balloon (10 mm proximal to B).

Imaging wire placement

Since the imaging wire is not torquable, we advance the over-the-wire occlusion balloon distal to the lesion to be assessed / stented segment to obtain a distal wire placement. Unlike the IVUS transducer, the optical sensor is invisible under fluoroscopy (Figure 3C) and therefore one must estimate the correct position, using the distal 15 mm radiopaque tip (Figure 3D) of the imaging wire and the two markers of the balloon catheter (Figure 3A, 3B). When fully advanced, the sensor is located 6-7 mm proximal to the radiopaque part as easily confirmed by direct observation of the position of the red light emitted when the imaging wire is handled out of the body. As there are no direct radiopaque markers for the infrared sensor, and despite meticulous attention, it is still possible to miss imaging an area of interest resulting in incomplete distal

lesion edge assessment. Imaging after stent implantation facilitates positioning because it is sufficient to advance the proximal end of the radiopaque wire tip at least 1 cm distal to the stent struts to image the entire stented segment. For imaging prior to treatment, it is important to note that the occlusion balloon is too bulky to cross severe stenoses before pre-dilatation and that the imaging wire should be advanced distal to the lesion to ensure that the segment of interest is fully visualised.

Proximal occlusion balloon

Although the company's instruction manual advises the use of diluted contrast (30-50% mix) to inflate the occlusion balloon, we use 0.9% normal saline. Saline takes less time for the occlusion balloon to be both fully dilated (to occlude blood flow) and deflated (to restore flow), resulting in a shorter period of ischaemia. The disadvantage of this method is that the balloon is not identifiable under fluoroscopy, however complete occlusion of the target vessel can be confirmed with test injection of contrast through the guiding catheter.

Intra-coronary flush

We use Ringer's lactate during infusion because we expect it to be less arrhythmogenic than other crystalloid solutions. In most cases, we use a pump with an injection rate of 0.7 or 1.2 ml/sec of intracoronary flush with good clearance of blood (Figure 4A). Some particularly large vessels, those receiving good collateral flow or those with large side branches require higher flushing rates, with the potential for endothelial damage. Fortunately, however, thus far we have not experienced any complications such as coronary dissection, target vessel failure or clinical adverse events at index procedure or at follow- up. For a large coronary the flow rates required are still in a physiological range (0.5–1.5 ml/sec) resulting in a physiological pressure rise. The Y-connector attached to the guiding catheter must be fastened securely enough to prevent leakage of the flushing solution but not too tight as to damage the optical fibre during pull-back.

Complementary flush

The proximal occlusion balloon can be dilated up to 4.0 mm in diameter, but if it fails to completely occlude the vessel being assessed, blood will escape. This will, depending on the severity, compromise image quality considerably (Figure 4B) or only partially (Figure 4C) where you may continue to visualise the vessel wall albeit in a suboptimal fashion. Even for partially insufficient imaging like figure 4C, inflating the occlusion balloon to 0.7 atm (max) and increasing flush volume do not always resolve the issue. Repositioning of the occlusion balloon or complementary manual injection through the guiding catheter are alternative solutions. Despite all efforts, chronically occluded segments following recanalisation are difficult to evaluate as collateral flow synchronised to cardiac motion complicates blood removal rendering strut assessment every sec (mm) almost impossible (Figure 4D-4F).

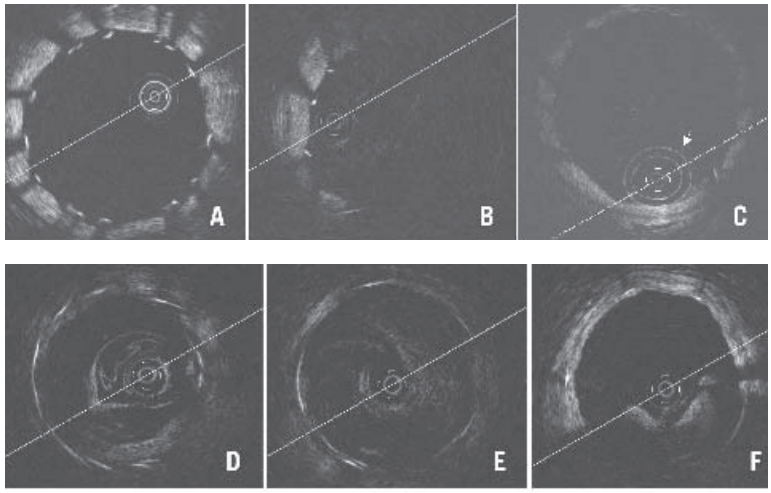

Figure 4. Optimal and various patterns of suboptimal blood removal. Optimal imaging clearly shows all struts with shadows cast (A), (B) indicates considerably deteriorated imaging with bright layers of blood lacking circumferential visualisation of vessel wall and (C) indicates minimally deteriorated imaging showing some blood speckles inside the lumen and circumferential vessel wall but without clear strut identification compared with (A). Double white rings (arrow) are shadows of the proximal balloon catheter tip. (D-F) indicate typical patterns of suboptimal blood removal immediately following recanalisation of chronically occluded segments. Blood removal was not easy during pull-back because of the collateral blood flow synchronised to cardiac motion rendering strut assessment difficult. In the image of (F) some struts can be evaluated, but contiguous assessment at every sec (mm) was almost impossible.

Usage of the fragile imaging wire

In multiple attempts for pre- and post-procedural assessment or multi-vessel observation, it is important to be meticulous in handling the imaging wire: leaving it straight on the table rather than keeping it back in the hoop helps to avoid damaging the fragile optical fibre. Furthermore, the imaging sensor should not be advanced when either the wire is being inserted or pulled out of the guiding catheter or when it is within the hoop.

Quantitative analysis with OCT: focus on strut apposition

OCT offers the possibility of a detailed analysis of the superficial plaque components, with resolution far superior to IVUS (Figure 5) (8,9). However, the assessment remains largely qualitative with the notable exception of the measurement of the thickness of the fibrous cap covering necrotic areas. Unless spectroscopy is introduced in the analysis package, with major changes in the hardware required to allow dual light emission, OCT cannot quantify the various plaque components as IVUS does using radiofrequency analysis (10). The other limitation of OCT for plaque quantification is the inability to provide a full thickness analysis of large plaques because of its limited penetration. OCT however, offers obvious advantages when dealing with superficial structures such as the fibrous plaques and stent struts. In the remaining part of this review we will focus on the methods we use to assess strut apposition.

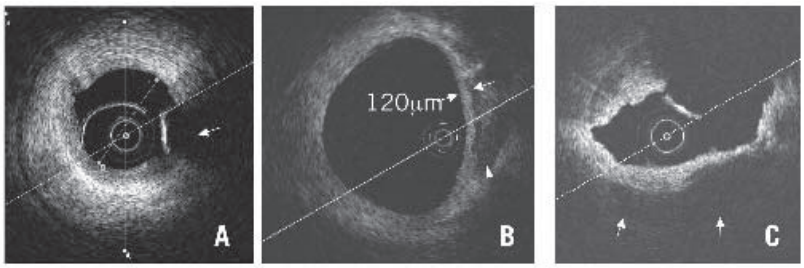

Figure 5. Qualitative analysis of superficial plaque components. A) Fibrous plaque: Homogeneous signal-rich plaque extending circumferentially (arrow: guidewire artefact). B) Fibroatheroma: Heterogeneous plaque includes signal poor regions (arrowhead) with diffuse border indicating lipid components. Cap thickness can also be measured. C) Calcified plaque: Image acquired following balloon dilatation of chronically occluded segments showing calcium characterised by well delineated signal poor regions extending from 3 to 7 o'clock positions (arrows)

Off-line analysis of contiguous cross sections within the stented segment is performed at 1 mm intervals. Firstly, the distal end should be detected with images of circumferential struts. From the identified distal end of the stent, every 15 frames (almost equivalent to 1 mm with an acquisition rate of 15.4 frames/sec) cross sections are checked and the best images with clearly identifiable vessel wall and struts within 2 frames distal or proximal are selected for evaluation of strut apposition ('Selected cross sections'). A proximal end with circumferential struts is also detected, and the interval from identified distal to proximal stent end is defined as the 'scanned stent length (mm)'. 'Percent (%) scanned stent length' is calculated as scanned stent length divided by total stent length implanted for the lesion. Detected overlapping length should be added to the scanned length for this calculation when two or more stents have been implanted in an overlapping fashion. In each selected cross section 'Complete cross sectional imaging' is defined as entirely circumferential image acquisition of the luminal border (Figure 6). 'Percent (%) complete cross sectional imaging' is calculated as the rate of complete cross sectional imaging divided by the number of selected cross sections.

Stent struts appear as highly reflective surfaces and cast shadows on the vessel wall behind. When the strut is not fully attached to the vessel wall by visual estimate (almost equivalent to > 50 μm), the position of a stent strut relative to the vessel wall is measured by magnifying the individual stent strut to maximise accuracy. Firstly, one pointer is placed on the endo-luminal surface of the reflection, followed by another at the surface of the vessel wall within the stent strut shadow using the reflections of the wall on either side of the strut shadow. The measurement line should be as perpendicular to the strut and vessel wall as possible (Figure 7). In case a strut protrudes into a side branch ostium, this should be classified as 'malapposed' and excluded from quantitative strut analysis.

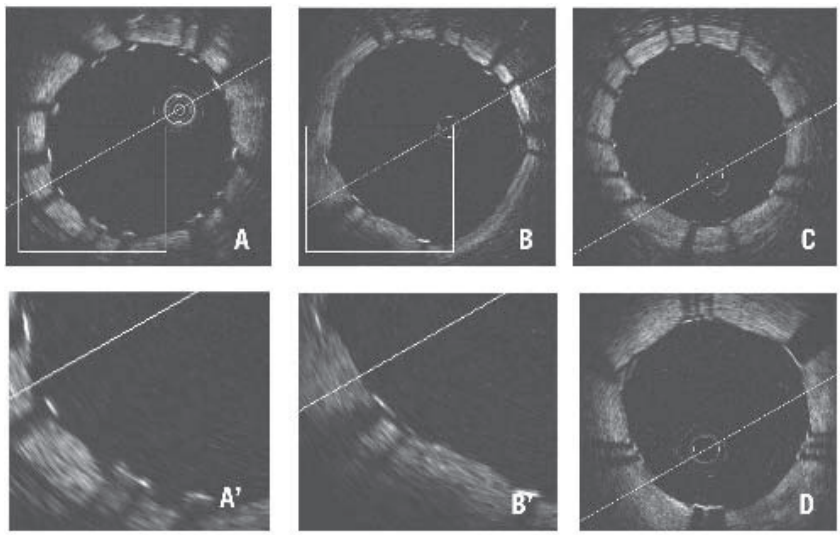

Figure 6. Complete cross sectional imaging of drug-eluting stents with apposed struts. (A) Cypher Select, (B) Taxus Liberte, (C) Endeavor, (D) CoStar. Cypher struts appear wider than the other 3, but all of their strut thicknesses are underestimated because of limited penetration of OCT.

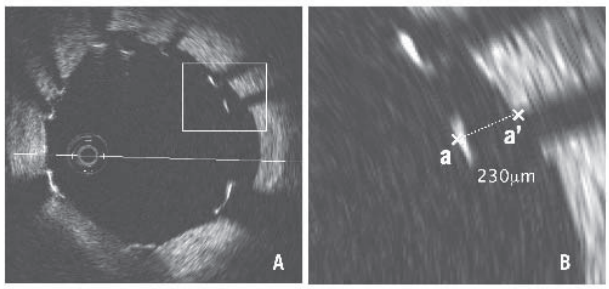

Figure 7. Measurement of strut apposition. The distance between the endo-luminal surface of the strut reflection and the vessel wall is measured prolonging and joining the contours of the wall on either side of the strut shadow with a measurement line as perpendicular as possible to the strut and vessel wall. The distance between (a) and (a') is equal to 230 mm.

Definition of strut apposition in DES

Since OCT can show only the endo-luminal surface of the strut due to limited penetration through the metal (Figure 8), strut and polymer thickness should be considered in assessing apposition for each type of DES design. Apart from Yukon® DES stent (Translumina GmbH, Hechingen, Germany) with 115 μm (0.0045") metal strut thickness, no polymer and an uneven rapamycin sprayed coating, four types of DES are clinically available in Europe presently: Cypher Select™ stent (Cordis, Johnson and Johnson Co., Miami Lake, FL, USA) with 140 μm strut and 7 μm polymer, Taxus® Liberte™ (Boston Scientific, Natick, MA, USA) with 97 μm and 15 μm, Endeavor™ (Medtronic AVE, Santa Rosa, CA, USA) with 91 μm and 8 μm and CoStar™

(Conor Medsystems, Inc., Hamilton Court Menlo Park, CA, USA) with 89 μm strut with no polymer around the struts.

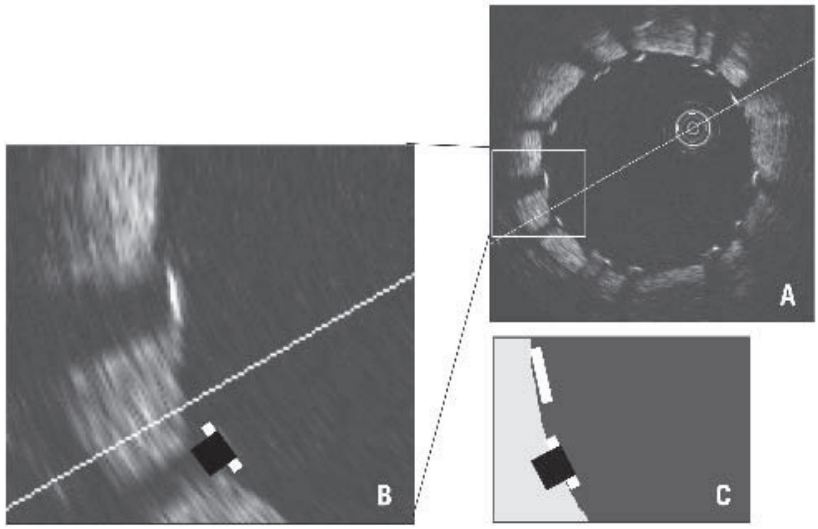

Figure 8. Visible and real strut thickness and width. A and B: OCT can show only the endo-luminal surface of the strut (bright white line) due to limited penetration through the metal; B and C: strut width is overestimated compared with the actual profile (black square) due to lateral resolution of 25-40 mm and there is a shadow behind struts where the vessel wall is not visible.

As a composite of metal strut and polymer, the thicknesses of each type of DES differ. Consequently, we define 'malapposed' stent struts as struts with detachment from the vessel wall > 160 μm for Cypher Select, > 130 μm for Taxus Liberte, > 110 μm for Endeavor and > 90 μm for CoStar. Struts with distances less than half of the above cut-off values are defined as 'embedded' while all others are defined as 'protruding'. In combination, both embedded and protruding struts are considered apposed to the vessel wall (Figure 9). This classification may also be adopted to assess persistent or acquired late malapposition.

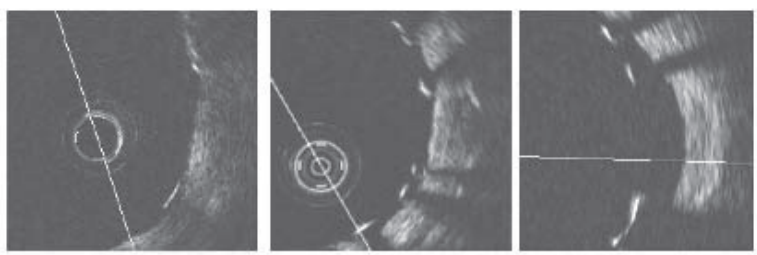

Figure 9. Definition of stent strut apposition. Note only endo-luminal surface of the metal can be identified with Optical Coherence Tomography. Different cut-offs should be adopted for each stent type. A strut is classified as embedded when less than half of a whole strut thickness is protruding into the lumen.

Assessment of tissue coverage following DES implantation

Unlike conventional stents which developed circumferential coverage with an average thickness of 500 μm or more, well visualised with IVUS and angiography (1mm late loss), DES delay and prevent the hyperplastic response so that the average late lumen loss for sirolimus- or paclitaxel-eluting stents can be as low as 0.1 or 0.2 mm which means the amount of intimal thickening will not be detectable with IVUS (11-13). OCT offers a potential alternative to detect and measure these tiny layers of intimal coverage (Figure 10) and to assess late strut malapposition that can be distinguished, if images immediately after implantation are also available, into persistent (present already at the time of stent implantation) and acquired (negative remodelling or disappearance of superficial components behind struts such as thrombus).

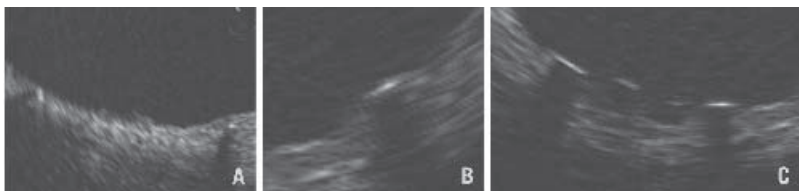

Figure 10. Definition of late strut coverage. Classified into 3 groups. A: Complete - fully embedded in the tissue or circumferentially covered if a strut is protruding. B: Incomplete - partially covered with tissue. C: Absent - no visible tissue around a strut.

Limitations

Current intravascular OCT has some limitations. The imaging wire is extremely difficult to manipulate for delivery and the occlusion balloon needs to be advanced over the lesion, with a 2.3 Fr tip and 4.0 Fr shaft (proximal to the balloon) that may not cross a tight lesion or have difficulty being advanced over stented lesions. This last limitation is, however, common to IVUS catheters as well. Ostial and very proximal lesions are not suitable for this system using the proximal occlusion balloon, because of the length of the tip, approximately 12 mm, and long occlusion balloon of 6.5 mm (Figure 1). This is currently under refinement. It should be noted however that, an image can still be acquired within the distal catheter end and through the balloon. OCT is more accurate in assessing strut apposition compared with IVUS because of higher resolution, but its poor penetration (1.5 mm approximately) makes it inferior to IVUS in assessing stent expansion. Even if the stent struts are well apposed to the vessel wall (well attached to the intimal plaque) the stent may not be optimally expanded because balloon sizing with OCT is more difficult as it is often impossible to identify the external elastic membrane and the lumen of the distal vessel reference may be collapsed.

The system requires 30 seconds of complete coronary flow occlusion to observe a lesion of the length of 30 mm with the minimal pull-back speed of 1.0 mm/sec. The pull-back speed can be increased from 1.0 to 2.0 mm/sec with fixed frame rates of 15.4/sec, but the quality of imaging degrades with faster pull-back speeds. We have not experienced any haemodynamic instability or arrhythmias, but are compulsive in deflating the balloon and stopping flushing if significant ischaemic changes begin to develop. In some cases we have had to perform multiple pull-backs

for periods shorter than 30 seconds because of ischaemia. All laborious manipulations with multiple pull-backs complicate the procedure and tend to result in incomplete blood removal and thereby hamper the quantitative analysis. Uneven images (shifted to one side due to wire bias) are often seen in large and tortuous vessels and cause elliptical distortion of the lumen with part of the vessel outside the imaging screen. This is at present the most annoying limitation of the current software which has a limited scan range of 5 mm. The next generation ImageWire™ will offer improved durability and trackability. Similarly, the Helios™ occlusion balloon catheter will be modified to have a shorter tip and a more kink resistant shaft. The M2 system (OCT hardware) will be improved to offer smoother L-mode (longitudinal) acquisition and edge-detection software. Eventually, automatic plaque morphology detection will also be included. Even after these changes, OCT will still be limited by suboptimal tissue penetration, because high resolution and penetration are mutually exclusive.

Conclusions

Although the current intravascular OCT system still needs some refinement for better handling and image quality, it should be considered the new gold standard in assessing apposition of stent struts quantitatively. The techniques and classifications discussed in this review can also be used for assessment of late stent malapposition taking into consideration tissue (fibrin or intimal) coverage. Clinical relevance between stent strut apposition and late adverse events such as stent thrombosis and restenosis in the DES era may also be clarified by OCT.

References

1. Colombo A, Hall P, Nakamura S, Almagor Y, Maiello L, Martini G, Gaglione A, Goldberg SL, Tobis JM. Intra-coronary stenting without anticoagulation accomplished with intravascular ultrasound guidance. Circulation. 1995;91(6):1676-88.
2. Mintz GS, Weissman NJ. Intravascular ultrasound in the drug-eluting stent era. J Am Coll Cardiol. 2006;48(3):421-9.
3. Tanabe K, Serruys PW, Degertekin M, Grube E, Guagliumi G, Urbaszek W, Bonnier J, Lablanche JM, Siminiak T, Nordrehaug J, Figulla H, Drzewiecki J, Banning A, Hauptmann K, Dudek D, Bruining N, Hamers R, Hoye A, Ligthart JM, Disco C, Koglin J, Russell ME, Colombo A. TAXUS II Study Group. Incomplete stent apposition after implantation of paclitaxel-eluting stents or bare metal stents: insights from the randomized TAXUS II trial. Circulation. 2005;111(7):900-5.
4. Hong MK, Mintz GS, Lee CW, Park DW, Park KM, Lee BK, Kim YH, Song JM, Han KH, Kang DH, Cheong SS, Song JK, Kim JJ, Park SW, Park SJ. Late stent malapposition after drug-eluting stent implantation: an intravascular ultrasound analysis with long-term follow-up. Circulation. 2006;113(3):414-9.
5. Diaz-Sandoval LJ, Bouma BE, Tearney GJ, Jang IK. Optical coherence tomography as a tool for percutaneous coronary interventions. Catheter Cardiovasc Interv. 2005;65(4):492-6.
6. Bouma BE, Tearney GJ, Yabushita H, Shishkov M, Kauffman CR, DeJoseph Gauthier D, MacNeill BD, Houser SL, Aretz HT, Halpern EF, Jang IK. Evaluation of intracoronary stenting by intravascular optical coherence tomography. Heart. 003;89(3):317-20.
7. Kawase Y, Hoshino K, Yoneyama R, McGregor J, Hajjar RJ,Jang IK, Hayase M.;In vivo volumetric analysis of coronary stent using optical coherence tomography with a novel balloon occlusion-flushing catheter: a comparison with intravascular ultrasound. Ultrasound Med Biol. 2005;31(10):1343-9.
8. Yabushita H, Bouma BE, Houser SL, Aretz HT, Jang IK, Schlendorf KH, Kauffman CR, Shishkov M, Kang DH, Halpern EF,

Tearney GJ. Characterization of human atherosclerosis by optical coherence tomography. Circulation. 2002;106(13):1640-5.
9. Jang IK, Tearney GJ, MacNeill B, Takano M, Moselewski F, Iftima N, Shishkov M, Houser S, Aretz HT, Halpern EF, Bouma BE. In vivo characterization of coronary atherosclerotic plaque by use of optical coherence tomography. Circulation. 2005;111(12):1551-5.
10. Rodriguez-Granillo GA, Garcia-Garcia HM, Valgimigli M, Schaar JA, Pawar R, van der Giessen WJ, Regar E, van der Steen AF, de Feyter PJ, Serruys PW. In vivo relationship between compositional and mechanical imaging of coronary arteries. Insights from intravascular ultrasound radiofrequency data analysis. Am Heart J. 2006;151(5):1025.e1-6.
11. Morice MC, Serruys PW, Sousa JE, Fajadet J, Ban Hayashi E, Perin M, Colombo A, Schuler G, Barragan P, Guagliumi G, Molnar F, Falotico R; RAVEL Study Group. Randomized Study with the Sirolimus- Coated Bx Velocity Balloon-Expandable Stent in the Treatment of Patients with de Novo Native Coronary Artery Lesions. Randomized Study with the Sirolimus-Coated Bx Velocity Balloon-Expandable Stent in the Treatment of Patients with de Novo Native Coronary Artery Lesions. A randomized
comparison of a sirolimus-eluting stent with a standard stent for coronary revascularization. N Engl J Med. 2002;346(23):1773-80.
12. Moses JW, Leon MB, Popma JJ, Fitzgerald PJ, Holmes DR, O'Shaughnessy C, Caputo RP, Kereiakes DJ, Williams DO, Teirstein PS, Jaeger JL, Kuntz RE. SIRIUS Investigators. Sirolimus-eluting stents versus standard stents in patients with stenosis in a native coronary artery. N Engl J Med. 2003;349(14):1315-23.
13. Stone GW, Ellis SG, Cox DA, Hermiller J, O'Shaughnessy C, Mann JT, Turco M, Caputo R, Bergin P, Greenberg J, Popma JJ, Russell ME; TAXUS-IV Investigators. A polymer-based, paclitaxel-eluting stent in patients with coronary artery disease. N Engl J Med. 2004;350(3):221-31.

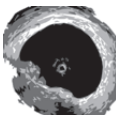

Chapter 6

A Novel approach for quantitative analysis of intracoronary optical coherence tomography: High inter-observer agreement with semi-automated contour detection in native and in stented human coronary arteries

Shuzou Tanimoto, Gaston Rodriguez-Granillo, Peter Barlis, Sebastiaan de Winter, Nico Bruining, Ronald Hamers, Michiel Knappen, Stefan Verheye, Patrick W. Serruys, Evelyn Regar

***Objective**: This study aims to examine observer related variability of quantitative optical coherence tomography (OCT) derived measurements from both in-vitro and in-vivo pullback data*

***Background:** Intravascular OCT is a new imaging modality using infrared light and offering 10 times higher image resolution (15µm) compared to intravascular ultrasound. The quantitative analysis of in-vivo intracoronary OCT imaging is complicated by the presence of blood, motion artifacts and the large quantity of information that has to be processed.*

***Methods:** We developed a standardized, automated quantification process for intracoronary OCT pullback data with inter-observer variability assessed both in-vitro using post-mortem human coronary arteries and in-vivo by studying simple and complex coronary pathology and outcomes following stent implantation. The consensus between measurements by two observers was analyzed using the intra- and interclass correlation coefficient and the reliability coefficients. Bland-Altman plots were generated to assess the relationship between variability and absolute measurements.*

***Results:** In-vitro OCT assessment was performed in 9 post-mortem coronary arteries. The time needed for semi-automated contour detection of a 15mm long coronary segment was approximately 40 min. The absolute and relative difference between lumen area measurements derived from 2 observers was low (0.02±0.10mm^2; 0.3±0.5% respectively) with excellent correlation confirmed by linear regression analysis (R^2 0.99; p<0.001). Similarly, in-vivo measurements demonstrated a high correlation with the main source of inter-observer variation occurring as a result of coronary dissection and motion artifact. The absolute and relative difference between measurements were 0.11±0.33mm^2 (1.57±0.05%) for lumen area (R^2 0.98; p<0.001), 0.17±0.68mm^2 (1.44±0.08%) for stent area (R^2 0.94; p<0.001) and 0.26±0.72mm^2 (14.08±0.37%) for neointimal area (R^2 0.78; p<0.001).*

***Conclusions**: Highly accurate computer-assisted quantitative analysis of intracoronary OCT pullbacks is feasible with low inter-observer variability. The presented approach allows for observer independent analysis of detailed vessel structures and may be a valuable tool for future longitudinal studies incorporating OCT.*

Optical coherence tomography (OCT) is a light-based imaging modality that can be used to study biological tissues *in vivo* (1). Recently, the concept of catheter-based intracoronary OCT has been introduced (2-4) allowing *in-vivo* imaging of the coronary vessel wall with a lateral resolution of 15µm and an axial resolution of 25µm (5). The currently accepted gold standard, intravascular ultrasound (IVUS), operates at a lateral resolution of approximately 120µm and axial resolution of 80µm. The unique high-resolution OCT imaging modality permits the analysis of coronary structures in greater detail. The measurement accuracy of intracoronary OCT has been established in post-mortem human coronary arteries and showed good correlation to histo-morphometry (6). However, compared to *ex-vivo* imaging, quantitative analysis of *in-vivo* intracoronary imaging is more complicated due to the presence of blood and motion artifacts during cardiac cycle. Furthermore, the OCT dataset acquired during motorized pullback in-vivo is much larger than local imaging of selected cross sections as performed in post mortem studies. A pullback through the region of interest (ROI) is necessary in order to visualize the three-dimensional morphology of the coronary artery. The present research proposes a standardized automated quantification process for intracoronary OCT pullback data. To test its accuracy, inter-observer variability was assessed *in-vitro* and *in-vivo* including, both, simple and complex vessel anatomy, represented by native coronary arteries before and after stent implantation.

Methods

OCT imaging system

We used a commercially available system for intravascular OCT imaging (LightLab Imaging Inc., Westford, MA, USA). The light source was a 1310nm broadband super luminescent diode with an output power in the range of 8.0mW. The imaging depth was approximately 1.5mm with an

axial and lateral resolution of 15μm and 25μm, respectively. The imaging probe (ImageWire ™ LightLab Imaging Inc., Westford, MA, USA) had a maximum outer diameter of 0.019 inch and contained a single-mode fiber optic core within a translucent sheath. The image wire was connected at its proximal end to the imaging console that permitted real-time data processing and two-dimensional representation of the backscattered light in a cross-sectional plane. Images were acquired at 15 frames per second. The fiber optic core was withdrawn within the catheter sheath using automated pullback at 1.0 mm/s.
The accuracy of the OCT system has been recently reported. Diameters of phantoms with precision-drilled circular holes were measured in-vitro using proprietary software from LightLab with excellent accuracy (-0.03) and precision (0.02)(7).

Human coronary arteries – post mortem study

In all cases (n=9), the left anterior descending artery was studied after pressure fixation using 10% buffered formalin. The take off of the first diagonal branch was used as proximal landmark. Both, the proximal and the distal end of the coronary specimen were sutured to a 6F introducer sheath and positioned in a saline bath at 37° C. The OCT imaging wire was introduced via the proximal sheath into the specimen and positioned in such a way that the distal OCT catheter tip was fixed in the distal sheath and an automated OCT pullback was performed.

Human coronary arteries – clinical studies

Patients undergoing a stent-implantation procedure (n=10) or a 6-month follow-up angiogram post stent implantation (n=10) were studied. A standard femoral approach with 7F guiding catheters was used. All patients received weight-adjusted intravenous heparin in order to maintain the activated clotting time > 300 sec and intravenous analgesics before imaging. First, a dedicated compliant occlusion catheter (Helios, Goodman Inc, Japan) was introduced into the artery and positioned proximally to the region of interest (ROI). The occlusion catheter allows (a) for limiting the coronary blood flow by very low-pressure (0.3 atm) inflation of a short (6.0mm length) balloon, (b) for simultaneous clearing of the artery by delivering flush distally to the balloon into the lumen, (c) for introduction of the OCT imaging wire into the artery. After positioning the occlusion catheter in over the wire technique, the standard 0.014" guide wire was withdrawn and the OCT imaging wire introduced via the central lumen distal into the target vessel. An automated OCT pullback was then performed. During OCT image acquisition, the artery was cleared with lactated ringer's solution (flow rate 0.5ml/s; temperature 37° C). Sufficient occlusion of the lumen was documented by contrast injection via the guiding catheter and the balloon pressure increased to 0.5 atm if necessary.

Quantitative OCT (QOCT)

The digitized tomographic OCT image dataset was transformed from digital movie file format (AVI) into the medical DICOM image standard and stored onto a picture archiving system. Quantitative OCT analysis was performed using dedicated software (CURAD vessel analysis, CURAD BV, Wijk bij Duurstede, Netherlands)(8) (Figure 1).

Every 3rd frame of the pullback of long segments was entered. This reduced the number of frames in the Curad software from n to at most (n/2)+1 per set. Two blinded observers experienced in the theory and practice of OCT performed the analysis. In non-stented arteries, the lumen area was directly traced and the mean lumen diameter calculated using a circular model. In stented arteries, lumen- and stent area were both directly traced, the mean lumen- and mean stent diameter were calculated. Neointimal area was calculated as stent area minus lumen area.

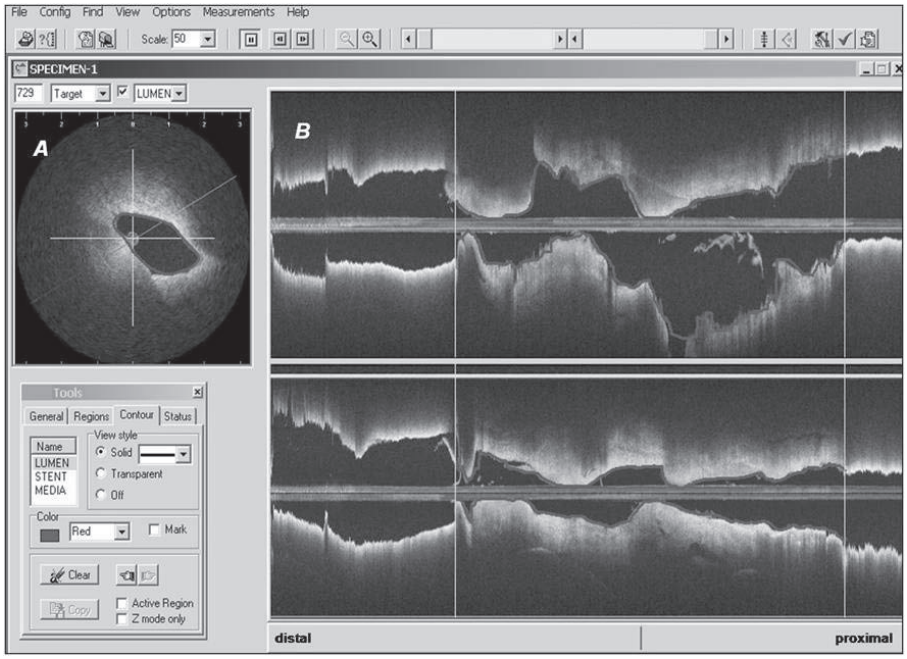

Figure 1: Example of quantitative OCT analysis in an ex-vivo coronary artery. The digitized tomographic OCT image dataset was transformed from digital movie file format (AVI) into the medical DICOM image standard and stored onto a picture archiving system. The dedicated software (CURAD) allows for simultaneous display of a cross sectional view (A) and two longitudinal cut planes (B). After a selection of a region of interest, the lumen contours are traced using automated contour detection whereby both, the cross sectional and the longitudinal image information is exploited.

OCT cross sections with a major side branch (diameter >2mm; or side branch take off occupying more than 60 degrees of the lumen circumference of the parent vessel) were excluded from analysis as well as cross sections in which the complete lumen circumference of 360 degrees could not be visualized due to motion artifacts during the cardiac cycle.

Statistical analysis

Statistical analyses were performed using SPSS 12.0.1 for Windows (SPSS Inc., Chicago, IL). Data are expressed as mean ± SD or median and inter-quartile range, if appropriate. Inter-observer agreement was determined by comparing measurements of each observer (observer 1 vs. observer 2) using the Bland-Altman method (9). Data are given as plots showing the absolute difference between corresponding measurements of both observers (y-axis) against the average of both observers (x-axis). The relative difference between measurements (absolute difference divided by the average) gives the bias, its standard deviation gives the random variation. The limits of agreement were calculated as mean bias ± 2 SD. Confidence intervals (95%) were calculated. In addition, absolute data were analyzed for correlation by regression analysis as necessary, but not sufficient, condition for agreement. The regression line was forced through the origin. A p-value less than 0.05 (two-tailed students T-test) was considered statistically significant.

Results

In-vitro coronary arteries

OCT imaging was successfully performed in all specimens (n=9). Computer-assisted contour detection was possible in all pullbacks. In each coronary artery, a ROI of 15mm in length was selected for analysis. The time needed for computer-assisted contour detection of a 15mm long coronary segment was approximately 40 min. Data for lumen dimensions by both observers are given in Table 1. The absolute difference in lumen area between the observers was low ($0.02\pm0.10mm^2$). Linear regression analysis confirmed these observations and showed excellent correlation between measurements (R^2 0.99). Bland Altman plots for lumen area and lumen diameter are shown in Figure 2.

	Lumen area	Lumen diameter
Observer 1		
Median (IQR)	2.48 (1.81) mm^2	1.78 (0.64) mm
Mean ± 1SD	$3.03\pm1.95mm^2$	$1.88\pm0.58mm$
Observer 2		
Median (IQR)	2.49 (1.75) mm^2	1.78 (0.62) mm
Mean ± 1SD	$3.02\pm1.93mm^2$	$1.87\pm0.58mm$
Absolute difference	$0.02\pm0.10mm^2$	$0.00\pm0.04mm$
Relative difference	$0.3\pm0.5\%$	$0.1\pm0.2\ \%$
Linear regression		
Slope	0.9904x	0.9905x
Intercept	0.0125	0.0135
R^2	0.9974	0.9957
p	<0.001	<0.001

Table 1: Comparison of lumen measurements in ex-vivo coronary arteries, n=772 frames

In-vivo native coronary arteries

OCT imaging could be successfully performed without complications in all patients. The majority of patients (90%) developed transient ECG changes indicative of ischemia during imaging. Ten coronary segments of 28±9mm lengths were studied. A total of 1807 frames were included in the analysis and 399 frames were excluded due to the presence of a major side branch or due to incomplete visualization of the lumen circumference due to motion artifacts. OCT data are summarized in Table 2. The absolute difference between observers was low (lumen area $0.04\pm0.14mm^2$) and in the same order of magnitude as for in-vitro measurements. Linear regression analysis confirmed these observations and showed high correlation between measurements (R^2 0.99). Bland Altman plots for lumen area and lumen diameter are shown in Figure 3. The bias between the observers was again very low. Main sources of disagreement

between observers were situations, in which lumen borders were ambiguous due to anatomical factors (e.g. dissections) or due to motion artifacts during the cardiac cycle.

FIGURE 2: Ex-vivo coronary arteries (n=772 frames)

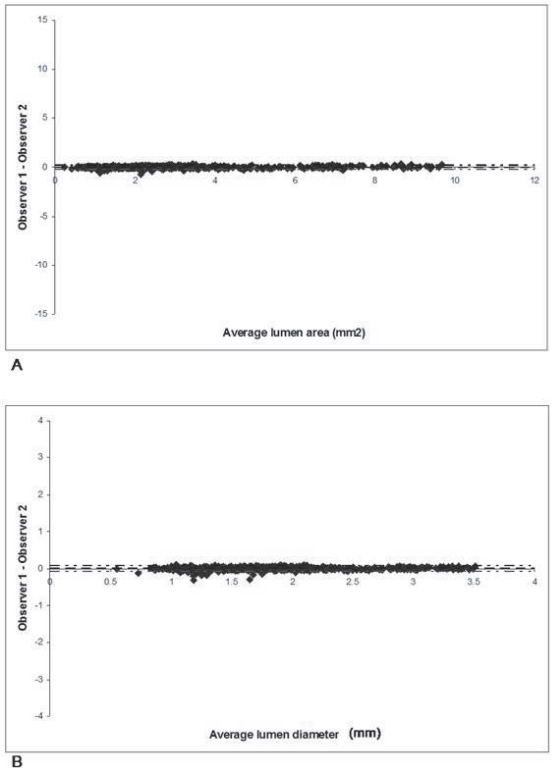

Figure 2: Bland Altman plots for measurements in ex-vivo coronary arteries. The x- axis shows the mean cross sectional area, and the Y axis shows the difference between the cross sectional measurements by observer 1 and observer 2. The dotted lines indicate the limits of agreement (bias ±2 SD). A) Lumen area B) Lumen diameter

	Lumen area	**Lumen diameter**
Observer 1		
Median (IQR)	4.34 (2.21) mm^2	2.35 (0.6) mm
Mean ± 1SD	4.29±1.37mm^2	2.30±0.40mm
Observer 2		
Median (IQR)	4.36 (2.19) mm^2	2.36 (0.59)mm
Mean ± 1SD	4.25±1.34mm^2	2.30±0.39mm
Absolute difference	0.04±0.14mm^2	0.01±0.04mm
Relative difference	0.6±0.4%	0.3±0.2 %
Linear regression		
Slope	0.9755	0.9731
Intercept	0.0647	0.0523
R^2	0.9904	0.9894
p	<0.001	<0.001

Table 2: Comparison of measurements in in-vivo coronary arteries, n=1807 frames

FIGURE 3: In-vivo coronary arteries (n=1807 frames)

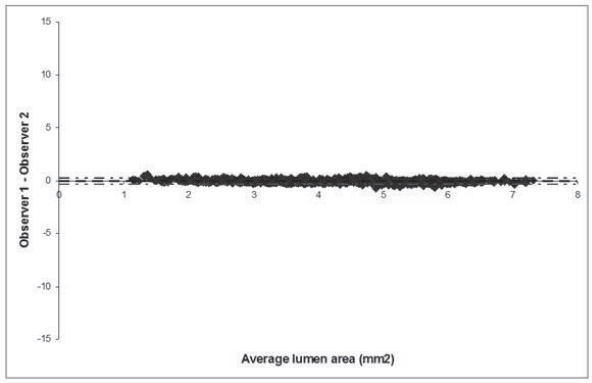

A

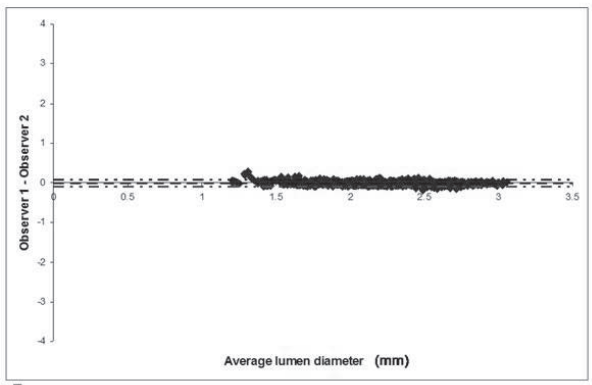

B

Figure 3: Bland Altman plots for measurements in in-vivo coronary arteries. The x- axis shows the mean cross sectional area, and the Y axis shows the difference between the cross sectional measurements by observer 1 and observer 2. The dotted lines indicate the limits of agreement (bias ±2 SD). A) Lumen area B) Lumen diameter

In-vivo stented coronary arteries at follow-up

Ten coronary segments of 25±11mm lengths were studied. Stent struts covered by neotinimal tissue were clearly visible in all segments and in all cross sections. Inter-observer agreement on the presence of neointimal tissue was 100%. A total of 2331 cross sections were included for analysis. In two patients, totally of 80 cross sections were excluded from analysis because of the take-off of a major side branch, and another 73 cross sections because of incomplete visualization of the lumen circumference due to motion artifacts.
OCT data for lumen, stent and neointimal area are summarized in Table 3. Bland Altman plots for lumen stent and neointimal area, as well as lumen and stent diameter are shown in Figure 4. As expected, the bias for the calculated variable of neointimal area was somewhat higher than for directly traced stent and lumen area with greater variability observed in assessing stent area. This relates to the operator having to manually trace each individual stent strut compared to a sharply demarcated lumen/vessel border when assessing lumen area.

	Lumen area	Lumen diameter	Stent area	Stent diameter	Neointima area
Observer					
Median	6.1 (3.45) mm2	2.79 (0.815) mm	9.28 (4.055)	3.44 (0.77) mm	2.96 (2.105) mm2
Mean ±1	5.97±2.41mm2	2.69±0.58mm	9.02±2.77mm2	3.34±0.55mm	3.05±1.48mm2
Observer					
Median	6.2 (3.63) mm2	2.81 (0.85) mm	9.07 (3.915)	3.4 (0.75) mm	2.77 (2.14) mm2
Mean ±1	6.07±2.46mm2	2.72±0.59mm	8.84±2.63mm2	3.31±0.52mm	2.79±1.53mm2
Absolute	0.11±0.33mm2	0.023±0.07mm	0.17±0.68mm2	0.03±0.13mm	0.26±0.72mm2
Relative	1.57±0.05%	0.79±0.03%	1.44±0.08%	0.72±0.04%	14.08±0.37%
Linear	0.9699x+0.077	0.9763x+0.0416	0.9191x+0.5561	0.924x+0.2255	0.8556x+0.6645
R2	0.9818	0.9849	0.9407	0.9471	0.7827
p	<0.001	<0.001	<0.001	<0.001	<0.001

Table 3: Comparison of measurements in in-vivo stented coronary arteries, n=2331 frames

Discussion

The main findings of this study are: (1) Inter-observer variability for lumen dimensions as measured by computer-assisted QOCT is extremely low and in a similar range for both in-vitro as well for in-vivo studies, despite the occurrence of motion induced artifacts during the acquisition in-vivo. (2) Similarly, inter-observer variability in complex vessel anatomy as represented by chronic coronary stents was very low.

Optical coherence tomography

OCT is a new intravascular imaging technology that permits the visualization of vascular microstructures with high precision. Its unique image resolution, in the range of 15μm, is in the magnitude of 10 times higher than the current golden standard, IVUS. Further, the visualization of plaque morphology in close proximity to the vessel lumen is superior to that obtained with IVUS (10). To date, findings based on single frame analysis only in distinct areas within the coronary tree have been published. The clinical application of intracoronary OCT has already been demonstrated in both in stable and unstable patients (11). Potential future applications are manifold. They may include in-vivo visualization of features associated with vulnerable plaque (e.g. thin fibrous cap) (12), analysis of early atherosclerotic lesions (e.g. local intimal thickening), the assessment of progression mechanisms of coronary artery disease and the analysis of the impact of pharmacological or catheter-based interventions on plaque structures and vessel architecture. Intracoronary OCT also provides detailed information relating to stent apposition while allowing the accurate quantification of neointimal stent coverage at follow-up. Such analyses, however, require OCT studies over relatively long epicardial artery segments. We therefore used a dedicated OCT system that allows for data acquisition over long coronary segments using an automated motorized pullback.

Computer-assisted analysis approach

During a motorized OCT pullback a large quantity of cross-sectional images of the coronary artery are acquired. For example, at a rate of 15 frames/sec and a pullback speed of 1.0mm/sec a ROI of 30mm will result in 450 individual cross-sections. Separate analysis of all these individual

cross-sections is cumbersome and time-consuming. In this study, a method similar to established quantitative IVUS (QCU) was adapted and applied. This resulted in a user-friendly analysis system that allows rapid and observer-independent quantitative analysis. This particular QCU software has been validated in the past (8) and is in use as the golden standard for the analysis of IVUS studies, having been applied in numerous multi-center trials (13-16).

FIGURE 4: In-vivo stented coronary arteries (n=2332 frames)

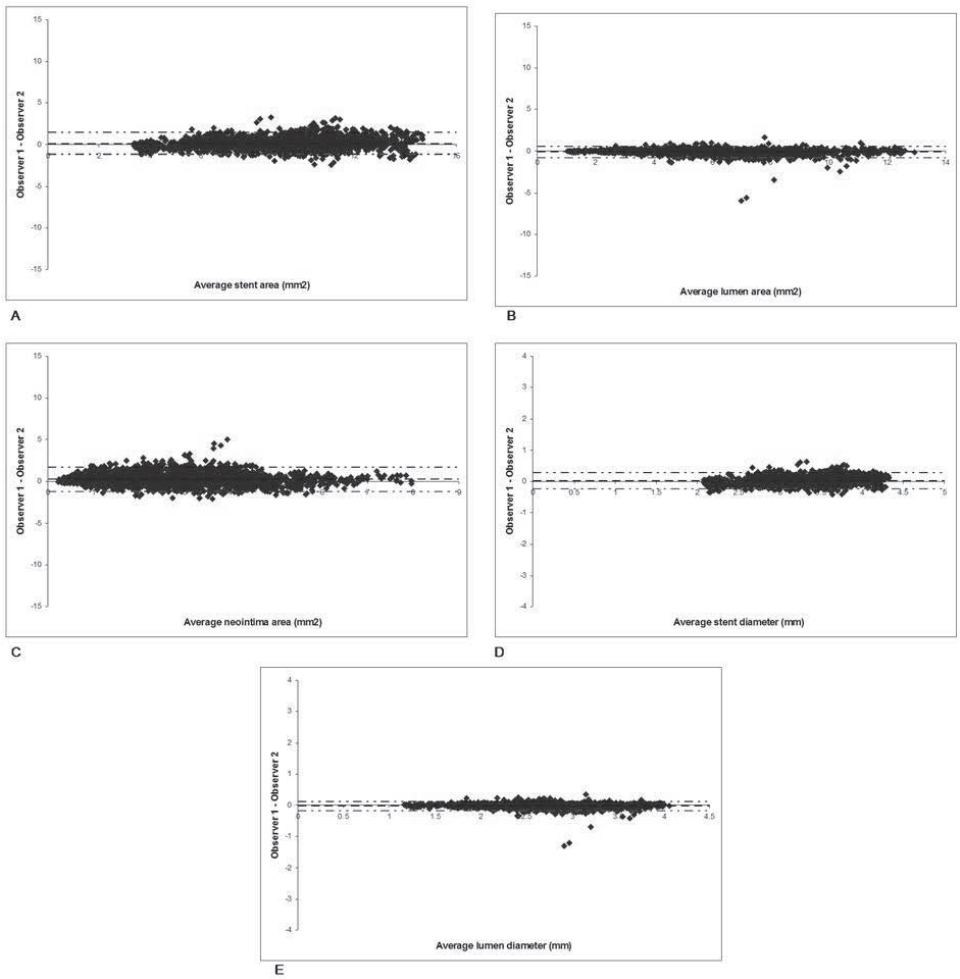

Figure 4: Bland Altman plots for measurements in in-vivo stented coronary arteries. The x- axis shows the mean cross sectional area, and the Y axis shows the difference between the cross sectional measurements by observer 1 and observer 2. The dotted lines indicate the limits of agreement (bias ±2 SD). A) Stent area B) Lumen area C) Neointimal area D) Stent diameter E) Lumen diameter

Comparison to previous studies

In a study using IVUS, inter-observer agreement for the presence of neointimal tissue was 62% with discrepancy between observers exclusively in very thin neointmal layers and a neointimal area <2mm^2 (17). In the present study, the inter-observer agreement on the presence of

neointimal tissue was 100% with neointima visible in all cross sections, whereby 23% of cross section had a neointimal area <2mm^2. The higher resolution of OCT compared to IVUS makes this imaging modality more sensitive at detecting even small quantities of intimal tissue, and this remains one of the major advantages, particularly in the era of drug-eluting stents.
Recent reports using OCT to assess tissue coverage after stent implantation (18,19) have used proprietary off-line software provided by LightLab Imaging Inc. Such an approach involves the operator individually measuring each stent strut at 1mm intervals (approximately each 15 frames) followed by manually tracing both the stent and lumen area, to derive the neointimal area. We have found this technique to be quite cumbersome and heavily operator dependent with each analysis of a stented segment taking between 120 to 240 minutes to complete, depending on the stent length. The method presented in this study achieves a more robust and reproducible analysis in a time and cost-effective fashion.

Clinical implications

OCT is a unique intravascular imaging modality with the sensitivity to delineate mural and luminal structures. As a result, the scope of OCT as both a research and clinical tool remains vast. Such a technology allows the precise assessment of lumen dimensions, plaques, thrombi and dissections (20), while also being able to assess both immediate and late results of stent implantation. While OCT provides additional morphologic information than IVUS, a considerable quantity of information still needs to be processed. Adopting a semi-automated, computer assisted approach with contour detection remains pivotal in making future studies incorporating OCT more reliable and reproducible with less potential sources of operator error.

Limitations

This study is obviously limited by the number of observations and the narrow range of arterial dimensions evaluated. However, the target vessel dimensions represent the majority of clinically relevant dimensions in patients. Motion artifacts during the cardiac cycle hampered the visualization of the complete vessel circumference in 9% of the cross sections using the current OCT software. Modifications in software, OCT imaging catheter design and ECG gated data acquisition (21) or retrospective image-based gating (22) of acquired IVUS data might alleviate such limitations in the future. The high resolution of OCT is at the expense of penetration depth, which is typically limited to approx 1-2mm into the vessel wall limiting analysis to structures that are relatively close to the inner lumen border.

Conclusions

Computer-assisted contour analysis of intracoronary OCT pullback is feasible and enables OCT morphometry with low inter-observer variability. This approach allows for observer independent QOCT analysis and may be a valuable tool for future longitudinal studies incorporating OCT.

References

1. Huang D, Swanson E, Lin C, et al. Optical coherence tomography. Science 1991;254:1178-81.
2. Brezinski ME, Tearney GJ, Bouma BE, et al. Imaging of coronary artery microstructure (in vitro) with optical coherence tomography. Am J Cardiol 1996;77:92-3.
3. Fujimoto JG, Boppart SA, Tearney GJ, Bouma BE, Pitris C, Brezinski ME. High resolution in vivo intra-arterial imaging with optical coherence tomography. Heart 1999;82:128-33.
4. Tearney GJ, Jang IK, Kang DH, et al. Porcine coronary imaging in vivo by optical coherence tomography. Acta Cardiol 2000;55:233-7.
5. Schmitt J, Petersen C, Mont E, Virmani R. imaging and characterization of coronary lesions with optical coherence tomography. ieee j. 2002:106 -109.

6. Kume T, Akasaka T, Kawamoto T, et al. Assessment of coronary intima--media thickness by optical coherence tomography: comparison with intravascular ultrasound. Circ J 2005;69:903-7.
7. Tsuchida K, van der Giessen WJ, Patterson M, et al. In-vivo validation of a novel three-dimensional quantitative coronary angiography system (CardioOp-B TM): comparison with a conventional two-dimensional system (CASS II TM) and with special reference to optical cohence tomography. EuroInterv. 2007;3:100-108.
8. Hamers R, Bruining N, Knook M, Sabate M, Roelandt JRTC. A novel approach to quantitative analysis of intravscular ultrasound images. IEEE J. 2001;28:589-592.
9. Bland JM, Altman DG. Statistical methods for assessing agreement between two methods of clinical measurement. Lancet 1986;1:307-10.
10. Jang IK, Bouma BE, Kang DH, et al. Visualization of coronary atherosclerotic plaques in patients using optical coherence tomography: comparison with intravascular ultrasound. J Am Coll Cardiol 2002;39:604-9.
11. Jang I-K, Tearney GJ, MacNeill B, et al. In Vivo Characterization of Coronary Atherosclerotic Plaque by Use of Optical Coherence Tomography. Circulation 2005;111:1551-1555.
12. Regar E, Schaar J, McFadden E, et al. Real-time, high resolution optical coherence tomography (OCT) – a potential tool to detect features of vulnerable plaque in-vivo? Eur Heart J 2005:3677 (abstract).
13. Degertekin M, Lemos PA, Lee CH, et al. Intravascular ultrasound evaluation after sirolimus eluting stent implantation for de novo and in-stent restenosis lesions. Eur Heart J 2004;25:32-8.
14. Serruys PW, Degertekin M, Tanabe K, et al. Vascular responses at proximal and distal edges of paclitaxel-eluting stents: serial intravascular ultrasound analysis from the TAXUS II trial. Circulation 2004;109:627-33.
15. Tanabe K, Serruys PW, Degertekin M, et al. Incomplete stent apposition after implantation of paclitaxel-eluting stents or bare metal stents: insights from the randomized TAXUS II trial. Circulation 2005;111:900-5.
16. Aoki J, Colombo A, Dudek D, et al. Peristent remodeling and neointimal suppression 2 years after polymer-based, paclitaxel-eluting stent implantation: insights from serial intravascular ultrasound analysis in the TAXUS II study. Circulation 2005;112:3876-83.
17. Regar E, Werner F, Siebert U, et al. Reproducibility of neointima quantification with motorized intravascular ultrasound pullback in stented coronary arteries. Am Heart J 2000;139:632-637.
18. Matsumoto D, Shite J, Shinke T, et al. Neointimal coverage of sirolimus-eluting stents at 6-month follow-up: evaluated by optical coherence tomography. Eur Heart J 2007;28:961-7.
19. Takano M, Inami S, Jang IK, et al. Evaluation by optical coherence tomography of neointimal coverage of sirolimus-eluting stent three months after implantation. Am J Cardiol 2007;99:1033-8.
20. Gerckens U, Buellesfeld L, McNamara E, Grube E. Optical Coherence Tomography (OCT). Potential of a new high-resolution intracoronary imaging technique. Herz. 2003;28: 496-500.
21. von Birgelen C, de Vrey EA, Mintz GS, et al. ECG-gated three-dimensional intravascular ultrasound: feasibility and reproducibility of the automated analysis of coronary lumen and atherosclerotic plaque dimensions in humans. Circulation 1997;96:2944-52.
22. De Winter SA, Hamers R, Degertekin M, et al. Retrospective image-based gating of intracoronary ultrasound images for improved quantitative analysis: the intelligate method. Catheter Cardiovasc Interv 2004;61:84-94.

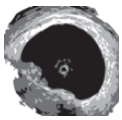

Chapter 7

Quantitative analysis of intracoronary optical coherence tomography measurements of stent strut apposition and tissue coverage

Peter Barlis, Konstantinos Dimopoulos, Jun Tanigawa, Ewa Dzielicka, Giuseppe Ferrante, Francesca Del Furia, Carlo Di Mario

Background: *The introduction of optical coherence tomography (OCT) as an intracoronary imaging modality has allowed accurate assessment of strut apposition and neointimal tissue coverage. This study set out to assess the inter and intraobserver variability of measurements of acute stent apposition and strut tissue coverage using OCT.*
Methods: *Thirty patients were studied (14 immediately after stent implantation and 16 during follow-up angiography [mean of 4.7±2.8 months]) using OCT. Data analysis was performed by 2 experienced observers. Struts were classified as embedded, protruding or malapposed to the vessel well. Intimal coverage at follow-up was measured as the thickness of tissue covering each strut (μm). Intra and interobserver variability was assessed by Bland-Altman plots and the intraclass correlation coefficient (ICC).*
Results: *An average of 3967 struts was examined by each observer and, overall, 53.7% of struts were embedded, 36.4% protruding and 9.9% malapposed. Low intraobserver variability for all measures of strut apposition was found, with repeatability coefficients that ranged between 5.1% and 9.3% and ICC exceeding 95% in all cases. Interobserver variability was also low (repeatability coefficients 6.6-10.8 and ICC>91.3%). Mean intimal thickness in the follow-up group was 172.5μm. Bland-Altman plots demonstrated a low intraobserver and interobserver variability for intimal thickness, with repeatability coefficients 26.7μm and 24.1μm, respectively and ICC exceeding 98.6% for both*
Conclusions: *Low intra and interobserver variability can be expected when analyzing OCT data for stent apposition and tissue coverage. This supports the validity of OCT as a clinical and research tool in the setting of intracoronary stent imaging.*

Optical coherence tomography (OCT) is rapidly achieving widespread diffusion in catheterization laboratories worldwide. Its advantage over intravascular ultrasound (IVUS) is its superior resolution (15μm) and fewer artifacts. The current technology permits image acquisition using a 1310 nm near-infrared light source that detects backscattering of light from superficial microstructures within the coronary wall. OCT has been used as an intra-coronary imaging tool for the assessment of stent apposition, neointimal tissue coverage and plaque characterization.(1-10) To date, there is only one commercially available OCT system which uses a proprietary software for offline analysis of acquired images. We sought to assess the inter- and intra-observer variability of the current OCT system for stent strut apposition immediately following stent deployment and for tissue coverage at follow-up.

Methods

A total of 30 patients were prospectively included in this study. OCT was performed immediately after stent deployment in 14 patients and on follow-up angiography in a separate group of 16 patients, using the LightLab system (Westford, Massachusetts, US). Blood clearance was achieved using a proximal occlusion balloon (Helios, Goodman, Japan) with intra-coronary flush of lactated Ringer's solution through the end-hole of the balloon catheter (flow rate 0.6-0.9ml/sec) during simultaneous image acquisition at 1.0mm/sec using the dedicated ImageWire (LightLab Imaging, Westford, Massachusetts, US) at 15.6 frames/second.

OCT data analysis

Offline OCT images were analyzed by 2 experienced observers. For intraobserver variability, measurements were repeated 3-months after the initial assessment by the same observer, who was blinded to the previous results. For interobserver variability, measurements were carried out independently by the two observers, blinded to each other's analysis.

Acute stent strut apposition

Analysis of contiguous cross-sections within the stented segment was performed at 1mm intervals. In each selected cross section, the distance between the endoluminal border of the strut and the intima was measured. As OCT can only image the endoluminal strut border, distances were adjusted based on the thickness of the strut, including the polymer, for each of the stent types used.(9) Struts were classified as "embedded" when buried into the vessel wall, "protruding" when in contact with the vessel wall but protruding into the lumen and "malapposed" when no contact between the intima and the strut was detected (Figure 1).

see colour section

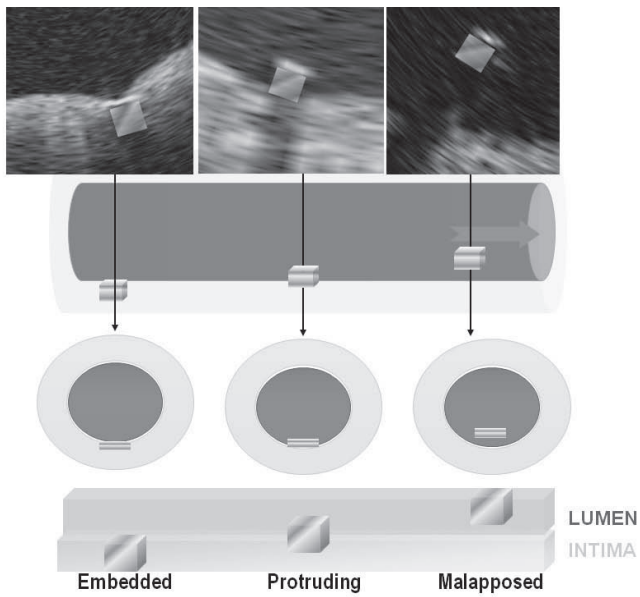

Figure 1 Optical coherence tomography classification of stent apposition into embedded, protruding or malapposed.

Strut tissue coverage

Tissue coverage was assessed by OCT at a minimum of 3 months post-implantation of different stents types and the thickness of the tissue overlying each stent strut was measured.

Statistical Analysis

Statistical analyses and generation of plots was performed using R version 2.6.1 (The R Foundation for Statistical Computing, Vienna, Austria). To assess intra and inter-observer agreement, Bland-Altman plots were produced and mean difference and 95% limits of agreement with 95% confidence intervals were calculated. The repeatability coefficient (within which 95% of all differences are included) was calculated as twice the standard deviation of the differences between measurements on the same segment, as described by Bland and Altman. (11) Intra-class correlation coefficients (ICC) with 95% confidence intervals were also calculated as an additional measure of intra and inter-examiner reliability.

Results

Acute stent strut apposition

Clinical and angiographic and procedural characteristics of the 14 patients having OCT immediately following stent implantation are shown in Table 1. The target vessel was the left anterior descending artery (LAD) in 50%, left circumflex artery (LCx) in 21.4% and the right coronary artery (RCA) in 28.6%. OCT was performed uneventfully in all cases.

	Assessment of Acute Apposition (n=14)	**Assessment of intimal coverage (n=16)**
Age (yrs)	62 ± 11	60±7
Men	11 (78.6%)	15 (93.7%)
Hypertension	6 (42.9%)	8 (50%)
Diabetes Mellitus	1 (7.1%)	5 (31.2%)
Hypercholesterolemia*	12 (85.7%)	10 (62.5%)
Current smoker	4 (28.6%)	3 (18.7%)
Prior myocardial infarction	5 (35.7%)	7 (43.7%)
Prior coronary artery bypass grafting	0 (0%)	3 (18.7%)
Prior percutaneous coronary intervention	3 (21.4%)	16 (100%)
1-vessel disease	8 (57.1%)	6 (37.5%)
2-vessel disease	4 (28.6%)	6 (37.5%)
3-vessel disease	2 (14.3%)	4 (25.0%)
Clinical presentation		
Stable Angina Pectoris	8 (57.1%)	10 (62.5%)
Unstable Angina Pectoris	6 (42.9%)	6 (37.5%)
Time to optical coherence tomography (months)	-	4.7±2.8
Artery treated and imaged		
Left anterior descending	7 (50%)	8 (50.0%)
Left circumflex	3 (21.4%)	3 (18.8%)
Right	4 (28.6%)	5 (31.2%)
Number of stents/patient	1.8±0.9	1.6±0.6
Stent type		
Cypher stent	8 (57.1%)	6 (37.5%)
Taxus stent	4 (28.6%)	3 (18.8%)
Endeavour stent	1 (7.1%)	2 (12.5%)
Costar stent	2 (14.2%)	1 (6.2%)
Yukon	0 (0%)	4 (25.0%)

Table 1: Baseline clinical, lesion and procedural characteristics

A mean of 3930 struts were examined by observer 1 and 4042 by observer 2. The average percent embedded, protruding and malapposed struts for observer 1 was 52.1%, 38.2% and 9.7%, respectively, and for observer 2, 55.3%, 34.6%, and 10.1%, respectively.

The Bland-Altman plots showed low intra-observer variability for all measures of strut apposition, with repeatability coefficients that ranged between 5.1% and 9.3% (Figure 2, Table

2). The intraclass correlation coefficient, exceeding 95% in all cases, confirmed the high intra-observer repeatability of the OCT measurements. No consistent bias was observed (mean absolute difference between observations ranging between 0.0-1.8%).

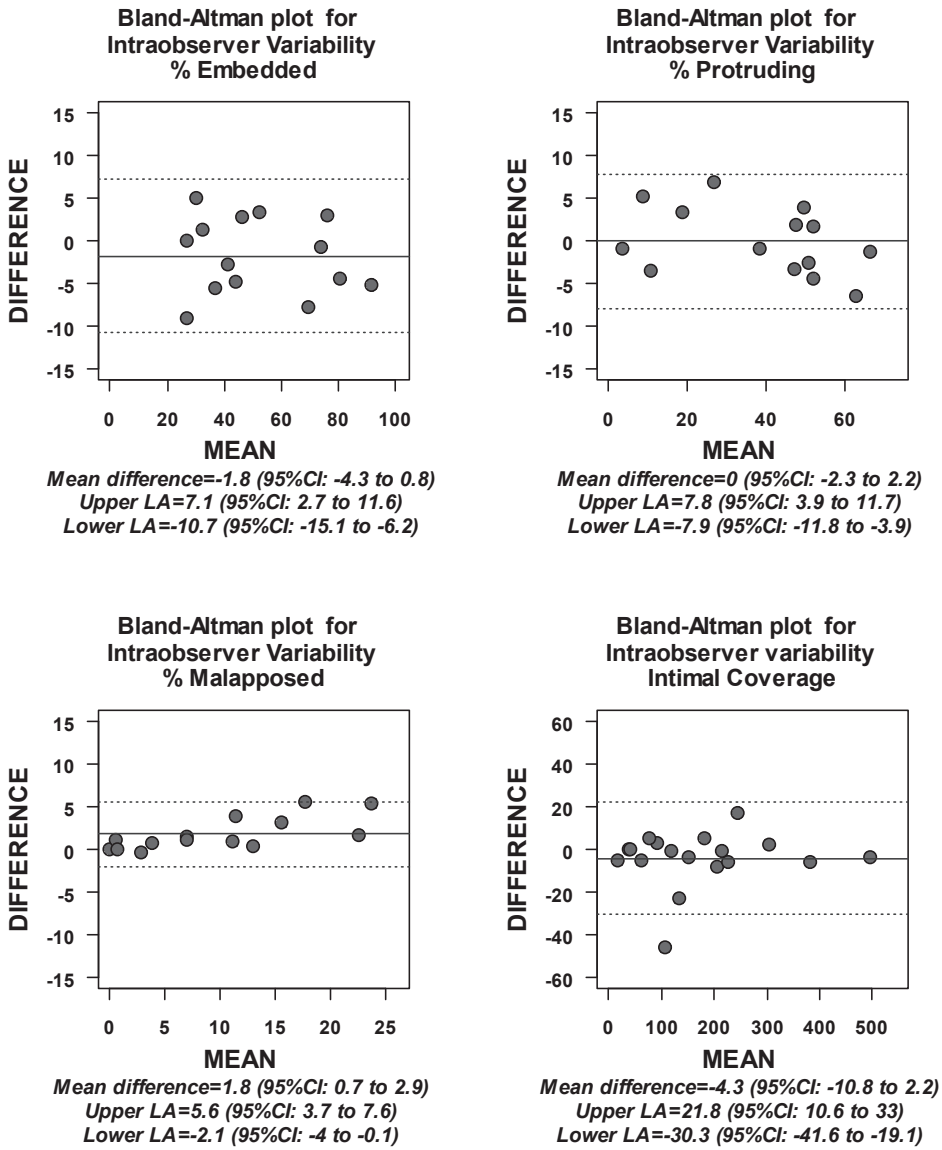

Figure 2 Bland-Altman plots of intraobserver variability

	Reproducibility coefficient	ICC	95%CI
Acute strut apposition			
Intra-observer			
Embedded	9.2%	97.8%	93.5 - 99.2%
Protruding	7.5%	98.4%	95.2 - 99.4%
Malapposed	5.1%	94.9%	85.5 - 98.3%
Inter-observer			
Embedded	10.8%	98.3%	95.1 - 99.4%
Protruding	8.6%	97.3%	92.2 - 99.1%
Malapposed	6.6%	91.3%	75.8 - 97.0%
Neointimal tissue coverage			
Intra-observer	26.7μm	99.4%	98.6 - 99.8%
Inter-observer	24.1μm	99.6%	98.8 - 99.8%

ICC-intraclass coefficient, CI-confidence interval;

Table 2: Reproducibility coefficient and intraclass correlation coefficient (expressed as %)

Good agreement was also found between observers for measures of strut apposition, with narrow limits of agreement on the Bland-Altman plots. Repeatability coefficients ranged between 6.6-10.8%, with intraclass correlation coefficients exceeding 91%. No consistent bias was observed (mean absolute difference between observations ranged between 1.2-3.5%).

Strut tissue coverage

Sixteen patients underwent OCT evaluation of late stent strut tissue coverage at a mean follow-up 4.7±2.8 months from stent implantation. Clinical, angiographic and procedural characteristics of this population are also depicted in Table 1. Mean intimal thickness for observers 1 and 2 was 169.6μm and 175.5μm, respectively. The Bland-Altman plots demonstrated a low intraobserver variability for intimal thickness, with no bias (Figure 3). The repeatability coefficient was 26.7μm, with a high ICC (98.6%). A high degree of agreement between different observers was also found. Limits of agreement were narrow and the repeatability coefficient was 24.1μm. ICC was very high (99.6%).

Discussion

This is the first systematic study to evaluate inter and intra-observer variability for both acute stent apposition and late tissue stent strut coverage using OCT. With its high resolution, OCT permits a detailed assessment of coronary structures while giving unique insights into tissue responses following stent implantation. Our study shows that OCT analysis gives highly reproducible data for both the assessment of acute stent strut apposition and late strut tissue coverage.

Stent strut apposition

Until recently, IVUS has been the gold standard for the assessment of acute and late stent strut apposition. Many studies have examined the implications of incomplete stent apposition with some showing no relation to adverse events (12,13) while others finding a link with in-stent restenosis and stent thrombosis.(14-16) Such inconsistencies are likely explained by the known

limitations of IVUS, namely its low resolution (100 μm) and the presence of artifacts. OCT uses near infra-red light with 10 times higher resolution than IVUS. This unique imaging modality gives precise quantification of stent struts and their relation to the vessel wall without the artifacts associated with echo.

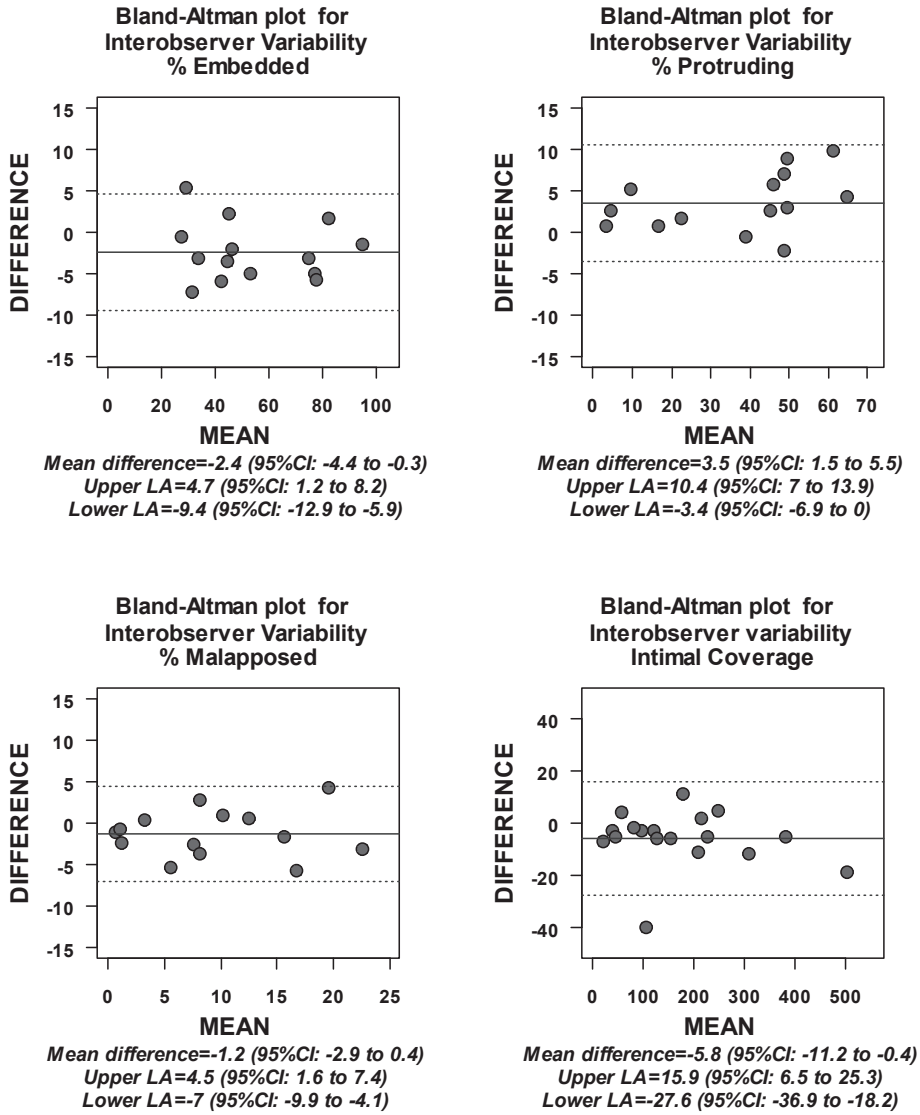

Figure 3- Bland-Altman plots of Interobserver variability

The infra-red light used by OCT is, however, unable to penetrate metal, thus producing dorsal shadowing behind the endoluminal aspect of the stent struts (Figure 2, arrow). As a result, when evaluating strut apposition, the additional thickness of the strut must also be taken into account (including the metal and polymer thickness) when assessing the distance between the strut and the intima. Moreover, position of the intima behind the strut of interest must be deduced from the adjacent intimal border, which is shadow-free. Despite these limitations of OCT, the low inter and intra observer variability found in this study reflects the high definition of this technology for microstructures such as stent struts.

The classification of strut apposition used in this study was previously proposed by our group. (9) (Figure 1) The rationale of this classification into "embedded", "protruding" and "malapposed" derives from the concept that struts buried into the intima (embedded) have a lower % exposed surface to flow and a higher probability of being covered by the intima in a timely fashion. Protruding struts, although in contact with the intima, have a higher % of exposed surface area to blood, which may affect local flow dynamics and potentially lead to delayed tissue coverage. Malapposed struts are not in contact with the intima, with 100% of their surface exposed to blood flow, possibly resulting in very delayed or no intimal coverage. This may have a bearing both on short and long-term risk of stent thrombosis, given that post-mortem studies have shown a clear link between malapposed struts, lack of tissue coverage and stent thrombosis. (15,17) This study showed a very high degree of inter and intraobserver agreement using the above classification. Serial OCT studies with long-term follow-up are needed demonstrate the clinical relevance of acute strut apposition classified in this manner.

Stent strut tissue coverage

OCT is likely to become the new gold standard for assessing stent tissue coverage in-vivo. Several studies have recently been published highlighting the application of OCT in the detection of stent tissue coverage at follow-up. Matsumoto et al (18) studied 34 patients following sirolimus-eluting stent (SES) implantation. The mean neointima thickness was 52.5 μm. We found comparable intra and interobserver variability to Matsumoto et al, despite a much higher mean neontimal thickness (170 in our study versus 52), likely due to the use of different stent types. The low variability is reassuring, given the potential application and importance of tissue coverage to the clinical setting, with studies having found a link between delayed or incomplete endothelialization and stent thrombosis. (19,20)

Clinical implications

When considering the valuable information gained from OCT, in particular its ability to detect minute tissue coverage over stent struts in-vivo, the intense interest now shown in this field is understandable. OCT is fast becoming an integral component of large clinical stent trials in an attempt to assess tissue coverage and possibly address the incidence of incomplete stent endothelialization in different stent types. Knowledge of intra and interobserver variability of OCT measurements is essential when designing such trials and when considering OCT findings as a surrogate marker of possible late thrombosis.

Limitations

Even though our study included a limited number of patients, a very large number of struts were examined using a highly sensitive imaging modality, resulting in very small intra and interobserver variability. Given the relatively recent introduction of OCT for the coronary circulation, only one system with its proprietary analysis software is currently available. Measurements of apposition and intimal tissue are currently performed manually, and are thus extremely time-consuming. In the near future, developments in analysis and data systems will see

the extension of IVUS based analysis packages to OCT data. New semi-automated or automated software will be developed and will need to be validated against the current proprietary software. Furthermore, until a precise threshold for the percentage of struts malapposed within a stent is defined by large series of patients undergoing serial OCT, the clinical relevance of the intra and interobserver variability found in our study will remain unclear. Regardless, a high degree of intra and interobserver agreement was present for all measures of apposition.

Conclusions

Low intra and interobserver variability can be expected when analyzing intracoronary derived OCT data for stent strut apposition and intimal coverage. This supports the validity of OCT as a clinical and research tool in the setting of intracoronary stent imaging.

References

1. Tanigawa J, Barlis P, Dimopoulos K, Di Mario C. Optical coherence tomography to assess malapposition in overlapping drug-eluting stents. EuroIntervention 2008;3:580-83.
2. Takano M, Inami S, Jang IK, et al. Evaluation by optical coherence tomography of neointimal coverage of sirolimus-eluting stent three months after implantation. Am J Cardiol 2007;99:1033-8.
3. Raffel OC, Tearney GJ, Gauthier DD, Halpern EF, Bouma BE, Jang IK. Relationship between a systemic inflammatory marker, plaque inflammation, and plaque characteristics determined by intravascular optical coherence tomography. Arterioscler Thromb Vasc Biol 2007;27:1820-7.
4. Kubo T, Imanishi T, Takarada S, et al. Assessment of culprit lesion morphology in acute myocardial infarction: ability of optical coherence tomography compared with intravascular ultrasound and coronary angioscopy. J Am Coll Cardiol 2007;50:933-9.
5. Tearney GJ, Jang IK, Bouma BE. Optical coherence tomography for imaging the vulnerable plaque. J Biomed Opt 2006;11:021002.
6. Jang IK, Tearney GJ, MacNeill B, et al. In vivo characterization of coronary atherosclerotic plaque by use of optical coherence tomography. Circulation 2005;111:1551-5.
7. Tearney GJ, Yabushita H, Houser SL, et al. Quantification of macrophage content in atherosclerotic plaques by optical coherence tomography. Circulation 2003;107:113-9.
8. Barlis P, Tanigawa J, Di Mario C. Coronary bioabsorbable magnesium stent: 15-month intravascular ultrasound and optical coherence tomography findings. Eur Heart J 2007;28:2319.
9. Tanigawa J, Barlis P, Di Mario C. Intravascular Optical Coherence Tomography: Optimisation of image acquisition and quantitative assessment of stent strut apposition. EuroIntervention 2007;3:128-136.
10. Tanimoto S, Rodriguez-Granillo G, Barlis P, et al. A novel approach for quantitative analysis of intracoronary optical coherence tomography: high inter-observer agreement with computer-assisted contour detection. Catheter Cardiovasc Interv 2008:DOI: 10.1002/ccd.21482.
11. Bland JM, Altman DG. Statistical methods for assessing agreement between two methods of clinical measurement. Lancet 1986;1:307-10.
12. Tanabe K, Serruys PW, Degertekin M, et al. Incomplete stent apposition after implantation of paclitaxel-eluting stents or bare metal stents: insights from the randomized TAXUS II trial. Circulation 2005;111:900-5.
13. Hong MK, Mintz GS, Lee CW, et al. Late stent malapposition after drug-eluting stent implantation: an intravascular ultrasound analysis with long-term follow-up. Circulation 2006;113:414-9.
14. Fujii K, Carlier SG, Mintz GS, et al. Stent underexpansion and residual reference segment stenosis are related to stent thrombosis after sirolimus-eluting stent implantation: an intravascular ultrasound study. J Am Coll Cardiol 2005;45:995-8.
15. Cook S, Wenaweser P, Togni M, et al. Incomplete stent apposition and very late stent thrombosis after drug-eluting stent implantation. Circulation 2007;115:2426-34.
16. Uren NG, Schwarzacher SP, Metz JA, et al. Predictors and outcomes of stent thrombosis: an intravascular ultrasound registry. Eur Heart J 2002;23:124-32.
17. Joner M, Finn AV, Farb A, et al. Pathology of drug-eluting stents in humans: delayed healing and late thrombotic risk. J Am Coll Cardiol 2006;48:193-202.

18. Matsumoto D, Shite J, Shinke T, et al. Neointimal coverage of sirolimus-eluting stents at 6-month follow-up: evaluated by optical coherence tomography. Eur Heart J 2007;28:961-7.
19. Bouma BE, Tearney GJ, Yabushita H, et al. Evaluation of intracoronary stenting by intravascular optical coherence tomography. Heart 2003;89:317-20.
20. Diaz-Sandoval LJ, Bouma BE, Tearney GJ, Jang IK. Optical coherence tomography as a tool for percutaneous coronary interventions. Catheter Cardiovasc Interv 2005;65:492-6.

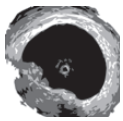

Chapter 8

Comparison of an occlusive versus non-occlusive technique in the acquisition of intra-coronary optical coherence tomography imaging

Peter Barlis, Francesca Del Furia, Giuseppe Ferrante, Konstantinos Dimopoulos, Pablo Aguiar-Souto, Savio D' Souza Carlo Di Mario

Aims: *The established technique for acquiring optical coherence tomography (OCT) images depends on temporary balloon occlusion of the proximal vessel with subsequent flush of crystalloid solution distally to clear blood. A new technique of flushing viscous contrast through the guiding catheter is increasingly being used although has not been compared to the established method. This study sought to compare the non-occlusive with the traditional occlusive technique for intracoronary OCT imaging.*

Methods and Results: *Eighty-two patients underwent OCT imaging. Fifty (61.0%) had images acquired during proximal balloon occlusion with coronary blood flow replaced by infusion of Ringer's lactate. Thirty-two (39.0%) patients underwent OCT imaging using the non-occlusive technique with flushing of iso-osmolar contrast through the guiding catheter. The additional procedure time for OCT imaging was shorter with the non-occlusive compared to occlusive technique (8.5±5.2 versus 19.9±8.5 min, p<0.001). The non-occlusive technique allowed for a shorter pullback time, achieving a longer pullback distance (37.8±9.0mm versus 28.2±6.2mm, p<0.001) and thus a greater length of vessel visualized. This was also better tolerated by patients with significantly less chest pain (68% versus 15.6%, p<0.001). Contrast use was higher for the non-occlusive technique (30.3±11.0ml versus 3.4±3.0ml, p<0.001).*

Conclusions: *The non-occlusive technique for OCT imaging is simpler and better tolerated by patients and allows for a more comprehensive assessment of the coronary tree. New developments with even faster acquisition speeds and the use of alternative, non-contrast based flushing solutions will mean quicker OCT assessments with even less contrast load.*

Optical coherence tomography (OCT) has been a welcome addition to the armamentarium of interventional cardiologists and researchers world-wide. The first generation system (M2, LightLab Imaging Inc., Westford, MA, USA) introduced commercially in 2004, demands transient vessel occlusion, achieved by dilatation of a balloon in the proximal vessel, with simultaneous flush of crystalloids (Ringer's lactate) through the end hole of the catheter. Refinements in OCT technology, with faster acquisition speeds (currently peaking at 3mm/sec but with 20mm/sec in the foreseeable future with the new generation Fourier domain OCT) have seen a gradual shift from the cumbersome occlusive technique to a simpler non-occlusive approach with flushing of viscous contrast through the guiding catheter. Even though initial reports have shown this to be feasible, (1) it continues to remain "off-label". The non-occlusive technique offers many potential advantages (Table 1) and reduces the risk of balloon-related vessel injury, but its application into clinical practice has not been tested in comparison to the conventional occlusive technique. This study is a single-center comparison of the non-occlusive and occlusive techniques for the acquisition of intra-coronary OCT images in 2 consecutive groups of patients examined between February 2006-March 2007 and March 2007–January 2008, respectively.

Methods

Eighty-two patients underwent OCT imaging at the time of percutaneous coronary intervention (PCI), or during follow-up angiography. Fifty (61.0%) patients had images acquired during proximal balloon occlusion (Helios, Goodman Inc, Nagoya, Japan) with a dedicated indeflator used to inflate the balloon between 0.5-0.7atm and coronary blood flow replaced by continuous infusion of Ringer's lactate at a rate of 0.5-1.2ml/sec using a power injector (Mark-V ProVis, Medrad, Inc. Indianola, PA, US). Images were acquired with a pullback speed of 1.0mm/sec. Thirty-two (39.0%) patients underwent OCT imaging with an upgraded OCT system (M3, LightLab Imaging Inc., Westford, MA, USA), using the non-occlusive technique with flushing of viscous iso-osmolar contrast (Iodixanol 320, Visipaque™, GE Health Care, Cork, Ireland) through the guiding catheter at a pullback speed of 3 mm/sec. As the OCT image wire is fragile

and does not have the handling properties of a guidewire, its passage distal to the region of interest must be facilitated by the use of a catheter. In our experience, we have found both single lumen (e.g. Transit, Cordis, Johnson & Johnson, Miami, FL, US) or double lumen (e.g.0.023" TwinPass, Vascular Solutions Inc, Minneapolis, Minnesota, US) catheters useful in this respect.

ADVANTAGES	DISADVANTAGES
▪ Expensive dedicated occlusive balloon not required ▪ Minimal vessel instrumentation (over-the-wire catheter for wire exchange) ▪ Ostial and proximal segments can be imaged ▪ Examination of long segments is simplified ▪ Better and more consistent image quality ▪ Patient discomfort and ECG changes are minimized	▪ Potentially nephrotoxic and expensive contrast is used ▪ Requires a well positioned guiding catheter at the ostium of the left or right coronary artery to facilitate adequate flush and blood clearance

Table 1: Advantages and disadvantages of the non-occlusive technique

Results

Clinical and procedural characteristics are shown in Table 2. The non-occlusive technique allowed visualization of larger numbers of ostial and proximal coronary segments, including the left main, many of which could not be examined using the occlusive technique (which requires the use a balloon proximal to the region of interest). Moreover, using the non-occlusive technique, we were able to perform multi-vessel imaging in a significantly higher number of patients. The additional procedure time for OCT imaging was significantly shorter with the non-occlusive compared to occlusive technique (8.5±5.2 vs. 19.9±8.5 min, $p<0.001$).

Of note, the non-occlusive technique allowed for a shorter pullback time thanks to the faster acquisition speed, despite achieving a longer pullback distance (37.8±9.0mm vs. 28.2±6.2mm, $p<0.001$) and thus a greater length of vessel visualized. The non-occlusive technique was also better tolerated by patients, with a significantly reduced incidence of procedure-related chest pain (68% vs. 15.6%, $p<0.001$).

Contrast volume for OCT imaging was higher for the non-occlusive compared with occlusive technique (30.3±11.0ml vs. 3.4±3.0ml, $p<0.001$). Although the occlusive technique uses Ringer's lactate, a small amount of contrast is required to guide positioning of the balloon and image wire. However, there were no cases of contrast nephropathy or significant post-procedural rises in creatinine concentration in either group.

Discussion

This is the first report comparing the two different approaches to intra-coronary OCT image acquisition in clinical practice. The "off-label" non-occlusive technique resulted in a shorter OCT procedure time and was able to provide a larger amount of information with a longer pullback distance achieved. This technique was also applicable to more ostial and proximal coronary segments and resulted in significantly less patient discomfort, overcoming the limitations inherent with the use of balloon occlusion. This was, however, at the expense of a larger contrast load.

	Entire group (n=82)	Occlusive technique (n=50)	Non-occlusive technique (n=32)	p value
Age (years)	64.7 ± 9.1	63.1 ± 9.6	67.0 ± 7.7	0.061
Male gender	62 (76)	39 (78)	23 (72)	0.528
Diabetes mellitus	19 (23)	10 (20)	9 (28)	0.423
Hypertension	57 (69)	31 (62)	26 (81)	0.064
Current/Ex Smoker	48 (58)	31 (62)	17 (53)	0.559
Dyslipidemia	73 (89)	41 (82)	32 (100)	0.011
Prior CABG	9 (11)	1 (2)	8 (25)	0.001
Baseline serum creatinine (µmol/l)	95 ± 22	93 ± 25	94 ± 23	0.872
Indication for OCT imaging				
Lesion/plaque characterization	8 (10)	6 (12)	2 (6)	0.392
PCI guidance (post-stenting)	47 (57)	32 (64)	15 (47)	0.126
Stent tissue coverage assessment	27 (33)	12 (24)	15 (47)	0.031
Target vessel imaged				
N	**105**	**58**	**47**	
Left main stem	1 (1)	0 (0)	1 (2)	0.447
Left anterior descending	46 (44)	28 (48)	18 (38)	0.301
Left circumflex	26 (25)	12 (21)	14 (30)	0.283
Right	28 (26)	18 (31)	10 (21)	0.261
Graft	4 (4)	0 (0)	4 (9)	0.037
Vessel segment imaged				
Ostial	12 (11)	2 (3)	10 (21)	0.005
Proximal	38 (36)	14 (24)	24 (51)	0.004
Mid	36 (34)	23 (40)	13 (28)	0.198
Distal	14 (13)	7 (12)	7 (15)	0.672
Multi-vessel imaging	18 (22)	7 (14)	11 (34)	0.030
Mean OCT procedural time (min)	14.4±9.1	19.9±8.5	8.5±5.2	<0.001
Mean contrast volume for OCT imaging (ml)	15.6±15.5	3.4±3.0	30.3±11.0	<0.001
Mean OCT pullback length (mm)	32.7 ± 9.1	28.2 ± 6.2	37.8±9.0	<0.001
OCT tolerability/safety				
Patient chest pain	39 (47.5)	34 (68)	5 (15.6)	<0.001
Major arrhythmia (AV block, AF, VT,	0	0	0	-
Contrast induced nephropathy	0	0	0	-
Vessel dissection/perforation	0	0	0	-

CABG-coronary artery bypass surgery; PCI-percutaneous coronary intervention; OCT-optical coherence tomography; AV-atrio-ventricular; AF-atrial fibrillation; VT-ventricular tachycardia; VF-ventricular fibrillation;

Table 2: Clinical and procedural characteristics

The highly detailed images obtained by OCT have given a new dimension to the understanding of atherosclerotic plaque and coronary stenting.(2-10) Despite its widespread use, the technique is highly specialized and requires adequate proctorship. Such a demanding image acquisition process has led to reservation amongst many interventionalists as to the true advantage of OCT compared to traditional intravascular ultrasound (IVUS), which, although at a lower resolution, is generally well tolerated by patients and simpler to use. The use of an occlusive balloon remains quite cumbersome and, in the vast majority of cases, results in patient discomfort with associated electrocardiographic changes, even though such events are usually transient and resolve completely when the balloon is deflated. Hence, a non-occlusive technique is attractive on a number of fronts, and could result in wider diffusion amongst the interventional community.

The improved patient tolerance, quicker procedural time and simpler procedural requirements, meant that OCT could be applied to multi-vessel imaging, thereby allowing a more comprehensive assessment of the coronary tree. Pathological and OCT studies have confirmed the predilection of thin cap fibroatheroma, notoriously associated with the risk of sudden cardiac

death and acute coronary syndromes, in proximal parts of the coronary arteries. (2,11,12) Therefore, the ability to image such segments with OCT, which can quantify cap thickness, is crucial for characterizing plaques in-vivo.
The contrast load required to achieve blood clearance during non-occlusive OCT imaging is an important consideration. Contrast is more viscous that other flush solutions (e.g. saline, ringer's lactate) and it is this property that ensures excellent blood clearance during imaging. An average 30ml additional contrast needs to be balanced against the clinically relevant information provided by OCT compared to traditional imaging techniques such as IVUS. Moreover, we found no rise in post-procedural creatinine levels, despite most patients (57%) undergoing PCI in the same session.

Conclusions

Both modalities of OCT imaging can be safely performed in clinical practice. The non-occlusive technique is simpler and better tolerated by patients and allows for a more comprehensive assessment of the coronary tree. New developments with even faster acquisition speeds and the use of alternative, non-contrast based flushing solutions will mean quicker OCT assessments with even less contrast load.

REFERENCES

1. Prati F, Cera M, Ramazzotti V, Imola F, Giudice R, Albertucci M. Safety and feasibility of a new non-occlusive technique for facilitated intracoronary optical coherence tomography (OCT) acquisition in various clinical and anatomical scenarios. EuroIntervention 2007;3:365-70.
2. Barlis P, Serruys PW, Gonzalo N, van der Giessen WJ, de Jaegere PJ, Regar E. Assessment of culprit and remote coronary narrowings using optical coherence tomography with long-term outcomes. Am J Cardiol 2008;102:391-5.
3. Tanigawa J, Barlis P, Dimopoulos K, Dalby M, Moore P, Di Mario C. The influence of strut thickness and cell design on immediate apposition of drug-eluting stents assessed by optical coherence tomography. Int J Cardiol 2008.
4. Gonzalo N, Serruys PW, Barlis P, Ligthart J, Garcia-Garcia HM, Regar E. Multi-modality intra-coronary plaque characterization: A pilot study. Int J Cardiol 2008.
5. Barlis P, Sianos G, Ferrante G, Del Furia F, D'Souza S, Di Mario C. The use of intra-coronary optical coherence tomography for the assessment of sirolimus-eluting stent fracture. Int J Cardiol 2008.
6. Barlis P, Ferrante G, Del Furia F, Di Mario C. In-vivo characterisation of coronary atherosclerosis with optical coherence tomography. Med J Aust 2008;188:728.
7. Barlis P, Serruys PW, Devries A, Regar E. Optical coherence tomography assessment of vulnerable plaque rupture: predilection for the plaque 'shoulder'. Eur Heart J 2008;29:2023.
8. Tanigawa J, Barlis P, Di Mario C. Heavily calcified coronary lesions preclude strut apposition despite high pressure balloon dilatation and rotational atherectomy: in-vivo demonstration with optical coherence tomography. Circ J 2008;72:157-60.
9. Tanigawa J, Barlis P, Di Mario C. Intravascular Optical Coherence Tomography: Optimisation of image acquisition and quantitative assessment of stent strut apposition. EuroIntervention 2007;3:128-136.
10. Tanigawa J, Barlis P, Dimopoulos K, Di Mario C. Optical coherence tomography to assess malapposition in overlapping drug-eluting stents. EuroIntervention 2008;3:580-83.
11. Kolodgie FD, Burke AP, Farb A, et al. The thin-cap fibroatheroma: a type of vulnerable plaque: the major precursor lesion to acute coronary syndromes. Curr Opin Cardiol 2001;16:285-92.
12. Cheruvu PK, Finn AV, Gardner C, et al. Frequency and distribution of thin-cap fibroatheroma and ruptured plaques in human coronary arteries: a pathologic study. J Am Coll Cardiol 2007;50:940-9.

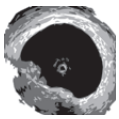

Chapter 9

Reproducibility of quantitative optical coherence tomography for stent analysis

Nieves Gonzalo, Hector M. Garcia-Garcia, Patrick W. Serruys, Koen H. Commissaris, Hiram Bezerra, Peter Barlis, Pierre Gobbens, Marco Costa, Evelyn Regar

Aims: *To assess the inter and intra observer reproducibility for strut count, strut apposition and strut tissue coverage measurements with optical coherence tomography (OCT).*

Methods and results: *Ten drug-eluting stents (244 frames, 1712 struts) imaged with OCT 9 months after implantation were analyzed by 2 independent analysts. One of the analysts repeated the analysis of 5 stents (120 frames, 795 struts) one week later. Offline analysis was performed with the proprietary LightLab Imaging software. The number of struts was counted and lumen and stent area contours were traced. Tissue coverage thickness was measured at 360 degrees of vessel circumference and in front of every individual strut. The number of malapposed struts was determined. There was good agreement for strut number count (Kendall's Tau-b 0.90 for inter and 0.94 for intraobserver variability). The relative difference for lumen area, stent area and tissue coverage measurements were around 1%. There was complete inter and intraobserver agreement for malapposed struts classification (4 out of 1708 struts, Kappa=1).*

Conclusions: *In a corelab setting, the inter and intra observer reproducibility for strut count, strut apposition and strut tissue coverage measurements with OCT is excellent. This emphasizes the value of OCT as a tool for the clinical long-term assessment of stents.*

Optical coherence tomography (OCT) is a light-based imaging modality that can provide in vivo high-resolution images of the coronary artery(1). This technique offers the possibility to identify coronary stents and individual stent struts(2). Further, it is able to provide detailed information about struts apposition and tissue coverage. This is of special interest in drug-eluting stents (DES) in which the neointimal proliferation is inhibited to such extent that might not be visualized with conventional intracoronary IVUS(3). Animal studies demonstrated good correlation between intracoronary OCT and pathology for neointimal thickness measurements (4,5). However, no criteria have been established for the quantitative analysis of stents on a per strut level with OCT. The objective of the present study was to assess the inter and intra observer reproducibility for strut count, strut apposition and strut tissue coverage measurements with OCT.

Methods

Study population

Ten stents (244 frames, 1712 struts) were analyzed in 8 asymptomatic patients undergoing an intracoronary OCT study 9 months after sirolimus (Cypher Select, Cordis, Johnson & Johnson, Miami, FL; 40%) or biolimus-eluting (Biomatrix III, Biosensors, Morges, Switzerland; 60%) stent implantation. The target vessel was the LAD in 50%, the LCX in 20% and the RCA in the 30% of the cases.

OCT acquisition

The OCT acquisition was performed using a commercially available system for intracoronary imaging (LightLab Imaging Inc, Westford, Massachusetts, US). The ImageWire (LightLab Imaging Inc, Westford, Massachusetts, US) consists of an optical fiber core (125 μm) covered by a protective sheath with a maximum outer diameter of 0.019". It was positioned distal to the region of interest using a double lumen catheter (Twin Pass catheter, Vascular Solutions Inc) that had been previously placed in the artery over a conventional guide wire. The automated pullback was performed at 3 mm/s while the blood was removed by the continuous injection of iso-

osmolar contrast (Iodixanol 370, Visipaque™, GE Health Care, Ireland) at 37° Celsius through the guiding catheter. The data was stored on CD for offline analysis.

OCT quantitative analysis

The analysis was performed with the proprietary LightLab software for off-line analysis (LightLab Imaging, Westford, Massachusetts, US). The data was imported in the workstation using the LightLab database format.

Z-Offset correction

The Z-Offset was adjusted in the catheterization laboratory before image acquisition while holding the ImageWire between two fingers. The Z-Offset is set properly when the ImageWire sheath is aligned with the yellow fiducials in the OCT image. During image acquisition, the optical fibres can stretch, especially at the beginning of the pullback. This may produce changes in the size of the Z-Offset along the pullback that can affect the accuracy of the measurements. Therefore, the Z-Offset was checked and modified if necessary in all the pullbacks before performing any measurement. To correct the Z-offset in saved pullbacks a frame in which the ImageWire sheath was in direct contact with the vessel wall was selected. In this frame the Z-Offset was corrected aligning the ImageWire sheath and the vessel wall with the yellow fiducials. This value of the Z-Offset was applied at the beginning of the pullback. If needed, the Z-Offset was recalibrated again along the pullback. The corrected Z-Offset was the same for both analysists.

Definition of the region of interest and frame selection

The region of interest (ROI) comprised the stented region and the reference segments. The ROI was systematically analysed in longitudinal intervals throughout the pullback. The stented region was defined as the region comprised between the first and the last frame with circumferentially visible struts. The reference segments were defined as the 5 mm proximal and distal to the stent. Frames were excluded when they presented severe artefacts such as incomplete blood clearance or non-uniform rotation distortion. When a frame was not analyzable an alternative frame located within the 2 proximal or distal frames was selected for analysis. No overlapping stent segments were included in the analysis.

Lumen analysis

The lumen contour was obtained with an automated detection algorithm available in the LightLab proprietary software and additional manual corrections were performed if necessary.

Stent analysis

Strut definitions: stent struts can show different appearances in OCT. In the present study structures were considered struts according to the following definitions.

a) Highly reflective surfaces (metal) with cast dorsal, radial shadows.
b) Highly reflective surfaces without dorsal shadowing.
c) Sector shaped shadows with sharp defined borders radial to the lumen.

Stent area

The stent contour was traced using a multiple point detection function. A support point for the contour was set in the middle of the endoluminal border of each stent strut. A semi-automated contour was then applied linking the points.

Struts coverage definitions and measurements

The tissue coverage area was calculated as stent area minus lumen area. Assessment of tissue coverage thickness was performed using a new function of the software which provides 360 degrees measurements, at 1 degree incremental, around the circumference of a given cross sectional image, developed in collaboration by Cardialysis-Cleveland, Cardialysis-Rotterdam and Lightlab (Figure 1). This also permits the measurement of the tissue located in front of every strut that was defined as strut coverage. The mean, maximum and minimum tissue coverage per strut were calculated.

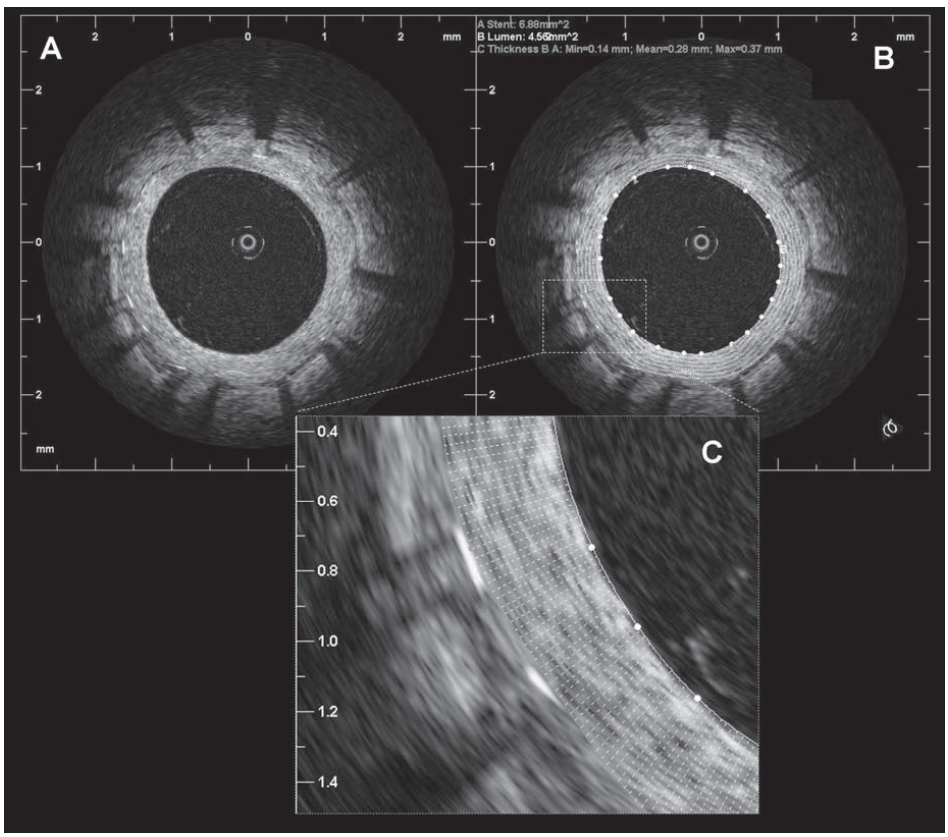

Figure 1: Tissue coverage measurement. A. Sirolimus eluting stent 9 months after stent implantation. B. The figure shows the lumen contour (white) and the stent contour (green). The tissue coverage area was calculated as stent area minus lumen area. The tissue coverage thickness was measured in 360 points (represented by the white chords). C. Magnification of 2 struts showing all the measurements (white chords) of the tissue coverage in front of every strut. For every strut the minimum, maximum and mean strut coverage was calculated.

see colour section

Malapposition definitions and measurements

Malapposition was defined as separation of at least one stent strut from the vessel wall. To evaluate apposition by OCT, especially with DES, some considerations must be taken into account. Most DES are constituted by a metal body covered by a polymer. Since OCT can show only the endoluminal surface of the strut due to limited penetration through the metal, strut and polymer thickness must be considered in assessing apposition for each type of stent design. For the present study a strut was considered malapposed if the distance from its endo-luminal surface to the vessel wall was higher than the sum of the metal and polymer thickness (Figure 2).

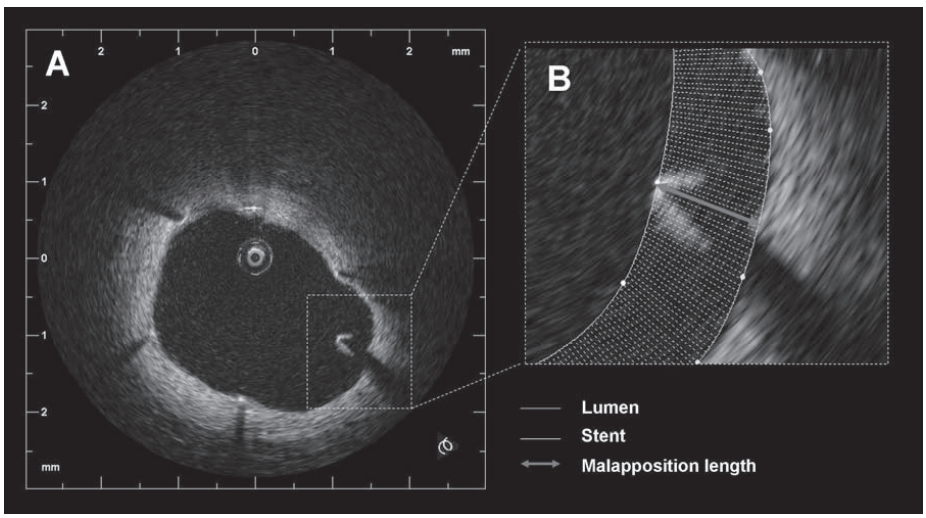

Figure 2: Malapposition. A. Example of a malapposed strut in a sirolimus eluting stent at 9 months follow up. **B**. Magnification of the malapposed strut. The yellow line represents the lumen contour and the white line corresponds to the stent contour. The distance from the endoluminal surface of the strut to the vessel wall (red arrow) was 440 μm (higher than the sum of the metal and polymer thickness for this type of stent).

see colour section

Reproducibility design

The reproducibility for the struts count and the malapposition and tissue coverage thickness measurements were tested independently.

Strut count reproducibility

In order to assess the interobserver variability for the struts count, two experienced observers analyzed independently 100 cross sections and counted the number of struts in each one. To test the intraobserver variability one of the two observers repeated the analysis of 50 randomly selected cross sections one week later.

Strut apposition and tissue coverage reproducibility

Two experienced observers analyzed independently 10 stents in order assess the interobserver variability for the struts apposition and tissue coverage measurements. One of the observers repeated the analysis in 5 of the cases one week later to evaluate the intraobserver variability.

Statistical analysis

The agreement of the number of struts counted in the same frame was estimated by calculating the Kendall's Tau-b rank correlation coefficient with its 95% confidence interval.
The inter and intraobserver reproducibility for lumen, stent and tissue coverage measurements were tested at 3 levels: per stent, per frame and per strut.
On a per stent level the mean and minimum lumen and stent area and the mean lumen and stent diameters were compared. The mean tissue coverage area and the mean, minimum and maximum tissue coverage thickness and strut coverage were also compared. The lumen, stent and tissue coverage volume were calculated by Trapezoidal rule. In the proximal and distal reference, the mean luminal area, diameter and volume were compared.
On a per frame level the luminal and stent areas and diameters were compared as well as the tissue coverage area and the mean, minimum and maximum tissue coverage thickness and strut coverage. In the frames corresponding to the proximal and distal edge, the mean luminal area and diameter were compared.
On a per strut level the mean, minimum and maximum tissue coverage in front of every strut were compared.
The reproducibility was calculated by estimating the residual standard deviation in an ANOVA model. The true value is expected to be within 1.96 times the calculated reproducibility of the single measurement for 95% of the observations. In addition the agreement between both observations has been expressed in Bland-Altman plots. The Bland-Altman plot depicts the differences of each pair of observations versus their mean values with reference lines for the mean difference of all paired observations and its 95% confidence limits, the so-called limits of agreement.
The Kappa coefficient for the agreement between observers for struts classification as incompletely apposed was tested for being not equal to zero.

Results

A total of 244 frames and 1712 struts were evaluated for the interobserver reproducibility and 120 frames, 795 struts were evaluated for the intraobserver variability.

Strut count reproducibility

Interobserver variability

There was complete agreement in the number of struts between the two observers in 55% of the cross sections, difference of 1 strut in 31%, difference of 2 struts in 9% and difference of more than 2 struts in only 5% of the cross sections. The correlation between both observers was high, i.e. Kendall's Tau-b was 0.90 (95% confidence interval 0.85 – 0.94).

Intraobserver variability

There was complete agreement in the number of struts in 72% of the cross sections, difference of one strut in 24% and difference of 2 struts in 4% of the cross sections. The correlation between both observations was very high, i.e. Kendall's Tau-b was 0.94 (95% confidence interval 0.91 – 0.97).

Lumen, stent and tissue coverage measurements reproducibility

Stent level

The results for the inter and intraobserver reproducibility at the stent level are summarized in Tables 1 and 2 respectively.

Table 1				Difference			Limits of Agreement[aaa]	
		Observation 1	Observation 2	Absolute	Relative (Obs1/Obs2)	Reproducibility[aa]	Lower	Upper
Stent	**Mean Stent Area (mm^2)**	5.44 ± 1.6	5.47 ± 1.5	-0.02 ± 0.2	1.0	0.1043	-0.32	0.28
	Mean Luminal Area (mm^2)	4.71 ± 1.5	4.70 ± 1.5	0.00 ± 0.0	1.0	0.0173	-0.05	0.05
	Mean Tissue Coverage Area (mm^2)	0.60 ± 0.5	0.63 ± 0.5	-0.03 ± 0.1	0.9	0.0780	-0.25	0.20
	Min Stent Area (mm^2)	3.89 ± 1.2	3.84 ± 1.1	0.05 ± 0.2	1.0	0.1549	-0.39	0.49
	Min Luminal Area (mm^2)	3.24 ± 1.1	3.26 ± 1.1	-0.01 ± 0.0	1.0	0.0158	-0.05	0.02
	Mean Tissue Coverage Thickness (mm)	0.08 ± 0.1	0.08 ± 0.1	0.00 ± 0.0	0.9	0.0100	-0.03	0.02
	Min Tissue Coverage Thickness (mm)	0.00 ± 0.0	0.00 ± 0.0	0.00 ± 0.0		0.0000	0.00	0.00
	Max Tissue Coverage Thickness (mm)	0.33 ± 0.1	0.33 ± 0.1	0.01 ± 0.0	1.1	0.0179	-0.04	0.06
	Mean Strut Coverage (mm)	0.08 ± 0.1	0.09 ± 0.1	-0.01 ± 0.0	0.9	0.0066	-0.02	0.01
	Min Strut Coverage (mm)	0.00 ± 0.0	0.00 ± 0.0	0.00 ± 0.0	0.0	0.0067	-0.02	0.02
	Max Strut Coverage (mm)	0.31 ± 0.1	0.32 ± 0.1	0.00 ± 0.0	1.0	0.0158	-0.05	0.04
	Mean Stent Diameter (mm)	2.60 ± 0.4	2.61 ± 0.4	-0.01 ± 0.0	1.0	0.0253	-0.08	0.07
	Mean Luminal Diameter (mm)	2.41 ± 0.4	2.41 ± 0.4	0.00 ± 0.0	1.0	0.0038	-0.01	0.01
	Stent Volume (mm^3)	101.58 ± 48.2	102.15 ± 48.3	-0.58 ± 2.7	1.0	1.8894	-5.97	4.81
	Luminal Volume (mm^3)	91.76 ± 48.0	91.67 ± 47.9	0.09 ± 0.5	1.0	0.3347	-0.87	1.05
	Tissue Coverage Volume (mm^3)	13.49 ± 11.6	14.13 ± 10.3	-0.65 ± 2.5	0.9	1.7454	-5.57	4.27

Table 1				Difference			Limits of Agreement[aaa]	
		Observation 1	Observation 2	Absolute	Relative (Obs1/Obs2)	Reproducibility[aa]	Lower	Upper
	In-stent Obstruction Volume (%)	13.73 ± 10.3	14.46 ± 9.0	-0.73 ± 2.2	0.9	1.5341	-4.95	3.49
Distal reference	**Mean Luminal Area (mm²)**	4.13 ± 1.5	4.14 ± 1.4	0.00 ± 0.0	1.0	0.0085	-0.03	0.02
	Mean Luminal Diameter (mm)	2.20 ± 0.3	2.20 ± 0.3	0.00 ± 0.0	1.0	0.0067	-0.02	0.02
	Luminal Volume (mm³)	18.39 ± 11.1	18.40 ± 11.1	-0.02 ± 0.1	1.0	0.0492	-0.16	0.12
Proximal reference	**Mean Luminal Area (mm²)**	5.33 ± 2.4	5.27 ± 2.3	0.06 ± 0.1	1.0	0.1051	-0.23	0.35
	Mean Luminal Diameter (mm)	2.55 ± 0.6	2.54 ± 0.6	0.01 ± 0.0	1.0	0.0198	-0.04	0.07
	Luminal Volume (mm³)	23.05 ± 8.6	22.87 ± 8.5	0.17 ± 0.4	1.0	0.3030	-0.67	1.01

Table 1. Interobserver reproducibility at stent level. N=10 stents. Min: minimum. Max: maximum. Obs1: observer 1 Obs2: observer 2. [aa] Reproducibility defined as residual standard deviation. [aaa] Bland-Altman limits of agreement defined as mean ± 1.96 SD of absolute difference.

Frame level

The results for the inter and intraobserver reproducibility at the frame level are summarized in Tables 3 and 4 respectively. Figures 3 and 4 show the results for the lumen, stent and tissue coverage area and mean neointimal thickness for inter and intraobserver reproducibility respectively.

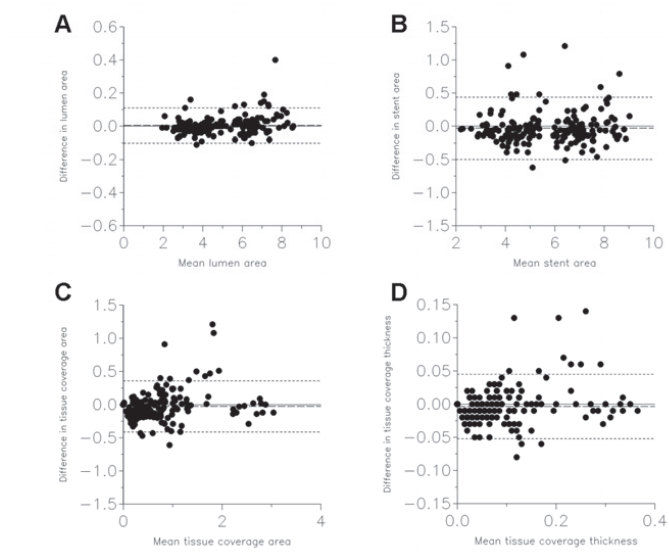

Figure 3: Interobserver reproducibility. Bland-Altman plots for the interobserver variability for mean lumen (A), stent (B) and tissue coverage area (C) and mean tissue coverage thickness (D).

	Table 2			Difference			Limits of Agreement[aaa]	
		Observation 1	Observation 2	Absolute	Relative (Obs1/Obs2)	Reproducibility[aa]	Lower	Upper
Stent	**Mean Stent Area (mm²)**	5.95 ± 1.7	5.90 ± 1.6	0.05 ± 0.1	1.0	0.0621	-0.11	0.21
	Mean Luminal Area (mm²)	4.97 ± 1.6	4.98 ± 1.6	-0.01 ± 0.0	1.0	0.0186	-0.06	0.05
	Mean Tissue Coverage Area (mm²)	0.80 ± 0.7	0.76 ± 0.8	0.04 ± 0.1	1.1	0.0518	-0.09	0.17
	Min Stent Area (mm²)	4.01 ± 1.0	3.88 ± 0.9	0.13 ± 0.2	1.0	0.1487	-0.24	0.49
	Min Luminal Area (mm²)	3.14 ± 0.6	3.14 ± 0.6	0.00 ± 0.0	1.0	0.0077	-0.02	0.02
	Mean Tissue Coverage Thickness (mm)	0.10 ± 0.1	0.09 ± 0.1	0.00 ± 0.0	1.1	0.0060	-0.01	0.02
	Min Tissue Coverage Thickness (mm)	0.00 ± 0.0	0.00 ± 0.0	0.00 ± 0.0		0.0000	0.00	0.00
	Max Tissue Coverage Thickness (mm)	0.37 ± 0.1	0.35 ± 0.2	0.02 ± 0.0	1.1	0.0161	-0.02	0.05
	Mean Strut Coverage (mm)	0.11 ± 0.1	0.11 ± 0.1	0.00 ± 0.0	1.1	0.0029	-0.01	0.01
	Min Strut Coverage (mm)	0.00 ± 0.0	0.00 ± 0.0	0.00 ± 0.0		0.0000	0.00	0.00
	Max Strut Coverage (mm)	0.35 ± 0.2	0.34 ± 0.2	0.01 ± 0.0	1.1	0.0122	-0.01	0.04
	Mean Stent Diameter (mm)	2.72 ± 0.4	2.71 ± 0.4	0.01 ± 0.0	1.0	0.0138	-0.02	0.05
	Mean Luminal Diameter (mm)	2.48 ± 0.4	2.48 ± 0.4	0.00 ± 0.0	1.0	0.0043	-0.01	0.01
	Stent Volume (mm³)	112.26 ± 58.0	111.37 ± 57.3	0.89 ± 1.5	1.0	1.1265	-2.00	3.78
	Luminal Volume (mm³)	98.63 ± 58.2	98.74 ± 58.3	-0.11 ± 0.5	1.0	0.3502	-1.17	0.94
	Tissue Coverage Volume (mm³)	18.05 ± 15.2	17.03 ± 16.0	1.02 ± 1.6	1.1	1.2617	-2.18	4.23
	In-stent Obstruction Volume (%)	16.81 ± 13.8	16.07 ± 13.9	0.74 ± 1.1	1.1	0.8790	-1.44	2.93

	Table 2			Difference			Limits of Agreement[aaa]	
		Observation 1	Observation 2	Absolute	Relative (Obs1/Obs2)	Reproducibility[aa]	Lower	Upper
Distal reference	**Mean Luminal Area (mm²)**	3.93 ± 1.4	3.93 ± 1.4	0.00 ± 0.0	1.0	0.0039	-0.01	0.01
	Mean Luminal Diameter (mm)	2.19 ± 0.3	2.19 ± 0.3	0.00 ± 0.0	1.0	0.0023	-0.01	0.01
	Luminal Volume (mm³)	17.14 ± 8.6	17.14 ± 8.6	-0.01 ± 0.0	1.0	0.0239	-0.08	0.07
	Luminal Volume[a] (mm³)	17.68 ± 9.2	17.69 ± 9.2	-0.01 ± 0.0	1.0	0.0196	-0.07	0.04
Proximal reference	**Mean Luminal Area (mm²)**	5.86 ± 4.9	5.79 ± 4.8	0.07 ± 0.1	1.0	0.0628	-0.07	0.21
	Mean Luminal Diameter (mm)	2.60 ± 1.2	2.58 ± 1.2	0.02 ± 0.0	1.0	0.0121	-0.01	0.04
	Luminal Volume (mm³)	18.61 ± 14.4	18.38 ± 14.2	0.23 ± 0.3	1.0	0.2035	-0.27	0.72
	Luminal Volume[a] (mm³)	18.46 ± 15.3	18.23 ± 15.1	0.23 ± 0.2	1.0	0.1977	-0.21	0.67

Table 2. Intraobserver reproducibility at stent level. N=5 stents. Min: minimum. Max: maximum. Obs1: observation 1. Obs2: observation 2. [aa] Reproducibility defined as residual standard deviation. [aaa] Bland-Altman limits of agreement defined as mean ± 1.96 SD of absolute difference.

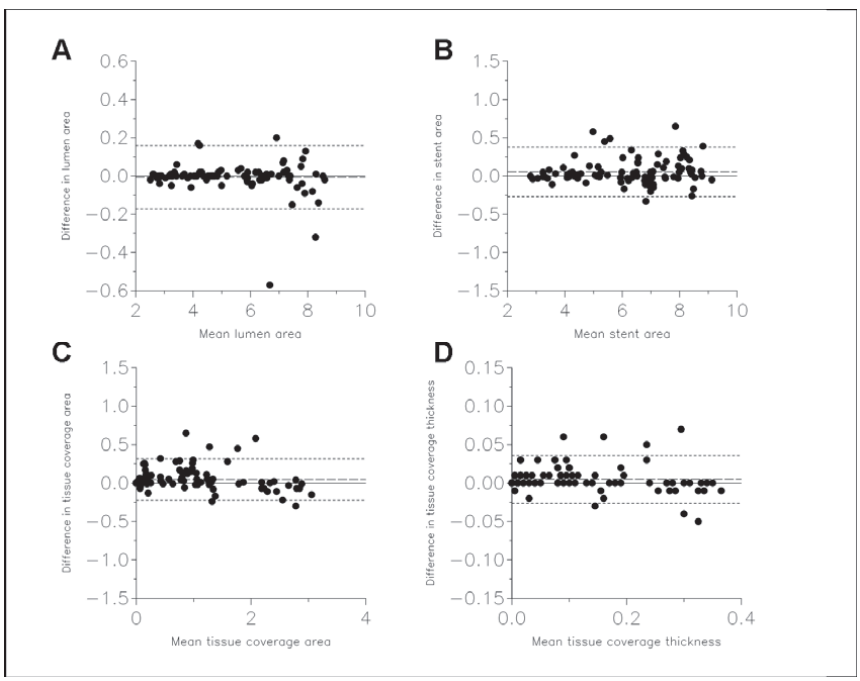

Figure 4: Intraobserver reproducibility. Bland-Altman plots for intraobserver variability for mean lumen (A), stent (B) and tissue coverage area (C) and mean tissue coverage thickness (D).

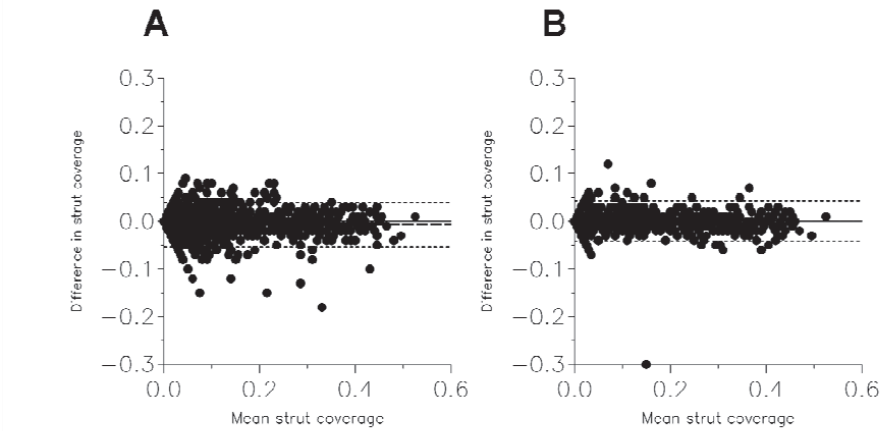

Figure 5: Strut coverage measurement reproducibility. Bland-Altman plots for the inter (A) and intraobserver (B) reproducibility for mean strut coverage measurements.

Strut level

Tables 5 and 6 show the inter (A) and intraobserver (B) reproducibility for the measurements at the strut level. Figure 5 shows the variability for the mean strut coverage.

Malapposition classification reproducibility

The observers had complete agreement for the classification of malapposed struts (4 out of 1712 struts malapposed, Kappa coefficient 1). The intraobserver analysis show the same result (4 out of 795 struts malapposed, Kappa coefficient 1)

Discussion

Due to its high resolution OCT can be a very valuable tool for the evaluation of the acute and long-term impact of stent implantation. OCT offers the possibility to assess stent apposition in great detail and allows the visualization and measurement of the tissue covering the struts even if this consists on tiny layers as it is frequently observed in DES(3). As the use of OCT is increasing rapidly, standardization of the methodology to measure and report stent apposition and tissue coverage is needed as well as data about the reproducibility of these measurements. Our results show that the methodology described in the present study allows analysis of stents by experienced analysts in a highly reproducible way.

Stent struts can have different appearances by OCT. The reproducibility of struts count has not been previously reported. Our data suggests that the inter and intraobserver variability for strut count is low when applying strict strut definitions. For the intraobserver variability, only in 4% of the cases the difference between the 2 observations was more than one single strut while for the interobserver in only 5% of the cases the difference was higher than 2 struts.

High accuracy and precision for diameters measurement in vitro using proprietary software from LightLab has been reported(6) . Tanimoto et al reported a low interobserver variability for lumen and stent area measurements with OCT using dedicated computer-assisted contour analysis(7).

Table 3				Difference			Limits of Agreement[aa]	
		Observer 1	Observer 2	Absolute	Relative (Obs1/Obs2)	Reproducibility[a]	Lower	Upper
Stent	**Stent Area (mm²)**	5.67 ± 1.7	5.71 ± 1.7	-0.03 ± 0.2	1.0	0.1694	-0.50	0.44
	Luminal Area (mm²)	4.95 ± 1.7	4.95 ± 1.7	0.00 ± 0.1	1.0	0.0380	-0.10	0.11
	Tissue Coverage Area (mm²)	0.56 ± 0.7	0.59 ± 0.6	-0.03 ± 0.2	0.9	0.1400	-0.41	0.36
	Mean Tissue Coverage Thickness (mm)	0.07 ± 0.1	0.07 ± 0.1	0.00 ± 0.0	0.9	0.0177	-0.05	0.05
	Min Tissue Coverage Thickness (mm)	0.02 ± 0.0	0.02 ± 0.0	0.00 ± 0.0	0.4	0.0132	-0.04	0.03
	Max Tissue Coverage Thickness (mm)	0.15 ± 0.1	0.15 ± 0.1	0.00 ± 0.0	1.0	0.0207	-0.06	0.06
	Mean Strut Coverage (mm)	0.08 ± 0.1	0.08 ± 0.1	-0.01 ± 0.0	0.9	0.0099	-0.03	0.02
	Min Strut Coverage (mm)	0.03 ± 0.1	0.04 ± 0.1	-0.01 ± 0.0	0.6	0.0125	-0.04	0.03
	Max Strut Coverage (mm)	0.14 ± 0.1	0.14 ± 0.1	0.00 ± 0.0	1.0	0.0141	-0.04	0.04
	Stent Diameter (mm)	2.66 ± 0.4	2.66 ± 0.4	-0.01 ± 0.1	1.0	0.0409	-0.12	0.10
	Luminal Diameter (mm)	2.47 ± 0.4	2.47 ± 0.4	0.00 ± 0.0	1.0	0.0090	-0.02	0.03
Distal reference	**Luminal Area (mm²)**	4.34 ± 1.6	4.35 ± 1.6	-0.01 ± 0.0	1.0	0.0148	-0.05	0.03
	Luminal Diameter (mm)	2.28 ± 0.4	2.28 ± 0.4	0.00 ± 0.0	1.0	0.0077	-0.02	0.02
Proximal reference	**Luminal Area (mm²)**	5.25 ± 2.1	5.20 ± 2.0	0.05 ± 0.1	1.0	0.0944	-0.21	0.30
	Luminal Diameter (mm)	2.54 ± 0.5	2.53 ± 0.5	0.01 ± 0.0	1.0	0.0180	-0.04	0.06

Table 3. Interobserver reproducibility at frame level. N=244 frames. Min: minimum. Max: maximum. Obs1: observer 1 Obs2: observer 2. [a] Reproducibility defined as residual standard deviation. [aa] Bland-Altman limits of agreement defined as mean ± 1.96 SD of absolute difference.

Table 4				Difference			Limits of Agreement[aa]	
		Observer 1	Observer 2	Absolute	Relative (Obs1/Obs2)	Reproducibility[a]	Lower	Upper
Stent	**Stent Area (mm²)**	6.28 ± 1.7	6.23 ± 1.7	0.05 ± 0.2	1.0	0.1224	-0.27	0.38
	Luminal Area (mm²)	5.33 ± 1.8	5.34 ± 1.8	-0.01 ± 0.1	1.0	0.0596	-0.17	0.16
	Tissue Coverage Area (mm²)	0.75 ± 0.9	0.70 ± 0.9	0.05 ± 0.1	1.6	0.1021	-0.22	0.32
	Mean Tissue Coverage Thickness (mm)	0.09 ± 0.1	0.08 ± 0.1	0.00 ± 0.0	1.2	0.0117	-0.03	0.04
	Min Tissue Coverage Thickness (mm)	0.03 ± 0.1	0.03 ± 0.1	0.00 ± 0.0	1.1	0.0197	-0.06	0.05
	Max Tissue Coverage Thickness (mm)	0.17 ± 0.2	0.17 ± 0.2	0.00 ± 0.0	1.1	0.0168	-0.04	0.05
	Mean Strut Coverage (mm)	0.10 ± 0.1	0.10 ± 0.1	0.00 ± 0.0	1.1	0.0083	-0.02	0.02
	Min Strut Coverage (mm)	0.05 ± 0.1	0.05 ± 0.1	0.00 ± 0.0	1.1	0.0181	-0.05	0.05
	Max Strut Coverage (mm)	0.17 ± 0.2	0.16 ± 0.2	0.00 ± 0.0	1.1	0.0125	-0.03	0.04
	Stent Diameter (mm)	2.80 ± 0.4	2.79 ± 0.4	0.01 ± 0.0	1.0	0.0272	-0.06	0.08
	Luminal Diameter (mm)	2.57 ± 0.4	2.57 ± 0.4	0.00 ± 0.0	1.0	0.0131	-0.04	0.04
Distal reference	**Luminal Area (mm²)**	3.98 ± 1.6	3.98 ± 1.6	0.00 ± 0.0	1.0	0.0109	-0.03	0.03
	Luminal Diameter (mm)	2.20 ± 0.4	2.20 ± 0.4	0.00 ± 0.0	1.0	0.0041	-0.01	0.01
Proximal reference	**Luminal Area (mm²)**	5.86 ± 3.8	5.79 ± 3.7	0.07 ± 0.1	1.0	0.0826	-0.12	0.27
	Luminal Diameter (mm)	2.60 ± 0.9	2.58 ± 0.9	0.02 ± 0.0	1.0	0.0164	-0.02	0.05

Table 4. Intraobserver reproducibility at frame level. N=120 frames. Min: minimum. Max: maximum. Obs1: observation 1. Obs2: observation 2. [a] Reproducibility defined as residual standard deviation. [aa] Bland-Altman limits of agreement defined as mean ± 1.96 SD of absolute difference.

Table 5			Difference			Limits of Agreement[aa]	
	Observer 1	Observer 2	Absolute	Relative (Obs1/Obs 2)	Reproducibility[a]	Lower	Upper
Min Coverage Strut (mm)	0.09 ± 0.1	0.10 ± 0.1	-0.01 ± 0.0	0.9	0.0179	-0.05	0.04
Mean Coverage Strut (mm)	0.10 ± 0.1	0.11 ± 0.1	-0.01 ± 0.0	0.9	0.0174	-0.05	0.04
Max Coverage Strut (mm)	0.11 ± 0.1	0.11 ± 0.1	-0.01 ± 0.0	0.9	0.0175	-0.05	0.04

Table 5. Interobserver reproducibility at strut level. N=1712 struts. Min: minimum. Max: maximum. [a] Reproducibility defined as residual standard deviation.
[aa] Bland-Altman limits of agreement defined as mean ± 1.96 SD of absolute difference.

Table 6			Difference			Limits of Agreement[aa]	
	Observer 1	Observer 2	Absolute	Relative (Obs1/Obs2)	Reproducibility[a]	Lower	Upper
Min Coverage Strut (mm)	0.13 ± 0.1	0.13 ± 0.1	0.00 ± 0.0	1.1	0.0161	-0.04	0.05
Mean Coverage Strut (mm)	0.14 ± 0.1	0.13 ± 0.1	0.00 ± 0.0	1.1	0.0153	-0.04	0.04
Max Coverage Strut (mm)	0.14 ± 0.1	0.14 ± 0.1	0.00 ± 0.0	1.0	0.0154	-0.04	0.04

Table 6. Intraobserver reproducibility at strut level. N=795 struts. Min: minimum. Max: maximum. [a] Reproducibility defined as residual standard deviation.
[aa] Bland-Altman limits of agreement defined as mean ± 1.96 SD of absolute difference.

However, no specific study to assess the reproducibility of strut apposition and strut tissue coverage measurements by OCT has been reported.
Recently several OCT studies evaluating the struts apposition and tissue coverage in DES in humans at different time intervals using proprietary off-line software provided by LightLab Imaging have been published (8-11).
In most of these studies, the operator manually traced the stent and lumen area, to derive the tissue coverage area. Stent struts apposition and tissue coverage are usually individually measured at 1-mm intervals. However the way of reporting the tissue coverage varies between studies.

Some authors report just tissue coverage thickness without detailed methodology (8,12). Other studies report the minimum, maximum or average tissue coverage but the selection method, the number of measurements and calculations method was not specified (9,10). The methodology used in the present study provides 360 data points for tissue coverage thickness for each cross section. Further the mean, the minimum and the maximum tissue coverage is reported for each individual strut. The mean tissue coverage per strut is derived from all the measurements at equidistant intervals along the strut.

Prati et al reported high inter and intraobserver reproducibility for neointima thickness measurements with OCT in carotid rabbit model (r^2 0.88 and 0.90 respectively)(4). Another study in humans comparing tissue coverage between SES and BMS reported 6 ± 8 μm and 8±8 μm intra and interobserver variability for the measurement of tissue coverage(8). However the authors did not specify if the measurements correspond to mean, minimum or maximum tissue coverage, how many measurements were performed per strut or in which part of the strut measurements were taken.

In the present study we observed absolute differences around 10 μm for the maximum and minimum strut coverage in repeated measurements. Those differences are in the limit of resolution of the technique. The absolute differences for tissue coverage area were 0.06±0.02 mm^2 and 0.04±0.02 mm^2 for the intra and interobserver variability respectively. Similar results were found when comparing stent and lumen area. A very good reproducibility for lumen measurement was expected as the automatic contour detection was used and not modified by the analyst in the majority of cases. The differences found in the present study are smaller than the ones reported previously by Xie et al for area measurements with OCT (0.3 ±0.5 mm^2 and 0.2±0.4 mm^2 for the intra and interobserver variability respectively). There are no reports on the reproducibility of lumen, stent and tissue coverage volumes derived from OCT. We found absolute differences around 1 mm^3 for the intra and 0.65 mm^3 for the interobserver variability for tissue coverage volume. Similar values (0.99 and 0.55 mm^3 for the intra and interobserver respectively) were obtained for the stent volume. As expected, the lumen volume variability was even lower (around 0.10 mm^3) as it was derived from automatic contour detection.

The higher resolution of OCT makes this technique superior to IVUS for the detection and measurement of tissue covering the stent struts. An IVUS study reported 62% of inter-observer agreement for the presence of neointimal tissue with discrepancy between observers in very thin neointimal layers and when the neointimal area was <2 mm^2(13). In the present study evaluating DES, a very good agreement was found between observers for the measurement of tissue coverage even when the mean tissue coverage area was less than 1 mm^2. An increased variability in the classification of individual struts was observed when the tissue coverage was below 50 μm. This may be related to the image resolution but also to software limitations. Automatic algorithms for detecting stent coverage from OCT datasets are under development(14). This could help eliminating the remaining small observer-related variability found in our study.

Kubo et al reported a good intra and interobserver agreement (Kappa=0.90 and 0.75 respectively) for malapposed struts classification in sirolimus eluting stents(15). Those results are in line with our study in which the agreement between observers for malapposed struts was excellent (kappa=1) even when applying customized cut-off points for each stent. However our results are limited by the small number of malapposed struts found in our population.

Clinical implications

The evaluation of strut apposition is essential in the evaluation of new stents designs as IVUS data have suggested a possible relation between apposition and the risk of stent thrombosis in DES(16,17). However interpretation of malapposition as assessed by OCT requires caution. Due to the high image resolution, malapposition of stent struts is a relatively common finding by OCT(8) but its clinical implications remain poorly understood. Incomplete endothelial struts coverage has been identified in pathology as the most powerful histological predictor of stent thrombosis(18,19). Pathological data in human suggests that neointimal coverage of stent struts could be used as a surrogate marker of endothelialization due to the good correlation between strut coverage and endothelialization. Animal data suggest good correlation between mean neointimal thickness measured by histology and OCT (4). The present study confirms that the tissue covering the strut can be measured with high reproducibility. However, the clinical relevance of uncovered struts as detected by OCT is not clear as some studies have reported presence of uncovered struts at follow-up not associated to clinical events(15). Further investigation and studies with longer follow up are needed in this field.

Although OCT has proved to be a highly informative imaging technique in assessing stents, standardization of the analysis of such images is not yet in place. In addition, OCT is a rapidly evolving imaging technology, and there is lack of large stent trials with long-term clinical follow-up linking OCT findings and clinical events. Thereby this methodology of analysis is prone to changes in the future in order to adjust to the new clinical needs.

Conclusions

In a corelab setting, the inter and intra observer reproducibility for strut count, strut apposition and strut tissue coverage measurements with OCT is excellent. This finding emphasizes the value of OCT as a tool for the clinical long-term assessment of stents.

References

1. Regar E, van Leeuwen A, Serruys PW. 2007. Optical coherence tomography in cardiovascular research.London: Informa Healthcare. 338 p.
2. Gonzalo N, Serruys PW, Regar E. Optical coherence tomography: clinical applications and the evaluation of DES. Minerva Cardioangiol 2008;56(5):511-25.
3. Aoki J, Colombo A, Dudek D, Banning AP, Drzewiecki J, Zmudka K, Schiele F, Russell ME, Koglin J, Serruys PW. Peristent remodeling and neointimal suppression 2 years after polymer-based, paclitaxel-eluting stent implantation: insights from serial intravascular ultrasound analysis in the TAXUS II study. Circulation 2005;112(25):3876-83.
4. Prati F, Zimarino M, Stabile E, Pizzicannella G, Fouad T, Rabozzi R, Filippini A, Pizzicannella J, Cera M, De Caterina R. Does optical coherence tomography identify arterial healing after stenting? An in vivo comparison with histology, in a rabbit carotid model. Heart 2008;94(2):217-21.
5. Suzuki Y, Ikeno F, Koizumi T, Tio F, Yeung AC, Yock PG, Fitzgerald PJ, Fearon WF. In Vivo Comparison Between Optical Coherence Tomography and Intravascular Ultrasound for Detecting Small Degrees of In-Stent Neointima after Stent Implantation. J Am Coll Cardiol Intv 2008;1:168-73.

6. Tsuchida K, vd Giessen W, Patterson M,Tanimoto S,Garcia-Garcia H,Regar E,Ligthart J,Maugenest AM,Maatrijk G,Wentzel JJ, Serruys P.W. In-vivo validation of a novel three-dimensional quantitative coronary angiography system (CardioOp-B TM): Comparison with a conventional two-dimensional system (CASS II TM) and with special reference to optical cohence tomography. Eurointervention 2007;3:100-108.
7. Tanimoto S, Rodriguez-Granillo G, Barlis P, de Winter S, Bruining N, Hamers R, Knappen M, Verheye S, Serruys PW, Regar E. A novel approach for quantitative analysis of intracoronary optical coherence tomography: high inter-observer agreement with computer-assisted contour detection. Catheter Cardiovasc Interv 2008;72(2):228-35.
8. Xie Y, Takano M, Murakami D, Yamamoto M, Okamatsu K, Inami S, Seimiya K, Ohba T, Seino Y, Mizuno K. Comparison of neointimal coverage by optical coherence tomography of a sirolimus-eluting stent versus a bare-metal stent three months after implantation. Am J Cardiol 2008;102(1):27-31.
9. Chen BX, Ma FY, Luo W, Ruan JH, Xie WL, Zhao XZ, Sun SH, Guo XM, Wang F, Tian T and others. Neointimal coverage of bare-metal and sirolimus-eluting stents evaluated with optical coherence tomography. Heart 2008;94(5):566-70.
10. Matsumoto D, Shite J, Shinke T, Otake H, Tanino Y, Ogasawara D, Sawada T, Paredes OL, Hirata K, Yokoyama M. Neointimal coverage of sirolimus-eluting stents at 6-month follow-up: evaluated by optical coherence tomography. Eur Heart J 2007;28(8):961-7.
11. Takano M, Yamamoto M, Inami S, Murakami D, Seimiya K, Ohba T, Seino Y, Mizuno K. Long-term follow-up evaluation after sirolimus-eluting stent implantation by optical coherence tomography: do uncovered struts persist? J Am Coll Cardiol 2008;51(9):968-9.
12. Yao ZH, Matsubara T, Inada T, Suzuki Y, Suzuki T. Neointimal coverage of sirolimus-eluting stents 6 months and 12 months after implantation: evaluation by optical coherence tomography. Chin Med J (Engl) 2008;121(6):503-7.
13. Regar E, Werner F, Siebert U, Rieber J, Theisen K, Mudra H, Klauss V. Reproducibility of neointima quantification with motorized intravascular ultrasound pullback in stented coronary arteries. Am Heart J 2000;139(4):632-7.
14. Bonnema GT, Cardinal KO, Williams SK, Barton JK. An automatic algorithm for detecting stent endothelialization from volumetric optical coherence tomography datasets. Phys Med Biol 2008;53(12):3083-98.
15. Kubo T IT, Kitabata H, Kuroi A, Ueno S, Yamano T, Tanimoto T, Matsuo Y, Masho T, Takarada S, Tanaka A, Nakamura N, Mizukoshi M, Tomobuchi Y, Akasaka T. Comparison of vascular response after sirolimus eluting stent implantation between patients with unstable and stable angina pectoris. . J Am Coll Cardiol Img 2008;1:475-84.
16. Alfonso F, Suarez A, Perez-Vizcayno MJ, Moreno R, Escaned J, Banuelos C, Jimenez P, Bernardo E, Angiolillo DJ, Hernandez R, Macaya C. Intravascular ultrasound findings during episodes of drug-eluting stent thrombosis. J Am Coll Cardiol 2007;50:2095-2097.
17. Cook S, Wenaweser P, Togni M, Billinger M, Morger C, Seiler C, Vogel R, Hess O, Meier B, Windecker S. Incomplete stent apposition and very late stent thrombosis after drug-eluting stent implantation. Circulation 2007;115(18):2426-34.
18. Finn AV, Joner M, Nakazawa G, Kolodgie F, Newell J, John MC, Gold HK, Virmani R. Pathological correlates of late drug-eluting stent thrombosis: strut coverage as a marker of endothelialization. Circulation 2007;115(18):2435-41.
19. Joner M, Finn AV, Farb A, Mont EK, Kolodgie FD, Ladich E, Kutys R, Skorija K, Gold HK, Virmani R. Pathology of drug-eluting stents in humans: delayed healing and late thrombotic risk. J Am Coll Cardiol 2006;48(1):193-202.

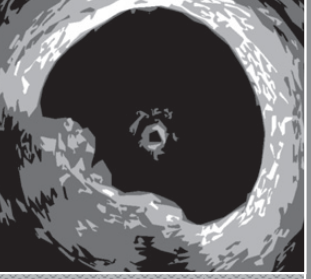

Part 3

OCT Clinical Applications
Coronary Stents

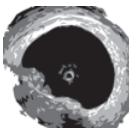

Chapter 10

Intra-coronary optical coherence tomography and the evaluation of stents

Peter Barlis, Gijs van Soest, Patrick W. Serruys, Evelyn Regar

Optical coherence tomography (OCT) is a light-based imaging modality long been applied to the field of ophthalmology, now also showing tremendous potential in the coronary circulation. Compared to traditional intravascular ultrasound (IVUS), OCT has a ten-fold higher resolution given the use of light rather than sound. This advantage has seen OCT successfully applied to the assessment of atherosclerotic plaque (including thin cap fibroatheroma and macrophage distribution within a culprit lesion), stent apposition and tissue coverage, introducing a new era in intravascular coronary imaging. (1-13) The issue of stent tissue coverage is particularly pertinent given that autopsy series have identified a link between incomplete stent endothelialisation and long-term stent thrombosis. (14) Therefore, the detailed imaging afforded by OCT may give further crucial insights into this condition, which, although uncommon, is catastrophic.

This chapter will address the application of OCT to the coronary arteries, with particular reference to the assessment of coronary stents. This field has emerged as one of the more promising for interventional cardiology with OCT able to traverse some of the limitations of IVUS by giving unique insights into tissue coverage, an 'intensely' debated topic in the current discussion surrounding drug-eluting stents (DES) and their long-term safety.

OCT principles

OCT utilises a near infrared light source (1310nm wavelength) in combination with advanced fibre-optics to create a dataset of the coronary artery. Both the bandwidth of the infrared light used and the wave velocity are orders of magnitude higher than in medical ultrasound (Table 1).

	IVUS	OCT
Dynamic range	40-60dB	90-110dB
Resolution		
axial	100-150μm	10-15μm
lateral	150-300 μm	25-40μm
Penetration (tissue)	4-8mm	1.5mm
Frame rate	30/sec	15-20/sec
Pull-Back Speed	0.5-1.0mm/sec	1.0-3.0mm/sec
Wire artefact	++	+
Complexity	+	+++

Table 1: Comparison between optical coherence tomography (OCT) and intravascular ultrasound (IVUS)

The resulting resolution depends primarily on the ratio of these parameters, and is one order of magnitude larger than that of IVUS: the axial resolution of OCT is about 15 μm. The lateral resolution is mainly determined by the imaging optics in the catheter and is approximately 25 μm. The imaging depth of approximately 1.0-1.5mm within the coronary artery wall is limited by the attenuation of light in the tissue. Analogous to ultrasound imaging, the echo time delay of the emitted light is used to generate spatial image information, the intensity of the received (reflected or scattered) light is translated into a (false) colour scale. As the speed of light is much faster than that of sound, an interferometer is required to measure the backscattered light. (15,16)

The interferometer splits the light source into two "arms" – a reference arm and a sample arm, which is directed into the tissue. The light from both arms is recombined at a detector, which registers the so-called interferogram, the sum of reference and sample arm fields. Because of the large source bandwidth, the interferogram is non-zero only if the sample and reference arms are of equal length, within a small window equal to the coherence length of the light source. (17) In the most straightforward embodiment of OCT (called time-domain OCT; TD-OCT), the length

of the reference arm is scanned over a distance of typically a few millimetres, by moving a mirror. The point from which intensity is collected from the sample arm is moved through the tissue accordingly, and the amplitude of the recorded interferogram in a scan corresponds to the reflectivity of the tissue along the direction of the sample beam. By scanning the beam along the tissue, in a rotary fashion for intravascular imaging, an image is built up out of neighbouring lines.

The imaging catheter

A catheter for intracoronary OCT imaging is part of the sample arm of the interferometer described above. The optical signal is transmitted by a single-mode fibre, which is fitted with an integrated lens micro-prism assembly to focus the beam and direct it towards the tissue. The focus is approximately 1mm outside the catheter.

The first commercial system used a design in which the fibre itself is rotating inside a stationary sheath, but other realisations are possible. Designs involving a high-torque speedometer cable transmitting the rotation has been demonstrated, (18) where the fibre is inside the hollow cable. In order to scan the vessel lengthwise, the catheter-imaging tip is pulled back while rotating, usually inside a transparent sheath, allowing to collect a three dimensional dataset of the coronary artery. Both rotary and pullback motion are driven proximally by a motor outside the patient. The current commercially available imaging probe (ImageWire™ LightLab Imaging Inc., Westford, MA, USA) has a maximum outer diameter of 0.019″ (with a standard 0.014" radiolucent coiled tip) and contains a single-mode fibre optic core within a translucent sheath. The image wire is connected at its proximal end to the imaging console that permitted real-time data processing and two-dimensional representation of the backscattered light in a cross-sectional plane.

Technical considerations

As infra-red light is unable to penetrate through red blood cells, OCT imaging must be performed in a blood-free environment. This has traditionally been performed with the use of a proximal balloon positioned in the coronary artery which is transiently inflated to occlude the vessel. A 30 second time limit is set into the console and imaging should be terminated prematurely at any stage should there be patient intolerance, arrhythmia or hemodynamic instability. As a result of the proximal balloon occlusion, such coronary segments are therefore unable to be optimally imaged with first generation OCT. Large vessels, such as the left main are also prohibitive with the balloon occlusion method, although increasingly, a non-occlusive technique is being adopted.

Balloon occlusion method

An OCT catheter is initially advanced distal to the area of interest over a conventional coronary guide wire, which is then replaced with the OCT imaging wire. The OCT catheter is then withdrawn proximal to the stented segment that is visualised using an automated pullback system. During image acquisition, coronary blood flow is replaced by continuous flushing of Ringer's lactate at 0.5-1.0ml/sec using a power injector (e.g. Mark V ProVis, Medrad, Inc. Indianola, PA, US). The highly compliant occlusion balloon remains inflated proximal to the lesion at 0.8atm for a maximum of 30sec.

Non-occlusive technique

With refinements in the OCT system, higher acquisition speeds permit imaging without the need for proximal vessel balloon occlusion. (19) Here, the optical wire is advanced distal to the area of

interest, with the position confirmed by fluoroscopy. To facilitate passage of the wire distal to the area of interest, a single lumen (e.g. Transit, Cordis, Johnson & Johnson, US) or dual lumen catheter (0.023" TwinPass, Vascular Solutions Inc, Minneapolis, Minnesota, US) is required over a conventional guide wire. An automated pullback is commenced during simultaneous contrast infusion of a viscous iso-osmolar contrast (e.g. Iodixanol 320, Visipaque™, GE Health Care, Cork, Ireland) at 37 degree Celsius connected to the standard Y-piece of the guiding catheter. Flushing can either be performed manually or using an infusion pump at a rate of between 2-4ml/sec. The pullback is stopped after visualisation of the complete stented segment or in case of significant signs of ischaemia, arrhythmia or patient intolerance.

The non-occlusive technique avoids the cumbersome balloon occlusion requirements and involves flushing of contrast via the guiding catheter during simultaneous imaging, usually at a pullback of 3 mm/sec (see below). In our experience, the non-occlusive technique is less time consuming, results in less patient chest pain and permits visualisation of ostial and proximal coronary segments.

OCT Safety

Several groups have reported their clinical experience with OCT over the last few years.(7,10,11,13,20-26) Nevertheless, only limited information about acute complications of this procedure is available. Recently, Yamaguchi et al (27) examined the feasibility of OCT and IVUS imaging in 76 patients. Although transient chest pain and electrocardiographic changes caused by imaging were not considered as part of their study, there were no adverse events reported following both IVUS and OCT, with the latter being performed exclusively using the occlusive method.

A number of risks need to be considered. Thrombus has been reported (28) during OCT instrumentation and highlights the need for careful systemic anticoagulation, usually with weight adjusted heparin. Transient chest pain and ST segment depression on the electrocardiogram are not uncommon and usually resolve immediately following OCT pullback. Arrhythmias are uncommon yet must be immediately recognised and treated. Several studies have shown the incidence of ventricular fibrillation (VF) during coronary angioplasty is about 1.5%,(29,30) with the rate dropping down to around 0.6% for diagnostic procedures.(31,32) In addition to ischaemia, other mechanisms have also been identified including reperfusion, electrolyte imbalances, coronary instrumentation, osmolarity and electrolyte composition of contrast agents and intra-coronary thrombus. (33-39).To reduce the incidence of VF during OCT imaging, iso-osmolar contrast such as Iodixanol (Visipaque™, GE Health Care, Cork, Ireland) is recommended with the non-occlusive technique. The advantage lies in its higher viscosity relative to other agents, which permits optimal blood clearance for OCT imaging at the given flush volumes through the guiding catheter. This agent has also been shown to have a lower propensity to cause VF given its lower osmolality, higher viscosity and higher concentration of sodium and calcium chloride molecules compared to other non-ionic media. (40-43)

The role of OCT in stent imaging

Coronary artery lesions and results following percutaneous coronary intervention (PCI) are usually assessed angiographically. This luminogram technique provides a unique overview of the coronary tree, information regarding anatomy and topography and can confirm the presence of atherosclerosis with high specificity. The prognostic relevance for subsequent cardiac events, such as myocardial infarction, however, is limited. Furthermore, stent implantation and optimisation undertaken using angiographic guidance alone has been shown to result in more

frequent incomplete stent expansion and an increased future risk of target vessel revascularisation when compared to guidance with IVUS. (44-47)

Unlike conventional stents, which develop circumferential coverage with an average thickness of 500μm or more, well visualised with IVUS and angiography, DES delay and prevent the hyperplastic response so that the average late lumen loss for DES can be lower than 100μm, (48) which means this amount of intimal thickening will not be detectable by IVUS.

Coronary angioscopy is able to visualise strut tissue coverage, but this highly specialised technique lacks the ability for quantification. Hence, OCT is an attractive alternative, able to circumvent many of these limitations, and, with its high-resolution, can precisely assess the in-vivo tissue responses following stent implantation. OCT is also becoming an integral tool to assess emerging stent technologies that are increasingly becoming more sophisticated such as bioabsorbable polymers and biodegradable magnesium alloy stents, (49) and thus demanding highly detailed assessments both in the initial animal testing phases but also in the clinical trial setting.

OCT for the assessment of acute stent apposition

Traditionally, IVUS has been the imaging modality to assess stent apposition, both acutely and, at follow-up. Inherent with its use however is the limited resolution. Two studies (50,51) using conventional IVUS suggested that stent malapposition did not increase the risk of major adverse cardiac events. Nevertheless, both studies detected a surprisingly small number of malapposed stents using the IVUS derived criterion of at least 1 malapposed strut (51/708 cases, 7.2% and 16/229 cases, 7.0% respectively).

Studies using OCT in the acute setting following stent implantation have demonstrated a high proportion of malapposed struts, even after optimal high pressure post-dilatation, with this phenomenon being particularly evident in regions of stent overlap.(11) In an evaluation of OCT findings following stent implantation to complex coronary lesions, Tanigawa et al (20,52) examined a total of 6,402 struts from 23 patients (25 lesions) and found 9.1±7.4% of all struts in each lesion treated were malapposed. Univariate predictors of malapposition on multilevel logistic regression analysis where: implantation of a sirolimus-eluting stent (SES), presence of overlapping stents, longer stent length and type C lesions. Likely mechanical explanations for malapposition of stent struts include increased strut thickness, closed cell design or acute stent recoil. The latter has been demonstrated in SES to be in the range of 15%, despite the use of high pressure balloon dilatation. (53) The long-term sequeale of malapposed struts found immediately following implantation using OCT however is currently unknown.

OCT for the assessment of stent tissue coverage

Several small studies have recently been published highlighting the application of OCT in the detection of stent tissue coverage at follow-up. Importantly, OCT permits the quantification of tissue coverage with high reliability. (54) Matsumoto et al (6) studied 34 patients following SES implantation. The mean neointima thickness was 52.5 microns, and the prevalence of struts covered by thin neointima undetectable by IVUS was 64%. The average rate of neointima-covered struts in an individual SES was 89%. Nine SES (16%) showed full coverage by neointima, whereas the remaining stents had partially uncovered struts. (6)

Similarly, Takano et al (10) studied 21 patients (4,516 struts) 3 months following SES implantation. Rates of exposed struts and exposed struts with malapposition were 15% and 6%, respectively. These were more frequent in patients with ACS than in those with non-ACS (18% vs 13%, $p < 0.001$; 8% vs 5%, $p < 0.005$, respectively). The same group have recently reported 2

year follow-up OCT findings with the thickness of neointimal tissue at 2-years being greater than that at 3-months (71 ±93 μm vs. 29 ± 41 μm, respectively; $p<0.001$). Frequency of uncovered struts was found to be lower in the 2-year group compared to the 3-month group (5% vs. 15%, respectively; $p<0.001$) and, in contrast, prevalence of patients with uncovered struts did not differ between the 3-month and the 2-year group (95% vs. 81%, respectively) highlighting that exposed struts continued to persist at long-term follow-up. (21)
Chen et al (55) recently used OCT to image SES and BMS at different time points following implantation. Of the 10 SES and 13 BMS imaged, the authors identified a significantly higher number of incompletely apposed and uncovered stent struts in patients receiving SES compared to BMS. The results of these small observational studies are compatible with evidence from animal and human post-mortem series showing that DES cause significant impairment in arterial healing resulting in incomplete re-endothelialisation with persistence of fibrin. (14,56) The importance of this is heightened by autopsy data implicating incomplete endothelialisation as a possible substrate for late stent thrombosis. (57)

With the reduction of in-stent hyperplasia induced by DES, other mechanisms of restenosis due to mechanical stent failure have become apparent. The causes behind DES failures remain complex and multi-factorial. Of the two established first generation DES, the SES (Cordis, J&J, Miami, Florida, US) has been particularly linked to cases of stent fracture, likely as a result of its closed cell design compared with other DES employing an open cell system. (58) The higher imaging resolution of OCT compared to IVUS permits a detailed assessment in such cases, as demonstrated recently by Shite et al. (6) and Barlis et al. (59)

In addition to quantifying the amount of neointima present, OCT can also characterise this tissue in a qualitative manner. Neointimal tissue can show a variety of morphologies ranging from homogenous, bright, uniform tissue to inhomogeneous or eccentric. OCT findings can possibly reflect fibrin deposition and incomplete healing (60) as well as rapid lesion progression (61) and neovascularisation. (62) OCT may also be used to provide complimentary information on stent apposition and other conditions not infrequently observed following stenting, including dissection, tissue prolapse, restenosis, fracture and thrombosis. (1,59,63). van Beusekkom et al (1) have also reported on the OCT features of the coronary artery following treatment with vascular brachytherapy. Here, the treated area shows several changes in vascular architecture, namely the appearance of a three layered artery with the intima becoming more pronounced and the media and adventitial layers becoming more reflective, indicating collagen deposition, the appearance of eccentric neointimal tissue and the disappearance of a clear demarcation between media and adventitia, indicating disappearance or fibrosis of the media with inward remodelling. (1) Figures 1 and 2 demonstrate the application of OCT post-stenting and show the diverse pathology able to be visualised in-vivo by this unique technique.

Typical Stent imaging artefacts

Although OCT has enabled a clear visualisation of stents and their relation to the vessel wall, a number of imaging artefacts need to be recognised.

Shadowing behind stent struts

The light source used for OCT is unable to penetrate metal resulting in dorsal shadowing behind the stent strut (Figure 3A). When interpreting OCT images, the thickness of the whole stent strut (including metal and polymer) must be taken into consideration rather than only the visible endo-luminal strut surface. Shadowing also limits the interpretation of structures behind the

stent strut and this remains a limitation of OCT, particularly also given its poor tissue penetration (< 1.5mm). Furthermore, the OCT imaging plane rarely intersects the stent struts perpendicularly thereby resulting in shadows much larger than the actual width of the stent strut.

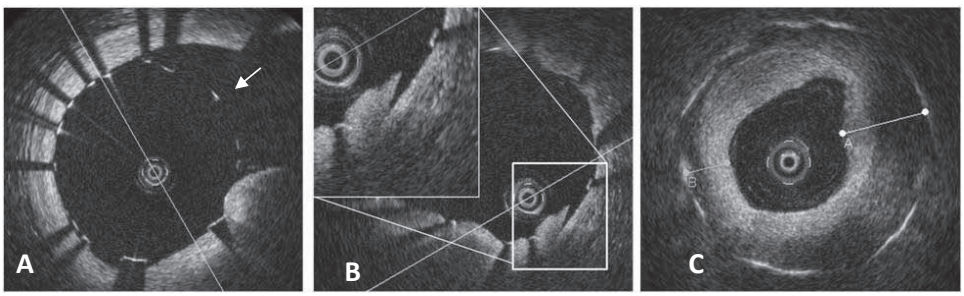

see colour section

Figure 1 The application of optical coherence tomography (OCT) post-stenting. **A:** shows a stent immediately following implantation across a bifurcation. The struts at the carina are clearly seen to be malapposed (arrow) **B:** OCT cross section with magnification (insert, top left) showing a dissection flap immediately following *implantation of a stent* ***C:*** *Demonstrates significant intimal hyperplasia occurring 8 months following* stent implantation. The intimal tissue is seen to have a layered pattern with the endo-luminal aspect showing a bright, reflective and homogenous appearance in contrast to the layer abutting the stent struts which is seen to be poorly reflective. The thickness measured at the 2 points indicated was A-0.82mm and B-0.40mm

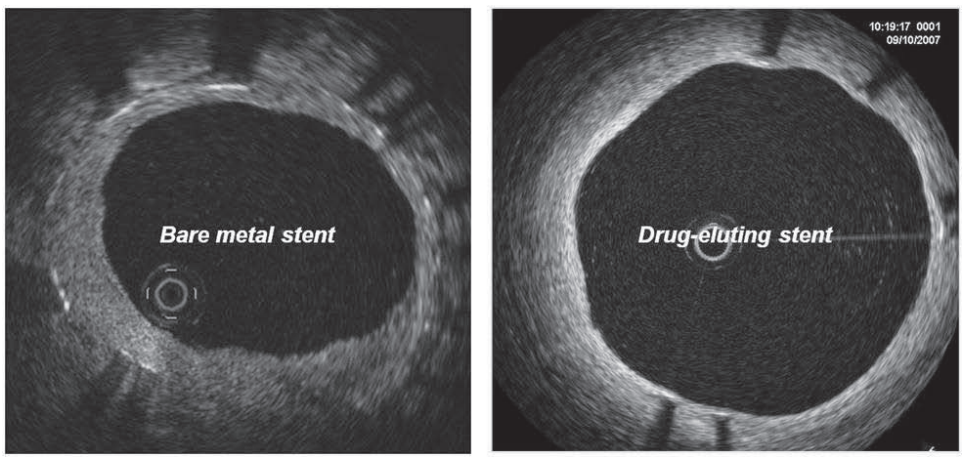

see colour section

Figure 2 – Shows the contrasting amount of tissue covering struts in a bare metal (BMS) and drug-eluting stent (DES). The tissue thickness overlying the BMS measured between 0.14 and 0.42mm. In contrast, the DES was covered by a thin, concentric layer of tissue measuring 0.09mm.

Bright reflections saturating an entire line (spikes)

If the imaging beam hits a strut perpendicularly, it reflects a very large fraction of the beam back towards the catheter. This strong signal may saturate the detector registering the interferogram, producing a readily recognisable artefact of bright radial streaks centred on struts. (Figure 3B)

Multiple reflections (stent – catheter – stent)

In a similar geometry, near-specular reflection, light may bounce back between catheter and strut more than once. The optical catheter itself reflects part of the received light back into the tissue. Strong reflectors, such as struts, may produce an appreciable signal in the second reflection. The optical path length of light in the secondary reflection is double that of the primary feature. Hence, a double reflection will show up as an apparent second strut appearing behind the first at twice the distance from the catheter. (Figure 3C)

see colour section

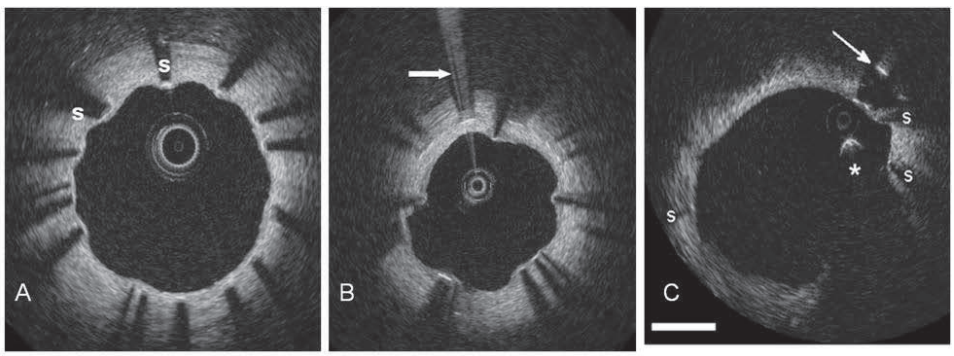

Figure 5 – A: Circumferential stent struts are shown covered by a thin layer of tissue. Dorsal shadowing is evident behind the stent struts (S) with only the luminal surface of the strut visible with OCT. **B:** demonstrates circumferential stent struts with shadowing and bright reflections caused by saturation of the detector registering the inferogram (arrow) **C:** Arrow indicates a double reflection between stent and catheter. This can occur if a stent strut is imaged face-on, and reflects the OCT beam specularly. Shadows of other stent struts are marked by s; stent struts that do not show up as the typical bright dot, but do cast a shadow, are imaged under an oblique angle. * is a guide wire artefact. White bar is 1 mm.

Summary: OCT for stent imaging

To date, OCT has shown a broad application in interventional cardiology both for the immediate and late follow-up of coronary stents. The ability to give highly detailed images in-vivo has shed greater light on the tissue responses following stenting and will provide essential feedback regarding emerging stent technologies. Nevertheless, current OCT requires an intricate imaging procedure and is not suited to tortuous or large calibre coronary arteries. OCT is unable to provide functional details about the neointima with a prior histological study confirming neointimal tissue can still be present over stent struts but can show limited functionality, best demonstrated by the Evans blue dye-exclusion test. (64) Furthermore, a number of interesting appearances have also been described including 'hypodense' regions beneath stent struts. (61,65) Such appearances remain an intense area of ongoing research with thoughts that they may represent areas of fibrinoid necrosis.(66) An example is demonstrated in figure 4_from a patient who had a DES implanted 9 months prior.

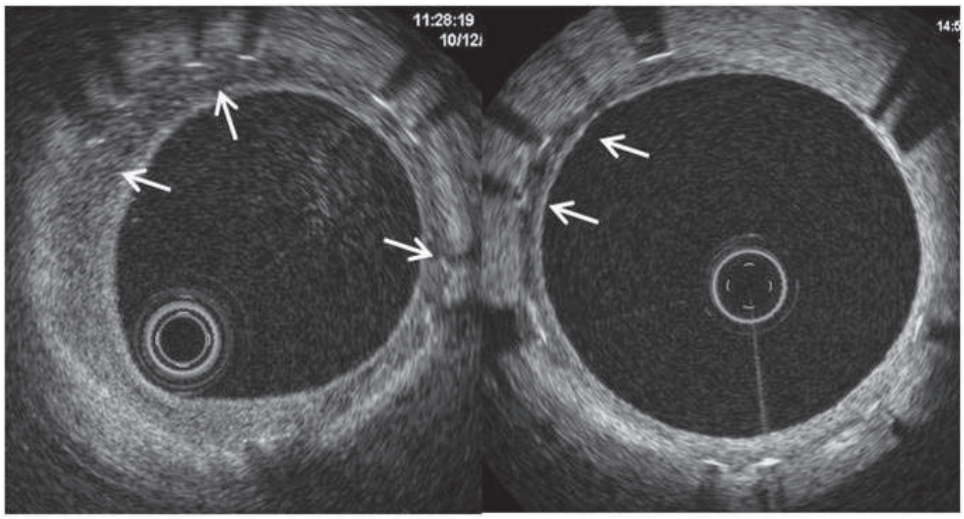

Figure 4 – Hypodense areas (arrows) imaged at 9 month following drug-eluting stent implantation. Such areas may represent fibrinoid necrosis although intense research is ongoing to delineate such regions further.

see colour section

OCT – emerging developments

The real benefit of OCT lies in its ability to provide high-resolution imaging in-vivo. New stents including bioabsorbable magnesium stents or those made with poly-lactic acid offer an exciting era into the management of coronary artery disease with the potential to eliminate some of the problems related to permanent metallic stents. The development of such technologies however remains time consuming and expensive, often necessitating the sacrifice of animals to retrieve the stents. (67) The high-resolution imaging capabilities of OCT gives the potential for rapid in-vivo assessment of tissue response to various stent designs, thereby also limiting the dependency on large numbers of animals. (67) The use of OCT serially is also an attractive concept giving unique insights into the time course of stent endothelialisation following implantation.

OCT remains a specialised intra-coronary imaging technique with dedicated procedural requirements and thus should only be performed by trained operators. As has been seen above, to accomplish adequate images, blood must be temporarily cleared and this task adds a new element to the procedure, particularly for operators trained in IVUS where a relatively simple, rapid-exchange imaging catheter is advanced over a standard guide wire. The need for balloon occlusion and intra-coronary flush are at the forefront of emerging developments to simplify the OCT image acquisition process. Faster pullback speeds offer the potential to scan an entire stent within a matter of 5-6 seconds. Such speeds are currently under development in OCT systems using optical frequency domain imaging (OFDI).

Optical frequency domain imaging (OFDI)

The development of faster image acquisition speeds, with greater penetration depth, without loss of vital detail and resolution is a great advancement on current OCT systems. Rather than using a broadband light source as in conventional OCT systems, OFDI incorporates a novel wavelength-swept laser source, the reason for its alternative moniker "swept-source OCT" (SS-OCT) (68-70). From the signal received in one wavelength sweep, the depth profile can be

constructed by the Fourier transform operation that is performed electronically in the data processing unit. All other components of an OFDI system (the interferometer, the catheter, including the imaging optics, display) are comparable in principle to those in a conventional OCT system. The scan speed, or line rate, in a TD-OCT system are limited by the achievable mechanical scan speed of the reference arm mirror, and by the sensitivity of the signal detection.(71) The source wavelength in OFDI can be swept at a much higher rate than the position scan of the reference arm mirror in a TD-OCT system. In addition, SS-OCT has a higher sensitivity than TD-OCT at large line rates and scan depths (72-74). These features can be put to good use in larger scan speeds, of the order of 10^5 lines per second. In an OFDI system, the wavelength range of the sweep determines the resolution of the image, while the imaging depth is inversely related to the instantaneous spectral width of the source.
The increased sensitivity of SS-OCT/OFDI also allows for larger imaging depths. The attenuation of light by the tissue is the same for TD-OCT and OFDI, but the lower noise of the latter makes it possible to discern weaker signals that would be indistinguishable from the background in TD-OCT (73). The depth range from which useful anatomical information can be extracted is extended by a factor of about 3. (75) Clinically, this advantage enables the assessment of coronary micro-structures well beyond the arterial-lumen border.

In the five years since the inception of SS-OCT, a continuous increase in scan speed was achieved. The first demonstrated system (68) exhibited a fourfold increase in scan speed at 15,600 lines per second, while fastest, fully functioning SS-OCT systems to date reach a line rate of 370,000 lines per second. (76) An experimental system with 5 MHz line rate has been demonstrated. (77) This development begs the question where the OCT speed limit lies, and to what use this tremendous gain in speed can be put.

OFDI and other swept-source systems produce images much faster than standard video-rate, so recorded data has to be replayed for inspection by the operator. Currently, OCT systems scan 200-500 angles per revolution (frame), and 5-10 images per mm in a pullback. If these parameters are maintained with high-speed systems, 2 cm/s (or higher) pullback speeds are possible at the same sampling density as conventional OCT data. This high pullback speed and the need for a fast-revolving imaging tip pose high demands on the mechanics of the disposable catheter.

At present, SS-OCT data acquisition is limited by the data transfer rate from the acquisition system to the processing system. With state of the art electronics, the data acquisition rate of the newest SS-OCT systems is higher than the transfer rate, so all data has to be stored on the acquisition board, (76) limiting acquisition time.
The high scan speeds have been employed for real-time volumetric imaging of dynamic phenomena including fast pullbacks for intra-coronary imaging with minimal ischaemia, (75) and retinal scans with minimal motion artefacts. (78) Imaging of dynamic phenomena in time, or rather removing motion artefacts, are the prime applications of high-speed OCT. 3-Dimensional rendering of volumes becomes possible if motion during the scan is limited.
A 3-D representation of a stent in porcine coronaries has been demonstrated, (75) although its construction was still off-line. Advances in data processing could lead to real-time construction of volume-rendered 3D datasets, providing further insight into stent positioning. The high data rate of novel OCT technologies could also be used to increase sampling density, either in the longitudinal (pullback) or angular direction. A smaller spacing between frames in a pullback would lead to a better sampling of small scale features in the arterial or stent geometry that would be missed at 100 μm inter-frame distance. Denser sampling in the angular direction would facilitate speckle filtering in OCT images. Speckle is a major obstacle for the development of parametric and quantitative imaging techniques. These possibilities are still largely unexplored.

Clinical applications of OFDI

Clinically, OFDI has been introduced to select catheterization laboratories and has been successfully used to assess coronary stents and atherosclerotic plaque.(79) Our first experience with the OFDI system at the Thoraxcenter (Erasmus MC, Rotterdam, The Netherlands) has been promising. The OCT catheter is easily advanced into the coronary artery, similar to conventional IVUS. Large coronary arteries can be visualized over the complete vessel circumference, ostial lesions and left main lesions can be imaged. Automated pullback speeds up to 20mm/sec allow for a very fast imaging procedure, thereby minimising ischemia. As a result, long pullbacks can be performed with a significant reduction in the amount of flush required.

Summary and Conclusions

OCT has caused intense interest in interventional cardiology. Its application to the assessment of coronary stents has been greeted with strong enthusiasm and is now also being incorporated into large multi-centre randomised stent trials aimed at complementing angiographic and clinical endpoints. Such applications are currently unique to OCT and, despite the recent progress of non-invasive techniques such as 64 multi-slice computed tomography (MSCT), conventional stents still represent a challenge to distinguish lumen and intimal hyperplasia within the stent. Reports showing that reconstruction of MSCT images using specific kernels offer good correlation with angiography are encouraging but unlikely to make this technique a reliable alternative at the present time.

The ability to provide high-resolution imaging in-vivo is the most significant concept circumventing the limitations of other imaging modalities such as IVUS or the need for multiple animal experiments. Refinements in acquisition speeds with OFDI will also make the technique less procedurally demanding and thus able to be applied to many more centres, thereby remaining a key tool in the armamentarium of researchers and interventional cardiologists alike.

References

1. Van Beusekom HM, Regar E, Peters I, Van der Giessen WJ. Long-term effects of endovascular radiation after balloon angioplasty: assessment by OCT and histology. In: Regar E, van Leeuwen AMGJ, Serruys PW, eds. Optical coherence tomography in cardiovascular research. London: Informa Healthcare, 2007.
2. Tearney GJ, Yabushita H, Houser SL, et al. Quantification of macrophage content in atherosclerotic plaques by optical coherence tomography. Circulation 2003;107:113-9.
3. Regar E, Schaar JA, Mont E, Virmani R, Serruys PW. Optical coherence tomography. Cardiovasc Radiat Med 2003;4:198-204.
4. Jang IK, Tearney GJ, MacNeill B, et al. In vivo characterization of coronary atherosclerotic plaque by use of optical coherence tomography. Circulation 2005;111:1551-5.
5. Tearney GJ, Jang IK, Bouma BE. Optical coherence tomography for imaging the vulnerable plaque. J Biomed Opt 2006;11:021002.
6. Shite J, Matsumoto D, Yokoyama M. Sirolimus-eluting stent fracture with thrombus, visualization by optical coherence tomography. Eur Heart J 2006;27:1389.
7. Tanigawa J, Barlis P, Di Mario C. Intravascular Optical Coherence Tomography: Optimisation of image acquisition and quantitative assessment of stent strut apposition. EuroIntervention 2007;3:128-136.
8. Tanigawa J, Barlis P, Di Mario C. Do unapposed stent struts endothelialise? In vivo demonstration with optical coherence tomography. Heart 2007;93:378.
9. Prati F, Zimarino M, Stabile E, et al. Does optical coherence tomography identify arterial healing after stenting? An in vivo comparison with histology, on a rabbit carotid model. Heart 2007.
10. Takano M, Inami S, Jang IK, et al. Evaluation by optical coherence tomography of neointimal coverage of sirolimus-eluting stent three months after implantation. Am J Cardiol 2007;99:1033-8.

11. Tanigawa J, Barlis P, Dimopoulos K, Di Mario C. Optical coherence tomography to assess malapposition in overlapping drug-eluting stents. EuroIntervention 2008;3:580-83.
12. Barlis P, Serruys PW, DeVries A, Regar E. Optical coherence tomography assessment of vulnerable plaque rupture: predilection for the plaque 'shoulder'. Eur Heart J 2008:ehn085.
13. Barlis P, Serruys PW, Gonzalo N, van der Giessen WJ, de Jaegere PJ, Regar E. Assessment of culprit and remote coronary narrowings using optical coherence tomography with long-term outcomes. Am J Cardiol 2008;102:391-5.
14. Finn AV, Joner M, Nakazawa G, et al. Pathological correlates of late drug-eluting stent thrombosis: strut coverage as a marker of endothelialization. Circulation 2007;115:2435-41.
15. Michelson AA, Morley EW. On the relative motion of the earth and the luminiferous aether. Philos. Mag 1887;S5 449-463.
16. Schmitt JM, Knuttel A, Yadlowsky M, Eckhaus MA. Optical-coherence tomography of a dense tissue: statistics of attenuation and backscattering. Phys Med Biol 1994;39:1705-20.
17. Schmitt JM. Optical coherence tomography (OCT): A review. IEEE J. Sel. Top. Quant. Elec 1999;5:1205-1215.
18. Bouma BE, Tearney GJ. Power-efficient nonreciprocal interferometer and linear-scanning fiber-optic catheter for optical coherence tomography. Opt Lett 1999;24:531-3.
19. Prati F, Cera M, Ramazzotti V, et al. From bench to bedside. Circ J 2008;72:839-43.
20. Tanigawa J, Barlis P, Kaplan S, Goktekin O, Di Mario C. Stent strut apposition in complex lesions using optical coherence tomography. Am J Cardiol 2006;98:Suppl 1: 97M.
21. Takano M, Yamamoto M, Inami S, et al. Long-term follow-up evaluation after sirolimus-eluting stent implantation by optical coherence tomography: do uncovered struts persist? J Am Coll Cardiol 2008;51:968-9.
22. Prati F, Cera M, Ramazzotti V, Imola F, Giudice R, Albertucci M. Safety and feasibility of a new non-occlusive technique for facilitated intracoronary optical coherence tomography (OCT) acquisition in various clinical and anatomical scenarios. EuroIntervention 2007;3:365-70.
23. Matsumoto D, Shite J, Shinke T, et al. Neointimal coverage of sirolimus-eluting stents at 6-month follow-up: evaluated by optical coherence tomography. Eur Heart J 2007;28:961-7.
24. Chen BX, Ma FY, Wei L, et al. Neointimal Coverage of Bare Metal and Sirolimus-Eluting Stents Evaluated with Optical Coherence Tomography. Heart 2007:hrt.2007.118679.
25. Kubo T, Imanishi T, Takarada S, et al. Assessment of culprit lesion morphology in acute myocardial infarction: ability of optical coherence tomography compared with intravascular ultrasound and coronary angioscopy. J Am Coll Cardiol 2007;50:933-9.
26. Tanigawa J, Barlis P, Di Mario C. Heavily calcified coronary lesions preclude strut apposition despite high pressure balloon dilatation and rotational atherectomy: in-vivo demonstration with optical coherence tomography. Circ J 2008;72:157-60.
27. Yamaguchi T, Terashima M, Akasaka T, et al. Safety and feasibility of an intravascular optical coherence tomography image wire system in the clinical setting. Am J Cardiol 2008;101:562-7.
28. Kim JS, Choi EY, Choi D, Jang Y. Images in cardiovascular medicine. Catastrophic thrombus formation during optical coherence tomography. Circulation 2008;118:e101-2.
29. Bredlau CE, Roubin GS, Leimgruber PP, Douglas JS, Jr., King SB, 3rd, Gruentzig AR. In-hospital morbidity and mortality in patients undergoing elective coronary angioplasty. Circulation 1985;72:1044-52.
30. Dorros G, Cowley MJ, Simpson J, et al. Percutaneous transluminal coronary angioplasty: report of complications from the National Heart, Lung, and Blood Institute PTCA Registry. Circulation 1983;67:723-30.
31. Davis K, Kennedy JW, Kemp HG, Jr., Judkins MP, Gosselin AJ, Killip T. Complications of coronary arteriography from the Collaborative Study of Coronary Artery Surgery (CASS). Circulation 1979;59:1105-12.
32. Nishimura RA, Holmes DR, Jr., McFarland TM, Smith HC, Bove AA. Ventricular arrhythmias during coronary angiography in patients with angina pectoris or chest pain syndromes. Am J Cardiol 1984;53:1496-9.
33. Goldstein JA, Butterfield MC, Ohnishi Y, Shelton TJ, Corr PB. Arrhythmogenic influence of intracoronary thrombosis during acute myocardial ischemia. Circulation 1994;90:139-47.
34. Gorenek B. Tachyarrhythmias in percutaneous coronary interventions. J Electrocardiol 2006;39:412 e1-5.

35. Huang JL, Ting CT, Chen YT, Chen SA. Mechanisms of ventricular fibrillation during coronary angioplasty: increased incidence for the small orifice caliber of the right coronary artery. Int J Cardiol 2002;82:221-8.
36. Missri J, Jeresaty RM. Ventricular fibrillation during coronary angiography: reduced incidence with nonionic contrast media. Cathet Cardiovasc Diagn 1990;19:4-7.
37. Pedersen HK, Jacobsen EA, Mortensen E, Refsum H. Contrast-medium-induced ventricular fibrillation: arrhythmogenic mechanisms and the role of antiarrhythmic drugs in dogs. Acad Radiol 1995;2:1082-8.
38. Quigley PJ, Maurer BJ. Ventricular fibrillation during coronary angiography: association with potassium-containing glyceryl trinitrate. Am J Cardiol 1985;56:191.
39. Rudoff J, Phillips L. High-osmolality and low-osmolality contrast agents. N Engl J Med 1992;327:203-4.
40. Baath L, Almen T. Reducing the risk of ventricular fibrillation by adding sodium to ionic and non-ionic contrast media with low iodine concentration. Coronary perfusion of the isolated rabbit heart with meglumine diatrizoate or iopentol at 140 mg I/ml and 0-154 mmol Na+/l. Acta Radiol 1989;30:207-12.
41. Hayakawa K, Yamashita K. Low-osmolality contrast media-induced ventricular fibrillation. Invest Radiol 1989;24:298-301.
42. Morris TW, Ventura J. Incidence of fibrillation with dilute contrast media for intra-arterial coronary digital subtraction angiography. Invest Radiol 1986;21:416-8.
43. Chai CM, Karlsson JO, Almen T. Incidence of ventricular fibrillation during left coronary arteriography in pigs: comparison of a solution of the nonionic dimer iodixanol with solutions of five different nonionic monomers. Acta Radiol 2008;49:150-6.
44. Albiero R, Rau T, Schluter M, et al. Comparison of immediate and intermediate-term results of intravascular ultrasound versus angiography-guided Palmaz-Schatz stent implantation in matched lesions. Circulation 1997;96:2997-3005.
45. Schiele F, Meneveau N, Seronde MF, Deforet MF, Gupta S, Bassand JP. Predictors of event-free survival after repeat intracoronary procedure for in-stent restenosis; study with angiographic and intravascular ultrasound imaging. Eur Heart J 2000;21:754-62.
46. Iakovou I, Mintz GS, Dangas G, et al. Optimal final lumen area and predictors of target lesion revascularization after stent implantation in small coronary arteries. Am J Cardiol 2003;92:1171-6.
47. Cheneau E, Satler LF, Escolar E, et al. Underexpansion of sirolimus-eluting stents: incidence and relationship to delivery pressure. Catheter Cardiovasc Interv 2005;65:222-6.
48. Fujii K, Mintz GS, Kobayashi Y, et al. Contribution of stent underexpansion to recurrence after sirolimus-eluting stent implantation for in-stent restenosis. Circulation 2004;109:1085-8.
49. Barlis P, Tanigawa J, Di Mario C. Coronary bioabsorbable magnesium stent: 15-month intravascular ultrasound and optical coherence tomography findings. Eur Heart J 2007;28:2319.
50. Hong MK, Mintz GS, Lee CW, et al. Late stent malapposition after drug-eluting stent implantation: an intravascular ultrasound analysis with long-term follow-up. Circulation 2006;113:414-9.
51. Tanabe K, Serruys PW, Degertekin M, et al. Incomplete stent apposition after implantation of paclitaxel-eluting stents or bare metal stents: insights from the randomized TAXUS II trial. Circulation 2005;111:900-5.
52. Tanigawa J, Barlis P, Dimopoulos K, Dalby M, Moore P, Di Mario C. The influence of strut thickness and cell design on immediate apposition of drug-eluting stents assessed by optical coherence tomography. Int J Cardiol 2008;doi:10.1016/j.ijcard.2008.05.069
53. Regar E, Schaar J, Serruys PW. Images in cardiology. Acute recoil in sirolimus eluting stent: real time, in vivo assessment with optical coherence tomography. Heart 2006;92:123.
54. Tanimoto S, Rodriguez-Granillo G, Barlis P, et al. A novel approach for quantitative analysis of intracoronary optical coherence tomography: high inter-observer agreement with computer-assisted contour detection. Catheter Cardiovasc Interv 2008:DOI: 10.1002/ccd.21482.
55. Chen BX, Ma FY, Wei L, et al. Neointimal Coverage of Bare Metal and Sirolimus-Eluting Stents Evaluated with Optical Coherence Tomography. Heart 2007.
56. Finn AV, Nakazawa G, Joner M, et al. Vascular responses to drug eluting stents: importance of delayed healing. Arterioscler Thromb Vasc Biol 2007;27:1500-10.

57. Joner M, Finn AV, Farb A, et al. Pathology of drug-eluting stents in humans: delayed healing and late thrombotic risk. J Am Coll Cardiol 2006;48:193-202.
58. Lee SH, Park JS, Shin DG, et al. Frequency of stent fracture as a cause of coronary restenosis after sirolimus-eluting stent implantation. Am J Cardiol 2007;100:627-30.
59. Barlis P, Sianos G, Ferrante G, Del Furia F, D'Souza S, Di Mario C. The use of intra-coronary optical coherence tomography for the assessment of sirolimus-eluting stent fracture. Int J Cardiol 2008.
60. Surmely J, Takeda Y, Ita T, Suzuki T. Acute optical coherence tomography findings after stenting. In: Regar E, van Leeuwen AMGJ, Serruys PW, eds. Optical coherence tomography in cardiovascular research. London: Informa Healthcare, 2007.
61. Tanimoto T, Aoki J, Serruys PW, Regar E. Paclitaxel-eluting stent restenosis shows three - layer appearance by optical coherence tomography. EuroIntervention 2006;1:484.
62. Regar E, van Beusekom HM, van der Giessen WJ, Serruys PW. Images in cardiovascular medicine. Optical coherence tomography findings at 5-year follow-up after coronary stent implantation. Circulation 2005;112:e345-6.
63. Bouma BE, Tearney GJ, Yabushita H, et al. Evaluation of intracoronary stenting by intravascular optical coherence tomography. Heart 2003;89:317-20.
64. van Beusekom HM, Whelan DM, Hofma SH, et al. Long-term endothelial dysfunction is more pronounced after stenting than after balloon angioplasty in porcine coronary arteries. J Am Coll Cardiol 1998;32:1109-17.
65. Barlis P, Di Mario C, Van Beusekom HM, Gonzalo N, Regar E. Novelties in cardiac imaging: Optical coherence tomography. EuroIntervention 2008;4:C22-C26.
66. van Beusekom HM, Saia F, Zindler JD, et al. Drug-eluting stents show delayed healing: paclitaxel more pronounced than sirolimus. Eur Heart J 2007;28:974-9.
67. Bonnema GT, Cardinal KO, McNally JB, Williams SK, Barton JK. Assessment of blood vessel mimics with optical coherence tomography. J Biomed Opt 2007;12:024018.
68. Yun SH, Tearney GJ, de Boer JF, Iftimia N, Bouma B. High-speed optical frequency-domain imaging. Optics Express 2003;11:2953-63.
69. Fercher AF, Hitzenberger CK, Kamp G, Elzaiat SY. Measurement of intraocular distances by backscattering spectral interferometry. Optics Communications 1995;117:43-48.
70. Chinn SR, Swanson EA, Fujimoto JG. Optical coherence tomography using a frequency-tunable optical source. Optics Letters 1997;22:340-342.
71. Rollins AM, Kulkarni MD, Yazdanfar S, Ung-arunyawee R, Izatt JA. In vivo video rate optical coherence tomography. Optics Express 1998;3:219-229.
72. Leitgeb R, Hitzenberger CK, Fercher AF. Performance of fourier domain vs. time domain optical coherence tomography. Optics Express 2003;11:889-894.
73. Choma M, Sarunic M, Yang C, Izatt J. Sensitivity advantage of swept source and Fourier domain optical coherence tomography. Opt. Express 2003;11:2183-2189.
74. de Boer JF, Cense B, Park BH, Pierce MC, Tearney GJ, Bouma BE. Improved signal-to-noise ratio in spectral-domain compared with time-domain optical coherence tomography. Optics Letters 2003;28:2067-2069.
75. Yun SH, Tearney GJ, Vakoc BJ, et al. Comprehensive volumetric optical microscopy in vivo. Nat Med 2006;12:1429-33.
76. Huber R, Adler DC, Fujimoto JG. Buffered Fourier domain mode locking: Unidirectional swept laser sources for optical coherence tomography imaging at 370,000 lines/s. Opt Lett 2006;31:2975-7.
77. Moon S, Kim DY. Ultra-high-speed optical coherence tomography with a stretched pulse supercontinuum source. Optics Express 2006;14:11575-84.
78. Lim H, Mujat M, Kerbage C, et al. High-speed imaging of human retina in vivo with swept-source optical coherence tomography. Optics Express 2006;14:12902-08.
79. Tearney G, Waxman S, Shishkov M, et al. Three-Dimensional Coronary Artery Microscopy by Intracoronary Optical Frequency Domain Imaging. J. Am. Coll. Cardiol. Img 2008;1:752 - 761.

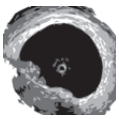

Chapter 11

An Optical Coherence Tomography Study of a Biodegradable versus Durable Polymer-Coated Limus-Eluting Stent: A LEADERS Trial Sub-Study

Peter Barlis, Evelyn Regar, Patrick W. Serruys, Konstantinos Dimopoulos, Willem J. van der Giessen, Robert-Jan M. van Geuns, Giuseppe Ferrante, Simon Wandel, Stephan Windecker, Gerrit-Anne van Es, Pedro Eerdmans, Peter Jüni, Carlo Di Mario

Objectives: *This study sought to evaluate tissue coverage of stents using optical coherence tomography (OCT) in a group of patients from the randomized LEADERS trial.*

Background: *Delayed and incomplete stent strut endothelialization is the most likely explanation of late stent thrombosis, a rare but devastating phenomenon, more frequent after drug-eluting stent (DES) implantation. OCT has 10 times greater resolution than intravascular ultrasound and thus appears to be a valuable modality for the assessment of stent strut coverage. The LEADERS trial was a multicenter, randomized comparison of a biolimus-eluting stent (BES) with biodegradable polymer with a sirolimus-eluting stent (SES) using a durable polymer.*

Methods: *Fifty-six consecutive patients received OCT during angiographic follow-up at 9 months. OCT images were acquired using a non-occlusive technique at a pullback speed of 3mm/sec. Data were analyzed using a Bayesian hierarchical random-effects model, which accounted for the correlation of lesion characteristics within patients and implicitly assigned analytical weights to each lesion depending on the number of struts observed per lesion.*

Results*: Twenty patients were included in the analysis in the BES group (29 lesions with 4592 struts) and 26 patients in the SES group (35 lesions with 6476 struts). A total of 83 struts were uncovered in the BES group and 407 out of 6476 struts were uncovered in the SES group (weighted difference -1.4%, 95% CI -3.7 to 0.0%, p=0.04). Results were similar after adjustment for pre-procedure lesion length, reference vessel diameter, number of implanted study stents and presence of stent overlap. There were 3 lesions in the BES and 15 lesions in the SES group that had ≥5% of all struts uncovered (difference -33.1% 95% CI -61.7 to -10.3%, p<0.01).*

Conclusions: *Strut coverage at an average follow-up of 9 months appears to be more complete in patients allocated to BES as compared with SES. The impact of this difference on clinical outcome and, in particular, on the risk of late stent thrombosis, is yet to be determined.*

Until recently, trials comparing drug-eluting stents (DES) and bare metal stent (BMS) used intravascular ultrasound (IVUS) to confirm that DES reduce restenosis and intimal proliferation. (1-5) However, the thin layer of neointima observed after implantation of DES is often below the 100 μm axial resolution of IVUS. Incomplete stent strut endothelialization has recently received attention with studies suggesting an association with the long-term risk of stent thrombosis, (6) but it cannot be detected by IVUS. Optical coherence tomography (OCT) has 10 times greater resolution than IVUS and thus appears to be the ideal imaging modality for the assessment of tissue coverage of DES. Observational data using OCT in first generation sirolimus-eluting stents suggest that stent struts may still remain uncovered 2 years after implantation. (7) Evidence of a small but clear increase of late stent thrombosis has led to the increase in the duration of dual anti-platelet therapy beyond the customary 3-6 month period of the initial DES trials, (8,9) with 1 year now recommended by the AHA/ACC/SCAI guidelines, (10) mainly based on theoretical reasoning, without robust studies supporting this recommendation.

The LEADERS (Limus Eluted from A Durable versus ERodable Stent coating) study, was a multi-center, randomized non-inferiority trial comparing a biolimus-eluting stent (BES) using a biodegradable polymer with a widely used sirolimus-eluting stent (SES) with durable polymer. At 9 months, BES were non-inferior to SES for the primary composite endpoint of cardiac death, myocardial infarction (MI), or clinically-indicated target vessel revascularization (TVR). (11) Frequency of cardiac death, MI and clinically-indicated TVR were similar for both stent types (composite endpoint of 9.1% for BES, 9.9% for SES, p=0.59). In the angiographic sub-study, BES were non-inferior to SES in in-stent percentage diameter stenosis at 9 month follow-up with an in-stent restenosis rate of 5.5% versus 8.7% (p=0.20), respectively. (11)

Durable polymer surface coatings may be one of the causes for incomplete endothelialization of first-generation DES. The BES uses biodegradable polylactic acid, which is co-released with biolimus during 6–9 months and degrades into carbon dioxide and water. Since the stainless steel surface of BES is free of additional primer polymer coatings, only the metal stent backbone remains in situ once the polymer has degraded. A second feature distinguishing BES and SES is that the coating is only abluminal, possibly favoring endothelialization of the stent. In a sub-study of the LEADERS trial we therefore set out to compare tissue coverage between BES and SES using OCT.

Methods

The design of the LEADERS study has been published elsewhere. (11) The study applied an 'all-comers' approach including patients aged 18 years or older with chronic stable coronary artery disease or acute coronary syndromes, including non-ST-elevation and ST-elevation MI. There was no limit for the number of treated lesions, vessels, or lesion length and no patients were excluded on the basis of co-morbid disorders or age, apart from the following pre-specified criteria: known allergy to acetylsalicylic acid, clopidogrel, heparin, stainless steel, sirolimus, biolimus, or contrast material; planned surgery within 6 months of percutaneous coronary intervention (PCI) unless the dual anti-platelet therapy could be maintained throughout the peri-surgical period; pregnancy; participation in another trial before reaching the primary endpoint; and inability to provide informed consent. All patients were discharged on acetylsalicylic acid of at least 75 mg daily indefinitely and clopidogrel 75 mg daily for at least 12 months.The study complied with the declaration of Helsinki and was approved by all institutional ethics committees. The trial is registered with ClinicalTrials.gov, number NCT00389220. All patients provided written, informed consent for participation in this trial.

Randomization was done centrally after diagnostic coronary angiography and before PCI by use of a telephone allocation service. Patients were randomly allocated on a 1:1 basis to treatment with BES (BioMatrix Flex, Biosensors Inc, Newport Beach, CA, USA) or SES (Cypher SELECT, Cordis, Miami Lakes, FL, USA), and to active angiographic follow-up at 9 months or clinical follow-up only on a 1:3 basis using a factorial design. The OCT sub-study was performed at 2 of the 10 LEADERS sites (Royal Brompton Hospital, London, UK and Thoraxcenter, Erasmus Medical Center, Rotterdam, The Netherlands). Randomized patients were eligible if they underwent follow-up angiography. Exclusion criteria specific to follow-up with OCT imaging were renal impairment (serum creatinine $\geq$ 200 mmol/L) and left ventricular ejection fraction (LVEF) < 30%. The OCT sub-study was approved by the trial Steering Committee and local Institutional Review Boards.

Optical coherence tomography

For the purpose of the sub-study, OCT was performed at follow-up only using the M3 system (LightLab Imaging, Westford, MS, USA) at 20 frames per second allowing retrieval of the imaging core at 3mm/sec for 30 seconds (90mm) with a non-occlusive imaging technique (12), following administration of intravenous heparin and intra-coronary nitrates. A standard guide wire was advanced distally in the target vessel. A single lumen (e.g. Transit, Cordis, Johnson & Johnson, Miami, FL, USA or ProGreat, Terumo Co, Tokyo, Japan) or a double lumen catheter (0.023" TwinPass, Vascular Solutions Inc, Minneapolis, MN, USA) was then advanced distal to the previously stented region. Following withdrawal of the guide wire, the optical ImageWire (LightLab Imaging, Westford, MS, USA) was passed through the catheter and OCT imaging commenced at a pullback of 3.0mm/sec, during flush of 2-4 ml/sec of iso-osmolar contrast (Iodixanol 320, Visipaque™, GE Health Care, Cork, Ireland) through the guiding catheter to replace blood flow and permit visualization of the stented segment and intima-lumen interface. Scanning was prematurely terminated if there was any hemodynamic instability, arrhythmia or

patient intolerance. If the stented segment was too long to be safely imaged in a single pull-back, image acquisition was stopped and recommenced from the same position during a second contrast injection. Anatomic landmarks such as side branches, calcifications or stent overlap segments were used for longitudinal view orientation.

Offline OCT data analysis was undertaken by an independent core laboratory (Cardialysis BV, Rotterdam, The Netherlands) blinded to stent type allocation, clinical and procedural characteristics of the patients. Analysis of contiguous cross-sections at 1mm longitudinal intervals within the stented segment was performed using proprietary software (LightLab Imaging, Westford, Massachusetts, US). Intra and inter observer reliability were evaluated in previous studies and found to be >0.95, (13-15) as could be expected in view of the clear visualization of intimal tissue and struts allowed by OCT. Recently, Barlis et al (16) demonstrated a low intra and inter-observer variability when assessing OCT strut tissue coverage at follow-up (reproducibility coefficients 26.7μm and 24.1μm, intraclass correlation coefficient 99.4% and 99.6%, respectively).
Metallic stent struts typically appear as bright, signal intense structures with dorsal shadowing. The number of stent struts was determined in each cross section. Stent coverage was classified as not visible/incomplete when there were points of the stent struts with no visible tissue coverage or as complete when tissue was seen overlying the strut. Thickness (μm) of the tissue coverage on the luminal side of each strut was measured at the middle of the long axis of the strut. A linear measurement line was drawn from the endoluminal leading edge perpendicular to the long axis of the strut towards the luminal leading edge of the strut Struts were classified as apposed (when the strut was in contact with the vessel wall) or malapposed if protruding into the lumen at a distance greater than the strut thickness (154μm for the SES and 112μm for the BES).

For malapposed struts, the presence of tissue was qualitatively assessed also on the abluminal surface to confirm circumferential coverage.

Sample Size Calculation and Statistical Analysis

The OCT sub-study was a superiority study. To estimate differences between BES and SES, we used a Bayesian hierarchical random-effects model based on Markov chain Monte Carlo simulation methods with vague priors. (17) The model included random-effects at the level of lesions and patients, fully accounting for the correlation of lesion characteristics within patients and implicitly assigning analytical weights to each lesion depending on the number of struts observed per lesion. The pre-specified primary endpoint of the sub-study was the difference in percentage of uncovered struts between BES and SES. Assuming average numbers of 1.5 lesions per patients and 160 struts per lesion and a design factor of 1.5 (defined as standard error derived from the Bayesian hierarchical random-effects model assuming clustering of lesions within patients divided by the crude standard error derived from conventional analysis assuming independency of lesions), we estimated that the inclusion of 22 patients per group would yield greater than 90% power to detect a difference in uncovered struts of 4% between BES and SES at a two-sided type I error of 0.05. Secondary endpoints were the differences in percentage of malapposed struts and in percentage of malapposed and uncovered struts. After logarithmic transformation of the data, we also estimated the difference between groups in neointimal thickness. Finally, we determined differences in the percentage of lesions with any struts with unfavourable outcome, with at least 5%, and with at least 10% of struts with unfavourable outcome, with unfavourable outcomes defined in accordance with definitions used for primary and secondary endpoints.

Differences between groups were estimated from the median of the posterior distribution of the 50,001 to 100,000 iteration, with the initial 50,000 iterations discarded as 'burn-in'. We derived 95% credibility intervals (95% CI) from the 2.5th and 97.5th percentiles of the posterior

distribution, also calculating two-sided p-values from the posterior distribution. 95% credibility intervals and p-values from posterior distributions can be interpreted similarly to conventional 95% confidence intervals and p values. Sensitivity analyses were adjusted for pre-procedure lesion length, reference vessel diameter, number of implanted study stents and presence of stent overlap. Finally, we restricted the analysis of the primary endpoint to patients with analyzable OCT data who had been randomly allocated to angiographic follow-up. Baseline characteristics of lesions, procedural results and angiographic follow-up data were analyzed as previously described, (8) using mixed maximum-likelihood logistic and linear regression models that allowed for correlation of more than one lesion within patients. Statistical analyses were performed using WinBUGS version 1.4.3 (Imperial College and MRC, United Kingdom) and Stata, version 10.0 (StataCorp, College Station, TX).

Results

Figure 1 shows the profile of the OCT sub-study. Twenty eight patients allocated to BES and 32 patients allocated to SES were eligible for the sub-study, and 26 and 30 patients respectively received OCT, all undertaken using the non-occlusive technique. Figure 2 presents some examples of the spectrum of OCT findings observed. Six patients in the BES and 4 patients in the SES group were excluded from the analysis because of low quality of OCT images. Twenty patients were included in the analysis in the BES group (29 lesions with 4592 struts) and 26 patients in the SES group (35 lesions with 6476 struts).

Baseline clinical and angiographic characteristics of the 46 patients are presented in Tables 1 and 2. Characteristics were similar in both groups, except for differences in the percentage of patients with small-vessel disease and in reference vessel and minimal lumen diameter at lesion level. In addition, more patients had a history of hypercholesterolemia in the SES group, even though overall cholesterol levels were comparable between groups (4.31 mmol/l in the BES versus 4.17 mmol/l in the SES group, difference -0.13, 95% confidence interval -0.90 to 0.63, p=0.73). The left anterior descending artery (LAD) and the right coronary artery (RCA) were the most frequently imaged vessels (Table 2). Procedural results were similar between groups, with a trend towards smaller minimal lumen diameters in-stent in patients allocated to SES (Table 3). Control angiography was performed at a median of 9.1 months (interquartile range 9.0 to 9.3 months). Table 4 presents results of angiographic follow-up, which were similar between groups and compatible with results of the main trial. (8)

OCT analysis

Figure 3 shows a graphical representation of stent strut coverage in lesions. Table 5 (top) presents results of the principal analysis of the primary endpoint. A total of 83 out of 4592 struts in 29 lesions were uncovered in the BES group (weighted estimate 0.6%, 95% CI 0.2 to 1.6%) and 407 out of 6476 struts in 35 lesions were uncovered in the SES group (2.1%, 95% CI 0.9 to 4.4), with a weighted difference between groups of -1.4% (95% CI -3.7 to 0.0%, p=0.04). Results were similar after adjustment for pre-procedure lesion length, reference vessel diameter, number of implanted study stents and presence of stent overlap (difference -2.0%, 95% CI -5.7 to -0.1, Table 6). There were 2 and 8 lesions that had ≥10% uncovered struts in BES and SES groups, respectively (difference -10.2%, 95% CI -30.9 to 1.3%, p 0.08), 3 and 15 lesions had ≥5% uncovered struts (difference -33.1% 95% CI -61.7 to -10.3% p <0.01) and 17 and 24 lesions had any uncovered struts (difference -11.1%, 95% CI -44.8 to 19.7% p 0.48). A total of 28 and 86 struts were malapposed in BES and SES groups, respectively (difference -0.2%, 95% CI -0.8 to

0.2%, p=0.19). Results were similar in adjusted analyses (difference -0.3%, 95% CI -0.6 to 0.0% p 0.08, Table 6). A total of 0 and 1 lesions had ≥10% malapposed struts in BES and SES groups, respectively (difference -0.4%, 95% CI –7.6 to 0.0% p 0.05), 1 and 6 lesions had ≥5% malapposed struts (difference -8.4% 95% CI -25.5 to -0.1% p 0.05) and 11 and 17 lesions had any malapposed struts (difference -13.7%, 95% CI -47.8 to 20.9% p 0.42). A total of 11 and 41 struts were both malapposed and uncovered in the BES and SES groups, respectively (difference -0.1%, 95% CI -0.4 to 0.0%, p=0.13). Results were similar in adjusted analyses (difference -0.2%, 95% CI -0.6 to 0.0% p 0.08, Table 6). None of the lesions had ≥10% struts, which were both malapposed and uncovered, 0 and 2 lesions had ≥5% (difference -5.1% 95% CI -20.1 to 1.5% p 0.12) and 6 and 14 lesions had any malapposed and uncovered struts (difference -21.0%, 95% CI -48.7 to 5.9% p 0.12).

Figure 4 presents the distribution of neointimal thickness across all struts. For 67% of all struts, tissue thickness was below 100 micron, the resolution of IVUS. The average tissue thickness was 67.6 μm (95% CI 56.0 to 81.7μm) in the BES and 57.1μm (95% CI 48.4 to 67.6μm) in the SES group, respectively (p=0.19).

Safety of OCT

Mean contrast volume used for coronary flushing was 37.4 ml (SD 12.3). There were no cases of contrast-induced nephropathy. In 1 patient, contrast flushing during OCT imaging induced ventricular fibrillation. Sinus rhythm was promptly restored following external cardioversion. Deep guide catheter intubation during contrast injection was thought to have caused the arrhythmia. The patient made an uneventful recovery and was discharged as planned the following day.

Discussion

The LEADERS trial is the first, large, multi-center randomized study to incorporate an OCT sub-study to help address the issue of tissue coverage following DES implantation. Quantitative coronary angiography (QCA) and IVUS lack the spatial resolution to accurately quantify tissue coverage. Hence, OCT, with a resolution of approximately 15 μm, is ideal for the purpose of comparing presence and extent of tissue coverage in the 2 stents studied.

The SES was the first DES to be introduced and is covered by two layers of durable polymer with a top coating for slow drug release. The availability of up to 8 years clinical follow-up after SES implantation and evidence of greater efficacy in reducing restenosis and late lumen loss in direct or indirect comparison with other DESs (9,18-20) has made SES the current gold standard of treatment. Pathological follow-up examinations at autopsy following implantation of a SES have shown that neointimal healing is still incomplete after 16 months, (21) a specific problem which may prolong the period of thrombotic risk. Struts directly exposed to the blood flow may be surrogates for thrombotic risk given that pathological studies have identified a lack of tissue healing in cases of stent thrombosis. (6,22) Furthermore, exposed struts, particularly if malapposed, are also likely to result in flow disturbance which can be pro-thrombotic. (23,24)

The polymer coating as a system for drug delivery has been implicated as being pro-inflammatory and retard healing and coverage. (22) A number of OCT results after implantation of DES have been reported (13,14,25-27) Takano et al,[10] undertook OCT examination at 3 months and 2 years following SES implantation in 21 patients. The thickness of tissue at 2-years was greater than that at 3-months (71±93μm versus 29±41μm, respectively; p<0.001). Frequency of struts with no visible coverage was lower in the 2-year group compared to the 3-month group (5% versus 15%, respectively; p< 0.001), with a prevalence of patients with uncovered struts between 3 months

and 2 years falling from 95% to 81%, respectively. Matsumoto et al[11] examined 57 SES in 34 patients at 6 months after implantation and found the median tissue thickness to be 52.5μm with 89% of struts covered and 11% exposed. These studies are limited by the small sample size and by the fact the population consisted almost exclusively of single short SES because of the limitations of the balloon occlusive technique used for OCT image acquisition.
Recently, results from a randomized trial of OCT in long lesions requiring overlap stenting were presented. (26) In 22 patients receiving SES, 6% of all struts had no visible coverage at 6 month follow-up. In our study, 407 out of 6476 struts were uncovered among patients allocated to SES, which corresponds to approximately 6% in a naive analysis ignoring the clustered nature of the data. Accounting for the nature of the data in a Bayesian hierarchical random-effects model yields a lower estimate of 2.1% is observed in this study, which suggests that the type of analysis has dramatic effects not only on the precision of estimates, but also on their estimated magnitude.
The duration of dual anti-platelet therapy after SES already extends far beyond the 2–3 months of treatment required in the initial SES studies. (8) The empirical solution of one year is recommended by the ACC/AHA/SCAI guidelines but this recommendation partially contradicts the ESC Guidelines of PCI (6-12 months) and is often not adhered to by individual cardiologists. The duration of dual anti-platelet treatment is often prolonged to 2 or more years or lifelong because physicians fear that the extension of percutaneous treatment to complex lesions facilitated by the low restenosis rate of SES has increased the risk of late stent thrombosis, (28-32), particularly with the use of multiple stents and kissing stents for bifurcation lesions.
We exclusively used a non-occlusive method to acquire OCT images performed during contrast flush via the guiding catheter with no requirement for the cumbersome occlusion balloon method used in all the other published studies. This ensured that the broad 'all-comer' inclusion criteria for the LEADERS trial were reproduced in the OCT sub-study in which ostial, proximal and multi-vessel stenting were all imaged by OCT.
The OCT results of our study in all comers with great lesion complexity confirms previous studies by showing that only a small percentage of SES struts are not covered with tissue 9 months after SES implantation. Still, only a minority of lesions after SES implantation had full lesion coverage at 9 months and half the lesions treated had less than 95% tissue coverage. The absence of longitudinal studies correlating intimal coverage of DES and late stent thrombosis is the main limitation of this and other OCT studies at this stage. Although OCT has a high resolution permitting clear visualization of the tissue surrounding stent struts, we can only hypothesize as to its exact composition, particularly around unapposed struts. With its homogenous, highly reflective appearance, it is likely in keeping with neointimal proliferation (especially at 9 month follow-up) rather than fibrin or unendothelialized tissue which typically has a heterogeneous appearance.

Contemporary DES technologies are now geared toward eliminating the potential causes of poor tissue coverage and hence, to develop a stent that has similar anti-proliferative properties to the first generation SES but with the added advantage of no or a lower risk of late stent thrombosis. The low incidence of stent thrombosis with first generation DES also means that comparison studies need thousands of patients and several years of follow-up to show differences in clinical outcome and this makes any surrogate end-point highly valuable.

The BES did not differ from SES in the quantity of tissue overlying the stent struts (67.6 □ m compared with 57.1□□ m for the SES, p=0.19), suggesting similar efficacy in preventing restenosis to SES, as confirmed by the results of the main study. (8) The BES contained fewer exposed stent struts, which translated into more than 95% of the stents showing near complete coverage versus less than 2/3 in the SES group. These results suggest that better intimal coverage may be achieved with the BES compared with the SES. This difference may have a bearing on long-term thrombotic risk and may help address the vexing issue of the optimum duration of dual anti-platelet therapy while implicating the polymer as a potential source of failure to endothelialize stent struts long-term.

The presence of the abluminal coating and the biodegradable polymer is not the only reason which possibly explained this difference. The better apposition observed at 9 month follow-up can be explained by fewer instances of late acquired malapposition due to the absence of hypersensitivity reaction against the biodegradable polymer. It may also reflect a better initial apposition immediately after stent implantation, allowed by the thinner more pliable struts and different stent design. A previous study using OCT immediately following SES or paclitaxel-eluting stent (PES, Taxus, Boston Scientific, Natick, US) implantation found a significantly higher proportion of SES struts to be malapposed compared with the PES. (33) This is likely, in part, to be due to the closed cell design and the thicker strut profile of the SES. (33)

Study limitations

Stent strut coverage is not a clinical outcome, but only a surrogate for long-term stent thrombosis and safety. The presence or absence of neointimal coverage is limited by the resolution of OCT and struts reported as bare could have a very thin covering of tissue (<10μm), though the biological protection offered by such a thin coverage is debatable. (34) Furthermore, the number of patients included was small, enrolled only in two centers and differences in patient and lesion characteristics may have clouded our conclusions despite the randomized nature of the trial and the robustness of results to adjusting for lesion characteristics.

The choice of a 9 month OCT examination was empiric and in line with the follow-up arm of the main LEADERS trial. An earlier OCT assessment may have helped to assess the rapidity of tissue coverage while a later examination may have offered more relevant information for the process of very late (>1 year) stent thrombosis. A recent OCT follow-up study with SES confirmed the presence of ongoing uncovered stent struts even at 2 years follow-up indicating that failure of early tissue coverage might become a permanent observation. (7) OCT was not carried out immediately following stent implantation so that the mechanism of malapposition of struts cannot be accurately determined so that we are unable to distinguish persisting or late acquired malapposition.

Multilevel analysis was used in this study as standard statistical approaches are inappropriate in data with significant clustering. In fact, even though more than 10,000 strut-related data points were available, these were not independent observations (struts within the same lesion and lesions within the same patient are likely to be similar), thus violating a fundamental assumption of classic statistical tests. Formal sample size calculations are difficult in this situation and no power calculation algorithm exists, which is based on generally accepted assumptions regarding intra-cluster correlation and design factors.

Conclusions

Strut coverage appears to be more complete in patients allocated to BES as compared with SES. The impact of this difference on clinical outcome and, in particular, on the risk of late stent thrombosis, is yet to be determined.

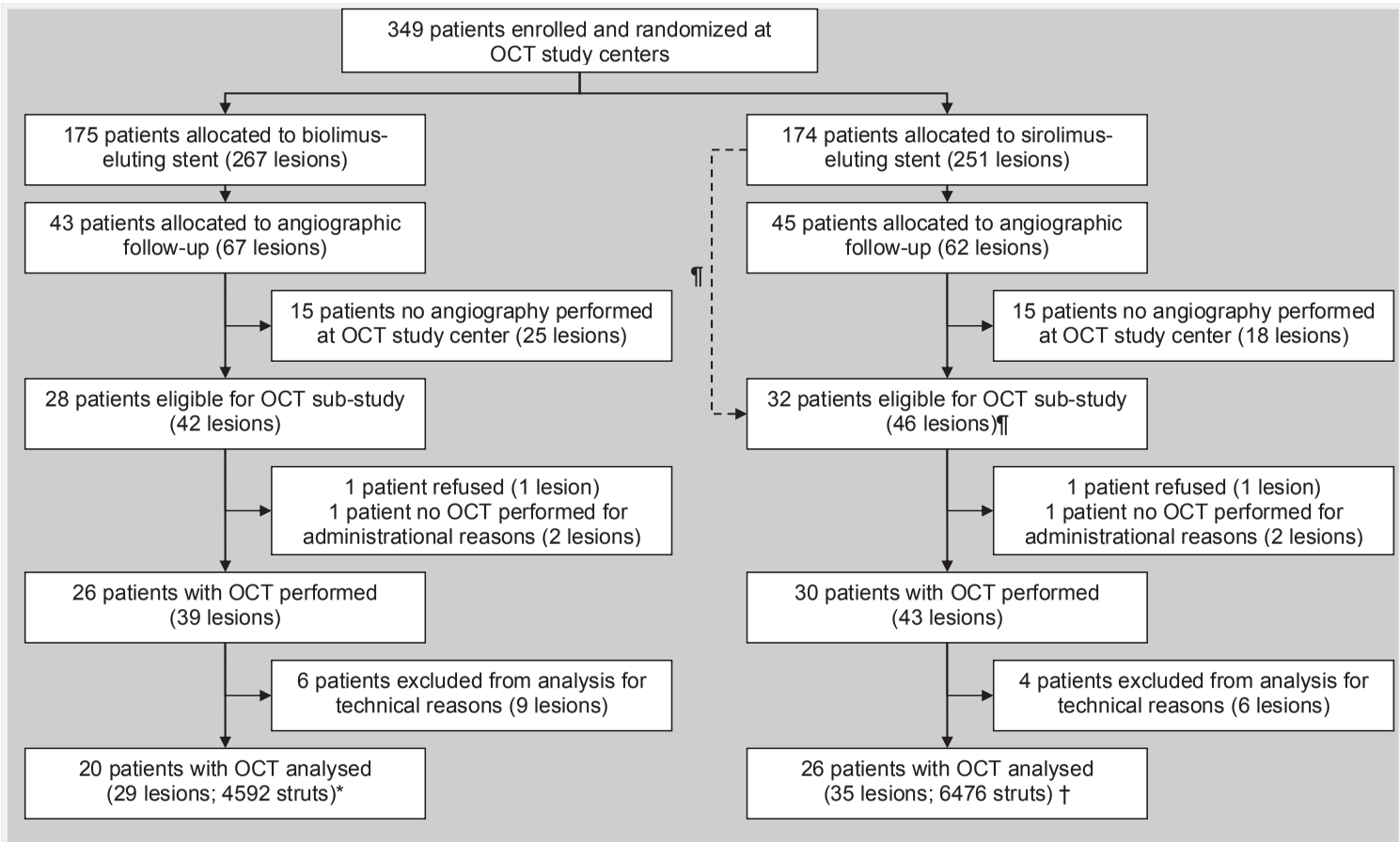

Figure 1: Trial protocol: ¶2 patients allocated to SES and clinical follow-up only (2 lesions) had a clinically indicated angiography and underwent OCT; *1 patient allocated to BES (2 lesions) had 1 lesion excluded from the analysis for technical reasons; †2 patients allocated to SES (4 lesions) had 1 lesion excluded each from the analysis for technical reasons.

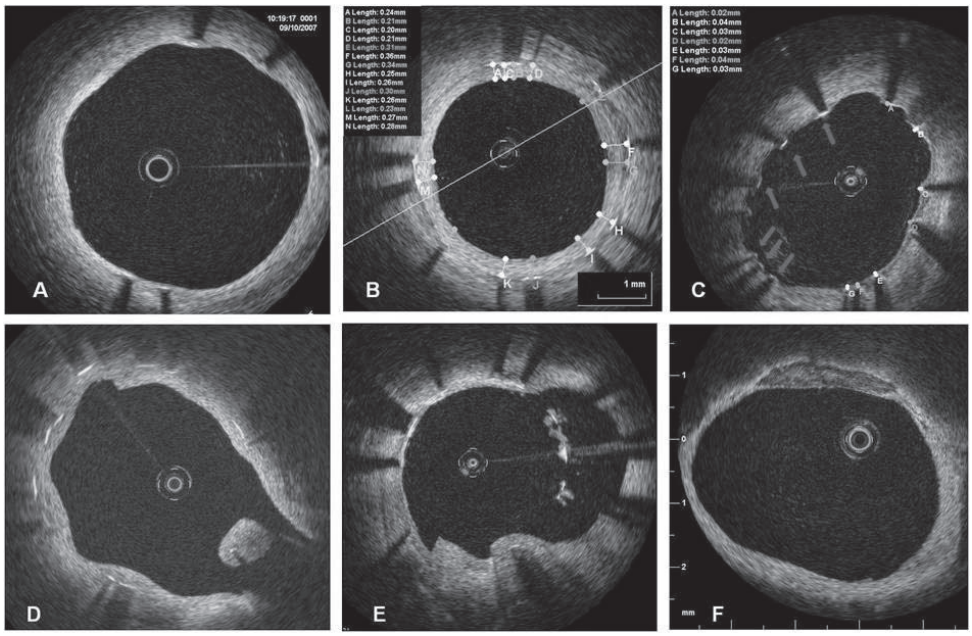

see colour section

Figure 2: Examples of OCT findings

A. This 73 year old male received a biolimus-eluting stent (BES) 9 months prior to the right coronary artery. The stent is seen covered by a thin, uniform layer of tissue overlying all stent struts that are well apposed to the vessel wall.

B. Offline OCT analysis. A total of 14 stent struts are visible in this cross section with the observer having measured the thickness of tissue overlying each of the struts, expressed in the colored panel (top left) in mm. The mean neointimal thickness in this frame was 0.27mm (270μm).

C. Sirolimus-eluting stent (SES) struts are observed circumferentially. Struts between 7 and 11 o'clock are apposed but uncovered by tissue. Struts from 1 – 5 o'clock are observed covered with a very thin layer of tissue (mean thickness 0.03mm or 30μm). The stent was implanted in a patient who received 2 SES to the mid left anterior descending artery (LAD) 9 months prior following a presentation with a non-ST elevation myocardial infarction. He was asymptomatic at 9 month follow-up.

D. Nine month follow-up of a BES implanted in the LAD across the diagonal bifurcation. A solitary strut is observed (arrow) malapposed at the level of the carina. The strut was seen covered by a thick, uniform and homogenous tissue.

E. This OCT pullback frame from a 78 year-old male with prior stenting to the LAD/diagonal bifurcation with a SES. Struts are observed (1-3 o'clock) to be malapposed to the vessel wall with a heterogeneous tissue with different signal attenuations that may represent thrombotic material. The patient was asymptomatic at 9 month follow-up and on dual anti-platelet therapy.

F. Left main coronary artery OCT. This patient had a proximal LAD stent implanted 9 months prior. We extended the pullback beyond the stent into the left main coronary artery which demonstrates a well demarcated, non-flow limiting, low attenuation plaque (12 o'clock) consistent with calcium. Our sub-study exclusively used a non-occlusive technique for OCT imaging which requires pullback of the image wire during simultaneous flush of contrast via the guiding catheter. This is a significant advance over the traditional method of OCT imaging in which a proximally positioned balloon is inflated during image acquisition. Hence, ostial and proximal segments of coronary arteries were all able to be imaged thereby supporting the 'all comer' design of the LEADERS trial without any OCT anatomical exclusions.

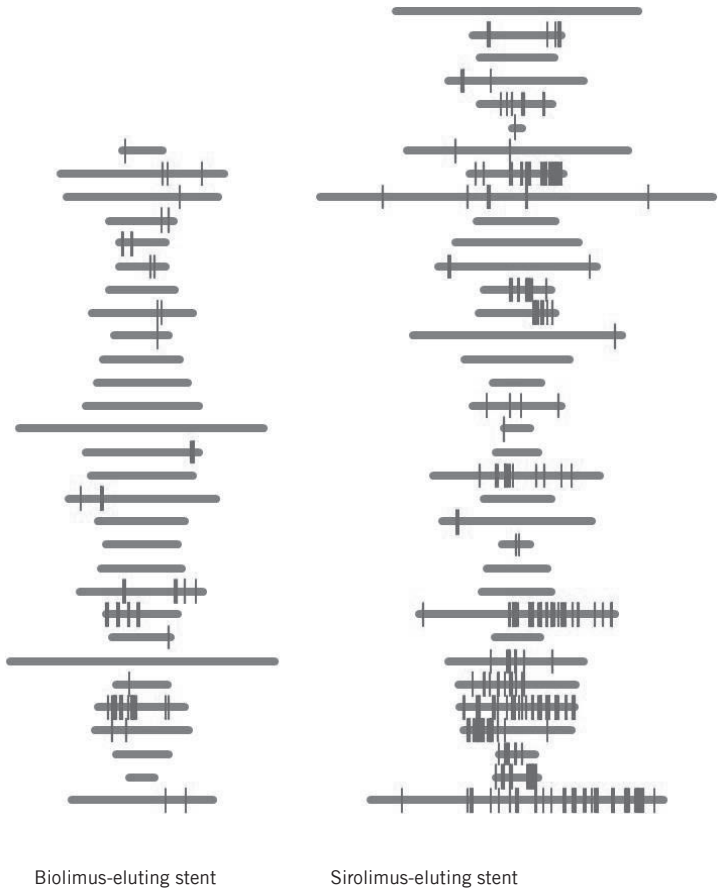

Figure 3: Graphical representation of stent coverage in lesions.

Grey horizontal bars represent lesions. Each uncovered strut is represented by a red line.

see colour section

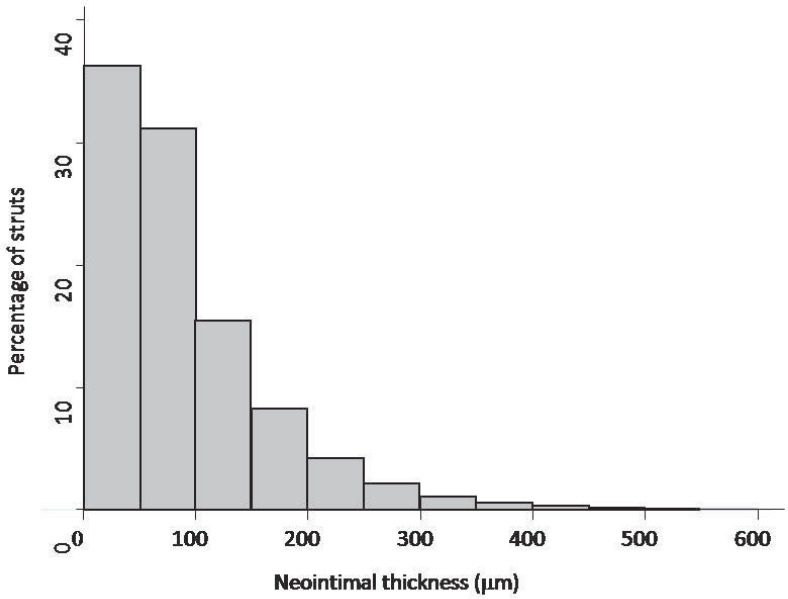

Figure 4: Distribution of neointimal thickness.

Note that dimensions <100µm are below the resolution of intravascular ultrasound (IVUS).

see colour section

Table 1: Baseline characteristics of patients

	Biolimus-eluting stent (N = 20)	**Sirolimus-eluting stent (N = 26)**	**p value**
Age (years)	64.9 (10.2)	63.0 (11.4)	0.56
Males	14 (70.0%)	18 (69.2%)	0.96
Diabetes mellitus	4 (20.0%)	5 (19.2%)	0.95
Diabetes requiring insulin	2 (10.0%)	1 (3.9%)	0.40
Hypertension	10 (50.0%)	17 (65.4%)	0.29
Hypercholesterolemia	9 (45.0%)	20 (76.9%)	0.03
Current smoker	5 (25.0%)	10 (38.5%)	0.33
Family history of CAD	11 (55.0%)	17 (65.4%)	0.47
History of MI	5 (25.0%)	9 (34.6%)	0.96
History of PCI	3 (15.0%)	6 (32.1%)	0.49
With drug-eluting stent	2 (10.0%)	1 (3.9%)	0.40
Previous CABG	1 (5.0%)	4 (15.4%)	0.26
Stable angina pectoris	12 (60.0%)	16 (61.5%)	0.92
Acute coronary syndrome	8 (40.0%)	10 (38.5%)	0.43
Unstable angina	1 (5.0%)	4 (15.4%)	
Non-ST-elevation MI	2 (10.0%)	2 (7.7%)	
ST-elevation MI	5 (25.0%)	4 (15.4%)	
Multi-vessel disease	5 (25.0%)	3 (11.5%)	0.23
Small-vessel disease (RVD < 2.75 mm)	8 (40.0%)	21 (80.8%)	< 0.001
Study lesions per patient			0.37
One	12 (60.0%)	17 (65.4%)	
Two	7 (35.0%)	7 (26.9%)	
Three	0 (0.0%)	2 (7.7%)	
Four or more	1 (5.0%)	0 (0.0%)	
De-novo lesions only	18 (90.0%)	25 (96.2%)	0.40
Long lesions (> 20 mm)	7 (35.0%)	13 (50.0%)	0.31
Number of lesions per patient	1.5 (0.8)	1.4 (0.6)	0.71
Off-label use	14 (70.0%)	23 (88.5%)	0.12

Data are mean (SD) or number (%). CAD = coronary artery disease. PCI = percutaneous coronary intervention. CABG = coronary artery bypass grafting. MI = myocardial infarction. RVD = reference vessel diameter. p values are from t-test for continuous and chi2-test for categorical data.

Table 2: Baseline characteristics of lesions

	Biolimus-eluting stent	Sirolimus-eluting stent	p value
Target lesion coronary artery			0.15
Left main	0/29 (0.0%)	0/35 (0.0%)	
Left anterior descending	15/29 (51.7%)	12/35 (34.3%)	
Left circumflex	3/29 (10.3%)	10/35 (28.6%)	
Right	11/29 (37.9%)	13/35 (37.1%)	
Bypass graft	0/29 (0.0%)	0/35 (0.0%)	
De novo lesions	27/29 (93.1%)	34/35 (97.1%)	0.45
Lesion length (mm)			
Assessed*	14.3 (14.5)	13.3 (9.1)	0.80
Assessed or estimated†	17.3 (14.7)	20.9 (19.0)	0.41
Reference vessel diameter (mm)†	2.7 (0.6)	2.4 (0.5)	0.02
Minimal lumen diameter (mm)§	0.93 (0.60)	0.63 (0.53)	0.04
Stenosis (% lumen diameter) §	66.9 (20.3)	73.4 (21.0)	0.20
Total occlusion	5/28 (17.9%)	9/34 (26.5%)	0.42
Severe Calcification	3/29 (10.3%)	3/33 (9.1%)	0.87
Pre-procedure TIMI flow			0.30
Grade 3	5/28 (17.9%)	9/34 (26.5%)	
Grade 2	1/28 (3.6%)	3/34 (8.8%)	
Grade 3	1/28 (3.6%)	4/34 (11.8%)	
Grade 4	21/28 (75.0%)	18/34 (52.9%)	

Data are mean (SD) or number of lesions/number assessed (%). Assessments were not possible in all 64 lesions with angiographic assessments; therefore the number of lesions differs according to outcome. TIMI = thrombolysis in myocardial infarction. * 21 lesions assessed in the biolimus-eluting stent group and 22 in the sirolimus-eluting stent group. † 29 lesions assessed in the biolimus-eluting stent group and 35 in the sirolimus-eluting stent group. § 27 lesions assessed in the biolimus-eluting stent group and 34 in the sirolimus-eluting stent group

Table 3: Procedural results

	Biolimus-eluting stent	Sirolimus-eluting stent	Difference	
			Estimate (95% CI)	p value
No. of study stents per lesion*	1.4 (0.7)	1.7 (0.9)	-0.3 (-0.7 to 0.1)	0.18
Maximal stent diameter per lesion (mm)*	3.1 (0.4)	2.9 (0.5)	0.2 (-0.1 to 0.4)	0.17
Total stent length per lesion (mm)*	26.7 (18.6)	33.5 (24.3)	-5.7 (-19.4 to 7.0)	0.38
Direct stenting	15/29 (51.7%)	14/35 (40.0%)	11.7 (-10.9 to 34.4)	0.31
Implantation of study stent	29/29 (100.0%)	35/35 (100.0%)	0 (n/e)¶	1.00
Device success	29/29 (100.0%)	35/35 (100.0%)	0 (n/e)¶	1.00
Lesion success	29/29 (100.0%)	35/35 (100.0%)	0 (n/e)¶	1.00
Minimal lumen diameter (mm)*				
In-stent	2.40 (0.47)	2.22 (0.43)	0.18 (-0.05 to 0.40)	0.13
In-segment	2.06 (0.55)	1.95 (0.45)	0.09 (-0.17 to 0.35)	0.49
Diameter stenosis (%)*				
In-stent	13.13 (6.37)	15.18 (6.97)	-2.12 (-5.74 to 1.50)	0.25
In-segment	23.24 (8.27)	22.90 (7.70)	0.64 (-3.54 to 4.83)	0.76
Acute gain (mm)†				
In-stent	1.50 (0.57)	1.58 (0.45)	-0.05 (-0.36 to 0.25)	0.73
In-segment	1.15 (0.63	1.31 (0.44)	-0.17 (-0.50 to 0.15)	0.30

Data are mean (SD) or number of lesions/number assessed (%), unless otherwise stated. Mixed maximum-likelihood logistic regression models were used for comparisons between groups for dichotomous variables and mixed maximum-likelihood linear regression models for continuous variables to account for the correlation of multiple lesions within patients. * 29 lesions assessed in the biolimus-eluting stent group and 35 in the sirolimus-eluting stent group. † 27 lesions assessed in the biolimus-eluting stent group and 34 in the sirolimus-eluting stent group. n/e confidence interval for difference in percentages could not be estimated.

Table 4: Angiographic follow-up results

	Biolimus-eluting stent	Sirolimus-eluting stent	Difference	
			Estimate (95% CI)	p value
Reference vessel diameter (mm)*	2.84 (0.44)	2.60 (0.57)	0.23 (-0.05 to 0.52)	0.11
Minimal lumen diameter (mm)				
In-stent	2.24 (0.69)	2.03 (0.57)	0.19 (-0.15 to 0.53)	0.27
In-segment	2.01 (0.63)	1.83 (0.54)	0.15 (-0.17 to 0.47)	0.37
Diameter stenosis (%)†				
In-stent	21.54 (19.51)	21.89 (13.56)	-0.10 (-9.21 to 9.01)	0.98
In-segment	27.85 (17.87)	27.55 (12.33)	0.69 (-7.61 to 8.99)	0.87
Late loss (mm) †				
In-stent	0.16 (0.41)	0.18 (0.39)	0.00 (-0.22 to 0.22)	0.99
In-segment	0.06 (0.35)	0.09 (0.36)	-0.03 (-0.22 to 0.16)	0.77
Binary restenosis†				
In-stent	2/29 (6.9%)	1/33 (3.0%)	3.9 (-7.1 to 14.9)	0.49
In-segment	2/29 (6.9%)	2/33 (6.1%)	0.8 (-11.4 to 13.1)	0.89

Data are mean (SD) or number of lesions/number assessed (%). Angiographic assessments were not possible in all lesions, therefore the number of lesions differs according to outcome. 95%-CI and P-values are two-sided, from superiority testing. 29 lesions were assessed in the biolimus-eluting stent group and 35 in the sirolimus-eluting stent group unless indicated otherwise. *28 lesions assessed in the biolimus-eluting stent group and 33 in the sirolimus-eluting stent group. †29 lesions assessed in the biolimus-eluting stent group and 33 in the sirolimus-eluting stent group.

Table 5: Results of principal analyses

	Biolimus-eluting stent	**Sirolimus-eluting stent**	**Difference in percentage**	
	Percentage (95% CI)	Percentage (95% CI)	Estimate (95% CI)	p value
Uncovered struts	0.6 (0.2 to 1.6)	2.1 (0.9 to 4.4)	-1.4 (-3.7 to 0.0)	0.04
Lesions with				
at least 10% uncovered struts	2.2 (0.2 to 12.1)	13.3 (3.4 to 33.5)	-10.2 (-30.9 to 1.3)	0.08
at least 5% uncovered struts	3.8 (0.4 to 16.9)	38.3 (16.4 to 65.5)	-33.1 (-61.7 to -10.3)	<0.01
any uncovered struts	63.3 (35.2 to 86.4)	74.9 (51.7 to 91.8)	-11.1 (-44.8 to 19.7)	0.48
Malapposed struts	0.2 (0.1 to 0.5)	0.4 (0.2 to 1.0)	-0.2 (-0.8 to 0.2)	0.19
Lesions with				
at least 10% malapposed struts	0.0 (0.0 to 0.3)	0.5 (0.0 to 7.6)	-0.4 (-7.6 to 0.0)	0.05
at least 5% malapposed struts	0.9 (0.0 to 8.2)	10.0 (2.2 to 27.2)	-8.4 (-25.5 to -0.1)	0.05
any malapposed struts	33.5 (12.3 to 60.1)	47.8 (24.0 to 72.4)	-13.7 (-47.8 to 20.9)	0.42
Malapposed and uncovered struts	0.1 (0.0 to 0.2)	0.2 (0.1 to 0.5)	-0.1 (-0.4 to 0.0)	0.13
Lesions with				
at least 10% malapposed and uncovered struts	0.0 (0.0 to 0.1)	0.0 (0.0 to 0.1)	0.0 (0.0 to 0.1)	0.70
at least 5% malapposed and uncovered struts	0.8 (0.0 to 7.4)	6.5 (1.2 to 21.8)	-5.1 (-20.1 to 1.5)	0.12
any malapposed and uncovered struts	12.9 (2.8 to 34.0)	35.5 (14.4 to 59.6)	-21.0 (-48.7 to 5.9)	0.12

4508 struts in 29 lesions assessed in the biolimus-eluting stent group and 6083 struts in 35 lesions in the sirolimus-eluting stent group. 95%-CI and P-values derived from Bayesian hierarchical models are two-sided, from superiority testing.

Table 6: Sensitivity analyses

	Biolimus-eluting stent	**Sirolimus-eluting stent**	**Difference in percentage**	
	Percentage (95% CI)	Percentage (95% CI)	Estimate (95% CI)	p value
Uncovered struts	0.7 (0.3 to 1.8)	2.7 (1.1 to 6.4)	-2.0 (-5.7 to -0.1)	0.04
Lesions with				
at least 10% uncovered struts	1.4 (0.1 to 10.6)	17.1 (3.4 to 45.1)	-14.7 (-43.3 to 0.0)	0.05
at least 5% uncovered struts	3.5 (0.3 to 18.1)	50.5 (20.1 to 80.2)	-45.5 (-76.9 to -14.3)	<0.01
any uncovered struts	70.0 (37.8 to 91.2)	80.5 (53.3 to 94.8)	-9.5 (-44.9 to 22.8)	0.54
Malapposed struts	0.2 (0.1 to 0.5)	0.5 (0.2 to 1.3)	-0.3 (-0.6 to 0.0)	0.08
Lesions with				
at least 10% malapposed struts	n/e	n/e	n/e	n/e
at least 5% malapposed struts	0.3 (0.0 to 4.2)	6.7 (0.8 to 26.3)	-5.9 (-25.5 to -0.2)	0.04
any malapposed struts	31.4 (9.2 to 64.2)	49.8 (20.1 to 78.7)	-16.9 (-56.5 to 24.6)	0.42
Malapposed and uncovered struts	0.1 (0.0 to 0.2)	0.3 (0.1 to 0.7)	-0.2 (-0.6 to 0.0)	0.08
Lesions with				
at least 10% malapposed and uncovered struts	n/e	n/e	n/e	n/e
at least 5% malapposed and uncovered struts	0.2 (0.0 to 3.7)	4.3 (0.6 to 22.5)	-3.8 (-21.9 to 0.2)	0.06
any malapposed and uncovered struts	12.3 (2.3 to 38.5)	37.8 (13.9 to 69.5)	-24.0 (-59.8 to 8.8)	0.14

4508 struts in 29 lesions assessed in the biolimus-eluting stent group and 6083 struts in 35 lesions in the sirolimus-eluting stent group. 95%-CI and P-values derived from Bayesian hierarchical model are two-sided, from superiority testing. All analyses are adjusted for pre-procedure lesion length, reference vessel diameter, number of implanted study stents and presence of stent overlap. n/e, could not be estimated

References

1. Serruys PW, Degertekin M, Tanabe K, et al. Intravascular ultrasound findings in the multicenter, randomized, double-blind RAVEL (RAndomized study with the sirolimus-eluting VElocity balloon-expandable stent in the treatment of patients with de novo native coronary artery Lesions) trial. Circulation 2002;106:798-803.
2. Degertekin M, Serruys PW, Foley DP, et al. Persistent inhibition of neointimal hyperplasia after sirolimus-eluting stent implantation: long-term (up to 2 years) clinical, angiographic, and intravascular ultrasound follow-up. Circulation 2002;106:1610-3.
3. Sonoda S, Morino Y, Ako J, et al. Impact of final stent dimensions on long-term results following sirolimus-eluting stent implantation: serial intravascular ultrasound analysis from the sirius trial. J Am Coll Cardiol 2004;43:1959-63.
4. Weissman NJ, Koglin J, Cox DA, et al. Polymer-based paclitaxel-eluting stents reduce in-stent neointimal tissue proliferation: a serial volumetric intravascular ultrasound analysis from the TAXUS-IV trial. J Am Coll Cardiol 2005;45:1201-5.
5. Park SJ, Shim WH, Ho DS, et al. A paclitaxel-eluting stent for the prevention of coronary restenosis. N Engl J Med 2003;348:1537-45.
6. Finn AV, Joner M, Nakazawa G, et al. Pathological correlates of late drug-eluting stent thrombosis: strut coverage as a marker of endothelialization. Circulation 2007;115:2435-41.
7. Takano M, Yamamoto M, Inami S, et al. Long-term follow-up evaluation after sirolimus-eluting stent implantation by optical coherence tomography: do uncovered struts persist? J Am Coll Cardiol 2008;51:968-9.
8. Stettler C, Allemann S, Wandel S, et al. Drug eluting and bare metal stents in people with and without diabetes: collaborative network meta-analysis. BMJ 2008;337:a1331.
9. Stettler C, Wandel S, Allemann S, et al. Outcomes associated with drug-eluting and bare-metal stents: a collaborative network meta-analysis. Lancet 2007;370:937-48.
10. King SB, 3rd, Smith SC, Jr., Hirshfeld JW, Jr., et al. 2007 focused update of the ACC/AHA/SCAI 2005 guideline update for percutaneous coronary intervention: a report of the American College of Cardiology/American Heart Association Task Force on Practice guidelines. J Am Coll Cardiol 2008;51:172-209.
11. Windecker S, Serruys PW, Wandel S, et al. Biolimus-eluting stent with biodegradable polymer versus sirolimus-eluting stent with durable polymer for coronary revascularisation (LEADERS): a randomised non-inferiority trial. Lancet 2008;372:1163-73.
12. Prati F, Cera M, Ramazzotti V, et al. From bench to bedside: a novel technique of acquiring OCT images. Circ J 2008;72:839-43.
13. Matsumoto D, Shite J, Shinke T, et al. Neointimal coverage of sirolimus-eluting stents at 6-month follow-up: evaluated by optical coherence tomography. Eur Heart J 2007;28:961-7.
14. Takano M, Inami S, Jang IK, et al. Evaluation by optical coherence tomography of neointimal coverage of sirolimus-eluting stent three months after implantation. Am J Cardiol 2007;99:1033-8.
15. Van Beusekom HM, Regar E, Peters I, Van der Giessen WJ. Long-term effects of endovascular radiation after balloon angioplasty: assessment by OCT and histology. In: Regar E, van Leeuwen AMGJ, Serruys PW, eds. Optical coherence tomography in cardiovascular research. London: Informa Healthcare, 2007.
16. Barlis P, Dimopoulos K, Tanigawa J, et al. Quantitative analysis of intracoronary optical coherence tomography measurements of stent strut apposition and tissue coverage. Int J Cardiol 2008;In press.
17. Spiegelhalter DJ, Abrams KR, Myles JP. Bayesian approaches to clinical trials and health care evaluation. Chichester: John Wiley & Sons, 2004.
18. Dibra A, Kastrati A, Mehilli J, et al. Paclitaxel-eluting or sirolimus-eluting stents to prevent restenosis in diabetic patients. N Engl J Med 2005;353:663-70.
19. Kastrati A, Dibra A, Eberle S, et al. Sirolimus-eluting stents vs paclitaxel-eluting stents in patients with coronary artery disease: meta-analysis of randomized trials. JAMA 2005;294:819-25.
20. Windecker S, Remondino A, Eberli FR, et al. Sirolimus-eluting and paclitaxel-eluting stents for coronary revascularization. N Engl J Med 2005;353:653-62.

21. Guagliumi G, Farb A, Musumeci G, et al. Images in cardiovascular medicine. Sirolimus-eluting stent implanted in human coronary artery for 16 months: pathological findings. Circulation 2003;107:1340-1.
22. Joner M, Finn AV, Farb A, et al. Pathology of drug-eluting stents in humans: delayed healing and late thrombotic risk. J Am Coll Cardiol 2006;48:193-202.
23. Davies PF, Spaan JA, Krams R. Shear stress biology of the endothelium. Ann Biomed Eng 2005;33:1714-8.
24. Dewey CF, Jr., Bussolari SR, Gimbrone MA, Jr., Davies PF. The dynamic response of vascular endothelial cells to fluid shear stress. J Biomech Eng 1981;103:177-85.
25. Chen BX, Ma FY, Luo W, et al. Neointimal coverage of bare-metal and sirolimus-eluting stents evaluated with optical coherence tomography. Heart 2008;94:566-70.
26. Guagliumi G, Musumeci G, Sirbu V, et al. A Prospective, Randomized, Controlled Study Using Optical Coherence Tomography to Evaluate Strut Coverage of Sirolimus-, Paclitaxel-, and Zotarolimus-Eluting Coronary Stents in Long Lesions Requiring Overlapping Transcatheter Cardiovascular Therapeutics. Washington, 2008.
27. Guagliumi G. Long-Term Strut Coverage of Paclitaxel Eluting Stents Compared with Bare-Metal Stents Implanted During Primary PCI in Acute Myocardial Infarction. A Prospective, Randomized, Controlled Study Performed with Optical Coherence Tomography. HORIZONS-OCT American Heart Association. New Orleans, 2008.
28. Iakovou I, Schmidt T, Bonizzoni E, et al. Incidence, predictors, and outcome of thrombosis after successful implantation of drug-eluting stents. Jama 2005;293:2126-30.
29. Kuchulakanti PK, Chu WW, Torguson R, et al. Correlates and long-term outcomes of angiographically proven stent thrombosis with sirolimus- and paclitaxel-eluting stents. Circulation 2006;113:1108-13.
30. Windecker S, Juni P. Safety of drug-eluting stents. Nat Clin Pract Cardiovasc Med 2008;5:316-28.
31. Windecker S, Meier B. Late coronary stent thrombosis. Circulation 2007;116:1952-65.
32. Schomig A, Dibra A, Windecker S, et al. A meta-analysis of 16 randomized trials of sirolimus-eluting stents versus paclitaxel-eluting stents in patients with coronary artery disease. J Am Coll Cardiol 2007;50:1373-80.
33. Tanigawa J, Barlis P, Dimopoulos K, Dalby M, Moore P, Di Mario C. The influence of strut thickness and cell design on immediate apposition of drug-eluting stents assessed by optical coherence tomography. Int J Cardiol 2008;doi:10.1016/j.ijcard.2008.05.069.
34. Finn AV, Nakazawa G, Joner M, et al. Vascular responses to drug eluting stents: importance of delayed healing. Arterioscler Thromb Vasc Biol 2007;27:1500-10.

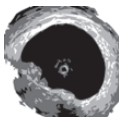

Chapter 12

A Randomised Optical Coherence Tomography Study of Coronary Stent Strut Coverage and Luminal Protrusion with Rapamycin-Eluting Stents

Phil Moore, Peter Barlis, Jonathan Spiro, Michael Roughton, Charles Isley, Carlo Di Mario, Rajesh Kharbanda, Miles Dalby

Objective: *We used optical coherence tomography (OCT) which has a resolution of <20μm to analyse thin layers of neointima in rapamycin-eluting coronary stents.*
Background: *Lack of neointimal coverage has been implicated in the pathogenesis of drug-eluting coronary stent (DES) thrombosis. Angiography and intracoronary ultrasound lack the resolution to examine this.*
Methods: *We conducted a randomised trial in patients receiving polymer-coated rapamycin-eluting stents (Cypher®, Cordis, Johnson & Johnson, Miami Fl, USA) and non-polymer rapamycin eluting stents (Yukon®, Translumina, Hechingen, Germany) to examine neointimal thickness, stent strut coverage and protrusion at 90 days. Twenty-four patients (n=12 for each group) underwent stent deployment and invasive follow-up at 90 days with OCT.*
Main outcome measure: *The primary end point was binary stent strut coverage. Co-primary end points were neointimal thickness and stent strut luminal protrusion.*
Results: *No patient had angiographic restenosis. For polymer-coated rapamycin-eluting and non-polymer rapamycin-eluting stents respectively, (mean (sd)), neointimal thickness was 77.2μm (25.6) versus 191.2μm (86.7) p<0.001. Binary stent strut coverage was 88.3% (11.8) versus 97.2% (6.1) p=0.030. Binary stent strut protrusion was 26.5% (17.5) versus 4.8%*
(8.6) p=0.001.
Conclusions: *Mean neointimal thickness for the polymer-coated rapamycin-eluting stent was significantly less than the non-polymer rapamycin-eluting stent but as a result coverage was not homogenous with >10% of struts being uncovered. High-resolution imaging allowed development of the concept of the protrusion index and >25% of struts protruded into the vessel lumen with the polymer-coated rapamycin-eluting stent compared with <5% with the non-polymer rapamycin-eluting stent. These findings may have important implications for the risk of stent thrombosis and therefore future stent design.*

Polymer-coated drug-eluting coronary stents reduce restenosis and repeat revascularisation.(1,2) Lack of endothelial coverage, however, has been reported as the most powerful predictor of stent thrombosis in post mortem series (3) which in turn carries a high mortality. (4,5,6) Coronary angiography and intravascular ultrasound lack the resolution to assess thin layers of coverage. In contrast, optical coherence tomography (OCT) is safe, feasible, has a resolution of <20μm, and has been correlated well with histological analysis of neointima making it suitable for this application. (7,8,9)

Methods

We undertook a randomised study comparing a polymer-coated rapamycin-eluting stent (Cypher®, Cordis, Johnson & Johnson, Miami, FL, USA) with a non-polymer rapamycin-eluting stent (Yukon®, Translumina, Hechingen, Germany) to examine whether one device was superior to the other with regard to the primary and co-primary end points of binary stent strut coverage, neointimal thickness, and luminal strut protrusion. Approximately 200 patients were screened for trial participation between October 2006 and July 2007, and 51 were randomised and underwent stent deployment as part of the study. Twenty-four patients completed the trial with 90-day angiography and OCT. Relatively slow recruitment and significant drop out were due in large part to patient concerns about the risks and inconvenience associated with follow up catheterisation and in particular the fact that OCT was a relatively new technology. Blocked randomisation was carried out by the use of sealed envelopes, with patients per block allocated in a 1:1 ratio between the polymer coated and non-polymer rapamycin-eluting stents. Follow-up used 90-day angiography with quantitative coronary angiography and OCT. Inclusion criteria were; age 18-75 years, stable angina pectoris or acute coronary syndrome pain-free for 24 hours. Exclusion criteria were: ST-elevation myocardial infarction, cardiogenic shock, chronic total occlusion, bifurcation procedure, left ventricular ejection fraction <30% and renal impairment (serum creatinine >200umol-1). Stent deployment was performed using angiography but without intracoronary imaging. Patients received loading doses of aspirin (300mg) and clopidogrel

(600mg) at least 2 hours before the index procedure if they were not on maintenance therapy, followed by planned lifelong aspirin 75mg daily and clopidogrel 75mg daily for a minimum of one year.
Ninety days was used as the study end point for two reasons. Firstly, early reports of OCT in a non-randomised series had presented data from 2 month follow up demonstrating a large and significant difference between stent strut coverage with bare metal and sirolimus eluting polymer coated stents on which the power calculation was based, (10) and secondly there was a clinical desire to gain mechanistic insight into the potential safety of the withdrawal of clopidogrel at this relatively early time in non-polymer rapamycin eluting stents, as compared with the usually recommended one year for polymer coated rapamycin eluting stents.

Optical coherence tomography image acquisition

OCT was performed with the M2 system (LightLab Imaging Inc., Westford, MA, USA) as previously described. (11) Briefly, an over-the-wire proximal occlusion balloon catheter (Helios™, Goodman Inc, Nagoya, Japan) was deployed and the imaging catheter advanced (ImageWire™, LightLab Inc., Westford, MA, USA) with the light source distal to the stent. The occlusion balloon was inflated to a maximum of 0.7 atmospheres for a maximum of 30 seconds with continual electrocardiographic monitoring whilst the coronary artery was infused with Ringer's lactate at 0.5-1.0ml/sec using a power injector (Mark V ProVis, Medrad, Inc. Indianola, PA, US). A motorised pullback at 1mm/sec was performed acquiring cross sectional images at 15.6 frames/sec. Frames analysed were those occurring at every 1mm (15 frames). In addition, the 2 adjacent frames both proximal and distal to the frame were also assessed to confirm tissue coverage or absence of tissue and apposition. If the stent could not be visualized with a single pullback (due to a long stent or patient intolerance), scanning was prematurely terminated and the pull-back stopped with a second pull-back started from the site where it was interrupted. Anatomic landmarks such as side branches, calcifications or stent overlap segments were used for longitudinal orientation.

Optical Coherence Tomography Analysis

OCT data analysis was performed offline using proprietary software (LightLab Imaging, Westford, Massachusetts, US). Analysis of angiographic images, QCA (Medis, Leiden, NL) and OCT was performed by experienced investigators (PB, PM). Regarding blinding, the very different presentation of the two stent types (including in particular the hub of the devices, and the angiographic appearances of the markers) made it impractical to blind the operators, however for the angiographic and OCT analysis investigators were blinded to the randomisation arm. The analyst was blinded to all clinical and procedural variables and thus, did not have any knowledge of stent sizes or stent type. When a strut was felt to be 'malapposed', the distance from the strut to lumen surface was recorded. Only after completion of the analysis was the stent type used to then confirm presence or absence of malapposition by incorporating the actual strut thickness for the 2 stents used. This is required as OCT is unable to penetrate through metal and thus can only visualise the luminal aspect of the stent strut. A blooming effect can result from hyperdense signals arising from metal struts. It is an optical property of the inferometer and hence an inevitable part of OCT. We did observe this and on the few occasions it was apparent, a frame immediately proximal or distal was selected without this effect. Although we are aware of such an effect, this was not an issue observed in the few stent struts malapposed. (12)
Neointimal thickness (µm) on the luminal side of each strut section was measured.
Neointimal area (mm2) was calculated by manually tracing and subtracting the stent and luminal areas. Percentage neointimal area was calculated as ([Stent area – lumen area]/Stent area) x 100. *Binary strut coverage (%)* was calculated as (number of strut sections covered /total number of strut sections examined) x100. *Apposition:* Strut sections in contact with the vessel wall were defined as

apposed. Strut sections were malapposed if protruding into the lumen at a distance greater to the strut thickness (154μm for the polymer-coated rapamycin-eluting stent and 90μm for the non-polymer rapamycin-eluting stent). *Protrusion* was defined as projection of the luminal surface of the strut section (whether covered or not) into the lumen, relative to the intima between the adjacent strut sections. The protrusion ratio (%) was calculated as (number of protruding strut sections/total number of strut sections) x 100. In the text, all parameters quoted are for the group level analysis of total number of strut sections studied in each stent type cohort. The terms apposition, protrusion and coverage are demonstrated in figure 1.

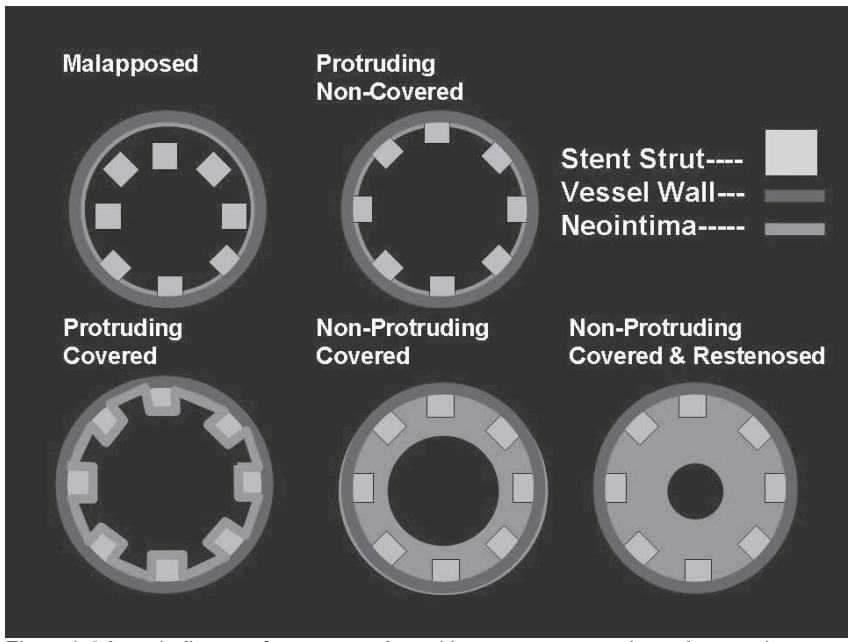

Figure 1: Schematic diagram of stent strut malapposition, coverage, protrusion and restenosis

Three-dimensional reconstruction

Representative OCT sections appearing to show protruding stent struts were subjected to 3-dimensional reconstruction for comparison with the known stent geometry to support validation of OCT for quantifying this characteristic. Intensity iso-contours delineating the lumen-wall interface were extracted from the OCT data.

Points on the extracted iso-contours were then used to reconstruct a triangulation of the lumen-wall interface. (13) Image coloration gives a qualitative indication of the local curvature of the surface and highlights particular features of the lumen wall interface.

Ethics and Trial Registration

The study was approved by the Brompton, Harefield and NHLI Ethics Committee, UK (06/Q0404/61). All patients enrolled gave written informed consent. International Randomised Controlled Trial Registration No ISRCTN42475919.

End points and Statistical methods

The primary end point was binary stent strut coverage (%). Co-primary end points were neointimal thickness (μm) and luminal strut protrusion (%).Secondary end points were

malapposition and stent, lumen and neointimal areas. The power calculation was based upon limited presented non randomised data available at the time suggesting a significant difference in stent strut coverage between bare metal (n=5) and polymer coated rapamycin eluting stents (n=12) with 2 month OCT follow up.10 In this study there was a large (>2 fold) difference in strut coverage between the two stent types, and we estimated that 12 patients in each group would be adequate to demonstrate a difference in coverage between the two stent types in our study based on the premise that the non-polymer rapamycin eluting stent would probably yield a coverage intermediate between that of a bare metal stent and the polymer coated rapamycin-eluting stent.
To account for the repeated measurements within each patient, the values for each endpoint were derived for each individual frame (n=623), and then the average of all that patient's frames was calculated to give a final summary value for each patient. Comparisons between the polymer coated and polymer free rapamycin eluting stent groups were made using t-tests. For the main outcomes the results are presented as mean (sd) along with the mean difference and the associated 95% confidence interval. A two-sided p-value of $p<0.05$ was considered to be statistically significant. In order for this trial to be considered as having a positive outcome, the primary end point had to achieve a p value of <0.05. Other p-values are exploratory in nature. Analysis was carried out using STATA 9.2 (StataCorp, Tx).

Results

Patient characteristics and procedural details are summarised in Table 1.

There were no significant complications of stent implantation. At follow up angiography and OCT analysis, chest pain or ST segment elevation on continuous ECG recording mandated balloon deflation, and in all cases this resulted in prompt resolution of pain and return of the ECG to baseline. There were no incidences of ventricular fibrillation or visible thrombus during the OCT. All study stents were patent at follow up with no cases of angiographic restenosis (defined as >50% diameter angiographic stenosis relative to the proximal reference segment).

A total of 5330 strut sections were analysed (polymer-coated rapamycin-eluting stent - 2465 and non-polymer rapamycin-eluting stent - 2865). The OCT outcome data is shown in Table 2, and summarised in figures 2-4 at both group and patient levels. The primary end point of binary stent strut coverage indicated significantly greater binary coverage with the non-polymer rapamycin-eluting stent than the polymer coated rapamycin-eluting stent.
A representative 3-dimensional reconstruction of a polymer-coated rapamycin-eluting stent with evidence of protruding struts matched closely with the known strut geometry of the bare in vitro stent and is compared with a non-protruding, non-polymer rapamycin-eluting stent (Figure 5).

Variable	polymer rapamycin stent	non-polymer rapamycin stent
Number	12	12
Age (years)	61.6 (55.0, 66.2)	62.3 (53.7, 63.8)
Male	11 (92)	10 (83)
Follow-up (mean days)	91 (85, 92)	91 (86, 96)
Hypertension	8 (67)	8 (67)
Diabetes	4 (42)	3 (25)
Hypecholesterolemia	10 (83)	11 (92)
Current or Ex-smoker	6 (50)	7 (58)
Vessel Treated		
LAD	9 (75)	6 (50)
Cx	2 (17)	4 (33)
RCA	1 (8)	2 (17)
Clinical syndrome		
Acute coronary syndrome	4 (33)	3 (25)
Chronic stable angina	6 (67)	9 (75)
Total number stents	19	18
Stent diameter (mm)	3.0 (2.8, 3.0)	3.0 (2.5, 3.0)
Stent length (mm)	18 (18, 18)	21 (18, 23)
Deployment pressure	17.5 (14.5, 20)	16 (14, 18)

Table 1: Baseline clinical and procedural characteristics

Variable	Polymer Coated rapamycin stent Mean (SD)	Non-Polymer Rapamycin stent Mean (SD)	Difference (95% CI)	p value
Neointimal thickness (um)	72.7 (25.6)	191.2 (86.7)	118.6 (64.4, 172.7)	<0.001
Strut Coverage (%)	88.3 (11.8)	97.2 (6.1)	8.9 (0.9, 16.8)	0.030
Protruding struts (%)	26.5 (17.5)	4.8 (8.6)	-21.7 (-33.34, -10.0)	0.001
Struts counted per frame (n)	8.2 (1.3)	8.4 (1.3)	0.2 (-0.9, 1.3)	0.700
Apposed and uncovered struts (%)	8.9 (12.4)	2.4 (6.0)	-6.6 (-16.0, 3.0)	0.170
Malapposed struts (%)	2.2 (2.1)	1.2 (1.1)	-0.9 (-3.2, 1.3)	0.380
Uncovered and malapposed struts (%)	1.7 (1.6)	0.4 (0.8)	-1.3 (-2.5, -0.1)	0.049
Covered and malapposed struts (%)	0.4 (0.8)	0.2 (0.4)	-0.2 (-0.8, 0.3)	0.410
Stent area (mm2)	8.8 (2.0)	8.0 (1.9)	-0.8 (-2.5, 0.8)	0.310
Lumen area (mm2)	8.0 (2.0)	6.1 (1.7)	-1.9 (-3.5, -0.4)	0.020
Neointimal area (mm2)	0.3 (0.2)	1.2 (0.8)	0.9 (0.3, 1.4)	0.002

Table 2: OCT analysis results

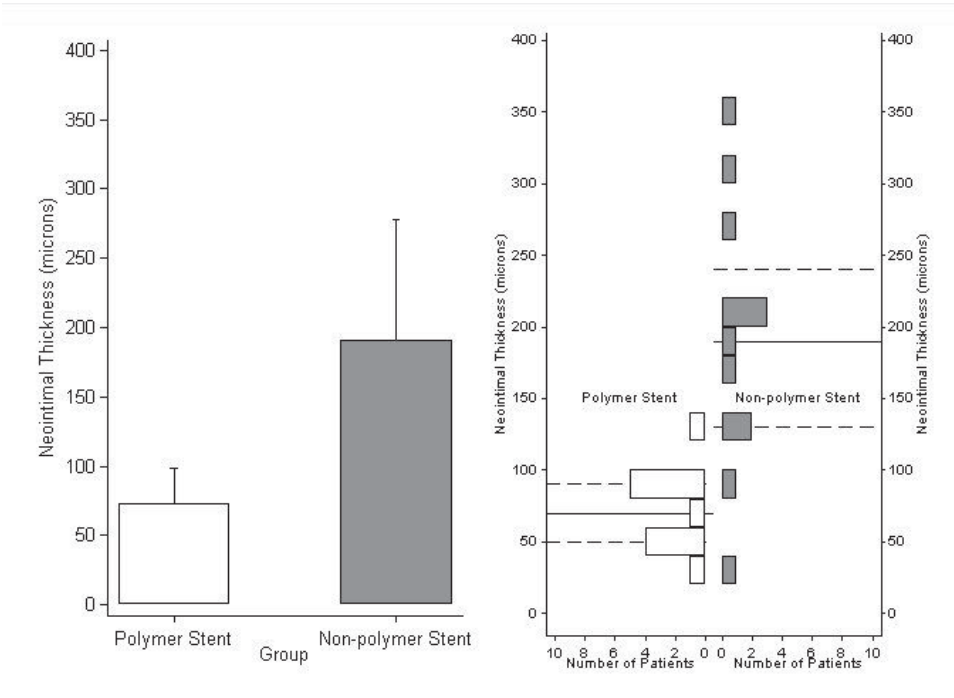

Figure 2: Combined results of neointimal thickness by the randomised stent groups [bar chart n= 5330 strut sections presented as mean (sd)] and by patient [histogram n=24 patients presented as median (IQR)].

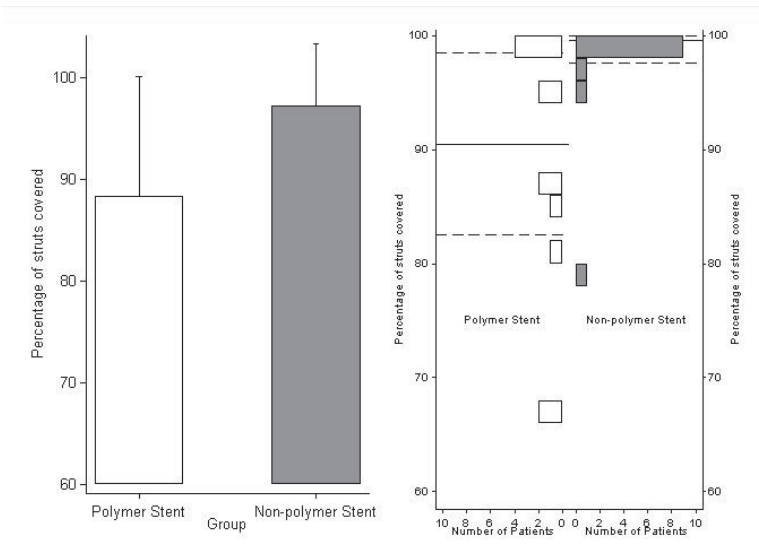

Figure 3 Combined results of binary strut coverage by the randomised stent groups [bar chart n= 5330 strut sections presented as mean (sd)] and by patient [histogram n=24 patients presented as median (IQR)].

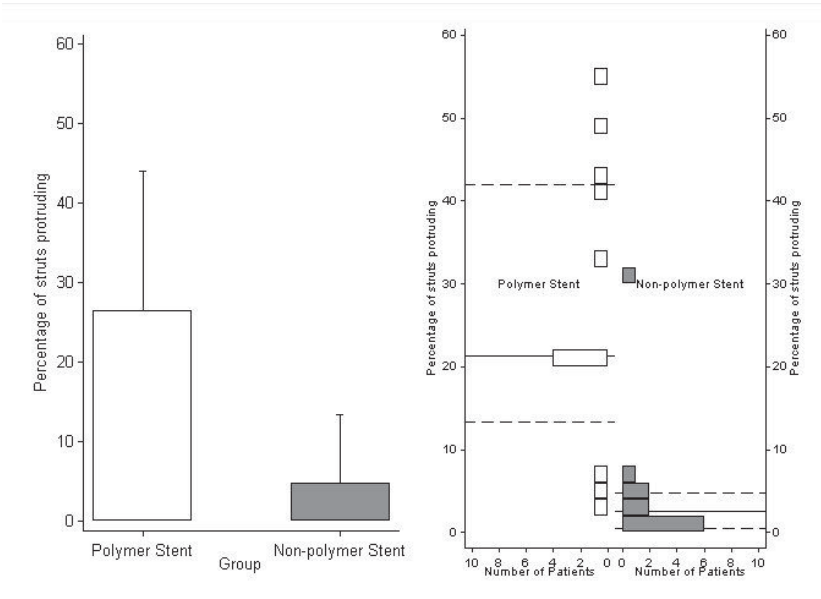

Figure 4 Combined results of binary luminal strut protrusion by the randomised stent groups [bar chart n= 5330 strut sections presented as mean (sd)] and by patient [histogram n=24 patients presented as median (IQR)]

Discussion

These data demonstrate that although the polymer-coated rapamycin-eluting stent shows reduced neointimal thickness compared with the non-polymer rapamycin-eluting stent, this is associated with a significantly higher number of uncovered and luminally protruding struts. Experimental data suggests these may be adverse features. Importantly, angiographic late loss is a parameter based focally upon the point of maximum neointimal hyperplasia, and therefore relevant when considering flow limitation. In contrast this methodology provides a more global picture of stent strut neointimal growth, coverage and protrusion, which are often non-uniform and is likely therefore to be more representative when considering potential predictors of thrombotic risk. Regarding the polymer coat as a system for drug delivery, evidence suggests that this may be pro-inflammatory in its own right and may retard healing and therefore coverage. (14) The etched porous surface of the non-polymer rapamycin-eluting stent as a drug delivery system in contrast has no potentially pro-inflammatory coating.

A number of OCT series have been reported; (15,16,17) however investigators are still working toward consensus with regard to which parameters are the most pathophysiologically relevant, what precise methodology should be used to analyse the images, and, as yet, have reported no randomised trial data. Observational studies using OCT have examined neointimal thickness in the polymer-coated rapamycin-eluting stent. Takano et al, (10) undertook OCT examination at 3 months and 2 years following polymer-coated rapamycin-eluting stent implantation in 21 patients. The neointimal thickness at 2-years was greater than that at 3-months (71±93μm versus 29±41μm, respectively; $p<0.001$). Frequency of uncovered struts was lower in the 2-year group compared to the 3-month group (5% versus 15%, respectively; $p< 0.001$). However, the prevalence of patients with uncovered struts did not differ between the 3-month and the 2-year group (95% versus 81%, respectively).

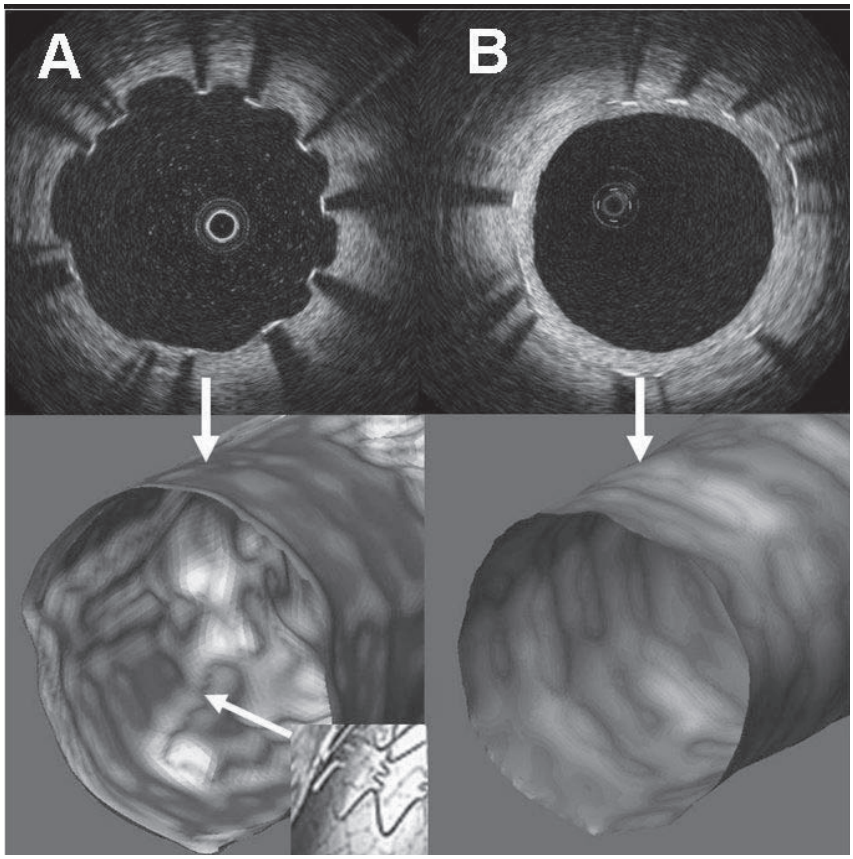

see colour section

Figure 5: Representative 2-dimensional optical coherence tomography image of stent strut sections of an uncovered polymer rapamycin-eluting stent and a covered non-polymer rapamycin-eluting stent with paired 3-dimensional reconstructions and reference photograph of a polymer-coated rapamycin-eluting stent.

Matsumoto et al (11) examined 57 polymer-coated rapamycin-eluting stents in 34 patients at 6 months after implantation and found the median neointimal thickness to be 52.5μm with 89% of struts covered and 11% exposed. This compares with our findings at 3 months post implantation, with a mean neointimal thickness of 77μm and 89% of struts covered.

Neointimal thickness

In the present study, the neointimal thickness seen with the non-polymer rapamycin-eluting stent was significantly greater than with the polymer-coated rapamycin-eluting stent. Dose ranging studies when compared with a bare metal stent, have indicated significant angiographic anti-restenotic efficacy for the non-polymer rapamycin-eluting stent (18) although it has not been formally compared with the polymer-coated rapamycin-eluting stent in a clinical trial. In the randomised ISARTest study, the non-polymer rapamycin-eluting stent however was seen to be noninferior to a polymer-coated paclitaxel-eluting stent (Taxus®, Boston Scientific Inc, Natick, US) (mean difference in angiographic late loss between the groups was 0.002mm p=0.02), with

no significant differences between angiographic restenosis rates or target vessel revascularisation (19). Furthermore, a recently published registry series of patients treated with more than 200 non-polymer rapamycin stents and the paclitaxel stent indicated no difference in major adverse cardiac event rates at 6 months. (20)

Strut protrusion

Although the concept of stent strut protrusion and flow disturbance as a potential contributor to stent thrombosis is not widely recognized, the protrusion of a foreign body into the coronary lumen will disturb flow at the blood-intima interface, potentially inducing complex flow patterns which may be thrombogenic in their own right. We suggest that the stent strut protrusion ratio may potentially be an important parameter when considering the safety of intracoronary stents. Regarding the 3d reconstruction, this was an exploratory technique which was applied to some representative OCT 2d images and is being further developed, but was not used quantitatively in this study.

Study limitations

Stent strut coverage is not a clinical outcome, but an important potential surrogate for thrombosis and therefore stent safety. The presence or absence of neointimal coverage is clearly as defined by the resolution of OCT and struts reported as bare could have had a thin covering of tissue (<10μm), though at this level the biological protection of the coverage has been debated. (21) The trial was small in terms of patient numbers; however, more than 5000 strut sections were analysed with on average more that 150 per patient driving the statistical power. From a statistical standpoint, there were some unequal variances, however, the t-test remains robust when variances are not equal and, furthermore, re-analysing all outcomes in table 3 using the Mann-Whitney test, which makes no distributional assumptions, gave extremely similar results in all cases. OCT was performed at a single, relatively early time point. This was considered appropriate in the light of the drive to develop drug-eluting stents in which dual anti-platelet therapy can potentially be stopped relatively early to reduce bleeding risk, allow non-cardiac surgery and reduce cost. Neointimal heterogeneity of optical signal in different stent types has been described; however, neointimal compositional analysis was beyond the scope of this study which focussed upon anatomical coverage. Finally, OCT was not performed immediately after stent deployment. Although this may have provided some useful comparative information, it was judged that at this point in the evolution of the technique two OCT procedures was excessive from an ethical standpoint.

Conclusions

This trial demonstrated that the polymer-coated rapamycin-eluting stent exhibited low neointimal thickness, however, this was at the expense of >10% of the struts being uncovered and > 25% protruding into the lumen at 90-days by OCT criteria. The non-polymer rapamycin-eluting stent in contrast exhibited greater neointimal thickness (with no angiographic or clinical restenosis) with <3% of struts uncovered and <5% protruding. These findings have to be interpreted in the context of reduced neointimal thickness being the very mechanism by which the efficacy of polymer coated rapamycin-eluting stents is achieved, with a proven reduction in subsequent target vessel revascularisation. Nevertheless, uncovered and protruding struts may be surrogates for thrombotic risk with the former indicating delayed healing, exposing the stent strut to the blood and the latter resulting in flow disturbance. These findings challenge the paradigm that less in-stent restenosis is better within a coronary stent and we hypothesize that at

least enough neointima to cover the stent struts and prevent protrusion may be important for safety. In addition it raises the possibility of earlier clopidogrel withdrawal in patients treated with non-polymer rapamycin-eluting stents than with polymer coated rapamycin-eluting stents. Proving these concepts will need clinical outcome trials, however, stent coverage and protrusion are logical parameters which can be employed in small scale trials to investigate the potential safety of new and existing coronary stent technologies.

References

1 Moses JW, Leon MB, Popma JJ, Fitzgerald PJ, Holmes DR, O'Shaughnessy C, Caputo RP, Kereiakes DJ, Williams DO, Teirstein PS, Jaeger JL, Kuntz RE. Sirolimus-eluting stents versus standard stents in patients with stenosis in a native coronary artery. N Engl J Med 2003;349:1315-23.
2 Weisz G, Leon MB, Holmes DR, Jr, Kereiakes DJ, Clark MR, Cohen BM, Ellis SG,
Coleman P, Hill C, Shi C, Cutlip DE, Kuntz RE, Moses JW. Two-year outcomes after sirolimus-eluting stent implantation: results from the Sirolimus-Eluting Stent in de
Novo Native Coronary Lesions (SIRIUS) trial. J Am Coll Cardiol 2006;47:1350-5.
3 Finn AV, Joner M, Nakazawa G, Kolodgie F, Newell J, John MC, Gold HK, Virmani
R. Pathological correlates of late drug-eluting stent thrombosis: strut coverage as a marker of endothelialization. Circulation 2007;115:2435-41.
4 Daemen J, Wenaweser P, Tsuchida K, Abrecht L, Vaina S, Morger C, Kukreja N,
Juni P, Sianos G, Hellige G, van Domburg RT, Hess OM, Boersma E, Meier B,
Windecker S, Serruys PW. Early and late coronary stent thrombosis of sirolimus-eluting and paclitaxel-eluting stents in routine clinical practice: data from a large two institutional cohort study. Lancet 2007;369:667-78.
5 Bavry AA, Kumbhani DJ, Helton TJ, Borek PP, Mood GR, Bhatt DL. Late thrombosis of drug-eluting stents: a meta-analysis of randomized clinical trials. Am J Med 2006;119:1056-61.
6 Pfisterer M, Brunner-La Rocca HP, Buser PT, Rickenbacher P, Hunziker P, Mueller C, Jeger R, Bader F, Osswald S, Kaiser C. Late clinical events after Clopidogrel discontinuation may limit the benefit of drug-eluting stents: an observational study of drug-eluting versus bare-metal stents. J Am Coll Cardiol 2006;48:2584-91.
7 Yamaguci T, Terashima M, Akasaka T, Hayashi T, Mizuno K, Muramatsu T et al Safety and feasibility of an intravascular optical coherence tomography image wire system in the clinical setting. Am J Cardiol. 2008 Mar 1;101(5):562-7
8 Suzuki, Yoriyasu, Ikeno, Fumiaki, Koizumi, Tomomi, Tio, Fermin, Yeung, Alan C., Yock, Paul G., Fitzgerald, Peter J., Fearon, William F. In Vivo Comparison Between Optical Coherence Tomography and Intravascular Ultrasound for Detecting Small Degrees of In-Stent Neointima After Stent Implantation. J Am Coll Cardiol Intv 2008 1: 168-173
9 Matsumoto D, Shite J, Shinke T, Otake H, Tanino Y, Ogasawara D et al Neointimal coverage of sirolimus-eluting stents at 6-month follow-up: evaluated by optical coherence tomography. Eur Heart J. 2007 8:961-7
10 Tatsuya I, Mitsuyasu T, Yoshihiro Optocal coherence tomography analysis of neointimal stent coverage in sirolimus eluting stents compared with bare metal stents. American College of Cardiology Scientific Sessions 2006 JACC 2006;47 Supplement A2906-73
11 Tanigawa J, Barlis P, Di Mario C. Intravascular Optical Coherence Tomography: Optimisation of image acquisition and quantitative assessment of stent strut apposition. EuroIntervention 2007;3:128-36.
12 Tanigawa J, Barlis P, Dimopoulos K, Dalby M, Moore P, Di Mario C. The influence of strut thickness and cell design on immediate apposition of drug-eluting stents assessed by optical coherence tomography. Int J Cardiol 2008 (*Sep 3).*
13 Giordana S, Sherwin SJ, Peiro J, Doorly DJ, Papaharilaou Y, Caro CG, Watkins N, Cheshire N, Jackson M, Bicknall C, Zervas V. Automated classification of peripheral distal by-pass geometries reconstructed from medical data. J Biomech 2005;38:47-62.

14 Joner M, Finn AV, Farb A, Mont EK, Kolodgie FD, Ladich E, Kutys R, Skorija K, Gold HK, Virmani R. Pathology of drug-eluting stents in humans: delayed healing and late thrombotic risk. J Am Coll Cardiol 2006;48:193-202.
15 Chen BX, Ma FY, Wei L, Ruan JH, Xie WL, Zhao XZ, Sun SH, Guo XM, Wang F, Tian T, Chu XW. Neointimal Coverage of Bare Metal and Sirolimus-Eluting Stents Evaluated with Optical Coherence Tomography. Heart 2007:hrt.2007.118679.
16Takano M, Inami S, Jang IK, Yamamoto M, Murakami D, Seimiya K, Ohba T, Mizuno K. Evaluation by optical coherence tomography of neointimal coverage of sirolimus-eluting stent three months after implantation. Am J Cardiol 2007;99:1033-8
17 Matsumoto D, Shite J, Shinke T, Otake H, Tanino Y, Ogasawara D, Sawada T, Paredes OL, Hirata K, Yokoyama M. Neointimal coverage of sirolimus-eluting stents at 6-month follow-up: evaluated by optical coherence tomography. Eur Heart J 2007;28:961-7.
18 Hausleiter J, Kastrati A, Wessely R, Dibra A, Mehilli J, Schratzenstaller T, Graf I, Renke-Gluszko M, Behnisch B, Dirschinger J, Wintermantel E, Schomig A.
Prevention of restenosis by a novel drug-eluting stent system with a dose-adjustable, polymer-free on-site stent coating. Eur. Heart J., 2005;26:1475-1481
19 Mehilli J, Kastrati A, Wessely R, Dibra A, Hausleiter J, Jaschke B, Dirschinger J, Schomig A. Randomized trial of a nonpolymer-based rapamycin-eluting stent versus a polymer-based paclitaxel-eluting stent for the reduction of late lumen loss. Circulation. 2006;113:273-279
20 Ruef J, Storger H, Schwarz F, et al. Comparison of a polymer-free rapamycin-eluting stent (Yukon) with a polymer-based paclitaxel-eluting stent (Taxus) in real world coronary artery lesions. Catheterization and Cardiovascular Interventions 2008;71:333-339
21 Finn A, Nakazawa G, Joner M, Kolodgie FD, Mont EK, Gold HK, Virmani R. Vascular responses to drug eluting stents: Importance of delayed healing. Arterioslcer. Thromb. Vasc. Biol. 2007;27:1500-1510

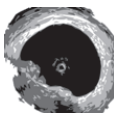

Chapter 13

Optical coherence tomography to assess malapposition in overlapping drug-eluting stents

Jun Tanigawa, Peter Barlis, Konstantinos Dimopoulos, Carlo Di Mario

Aim: *Overlapping drug-eluting stents (DES) are frequently implanted to cover long segments of diseased and injured vessel, or as a bailout technique for edge dissection or incomplete lesion coverage. DES overlap is, nevertheless, associated with strut malapposition and poor intimal coverage, which may increase the risk of stent thrombosis. The aim of this study is to evaluate stent strut apposition in overlapping DES.*

Methods and results: *We assessed strut apposition in 10 overlapped segments (20 DES, 10 patients, 661 struts) immediately after implantation, using optical coherence tomography (OCT). Struts were defined as malapposed when no contact with the intima was detected by OCT. Despite aggressive stent optimisation using balloons with a final balloon/artery ratio of 1.26±0.18 at a maximum inflation pressure of 18.0±1.9atm, 41.8±21.5% of struts were malapposed in the overlapping segment, compared to 20.1±17.6% in the proximal and 9.7±10.6% in the distal segment ($p < 0.05$ for both).*

Conclusion: *OCT revealed that 40% of struts within an overlapped DES segment were malapposed, and this may explain the reported delay in endothelialisation in such segments.*

Coverage of the entire injured and diseased vessel segment is an established principle in the deployment of drug-eluting stents (DES) and a key factor in optimising DES efficacy to limit restenosis. This strategy requires stent coverage from healthy to healthy segments, thus demanding the implantation of multiple stents when lesions are long. Implantation of multiple overlapping stents is also required following initial DES implantation when extensive dissection or residual stenosis is present. The use of overlapping stents may lead to local arterial toxicity with exposure to inappropriately high levels of anti-proliferative drug or polymer. This phenomenon remains a concern and may predispose to delayed endothelialisation. Moreover, overlapping layers of stent struts and sub-optimal stent expansion and apposition to the intima can also lead to stent thrombosis.(1) Optical coherence tomography (OCT) is a new intravascular imaging modality, which uses infrared light and offers ten-fold higher resolution (10-15µm) and fewer artefacts compared to intravascular ultrasound, thereby enabling precise assessment of stent optimisation.(2,3) The present study aimed to assess the frequency of DES strut malapposition within overlapped segments immediately following implantation and angiographic optimisation.

Methods

Study population

Between February and October 2006, 10 patients who received overlapping DES were assessed using OCT (20 stents, 10 lesions). The OCT examination took place following angiographic optimisation. Overlapping DES was used as a primary strategy for very long lesions or bailout for residual stenosis or dissection following the implantation of the first stent. Pre-dilatation or direct stenting and selection of stent type were left to the discretion of the operator, but the same type of DES was used for each lesion and stent implantation was always followed by high-pressure post-dilatation at the overlapping segment. Stent optimisation was accomplished with conventional angiographic guidance aiming at a residual diameter stenosis < 20% by visual estimate.

OCT procedure

The OCT system used in this study (LightLab Imaging Inc., Westford, MA, US) has been described previously.(3,4) In brief, lesions were imaged during proximal occlusion and continuous infusion of Ringer's lactate at 0.5-1.5ml/sec. An OCT catheter (Helios™ proximal occlusion catheter) and an OCT imaging wire (ImageWire™) were used. The lesion was visualised with an automated pullback system at 1.0mm/sec acquiring cross sectional images at 15.4 frames/sec. Off-line analysis of contiguous cross-sections in overlapped stents was performed at 1mm intervals. The overlapped struts were assessed as well as the 2 adjacent cross-sections immediately proximal and distal (Figure 1).

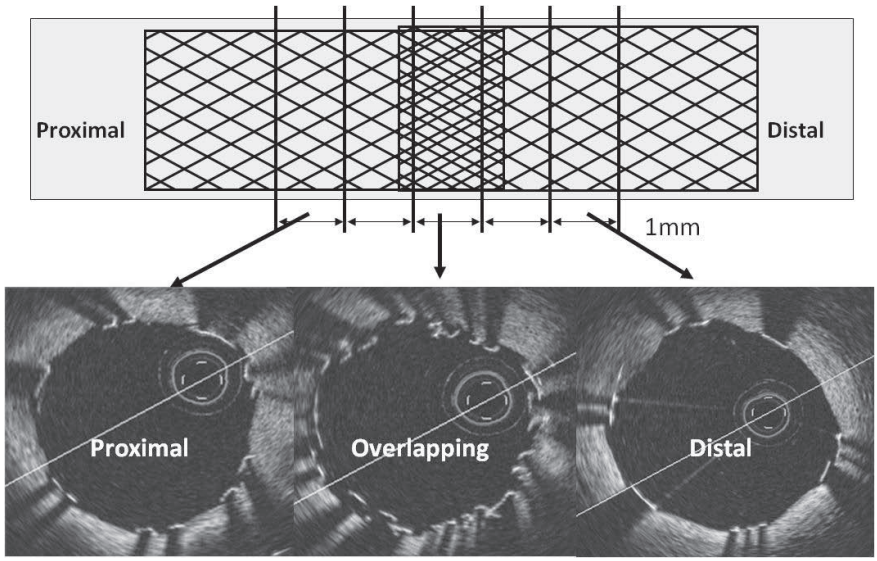

Figure 1: Schema of two overlapped stents demonstrating the areas assessed using optical coherence tomography

Strut malapposition was defined as no contact between the strut and intima. As OCT can show only the surface of stent struts due to its limited penetration through the metal, the measured distance between the strut surface and the luminal surface (Figure 2) was adjusted based on each stent thickness. Each cut-off was determined as the total of the metal and polymer thickness plus 10μm (OCT longitudinal resolution) (Table 1). Struts protruding into the ostium of a side branch were excluded from the analysis.

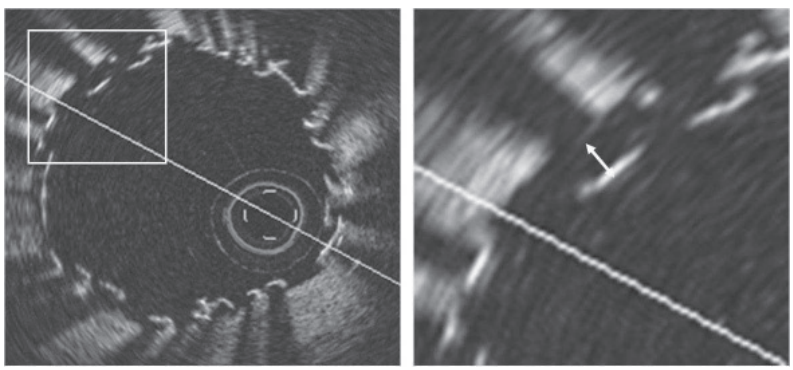

Figure 2: Measurement of distance between the endoluminal surface of the strut and intima Note that OCT can only show the endoluminal surface of the strut due to its limited penetration through metal.

	Metal thickness	Polymer thickness	Total thickness	Malapposed*
Cypher Select	140	7	154	≥ 170
Taxus Liberte	97	15	127	≥ 140
Co Star	89	No	89	≥ 100
Values are presented as μm				
*Distances from endoluminal surface to the intima				

Table 1. Strut thickness and classification of apposition of the drug-eluting stents used in this study

Statistical analysis

Statistical analysis was performed using R version 2.4.1 and StatView 5.0 (SAS Institute Inc., Cary, NC, US). Comparison between groups was performed using the two-sample Wilcoxon test for continuous variables. A two-tailed p-value of <0.05 was used as the criterion for statistical significance for all analyses.

Results

Clinical and lesion characteristics

Table 2 lists the clinical and lesion characteristics for the 10 patients. All lesions studied were complex (ACC/AHA classification type B or C), including 3 severely calcified lesions. Cypher Select (Cordis, Johnson and Johnson Co., Miami Lake, FL, US), CoStar (Conor Medsystems, Inc., Hamilton Court Menlo Park, CA, US) and Taxus Liberte (Boston Scientific, Natick, MA, US) stents were used in this study. There were no OCT-related complications such as haemodynamic instability or arrhythmias during image acquisition and no subsequent deterioration of flow or coronary dissection.

	Sex	Age	Prior MI	Diabetes	Hypert-ension	Current / former smoker	Dyslipi-demia	Clinical presentation	Target vessel	ACC / AHA lesion classification	Heavy calcific-ation
1	F	74	Yes	No	Yes	No	Yes	Stable angina	LCx	type C	No
2	M	71	No	No	No	Yes	No	Stable angina	LAD	type B	No
3	M	64	No	No	Yes	No	Yes	Stable angina	RCA	type C	Yes
4	M	65	Yes	No	No	No	Yes	Stable angina	RCA	Type C	Yes
5	F	54	No	Yes	Yes	Yes	Yes	ACS	LAD	Type B	No
6	M	66	Yes	No	No	Yes	Yes	Stable angina	LCx	Type C	Yes
7	M	54	Yes	No	No	Yes	Yes	Stable angina	LAD	Type C	No
8	M	79	No	No	No	Yes	Yes	Stable angina	RCA	Type C	No
9	M	65	No	Yes	Yes	No	Yes	Stable angina	LAD	Type C	No
10	M	66	Yes	No	Yes	Yes	No	ACS	RCA	Type B	No

MI – myocardial infarction; LCx – left circumflex artery; RCA – right coronary artery, LAD – left anterior descending artery

Table 2: Clinical and lesion characteristics

Angiographic and procedural characteristics

Table 3 lists the angiographic and procedural characteristics. The mean number of stents used per lesion was 2.2±0.4. In only one case was direct stenting performed. Mean total stent length was 47.9±7.3mm. Post-dilatation was used in all cases with non-compliant balloons at a mean pressure of 18.0±1.9atm. The balloon to artery ratio was 1.26±0.18. In 8 of 10 patients (80%), the distal stent was implanted first followed by the proximal stent in an overlap fashion.

Stent type, Cypher Select, n (%)	6 (60)
Stent type, Taxus Liberte, n (%)	1 (10)
Stent type, CoStar, n (%)	3 (30)
Number of stents	2.2±0.4
Average stent diameter (mm)	2.86 ± 0.31
Total stent length (mm)	47.9 ± 7.3
Pre-dilatation, n (%)	9 (90)
Post-dilatation, n (%)	10 (100)
Maximum balloon diameter (mm)	3.08 ± 0.24
Maximum balloon artery ratio	1.26 ± 0.18
Maximum balloon pressure (atm)	18.0 ± 1.9
Quantitative coronary angiographic results	
Pre-procedural	
Reference vessel diameter (mm)	2.49 ± 0.40
Minimal lumen diameter (mm)	1.00 ± 0.38
Diameter stenosis (%)	58.5 ± 18.1
Lesions length (mm)	28.9 ± 9.3
Post-procedural	
Reference vessel diameter (mm)	3.01 ± 0.38
Minimal lumen diameter (mm)	2.49 ± 0.35
Diameter stenosis (%)	17.4 ± 6.5
LAD: Left anterior descending artery, RCA: Right coronary artery, LCx: Left circumflex artery	

Table 3. Angiographic and procedural characteristics

OCT analysis

A total of 661 struts in 53 cross sections were analyzed (239 struts in the overlapping segment, 228 struts in the proximal segment and 194 struts in the distal segment). The proportion of malapposed struts differed significantly between the overlapped (41.8±21.5%) and both the proximal (20.1±17.6%) and distal (9.7±10.6%) non-overlapped segments (Figure 3).

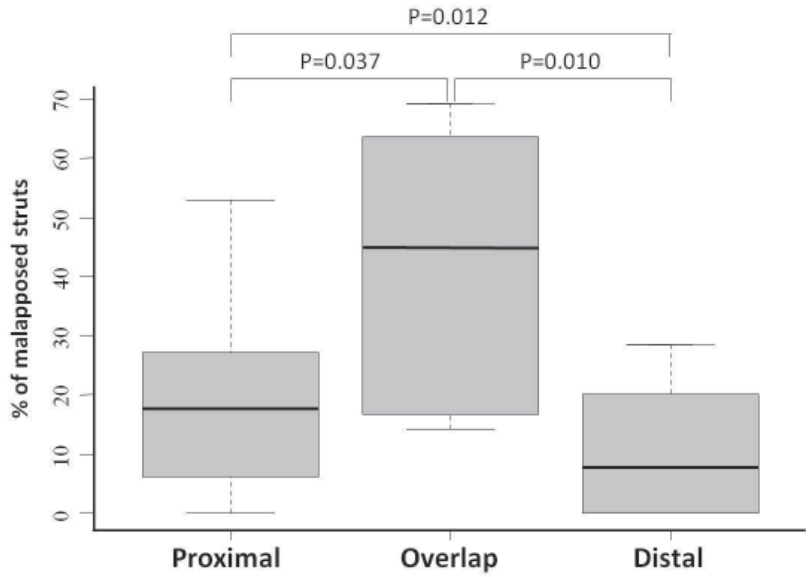

Figure 3: Percentage of malapposed struts

Discussion

Using high resolution intravascular imaging with OCT, our study has shown that a high proportion of the stent struts located within an overlapped segment remain malapposed, despite high pressure balloon dilatation with appropriately sized balloons. Furthermore, the region immediately proximal to the overlap segment has a greater number of malapposed struts.

OCT is a new intravascular imaging modality, which uses infrared light and offers 10 time's higher resolution (10-15μm) and fewer artefacts compared to IVUS. The clinical application of intracoronary OCT has already been demonstrated both in stable patients and in those with acute coronary syndromes (5) and was used without complication in our patients.

The high malapposition rate in the overlap segment immediately following DES implantation and aggressive optimisation is an important finding and one that has not previously been reported using OCT. Prior studies have raised concerns regarding the safety of overlapping DES, with particular reference to the phenomenon of 'double dose' of metal, polymer and drug in this stented segment.(6) One third of patients enrolled in SIRIUS, E-SIRIUS and TAXUS-VI study received multiple overlapping stents.(7-9) In a recent pooled analysis of five clinical trials of the sirolimus-eluting stent (SES, Cypher, Johnson & Johnson, Miami, USA), 575 patients with stent overlap (337 SES, 238 BMS) were compared to 1162 patients with single stents (697 SES, 465 BMS).(6) Stent overlap was associated with a greater late lumen loss in stent and more frequent angiographic restenosis, regardless of stent type.(6)

Concerns that stent overlap may increase the likelihood of stent strut malapposition and thus the propensity for restenosis and thrombosis therefore remain unanswered. An animal study, showed persistent inflammation, fibrin deposition, and delayed endothelialisation following DES implantation compared with bare metal stents, particularly at overlapping segments. (10) This may be related to excess inhibition of neointimal hyperplasia as a result of the double dose of sirolimus. Using OCT 6 months after SES implantation, Matsumoto et al (11) found that overlapping SES struts showed malapposition more frequently than did non-overlapping struts. The clinical

significance of this however remains unclear, particularly as this study did not assess stent strut apposition at implantation.
In our study, we found a significant difference in the rate of strut malapposition between the proximal and distal stented segments (20.1% vs. 9.7%, p=0.012). This difference could be due to vessel tapering or the deployment order of the overlapping stents. Since coronary dilatation balloons and stents have a longitudinally uniform size, it is less likely that struts in the proximal part of the stent become optimally apposed to the intima. Furthermore, when the intended strategy is that of overlapping stents, the distal stent is usually implanted first followed by the proximal stent. This may results in a funnelling effect with the proximal stent expansion being restricted by the already deployed distal stent. Deployment of the proximal stent first may limit this phenomenon, but may prove technically challenging.

Limitations

This was an observational study with a small sample size. For this reason, this report was limited to individual patient data and few overall summary statistics and comparisons. The sample size also precludes any formal assessment of predictors of strut malapposition in overlap segments with larger studies needed to address this and other concerns related to the long-term issues of DES safety and any differences that may exist between different stent platforms.

Conclusions

This preliminary study has shown that overlapping DES are associated with a considerable risk of immediate malapposition. Moreover, the segment proximal to the overlap appears more prone to malapposition compared to the distal stented segment, despite aggressive stent optimisation using adequately sized balloons with high pressures. This phenomenon, never before documented, may contribute to delayed endothelialisation and result in an increased risk of stent thrombosis although larger studies are needed to confirm these findings and determine their relation to late DES complications.

References

1. Joner M, Finn AV, Farb A, et al. Pathology of drug-eluting stents in humans: delayed healing and late thrombotic risk. J Am Coll Cardiol 2006;48:193-202.
2. Bouma BE, Tearney GJ, Yabushita H, et al. Evaluation of intracoronary stenting by intravascular optical coherence tomography. Heart 2003;89:317-20.
3. Tanigawa J, Barlis P, Di Mario C. Intravascular Optical Coherence Tomography: Optimisation of image acquisition and quantitative assessment of stent strut apposition. EuroIntervention 2007;3:128-136.
4. Kawase Y, Hoshino K, Yoneyama R, et al. In vivo volumetric analysis of coronary stent using optical coherence tomography with a novel balloon occlusion-flushing catheter: a comparison with intravascular ultrasound. Ultrasound Med Biol 2005;31:1343-9.
5. Jang IK, Tearney GJ, MacNeill B, et al. In vivo characterization of coronary atherosclerotic plaque by use of optical coherence tomography. Circulation 2005;111:1551-5.
6. Kereiakes DJ, Wang H, Popma JJ, et al. Periprocedural and late consequences of overlapping Cypher sirolimus-eluting stents: pooled analysis of five clinical trials. J Am Coll Cardiol 2006;48:21-31.
7. Dawkins KD, Grube E, Guagliumi G, et al. Clinical efficacy of polymer-based paclitaxel-eluting stents in the treatment of complex, long coronary artery lesions from a multicenter, randomized trial: support for the use of drug-eluting stents in contemporary clinical practice. Circulation 2005;112:3306-13.
8. Moses JW, Leon MB, Popma JJ, et al. Sirolimus-eluting stents versus standard stents in patients with stenosis in a native coronary artery. N Engl J Med 2003;349:1315-23.

9. Schofer J, Schluter M, Gershlick AH, et al. Sirolimus-eluting stents for treatment of patients with long atherosclerotic lesions in small coronary arteries: double-blind, randomised controlled trial (E-SIRIUS). Lancet 2003;362:1093-9.
10. Finn AV, Kolodgie FD, Harnek J, et al. Differential response of delayed healing and persistent inflammation at sites of overlapping sirolimus- or paclitaxel-eluting stents. Circulation 2005;112:270-8.
11. Matsumoto D, Shite J, Shinke T, et al. Neointimal coverage of sirolimus-eluting stents at 6-month follow-up: evaluated by optical coherence tomography. Eur Heart J 2006.

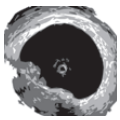

Chapter 14

Heavily calcified coronary lesions preclude strut apposition despite high pressure balloon dilatation and rotational atherectomy: In-vivo demonstration with optical coherence tomography

Jun Tanigawa, Peter Barlis, Carlo Di Mario

Heavily calcified lesions (HCL) continue to represent challenges not always solved by low profile, non-compliant high-pressure balloons, or bladed balloons. Uncrossable or unexpandable lesions need lesion modification using ablating devices such as rotational atherectomy. We assessed 3 HCL treated with drug-eluting stents using a new intravascular imaging device, Optical Coherence Tomography with tenfold superior resolution and fewer artifacts compared to conventional intravascualr ultrasound. Insights from this highly sensitive imaging technique outline the high prevalence of persistent stent strut malapposition in this group despite high-pressure dilatation or rotational atherectomy.

Crossing the lesion, initial dilatation by balloons and final stent expansion may present a challenge to the operator's skill and experience in heavily calcified lesions (HCL) due to a highly angulated lumen and resistance to optimal expansion (1,2). If balloons do not cross or expand and the poorly steerable thin uncoated Rotablator® (Boston Scientific, Natick, MA, US) wire can be advanced, rotational atherectomy provide favorable lesion modification, which can facilitate lesion dilatation and stent expansion (3,4). Other methods of lesion preparation (cutting balloon, high pressure pre- and post-dilatation) have been advocated to obtain optimal stent expansion and apposition. Based on the examination of 3 representative cases with optical coherence tomography (OCT), we explain why optimal strut apposition remains an elusive target in the presence of heavy eccentric calcified plaques.

Case report

CASE 1

A 66-year-old male admitted with typical angina pectoris on a background of hypertension, hyperlipidemia and previous myocardial infarction underwent coronary angiography. This demonstrated long segments of heavily calcified severe stenoses in the mid left circumflex artery (Figure 1). The lesions were sequentially dilated with both 1.5 and 2.0mm non-compliant balloons up to 16atm. Three sirolimus-eluting stent (SES, Cypher Select™, Cordis, Johnson and Johnson Co., Miami Lake, FL, US), 2.5x18, 3.0x13 and 3.0x23mm were implanted in an overlapping fashion and post-dilated with a non-compliant 3.0mm balloon to 22atm. Although his angiogram showed optimal lesion dilatation with only minimal lumen haziness (Figure 1C), OCT (LightLab Imaging Inc., Westford, MA, US) revealed sub-optimal stent expansion and poor stent strut apposition (5). Despite multiple high-pressure lesion dilatations, optimally circumferential expansion could not be achieved. Figure 2A shows elliptical stent expansion limited by heavily calcified superficial eccentric plaque (*). Irregular contours of the stent struts maintained a circular geometry and were unable to fully conform to the slit like lumen induced by the severe calcification. Although circumferential expansion shows greater minimal lumen diameter compared to elliptic expansion (3.17x2.86mm vs. 3.33x1.97mm), some struts still remain malapposed to the intima at the intimal tear between the superficial eccentric calcification and non-calcified intima (Figure 2). Although stent expansion was acceptable, matching the distal reference lumen area, the irregularity of the lumen contours due to protruding eccentric calcification precluded complete strut apposition. We administered IIb/IIIa inhibitors and recommended long-term dual anti-platelet treatment. Clinical follow-up at 4 months is uneventful.

CASE 2

A 71-year-old male admitted with angina pectoris on a background of hypertension, hyperlipidemia and previous myocardial infarction underwent coronary angiography. This demonstrated HCL in the mid right coronary artery. As no balloon could cross the stenosis, a rotablator wire was inserted and a 1.5mm burr used, followed by multiple sequential dilatations using a 2.0, 3.0 and 3.5mm non-compliant balloon up to 20Atm. A 3.5x28mm Cypher Select stent (Cordis, Johnson & Johnson, Miami, FL, USA) was implanted and post-dilated with a short

3.5mm non-compliant balloon up to 24atm (Figure 3). OCT (Figure 4) showed that rotational atherectomy created a small circular divot in the eccentric calcified plaque extending for half of the vessel circumference, which resulted in complex lumen geometry. This crater (E, F arrow heads) measured 1.60mm in diameter, almost equivalent to the rotablator burr size of 1.5mm, contributed to the incomplete expansion of the lesion despite high-pressure dilatation and preventing full stent strut apposition (E, double arrow).

CASE 3

A 57-year-old male with stable angina was electively transferred following unsuccessful balloon angioplasty of the mid left circumflex bifurcation lesion, resistant to expansion using conventional balloons due to heavy calcification. After engagement of 7Fr guiding catheter, rotational atherectomy using 1.75mm burr was successfully performed and followed by pre-dilatation using 3.0 and 3.5mm non-compliant balloon up to 20atm. Paclitaxel-eluting stent (Taxus Liberte™, Boston Scientific, Natick, MA, US) was implanted (4.0x16mm, 16atm) in the main vessel crossing the side branch and post-dilated using kissing inflation technique (3.5mm for the main vessel and 2.5mm for the side branch, up to 14atm, Figure 5). Although his angiogram showed an optimal result at the main vessel, OCT imaging demonstrated similar findings (Figure 6) as identified in case 2, a crater formation (arrow heads) with diameters of 1.69mm (A) and 1.83mm (B) beside the remaining fibro-calcified plaque (*), preventing complete lesion expansion and full stent strut apposition (arrows).

Discussion

Even in the HCL, the majority can be treated with balloon dilatation and stent implantation alone (3). Many, however, may not be optimally expanded and stent struts may not be fully apposed to the intima as shown in case 1. The importance of this is underscored with findings from the e-Cypher registry correlating HCL with future occurrence of stent thrombosis (6). At times, stent expansion and apposition are often confused. Stent expansion is defined in relation to the lumen diameter of the proximal or distal vessel (reference diameter), while stent apposition is a description of the strut's attachment to the intima (plaque or vessel wall), regardless of whether it is properly expanded or not. OCT remains inferior to IVUS in guiding stent expansion since the external elastic membrane diameter is not always detectable due to its limited penetration of around 1.5mm and scan range of approximately 5mm. Although it is still controversial, stent under expansion and sub-optimal strut apposition following drug-eluting stent (DES) implantation are suggested as possible causes of stent thrombosis (7). Both stent under expansion and strut malapposition were clearly identified in the 3 cases, even when rotational atherectomy was performed. Although there have not been any reports in the literature comparing expansion in HCL versus non-calcific lesions, in our experience malapposition and poor expansion are more frequent in the treatment of HCL and this may account for sub-optimal long-term result associated with HCL.

Rotational atherectomy for the HCL is quite useful to improve procedural success thanks to lesion modification (removal of dense calcification) leading better stent expansion (4). However, in cases 2 and 3, the superficial calcification was not completely cleared, preventing optimal stent expansion and apposition. Stent expansion and apposition are completely different concepts; stent expansion is defined in relation to the lumen diameter of the proximal or distal vessel, while stent apposition is a description of the strut's attachment to the intima (plaque or vessel wall), regardless of whether it is properly expanded or not. Both are desirable to optimize DES safety and efficacy. Even with maximum dilatation using adequately sized balloons at high-pressure and/or rotational atherectomy using small burrs acquiring angiographically optimal stent deployment, full stent expansion and apposition cannot be optimally achieved in HCL. Sizing-up

the burr might enable better lesion modification resulting in better stent expansion and strut apposition. It is, however, unknown whether routine usage of aggressive rotational atherectomy is superior to conventional balloon dilatation as a means of lesion modification followed by DES implantation due to a lack of systemic long-term results of such a strategy. Clinical consequences of such gross malapposition also remain unknown (e.g. long-term double anti-platelet therapy needed to prevent late stent thrombosis), but may impinge on the elution properties of DES, activate fibrin and platelet more and may result in accelerated intimal hyperplasia or stent thrombosis. In this case series, OCT clearly showed how HCL behave when dilated using conventional balloons and modified using rotational atherectomy. It is often a challenge to achieve optimal stent expansion and strut apposition in such lesions; however this remains one of the major benefits of DES.

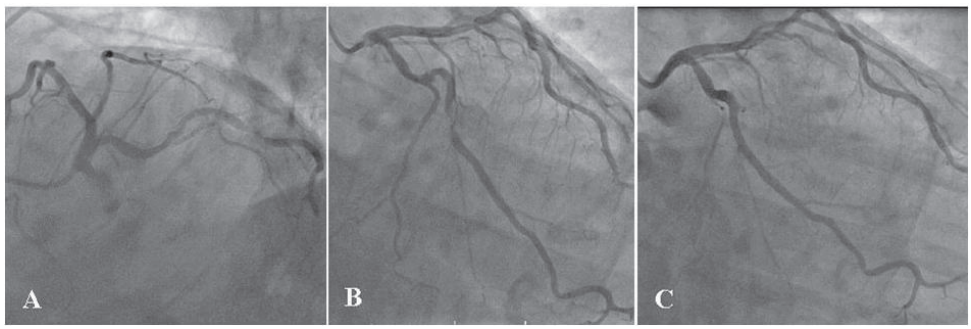

Figure 1: Case 1 - Coronary Angiography

A) Pre-procedural caudal left anterior oblique view showing tortuous diffuse stenosis in the mid left circumflex artery, B) Pre-procedural caudal right anterior oblique view, C) Post-procedural caudal right anterior oblique view. Optical Coherence Tomography assessment was performed using automatic pull-back system and arrows (a, b) correspond to OCT cross-sectional images as shown in Figure 2-a, b.

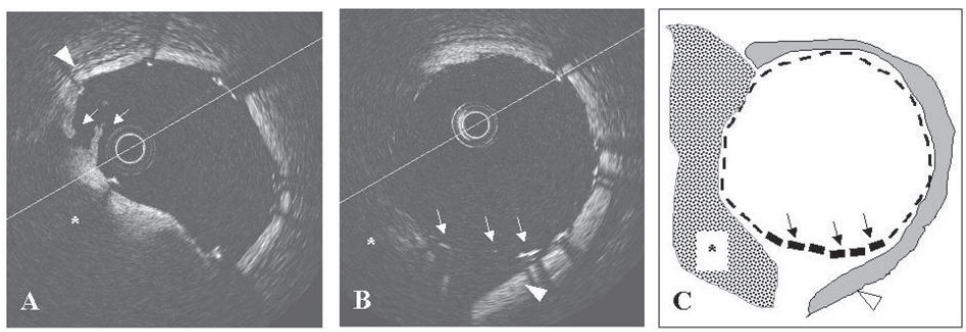

Figure 2: Optical Coherence Tomography findings following conventional balloon dilatation and stent implantation A) Elliptical stent expansion limited by superficial calcification (*) and intimal flaps (double arrows) outside the stent at the border between superficial calcification and non-calcified intima (white arrow head), B) Circular stent expansion with an intimal tear between the superficial calcification (*) and non-calcified intima (arrow head), where stent struts are malapposed. Intimal tear was distinguished from branches using adjacent cross-sectional OCT images and corresponding angiogram.

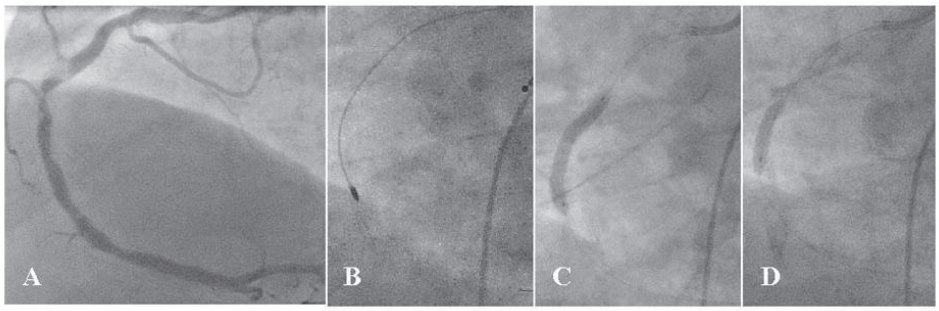

A) Figure 3: Coronary angiography of the right coronary artery in Case 2 Left anterior oblique view indicating severe calcification in the mid segment, B) Rotational atherectomy using 1.5mm burr, C) Cypher Select Stent 3.5x28mm, D) Post-dilatation using 3.5mm balloon up to24atm

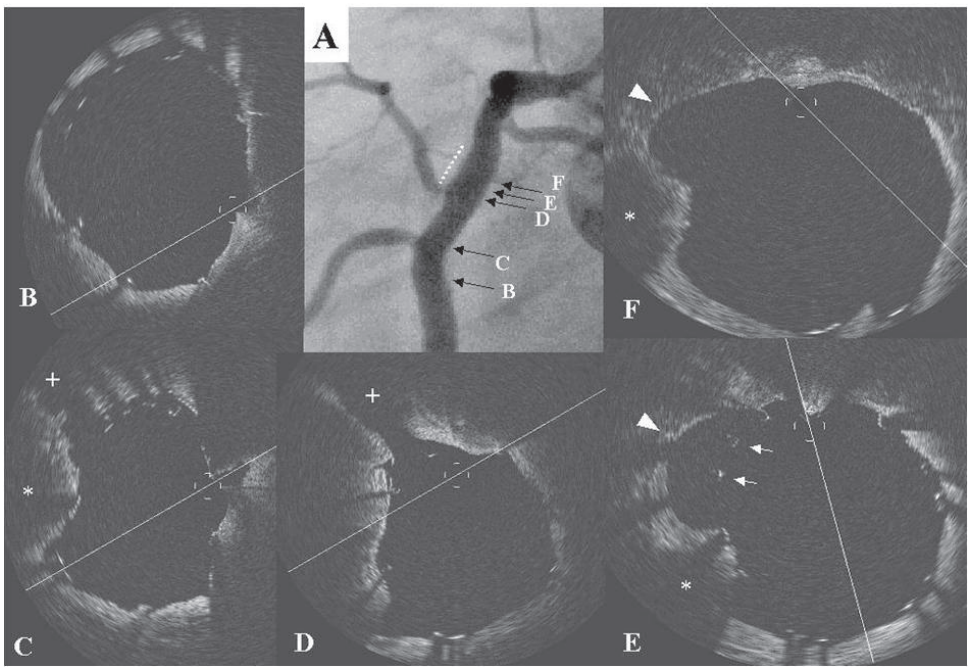

Figure 4: Final result of Case 2 and Optical Coherence Tomography findings
A) Angiographic result following stent implantation E, F) A crater formation (arrowhead) beside the remaining superficial eccentric calcification (*) located on the same side of the two branches (C,D +) where the Rotablator has shifted (wire bias) during ablation. The diameter of the crater was 1.60mm almost equivalent to the Rotablator burr size of 1.5mm. Note struts (arrows) are malapposed at the crater. This crater corresponded with the protuberance on the outer contour of the right coronary artery on angiography, just above the level of the side branch (5A, dotted line).

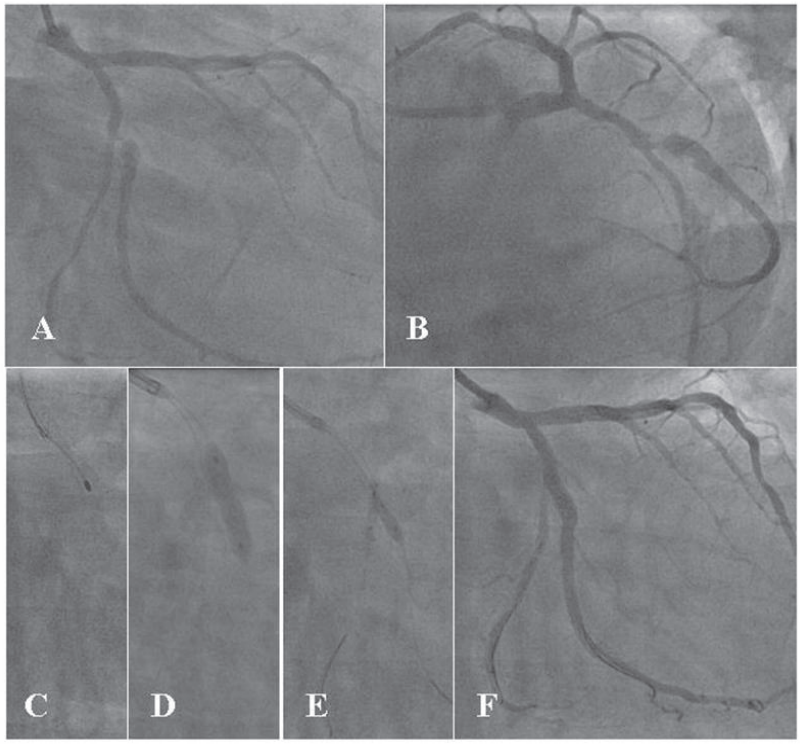

Figure 5: Pre- and post-procedural angiography and procedures (Case 3) Severe calcification in the mid left circumflex artery (A,B) was ablated using 1.75mm Rotablator burr (C) and followed by Taxus Liberte stent (4.0x16mm, 16atm) implantation (D) and final kissing inflation (E). Final result was optimal (E).

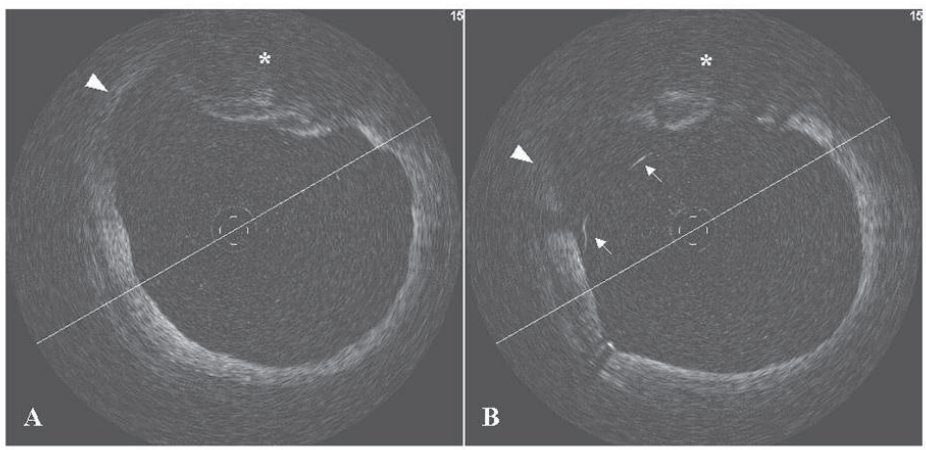

Figure 6: Optical Coherence Tomography findings of Case 3
As in Case 2, a crater formed by the rotational atherectomy burr beside the fibro-calcified plaque (A,B), where stent struts are malapposed (B). A crater formation (arrowhead) can be seen beside the remaining superficial eccentric calcification (*)

References

1. Fujii K, Ochiai M, Mintz GS, Kan Y, Awano K, Masutani M, Ashida K, Ohyanagi M, Ichikawa S, Ura S, Araki H, Stone GW, Moses JW, Leon MB, Carlier SG. Procedural implications of intravascular ultrasound morphologic features of chronic total coronary occlusions. Am J Cardiol. 2006;97:1455-62.
2. Wilensky RL, Selzer F, Johnston J, Laskey WK, Klugherz BD, Block P, Cohen H, Detre K, Williams DO. Relation of percutaneous coronary intervention of complex lesions to clinical outcomes (from the NHLBI Dynamic Registry). Am J Cardiol. 2002;90:216-21.
3. Clavijo LC, Steinberg DH, Torguson R, Kuchulakanti PK, Chu WW, Fournadjiev J, Satler LF, Kent KM, Suddath WO, Waksman R, Pichard AD. Sirolimus-eluting stents and calcified coronary lesions: Clinical outcomes of patients treated with and without rotational atherectomy. Catheter Cardiovasc Interv. 2006;68:873-8
4. Cavusoglu E, Kini AS, Marmur JD, Sharma SK. Current status of rotational atherectomy. Catheter Cardiovasc Interv. 2004;62:485-98.
5. Tanigawa J, Barlis P, Di Mario C. Intravascular Optical Coherence Tomography: Optimisation of image acquisition and quantitative assessment of stent strut apposition. EuroInterv. 2007;3128-36
6. Urban P, Gershlick AH, Guagliumi G, Guyon P, Lotan C, Schofer J, Seth A, Sousa JE, Wijns W, Berge C, Deme M, Stoll HP; e-Cypher Investigators. Safety of coronary sirolimus-eluting stents in daily clinical practice: one-year follow-up of the e-Cypher registry. Circulation. 2006;113:1434-41.
7. Joner M, Finn AV, Farb A, Mont EK, Kolodgie FD, Ladich E, Kutys R, Skorija K, Gold HK, Virmani R. Pathology of drug-eluting stents in humans: delayed healing and late thrombotic risk. J Am Coll Cardiol. 2006;48:193-202.

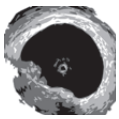

Chapter 15

The influence of strut thickness and cell design on immediate apposition of drug-eluting stents assessed by optical coherence tomography

Jun Tanigawa, Peter Barlis, Konstantinos Dimopoulos, Philip Moore, Miles Dalby, Carlo Di Mario

Background: *Stent strut malapposition correlates with poor intimal coverage and this may increase the risk of late stent thrombosis. At present, there is limited data on whether stent strut thickness and stent design impact on acute apposition. We aimed to investigate the influence of stent strut thickness and design on acute stent strut apposition (SSA) immediately following drug-eluting stent (DES) implantation using optical coherence tomography (OCT), a technique with higher resolution and fewer artefacts than intravascular ultrasound.*

Methods: *Thirty-six DES in 23 patients (25 lesions) were studied by OCT. SSA was defined as embedded when a strut was buried in the intima for more than half its thickness, protruding when apposed to the intima but not embedded and malapposed when there was no intimal contact.*

Results: *Cypher Select stents were implanted in 52%, Taxus Liberte in 32%, Costar in 12% and Endeavour in 4%. A total of 6,402 struts were evaluated. Despite stent optimisation using balloons with a final balloon/artery ratio of 1.26±0.19 at a maximum inflation pressure of 17.5±3.0atm, only 57.1±20.7% of struts were embedded, whereas 33.8±18.4% were protruding and 9.1±7.4% were malapposed. Stent type was a strong predictor of malapposition on logistic multilevel analysis (OR 3.95, 95%CI: 1.27-12.23, p=0.017). At 12 months follow-up, there were no adverse clinical events.*

Conclusion: *Despite angiographic optimisation with high pressures and adequately sized balloons, malapposed stent struts are frequently found in complex coronary lesions and more often following the implantation of Cypher Select stents which have a thicker stent strut and closed cell design. With no adverse clinical events at 12 months follow-up, this likely represents a benign phenomenon at least as long as combined anti-platelet therapy is maintained.*

Although drug-eluting stents (DES) have dramatically reduced restenosis compared to bare metal stents (BMS), restenosis and stent thrombosis continue to present a challenge, especially in complex coronary lesions (1-5). The issue of late and very late stent thrombosis has cast a cloud on the use of DES (6-9), resulting in an empirical increase in the duration of dual anti-platelet therapy beyond the customary 6-12 months. Although the magnitude of this phenomenon remains unclear, recent studies have found a link between sub-optimal stent strut apposition (SSA) and delayed endothelialisation which may predispose to stent thrombosis.(6,10,11) Previous studies have demonstrated a link between stent strut thickness and long-term restenosis and target lesion revascularisation (TLR),(4,12) there is currently no data specifically assessing the influence of stent strut thickness on apposition in the DES era.

Optical coherence tomography (OCT) is a relatively new intravascular imaging modality, which uses infrared light and offers 10 times higher resolution (10-15μm) and fewer artefacts compared to intravascular ultrasound (IVUS), thereby enabling precise assessment of stent optimisation. (13) The present study used OCT to identify predictors of sub-optimal apposition and, in particular, the influence of stent strut thickness and design and examine 12-month clinical outcomes.

Methods

Patient Enrolment and Pharmacological Treatment

From January 2005, OCT became the mainstay intravascular imaging modality used at our institution to assess results of stent implantation. For this particular study, we only enrolled patients undergoing percutaneous coronary intervention for complex coronary lesions defined as long (>20mm), heavily calcified or at a bifurcation. Clinical exclusion criteria were: poor renal function (serum creatinine >1.5mg/dL), left ventricular ejection fraction <30% and haemodynamic instability. Angiographic exclusion criteria were: residual thrombus or dissection; lumen diameter proximal to the stented lesion smaller than 2.5mm or greater than 4.0mm by visual estimate; ostial or very proximal lesion (<15mm from ostium); recanalised chronic total occlusion; severe tortuosity; final post-procedural Thrombolysis In Myocardial Infarction (TIMI)

grade flow <3. All patients provided written informed consent prior to the procedure approved by the local institutional ethics committee.
All patients were pre-treated with aspirin and clopidogrel (300-600mg loading dose) and both were continued for 1 year. Heparin was used to maintain an activated clotting time (ACT) ≥250 seconds. Upstream use of glycoprotein IIb/IIIa inhibitor therapy was left to the operator's discretion.

Definitions and Clinical Follow-up

Technical success was defined as restoration of TIMI flow grade 3 with stent implantation and residual stenosis <20% by visual estimate. Procedural success was defined as technical success in the absence of death, Q-wave or non-Q wave MI (> 3 fold increase of creatine kinase MB), stroke, pericardial effusion requiring pericardiocentesis, emergency coronary artery bypass grafting (CABG), defined as bypass surgery within 24 hours of the procedure. Confirmed stent thrombosis was defined as angiographically or pathologically documented stent occlusion with TIMI grade 0 or 1 flow or residual thrombus at the stent site occurring within 24 hours of the index procedure (acute), between 24 hours and 1 month after the procedure (sub-acute) or more than 1 month after the procedure (late thrombosis). Suspected stent thrombosis was defined as sudden death or MI with electrocardiographic changes in the territory of the treated artery without demonstration at angiography or on post-mortem examination.
Clinical follow-up was performed by outpatient visit and telephone enquiries. Patients were evaluated for survival-free of major adverse cardiac events (MACE), such as death, non-fatal MI or repeat target vessel revascularisation (TVR).

Coronary Interventions

Coronary interventions were performed electively according to standard practice with DES implantation through a 6 Fr guiding catheter with an inner diameter of 0.071". Stent optimization was accomplished with conventional angiographic guidance aiming at a residual diameter stenosis <10% by visual estimate. Implantation of multiple stents (≥2) with overlap was always followed by high pressure post-dilatation using non-compliant balloons. Four different DES were used in this study (Cypher Select™, Cordis, Johnson and Johnson Co., Miami Lake, FL, US, Taxus Liberte™ Boston Scientific, Natick, MA, US, Endeavor™ , Medtronic, Santa Rosa, CA, US and CoStar™ (Conor Medsystems, Inc., Hamilton Court Menlo Park, CA, US).

OCT Imaging

The OCT system used in this study (LightLab Imaging Inc., Westford, MA, US) has been described previously.(1) Briefly, an over-the-wire OCT catheter (Helios™ proximal occlusion catheter) is advanced distal to the stented lesion over a conventional coronary guide wire, which is then replaced with the OCT imaging wire (ImageWire™). The OCT catheter is then withdrawn proximal to the stented segment and the lesion visualised using an automated pullback system at 1.0mm/sec. During image acquisition, coronary blood flow is replaced by continuous infusion of Ringer's lactate at 0.5-1.5ml/sec using a power injector (Mark V ProVis, Medrad, Inc. Indianola, PA, US). The highly compliant occlusion balloon remains inflated proximal to the lesion at 0.5 or 0.7atm for a maximum of 30sec. Meticulous attention must be paid to haemodynamic monitoring of the patient during the proximal occlusion and intra-coronary flush.
Cross sectional images are acquired at 15.4 frames/sec. In case the lesion is not fully imaged in the first pullback, the imaging sensor is left in position and a second or occasionally third pullback is required to achieve complete lesion assessment. In such circumstances, the pullback is stopped as soon as a decision is taken to deflate the balloon and stop the infusion, and the new pullback is started after patient recovery from exactly the same position whilst the blood is being cleared by a new infusion.

Off-line OCT Analysis

Analysis of contiguous cross-sections within the stented segment was performed at 1 mm intervals. In each selected cross section, the distance between endoluminal edge of the strut and intima was measured. Measurements were classified into 3 grades of apposition: '*embedded*', '*protruding*' or '*malapposed*'.(1) Since only the endoluminal surface of struts can be identified with OCT, distances were adjusted based on the thickness of the strut including the polymer layer (Table 1). Struts buried in the intima for more than half of their thickness were defined as *'embedded'*, those apposed to the intima but not embedded were defined as '*protruding*' and those with no contact to the intima were defined as *'malapposed'* (Figure 1). Struts protruding into a side branch ostium were excluded from the analysis.

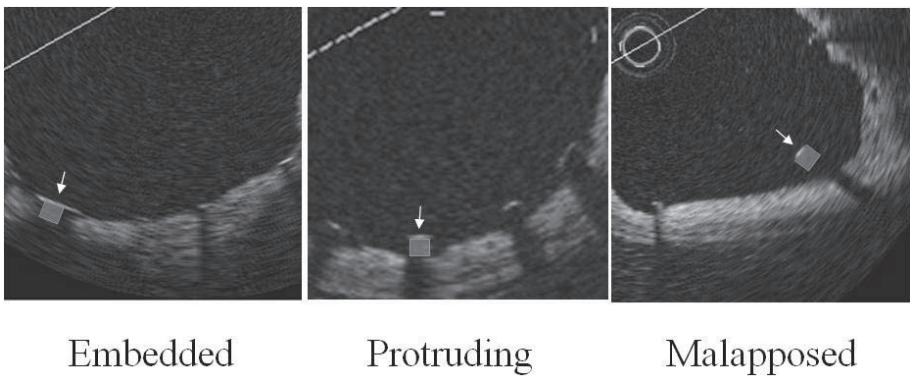

Figure 1: Classification of stent strut apposition
The distance between the endoluminal surface of the strut and the intima was measured by OCT and adjusted for strut thickness to calculate the gap between the strut and the intima. Based on this value, struts were classified into 3 grades: embedded, protruding and malapposed.

	Strut thickness					
	Metal Strut	**Polymer**	**Total Thickness**	**Embedded**	**Protruding**	**Malapposed**
Cypher Select	140	7	154	<80	80-160	≥160
Taxus Liberte	97	15	127	<65	65-130	≥130
Endeavor	91	8*	107	<55	55-110	≥110
Co Star	89	No	89	<45	45-90	≥90
Values are (μm), *Average thickness of uneven endo- and abluminal polymers						

Table 1. Strut thickness and classification of apposition of the DES used in this study

Statistical Analysis

Statistical analysis was performed using R version 2.4.1 (The R Foundation for Statistical Computing, Vienna, Austria) and MLwiN version 2.02 (Centre for multilevel modelling, University of Bristol, UK) with residual iterated generalised least squares and pseudoquasi-likelihood model specifications. Data are expressed as mean ± standard deviation for continuous variables and as percentages for categorical variables. Comparison between groups was performed using the two-sample Wilcoxon test for continuous variables and Fisher's exact test for count data. Distribution of strut-to-intima distance was graphically represented by means of

histograms of probability densities (with a total histogram area of 1). The Shapiro-Wilk test was used to assess normality of continuous variables.

Since the observation of struts in the same stent are not independent of each other, it would be wrong to use standard regression analysis to identify predictors of strut malapposition, as this assumes independence of observations. Given the hierarchical nature of the data (stent struts nested within lesions nested within patients), multilevel logistic regression with malapposition as the outcome variable was applied to address random and fixed effects at the strut, lesion and patient levels. At the lesion level, presence of calcification, type C lesions, stent type (Cypher versus non-Cypher), stent length, stent diameter, maximal balloon size and maximum inflation pressure were considered. At the patient level, age, sex and diabetes mellitus were considered. A two-tailed p-value of <0.05 was used as the criterion for statistical significance for all analyses.

Results

Baseline Clinical Characteristics

Between February 2006 and August 2006, 36 stents implanted in 25 complex lesions from 23 patients were assessed using OCT. Baseline clinical characteristics are shown in Table 2. Mean age of patients was 64.5±10.3 years with 91.3% male. Diabetes mellitus was a risk factor in 17.4% of patients with nearly half of the patients presenting with an acute coronary syndrome.

n=23 patients	
Age (years)	64.5±10.3
Male gender, n (%)	21 (91.3)
Hypertension, n (%)	14 (60.8)
Hyperlipidemia, n (%)	20 (86.9)
Diabetes Mellitus, n (%)	4 (17.4)
Smoker (current/former), n (%)	17 (73.9)
Familial history of IHD, n (%)	14 (60.1)
Stable angina, n (%)	14 (60.1)
ACS presentation, n (%)	11 (47.8)
Previous MI, n (%)	7 (30.4)
Previous CABG, n (%)	3 (13.0)

Table 2. Baseline Clinical Characteristics

Angiographic and Procedural Characteristics

Angiographic and procedural characteristics are shown in Table 3. All lesions were complex (ACC/AHA classification type B or C), including long and severely calcified lesions as well as bifurcations. The LAD was the target vessel in almost half of all cases.

Cypher Select™ (Cordis, Johnson and Johnson Co., Miami Lake, FL, US) and Taxus Liberte™ (Boston Scientific, Natick, MA, US) stents were predominantly used while Endeavor™ (Medtronic, Santa Rosa, CA, US) and CoStar™ (Conor Medsystems, Inc., Hamilton Court Menlo

Park, CA, US) stents were used in 4 cases. Overlap stenting was performed in 40% of cases due to long lesion length. During OCT acquisition, intra-coronary infusion with Ringer's lactate was performed at a rate of 0.92±0.25 (Range: 0.5-1.5) ml/sec. There was no haemodynamic instability or arrhythmias during acquisition and no subsequent coronary dissection. Only one patient had transient slow flow because of air embolisation after withdrawal of the occlusion catheter. Treatment with air aspiration and intra-coronary nitroprusside led to prompt restoration of TIMI-grade-3 flow. The patient had presented with an acute coronary syndrome and the peak post-procedural troponin I and creatine kinase were 1.23µg/L and 387U/L respectively.

OCT assessment of strut apposition

A total of 6,402 struts were evaluated (256±108 struts/lesion). An average of 57.1±20.7% struts were embedded, 33.8±18.4% protruding and 9.1±7.4% malapposed per lesion. The mean difference in SSA classification between the 2 observations made by the same operator was 1.8% (95% limits of agreement [LA]: -11 to 7.1%) for embedded, 0.043% (95% LA: -7.9 to 7.8%) for protruding and 1.8% (95% LA: -2.1 to 5.6%) for malapposed struts. Interclass correlation coefficient for the three categories was 0.98 (95% CI: 0.94-0.99) for embedded, 0.98 (95% CI: 0.95-0.99) for protruding and 0.95 (95% CI: 0.86-0.98) for malapposed.
The rate of malapposed struts per lesion ranged between 0 and 21.7% of the total struts assessed, with 88% of lesions having at least 1 malapposed strut.

Predictors of strut malapposition

Univariate predictors of malapposition on multilevel logistic regression analysis are shown in table 4 and figure 2. Implantation of a Cypher stent was a strong predictor of malapposition, together with the presence of a overlapping stents, a longer stent length, a type C lesion, performance of post-dilatation, a higher maximal inflation pressure and diabetes mellitus.

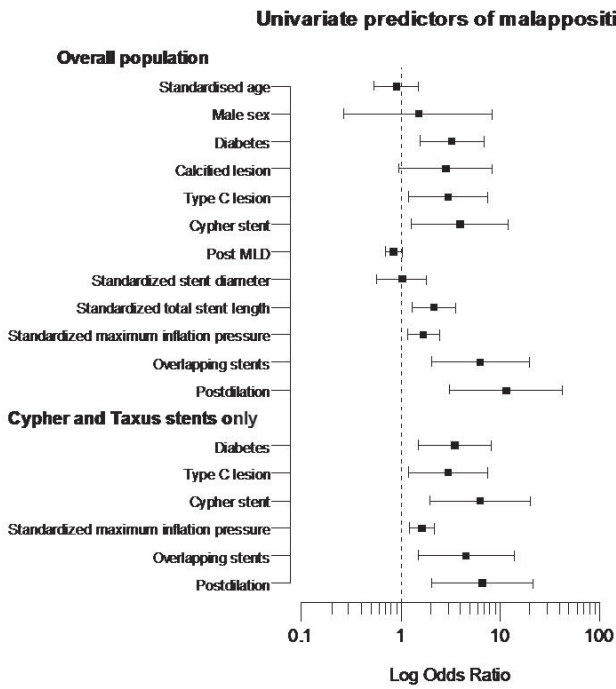

Figure 2: Predictors of malapposition on multilevel logistic regression analysis in the overall population and the subset of patients treated with either Cypher or Taxus stents (significant predictors only shown for the latter).

n=25 lesions	
Angiographic Characteristics	
ACC/AHA classification n, (%) **Type B** **Type C**	 16 (64) 9 (36)
Target vessels, n (%) **LAD** **RCA** **LCx**	 12 (48) 7 (28) 6 (24)
Location, n (%) **Proximal** **Mid** **Distal**	 5 (20) 15 (60) 5 (20)
Bifurcation, n (%)	12 (48)
Severe calcification, n (%)	6 (24)
Stent type	
Cypher Select, n (%)	13 (52)
Taxus Liberte, n (%)	8 (32)
Endeavor, n (%)	1 (4)
CoStar, n (%)	3 (12)
Average stent number per lesion	1.4 ± 0.6
Average stent diameter (mm)	2.97 ± 0.35
Total stent length (mm)	32.5 ± 14.4
Pre-dilatation (%)	19 (76)
Post-dilatation (%)	20 (80)
Maximum balloon diameter (mm)	3.09 ± 0.30
Maximum balloon artery ratio	1.26 ± 0.19
Maximum balloon pressure (atm)	17.5 ± 3.0
Multiple stenting (%overlapping/ %culotte)	10 (40)/ 4 (16)
QCA Pre-procedural	
Reference vessel diameter (mm)	2.51 ± 0.43
Minimal lumen diameter (mm)	1.07 ± 0.34
Diameter stenosis (%)	57.0 ± 14.0
Lesions length (mm)	18.9 ± 11.1
QCA Post-procedural	
Reference vessel diameter (mm)	2.98 ± 0.43
Minimal lumen diameter (mm)	2.59 ± 0.43
Diameter stenosis (%)	13.3 ± 6.1

Table 3. Angiographic and Procedural Characteristics

Difference of Stent Type: Cypher and Taxus

To further investigate the role of stent type on SSA, separate analysis was performed using only data from lesions in which the 2 most commonly used types of DES (Cypher Select, n=13 and Taxus Liberte, n=8) were implanted. Data on a total of 21 lesions were analysed. There were more overlapping stents in the Cypher group (6 (46.2%) versus 1 in the Taxus group (12.5%), p=0.173) and pre-MLD was lower in the Taxus group (0.95±0.28mm versus 1.22±0.27mm in the Cypher group, p=0.053).

A significant difference was found in % embedded (40.2±8.6% vs. 73.3±13.6%. p<0.0001), % protruding (48.1±10.1% vs. 23.0±10.5%, p<0.0001) and % malapposed (11.6±6.6% vs. 3.7±5.2%, p=0.007) struts between the Cypher and Taxus group (Figure 3). In fact, a wider distribution of the distance between the endoluminal surface of the strut and the intima was observed in the Cypher group, with more struts at less than 50μm from the intima in the Taxus group (Figure 4). Stent type was a strong predictor of malapposition on multilevel logistic regression analysis, together with overlap stenting, post-dilatation, type C lesions, diabetes mellitus and maximal balloon inflation pressure (Figure 2).

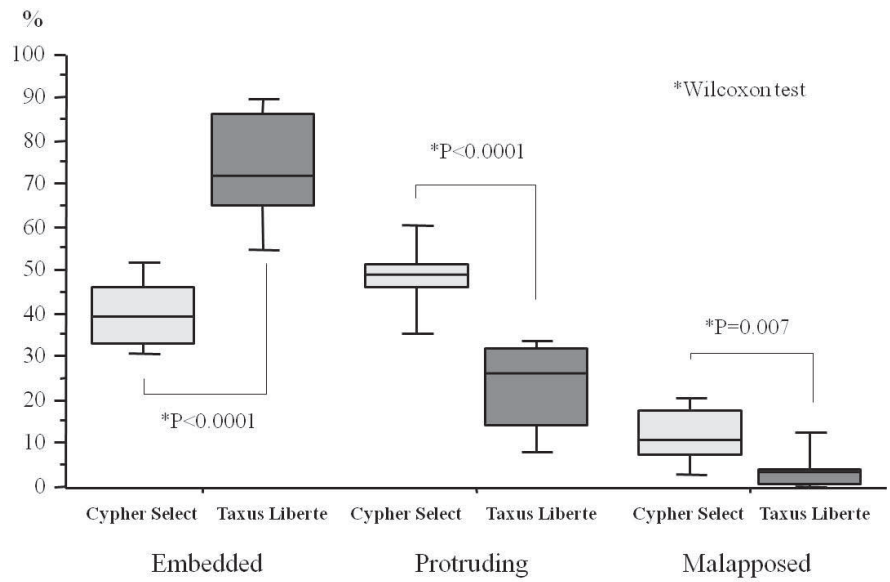

Figure 3: Differences in stent strut apposition: Cypher Select vs. Taxus Liberte
Cypher Select stent struts were less likely to be embedded and more likely to be protruding and malapposed compared with Taxus Liberte stents.

Clinical Outcomes

Twelve month follow-up was available for all patients. Five months after the index procedure, 1 patient had repeat angiography to evaluate chest pain and an equivocal exercise stress test. He had a heavily calcified long lesion of the LCx treated with 3 Cypher stents in an overlap fashion. Angiography showed an excellent result of the previously stented segment with no other coronary stenosis. There were no adverse events encountered and no episodes of stent thrombosis.

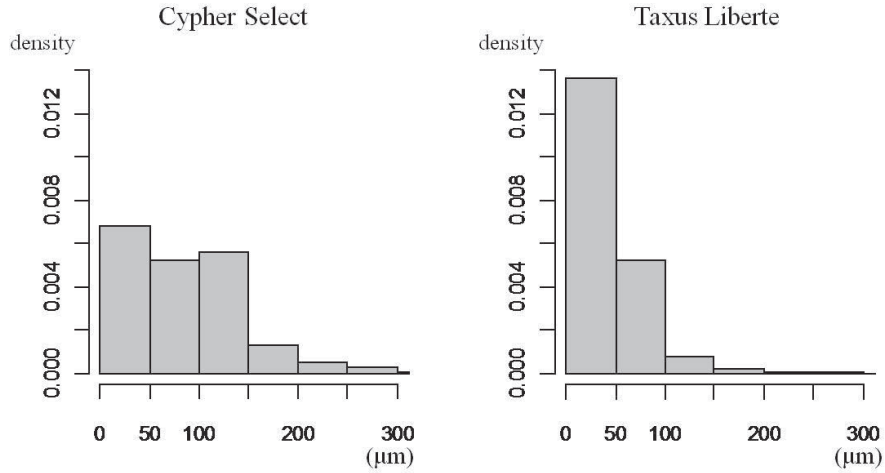

Figure 4: Histograms of probability densities of the distance between the endoluminal surface of the strut and the intima for the Cypher and Taxus Groups
A wider distribution of distances is seen for Cypher Select stents, with more struts lying at a greater distance from the intima compared to Taxus Liberte stents.

Discussion

This is the first study using OCT to assess stent strut apposition systematically following implantation. Our study has shown that in complex coronary lesions, stent strut malapposition persists despite angiographic optimisation. Further, the thinner struts of the Taxus Liberte stent with its open cell design were more likely to be embedded to the vessel wall compared to the thicker Cypher stent struts employing a closed-cell system. Nevertheless, using high pressure stent expansion with properly sized balloons, the absence of clinical events at 12 follow-up suggests that the frequent persistence of malapposed struts remains a benign phenomenon.

Comparison with previous studies

Information on what is currently known linking strut malapposition and stent thrombosis is primarily derived from pathological series. Ante-mortem correlations are scarce but 2 studies (14,15) using conventional intravascular ultrasound (IVUS) suggested that stent malapposition did not increase the risk of major adverse cardiac events. Nevertheless, both studies detected a surprisingly small number of malapposed stents using the IVUS derived criterion of at least 1 malapposed strut (51/708 cases, 7.2% and 16/229 cases, 7.0%). Our study found a greater proportion of malapposed struts, mainly because of the more detailed assessment afforded by OCT. Nevertheless, like the previous IVUS studies which found no adverse clinical outcomes as a result of malapposed struts, our study confirms this with mid-term follow-up.

Classification of apposition

In the present study, we propose novel OCT derived cut-off values to stratify SSA as embedded, protruding or malapposed. This classification takes into consideration the thickness of the different DES in current use. Our data suggest that just over half of all DES struts implanted in complex coronary lesions were optimally embedded in the vessel intima despite aggressive optimisation of stent deployment. It remains, however, unknown whether these minor degrees of strut protrusion or malapposition now detected with OCT are of clinical and prognostic significance beyond mid-term follow-up.

Causes of incomplete apposition

In our study, stent type was a strong predictor of strut malapposition. Cypher Select stents showed almost 50% less embedded struts compared to the Taxus Liberte stents (figure 3). The Cypher Select stent has thicker metal struts (140μm) compared to other stents (89-97μm) and this may affect the stent's conformability to the uneven intimal surface. Since the stents also have different design, it is difficult to know how much of the difference in apposition is due to strut thickness and how much is due to the close cell design of Cypher Select stent, which ensures more uniform coverage and radial support (16) but may be inferior to other designs in terms of conformability.

Higher pre-MLD and higher maximum dilatation pressure were associated with a lower number of embedded struts in our study. This sounds paradoxical, as one would expect optimal stent deployment in less severe lesions and with higher inflation pressures. Stent struts deployed in tighter lesions are more likely to be pressed against the intima and become embedded during balloon inflation compared to struts in milder lesions. Higher pressures were used by the operators when there was angiographic evidence of poor balloon or lumen expansion and reflect the presence of resistant fibrotic or calcific wall changes. As indicated in figure 5, there is no potential for full apposition in the non-circular geometry of eccentric focal heavy calcification and, higher pressures increase lumen expansion but may paradoxically increase malapposition under these circumstances.

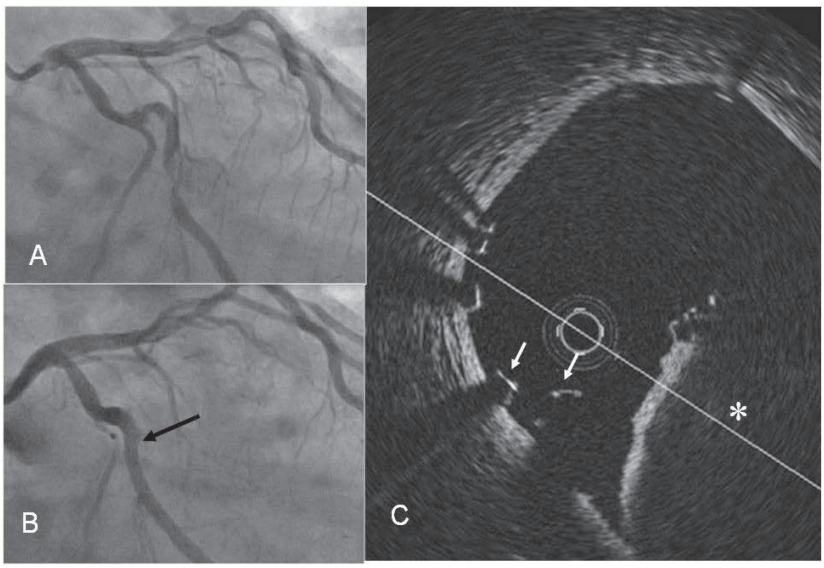

Figure 5: Optical coherence tomography of a severely calcified lesion

A. Right caudal view showing an eccentric and long calcific stenosis in the mid portion of the left circumflex.
B. Final angiographic result following Cypher stent implantation and high pressure post-dilatation. The black arrow indicates the region imaged by OCT.
C. OCT imaging showing transformation of stent geometry caused by the eccentric focal heavy calcification (*). Struts are completely malapposed to the intima at the segment between fibrous intima and area of superficial calcification (white arrows).

Clinical implications of malapposition

Considerable interest exists linking the use of DES with late and very late stent thrombosis. The aetiology for this relation however remains ill-defined. Malapposition has been found to correlate with poor intimal coverage and subsequent stent thrombosis in autopsy series.(7,10,11)

Conceptually, it is obvious that a strut fully embedded has a lower potential to trigger fibrin and platelet deposition than a strut floating in the lumen. Matsumoto et al (17) reported malapposed struts were more frequently incompletely covered with intima. Recently, Takano et al (18) also confirmed this finding investigating sirolimus-eluting stents with OCT 3 months after implantation. Bare struts were also more frequently observed in patients presenting with acute coronary syndrome (ACS) and, such struts were also more often malapposed (18).

Univariate predictors of % embedded			
	Estimate	**95% CI**	**p-value**
Stent Type: Taxus Liberte vs. Cypher Select	33.11	23.66-45.26	<0.001
Endeavor vs. Cypher Select	53.89	32.06-75.72	<0.001
CoStar vs. Cypher Select	34.20	20.73-47.67	<0.001
Pre-procedural Minimal Lumen Diameter	-27.08	-50.89- -3.26	0.028
Smoking	-18.50	-35.44- -1.56	0.034
Maximum Dilatation Pressure	-2.74	-5.45- -0.03	0.048
Multivariate predictors of % embedded			
Stent Type: Taxus Liberte vs. Cypher Select	33.11	23.66-45.26	<0.001
Endeavor vs. Cypher Select	53.89	32.06-75.72	<0.001
CoStar vs. Cypher Select	34.20	20.73-47.67	<0.001
Univariate predictors of % malapposed			
Stent Type: Taxus Liberte vs. Cypher Select	-7.93	-13.60- -2.26	0.009
Endeavor vs. Cypher Select	-11.63	-24.73- 1.47	0.080
CoStar vs. Cypher Select	3.84	-4.24 -11.92	0.337
Post Dilatation	9.59	3.00 -16.18	0.006
Multiple Stenting	7.21	1.82-12.61	0.011
Total Stent Number per Lesion	6.33	1.62-11.05	0.011
Maximum Dilatation Pressure	1.17	0.24-2.09	0.016
Total Stent Length	0.21	0.01-0.41	0.045
Post-procedural Diameter Stenosis	0.49	0.01-0.96	0.045
Multivariate predictors of % malapposed			
Stent Type: Taxus Liberte vs. Cypher Select	-5.84	-11.13- -0.54	0.03
Endeavor vs. Cypher Select	-9.03	-20.82- 2.76	0.13
CoStar vs. Cypher Select	6.44	-1.02 -13.90	0.09
Maximum Dilatation Pressure	1.03	0.21-1.84	0.02

Table 4. Univariate and Multivariate Predictors of % Embedded and Malapposed Struts

The lack however of adverse events at 1 year, even in patients with a high number of malapposed struts in our study and in previous IVUS studies suggests that other factors must be at play. All our patients were prescribed dual anti-platelet therapy for 12 months which, in itself, may act to

protect against thrombus formation on malapposed struts. After reviewing autopsy studies, Joner et al (7) identified that stent thrombosis was multi-faceted with predictors in addition to malapposition being a polymer induced hypersensitivity reaction, ostial and/or bifurcation stenting, restenosis and strut penetration into a necrotic core. Therefore, it appears malapposition is but one piece of the yet to be completed puzzle.

Limitations

As this was a small non-randomised study, it cannot be excluded that the difference observed between the Cypher and Taxus stents could be due to differences in baseline and treatment characteristics. Although multilevel logistic regression was used accounting for the hierarchical nature of the data, this was limited to univariate analyses and produced estimates with relatively large confidence intervals due to the small number of lesions and patients included in this study. Further, larger studies with longer follow-up and serial OCT examinations are essential to truly understand the importance of malapposition on strut coverage and its possible relation to late stent thrombosis.

Conclusions

Despite angiographic optimisation with high pressures and adequately sized balloons, malapposed stent struts are frequently found in complex coronary lesions and more often following the implantation of Cypher Select stents which have a thicker stent strut and closed cell design compared to other DES. With no adverse clinical events at 12 months follow-up, this likely represents a benign phenomenon at least as long as combined anti-platelet therapy is maintained.

References

1. Tanigawa J, Barlis P, Di Mario C. Intravascular Optical Coherence Tomography: Optimisation of image acquisition and quantitative assessment of stent strut apposition. EuroIntervention 2007;3:128-136.
2. Dawkins KD, Grube E, Guagliumi G, et al. Clinical efficacy of polymer-based paclitaxel-eluting stents in the treatment of complex, long coronary artery lesions from a multicenter, randomized trial: support for the use of drug-eluting stents in contemporary clinical practice. Circulation 2005;112:3306-13.
3. Urban P, Gershlick AH, Guagliumi G, et al. Safety of coronary sirolimus-eluting stents in daily clinical practice: one-year follow-up of the e-Cypher registry. Circulation 2006;113:1434-41.
4. Iakovou I, Schmidt T, Bonizzoni E, et al. Incidence, predictors, and outcome of thrombosis after successful implantation of drug-eluting stents. Jama 2005;293:2126-30.
5. Kuchulakanti PK, Chu WW, Torguson R, et al. Correlates and long-term outcomes of angiographically proven stent thrombosis with sirolimus- and paclitaxel-eluting stents. Circulation 2006;113:1108-13.
6. Cook S, Wenaweser P, Togni M, et al. Incomplete stent apposition and very late stent thrombosis after drug-eluting stent implantation. Circulation 2007;115:2426-34.
7. Joner M, Finn AV, Farb A, et al. Pathology of drug-eluting stents in humans: delayed healing and late thrombotic risk. J Am Coll Cardiol 2006;48:193-202.
8. Kotani J, Awata M, Nanto S, et al. Incomplete neointimal coverage of sirolimus-eluting stents: angioscopic findings. J Am Coll Cardiol 2006;47:2108-11.
9. Daemen J, Wenaweser P, Tsuchida K, et al. Early and late coronary stent thrombosis of sirolimus-eluting and paclitaxel-eluting stents in routine clinical practice: data from a large two-institutional cohort study. Lancet 2007;369:667-78.
10. Finn AV, Joner M, Nakazawa G, et al. Pathological correlates of late drug-eluting stent thrombosis: strut coverage as a marker of endothelialization. Circulation 2007;115:2435-41.

11. Finn AV, Nakazawa G, Joner M, et al. Vascular responses to drug eluting stents: importance of delayed healing. Arterioscler Thromb Vasc Biol 2007;27:1500-10.
12. Rittersma SZ, de Winter RJ, Koch KT, et al. Impact of strut thickness on late luminal loss after coronary artery stent placement. Am J Cardiol 2004;93:477-80.
13. Kawase Y, Hoshino K, Yoneyama R, et al. In vivo volumetric analysis of coronary stent using optical coherence tomography with a novel balloon occlusion-flushing catheter: a comparison with intravascular ultrasound. Ultrasound Med Biol 2005;31:1343-9.
14. Hong MK, Mintz GS, Lee CW, et al. Incidence, mechanism, predictors, and long-term prognosis of late stent malapposition after bare-metal stent implantation. Circulation 2004;109:881-6.
15. Tanabe K, Serruys PW, Degertekin M, et al. Incomplete stent apposition after implantation of paclitaxel-eluting stents or bare metal stents: insights from the randomized TAXUS II trial. Circulation 2005;111:900-5.
16. Suzuki Y, Ikeno F, Yeung AC. Drug-eluting stent strut distribution: a comparison between Cypher and Taxus by optical coherence tomography. J Invasive Cardiol 2006;18:111-4.
17. Matsumoto D, Shite J, Shinke T, et al. Neointimal coverage of sirolimus-eluting stents at 6-month follow-up: evaluated by optical coherence tomography. Eur Heart J 2007;28:961-7.
18. Takano M, Inami S. Evaluation by Optical Coherence Tomography of Neointimal Coverage of Sirolimus-Eluting Stent Three Months After Implantation. Am J Cardiol 2007.

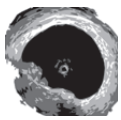

Chapter 16

The use of intra-coronary optical coherence tomography for the assessment of sirolimus-eluting stent fracture

Peter Barlis, Georgios Sianos, Giuseppe Ferrante, Francesca Del Furia, Savio D'Souza, Carlo Di Mario

Drug-eluting stents (DES) have made a tremendous impact on the practice of percutaneous coronary intervention. Recently however, long-term DES failures have become a focal point, particularly with restenosis and thrombosis. An uncommon, yet important cause of DES failure is stent fracture. Of the two established first generation DES, the sirolimus-eluting stent (SES) has been particularly linked to cases of stent fracture, likely as a result of its closed cell design compared with other DES employing an open cell system. We present 2 cases of SES fracture confirmed using high-resolution intravascular optical coherence tomography giving unique insights into the in-vivo appearance of this complication.

Drug-eluting stents (DES) have significantly reduced restenosis compared to bare metal stents (BMS) and have helped establish percutaneous coronary intervention (PCI) as the mainstay invasive therapy for patients with coronary artery disease. More recently however, attention has been drawn to the problems of late DES failures, particularly stent thrombosis. The causes behind DES failures remain complex and multi-factorial. When in-stent restenosis occurs, this is usually focal in nature while mechanical factors such as stent fracture have also been implicated [1]. Of the two established first generation DES, the sirolimus-eluting stent (SES, Cordis, J&J, Miami, Florida, US) has been particularly linked to cases of stent fracture, likely as a result of its closed cell design compared with other DES employing an open cell system [2]. We present 2 cases of SES fracture confirmed using high-resolution intravascular optical coherence tomography (OCT) giving unique insights into the in-vivo appearance of this complication.

Case 1

A 66-year-old diabetic male underwent coronary artery bypass grafting (CABG) in 2002 because of symptomatic angina. The right internal mammary artery (RIMA) was grafted to the left anterior descending (LAD) while the left internal mammary artery (LIMA) was grafted to the dominant left circumflex artery obtuse marginal branch. In 2004 he was admitted because of escalating angina. Angiography revealed a patent RIMA graft however the LIMA graft contained a critical stenosis in the highly angulated mid-segment (Figure 1A). Following pre-dilatation, two 3.5 mm bare metal Driver (Medtronic Inc., Minneapolis, US) stents were deployed giving a very good angiographic result (Figure 1B).

In 2005, he presented with a non-ST-elevation myocardial infarction and was found to have severe in-stent restenosis of the LIMA graft (Figure 1C). Following pre-dilatation, a 3.5 × 33 mm SES was implanted and post-dilated with a non-compliant balloon (Figure 1D).

In 2007, because of angina, a nuclear perfusion scan was arranged. This revealed extensive reversible perfusion defects in the infero-lateral wall. Repeat coronary angiography revealed that the LIMA graft had a significant stenosis at the hinge point within the previously stented segment (Figure 2). Using optical coherence tomography, we confirmed the presence of a fracture of the SES implanted in 2005 with gross hyperplasia and almost complete obliteration of the lumen (minimal lumen area 0.71 mm2). Further, the SES lacked circumferential struts with extensive disarray, consistent with fracture (Figure 2B–C).

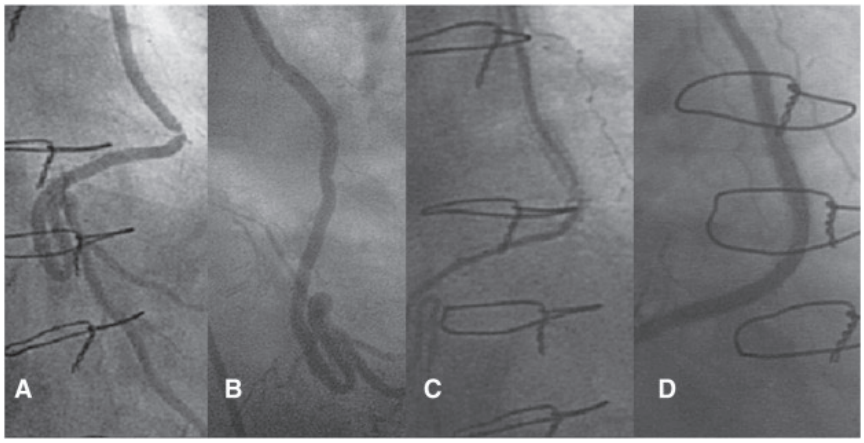

Figure 1 A: Illustrates the left internal mammary artery (LIMA) graft with a critical stenosis in the highly angulated mid-segment. B: Immediate angiographic appearance following pre-dilatation and implantation of two 3.5 mm bare metal Driver (Medtronic Inc., Minneapolis, US) stents. C: Angiography 12 months following initial stent implantation demonstrating critical in-stent-restenosis. D: Final angiographic result following treatment with a 3.5 × 33 mm sirolimus-eluting stent (SES).

see colour section

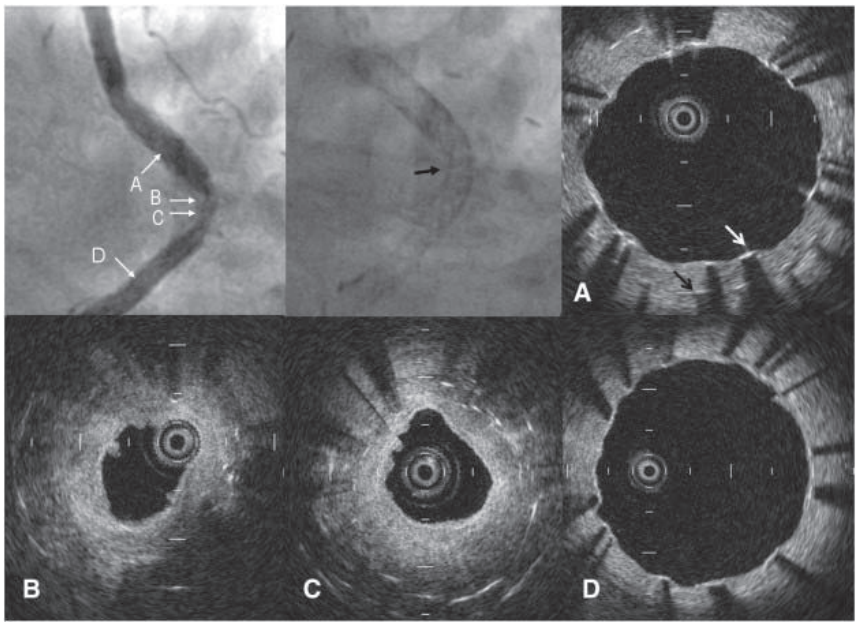

Figure 2 Two years following stenting, angiography confirmed a significant stenosis at the hinge point within the previously stented segment (black arrow). A: Optical coherence tomography (LightLab Imaging Inc., Westford, MA, USA) was acquired during simultaneous contrast flush through the guiding catheter at a pullback speed of 1 mm/s. This proximal cross-section shows 2 layers of stent struts coinciding with the previously deployed bare metal stent (black arrow) and the SES (white arrow). B–C: Imaging at the level of the stenosis reveals gross hyperplasia and almost complete obliteration of the lumen (minimal lumen area 0.71 mm^2) with absence of circumferential struts. D. OCT distal to the stenosis showed the struts of the SES were widely patent with thin coverage of neointimal tissue (10–30 μm).

see colour section

As a result of the previous failures, we were reluctant to implant a further stent and elected to attempt recanalisation of the occluded native proximal LCx. With bilateral femoral access, a guide wire was passed retrogradely through the LIMA graft through the anastomosis of the obtuse marginal in the direction of the native LCx. Using the retrograde wire as a guide (Figure 3A), we were able to pass a hydrophilic wire antegradely, pre-dilate the occlusion and, finally implant two Taxus Liberte stents (Boston Scientific, Natick, US), both expanded to 3.0 mm at high pressure (Figure 3B). The patient remains symptom-free 12 months following the recent procedure.

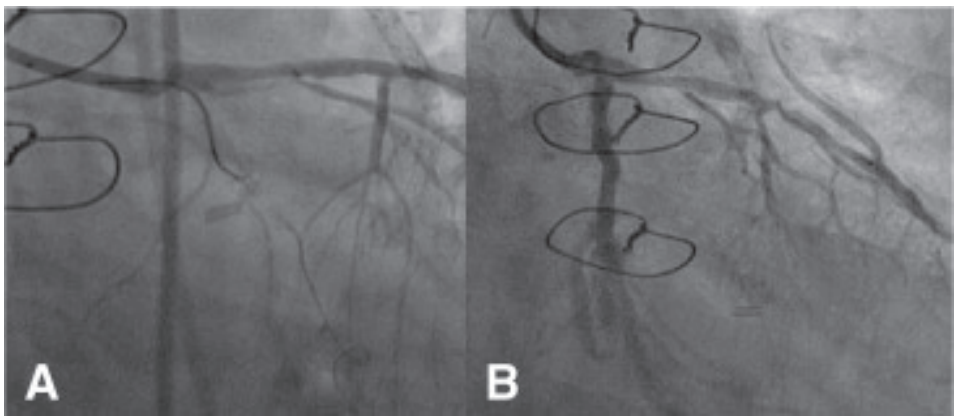

Figure 3. Recanalisation of the native occluded left circumflex artery was undertaken with the left coronary artery and the left internal mammary artery graft retrogradely. Using the retrograde wire as a guide, a hydrophilic wire was advanced antegradely. The occlusion was pre-dilated with final implantation of two Taxus Liberte stents (Boston Scientific, Natick, US).

Case 2

A 62-year-old man with strong family history of coronary artery disease developed new onset chest pain. He was found to have a high calcium score (> 2000) on computed tomography and subsequently underwent coronary angiography. This demonstrated a significant lesion in the proximal and mid-LAD that was sub-totally occluded together with diffuse disease in the diagonal branch (Figure 4A). Percutaneous coronary intervention was discussed and this was performed with the implantation of 2 SES in an overlapping fashion (2.25 × 23 mm followed by 2.5 × 18 mm proximally) post-dilated to 18 18 atm with a 2.5 mm balloon (Figure 4B). Nine months following the procedure, the patient presented with recurrent chest pain. Coronary angiography revealed 2 discrete areas of restenosis occurring within the previously implanted SES at 2 hinge points of the LAD (Figure 4C, white arrows). There was also disease progression in the proximal LAD. OCT was undertaken to assess the lesions in greater detail. Coinciding with the 2 regions of restenosis, OCT showed focal stent fracture with significant intimal hyperplasia, lack of circumferential stent struts and altered stent and vessel geometry (Figure 5). The lesions were treated with high-pressure balloon dilatation and with new stent implantation to the diseased proximal LAD segment (Figure 4D). The patient remains symptom-free at 9-month follow-up and with aggressive risk factor modification.

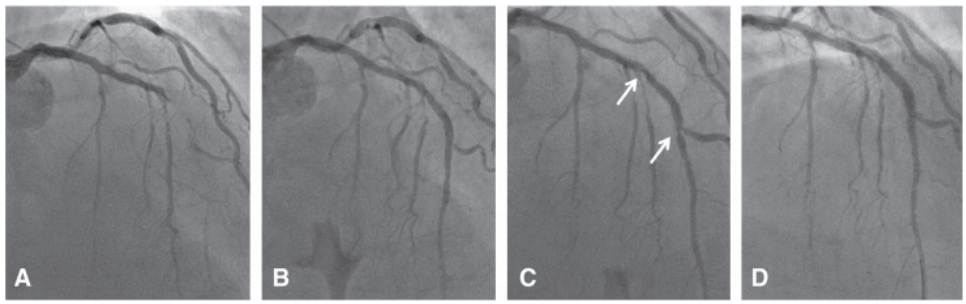

Figure 4. Antero-posterior cranial view showing the left anterior descending artery with significant stenosis in the mid-segment and diagonal branch. Immediately following implantation of 2 sirolimus-eluting stents. Nine-month follow-up angiography showed 2 sites of restenosis but no obvious fracture. Following high-pressure balloon dilatation and further stent implantation.

see colour section

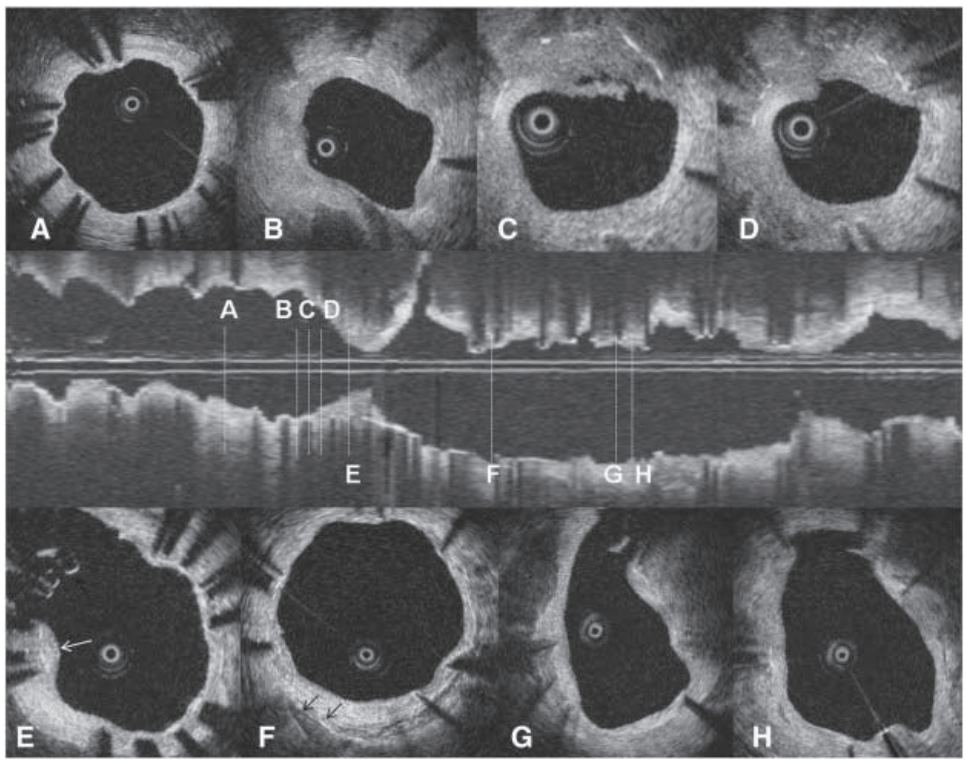

Figure 5. OCT demonstrating a widely patent stent with a thin layer of neointimal tissue. B–D: Shows the more distal lesion with significant luminal narrowing as a result of intimal hyperplasia. The cross-sections demonstrate the lack of circumferential stent struts and altered stent and vessel lumen geometry. E: Shows the OCT appearance at the level of the side branch. 3 stent struts are shown at the carina with no visible tissue coverage (black arrow) while the surround stent struts show an exaggerated intimal tissue response (white arrow). F: Demonstrates circumferential stent struts covered by a thin tissue layer. Also evident is a fibro-calcific plaque (black arrows) with its low reflective appearance and sharp margins. G–H: Shows the lack of circumferential stent struts resulting in considerable disruption of vessel and lumen geometry.

see colour section

Discussion

Although uncommon, stent fracture is increasingly being reported in the literature and, in the DES era, is more often associated with SES [3], [4], [5], [6] and [7]. In a recent study of 530 patients who received DES with follow-up angiography, Lee et al. [2] identified stent fracture in 10 (1.9%) patients, all restricted to those with SES. Similarly, Aoki et al. [6] studied 280 patients following SES implantation and identified stent fracture in 2.6% of cases. In this study, significant multivariate predictors of stent fracture were saphenous vein graft location (OR 35.88; 95% CI 2.73–471.6, p = 0.006), implanted stent length (OR 1.04; 95% CI 1.01–1.07, p = 0.02), and right coronary artery location (OR 10.00; 95% CI 1.11–89.67, p = 0.04). In another study, Lee et al. [8] followed up 588 patients and found 26 patients with SES in-stent restenosis (ISR) and 30 BMS ISR lesions. Of 26 cases of ISR lesions associated with SES, stent fracture was identified in 10. There were no cases of stent fracture in the BMS group. In 7 patients that received a single SES, the fracture occurred at the mid-segment of the stent. As a result of the lack of stent fracture within BMS, the authors concluded that the lack of stent protection by neointima at an early stage of stent implantation might contribute to stent fracture.

Stent fracture has been identified in cases of under or over-expanded stents, long stented segments, repetitive kinking caused by vessel movement during the cardiac cycle and in tortuous vessels. Furthermore, the closed cell design of the SES and thicker metal struts (metal and polymer thickness of 154 μm) may be critical in making this stent more rigid and inflexible compared with other stent types. This should be considered in situations where lesions occur at hinge points and the operator may then consider an alternative stent to implant.

The diagnosis of stent fracture has traditionally been limited to findings on coronary angiography. Recently however, Yamada et al. [7] demonstrated the limitations of angiography by studying 102 consecutive patients receiving SES. Angiography failed to detect any cases of stent fracture at 6 months whereas intravascular ultrasound (IVUS) identified 3 cases. Although IVUS remains the current gold standard for the detailed assessment of the results following stent implantation, this too has several limitations. The resolution of IVUS is in the realms of 150 mm and the sound echoes frequently cause artifacts. In our 2 cases, we used a relatively new imaging technology using near infra-red light with 10 times the resolution of IVUS and fewer artifacts.

The use of OCT to confirm stent fracture in our report highlights the unique detail afforded by this technique. In the first case, stent fracture was identified within an arterial conduit and was clearly related to the repeated hinge motion during the cardiac cycle. In the second case, no overt signs of fracture were evident on angiography however this was clearly demonstrated with OCT at 2 sites within the previously implanted stents. The excess intimal hyperplasia, altered stent geometry and complete fracture of the stents with lack of circumferential struts are dramatic on OCT. Furthermore, the power of the SES to inhibit neointimal tissue is shown in the relatively normal distal stented segments. Still, the advantage of DES over BMS remains their inherent ability to restrict this intimal tissue and therefore limit restenosis and, when this does occur, mechanical failure must be considered.

The treatment of stent fracture requires the operator to consider the underlying cause and then the likelihood of recurrence. As a result of this, in the first case, we elected not to introduce a

further stent but targeted the native vasculature as a means to improve perfusion. In the second case, post-dilatation at the sites of fracture and of the entire stented segment gave a very acceptable result and also addressed the issue of possible stent under-expansion following the initial implantation. When repeat stenting is considered, this may be accomplished using a different DES, while, more recently, Koh and Mathur described the successful implantation of a polytetrafluoroethylene-coated Jomed stent (Jomed International AB, Helsingborg, Sweden) within a saphenous vein graft stent fracture lesion [9]. This novel approach, using a stent with 2 layers, provides greater support and resistance to areas of high mechanical stress.

Although stent fracture remains uncommon, it is an increasingly reported cause of DES ISR, particularly with SES. A number of factors have been implicated, both vessel and stent specific that need to be considered when optimizing stent deployment to achieve a long lasting outcome.

References

[1] G. Sianos, S. Hofma and J.M. Ligthart et al., Stent fracture and restenosis in the drug-eluting stent sera, Catheter Cardiovasc Interv 2004; 61:111–116.
[2] M.S. Lee, D. Jurewitz, J. Aragon, J. Forrester, R.R. Makkar and S. Kar, Stent fracture associated with drug-eluting stents: clinical characteristics and implications, Catheter Cardiovasc Interv 2007; 69: 387–394.
[3] J. Wilczynska, A. Rdzanek, J. Kochman, G.J. Horszczaruk, A. Pietrasik and G. Opolski, Sirolimus eluting stent fracture following angioplasty of diffuse in-stent restenosis in the right coronary artery, Int J Cardiol 2007; 118: 126–127.
[4] P.K. Min, Y.W. Yoon and H. Moon Kwon, Delayed strut fracture of sirolimus-eluting stent: a significant problem or an occasional observation?, Int J Cardiol 2006; 106:404–406.
[5] A. Mehrle, T. Skelton and A. Almonacid, Stent fracture: an unusual cause of late restenosis after sirolimus-eluting stent placement, Catheter Cardiovasc Interv 2007; 69: 988–991.
[6] J. Aoki, G. Nakazawa and K. Tanabe et al., Incidence and clinical impact of coronary stent fracture after sirolimus-eluting stent implantation, Catheter Cardiovasc Interv 2007; 69:380–386
[7] K.P. Yamada, T. Koizumi and H. Yamaguchi et al., Serial angiographic and intravascular ultrasound analysis of late stent strut fracture of sirolimus-eluting stents in native coronary arteries, Int J Cardiol 2008;130:255-9.
[8] S.H. Lee, J.S. Park and D.G. Shin et al., Frequency of stent fracture as a cause of coronary restenosis after sirolimus-eluting stent implantation, Am J Cardiol. 2007; 100:627–630.
[9] T.W. Koh and A. Mathur, Coronary stent fracture in a saphenous vein graft to right coronary artery-successful treatment by the novel use of the Jomed coronary stent graft: case report and review of the literature, Int J Cardiol 2007; 119: e43–e45

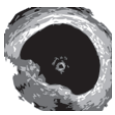

Chapter 17

Incomplete stent apposition and delayed tissue coverage are more frequent at long-term follow-up in drug-eluting stents implanted for ST-elevation myocardial infarction. Insights from optical coherence tomography

Nieves Gonzalo, Peter Barlis, Patrick W. Serruys, Hector M Garcia-Garcia, Yoshinobu Onuma, Jurgen Ligthart, Evelyn Regar

Objective: *To compare the frequency of incomplete stent apposition (ISA) and struts not covered by tissue at long term follow-up (as assessed by optical coherence tomography, OCT) in drug-eluting stents (DES) implanted during primary percutaneous coronary intervention (PCI) for ST-elevation myocardial infarction (STEMI) vs DES implanted for unstable and stable angina.*
Background: *ISA and the absence of strut endothelialization may be linked to stent thrombosis. DES implanted for STEMI may have higher risk of thrombosis.*
Methods: *Consecutive patients in whom OCT was performed at least 6 month following DES implantation were included in the study. Stent struts were classified based on the presence of absence of ISA and tissue coverage.*
Results: *Forty-seven lesions in 43 patients (1356 frames, 10140 struts) were analyzed (48.9% stable angina, 17% unstable angina, 34% STEMI). Median follow up time was 9 (range 7-72) months. DES implanted during primary PCI presented ISA more often than DES implanted in stable/unstable angina patients (75% vs 25.8% p=0.001). The frequency of uncovered struts was also higher in the STEMI group (93.8% vs 67.7% p=0.048). On multivariate analysis, DES implantation in STEMI was the only independent predictor of ISA (OR 9.8, 95%CI 2.4-40.4 p=0.002) and presence of uncovered struts at follow-up (OR 9.5 95%CI 1.0-90.3 p=0.049).*
Conclusions: *DES implanted for STEMI had higher frequency of incompletely apposed struts and uncovered struts as assessed by OCT at follow up. DES implantation during primary PCI in STEMI was an independent predictor of ISA and presence of uncovered struts at follow-up.*

Primary percutaneous coronary intervention (PCI) is the recommended treatment for ST elevation myocardial infarction (STEMI) (1). Stent implantation during primary PCI presents some challenges namely the presence of abundant thrombotic material that can potentially contribute to suboptimal stent deployment. The use of drug eluting stents (DES) in this setting is under debate due to the concerns about a potentially higher risk of stent thrombosis in this population (2). Recent IVUS studies suggest that the presence of incomplete stent apposition (ISA) is potentially linked to late stent thrombosis(3). Gradual absorption of the thrombus that was present during primary PCI has been postulated to contribute to late acquired stent malapposition (4). Endothelial struts coverage has been identified in pathological series as the most powerful histological predictor of stent thrombosis(5). DES inhibit neointimal proliferation to such extent that it might not be visualized with conventional intracoronary imaging techniques such as IVUS. Optical Coherence Tomography (OCT) is a high-resolution light-based imaging modality that can provide a very detailed assessment of stent apposition and tissue strut coverage.
The objective of the present study was to compare the frequency of ISA and uncovered struts (as assessed by OCT) at long term follow up in DES implanted during primary PCI for STEMI vs DES implanted for stable or unstable (IB/IIB/IIIB Braunwald classification) angina.

Methods

Patient sample

All consecutive patients between January 2007 and May 2008 in whom OCT was performed for follow-up of a DES implanted at least 6 months prior were included in the study. Exclusion criteria were repeated revascularization in the target vessel, depressed left ventricular function, coronary chronic total occlusions and impaired renal function. All patients gave written informed consent.

OCT acquisition

The OCT acquisition was performed using a commercially available system for intracoronary imaging (LightLab Imaging, Westford, Massachusetts, US). The ImageWire (LightLab Imaging, Westford, Massachusetts) was positioned distal to the region of interest using a double lumen

catheter (Twin Pass catheter, Vascular Solutions Inc) that had been placed in the artery over a conventional guide wire. The automated pullback was performed at 3 mm/s while the blood was removed by the continuous injection of iso-osmolar contrast (Iodixanol 320, Visipaque™, GE Health Care, Ireland) at 37° Celsius through the guiding catheter. The data was digitally stored for offline analysis.

OCT analysis

Offline analysis was performed with the proprietary LightLab software (LightLab Imaging, Westford, Massachusetts, US). The analysts (Cardialysis BV, Rotterdam, The Netherlands) were blinded to clinical and procedural characteristics. The stented region was defined as the region comprised between the first and the last frame with circumferentially visible struts. For this region one frame was selected every mm and the lumen and stent area contours were drawn. Stent longitudinal symmetry ratio was defined as minimum stent area /maximum stent area.

Incomplete stent apposition definitions and measurements

Incomplete stent apposition (ISA) was defined as separation of at least one stent strut from the vessel wall not related with a side branch (Figure 1). A strut was considered incompletely apposed if the distance from the endo-luminal surface of the strut to the vessel wall was higher than the sum of the metal and polymer thickness. The cut-off points used for each stent type were: paclitaxel eluting stent (Taxus, Boston Scientific Corp, Natick, MA) 130μm, sirolimus eluting stent (Cypher Select, Cordis, Johnson & Johnson, Miami, FL) 160μm, everolimus eluting stent (Xience V, Abbot Vascular, Santa Clara, CA) 90μm and biolimus eluting stent (Biomatrix III, Biosensors, Morges, Switzerland) 120μm. The number of malapposed struts, the maximal incomplete stent apposition length (maximum distance from the endo-luminal surface of the strut to the vessel wall) and the incomplete stent apposition area were measured. Calcification could not be accurately evaluated due to the shadow caused by stent struts in OCT.

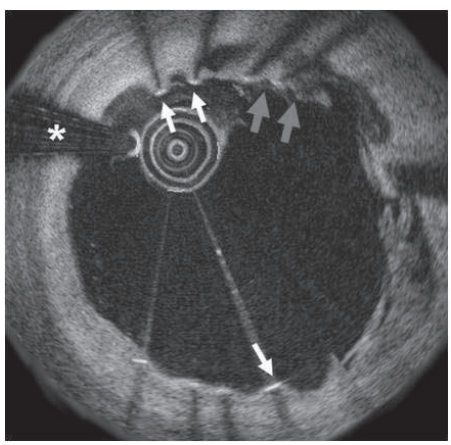

Figure 1: Incomplete stent apposition and uncovered struts.
Optical coherence tomography cross section corresponding to a patient treated with DES implantation during primary PCI in the right coronary artery due to an inferior ST elevation myocardial infarction 9 months before. The red arrows indicate incomplete stent apposition while the white arrows show some struts not covered by tissue. From 12 to 5 it can be observed behind the struts an irregular material suggestive of organized thrombus. * Guidewire artefact.

Struts coverage definitions and measurements

The struts were classified as uncovered when a tissue layer on the endoluminal surface could not been clearly distinguished. In the covered struts, the tissue coverage thickness was measured per strut as the distance from the central aspect of the endoluminal surface of the strut to the lumen. The total tissue coverage area was calculated as stent area – lumen area. The % of tissue coverage area was calculated as the tissue coverage area /stent area x 100. The tissue coverage volume was

calculated as the tissue coverage area x stent length. The % tissue coverage volume area was calculated as the tissue coverage volume/stent volume x 100. The tissue coverage symmetry per frame was analyzed using the following ratio: (Maximum tissue coverage thickness per frame – minimum tissue coverage thickness per frame)/Maximum tissue coverage thickness per frame. This ratio can have values between 0 and 1. The closer the ratio is to 1 the higher is the asymmetry of the tissue coverage (Figure 2). To evaluate the distribution of the uncovered struts along the stent we calculated the % of frames with at least one uncovered strut in the lesions that showed uncovered struts.

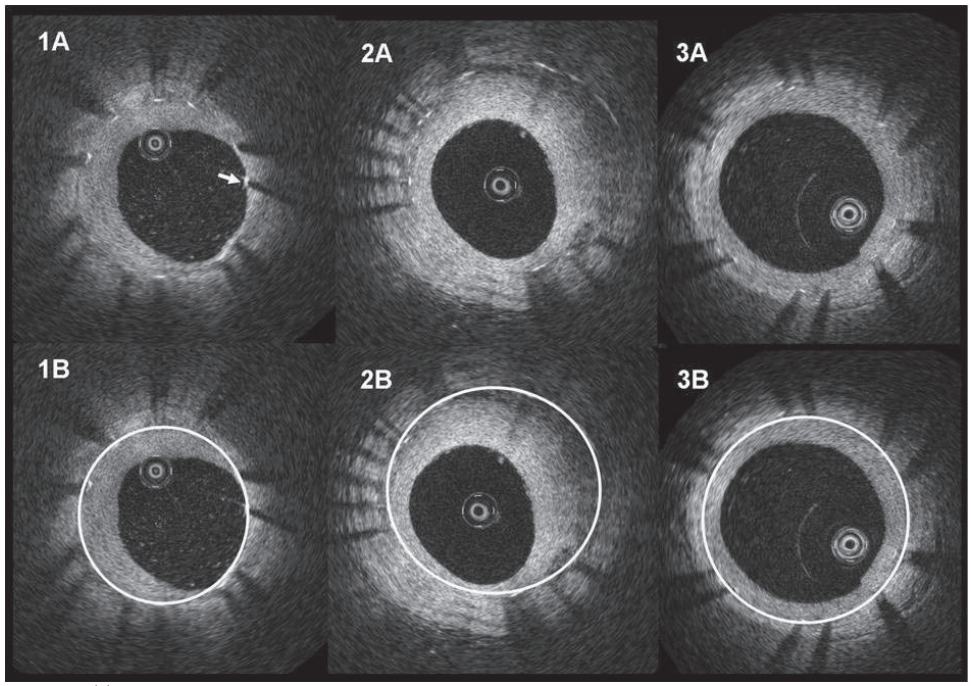

Figure 2: Tissue coverage symmetry patterns. 1A and 1B: Asymmetric tissue coverage with uncovered struts: while some struts are covered by a thick layer of tissue, other struts (from 2 to 5) are covered by a very thin layer and there is even one uncovered strut (indicated by the white arrow). 2B and 2B: Asymmetric tissue coverage without uncovered struts: all the struts are covered by tissue that shows very different thickness along the vessel circumference. 3A and 3C: Symmetric tissue coverage: all the struts are covered by tissue that shows similar thickness along the vessel circumference.

Statistical analysis

Statistical analysis was performed using SPSS 12.0.1 for Windows (SPSS Inc., Chicago, IL). Categorical variables are expressed as percentages and continuous variables are expressed as mean ± standard deviation, median and (range) or median and (interquartile range). ISA and strut coverage comparisons were performed per lesion. χ^2 was used for the comparisons of categorical variables between groups. For the comparisons of continuous variables Student t test or non parametric (Mann-Whitney) test were used according to their distribution. Multiple logistic regression analysis was performed to assess independent predictors of ISA and uncovered struts. Variables considered clinically relevant and with $p<0.15$ in the univariate analysis were included in the models.

Results

Clinical and procedural characteristics

Fifty patients followed up with OCT after DES implantation were initially enrolled in the study. Seven patients were excluded for image quality not appropriate for analysis. Finally 43 patients (47 vessels, 47 lesions) were included (16 STEMI, 27 stable/unstable angina).

The mean age was 64.5±11.7 years and 63.8% were males. Regarding cardiac risk factors, 47.8%, 21.3% and 70.2% had hypertension, diabetes mellitus, and hyperlipidemia, respectively and 19.1% were smokers. The studied vessel was the left anterior descending in 57%, the circumflex in 19% and the right coronary artery in 24% of the lesions. The indication for stent implantation was stable angina in 47% (20/43), unstable angina in 16% (7/43) and STEMI in 37% (16/43). The stent implanted was Taxus™ in 10.6%, Cypher Select™ in 55.3%, Xience V™ in 2.1%, and Biomatrix III™ in 32%. The median time to follow-up angiography and OCT examination was 9 (7-72) months. The mean stent diameter, stent number and stent imaged length were 2.9±0.3 mm, 1.8±0.8 and 28±15 mm respectively.

OCT quantitative analysis

A total of 10140 struts from1356 frames were analyzed. The mean lumen area, mean stent area and mean neointimal area were 6.42±2.11mm², 7.11± 2.06 mm² and 0.67±0.47 mm² respectively. The stent symmetry ratio was 0.63±0.16.

ISA frequency by OCT

The frequency of incompletely apposed struts was 68/10140 (0.6%). Forty-five out of the 68 incompletely apposed struts (66.1%) were not covered by tissue. Forty out of 1356 frames (2.9%) had at least one incompletely apposed strut. In 20 out of 47 lesions (42.6%) incomplete stent apposition of at least one strut was found. In the lesions with ISA the mean percentage of frames with ISA was 9.3±7.1%.

Struts coverage by OCT

The frequency of uncovered struts in the total sample was 6.1% (624/10140). Twenty-one percent (285/1356) of all the analyzed frames presented at least 1 strut uncovered. In 36 out of 47 lesions (76.6%) at least one uncovered strut was visualized. The mean neointima symmetry ratio was 0.73±0.13. Twenty-six struts out of the 10140 (0.2%) were covered by an irregular material suggestive of organized thrombus (Figure 3)

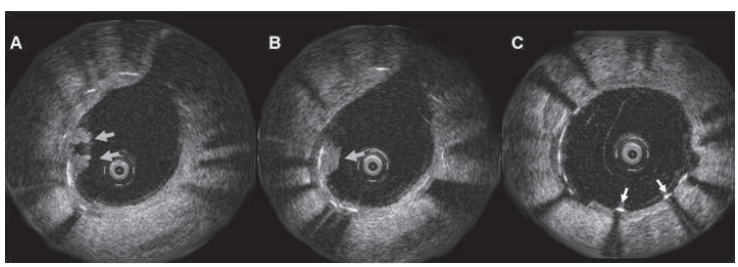

Figure 3: Struts covered by organized thrombus. Optical coherence tomography cross-sections corresponding to a DES implanted in the LAD more than 4 years ago due to an anterior ST elevation myocardial infarction. In A and B the blue arrows indicate the presence of an irregular highly reflective material (suggestive of organized thrombus) covering some struts. C represents a cross section more proximal where some uncovered struts can be observed (white arrows).

STEMI patients

Sixteen out the 47 lesions studied were treated with DES implantation during primary PCI due to STEMI. Table 1 shows the baseline characteristics of the STEMI patients in comparison with the rest of the sample. The time to follow up was 11.5 months (range 7-59) for the STEMI group and 9 months (range 9-72) for the rest of the patients. There were no significant differences in lumen area (6.5±2.0 Vs 6.4±2. for STEMI and stable/unstable angina respectively p=0.86), stent area (7.2±2.0 vs 7.0±2.0 for STEMI and stable/unstable angina respectively p=0.78) or stent symmetry ratio (0.58±0.17 vs 0.65±0.15 for STEMI and stable/unstable angina respectively p=0.13).

	STEMI	Stable/unstable angina	p-value
Age (years)	64±12	64±11	0.85
Male (%)	50.0	71.0	0.13
HTA (%)	50.0	46.7	0.53
DM (%)	31.3	16.1	0.2
Dyslipidemia (%)	75.0	67.7	0.43
Smoker (%)	31.3	12.9	0.13
Family history (%)	62.5	67.7	0.48
Vessel (%)			0.46
LAD	68.8	51.6	
LCX	18.7	19.4	
RCA	12.5	29.0	
Stent type (%)			0.48
Taxus™	13.3	9.7	
Cypher™	53.3	54.8	
Xience™	6.7	0.0	
Biomatrix™	26.7	35.5	
Number stents	1.53±0.52	2.03±0.94	0.08
Stent imaged length (mm)	24.9±10.5	29.9±17.6	0.3

Table 1. Baseline characteristics in ST elevation myocardial infarction (STEMI) and stable/unstable angina patients. Age, gender and cardiovascular risk factors are compared per patient (STEMI=16 stable/unstable angina=27). The rest of the variables are compared per lesion (STEMI=16 stable/unstable angina=31).

	STEMI (n=16)	Stable/unstable angina (n=31)	p-value
Number of incompletely apposed struts	2 (0-13)	0 (0-5)	0.001
Number of incompletely apposed uncovered struts	1 (0-13)	0 (0-4)	<0.001
Number of incompletely apposed covered struts	0.5 (0-3)	0 (0-5)	0.02
ISA area (mm^2)	0.28 (0.17-0.67)	0.35 (0.23-0.44)	0.5
Maximum ISA length (μm)	235 (162-297)	250 (230-600)	0.4

Table 2. Differences in incomplete stent apposition (ISA) between lesions treated with drug-eluting stent implantation for ST elevation myocardial infarction (STEMI) and lesions treated for stable/unstable angina. Number of struts is expressed as median and range. ISA area and maximum ISA length are expressed as median and IQ range.

ISA in STEMI patients

Figure 4 represents the frequency of ISA in lesions treated with DES implantation for STEMI and the rest of the lesions. Table 2 shows the differences in the number of incompletely apposed struts (covered and not covered), maximum ISA length and ISA area in lesions treated for STEMI and lesions treated for stable/unstable angina.

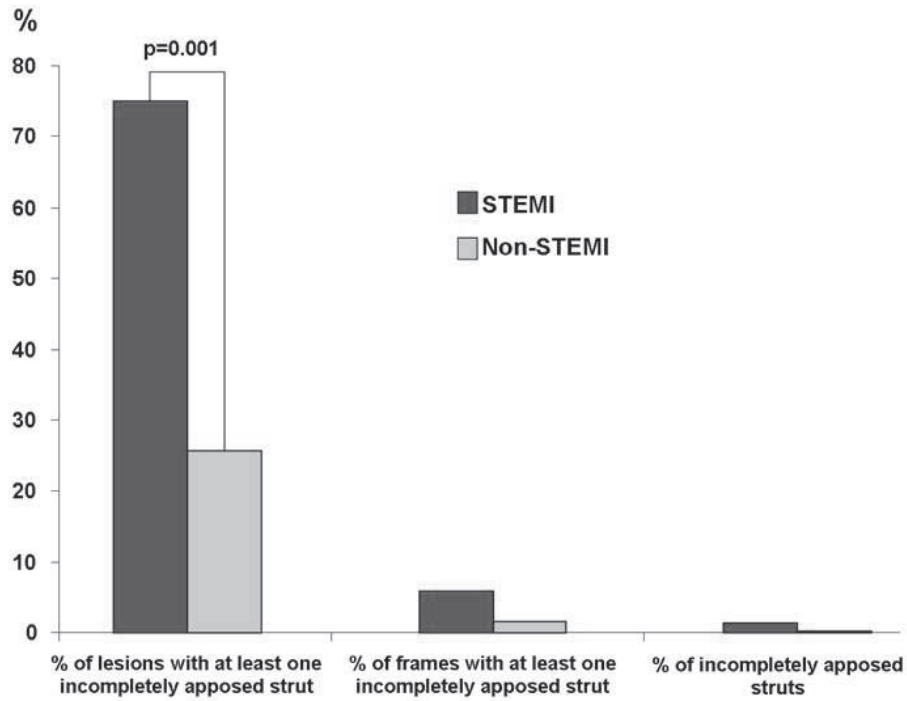

Figure 4: Difference in ISA frequency between ST elevation myocardial infarction (STEMI) patients and stable/unstable angina patients. ISA frequency is shown per lesion (number of lesions with at least one incompletely apposed strut/total number of lesions), per frame (number of frames with at least one incompletely apposed strut/total number of frames) and per strut (number of incompletely apposed struts/total number of struts).

Uncovered struts in STEMI patients

Figure 5 shows the difference in frequency of uncovered struts between lesions treated for STEMI and lesions treated for stable/unstable angina. The number of uncovered struts, the mean tissue coverage thickness, area and volume and the tissue coverage symmetry ratio in both groups are indicated in Table 3.

Predictors of incomplete stent apposition (ISA)

Multiple logistic regression analysis was performed to determine the independent predictors of ISA. The following variables were included in the model: age, time follow-up, stent length, stent symmetry ratio, stent implantation during primary PCI. The only independent predictor of ISA was DES implantation during primary PCI for STEMI (OR 9.8, 95%CI 2.4-40.4 p=0.002).

	STEMI (n=16)	Stable/unstable angina (n=31)	p-value
Number of uncovered struts	26.8±20.8	6.2±7.5	0.001
Uncovered strut distribution (%)	40.7±25.2	16.4±19.8	0.001
Mean tissue coverage area (mm^2)	0.72±0.63	0.65±0.37	0.68
% tissue coverage area	12.4±9.9	11.0±6.9	0.58
Tissue coverage volume (mm^3)	17.7±21.6	21.9±22.04	0.54
% tissue coverage volume	10.0±9.4	10.3±6.7	0.91
Tissue coverage thickness* (μm)	110±48	90±53	0.22
Tissue coverage symmetry ratio	0.79±0.23	0.70±0.13	0.02

Table 3. Differences in struts coverage between lesions treated with drug-eluting stent implantation for ST elevation myocardial infarction (STEMI) and lesions treated for stable/unstable angina.

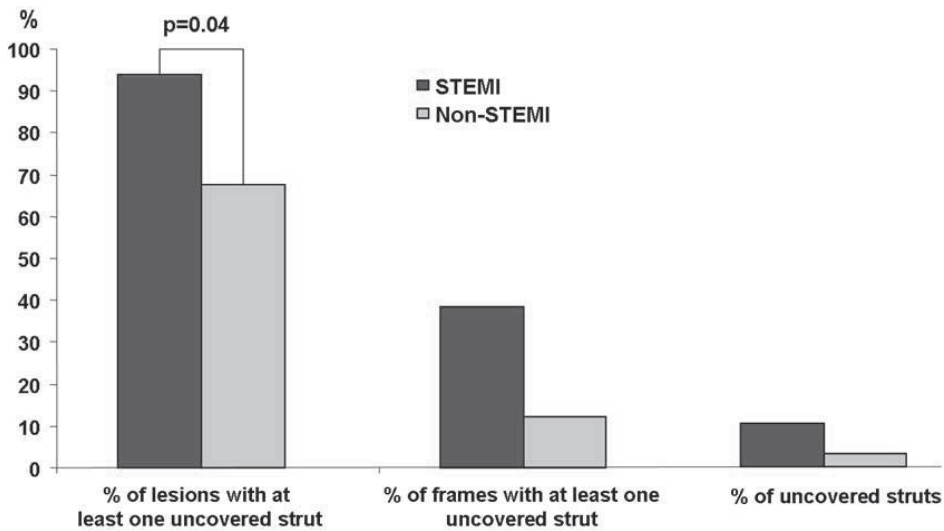

Figure 5: Difference in uncovered struts frequency between ST elevation myocardial infarction (STEMI) patients and stable/unstable angina patients. Data is shown per lesion (lesions with at least one uncovered strut/total number of lesions), per frame (frames with at least one uncovered strut/total number of frames) and per strut (number of uncovered struts/total number of struts).

Predictors of uncovered struts

In the multivariate model for uncovered struts predictors the following variables were included: age, time follow up, stent length, stent area and stent implantation during primary PCI. DES implantation during primary PCI for STEMI was the only independent predictor of uncovered struts at follow up (OR 9.5 95%CI 1.0-90.3 p=0.049).

Discussion

To our knowledge this is the first such study to use the high-resolution capabilities of intra-coronary OCT to examine stent strut apposition and tissue coverage at follow-up in patients with STEMI treated with primary PCI. The main findings are: 1. DES implanted for STEMI had a higher frequency of incompletely apposed and uncovered struts as assessed by OCT at follow up. 2. DES implantation during primary PCI in STEMI is an independent predictor of both ISA and presence of uncovered struts at follow up.

DES have consistently demonstrated a reduction in restenosis rates when compared to bare metal stents (BMS) in different clinical settings including primary PCI for the treatment of STEMI(6). However, concerns have been raised about a potentially higher risk of stent thrombosis following DES implantation during primary PCI (7). Further ISA and lack of complete stent endothelialization have been identified as factors related to stent thrombosis(4,5).

Incomplete stent apposition (ISA)

Overall the frequency of incompletely apposed struts was very low (0.6%). In our study patients with STEMI treated with DES implantation during primary PCI had a higher frequency of ISA. Our results are in concordance with IVUS studies that have identified a higher incidence of late ISA in STEMI patients specially when treated with DES. Hong et al reported an incidence of late ISA after primary PCI in STEMI of 11.5% after BMS implantation and 31.8% after DES implantation (8). In our sample 75% of the lesions treated with DES during primary PCI showed evidence of ISA. The higher frequency of ISA observed in the present study can be explained by the higher resolution of OCT in comparison with IVUS(9). The results of the present study are also in line with a recent OCT study that identified a higher incidence of ISA in sirolimus-eluting stents implanted in unstable vs stable angina patients (33% vs 4%)(10).

The dissolution of thrombus jailed after stent implantation during primary PCI has been postulated as one of the possible causes of the higher incidence of late ISA in STEMI patients(4). Plaque rupture (characterized by a necrotic core with an overlying thin-ruptured cap infiltrated by macrophages and with paucity of smooth muscle cells) is the most frequent underlying substrate in STEMI. Stent implantation over a ruptured plaque with strut penetration into necrotic core have also been related to ISA in acute coronary syndromes (11). The clinical implications of ISA are controversial. Several studies have reported that the presence of ISA after DES implantation is not associated with adverse events at long term follow up (8,12,13). However, recently published IVUS observations suggest a possible relation between incomplete DES apposition and subsequent stent thrombosis (3,4). The clinical significance of ISA as detected by OCT is poorly understood. In fact, incomplete apposition of stent struts is a relatively common finding by OCT, while the vast majority of the patients do not experience clinical events in the long-term(14) . In addition, not all patients that experience DES thrombosis show strut malapposition(15,16). In the present study none of the patients with ISA as assessed by OCT presented with adverse clinical events.

Strut coverage

DES inhibits neointimal proliferation to such extent that it may not be detectable by IVUS(17). The high resolution of OCT allows the visualization and measurement of tiny layers of tissue covering the stent struts(18). In the present study, the global frequency of uncovered individual struts was 6.1% and a high proportion of lesions (36/47) presented uncovered struts. This is in agreement with different OCT studies recently published reporting strut coverage in DES at follow up (14,19). A long-term follow up with OCT in a group of patients treated with SES revealed that 81% of the patients presented uncovered struts at 2 years follow-up(20). In the present study 8 out of the 9 lesions with more than 2 years follow-up demonstrated uncovered struts by OCT and interestingly in 6 out of those 8 lesions the DES were implanted during

primary PCI. The frequency of struts with no visible coverage was significantly higher in STEMI patients treated during primary PCI (15 out of 16 lesions). Likewise, the distribution of uncovered struts within the stent was more spread in STEMI patients (reflected in a higher proportion of frames with uncovered struts). The mean neointimal thickness did not differ between STEMI and stable/unstable angina patients but the neointima showed a more asymmetric distribution in STEMI patients. Our findings are in agreement with pathological studies showing delayed endothelialization at the culprit site in acute myocardial infarction patients treated with DES compared with the culprit site in patients receiving DES for stable angina(21).

A recent study reporting a lower incidence of full tissue coverage in unstable than in stable angina is also in line with our observations(10). Pathological data suggests a relation between arterial healing and underlying plaque morphology. In an autopsy study, Nakazawa et al found a higher percentage of uncovered struts in patients with stents implanted in plaques with high risk features (such as plaque rupture and TCFA) as compared with those with stable plaque morphology (21). Despite a lack of OCT assessment during the primary PCI procedure in our study, it is accepted that plaque rupture is the most frequent underlying event leading to STEMI(22). The stent contact with an avascular tissue such as necrotic core and the different drug distribution due to the presence of thrombus are some of the factors that could explain the delayed coverage of struts in unstable patients(21,23). The more asymmetric distribution in the cross section of the tissue covering the struts found in STEMI patients might also be related with the eccentricity and composition of the plaque underlying the stent implantation(24).

Endothelial struts coverage has been identified in pathological series as the most powerful histological predictor of stent thrombosis(5). Pathological data in human suggests that neointimal coverage of stent struts may be a surrogate marker of endothelialization (25). However, Kubo et al reported that the presence of a higher incidence of uncovered struts by OCT in unstable patients was not associated with adverse outcomes at 9 months(10). In the present study no adverse events occurred at follow up even when the frequency of uncovered struts was high. The clinical significance of the presence of uncovered struts as assessed by OCT remains unknown and would require specific long-term follow up studies. Despite the high resolution of the technique, coverage of the strut with an individual cell layer can not be excluded. Currently, OCT cannot well distinguish the tissue type covering the struts, e.g. a neointimal layer from fibrin. Furthermore, different types of neointimal tissue with different optical properties can be observed and may have different functionality(26). The development of quantitative tissue characterization by OCT might be helpful to better understand the clinical implications of strut tissue coverage.

Limitations

The present study is observational and non-randomized. No formal sample size calculation was performed. Another limitation is the lack of serial OCT assessments with OCT only performed at long-term follow-up. Therefore it was not possible to distinguish between persistent and late acquired ISA. The presence of positive remodelling as cause of late ISA (as demonstrated previously in IVUS) can not be excluded. Likewise, no information was available about the underlying plaque in which the stent was implanted. Only DES were included in the study. Therefore we can not exclude that BMS would not have behaved similarly when implanted in the setting of STEMI.

Conclusions

DES implanted for STEMI had higher frequency of incompletely apposed struts and uncovered struts as assessed by OCT at follow up. DES implantation during primary PCI in STEMI was an independent predictor of ISA and presence of uncovered struts at follow up. Whether these findings have a causal link to the heightened rate of stent thrombosis in STEMI patients remains to be confirmed by larger studies.

References

1. Boden WE, Eagle K, Granger CB. Reperfusion strategies in acute ST-segment elevation myocardial infarction: a comprehensive review of contemporary management options. J Am Coll Cardiol 2007;50:917-29.
2. Urban P, Gershlick AH, Guagliumi G, et al. Safety of coronary sirolimus-eluting stents in daily clinical practice: one-year follow-up of the e-Cypher registry. Circulation 2006;113:1434-41.
3. Alfonso F SA, Perez-Vizcayno MJ, Moreno R, Escaned J, Banuelos C, Jimenez P, Bernardo E, Angiolillo DJ, Hernandez R, Macaya C. Intravascular ultrasound findings during episodes of drug-eluting stent thrombosis. J Am Coll Cardiol 2007;50:2095-2097.
4. Cook S, Wenaweser P, Togni M, et al. Incomplete stent apposition and very late stent thrombosis after drug-eluting stent implantation. Circulation 2007;115:2426-34.
5. Joner M, Finn AV, Farb A, et al. Pathology of drug-eluting stents in humans: delayed healing and late thrombotic risk. J Am Coll Cardiol 2006;48:193-202.
6. Spaulding C, Henry P, Teiger E, et al. Sirolimus-eluting versus uncoated stents in acute myocardial infarction. N Engl J Med 2006;355:1093-104.
7. Daemen J, Tanimoto S, Garcia-Garcia HM, et al. Comparison of three-year clinical outcome of sirolimus- and paclitaxel-eluting stents versus bare metal stents in patients with ST-segment elevation myocardial infarction (from the RESEARCH and T-SEARCH Registries). Am J Cardiol 2007;99:1027-32.
8. Hong MK, Mintz GS, Lee CW, et al. Late stent malapposition after drug-eluting stent implantation: an intravascular ultrasound analysis with long-term follow-up. Circulation 2006;113:414-9.
9. Bouma BE, Tearney GJ, Yabushita H, et al. Evaluation of intracoronary stenting by intravascular optical coherence tomography. Heart 2003;89:317-20.
10. Kubo T IT, Kitabata H, Kuroi A, Ueno S, Yamano T, Tanimoto T, Matsuo Y, Masho T, Takarada S, Tanaka A, Nakamura N, Mizukoshi M, Tomobuchi Y, Akasaka T. Comparison of vascular response after sirolimus eluting stent implantation between patients with unstable and stable angina pectoris. A serial optical coherence tomography study. J Am Coll Cardiol Imaging 2008;1:475-484.
11. Finn AV NG, Ladich E, Kolodgie FD, Virmani R. Does Underlying plaque morphology play a role in vessel healing after drug eluting stent implantation? J Am Coll Cardiol Imaging 2008;1:485-488.
12. Degertekin M, Serruys PW, Tanabe K, et al. Long-term follow-up of incomplete stent apposition in patients who received sirolimus-eluting stent for de novo coronary lesions: an intravascular ultrasound analysis. Circulation 2003;108:2747-50.
13. Tanabe K, Serruys PW, Degertekin M, et al. Incomplete stent apposition after implantation of paclitaxel-eluting stents or bare metal stents: insights from the randomized TAXUS II trial. Circulation 2005;111:900-5.
14. Xie Y, Takano M, Murakami D, et al. Comparison of neointimal coverage by optical coherence tomography of a sirolimus-eluting stent versus a bare-metal stent three months after implantation. Am J Cardiol 2008;102:27-31.
15. Schinkel AFL vBH, Maugenest AM; van Wunnik S, Serruys PW, Regar E. OCT Findings in Very Late (4 Years) Paclitaxel-Eluting Stent Thrombosis. J Am Coll Cardiol Interventions 2008;In press.

16. Barlis P DMC, van Beusekom HMM, Gonzalo N, Regar E. Novelties in Cardiac Imaging – Optical Coherence Tomography (OCT). A critical appraisal of the safety concerns tempering the success of drug-eluting stents Eurointervention 2008;In press.
17. Serruys PW, Degertekin M, Tanabe K, et al. Intravascular ultrasound findings in the multicenter, randomized, double-blind RAVEL (RAndomized study with the sirolimus-eluting VElocity balloon-expandable stent in the treatment of patients with de novo native coronary artery Lesions) trial. Circulation 2002;106:798-803.
18. Prati F, Zimarino M, Stabile E, et al. Does optical coherence tomography identify arterial healing after stenting? An in vivo comparison with histology, in a rabbit carotid model. Heart 2008;94:217-21.
19. Matsumoto D, Shite J, Shinke T, et al. Neointimal coverage of sirolimus-eluting stents at 6-month follow-up: evaluated by optical coherence tomography. Eur Heart J 2007;28:961-7.
20. Takano M, Yamamoto M, Inami S, et al. Long-term follow-up evaluation after sirolimus-eluting stent implantation by optical coherence tomography: do uncovered struts persist? J Am Coll Cardiol 2008;51:968-9.
21. Nakazawa G, Finn AV, Joner M, et al. Delayed arterial healing and increased late stent thrombosis at culprit sites after drug-eluting stent placement for acute myocardial infarction patients: an autopsy study. Circulation 2008;118:1138-45.
22. Virmani R, Burke AP, Farb A, Kolodgie FD. Pathology of the vulnerable plaque. J Am Coll Cardiol 2006;47:C13-8.
23. Hwang CW, Levin AD, Jonas M, Li PH, Edelman ER. Thrombosis modulates arterial drug distribution for drug-eluting stents. Circulation 2005;111:1619-26.
24. Falk E, Shah PK, Fuster V. Coronary plaque disruption. Circulation 1995;92:657-71.
25. Finn AV, Joner M, Nakazawa G, et al. Pathological correlates of late drug-eluting stent thrombosis: strut coverage as a marker of endothelialization. Circulation 2007;115:2435-41.
26. Takano M, Xie Y, Murakami D, et al. Various optical coherence tomographic findings in restenotic lesions after sirolimus-eluting stent implantation. Int J Cardiol 2008. DOI: S0167-5273(08)00101-0 [pii]10.1016/j.ijcard.2007.12.110

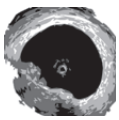

Chapter 18

A Critical Appraisal of the Safety Concerns Tempering the Success of Drug-Eluting Stents: Novelties in Cardiac Imaging – Optical Coherence Tomography

Peter Barlis, Carlo Di Mario, Heleen van Beusekom, Evelyn Regar

In order to improve our understanding of late stent thrombosis and to assess the individual risk of a patient or lesion, there is clinical need to assess vascular healing after stenting in vivo. We will discuss the potential and limitations of optical coherence tomography (OCT) for imaging of drug eluting stents (DES).

OCT, a light based imaging modality (1), has recently become available for intracoronary application (2-4). Because of the shorter wavelength of infrared light compared to ultrasound, OCT has a ten-fold higher image resolution than conventional intravascular ultrasound (IVUS), 150 micron for IVUS as compared to 15 micron for OCT. This advantage renders OCT particularly useful for the assessment of coronary stents.

OCT observations in drug-eluting stents immediately after implantation

For the past two decades, IVUS has been used to assess the acute result following stenting, giving valuable information on stent expansion, strut apposition and signs of vessel trauma including dissections and tissue prolapse (5,6). IVUS studies (7,8) suggested that stent strut malapposition is a relatively uncommon finding, observed in approx 7% of cases, and that strut malapposition does not increase the risk of subsequent major adverse cardiac events. In contrast, OCT can visualise the complex coronary arterial wall structure after stenting in much greater detail (9). As a result, OCT studies in the acute post stent setting (10) have demonstrated a relatively high proportion of stent struts, not completely apposed to the vessel wall, even after high pressure post-dilatation. Furthermore, this phenomenon is particularly evident at regions of stent overlap (11). Tanigawa et al (12) examined a total of 6,402 struts from 23 patients (25 lesions) and found 9.1±7.4% of all struts in each lesion treated were malapposed. Univariate predictors of malapposition where: implantation of a sirolimus-eluting stent (SES), presence of overlapping stents, longer stent length and type C lesions. Likely mechanical explanations for malapposition of stent struts include increased strut thickness, closed cell design or acute stent recoil. The latter has been demonstrated in SES to be in the range of 15%, despite the use of high pressure balloon dilatation (13). While these findings are impressive and helpful for the improvement of future stent designs, today the clinical relevance and potentially long-term sequeale of malapposed struts as detected by OCT are currently unknown.

OCT observations in drug eluting stents at long-term follow-up

Unlike conventional stents, which develop circumferential coverage with an average thickness of 500 micron or more, well visualised with IVUS and angiography, drug-eluting stents delay and prevent the hyperplastic response so that the average late lumen loss for drug-eluting stents can be lower than 100 micron (4) which means this thin layer of intimal thickening can be below the resolution of IVUS. Coronary angioscopy is able to visualise strut tissue coverage to a certain extent, but this highly specialised technique lacks the ability for quantification and the ability to assess thin amounts of neotinima. Hence, OCT is an attractive alternative, able to circumvent many of these limitations and, with its high-resolution, can precisely assess the in vivo tissue responses following stent implantation (14). Specific applications of OCT relevant for late stent thrombosis are discussed below.

a) Visualisation and quantification of stent strut tissue coverage

OCT can reliably detect early and very thin layers of tissue coverage on stent struts (Figure 1-4). Several small studies have recently been published highlighting the application of OCT in the detection of stent tissue coverage at follow-up. Importantly, OCT permits the quantification of tissue coverage with high reliability (15).

see colour section

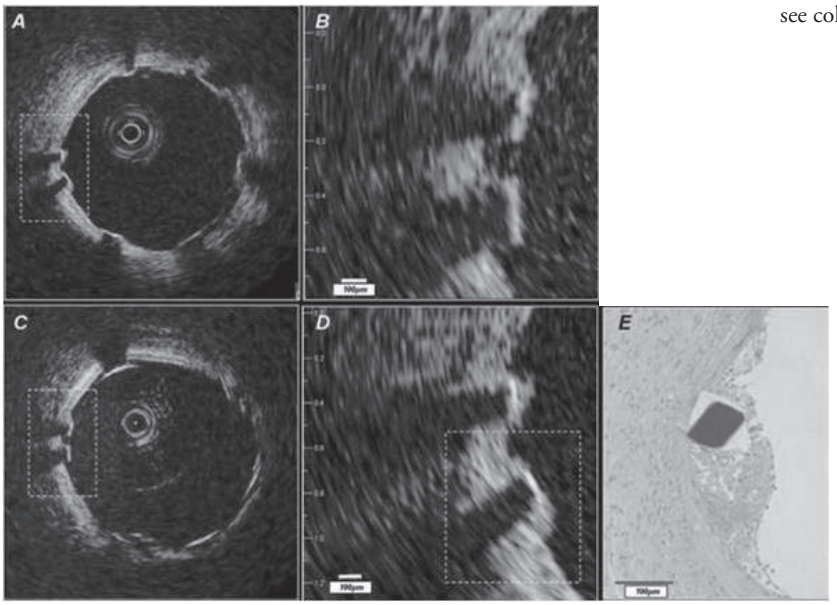

Figure 1. In vivo OCT (LightLab Imaging Boston, MA, USA) in a porcine coronary artery. A) Baseline OCT immediately after stent implantation shows adequate stent expansion and apposition of the struts against the normal coronary wall. B) Magnification demonstrating the stent strut vessel wall interface. C) Follow-up investigation at five days. The stent struts are clearly visible and show thin, bright reflective tissue coverage in the magnification D) Histology E) confirms the presence of a thin neointimal layer.

Matsumoto et al (16) studied 34 patients following sirolimus eluting stent (SES) implantation. The mean neointima thickness was 52.5 microns, and the prevalence of struts covered by thin neointima undetectable by IVUS was 64%. The average rate of neointima-covered struts in an individual SES was 89%. Nine SES (16%) showed full coverage by neointima, whereas the remaining stents had partially uncovered struts. Similarly, Takano et al (17) studied 21 patients (4,516 struts), three months following SES implantation. Rates of exposed struts and exposed struts with malapposition were 15% and 6%, respectively. These were more frequent in patients with acute coronary syndrome (ACS) than in those with non-ACS (18% vs 13%, $p < 0.001$; 8% vs 5%, $p < 0.005$, respectively). The same group recently reported two year follow-up OCT findings (18) with the thickness of neointimal tissue at 2-years being greater than that at 3-months (71±93micron vs. 29±41 micron, respectively; $p<0.001$). Frequency of uncovered struts was found to be lower in the 2-year group compared to the 3- month group (5% vs. 15%, respectively; $p<0.001$). Conversely, prevalence of patients with uncovered struts did not differ between the 3- month and the 2-year follow-up study (95% vs. 81%, respectively) highlighting that uncovered struts continued to persist at long-term follow-up. Chen et al (19) recently used

OCT to image SES and bare metal stents (BMS) at different time points following implantation. Of the 10 SES and 13 BMS imaged, the authors identified a significantly higher number of incompletely apposed and uncovered stent struts in patients receiving SES compared to BMS. The results of these small observational studies are compatible with evidence from animal and human post-mortem series showing that DES cause impairment in arterial healing, some with suggested incomplete re-endothelialisation and persistence of fibrin(oid) (20,21) possible triggering late stent thrombosis (22).

see colour section

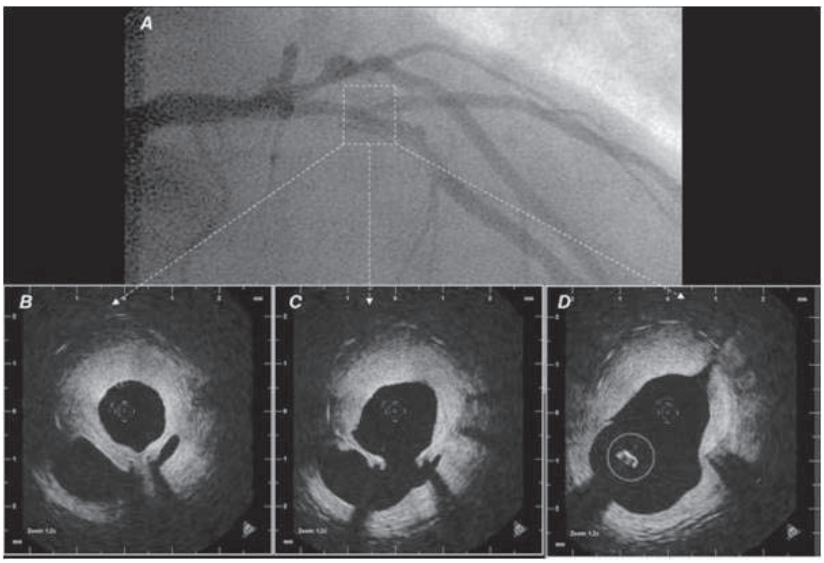

Figure 2. In vivo OCT (LightLabImaging™, Boston, MA, USA) in the LAD in a patient presenting with in-stent restenosis. A) The coronary angiogram shows a lumen narrowing within the stent that is covering the second diagonal branch. OCT visualises the complex coronary anatomy in great detail. The stent is covered by a thick neointima that shows a layered appearance with a bright, highly reflective luminal layer, an intermediate layer and a dark, signal poor layer surrounding the struts (B). The diagonal take off can be clearly seen (C) as well as a stent strut that is "floating" in the carina (D).

However, OCT observations need to be interpreted with caution. OCT is limited by its resolution of 15 micron which is greater than the thickness of an individual layer of endothelial cells. Therefore, coverage that is not visible by OCT does not exclude the presence of an endothelial layer. Second, the presence of tissue coverage does not necessarily imply the presence of a functionally intact endothelium. Early experimental stent data showed that endothelial function can vary considerably and show evidence of damage when subjected to the Evan's blue dye exclusion test (23), even in the presence of a well structured neotintimal layer. In consequence, morphology should not be confused with function.

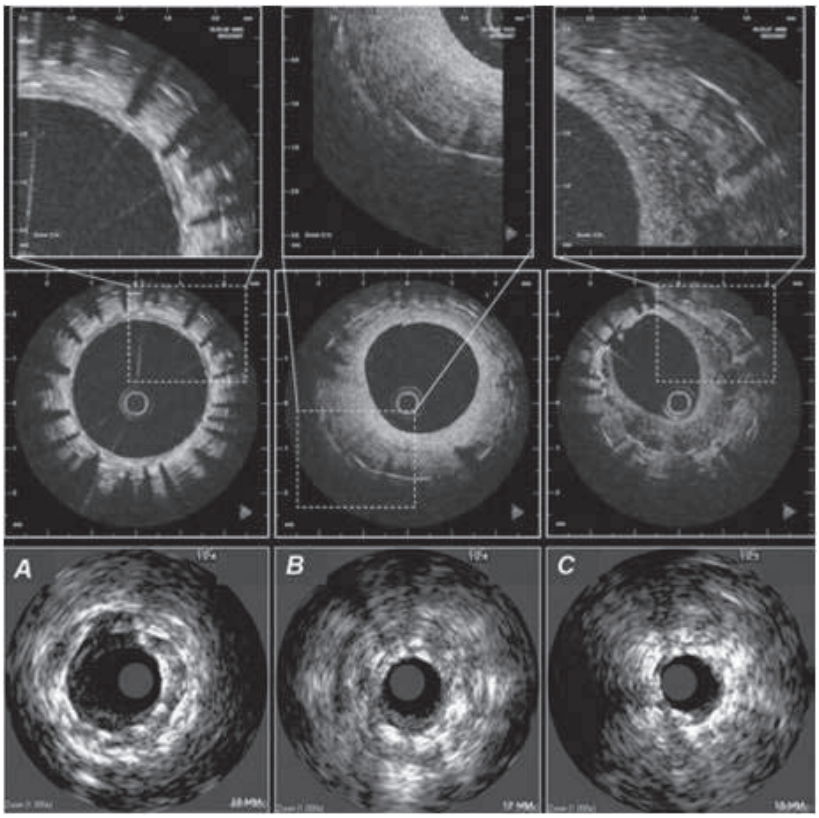

Figure 3. Demonstrates the information that can be gathered from IVUS (20Mhz, lower panels) and from OCT imaging (mid and upper panels, LightLabImaging™, Boston, MA, USA) in patients at follow-up after stent implantation. These are corresponding cross sections within a stent, imaged by both, OCT in the upper panels and by IVUS in the lower panels. The images represent the same spots within a coronary artery (A, B, C), and illustrates the different quality of information that can be obtained by OCT as compared to conventional grey scale IVUS. A) Three layers of stents can be seen. OCT is able to clearly visualise the individual stent struts, the neointimal layers separating the different stents and the very thin coverage of the most inner, luminal stent struts. B) a bright, eccentric and relatively thick neointimal layer can be seen C) an eccentric thick neointimal layer is visible, however, the structure of this neointima differs considerably from the example B) with a low-reflective and speckled appearance.

see colour section

b) Assessment of structural details of tissue coverage

OCT also permits the characterisation of neointimal tissue in a qualitative way. This is a great advantage as such information has not been available in vivo until now. The limited resolution, together with artefacts induced by metallic stent struts does not allow the characterisation of such details by IVUS. With OCT, neointimal tissue can show a variety of morphologies ranging from homogeneous, bright, uniform tissue to optically heterogeneous tissue or eccentric tissue of various thickness. Furthermore, structural details within the tissue can be observed such as intimal neovascularisation (24) or a layered appearance, typically observed in restenotic regions (25). Variations in the appearance of strut coverage can be seen within an individual patient, within an individual stent or within stents of different design. OCT findings, such as dark, signal-

poor halos around stent struts may reflect fibrin deposition and incomplete healing, as described in pathologic and animal experimental series (20,21). However, there is paucity of data demonstrating directly the OCT appearance of different components in neointimal tissue as defined by histology. Post-mortem imaging of DES in human coronaries is difficult and might be limited by the fact that the optical tissue properties show variations with temperature and fixation (26). Long-term animal OCT observations in DES are scarce.

see colour section

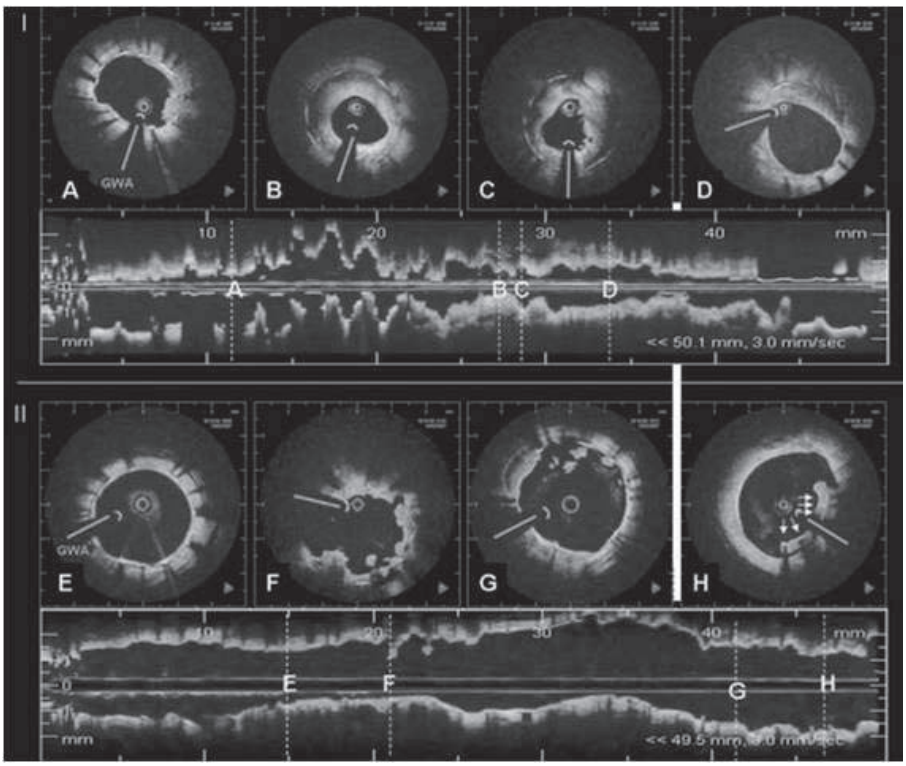

Figure 4. OCT (LightLab Imaging Boston, MA, USA) findings in two patients presenting with late drug-eluting stent (DES) thrombosis. OCT was performed in both cases immediately after thrombus aspiration and reveals completely different morphologic findings, possible suggesting two different mechanisms for late stent thrombosis, focal restenosis and incomplete strut coverage. I) Patient with late stent thrombosis three months after DES implantation in the left circumflex artery. OCT reveals an adequately expanded stent, all struts are well apposed against the vessel wall. All struts show tissue coverage, which is more pronounced in the proximal portion of the stent (D) as compared to the distal stent portion (A). There is focal in-stent restenosis (B, C) with severe lumen narrowing (MLA 1.63 mm2). The neointima shows a layered appearance with a luminal bright, highly reflective layer, an intermediate layer and a dark, signal poor layer surrounding the struts. Remnants of the thrombus are focally seen focally as irregular mural structures, protruding into the lumen (A, C). II) Patient with very late stent thrombosis four years after DES implantation in the left anterior descending artery. OCT reveals an adequately expanded stent, however, there is incomplete stent strut apposition at the proximal stent edge with incomplete tissue coverage in 21% of struts. (E) The distal stent portion, shows a well expanded and apposed stent with thin tissue coverage by OCT. F) irregular lumen borders with intraluminal remnants of the thrombus. G) proximal stent portion showing a strut without visible tissue coverage in 12 o'clock position and thrombus fragments in the lumen. H) proximal stent edge with incomplete apposition of five stent struts (arrows) against the vessel wall. The distance to the vessel wall is 200 micron. OCT shows tissue around the stent struts (DD thrombus, neointima). GWA: guidewire artefact.

c) Assessment of stent strut vessel wall interaction and strut apposition

The interest in the long-term stent strut vessel wall interaction is manifold and includes the assessment of the stability of the acute result, the visualisation of complex anatomy that is not accessible by angiography or IVUS and the clearer understanding of reasons for stent failures, when they do occur. The unique optical properties of OCT can also be applied to the study and evaluation of new stent designs including bioabsorbable stents. Morphologic changes of the absorbable, polylactic acid stent struts and the vessel wall during follow-up have been recently described and show the unique capabilities of this in vivo imaging modality (27). Stent strut malapposition remains an important consideration. Postulated causes for stent strut malapposition are various and include incomplete stent expansion, stent recoil or fracture, late outward vessel remodelling or the dissolution of thrombus that was compressed during PCI between the stent strut and the vessel wall. Regardless of the pathophysiologic mechanism, the major concern in stent malapposition remains in the assumption that areas of strut malapposition cause non-laminar and turbulent blood flow characteristics, which in turn can trigger platelet activation and thrombosis. Here, prospective, serial OCT observations immediately and at longer term follow-up after stenting may improve our understanding of these complex mechanisms and shed light on the likely clinical significance of this phenomenon. Reasons for DES failure are poorly understood. With the reduction of in-stent hyperplasia, other mechanisms of restenosis due to mechanical stent failure have become apparent. Of the two established first generation DES, the sirolimus-eluting stent (Cordis, Johnson & Johnson, Miami, FL, USA) has been particularly linked to cases of stent fracture, likely as a result of its closed cell design compared with other DES employing an open cell system (28). The higher imaging resolution of OCT compared to IVUS permits a detailed assessment in such cases, as demonstrated recently by Shite et al (29) and Barlis et al (30).

Conclusion & future developments

OCT is a light-based diagnostic tool that allows in vivo imaging of the coronary artery wall in unparalleled detail (31). OCT can reliably visualise very thin stent strut tissue coverage as early as five days after implantation, and permits for its qualitative and precise quantitative assessment. These unique capabilities favour OCT as the new golden standard for the evaluation of coronary stents. Recent improvements in OCT technology, with frequency-domain OCT, will allow for a simple imaging procedure and offer the potential for large scale, prospective studies, indispensable to address vexing clinical questions such as the relationship of drug-eluting stent deployment, vascular healing, the true time course of endothelial stent coverage and late stent thrombosis. This may also better guide the optimal duration of dual anti-platelet therapy that currently remains unclear and rather empiric.

References

1. Huang D, Swanson EA, Lin CP, Schuman JS, Stinson WG, Chang W, Hee MR, Flotte T, Gregory K, Puliafito CA, et al. Optical coherence tomography. Science, 1991;254:1178-81.
2. Brezinski ME, Tearney GJ, Bouma BE, Boppart SA, Hee MR, Swanson EA, Southern JF, Fujimoto JG. Imaging of coronary artery microstructure (in vitro) with optical coherence tomography. Am J Cardiol, 1996;77:92-3.
3. Fujimoto JG, Boppart SA, Tearney GJ, Bouma BE, Pitris C, Brezinski ME. High resolution in vivo intra-arterial imaging with optical coherence tomography. Heart, 1999;82:128-33.
4. Regar E, Schaar J, van der Giessen W, van der Steen A, Serruys P. Real-time, in-vivo optical coherence tomography of human coronary arteries using a dedicated imaging wire. Am J Cardiol 2002;90(suppl 6A): 129H.
5. Colombo A, Hall P, Nakamura S, Almagor Y, Maiello L, Martini G, Gaglione A, Goldberg SL, Tobis JM. Intracoronary stenting without anticoagulation accomplished with intravascular ultrasound guidance [see comments]. Circulation, 1995;91:1676-88.
6. de Jaegere P, Mudra H, Figulla H, Almagor Y, Doucet S, Penn I, Colombo A, Hamm C, Bartorelli A, Rothman M, Nobuyoshi M, Yamaguchi T, Voudris V, DiMario C, Makovski S, Hausmann D, Rowe S, Rabinovich S, Sunamura M, van Es GA. Intravascular ultrasound-guided optimized stent deployment. Immediate and 6 months clinical and angiographic results from the Multicenter Ultrasound Stenting in Coronaries Study (MUSIC Study. Eur Heart J, 1998;19:1214-23.
7. Meerkin D, Lee SH, Tio FO, Grube E, Wong SC, Hong MK. Effects of focused force angioplasty: pre-clinical experience and clinical confirmation. J Invasive Cardiol, 2005;17:203-6.
8. Tanabe K, Serruys PW, Degertekin M, Grube E, Guagliumi G, Urbaszek W, Bonnier J, Lablanche JM, Siminiak T, Nordrehaug J, Figulla H, Drzewiecki J, Banning A, Hauptmann K, Dudek D, Bruining N, Hamers R, Hoye A, Ligthart JM, Disco C, Koglin J, Russell ME, Colombo A; TAXUS II Study Group. Incomplete stent apposition after implantation of paclitaxeleluting stents or bare metal stents: insights from the randomized TAXUS II trial. Circulation, 2005;111:900-5.
9. Tearney GJ, Jang IK, Kang DH, Aretz HT, Houser SL, Brady TJ, Schlendorf K, Shishkov M, Bouma BE. Porcine coronary imaging in vivo by optical coherence tomography. Acta Cardiol, 2000;55:233-7.
10. Hauger C, Worz M, Hellmuth T. Interferometer for optical coherence tomography. Appl Opt,2003;42:3896-902.
11. Tanigawa J, Barlis P, Dimopoulos K, Di Mario C. Optical coherence tomography to assess malapposition in overlapping drug-eluting stents. EuroInterv., 2008;3:580-583.
12. Tanigawa J, Barlis P, Kaplan S, Goktekin O, Di Mario C. Stent strut apposition in complex lesions using optical coherence tomography. Am J Cardiol, 2006;98:Suppl 1: 97M.
13. Regar E, Schaar J, Serruys P. Acute recoil in sirolimus eluting stent: real time, in vivo assessment with optical coherence tomography. Heart, 2006;92:123.
14. Regar E, Ong A, McFadden EP, de Jaegere PPT, van Beusekom HMM, van der Giessen WJ, de Feyter P, Serruys PW. Long-term follow-up of drug-eluting stents (DES) - optical coherence tomography (OCT) findings. Eur Heart J, 2005:P4047 (abstract).
15. Tanimoto S, Rodriguez-Granillo G, Barlis P, de Winter S, Bruining N, Hamers R, Knappen M, Verheye S, Serruys PW, Regar E. A Novel Approach for Quantitative Analysis of Intracoronary Optical Coherence Tomography. High inter-observer agreement with computer-assisted contour detection. Catheter Cardiovasc Interv., 2008;Mar 6; [Epub ahead of print].
16. Matsumoto D, Shite J, Shinke T, Otake H, Tanino Y, Ogasawara D, Sawada T, Paredes OL, Hirata K, Yokoyama M. Neointimal coverage of sirolimus-eluting stents at 6-month follow-up: evaluated by optical coherence tomography. Eur Heart J, 2007;28:961-7.
17. Takano M, Inami S, Jang IK, Yamamoto M, Murakami D, Seimiya K, Ohba T, Mizuno K. Evaluation by optical coherence tomography of neointimal coverage of sirolimus-eluting stent three months after implantation. Am J Cardiol, 2007;99:1033-8.
18. Takano M, Yamamoto M, Inami S, Murakami D, Seimiya K, Ohba T, Seino Y, Mizuno K. Long-term follow-up evaluation after sirolimus-eluting stent implantation by optical coherence tomography: do uncovered struts persist? J Am Coll Cardiol, 2008;51:968-9.
19. Chen BX, Ma FY, Luo W, Ruan JH, Xie WL, Zhao XZ, Sun SH, Guo XM, Wang F, Tian T, Chu XW. Neointimal Coverage of Bare Metal and Sirolimus-Eluting Stents Evaluated with optical coherence tomography, Heart. 2008 May;94(5):566-70.

20. Finn AV, Joner M, Nakazawa G, Kolodgie F, Newell J, John MC, Gold HK, Virmani R. Pathological correlates of late drug-eluting stent thrombosis: strut coverage as a marker of endothelialization. Circulation, 2007;115:2435-41.
21. Finn AV, Nakazawa G, Joner M, Kolodgie FD, Mont EK, Gold HK, Virmani R. Vascular responses to drug eluting stents: importance of delayed healing. Arterioscler Thromb Vasc Biol 2007;27:1500-10.
22. Joner M, Finn AV, Farb A, Mont EK, Kolodgie FD, Ladich E, Kutys R, Skorija K, Gold HK, Virmani R. Pathology of drug-eluting stents in humans: delayed healing and late thrombotic risk. J Am Coll Cardiol, 2006;48:193-202.
23. van Beusekom HM, Whelan DM, Hofma SH, Krabbendam SC, van Hinsbergh VW, Verdouw PD, van der Giessen WJ. Long-term endothelial dysfunction is more pronounced after stenting than after balloon angioplasty in porcine coronary arteries. J Am Coll Cardiol, 1998;32:1109-17.
24. Regar E, van Beusekom HM, van der Giessen WJ, Serruys PW. Images in cardiovascular medicine. Optical coherence tomography findings at 5-year follow-up after coronary stent implantation. Circulation, 2005;112:e345-6.
25. Tanimoto S, Aoki J, Serruys PW, Regar E. Paclitaxel-eluting stent restenosis shows three - layer appearance by optical coherence tomography. Eurointerv., 2006 2006;1:484.
26. Meer FJvd, Faber DJ, Cilesiz I, Gemert MJCv, Leeuwen TGv. Temperature-dependent optical properties of individual vascular wall components measured by optical coherence tomography. Journal of Biomedical Optics, 2006;11:041120.
27. Ormiston JA, Serruys PW, Regar E, Dudek D, Thuesen L, Webster MW, Onuma Y, Garcia-Garcia HM, McGreevy R, Veldhof S. First-In-Man Evaluation of a Bioabsorbable-Everolimus Eluting Coronary Stent System (BVS) in the Treatment of Patients with Single de-novo Native Coronary Artery Lesions: The ABSORB Trial. The Lancet, 2 2008;371:899-907.
28. Lee SH, Park JS, Shin DG, Kim YJ, Hong GR, Kim W, Shim BS. Frequency of stent fracture as a cause of coronary restenosis after sirolimus-eluting stent implantation. Am J Cardiol, 2007;100:627-30.
29. Shite J, Matsumoto D, Yokoyama M. Sirolimus-eluting stent fracture with thrombus, visualization by optical coherence tomography. Eur Heart J, 2006;27:1389.
30. Barlis P, Sianos G, Ferrante G, Del Furia F, D'Souza S, Di Mario C. The use of intra-coronary optical coherence tomography for the assessment of sirolimus-eluting stent fracture. Int J Cardiol 2008. doi:10.1016/j.ijcard.2008.04.076
31. Regar E, van Leeuwen AMGJ, Serruys PW (Eds): Optical coherence tomography in cardiovascular research. London: Informa Healthcare. 2007. ISBN 1841846112.

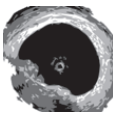

Chapter 19

Coronary Bioabsorbable Magnesium Stent: 15 Month Intravascular Ultrasound and Optical Coherence Tomography Findings

Peter Barlis, Jun Tanigawa, Carlo Di Mario

A 65-year-old man underwent elective percutaneous coronary intervention for a stenosis in the proximal left anterior descending artery (LAD). As part of the PROGRESS study (designed as a first-in-man coronary study in 65 patients in 7 European centres), a 3.5x15mm magnesium based bioabsorbable stent (Lekton Magic Stent, Biotronik, Bulach, Switzerland) was implanted achieving an excellent angiographic result. Fifteen months following the initial intervention, an exercise treadmill test to evaluate exertional dyspnoea was positive. Angiography revealed a new and separate lesion in the mid-LAD/diagonal artery that was treated successfully with 2 sirolimus-eluting stents (Cypher Select, Cordis, J&J) in a culotte fashion. In the previously treated proximal segment, the vessel lumen was patent with no signs of narrowing or edge effect (Panel A). Imaging using intravascular ultrasound (IVUS, Panel B) and optical coherence tomography (OCT, Panel C) showed absence of circumferential stent struts with shadowing. Small, scattered and circumscribed zones of high intensity (arrows) indicated the previous stent strut position (Panel B-C). All struts were covered by a thin neointimal layer with a thickness between 80 and 140 microns (Panel C).

The bioabsorbable stent is constructed from a magnesium alloy containing also Zirconium (<5%), Yttrium (<5%), and rare earth elements (<5%). The struts disappear over time but their position can still be identified due to the fact that the strut material is absorbed and the space filled in by calcium apatite complex, accompanied by a phosphorous compound. These stents are compatible with cardiac magnetic resonance imaging and multi-slice computed tomography and can be used as vehicles for possible drug and gene delivery. Such a novel technology may prove useful in negating some of the untoward complications of current permanent metallic stents, namely stent thrombosis and the need for prolonged dual anti-platelet therapy.

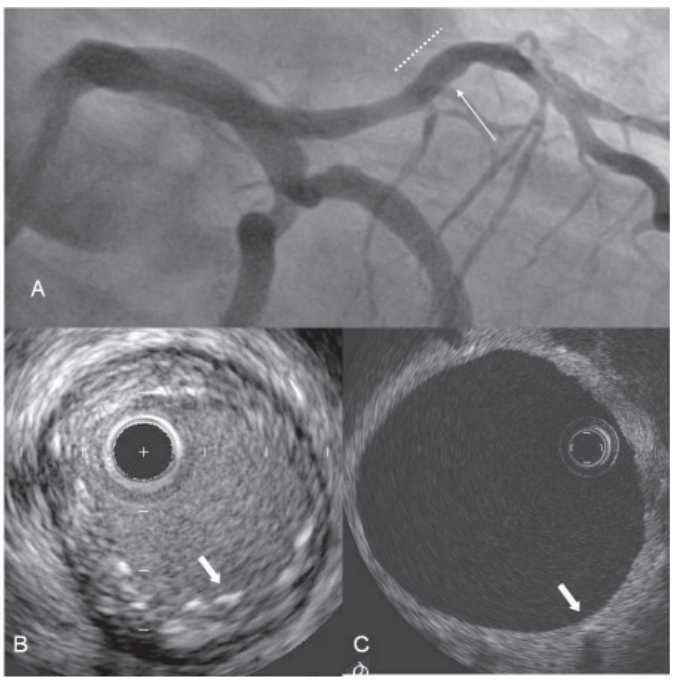

Panel A Coronary angiography in the right caudal view showing the proximal left anterior descending artery (LAD) 15 months after implantation of a magnesium bioabsorbable stent. The stented area is indicated by the dashed line. The arrow indicates the region imaged by IVUS and OCT.

Panel B and C B: IVUS and C: OCT imaging of the previously stented segment at 15 months follow-up. The vessel wall is without stent struts after absorption but small, well defined zones of high intensity (arrowheads) are scattered indicating the previous stent strut position. There is a thin, concentric layer of neointima with thickness between 80μm and 140μm (panel C).

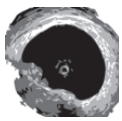

Chapter 20

Optical Coherence Tomography Findings in Very Late (4 Years) Paclitaxel-Eluting Stent Thrombosis

Arend Schinkel, Peter Barlis, Heleen van Beusekom, Patrick W. Serruys, Evelyn Regar

The mechanisms of late coronary stent thrombosis, a complication with high morbidity and mortality (1), are poorly understood. Late thrombosis in drug-eluting coronary stents has been associated with delayed endothelialization of the stent struts or systemic and intra-stent hypersensitivity reaction (2). We present in-vivo findings in a patient with very late stent thrombosis. In 2003, a 60-year-old man with a history of stable angina and smoking underwent elective placement of two overlapping paclitaxel-eluting stents (3.0x16 mm and 2.75x28mm, Boston Scientific, Natick, MA) and post-dilation with a noncompliant balloon, for a significant stenosis of the left anterior descending artery (LAD). The discharge medication consisted of aspirin, Clopidogrel (12 months), beta-blockers and statins. Four years after stenting, the patient presented with acute anterior myocardial infarction caused by late stent thrombosis while under chronic aspirin therapy (Figure 1). After thrombus aspiration intravascular ultrasound (IVUS) and intravascular optical coherence tomography (OCT) were performed, showing incomplete coverage of 21% of the stent struts, which may reflect delayed vascular healing (Figure 2 and 3). Pathology of the thrombotic material showed a recent multilayered thrombus (Figure 4). Post-procedure, the patient was treated with abciximab (Centocor, Leiden, Netherlands) and was discharged with sustained aspirin and Clopidogrel therapy.

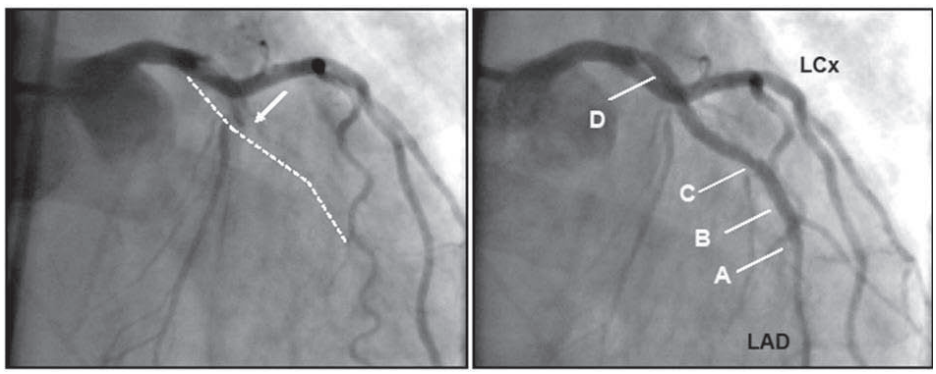

Figure 1: Coronary angiogram: Left: thrombotic occlusion of the LAD, dotted line indicates stented segment. Right: result after thrombus aspiration (Export catheter, Medtronic, Minneapolis, MI), with TIMI III antegrade flow and moderate residual stenosis in the mid-portion of the stented segment. A-D indicate locations of intracoronary imaging.

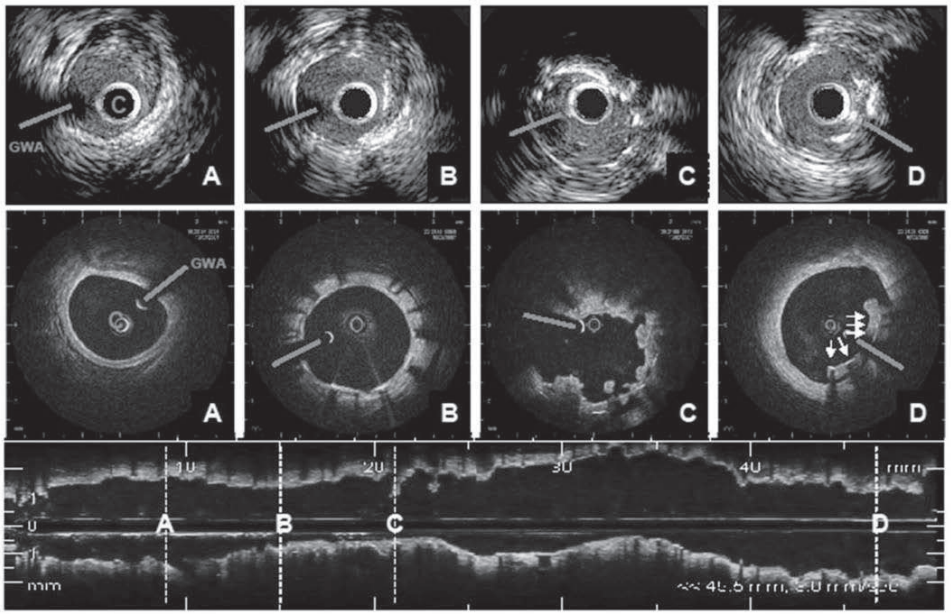

Figure 2: Intracoronary imaging after thrombus aspiration. Upper panels: IVUS (Atlantis, Boston Scientific, Natick, MA), lower panels: OCT (LightLab Imaging™, Boston, MA; cross sectional and longitudinal view) A) distal reference showing eccentric plaque in 11-4 o'clock position. B) distal stent portion, showing a well expanded and apposed stent with thin tissue coverage by OCT that is missed by IVUS. C) irregular lumen borders with intraluminal remnants of the thrombus D) proximal stent edge with incomplete apposition of 5 stent struts (arrows) against the vessel wall. The distance to the vessel wall is 200µm. OCT shows tissue around the stent struts (DD thrombus, neointima). Incomplete stent apposition may be caused initial malapposition or acquired malapposition caused by a vascular response to the stent. GWA= guide wire artefact; C= catheter artefact.

see colour section

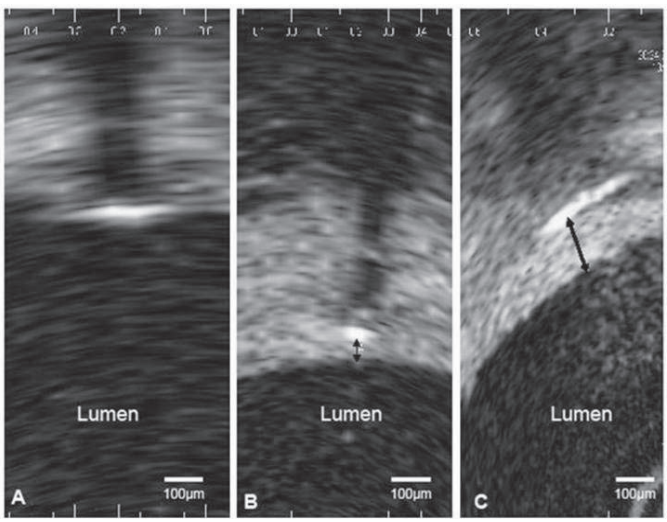

Figure 3: Spectrum of tissue coverage as seen by OCT in this stented segment. Tissue coverage was not visible in 21% (n=110) of the struts, while 79% (n=411 of 521) of the struts showed tissue coverage of various thickness. A) no visible coverage B) very thin coverage (40µm) C) maximal coverage (140 µm).

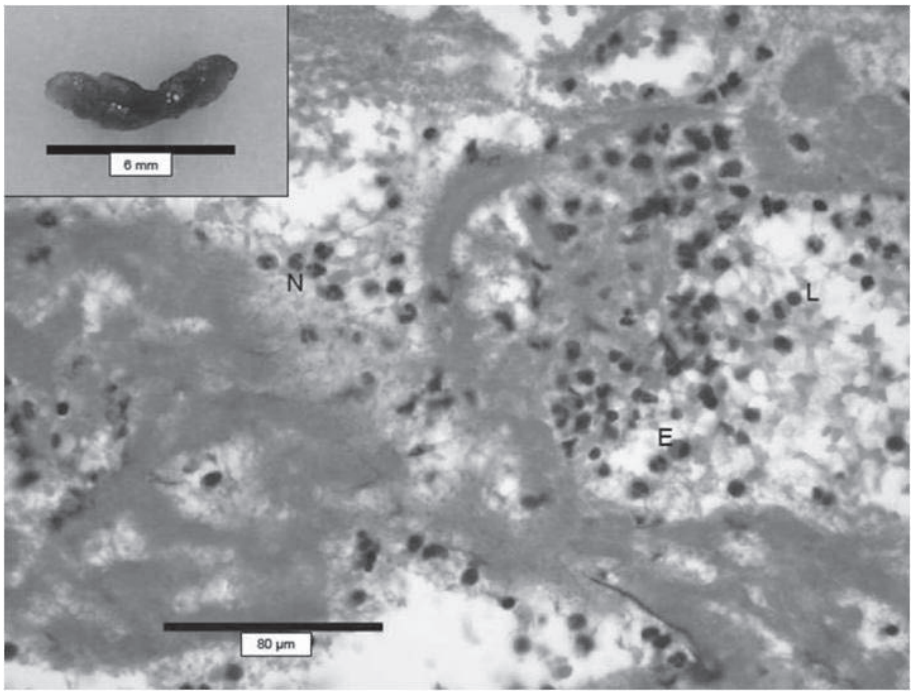

Figure 4: Histology of the aspirated thrombus: recent multilayered thrombus showing Zahn lines and containing abundant leukocytes consisting of eosinophils (E), neutrophils (N) and lymphocytes (L).

see colour section

References

1. McFadden EP, Stabile E, Regar E, et al. Late thrombosis in drug-eluting coronary stents after discontinuation of anti-platelet therapy. Lancet 2004;364:1519-21.
2. Nebeker JR, Virmani R, Bennett CL, et al. Hypersensitivity cases associated with drug-eluting coronary stents: a review of available cases from the Research on Adverse Drug Events and Reports (RADAR) project. J Am Coll Cardiol 2006;47:175-81.

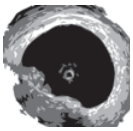

Chapter 21

Optical Coherence Tomography: A new Tool to Detect Tissue Coverage in Drug Eluting Stents

Carlo Di Mario, Peter Barlis

The nineties have seen a parallel growth of intravascular ultrasound (IVUS) and stent implantation, heralded and explained by the seminal observations that stents implanted at low pressure under angiographic guidance alone are frequently under-deployed and have higher risk of thrombosis.(1) With a high price to pay in terms of late hyperplasia in the first months after implantation, meticulous attention was paid to overexpansion as a potential remedy to reduce restenosis. Despite conflicting results of studies of IVUS guided stenting, (2,3) IVUS was largely applied to guide stenting in complex coronary lesions. (4) The introduction of drug-eluting stents (DES) has reset the boundary of optimal stent expansion to prevent thrombosis and restenosis, with risk thresholds as low as 4.5 mm^2, achievable in most cases without ultrasound guidance. (5) The new challenge for interventional cardiology became late stent thrombosis and IVUS seemed inadequate to prevent this new evil, with late malapposition (6) but not post-procedural malapposition (7) correlated with late thrombosis.

Unlike conventional stents which develop circumferential coverage with an average thickness of 500μm or more, well visualized with IVUS and angiography (1mm late loss),(8) DES delay and prevent the hyperplastic response so that the average late lumen loss for sirolimus- or paclitaxel-eluting stents can be lower than 100μm, (9) which means the amount of intimal thickening will not be detectable with IVUS because of its limited axial resolution and the presence of artifacts around struts.

Suzuki et al (10) suggest that another intravascular imaging technique may replace IVUS for the more refined assessment required by DES. In the 11 stents with a small hyperplastic response measured with histology, IVUS overestimated lumen area and underestimated in-stent hyperplasia. In this swine model of stent overexpansion, the optical coherence tomography (OCT) measurements were much closer to the histological measurements. The receiver operator curve of sensitivity-specificity showed a greater diagnostic accuracy, approaching the unity as opposed to a disappointing 0.78 with IVUS (see Suzuki et al, Figure 5). This was expected since OCT has a far greater resolution than IVUS and was initially introduced to study superficial plaque components, (11) with studies claiming the technique is also able to detect macrophages in unstable plaques. (12,13)

Several small studies have recently been published highlighting the application of OCT for the in-vivo detection of stent tissue coverage at follow-up.(14-16) The study by Matsumoto et al (17) used both IVUS and OCT in 34 patients following sirolimus-eluting stent (SES) implantation. The mean neointima thickness was 52.5 microns, and the prevalence of struts covered by thin neointima, undetectable by IVUS, was 64%. The average rate of neointima-covered struts in an individual SES was 89%. Nine SES (16%) showed full coverage by neointima, whereas the remaining stents had partially uncovered struts. This small series confirms the superiority of OCT over IVUS for the detection of thin layers of neointimal tissue following stent implantation.

The crisp OCT images obtained in swines by Suzuki et al (10) in their experimental model are perfectly reproducible in patients in daily clinical practice. A cumbersome technique of proximal balloon occlusion and sub-selective intra-coronary flushing with crystalloid solutions was used in this study. This strategy can be replaced by continuous injection of a viscous contrast medium via the guiding catheter.(18) The OCT image wire is not steerable but can be inserted via an over the wire (OTW) lumen larger than 0.019" using either a single lumen (e.g.Transit, Cordis, Johnson & Johnson, Miami FL, USA) or a double lumen Monorail-OTW catheter such as the TwinPass 0.023" (Vascular Solutions Inc, Minneapolis, Minnesota, US).
The use of the non-occlusive (flush-only) technique is compatible with OCT systems capable of acquisition speeds between 2 and 3mm/sec, thereby fast enough to generate interpretable images

in a safe and rapid manner, perfectly tolerated with no chest pain or major ECG changes or arrhythmias if an iso-osmolar contrast agent such as Iodixanol 370 (Visipaque™, GE Health Care, Ireland) is used. (8,19) The OCT procedure is also set to become greatly simplified with the introduction into clinical practice (within 1-2 years) of Fourier or optical frequency domain imaging (OFDI) technologies, (20) with acquisition speeds of 20mm/sec enabling complete pullbacks in only a matter of 3-5 seconds and eliminating the need for proximal vessel balloon occlusion.

The scary picture of DES associated with increased mortality and myocardial infarction (21,22) has lost credit (23-25). Still, the sirolimus-eluting stent Cypher (J&J, Cordis, Miami, FL,USA) and the paclitaxel-eluting stent TAXUS (BSC, Boston, MS, USA), the only 2 DES with sufficient number of observations at late follow-up, show a small but worrisome increase in late thrombosis. (23,26)

Trialists are faced with the challenge of studying a phenomenon so rare and so far in time from the initial treatment to require prolonged studies of tens of thousands of patients to provide meaningful answers. Studies of the magnitude of the largest secondary prevention or thrombolytic mega-trials are very difficult to be carried out because of cost and availability of patients and suitable centers. The duration of these trials is an equally important problem since their results risk being invalidated by the availability of new anti-platelet treatments and new DES, the latter with the potential to offer more safety because of thinner struts and more conformable designs and biologically tissue friendly coatings and drugs. OCT has the potential to offer surrogate end-points to test the ability of new DES to promote consistent tissue coverage of all struts. Studies of new DES should include OCT sub-studies of adequate size and with serial examinations at well selected time intervals after implantation. Such studies could identify the most promising DES and provide evidence to guide duration of anti-platelet treatment after different DES types.

References

1. Colombo A, Hall P, Nakamura S, et al. Intracoronary stenting without anticoagulation accomplished with intravascular ultrasound guidance. Circulation 1995;91:1676-88.
2. Albiero R, Rau T, Schluter M, et al. Comparison of immediate and intermediate-term results of intravascular ultrasound versus angiography-guided Palmaz-Schatz stent implantation in matched lesions. Circulation 1997;96:2997-3005.
3. Mudra H, di Mario C, de Jaegere P, et al. Randomized comparison of coronary stent implantation under ultrasound or angiographic guidance to reduce stent restenosis (OPTICUS Study). Circulation 2001;104:1343-9.
4. Moussa I, Di Mario C, Moses J, et al. Coronary stenting after rotational atherectomy in calcified and complex lesions. Angiographic and clinical follow-up results. Circulation 1997;96:128-36.
5. Fitzgerald PJ, Oshima A, Hayase M, et al. Final results of the Can Routine Ultrasound Influence Stent Expansion (CRUISE) study. Circulation 2000;102:523-30.
6. Cook S, Wenaweser P, Togni M, et al. Incomplete stent apposition and very late stent thrombosis after drug-eluting stent implantation. Circulation 2007;115:2426-34.
7. Kimura M, Mintz GS, Carlier S, et al. Outcome after acute incomplete sirolimus-eluting stent apposition as assessed by serial intravascular ultrasound. Am J Cardiol 2006;98:436-42.
8. Tanigawa J, Barlis P, Di Mario C. Intravascular Optical Coherence Tomography: Optimisation of image acquisition and quantitative assessment of stent strut apposition. EuroIntervention 2007;3:128-136.
9. Fujii K, Mintz GS, Kobayashi Y, et al. Contribution of stent underexpansion to recurrence after sirolimus-eluting stent implantation for in-stent restenosis. Circulation 2004;109:1085-8.

10. Suzuki Y, Ikeno F, Koizumi T, et al. In vivo Comparison Between Optical Coherence Tomography and Intravascular Ultrasound for Detecting Small Degrees of In-Stent Neointima after Stent Implantation. JACC: Cardiovascular Interventions 2008;In Press.
11. Jang IK, Bouma BE, Kang DH, et al. Visualization of coronary atherosclerotic plaques in patients using optical coherence tomography: comparison with intravascular ultrasound. J Am Coll Cardiol 2002;39:604-9.
12. Tearney GJ, Yabushita H, Houser SL, et al. Quantification of macrophage content in atherosclerotic plaques by optical coherence tomography. Circulation 2003;107:113-9.
13. MacNeill BD, Jang IK, Bouma BE, et al. Focal and multi-focal plaque macrophage distributions in patients with acute and stable presentations of coronary artery disease. J Am Coll Cardiol 2004;44:972-9.
14. Takano M, Inami S, Jang IK, et al. Evaluation by optical coherence tomography of neointimal coverage of sirolimus-eluting stent three months after implantation. Am J Cardiol 2007;99:1033-8.
15. Chen BX, Ma FY, Wei L, et al. Neointimal Coverage of Bare Metal and Sirolimus-Eluting Stents Evaluated with Optical Coherence Tomography. Heart 2007:hrt.2007.118679.
16. Matsumoto D, Shite J, Shinke T, et al. Neointimal coverage of sirolimus-eluting stents at 6-month follow-up: evaluated by optical coherence tomography. Eur Heart J 2007;28:961-7.
17. Matsumoto D, Shite J, Shinke T, et al. Neointimal coverage of sirolimus-eluting stents at 6-month follow-up: evaluated by optical coherence tomography. Eur Heart J 2006.
18. Prati F, Cera M, Ramazzotti V, Imola F, Giudice R, Albertucci M. Safety and feasibility of a new non-occlusive technique for facilitated intracoronary optical coherence tomography (OCT) acquisition in various clinical and anatomical scenarios. EuroIntervention 2007;3:365-70.
19. Chai CM, Almen T, Baath L, Besjakov J. Adding sodium and calcium ions to the contrast medium iodixanol reduced the risk of ventricular fibrillation during perfusion of the left coronary artery in pigs: effects of electrolytes, viscosity, and chemotoxicity of an isotonic perfusate. Acad Radiol 2004;11:583-93.
20. Yun SH, Tearney GJ, Vakoc BJ, et al. Comprehensive volumetric optical microscopy in vivo. Nat Med 2006;12:1429-33.
21. Camenzind E, Steg PG, Wijns W. Stent thrombosis late after implantation of first-generation drug-eluting stents: a cause for concern. Circulation 2007;115:1440-55; discussion 1455.
22. Lagerqvist B, James SK, Stenestrand U, Lindback J, Nilsson T, Wallentin L. Long-term outcomes with drug-eluting stents versus bare-metal stents in Sweden. N Engl J Med 2007;356:1009-19.
23. Stone GW, Moses JW, Ellis SG, et al. Safety and efficacy of sirolimus- and paclitaxel-eluting coronary stents. N Engl J Med 2007;356:998-1008.
24. James SK, Carlsson J, Lindbäck J, et al. Long term follow up of additional Swedish registry data does not indicate an increased mortality with drug-eluting stents but the benefit is limited and the risk of blood clots is sustained. European Socety of Cardiology. Vienna, 2007.
25. Jeremias A, Kirtane A. Balancing Efficacy and Safety of Drug-Eluting Stents in Patients Undergoing Percutaneous Coronary Intervention. Ann Intern Med 2007:0000605-200802050-00199.
26. Daemen J, Wenaweser P, Tsuchida K, et al. Early and late coronary stent thrombosis of sirolimus-eluting and paclitaxel-eluting stents in routine clinical practice: data from a large two-institutional cohort study. Lancet 2007;369:667-78.

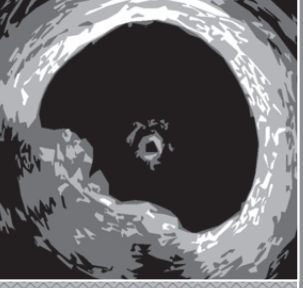

Part 4

OCT Clinical Applications
Atherosclerotic Plaque Assessment

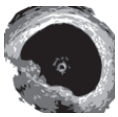

Chapter 22

Assessment of Culprit and Remote Coronary Narrowings Using Optical Coherence Tomography with Long-Term Outcomes

Peter Barlis, Patrick W. Serruys, Nieves Gonzalo, Willem J. van der Giessen, Peter J. de Jaegere, Evelyn Regar

Much of what is currently known about vulnerable plaque (VP) stems from post-mortem studies that have identified several characteristics of plaques making them prone to rupture, including the presence of a thin fibrous cap and a large lipid core. This study used optical coherence tomography (OCT) to assess culprit and remote coronary narrowings and to investigate whether intra-coronary OCT in living patients, was able to visualize morphologic features associated with VP in post-mortem studies. Twenty-three patients successfully underwent OCT prior to percutaneous coronary intervention. The culprit lesion and mild-moderate coronary narrowings remote from the target stenosis were investigated. By OCT, the culprit lesion was found to be fibrous in 39.1%, fibro-calcific in 34.4% and lipid-rich in 26.1% of cases. There were 2 patients meeting the criteria for thin-cap fibroatheroma (TCFA) (defined as the presence of a signal-rich fibrous cap covering a signal-poor lipid/necrotic core with a cap thickness <0.2mm). The majority of plaques at remote segments were proximal to the culprit lesion (73.9%) and predominantly fibrous and lipid-rich. OCT identified 7 TCFA lesions in 6 patients with a mean cap thickness of 0.19±0.05mm, extending for 103 ±49° of the total vessel circumference. At 24-months clinical follow-up, the only event occurred in a patient with in-stent restenosis who underwent repeat percutaneous revascularization. There were no clinically apparent plaque rupture-related events in the 6 patients found to have remote TCFA. This study has showed that OCT can be safely applied to image beyond the culprit lesion and that it can detect in-vivo morphologic features that have been associated with plaque vulnerability by retrospective pathologic examination. In conclusion, the detection of TCFA, particularly in stable patients is desirable and may principally allow for early intervention and prevention of adverse events.

Acute coronary syndromes (ACS) including myocardial infarction (MI) are leading causes of death in industrialized countries, often caused by rupture of vulnerable plaque (VP). The detection of VP in the early phase of coronary artery disease therefore remains essential to limit morbidity and mortality while helping to target specific therapeutic interventions. Through retrospective, post-mortem studies, several characteristics of plaques that are prone to rupture have been identified including: the presence of a thin fibrous cap (<65 microns in thickness); a large lipid core and activated macrophages near the cap. The limitation of such studies however remains their inability to provide crucial detail regarding the natural history and progression of VP, and, therefore prognosis. Several imaging modalities have been used to assess and identify VP including coronary angioscopy, intravascular ultrasound (IVUS) and magnetic resonance imaging.(1-3) Recently, there has been significant interest in the field of VP detection using optical coherence tomography (OCT)(1,4-13) as it permits high-resolution (10-20 microns) imaging, principally suited to detect and quantify the thickness of a thin cap fibroatheroma (TCFA) and to estimate macrophage distribution.(9,14,15) In this study, we investigated whether intra-coronary OCT in living patients, was able to visualize morphologic features that have been associated with VP in post-mortem studies.

Methods

Between February and August 2004, this single-center, observational pilot study examined patients with coronary artery disease. Twenty-three patients scheduled for coronary stent implantation underwent OCT before angioplasty. The culprit lesion and mild to moderate coronary lesions remote from the target stenosis were investigated. Patients were selected based on the presence of stable or unstable angina pectoris with objective evidence of ischemia. Clinical exclusion criteria were: poor renal function (serum creatinine >1.5mg/dL), left ventricular ejection fraction <30% and hemodynamic instability. Angiographic exclusion criteria were: lumen diameter proximal to the lesion <2.5mm or >4.0mm by visual estimate; ostial lesion; chronic total occlusion. All patients were pre-treated with aspirin and clopidogrel (600mg loading dose) and both were continued for 1 year. Heparin was used to maintain an activated clotting time >250 seconds. All patients provided written informed consent prior to the

procedure. Clinical follow-up was performed by regular outpatient visit and telephone interview up to two years.
The OCT system used in this study (LightLab Imaging Inc., Westford, MA, US) has been described previously.(1,16) Briefly, an OCT balloon catheter (Helios™, Goodman, Nagoya, Japan) is advanced distal to the lesion over a conventional coronary guide wire, which is then replaced with the OCT imaging wire (ImageWire™). The OCT catheter is then withdrawn proximally and the lesion and segments distal and proximal to the lesion visualized using an automated pullback system at 1.0mm/sec. During image acquisition, coronary blood flow is replaced by continuous infusion of Ringer's lactate at 0.8 ml/sec using a power injector (Mark V ProVis, Medrad, Inc. Indianola, PA, US). The highly compliant occlusion balloon remains inflated proximal to the lesion at 0.5 or 0.7atm for a maximum of 30sec. Cross-sectional images are acquired at 15.6 frames/sec.
Analysis of contiguous cross-sections was performed at 1mm intervals. In each selected cross section, plaque characterization was according to the following established OCT criteria: 1) Fibrous, 2) Fibrocalcific and 3) Lipid-rich.(17) Capped fibroatheroma was defined as the presence of a signal-rich fibrous cap covering a signal-poor lipid/necrotic core with a cap thickness <0.2mm and extending for more than one quadrant of the vessel circumference. The plaque had to be visualized in at least 5 consecutive frames.
Following OCT examination, coronary interventions were performed according to standard practice with stent implantation. Stent optimization was accomplished with conventional angiographic guidance aiming at a residual diameter stenosis <20% by online quantitative coronary angiography. Statistical analyses were performed using SPSS 12.0.1 for Windows (SPSS Inc., Chicago, IL). Data are expressed as mean ± standard deviation for continuous variables or as median (interquartile range) if appropriate and as percentages for categorical variables. In order to evaluate the interobserver agreement for plaque characterization, a subset of plaques was classified by a second observer and the kappa statistic was calculated. To assess the reproducibility of cap thickness a set of fibrous caps were also measured by a second independent observer; the absolute mean difference between two observers' measurements and its standard deviation was calculated.

Results

Baseline clinical and lesion characteristics are shown in Table 1. There was 1 case of transient atrio-ventricular block during OCT pullback in a 72 year-old man with single vessel disease. His further clinical course was uneventful and was discharged as planned the following day.
OCT analysis of the coronary artery wall was possible in all patients. Mean OCT pullback length was 28.8±12.2mm. Quantitative measurements at the culprit site showed a mean minimal lumen area (MLA) and mean minimal lumen diameter (MLD) of 2.38±0.93mm^2 and 1.45±0.33mm respectively. A wide spectrum of plaque morphologies was seen both at the culprit lesion and in remote segments.

The culprit lesion OCT characteristics are also shown in Table 1. The agreement between observers for determining plaque type was good (kappa value of 0.85). There were 2 patients meeting the criteria for TCFA. A 58-year-old female with type 1 diabetes mellitus and hypertension presented with non-ST elevation MI. Coronary angiography revealed single vessel disease in the LAD. OCT demonstrated a tight lesion with a MLA of 0.68mm^2 irregular lumen contours, signs of plaque fissure/rupture and mural thrombus. The other patient was a 62-year-old male with a history of prior MI, presenting with angina (CCS III). Angiographically, three-vessel disease was present with a culprit lesion in the LAD. OCT visualized a non-ruptured TCFA with a cap thickness of 180 μm and a circumferential extent of 100º with a MLA of 3.42mm^2. Both patients underwent uneventful coronary stent implantation.

Variable	n=23
Age (years)	61 ± 11
Men	18 (78)
Diabetes mellitus	2 (9)
Hypertension	13 (57)
Dyslipidemia*	11 (48)
Current smoker	5 (22)
Prior myocardial infarction	6 (26)
Number of coronary arteries narrowed >50%	
1	14 (61)
2	5 (22)
3	4 (17)
Clinical presentation	
Silent myocardial ischemia	1 (4)
Stable angina pectoris	18 (78)
Unstable angina pectoris	4 (17)
Target vessel	
Left anterior descending	14 (61)
Left circumflex	3 (13)
Right	6 (26)
Culprit lesion morphology assessed by optical coherence tomography	**23 lesions**
Fibrous	9 (39)
Fibrocalcific	8 (35)
Lipid-rich	6 (26)

* Total cholesterol ≥5.0 mmol/L or treatment with a lipid-lowering drug

Table 1: Baseline clinical and lesion characteristics

Most plaques (73.9%) at remote segments were found to be proximal to the culprit lesion. Fibrous and lipid-rich plaques were more common while there was one patient with a fibrocalcific plaque distal to the culprit lesion in the RCA (Figure 1).

OCT identified 7 TCFA lesions in 6 patients. One patient presented with stable angina, 3 with unstable angina, and 2 patients had a recent history of ACS. These latter patients underwent primary PCI for acute MI caused by thrombotic occlusion in another vessel 2 weeks prior and were re-scheduled for elective PCI to a residual lesion in a non-infarct related artery. The mean cap thickness was 0.19±0.05mm, extending for 103 ±49° of the total vessel circumference. Three of these TFCA lesions showed an irregular inner lumen contour with evidence of mural thrombi in two lesions (Figure 2). The reproducibility of fibrous cap measurements revealed an absolute mean difference between two observers of 0.010 +/- 0.016 mm, with the limits of agreement (i.e., 1.96SD of mean difference) of 0.043,-0.023.

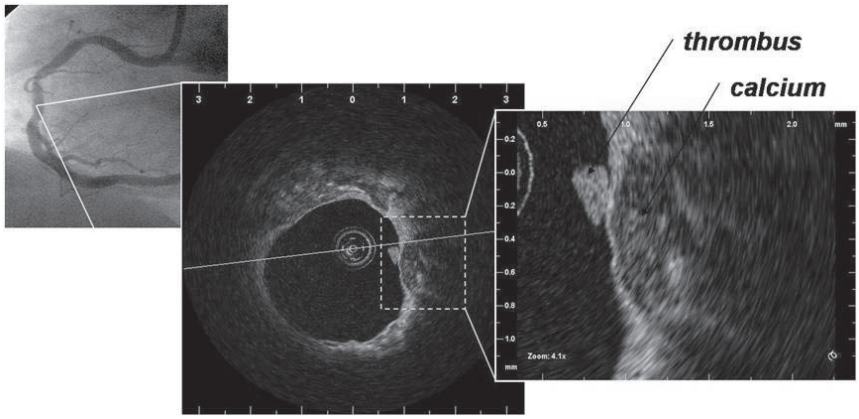

Figure 1: Angiography demonstrating a calcific mid-vessel lesion. A further calcific plaque with sharp and well-delineated margins was also observed by OCT remote and distal to the culprit lesion with attached mural thrombus

see colour section

Two year clinical follow-up was available in all patients. There were no deaths or MI. There was 1 case of target lesion revascularization due to in-stent restenosis in a 65-year-old male 8 months following the index procedure. The patient was successfully treated with repeat PCI. There were no adverse events in the patients with TCFA at remote segments during 24 months follow-up with most patients classified as CCS 1 angina pectoris. All patients were on treatment with statin therapy.

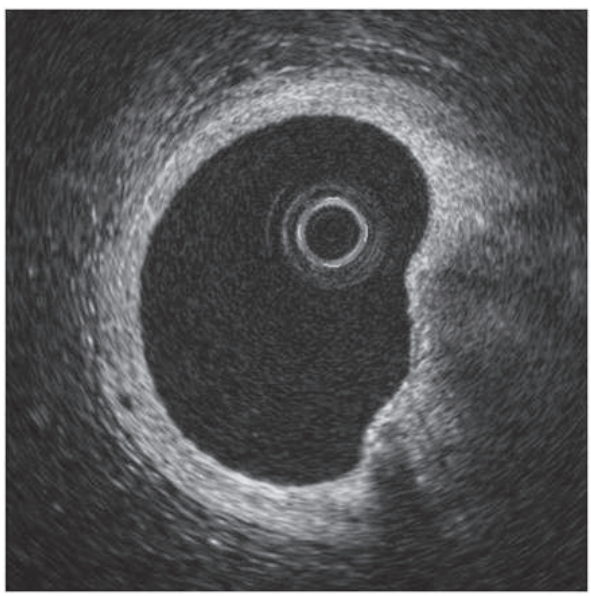

Figure 2: Thin-cap fibroatheroma (TCFA) assessed by OCT overlying a large lipid-rich plaque (2-5 o'clock position). The bright, highly reflective fibrous cap measured between 30-80 microns

see colour section

Discussion

The main findings of this study are: 1) OCT can be safely used in-vivo to demonstrate the heterogeneity of coronary plaques at culprit and remote sites 2) Intravascular OCT can detect in-vivo morphologic features that have been associated with plaque vulnerability by retrospective pathologic examination 3) the lack of long-term clinical events in our patients with TCFA gives a unique, ante-mortem insight into such lesions, even though the sample size is small.

The recent introduction of OCT has proven to be an innovative contribution to the in-vivo detection of VP and TCFA. Its unique image resolution, in the range of 10-15μm, is in the magnitude of 10 times higher than that of IVUS and permits superior visualization of plaque morphology.(18) Although OCT suffers from the inherent lack of tissue penetration (<2mm), it is ideally served to examine the arterial lumen and the lumen–vessel interface. Yabushita et al (17) performed an in-vitro study of more than 300 human atherosclerotic artery segments. When compared to histological examination, OCT had a sensitivity and specificity of 71-79% and 97-98% for fibrous plaques, 95-96% and 97% for fibrocalcific plaques, and 90-94.5% and 90-92% for lipid-rich plaques, respectively. Further, the inter-observer and intra-observer variability of OCT measurements were high (κ values of 0.88 and 0.91 respectively).

The use of OCT to assess culprit lesions in-vivo has shown favorable results. In 57 patients, Jang et al (8) found that lipid-rich plaques were found in 90%, 75% and 59% of patients presenting with recent acute MI, ACS and stable angina, respectively. The frequency of TCFA (defined as lipid-rich plaque with cap thickness <65μm) was 72%, 50%, and 20% in the AMI, ACS and stable patients, respectively (p=0.012). Our study, demonstrating TCFA predominantly in patients with a recent history of ACS seems to be in-line with this observation.

Of note, the study by Jang et al (8) did not use a motorized pullback for OCT image acquisition. The authors positioned the OCT wire at the level of the tightest stenosis, judged angiographically. This has several limitations, particularly the inability to detect continuous cross-sections of the coronary artery. Our study utilized an automated pullback at 1.0mm/sec with a relatively long pullback of the coronary artery permitting the visualization of additional plaques, both proximal and distal to the culprit lesion. We judged the severity of the culprit lesion using OCT rather than angiography which is associated with its inherent limitations, namely its low resolution and inability to accurately discriminate between plaques.

Recently, Kubo et al (4) used OCT, with IVUS and angioscopy to assess culprit plaque characteristics in 30 patients presenting with AMI. The imaging devices were consecutively used following initial mechanical thrombectomy. The incidence of plaque rupture by OCT was 73%, significantly higher than that detected by both angioscopy (47%, p= 0.035) and IVUS (40%, p =0.009). The incidence of TCFA was 83% in this patient population and only OCT was able to estimate the fibrous cap thickness (mean 49±21μm). Further, intracoronary thrombus was observed in all cases by OCT and angioscopy but was identified only in 33% of patients by IVUS (p< 0.001). The different patient populations evaluated likely explains the lower frequency of thrombi in our study as compared to that of Kubo et al. We did not recruit patients with AMI due to the relatively prolonged OCT imaging required to visualize both culprit and remote segments. Moreover, compared to the study by Kubo et al, our study extended OCT imaging beyond the culprit lesion, thereby giving a more representative indication about the presence of TCFA in non-culprit segments.

The presence of TCFA in regions remote to the culprit lesion in 26% of patients in our study is an interesting observation and one that has not been shown previously using OCT. One possible explanation relates to the widely accepted understanding that atherosclerosis is a systemic disease with focal manifestations. In a study using multi-slice computed tomography (MSCT), Kunimasa et al (19) assessed 21 patients with ACS and 53 patients with non-ACS. The presence of CT-low-density plaques (defined as a CT density of < 68 Hounsfield units), were more frequent in the ACS group than in the non-ACS group (81 vs 43%, p=0.03). In addition, the CT density of the non-culprit lesion was significantly lower in patients with ACS than in those with non-ACS.

While the presence of >1 unstable plaque is a relatively common occurrence in patients with ACS and AMI,(19,20) this does not provide a comprehensive explanation of our findings, particularly given patients with AMI were excluded, and, the majority of patients had presented with stable angina pectoris.
The localization of TCFA in the proximal coronary segments has not been previously reported using in-vivo OCT. Such a finding has been confirmed in post-mortem studies with a low incidence of TCFA in patients dying of sudden cardiac death (1.3±1.4 TCFA per heart) of which most were clustered in the proximal segment of the artery, particularly the LAD.(21,22). It is thought that focal areas of low shear stress in proximal segments contribute to this phenomenon resulting in the migration of lipids and monocytes into the vessel wall and accelerating the atherosclerotic process.(23-25)
The incidence of TCFA is dependent on the OCT criteria applied to make the diagnosis. We used rather conservative criteria requiring a relatively extensive lipid/necrotic core occupying more than one quadrant of the vessel circumference. This approach was chosen to exclude the chance for confusion with calcification, a potential limitation that has been described in a pathology series.(26) We applied a relatively high cut-off value of <200microns for cap thickness, possibly overestimating the incidence of true TCFA. However, it is difficult to translate a cut-off value defined by pathology into the clinical setting. Although the most accepted threshold to define a cap as "thin" has been set as <65 microns, this was based on post-mortem studies.(27) Extrapolation to in vivo studies requires caution. It is well established that anisotropic tissue shrinkage occurs during tissue fixation.(28) Shrinkage (particularly of collagen tissue, the main component of fibrous cap) of up to 60%, 15% and 80% can occur during critical-point-drying, free-drying and air-drying respectively.(29) Furthermore, post-mortem contraction of arteries is an additional confounding factor.(30) It is likely therefore that the threshold used to define a thin cap in vivo should be higher than 65 microns. Finally a number of important ex-vivo studies have used a higher (>200 microns) threshold.(31-33) Indeed, one of these studies identified a mean cap thickness of 260 μm and 360 μm for vulnerable and non-vulnerable plaques respectively.(33)

The present study is not randomized and includes a relatively small sample size. In addition, OCT was restricted to a relatively short coronary artery segment, therefore, and unlike pathological studies, does not allow us to draw conclusions on the incidence of TCFA within the complete coronary tree. Further, the study did not involve routine angiographic and OCT follow-up. Still, its prospective design and use of a sensitive imaging device has given the first insight into the potential time course of such lesions. Obviously, larger studies, possible using multimodal imaging which allows the assessment of macrophage accumulation and collagen composition will help make clearer the pathogenesis and natural history of such VP with a tremendous potential to reduce the burden of cardiovascular disease.

References

1. Regar E, Schaar JA, Mont E, Virmani R, Serruys PW. Optical coherence tomography. Cardiovasc Radiat Med 2003;4:198-204.
2. Garcia-Garcia HM, Goedhart D, Serruys PW. Relation of plaque size to necrotic core in the three major coronary arteries in patients with acute coronary syndrome as determined by intravascular ultrasonic imaging radiofrequency. Am J Cardiol 2007;99:790-2.
3. Garcia-Garcia HM, Gonzalo N, Granada JF, Regar E, Serruys PW. Diagnosis and treatment of coronary vulnerable plaques. Expert Rev Cardiovasc Ther 2008;6:209-22.
4. Kubo T, Imanishi T, Takarada S, et al. Assessment of culprit lesion morphology in acute myocardial infarction: ability of optical coherence tomography compared with intravascular ultrasound and coronary angioscopy. J Am Coll Cardiol 2007;50:933-9.

5. Chia S, Christopher Raffel O, Takano M, Tearney GJ, Bouma BE, Jang IK. In-vivo comparison of coronary plaque characteristics using optical coherence tomography in women vs. men with acute coronary syndrome. Coron Artery Dis 2007;18:423-7.
6. Tearney GJ, Jang IK, Bouma BE. Optical coherence tomography for imaging the vulnerable plaque. J Biomed Opt 2006;11:021002.
7. Giattina SD, Courtney BK, Herz PR, et al. Assessment of coronary plaque collagen with polarization sensitive optical coherence tomography (PS-OCT). Int J Cardiol 2006;107:400-9.
8. Jang IK, Tearney GJ, MacNeill B, et al. In vivo characterization of coronary atherosclerotic plaque by use of optical coherence tomography. Circulation 2005;111:1551-5.
9. Tearney GJ, Yabushita H, Houser SL, et al. Quantification of macrophage content in atherosclerotic plaques by optical coherence tomography. Circulation 2003;107:113-9.
10. Jang IK, Bouma BE, Kang DH, et al. Visualization of coronary atherosclerotic plaques in patients using optical coherence tomography: comparison with intravascular ultrasound. J Am Coll Cardiol 2002;39:604-9.
11. Tsuchida K, van der Giessen WJ, Patterson M, et al. In-vivo validation of a novel three-dimensional quantitative coronary angiography system (CardioOp-B TM): comparison with a conventional two-dimensional system (CASS II TM) and with special reference to optical cohence tomography. EuroInterv. 2007;3:100-108.
12. Barlis P, Serruys PW, DeVries A, Regar E. Optical coherence tomography assessment of vulnerable plaque rupture: predilection for the plaque 'shoulder'. Eur Heart J 2008:doi:10.1093/eurheartj/ehn085
13. Tanimoto S, Rodriguez-Granillo G, Barlis P, et al. A novel approach for quantitative analysis of intracoronary optical coherence tomography: high inter-observer agreement with computer-assisted contour detection. Catheter Cardiovasc Interv 2008:DOI: 10.1002/ccd.21482.
14. MacNeill BD, Jang IK, Bouma BE, et al. Focal and multi-focal plaque macrophage distributions in patients with acute and stable presentations of coronary artery disease. J Am Coll Cardiol 2004;44:972-9.
15. Raffel OC, Tearney GJ, Gauthier DD, Halpern EF, Bouma BE, Jang IK. Relationship between a systemic inflammatory marker, plaque inflammation, and plaque characteristics determined by intravascular optical coherence tomography. Arterioscler Thromb Vasc Biol 2007;27:1820-7.
16. Tanigawa J, Barlis P, Di Mario C. Intravascular Optical Coherence Tomography: Optimisation of image acquisition and quantitative assessment of stent strut apposition. EuroIntervention 2007;3:128-136.
17. Yabushita H, Bouma BE, Houser SL, et al. Characterization of human atherosclerosis by optical coherence tomography. Circulation 2002;106:1640-5.
18. Jang IK, Bouma BE, Kang DH, et al. Visualization of coronary atherosclerotic plaques in patients using optical coherence tomography: comparison with intravascular ultrasound. J Am Coll Cardiol 2002;39:604-9.
19. Kunimasa T, Sato Y, Sugi K, Moroi M. Evaluation by multislice computed tomography of atherosclerotic coronary artery plaques in non-culprit, remote coronary arteries of patients with acute coronary syndrome. Circ J 2005;69:1346-51.
20. Goldstein JA, Demetriou D, Grines CL, Pica M, Shoukfeh M, O'Neill WW. Multiple complex coronary plaques in patients with acute myocardial infarction. N Engl J Med 2000;343:915-22.
21. Cheruvu PK, Finn AV, Gardner C, et al. Frequency and distribution of thin-cap fibroatheroma and ruptured plaques in human coronary arteries: a pathologic study. J Am Coll Cardiol 2007;50:940-9.
22. Kolodgie FD, Burke AP, Farb A, et al. The thin-cap fibroatheroma: a type of vulnerable plaque: the major precursor lesion to acute coronary syndromes. Curr Opin Cardiol 2001;16:285-92.
23. Slager CJ, Wentzel JJ, Gijsen FJ, et al. The role of shear stress in the generation of rupture-prone vulnerable plaques. Nat Clin Pract Cardiovasc Med 2005;2:401-7.
24. Stone PH, Coskun AU, Kinlay S, et al. Effect of endothelial shear stress on the progression of coronary artery disease, vascular remodeling, and in-stent restenosis in humans: in vivo 6-month follow-up study. Circulation 2003;108:438-44.
25. Cunningham KS, Gotlieb AI. The role of shear stress in the pathogenesis of atherosclerosis. Lab Invest 2005;85:9-23.

26. Manfrini O, Mont E, Leone O, et al. Sources of error and interpretation of plaque morphology by optical coherence tomography. Am J Cardiol 2006;98:156-9.
27. Burke AP, Farb A, Malcom GT, Liang YH, Smialek J, Virmani R. Coronary risk factors and plaque morphology in men with coronary disease who died suddenly. N Engl J Med 1997;336:1276-82.
28. Cilingiroglu M, Oh JH, Sugunan B, et al. Detection of vulnerable plaque in a murine model of atherosclerosis with optical coherence tomography. Catheter Cardiovasc Interv 2006;67:915-23.
29. Boyde A TA. Dimensional changes during specimen preparation for scanning electron microscopy. . Scanning Electron Microscopy 1977:507-518.
30. Fishbein MC, Siegel RJ. How big are coronary atherosclerotic plaques that rupture? Circulation 1996;94:2662-6.
31. Felton CV, Crook D, Davies MJ, Oliver MF. Relation of plaque lipid composition and morphology to the stability of human aortic plaques. Arterioscler Thromb Vasc Biol 1997;17:1337-45.
32. Mann JM, Davies MJ. Vulnerable plaque. Relation of characteristics to degree of stenosis in human coronary arteries. Circulation 1996;94:928-31.
33. Schaar JA, De Korte CL, Mastik F, et al. Characterizing vulnerable plaque features with intravascular elastography. Circulation 2003;108:2636-41.

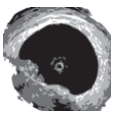

Chapter 23

Multi-modality intra-coronary characterization of atherosclerotic plaques using IVUS Grey-scale, IVUS Radiofrequency Data Analysis, Optical Coherence Tomography and Intravascular Magnetic Resonance: A Pilot Study

Nieves Gonzalo, Patrick W. Serruys, Peter Barlis, Jurgen Ligthart, Hector M. Garcia-Garcia, Evelyn Regar

Background: *The risk of rupture and subsequent thrombosis of the atherosclerotic coronary plaques is related to the presence of necrotic core with high lipid content. We conducted an exploratory pilot trial to compare the capability for lipid tissue detection using four intra-coronary diagnostic techniques: IVUS Greyscale (IVUS GS), IVUS Radiofrequency Data (IVUS RFD) Analysis, Optical Coherence Tomography (OCT) and Intravascular Magnetic Resonance Spectroscopy (IVMR).*

Methods: *Twenty-four matched target plaques were analyzed with the 4 techniques in non-culprit lesions in patients with stable angina. Following IVUS pullback, OCT and IVMR was performed. Plaque composition was assessed using established criteria of each technology.*

Results: *Atherosclerotic plaques classified as soft by IVUS GS were mainly composed by fibro-fatty (80%) or necrotic core (20%) by IVUS RFD. These soft plaques were classified as "lipid rich" by OCT in the majority of cases (80%). IVMR confirmed the presence of lipid with a lipid fraction index ranging between 36 and 79 in these soft plaques. Besides this good agreement for soft plaques, IVUS GS, IVUS RFD and OCT had 100% agreement in the identification of calcified plaques.*

Conclusion: *The present study explored multi-modality imaging of atherosclerotic plaque in-vivo. Assessing specifically lipid-rich plaques, there was generally good agreement for lesion components identified as soft by traditional IVUS GS with RFD and OCT whereas IVMR showed a varying amount of lipid in these regions. Nevertheless there continues to remain inherent variation, namely as a result of the different imaging resolutions and the lack of common nomenclature and classification.*

Acute coronary syndromes (ACS) are common initial manifestations of coronary atherosclerosis. The propensity of atherosclerotic lesions to destabilize is highly dependent on their composition, with autopsy studies of sudden cardiac death victims showing that the most frequent cause of the coronary occlusion is rupture of a thin-cap fibroatheroma (TCFA) plaque (1). Such lesions are characterized by a large necrotic core (tissue with lipid-rich necrotic areas containing remnants of foam cells, lymphocytes, cholesterol clefts and microcalcification) with a thin, fibrous cap, usually < 65 microns in thickness (2). Since the necrotic core is a tissue with high lipid content, discrimination of lipid-rich tissue may have an important impact on the detection of lesions prone to rupture.

Intravascular ultrasound (IVUS) greyscale (GS) is the most often employed diagnostic technique for the evaluation of extent and distribution of coronary atherosclerotic plaque (3), however, its specificity and sensitivity for tissue identification is limited (4,5). Spectral analysis of IVUS radiofrequency data (RFD) is a tool developed in the last few years for more reliable analysis of plaque composition (6,7). Optical coherence tomography (OCT) is a high-resolution imaging modality that uses reflected near-infrared light to visualize vascular microstructures and it has been successfully applied for the characterization of coronary atherosclerotic plaques in-vivo (8). Intravascular magnetic resonance spectroscopy (IVMR) is a new technique developed to identify specifically the lipid component of plaques based on the self-diffusion of water molecules that is translated into a lipid fraction index (LFI) (9).

These four imaging modalities have in common, the ability to give a detailed assessment of the composition of atherosclerotic plaques but do differ in the means of achieving this. Currently, it is unclear to what extent these techniques, with different physical properties and varying resolution, are able to give comparable results. We conducted this exploratory pilot trial to compare the capability for lipid tissue detection using these four intra-coronary diagnostic modalities (IVUS GS, IVUS RFD Analysis, OCT and IVMR) while comparing these findings to each other and to IVUS GS, the most widely used and standardized method for plaque characterization.

Methods

Study population

Patients with stable angina undergoing percutaneous coronary intervention (PCI) were included in this pilot study. Following treatment of the culprit vessel, an IVUS pullback was performed in a non-culprit vessel containing a non-flow limiting stenosis (defined as less than 50% diameter stenosis by online quantitative coronary angiography, QCA). Following the IVUS pullback, OCT and IVMR acquisitions were performed. Heavily calcified and tortuous vessels and those with a minimal lumen diameter <2mm were excluded. Patients with depressed left ventricular function, coronary chronic total occlusions and impaired renal function were also excluded. All patients gave written informed consent.

Coronary angiography

All angiograms were evaluated after intra-coronary administration of nitrates using commercially available software for QCA [Cardiovascular Angiography Analysis System II (CAAS II), Pie Medical, Maastricht, the Netherlands].

IVUS and RFD acquisition and analysis

IVUS was performed using the Eagle Eye 20-MHz catheter (Volcano Corporation, Rancho Cordova, USA) with an automatic continuous pullback at a rate of 0.5 mm/sec. The GS and the RFD were acquired during the same pullback (6). IVUS GS plaque analysis was performed by visual assessment and consensus of two experienced observers. Plaque type was classified according to the Consensus Document of the American College of Cardiology (10) as: normal vessel wall, soft plaque (echogenicity lower than the adventitia), fibrous plaque (intermediate echogenicity), and calcified plaque (echogenicity higher than the adventitia with acoustic shadowing).

The RFD analysis was performed offline with pcVH software (Volcano Corporation Rancho Cordova, USA) that permits semi-automated contour detection and provides the compositional structure of the vessel. The IVUS RFD analysis remains observer independent, using spectral analysis to classify the four different components of the atherosclerotic plaque and gives a colour-coded map distinguishing between fibrous tissue (green), fibro-lipid tissue (light green), necrotic core (red) and dense calcium (white).

OCT acquisition and analysis

The OCT acquisition was performed using a commercially available system for intracoronary imaging (LightLab Imaging, Westford, Massachusetts, US). It operates at a wavelength of 1310 nm and has an axial resolution of 10 μm and a lateral resolution of 20 μm. We used a 0.019" ImageWire (LightLab Imaging, Westford, Massachusetts) in combination with a proximal, low pressure (0.4 atm) occlusion balloon (Helios, Goodman Inc, Japan) with simultaneous distal flush delivery (lactated ringers at 37°Celsius; flow rate 0.5ml/sec). Images were acquired during a pullback rate of 1.0 mm/sec.

Plaque components were assessed by two experienced observers and classified according to previously published data as: normal vessel wall, fibrous plaque (homogeneous, signal-rich regions), lipid rich plaque (signal-poor regions with diffuse borders) and fibro-calcific plaque (well-delineated, signal-poor regions with sharp borders) (8).

IVMR acquisition and analysis

The IVMR system consisted of a self-contained 5.2 F over-the-wire IVMR catheter, without external magnets or coils, a patient interface unit and a console. A pullback through the region of interest was performed using a dedicated device allowing controlling stepwise rotation (120 degrees) and withdrawal (1.6mm) of the catheter. To eliminate motion artefacts, and to improve image resolution, the IVMR catheter was stabilized against the arterial wall by inflation of a partially occlusive, low-pressure balloon (1 atm). The time required for each acquisition was 51 seconds. The magnetic fields generated by the probe located at the tip of the catheter, created a sector shaped (60 degrees), field of view (FOV) looking sideways into the artery wall. Acquired data was displayed as colour-code sectors of the LFI for the FOV. Blue indicated no lipid; grey corresponded to intermediate lipid content and yellow indicated high lipid content.

Matching of the different diagnostic pullbacks to the target plaque

Documentation of all catheter positions was made using angiographic landmarks. The localization of the IVUS, OCT and IVMR probes in the vessel were filmed using bi-plane angiography both pre and post acquisition. Biplane angiography served to determine the target segment and for orientation of the catheter position in a longitudinal (IVUS, OCT, IVMR) and cross sectional (IVMR) plane. The longitudinal orientation of the probes was determined by angiographically visible side branches (Figure 1). The cross-sectional orientation of the probe was determined by the presence of side branches visible in the longitudinal and cross-sectional views of IVUS (11) and OCT and the specifically designed, radiopaque rotation markers for IVMR. Acquisitions, in which rotation of the probe could not be clearly confirmed by the marker, were excluded from the analysis.

Matched samples from all 4 diagnostic modalities were analysed in 1.6 mm longitudinal intervals, the target plaques were defined as 60 degrees sectors of the vessel wall in accordance to the acquired IVMR datasets (Figure 2A and 2B).

Statistical analysis

Data are expressed as mean ± standard deviation for continuous variables and as percentages for categorical variables.

Results

Patient and procedural characteristics

Twenty-four matched target plaques were collected from five patients. The intracoronary diagnostic devices were successfully advanced to the area of interest in all the patients. There were no cases of coronary spasm, dissection, acute closure or perforation. During OCT and IVMR pullbacks transient signs of ischemia with ST segment changes were documented. Following the procedure, all patients remained symptom-free with no detected elevation in the creatinine kinase -MB or Troponin-T enzymes.

IVUS GS, IVUS VH and OCT imaging were successfully performed in all target lesions. IVMR pullbacks contained 6 acquisition cycles in 3 patients and 4 in the remaining 2 patients due to chest pain or transient ECG changes that completely resolved immediately after balloon deflation. Two IVMR acquisitions were excluded, as complete, 120-degree rotation could not be judged definitively.

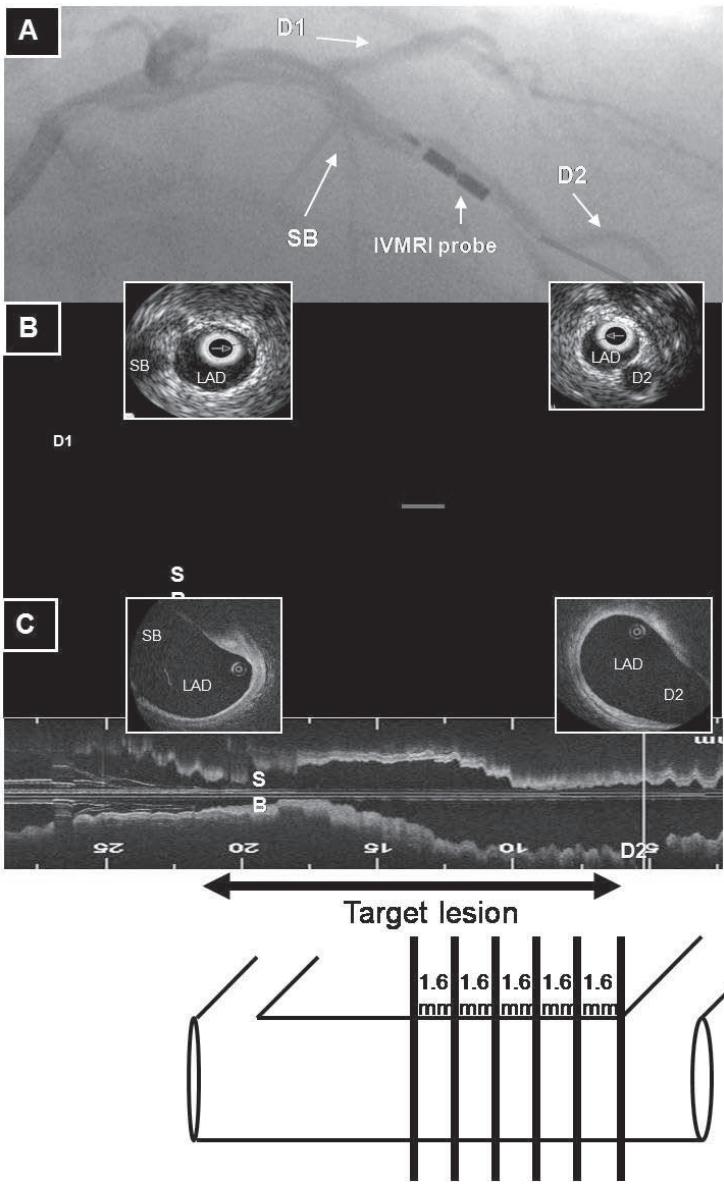

see colour section

Figure 1. Matching of the OCT and IVUS pullbacks. The position of the IVUS, Optical Coherence Tomography (OCT) and Intravascular Magnetic Resonance Spectroscopy (IVMR) probe along the vessel was filmed before and after each acquisition (A). The "matching" of the region of interest in the IVUS (B) and OCT (C) pullback was based on the presence of anatomical landmarks (e.g. side branches visible in the longitudinal and cross-sectional views). To determine the longitudinal position of the IVMR probe in the vessel, a side branch was used as a marker. From the landmark to the proximal part of the vessel one frame every 1.6 mm was selected. D1: first diagonal, D2: second diagonal, SB: septal branch, LAD: left anterior descendent coronary artery. CS: cross section.

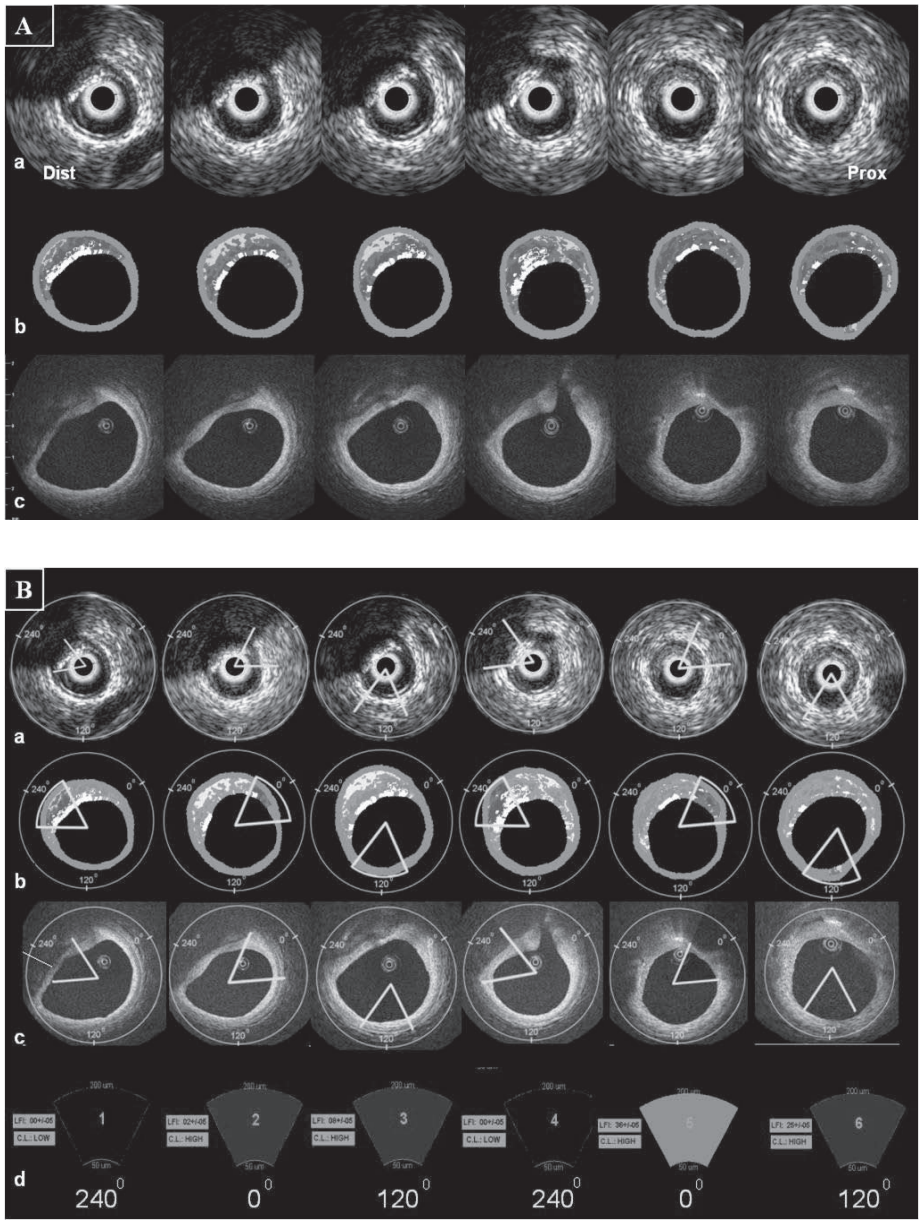

Figure 2. Analysis of the targeted matched plaques. 2A) Matching of the cross sections in a) IVUS greyscale b) IVUS Radiofrequency Data Analysis and c) Optical Coherence Tomography pullbacks. 2B) Analysis screen. After matching corresponding cross sections based on their longitudinal orientation, the region of interest is defined according to the orientation of the Intravascular Magnetic Resonance probe towards the vessel wall. The figure illustrates the results of the six target matched plaques (60 degrees sector) analyzed in one patient. Prox: proximal Dist: distal.

see colour section

Target plaque characteristics

The interrogated artery was the proximal LAD in 75% of the cases, and the proximal RCA in 25%. The reference vessel diameter, minimal lumen diameter and percent diameter stenosis were 3.2 ± 0.2 mm, 2.2 ± 0.4 mm and 34 ± 11%, respectively. By IVUS**,** the vessel area was 14.3 ± 4.9 mm^2, the mean luminal area was 8.3 ± 3.2 mm^2 and the mean plaque burden was 41± 22% in the imaged vessel.

Characteristics of the target plaques by the different techniques

We analyzed 24 matched target plaques using the four techniques.

Plaque morphology by IVUS Grey-scale

IVUS GS identified normal vessel wall, soft plaque, fibrous plaque and calcific plaque in 62.5%, 20.8%, 8.3% and 8.3% of cases respectively.

Plaque composition by IVUS RF analysis

Using IVUS RF, the analyzed target plaque was defined as normal vessel wall in 62.5% of the cases. The remainder were necrotic core (4.2%), fibro-fatty (16.7%) and fibrous (8.3%), Dense calcium was the main component in 8.3% of the cases.

Plaque morphology by OCT

The evaluated target plaque was considered normal by OCT in 54.2% of the cases, lipid rich plaque in 20.8%, fibrous plaque in 16.7% of the cases, and fibrocalcific plaque in 8.3% of the cases.

Plaque composition by IVMR

The result of the IVMR was yellow (high LFI) in 16.7%, grey (intermediate LFI) in 25% and blue (indicating low LFI) in 45.8% of the analyzed target plaques. In 12.5% the result was black, which indicates artefact. The minimum LFI was 0 and the maximum was 80, with a mean of 30 ± 48. The mean LFI was 73 ± 3.9 in the yellow regions, 42 ± 1.5 in the grey regions and 17.2 ± 2.8 in the blue regions.

Comparison of IVUS GS findings with other techniques (Table 1)

Comparison IVUS GS and IVUS RFD analysis

When the vessel was defined as normal by IVUS GS, it was normal by IVUS RF analysis in 100% (15/15) of the segments. When the plaque was defined as soft by IVUS GS, it was predominantly composed of fibro-fatty tissue by RF analysis in 80% (4/5) of the cases and necrotic core in 20% (1/5) of cases. The fibrous plaques by IVUS GS where also (2/2) fibrous in the RFD analysis. When the plaque was calcified by IVUS GS, it was composed predominantly of dense calcium in all the RFD analysis (2/2) matched plaques.

Comparison IVUS GS and OCT findings

When the vessel was normal by IVUS GS, it was normal by OCT in 80% (12/15) of the cases, but in 20% (3/15) of the matched sectors considered normal by IVUS GS examination, it was possible to identify fibrous plaques with OCT. When the plaque was defined as soft by IVUS GS it was mainly "lipid rich" by OCT (80% of the cases 4/5). The fibrous plaques by GS were fibrous by OCT in 50% of the cases (1/2) and normal vessel wall in another 50% (1/2). As with RFD analysis, all the calcified plaques by IVUS GS were also fibro-calcific plaques by OCT (2/2).

IVUS Grev-scale

IVUS RFD	Normal	Soft	Fibrous	Calcified	Total
Normal	**15**	0	0	0	15
NC	0	**1**	0	0	1
Fibrofatty	0	**4**	0	0	4
Fibrous	0	0	**2**	0	2
DC	0	0	0	**2**	2
Total	15	5	2	2	24
OCT	**Normal**	**Soft**	**Fibrous**	**Calcified**	**Total**
Normal	**12**	1	0	0	13
Lipid rich	0	**4**	1	0	5
Fibrous	3	0	**1**	0	4
Calcified	0	0	0	**2**	2
Total	15	5	2	2	24
IVMR	**Normal**	**Soft**	**Fibrous**	**Calcified**	**Total**
Blue	**10**	0	**1**	0	11
Grey	3	**3**	0	0	6
Yellow	1	**2**	1	0	4
Black	1	0	0	**2**	3
Total	15	5	2	2	24

Table 1. Results of the interrogated 24 matched target plaques with the four techniques. IVUS: Intravascular Ultrasound RFD: Radiofrequency Data OCT: Optical Coherence Tomography IVMR: Intravascular Magnetic Resonance Spectroscopy.

Comparison IVUS GS and IVMR findings

When the analyzed segment was normal by IVUS GS, it was blue by IVMR in 66% of cases (10/15). The normal vessel wall was identified as grey by IVMR in 20% (3/15) and as yellow in 6% (1/15). In 6% (1/15) of the normal vessel wall sectors the result of the IVMR was black. When the target plaque was described as soft by IVUS GS assessment, it was grey by IVMR in 60% (3/5) of the cases and yellow in 40% (2/5) of the cases. Of the two target plaques identified as fibrous by IVUS GS, one was classified as blue by the IVMR and the other as yellow. The calcified target plaques by IVUS GS were classified in 100% (2/2) of the cases as black (artefact) in the IVMR. The mean LFI was 52 ± 17 in the soft plaques, 46 ± 36 in the fibrous and 25 ± 21 in the normal vessel wall.

Discussion

A body of various clinical, post mortem and experimental observations suggest that the composition of atherosclerotic plaque is an important determinant for subsequent clinical outcome. This knowledge triggered the development of a variety of new technological approaches for the analysis of plaque structure and chemical composition. It is however challenging to estimate the accuracy of a given diagnostic method *in vivo* due to the fact that no 'gold standard' method is available. A pragmatic way to get an indication for the plausibility of the information acquired in the clinical setting can be the cross correlation of different techniques. In the present study, the ability of four different intra-coronary diagnostic modalities to detect the lipid components of atherosclerotic plaque was tested. The atherosclerotic plaques classified as soft by IVUS GS were mainly composed by fibro-fatty or necrotic core in the RFD analysis. These soft plaques were classified as "lipid rich" by OCT in most of the cases while IVMR always classified as intermediate or high lipid content the plaques identified as soft by IVUS GS. The 3 techniques of IVUS GS, IVUS RFD and OCT had a 100% agreement in the identification of calcified plaques. All these plaques were displayed as artefact by IVMR.

The detection of plaque components by IVUS is based on visual assessment of GS images and is highly influenced by the observer's experience and interpretation. It has been reported that soft (hypo-echoic) plaques usually have a high lipid content (12,13), but histological correlations have shown that IVUS GS, has low sensitivity (46%) for lipid detection (5,14). In the present study, when compared with the findings of the IVUS RFD, all plaques classified as soft by IVUS GS were composed of fibro-fatty or necrotic tissue. The spectral analysis of IVUS RFD has been validated with histopathology *ex-vivo* (15) and *in vivo* (16), demonstrating high predictive accuracy. This technique has the advantage of being observer independent and importantly, permits the identification of necrotic core. However, histological comparisons have shown some misclassification due to overlap between tissues in the RFD spectrum ((15)).

The use of OCT and IVUS GS showed good correlation for the detection of soft and lipid-rich plaques respectively. For lipid-rich plaques a sensitivity ranging from 90 to 94% and specificity ranging from 90% to 92% have been reported for OCT(8). Despite its high resolution, one drawback of current OCT systems is the limited penetration depth (1.5-2.0mm) that does not allow the detection of lipid pools or calcium behind thick fibrous caps. Further, the tissue characterization by OCT is observer dependent. An incorrect classification between calcium and lipid deposits by OCT has been described in comparisons with histology (17) and this may explain this phenomenon in a study by Jang et al where there was no difference in lipid-rich plaques defined by OCT criteria in ACS and stable angina patients (18). In the present study, we found concordance between the techniques for calcified and "lipid-rich" plaques with all plaques identified as fibro-calcific by OCT also found to be calcified by IVUS GS and RFD analysis and were displayed as black ("artefact") by the IVMR system.

IVMR is a technique specifically developed to identify the lipid composition of plaque. It has demonstrated a strong correlation with histology in lipid-rich tissue detection in both the aorta and coronary arteries of patients suspected of dying of cardiovascular causes (19). In the present study, plaques classified as soft by IVUS GS were identified as regions with intermediate to high LFI by IVMR. However there were 4 plaques that had intermediate or high lipid content by IVMR but were classified as normal vessel wall by IVUS GS and one fibrous plaque by IVUS showed high LFI in the IVMR analysis. This may reflect higher sensitivity of IVMR for lipid detection compared to IVUS. One of the main advantages of IVMR is that it is observer independent and that it allows the quantification of the lipid component. A previous *ex vivo* study suggested that IVMR could identify TCFA (19,20). However this application is not possible at present in the *in vivo* scenario where the scan area is restricted to 60 degrees sectors of the vessel wall. The small sample volume, the lack of structural information and the complex definition of the location of the probe in the arterial wall are the main limitations of the IVMR system at this point in time.

Presently, a number of imaging modalities are vying to accomplish plaque characterization and detection. Our study demonstrates the feasibility of assessing different physical aspects of atherosclerotic plaques in-vivo by multi-modality imaging. However, such an approach is complicated by a rather cumbersome matching process originating from varying sample volumes, resolutions and accuracies and, secondly, different terminologies, thresholds and cut-off values for the different technologies. Obviously, the "gold standard" for lipid detection is histopathology, but the reported classifications are qualitative and difficult to apply homogenously to the findings of all these in-vivo techniques. This may be aided by defining histological plaque composition based on quantitative and uniformly applied criteria (21). Currently, findings gained from different diagnostic modalities cannot be considered equivalent. This should be considered when interpreting and designing clinical trials involving plaque detection and characterization.

Limitations

The main limitations of the present study are: 1) the small sample size 2) lack of histological correlation 3) the localization of the sector scanned by IVMR was difficult to precisely assess due to the simplified spatial representation associated with the technique; however specifically designed rotation markers, meticulous inspection and exclusion of doubtful rotations were used to optimize data analysis.

Conclusions

The present study explored multi-modality imaging of atherosclerotic plaque in-vivo. Assessing specifically lipid-rich plaques, there was generally good agreement for lesion components identified as soft by traditional IVUS GS with RFD and OCT whereas IVMR showed a varying amount of lipid in these regions. Nevertheless there continues to remain inherent variation, namely as a result of the different imaging resolutions and the lack of common nomenclature and classification.

References

1. Virmani R, Kolodgie FD, Burke AP, Farb A, Schwartz SM. Lessons from sudden coronary death: a comprehensive morphological classification scheme for atherosclerotic lesions. Arterioscler Thromb Vasc Biol 2000;20:1262-75.
2. Virmani R, Burke AP, Farb A, Kolodgie FD. Pathology of the vulnerable plaque. J Am Coll Cardiol 2006;47:C13-8.
3. Rasheed Q DP, Anderson J, Hodgson JM. Intracoronary ultrasound-defined plaque composition: computer-aided plaque characterization and correlation with histologic samples obtained during directional coronary atherectomy. Am Heart J 1995;129:631-637.
4. Di Mario C TS, Madretsma S, van Suylen RJ, Wilson RA, Bom N, Serruys PW, Gussenhoven EJ, Roelandt JR. Detection and characterization of vascular lesions by intravascular ultrasound: an in vitro study correlated with histology. J Am Soc Echocardiogr. 1992;5:135-146.
5. Peters RJ, Kok WE, Havenith MG, Rijsterborgh H, van der Wal AC, Visser CA. Histopathologic validation of intracoronary ultrasound imaging. J Am Soc Echocardiogr 1994;7:230-41.
6. Rodriguez-Granillo GA, Garcia-Garcia HM, Valgimigli M, et al. Global characterization of coronary plaque rupture phenotype using three-vessel intravascular ultrasound radiofrequency data analysis. Eur Heart J 2006;27:1921-7.
7. Rodriguez-Granillo GA, Garcia-Garcia HM, Mc Fadden EP, et al. In vivo intravascular ultrasound-derived thin-cap fibroatheroma detection using ultrasound radiofrequency data analysis. J Am Coll Cardiol 2005;46:2038-42.
8. Yabushita H, Bouma BE, Houser SL, et al. Characterization of human atherosclerosis by optical coherence tomography. Circulation 2002;106:1640-5.

9. Regar E HB, Grube E, Halon D, Wilensky R.L, Virmani R, Schneiderman J, Sax S, Friedmann H, Serruys P. W, Wijns W. First-In-Man application of a miniature self-contained intracoronary magnetic resonance probe. A multi-centre safety and feasibility trial. Eurointervention 2006;2:77-83.
10. Mintz GS, Nissen, S. E, Anderson, W. D, Bailey, S. R, Erbel, R, Fitzgerald, P. J, Pinto, F. J, Rosenfield, K, Siegel, R. J, Tuzcu, E. M, Yock, P. G. American College of Cardiology Clinical Expert Consensus Document on Standards for Acquisition, Measurement and Reporting of Intravascular Ultrasound Studies (IVUS). A report of the American College of Cardiology Task Force on Clinical Expert Consensus Documents. J Am Coll Cardiol 2001;37:1478-92.
11. Fitzgerald PJ, Yock C, Yock PG. Orientation of intracoronary ultrasonography: looking beyond the artery. J Am Soc Echocardiogr 1998;11:13-9.
12. DeMaria AN, Narula J, Mahmud E, Tsimikas S. Imaging vulnerable plaque by ultrasound. J Am Coll Cardiol 2006;47:C32-9.
13. Gronholdt ML. Ultrasound and lipoproteins as predictors of lipid-rich, rupture-prone plaques in the carotid artery. Arterioscler Thromb Vasc Biol 1999;19:2-13.
14. Hiro T, Leung CY, De Guzman S, et al. Are soft echoes really soft? Intravascular ultrasound assessment of mechanical properties in human atherosclerotic tissue. Am Heart J 1997;133:1-7.
15. Nair A MP KB, Vince DG. Automated coronary plaque characterization with intravascular ultrasound backscatter: ex vivo validation. Eurointervention 2007;3:113-130.
16. Nasu K TE, Katoh, Vince DG, Virmani R, Surmely JF, Murata A, Takeda Y, Ito T, Ehara M, Matsubara T, Terashima M, Suzuki T. Accuracy of in vivo coronary plaque morphology assessment: a validation study of in vivo virtual histology compared with in vitro histopathology. . J Am Coll Cardiol 2006;47:2405-2412.
17. Manfrini O, Mont E, Leone O, et al. Sources of error and interpretation of plaque morphology by optical coherence tomography. Am J Cardiol 2006;98:156-9.
18. Jang IK, Bouma BE, Kang DH, et al. Visualization of coronary atherosclerotic plaques in patients using optical coherence tomography: comparison with intravascular ultrasound. J Am Coll Cardiol 2002;39:604-9.
19. Schneiderman J, Wilensky RL, Weiss A, et al. Diagnosis of thin-cap fibroatheromas by a self-contained intravascular magnetic resonance imaging probe in ex vivo human aortas and in situ coronary arteries. J Am Coll Cardiol 2005;45:1961-9.
20. Wilensky RL, Song HK, Ferrari VA. Role of magnetic resonance and intravascular magnetic resonance in the detection of vulnerable plaques. J Am Coll Cardiol 2006;47:C48-56.
21. Bruining N, Verheye S, Knaapen M, et al. Three-dimensional and quantitative analysis of atherosclerotic plaque composition by automated differential echogenicity. Catheter Cardiovasc Interv 2007;70:968-78.

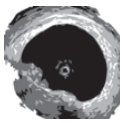

Chapter 24

Optical coherence tomography assessment of vulnerable plaque rupture: predilection for the plaque 'shoulder'

Peter Barlis, Patrick W. Serruys, Arie Devries, Evelyn Regar

Atherosclerosis as a disease entity remains an intensely researched field, given the tendency for considerable morbidity and mortality. This attention has given rise to exciting opportunities in developing tools aimed at early detection and possible targeting of specific therapeutic interventions. One such modality is optical coherence tomography (OCT) that permits high-resolution visualization of backscattered light. This has given unique insights into disease processes and with greater detail than traditional grey scale intravascular ultrasound (IVUS). We present a 69-year-old man with 1 week of crescendo angina 9 months following stent implantation to the left anterior descending artery (LAD). Angiography demonstrated a new lesion in the mid LAD and diagonal branches. Assessment of the region with OCT revealed a high lipid content plaque with a thin fibrous cap (maximal thickness 20 microns). In association, rupture of the thin cap was apparent, occurring at both shoulders of the plaque with associated mural thrombus. The patient was treated with further stent implantation and remains symptom-free at 3 months follow-up.

The predilection for plaque to rupture at the shoulder region is interesting. Pathological studies have shown that this region demonstrates intense inflammatory cell infiltrate, particularly with macrophage cells and lymphocytes. When activated, macrophages release matrix metalloproteinases in the vessel wall, which in-turn can induce 'weak spots' that become susceptible to rupture. Other factors also implicated in this increased vulnerability at the plaque shoulder include neovascularization with expression of adhesion molecules, and increased biomechanical stresses occurring around cellular microcalcification within the thin cap.

Several imaging modalities have been used to assess and identify vulnerable plaque (VP) including coronary angioscopy, IVUS and magnetic resonance imaging. Recently, there has been significant interest in the field of VP detection using OCT. This modality permits high-resolution (10-20 microns) imaging, in the vicinity of 10 times greater than IVUS and has become a key tool to detect and quantify thin cap fibroatheroma and macrophage distribution. This individual clinical observation supports the evidence gained from post mortem observations pointing to the plaque 'shoulder' as a site of vulnerability for rupture.

Panel Legend A. Angiography in the right cranial view demonstrated stenosis in the mid left anterior descending artery (LAD) involving both small diagonal branches. The previously implanted LAD stent proximally was widely patent. The region corresponding to the optical coherence tomography (OCT) images is shown with the black arrow. **B-C**. Intravascular OCT (LightLab Imaging, Westford, Massachusetts, US) was acquired using a non-occlusive technique with a 3.0mm/sec pullback. OCT clearly demonstrated the presence of a lipid-rich plaque in the 6 to 9 o/clock position characterized by low reflectivity, speckled appearance with diffuse margins. This was covered with a bright rim of fibrous tissue corresponding to thin-cap fibroatheroma (TCFA). Mural thrombus was evident in all OCT cross-sections. The TCFA measured 20 microns thick and was found to be ruptured at each of the two shoulders of the plaque (arrows).

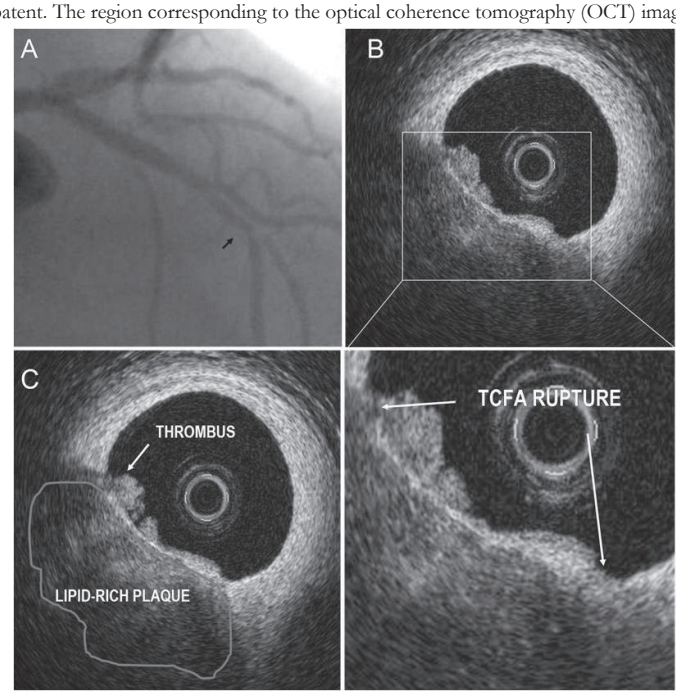

see colour section

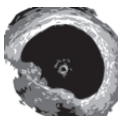

Chapter 25

In Vivo Assessment of High-risk Coronary Plaques at Bifurcations with Combined Intravascular Ultrasound Virtual Histology and Optical Coherence Tomography

Nieves Gonzalo, Hector Garcia-Garcia, Evelyn Regar, Peter Barlis, Jolanda Wentzel, Yoshinobu Onuma, Jurgen Lighthart, Patrick W. Serruys

Objectives: *Atherosclerotic plaque rich in necrotic core is prone to develop at bifurcations. This study aimed to evaluate the in-vivo frequency and distribution of high-risk plaques (i.e necrotic core rich) at bifurcations using a combined plaque assessment with IVUS virtual histology (IVUS-VH) and optical coherence tomography (OCT).*
Methods: *From 30 patients imaged with IVUS-VH and OCT, 103 bifurcations were selected. The main branch was analyzed at the proximal rim of the ostium of the side-branch, at the in-bifurcation segment and at the distal rim of the ostium of the side-branch. Plaques with more than 10% confluent necrotic core by IVUS-VH were selected and classified as fibroatheroma (FA) or thin-cap fibroatheroma (TCFA) depending on the thickness of the fibrous cap by OCT (> or ≤65μm for FA and TCFA respectively).*
Results: *27 FA (26.2%) and 18 TCFA (17.4%) were found. Overall the % of necrotic core decreases from proximal to distal rim (16.8% vs 13.5% respectively p=0.01) while the cap thickness showed an inverse tendency (130±105 vs 151±68μm for proximal and distal rim respectively p=0.05). The thin caps were more often located in the proximal rim (15/34, 44.1%), followed by the in-bifurcation segment (14/34, 41.2%) and were less frequent in the distal rim (5/34 14.7%).*
Conclusions: *The proximal rim of the ostium of the side-branch has been identified as a region more likely to contain thin fibrous cap and a greater proportion of necrotic core.*

High-risk atherosclerotic plaques (i.e. rich with necrotic core) are prone to develop at bifurcations due to the specific shear stress conditions present in these regions(1,2). Stented bifurcations lesions represent a complex lesion subset at high-risk of restenosis and thrombosis (3,4). These phenomena may reflect certain procedural aspects such as incomplete stent apposition, under-expansion or gap regions (5,6) but may also be associated with specific compositional and morphological plaque features in these regions. Thin-cap fibroatheroma (TCFA) has been described as the plaque with an increased risk of rupture (7). Such lesions are characterized by a large necrotic core with a thin fibrous cap, usually < 65 microns in thickness (8). Recently, it has been reported that TCFA detection could be improved by the combined use of intravascular ultrasound virtual histology (IVUS-VH) and optical coherence tomography (OCT)(9).
IVUS-VH uses spectral analysis of IVUS radiofrequency data to identify four tissue types in the atherosclerotic plaque, among them necrotic core (10). Optical coherence tomography (OCT) is a high-resolution imaging modality that uses reflected near-infrared light allowing a very precise visualization and measurement of vascular microstructures such as the fibrous cap (11). To our knowledge, in vivo characterization of necrotic core rich plaques at bifurcation regions has not been explored. The objective of the present study was therefore to evaluate *in-vivo* the frequency and distribution of high-risk plaques at bifurcation lesions using a combined plaque assessment with IVUS-VH and OCT.

Methods

Study population

All the patients admitted in our hospital between January 2005 and March 2008 in whom IVUS-VH and OCT were performed in the same vessel were investigated for bifurcations adequately visualized by both imaging techniques. The indication for the IVUS-VH and OCT was the assessment of intermediate, non-flow limiting lesions by angiography or post stent implantation assessment. Only regions located more than 5 mm beyond the stent were included. All patients gave written informed consent.

IVUS-VH acquisition

IVUS was performed using the Eagle Eye 20 MHz catheter (Volcano Corporation, Rancho Cordova, CA, USA) with an automatic continuous pullback at a rate of 0.5 mm/sec. Greyscale images and radiofrequency data required for VH analysis were acquired during the same pullback.

The VH processing was performed offline with pcVH 2.1 software (Volcano Corporation Rancho Cordova, USA) that permits semi-automated contour detection and provides the compositional structure of the vessel. The IVUS-VH uses spectral analysis to classify the four different components of the atherosclerotic plaque and gives a colour-coded map distinguishing between fibrous tissue (green), fibro-fatty tissue (light green), necrotic core (red) and dense calcium (white).

OCT acquisition

The OCT acquisition was performed using a commercially available system for intracoronary imaging and a 0.019" ImageWire (LightLab Imaging, Westford, Massachusetts, US). Red blood cells represent a non-transparent tissue causing multiple light scattering and substantial signal attenuation. Therefore, for adequate OCT image acquisition blood must be temporarily removed from the vessel. In seventy-seven percent of the cases this was achieved with the occlusion technique in which a proximal, low-pressure (0.4 atm) occlusion balloon (Helios, Goodman Inc, Nagoya, Japan) is inflated with simultaneous distal flush delivery (lactated ringer; flow rate 0.8ml/sec) to remove blood from the vessel lumen. Images were acquired during a pullback rate of 1.0 mm/sec. The possibility to increase the pullback speed up to 3 mm/s in the new OCT system permitted 23% of the cases to be acquired exclusively using a non-occlusive technique in which the blood was removed by the continuous injection of contrast (Iodixanol 370, Visipaque™, GE Health Care, Cork, Ireland) through the guiding-catheter. The non-occlusive technique reduces the procedural time and the incidence of chest pain and ECG changes during image acquisition without affecting the image quality(12).

Bifurcation selection and analysis

Simultaneous visual assessment of IVUS-VH and OCT pullbacks, in two contiguous screens, allowed the selection of all bifurcations that could be identified with both techniques (13). To ensure proper matching between two imaging modalities that have different lateral resolutions (20 μm for OCT and 300 μm for IVUS) and depth penetration, a strict selection of the frames was followed. Only the main branch was analyzed. The lesion analysis included: i. proximal rim of the ostium of the side-branch cross section (first frame proximal to the take-off of the side-branch); ii. in-bifurcation cross section (frame with the larger ostial diameter of the side-branch) and iii. distal rim of the ostium of the side-branch cross section (first frame distal to the take off of the side-branch) **(**Figure 1). In each bifurcation the plaque location in relation to the flow divider was analyzed (Figure 2).

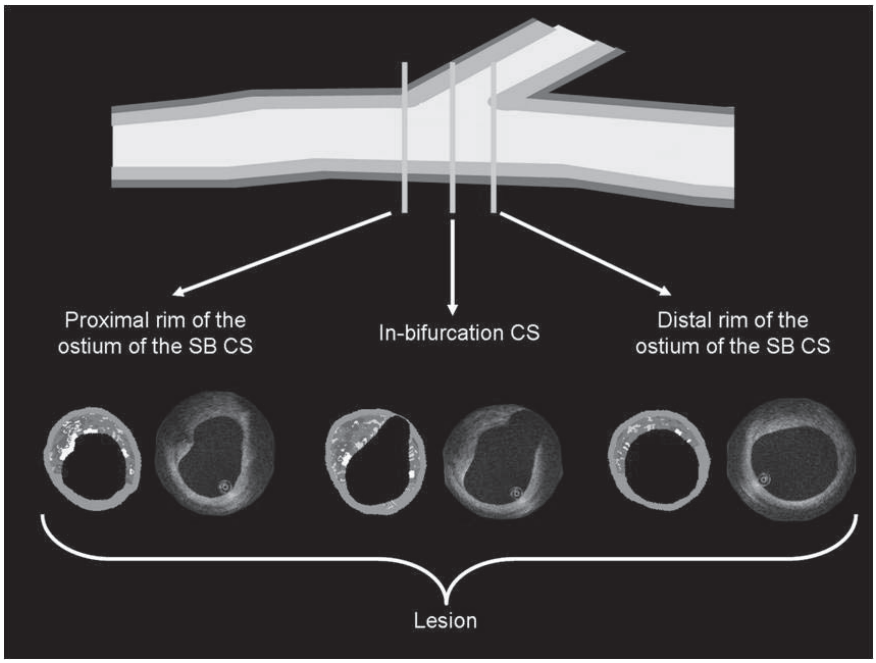

Figure 1: Bifurcation selection and analysis
Bifurcations that could be identified in both IVUS-VH and OCT pullbacks were included. A strict selection of the analyzed cross sections was followed to ensure correct matching between the two techniques. Plaques were analyzed only in the main branch. The lesion analysis included: i. proximal rim of the ostium of the side-branch cross section (first frame proximal to the take-off of the side-branch); ii. in-bifurcation cross section (frame with the larger ostial diameter of the side-branch) and iii. distal rim of the ostium of the side-branch cross section (first frame distal to the take off of the side-branch) SB: side-branch CS: cross section.

see colour section

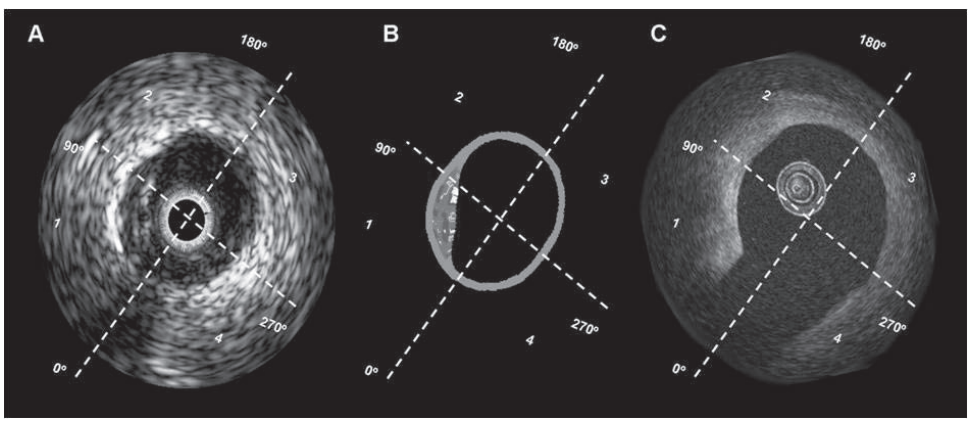

Figure 2: Location of the plaque in relation to the flow divider. To describe the plaque location in relation to the flow divider, the vessel cross section was divided in 4 quadrants according to the position of the side-branch. Quadrants 1 and 4 correspond to the ostium of the side-branch while quadrants 2 and 3 correspond to the part of the vessel wall located in front of the ostium of the side-branch. A: greyscale IVUS, B: virtual histology, C: optical coherence tomography.

see colour section

Plaque type classification

Two experienced observers jointly analyzed the IVUS-VH data and the OCT measurements in the selected frames to characterize the plaque type according to the following hierarchical classification:(7,14,15) **(Figure 3, 4 and 5):**

1. **Adaptive intimal thickening (AIT):** intimal thickening of less than 600 μm for less than 20% of the circumference.
2. **Pathological intimal thickening (PIT):** intimal thickening ≥600 μm for more than 20% of the circumference with more than 15% of fibro-fatty tissue, and no confluent necrotic core or dense-calcium
3. **Fibrotic plaque:** plaque constituted predominantly by fibrous tissue without confluent NC or dense-calcium.
4. **Fibrocalcific plaque:** more than 10% of confluent dense-calcium without confluent NC.
5. **Fibroatheroma (FA*)***: plaque characterized by the presence of more than 10% confluent NC covered by a fibrous cap thicker than 65 μm.
6. **Calcified fibroatheroma (CaFA):** fibroatheroma that contains more than 10% of confluent dense-calcium
7. **IVUS/OCT-derived Thin-Capped Fibroatheroma (TCFA):** defined as the presence of more than 10% confluent NC at the lumen covered by a thin fibrous cap (<65 μm).
8. **IVUS/OCT-derived Calcified Thin-Capped Fibroatheroma (CaTCFA):** TCFA that contains more than 10% of confluent dense-calcium.

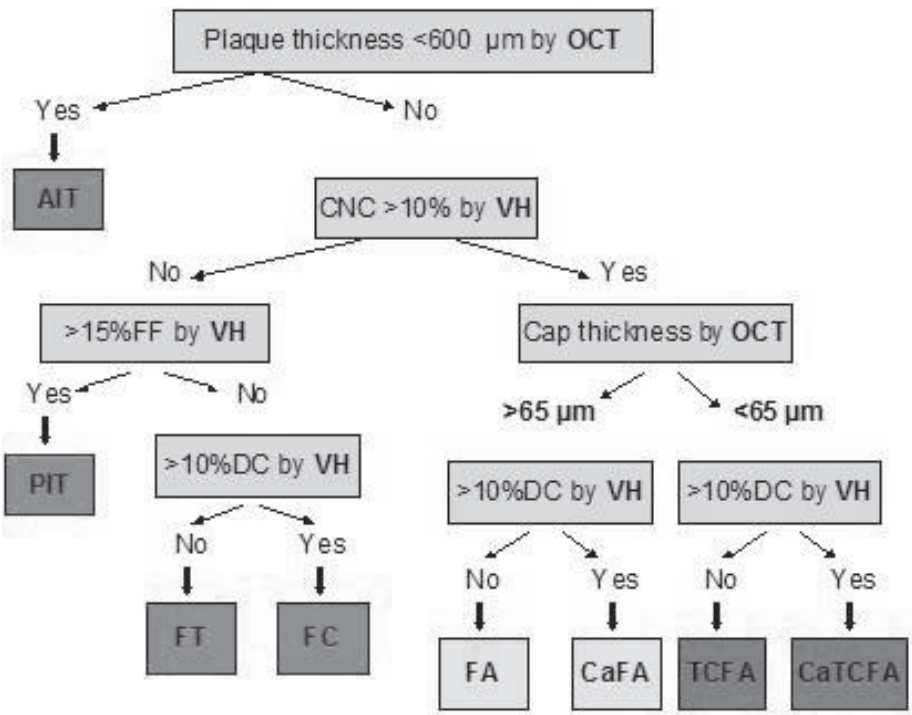

Figure 3: Plaque classification algorithm. OCT: optical coherence tomography, VH: virtual histology, CNC: confluent necrotic core, FF: fibrofatty, DC: dense calcium, AIT: adaptive intimal thickening, PIT: pathological intimal thickening, FC: fibrocalcic, FT: fibrotic, FA: fibroatheroma, CaFA: calcified fibroatheroma, TCFA: thin-cap fibroatheroma, CaTCFA: calcified thin-cap fibroatheroma.

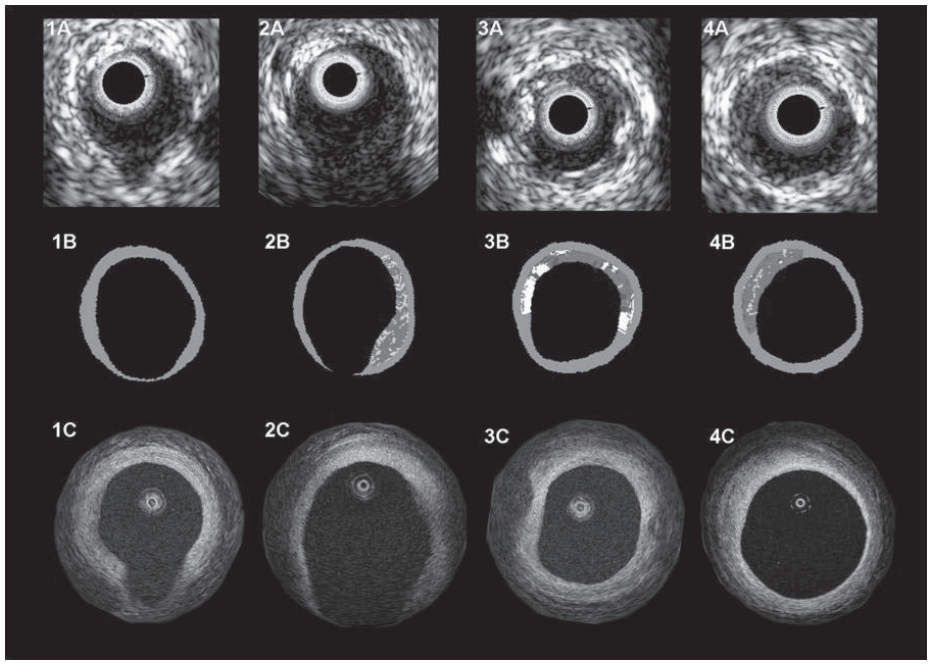

Figure 4: Low-risk plaques. Matched images of greyscale IVUS (A), virtual histology (B) and optical coherence tomography (C) for the 4 types of plaques considered of low-risk. 1: adaptive intimal thickening, 2: pathological intimal thickening, 3: fibrocalcific plaque 4: fibrotic plaque.

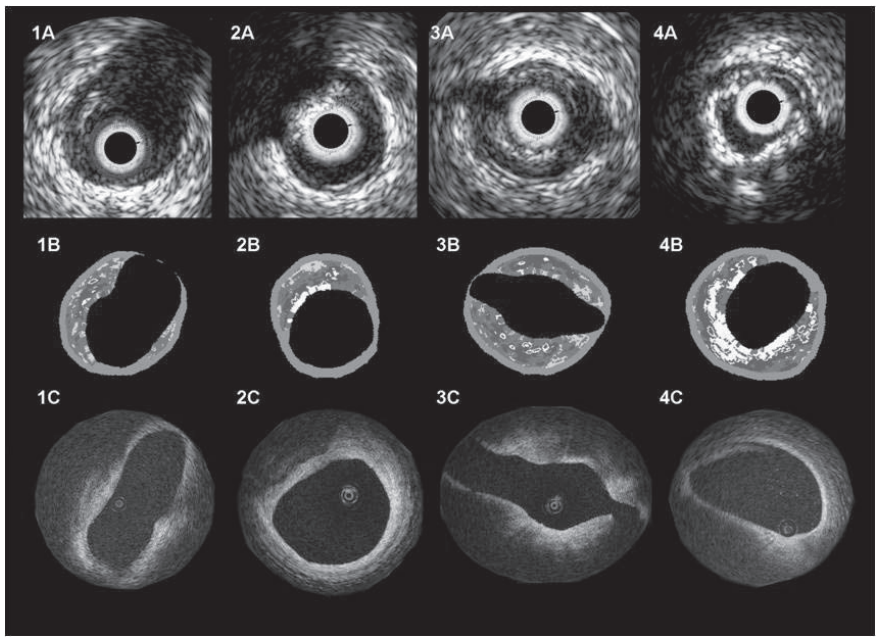

Figure 5: High-risk plaques. Matched images of greyscale IVUS (A), virtual histology (B) and optical coherence tomography (C) for the 4 types of plaques considered at high-risk of rupture. 1: fibroatheroma, 2: calcified fibroatheroma 3: thin-cap fibroatheroma 4: calcified thin-cap fibroatheroma.

see colour section

Fibroatheroma and TCFA are considered high-risk plaques in AHA and Virmani's classifications(7,16). The necrotic core was considered confluent when it was forming a major pool. This definition was used to avoid misclassification as high-risk plaques of lesions with isolated islets or individual pixels of necrotic core which can be artefacts. The presence of confluent NC >10% at the lumen was measured using dedicated in house developed software (MATLAB MathWorks, Natick, MA)(9). A validation with pathology of a similar algorithm was reported in the CAPITAL study(14). The diagnostic accuracy of IVUS-VH compared to histology in different carotid plaque types was 99.4% for TCFA, 96.1% for CaTCFA, 85.9% in FA, 85.5% for fibrocalcific, 83.4% in PIT, and 72.4% for CaFA. To overcome the limitations of IVUS-VH in the fibrous cap evaluation the classification used in our study combines the information about plaque composition provided by IVUS-VH and the measurements of fibrous cap as assessed by OCT(9). The thinnest part of the fibrous cap was measured by OCT in all the plaques that contain more than 10% of confluent NC to distinguish between FA and TCFA. The fibrous cap measurement by OCT was guided by the IVUS-VH to avoid misclassification between lipid pools and calcium. The cap was measured in the area where the NC was closer to the lumen. The reproducibility of fibrous cap measurements has previously been reported (12).
If different morphologies were present along the lesion, the highest degree plaque was established as the definite plaque type.

Statistical analysis

Statistical analyses were performed using SPSS 12.0.1 for Windows (SPSS Inc., Chicago, IL). Continuous variables are expressed as mean ± standard deviation. Categorical variables are expressed as percentages. The bifurcation (lesion) was the unit of analysis without corrections for correlated observations in the same subjects. To compare continuous variables between lesions, t test or ANOVA were used. To compare continuous variables between different segments of the bifurcation paired samples T test or Wilcoxon signed Ranks Test for 2 dependent samples were used. Comparison among groups for categorical variables was made with χ^2 method.

Results

Clinical and procedural characteristics

One hundred and three bifurcations were selected in 32 pullbacks performed in 30 patients. The mean age was 60±7 years and 73% were males. Regarding cardiac risk factors, 48.3% 6.9% and 72.4% had hypertension, diabetes mellitus, and hyperlipidemia, respectively and 27.6% were smokers. Seven percent had prior myocardial infarction and 43.3% had undergone a prior percutaneous coronary intervention. The clinical presentation was stable angina in 86.7%, unstable angina in 10% and acute myocardial infarction in 3.3%. The investigated vessel was LAD in 34%, LCX in 33% and RCA in 33% of the cases. The type of bifurcations studied were LAD/diagonal, LAD/septal branch, LCX/marginal and RCA/right ventricular branch in 21.4%, 12.6%, 33% and 33% of the cases respectively. The indication for IVUS-VH and OCT was assessment of intermediate, non-flow limiting lesions by angiography in 40% of the cases and post stent implantation assessment in the remaining 60% of cases. All studied lesions were considered non- significant by angiographic criteria and had a lumen area >4mm^2 by IVUS. Overall the mean vessel and lumen area and plaque burden (PB) were 13.9 ± 3.7 mm^2, 7.7 ± 2.2 and 43.2 ± 13% respectively. Table 1 shows the number of quadrants containing plaque and the location of the thickest part of the plaque in relation to the side-branch.

Number of quadrants containing plaque	
1	25/103 (24.3%)
2	33/103 (32.0%)
3	29/103 (28.2%)
4	16/103 (15.5%)
Location of the thickest part of the plaque	
Quadrant 1	28/103 (27.2%)
Quadrant 2	18/103 (17.5%)
Quadrant 3	26/103 (25.2%)
Quadrant 4	31/103 (30.1%)

Table 1. Number of quadrants containing plaque and location of the thickest part of the plaque in relation to the flow divider.

Frequency of plaque type

The plaque type was analyzed in 103 lesions and 293 cross sections. Eight distal and 8 proximal rims could not be analyzed due to artefacts. Overall, the frequency of each plaque type per lesion was: AIT 20 (19.4%), PIT 16 (15.5%), fibrocalcific 15 (14.6%), fibrotic 7 (6.8%), FA 8 (7.8%), CaFA 19 (18.4%), TCFA 10 (9.7%) and CaTCFA 8 (7.8%). In the analyzed cross sections the distribution was as follows: AIT 76 (25.9%), PIT 53 (18.1%), fibrocalcific 42 (14.3%), fibrotic 28 (9.6%), FA 18 (6.1%), CaFA 42 (14.3%), TCFA 21 (7.2%) and CaTCFA 13 (4.4%).

Necrotic core and cap thickness distribution

The NC and cap thickness distribution in the proximal rim, in-bifurcation and distal rim cross sections are shown in Figure 6. Overall, the mean NC area and mean percentage of NC decreased from proximal to distal while the mean cap thickness showed an inverse tendency.

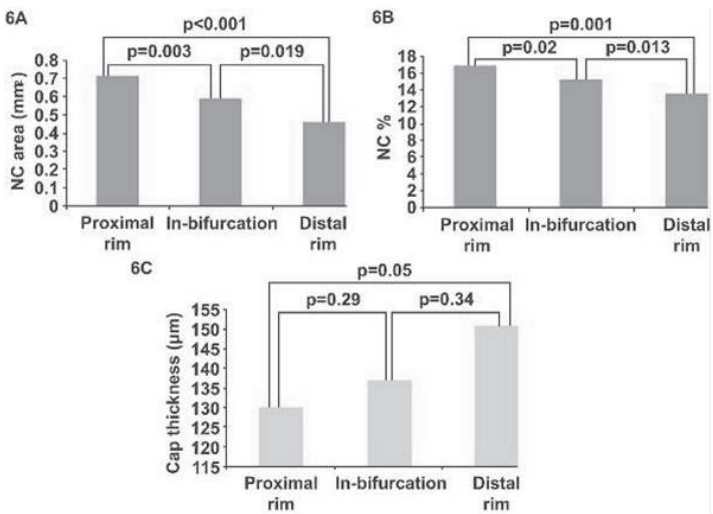

Figure 6: Necrotic core (NC) area (6A), necrotic core percentage (6B) and cap thickness (6C) distribution in the proximal rim of the ostium of the side-branch, in-bifurcation and distal rim cross sections.

High-risk plaques distribution, compositional and geometrical analysis

The distribution of the different plaque types in relation to the location is shown in Table 2. Figure 7 shows the number of cross sections with high-risk plaque morphology in the proximal rim, in-bifurcation and distal rim.

	AIT	PIT	FC	FT	FA	CaFA	TCFA	CaTCFA	Total
Proximal rim	21 (22.1%)	19 (20%)	13 (13.7%)	5 (5.3%)	8 (8.4%)	14 (14.7%)	10 (10.5%)	5 (5.3%)	95
In-bifurcation	24 (23.3%)	18 (17.5%)	15 (14.6%)	12 (11.7%)	5 (4.9%)	15 (14.6%)	8 (7.8%)	6 (5.8%)	103
Distal rim	31 (32.6%)	16 (16.8%)	14 (14.7%)	11 (11.6%)	5 (5.3%)	13 (13.7%)	3 (3.2%)	2 (2.1%)	95

Table 2. Distribution of the different plaque types in the proximal rim of the ostium of the side branch, in bifurcation and distal rim cross sections. N=293 cross sections. AIT: Adaptative intimal thickening, PIT: pathological intimal thickening, FC: fibrocalcic, FT: fibrotic, FA: fibroatheroma, CaFA: calcified fibroatheroma, TCFA: thin cap fibroatheroma, CaTCFA: calcified thin cap fibroatheroma.

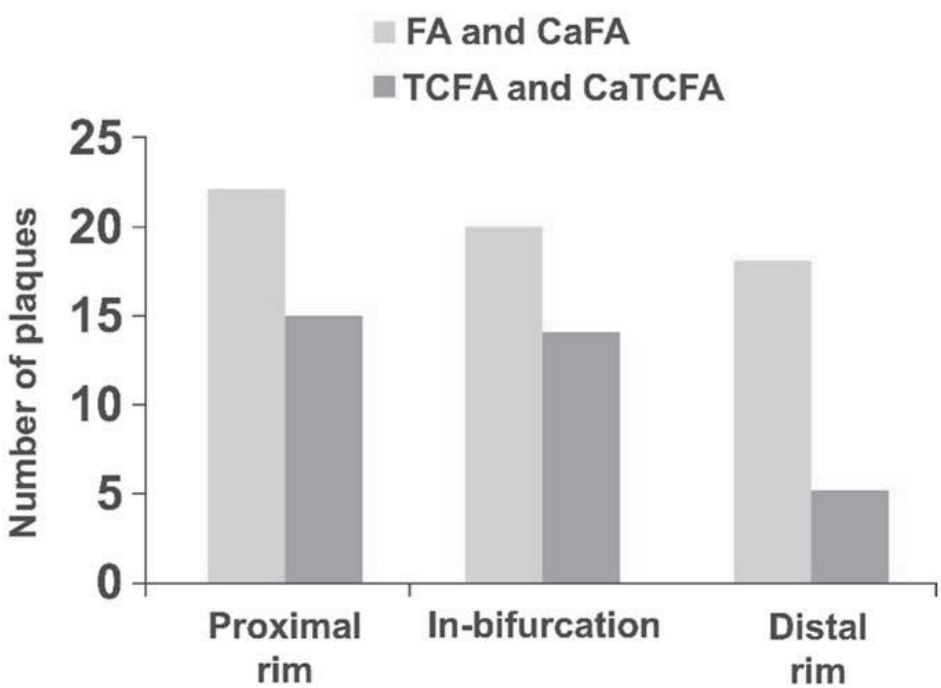

Figure 7: Distribution of the high-risk plaques in the proximal rim of the ostium of the side-branch, in-bifurcation and distal rim cross sections. Number of cross sections with high-risk plaque morphology in the proximal rim, in-bifurcation and distal rim FA: fibroatheroma, CaFA: calcified fibroatheroma TCFA: thin-cap fibroatheroma CaTCFA: calcified thin-cap fibroatheroma.

The thin caps were more often located in the proximal rim (15/34, 44.1%), followed by the in-bifurcation (14/34, 41.2%) and were less frequent in the distal rim (5/34, 14.7%). The location of the thin cap in the 18 lesions classified as TCFAs was as follows: In 4 cases the thinning of the cap extended from the proximal rim into the distal rim, in 7 cases the thin cap was located in the proximal rim and in the in-bifurcation; in 3 TCFAS the thinning of the cap was located only in the in-bifurcation and in 3 only in the proximal rim; there was one TCFA that presented the thin cap at both rims while the cap at the in-bifurcation frame was thicker. There were no cases in which the thin cap was located only in the distal rim. The mean cap thickness in proximal rim, in-bifurcation and distal rim in TCFAs is shown in Figure 8.

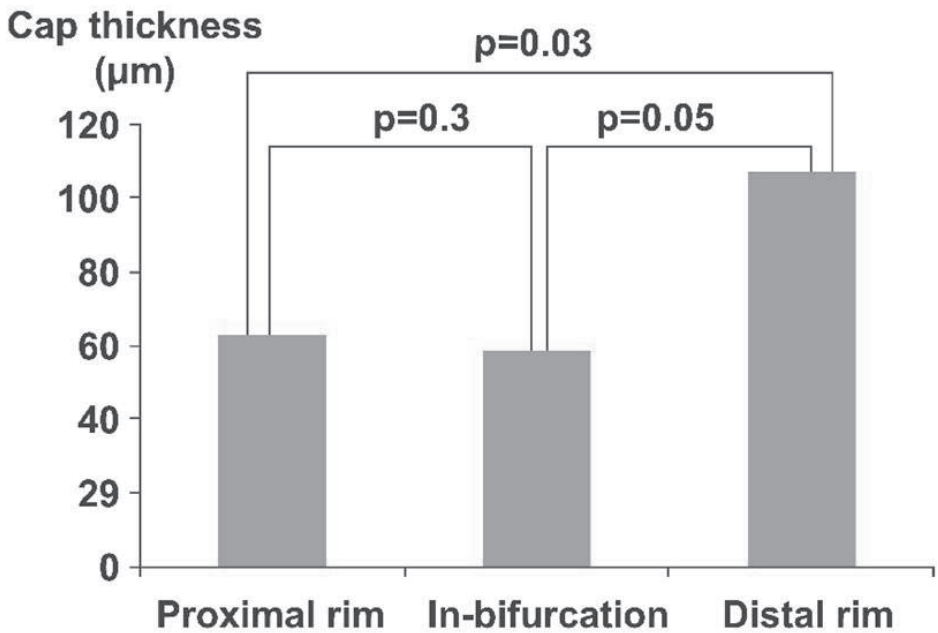

Figure 8: Mean cap thickness in the proximal rim of the ostium of the side-branch, in-bifurcation and distal rim cross sections in thin-cap fibroatheromas.

The vessel area and the plaque burden was significantly greater in the subgroup of lesions considered high-risk (FA, CaFA, TCFA and CaTCFA) than in the rest of lesions (16.5 ± 3 mm^2 vs 14.1 ± 3 mm^2 p=0.002 and 55 ± 9% vs 42 ± 12% p<0.001 for vessel area and plaque burden respectively) while the lumen area was not significantly different (6.8 ± 2 mm^2 vs 7.1 ± 2 mm^2 p=0.39). Table 3 shows the PB, NC percentage and cap thickness in FA, CaFA, TCFA and CaTCFA.

Plaque type in relation to the clinical presentation

As exploratory analysis, patients with acute coronary syndromes (ACS) had a significant higher proportion of lesions with high-risk morphology plaques than stable patients [17/23 (73.9%) vs 28/80 (35%) p=0.002]. Specifically the number of lesions with TCFA morphology was 6/23 (26.1%) vs 12/80 (15%) p=0.2, for ACS and stable patients respectively and the number of lesions with FA morphology was 11/23 (47.8%) vs 16/80 (20%) p=0.01 for ACS and stable patients respectively.

	FA (n=8)	CaFA (n=19)	TCFA (n=10)	CaTCFA (n=8)	p-value
PB (%)	51.7 ± 11	53.7 ± 10	54.2 ± 6	61.8 ± 5	0.13
NC (%)	20.1 ± 5.3	27.1 ± 6	33.0 ± 8	31.7 ± 8	0.002
Cap thickness (μm)	165 ± 59	174 ± 88	49 ± 15	51 ± 13	<0.001

Table 3. Plaque burden (PB), necrotic core (NC) % and cap thickness in fibroatheromas (FA), Calcified fibroatheromas (CaFA), thin cap fibroatheromas (TCFA) and calcified thin cap fibroatheromas (CaTCFA).

Discussion

To our knowledge this is the first in-vivo study evaluating the frequency and distribution of high-risk plaques at bifurcations in coronary arteries using a combined plaque assessment with IVUS-VH and OCT. The main finding is that the thinning of the fibrous cap occurs more often in the proximal rim of the ostium of the side-branch. The NC shows also a differential distribution along the bifurcation being higher at the proximal rim.

Multi-modality plaque assessment

The detection of plaques at potentially high-risk of rupture could prevent future occurrence of acute coronary syndromes. At present, multiple techniques are available that evaluate different aspects of the atherosclerotic plaque such as its structure, composition or mechanical properties (17). The combined information provided by the different methods is essential for better identification of high-risk coronary lesions. In this study, a combined approach with IVUS-VH and OCT was used. IVUS-VH allows the detection and quantification of NC, one of the main components of high-risk plaques. However, the limited axial resolution of IVUS (around 200 μm) does not permit an accurate evaluation of the fibrous cap. On the contrary, OCT has a very high resolution (10-20 μm) allowing a very precise measurement of the fibrous cap. Sawada et al, recently reported the combined use of IVUS-VH and OCT improved the accuracy for TCFA detection(9). They studied 126 plaques in 56 patients with angina. Of the sixty-one plaques diagnosed as TCFA by IVUS-VH criteria, only 28 had a thin fibrous cap, as measured by OCT. In addition, eight OCT-derived TCFA did not have NC in the VH analysis, mainly due to the misinterpretation in the OCT analysis caused by dense calcium. This source of error in plaque characterization by OCT has previously been described and indicates the difficulty in identify TCFAs using only OCT(18). To avoid this misclassification in our study the measurement of the fibrous cap in OCT was guided by IVUS-VH. At the present stage neither modality independently is sufficient for detecting the highest risk plaques; the combined approach seems to be mandatory for the accurate diagnosis of TCFA *in vivo*.

High-risk plaque frequency, distribution, composition and geometrical analysis

The *in- vivo* frequency of TCFAs at bifurcations is not known. In our study, in which a highly selected population was included, 18 out of 103 bifurcations presented TCFAs (17%). Considering that the number of bifurcations in the complete coronary tree is around 15(19), the frequency of TCFAs per heart would be around 2.5. This is in agreement with reported pathological data(7). The bifurcation left main/LAD has been studied with IVUS-VH showing that the plaque burden and the amount of necrotic core are higher in the LAD than in the left main. However, plaque morphology in the different segments of other bifurcations has not been

previously evaluated in vivo. The present study, which extended the assessment of bifurcation lesions beyond the left main, showed that the amount of necrotic core is higher at the proximal rim of the ostium of the side-branch with a thin fibrous cap more often identified in the proximal rim. The fibrous cap thickness is determined by the balance between matrix synthesis by the smooth muscle cells and matrix degradation by metalloproteinases (MMP) produced by macrophages(20). It has been demonstrated that the distribution of inflammatory cells in atherosclerotic plaques relates to the direction of the flow with higher concentration of macrophages and MMP activity in the upstream or proximal part(21). One of the mechanisms that have been proposed for the differential distribution of the high-risk plaques along the artery is the influence of endothelial shear-stress. Bifurcations are geometrically irregular regions where disturbed laminar flow occurs generating abnormal endothelial shear-stress patterns that may play a role in plaque destabilization. Previous studies showed that atherosclerosis develops preferentially at low shear stress locations such as the outer wall of bifurcations (2). However in our data the thickest part of the plaque did not show a preferential location for this region.
Different pathological and IVUS studies have confirmed that plaques rupture occurs usually at sites of significant plaque accumulation associated with positive remodelling(2,22). This is in agreement with our data showing how the vessel area and the plaque burden were higher in high-risk plaques compared to stable lesions. In line with pathological series, TCFAs in our study were located in areas with non-significant lumen compromise, with a mean luminal area of 6.8 ± 2 mm^2(8). Similarly, NC in TCFAs in this population is concordant with previously published pathological findings (8).

High-risk plaques in relation to clinical presentation

Although the comparison between ACS and stable patients in this study was exploratory, patients with unstable clinical presentation showed a high-risk profile of plaque types at bifurcations with a higher proportion of TCFAs and FA. This is in agreement with previous data regarding TCFA detection with IVUS-VH demonstrating that acute coronary syndrome (ACS) patients present a significantly higher prevalence of IVUS derived TCFA than stable patients(10).

Limitations

Currently VH derived necrotic core rich plaques can only be consider as allegedly high-risk lesions as it has not been demonstrated if they are associated with a higher incidence of clinical events at follow up. In the present study OCT and VH were restricted to one or two vessels, therefore, and unlike pathological studies, does not allow us to draw conclusions on the incidence of TCFA in bifurcations within the complete coronary tree. No comparison with non-bifurcation lesions was performed. Still the detailed plaque assessment combining two imaging modalities has given the first insight into the distribution of these allegedly high-risk lesions at bifurcations.

Conclusions

This study, has given unique, in vivo data on the localization of plaque occurring at bifurcation lesions. Further, the proximal rim of the ostium of the side-branch has been identified as a region more likely to contain thin fibrous cap and a greater proportion of necrotic core.

References

1. Virmani R, Burke A, Farb A, Kolodgie FD, Finn AV, Gold HK. Pathology of the vulnerable plaque. London: Informa Healthcare, 2007.
2. Slager CJ, Wentzel JJ, Gijsen FJ, et al. The role of shear stress in the generation of rupture-prone vulnerable plaques. Nat Clin Pract Cardiovasc Med 2005;2:401-7.

3. Al Suwaidi J, Berger PB, Rihal CS, et al. Immediate and long-term outcome of intracoronary stent implantation for true bifurcation lesions. J Am Coll Cardiol 2000;35:929-36.
4. Iakovou I, Schmidt T, Bonizzoni E, et al. Incidence, predictors, and outcome of thrombosis after successful implantation of drug-eluting stents. Jama 2005;293:2126-30.
5. Costa RA, Mintz GS, Carlier SG, et al. Bifurcation coronary lesions treated with the "crush" technique: an intravascular ultrasound analysis. J Am Coll Cardiol 2005;46:599-605.
6. Alfonso F SA, Perez-Vizcayno MJ, Moreno R, Escaned J, Banuelos C, Jimenez P, Bernardo E, Angiolillo DJ, Hernandez R, Macaya C. Intravascular ultrasound findings during episodes of drug-eluting stent thrombosis. J Am Coll Cardiol 2007;50:2095-2097.
7. Virmani R, Kolodgie FD, Burke AP, Farb A, Schwartz SM. Lessons from sudden coronary death: a comprehensive morphological classification scheme for atherosclerotic lesions. Arterioscler Thromb Vasc Biol 2000;20:1262-75.
8. Virmani R, Burke AP, Farb A, Kolodgie FD. Pathology of the vulnerable plaque. J Am Coll Cardiol 2006;47:C13-8.
9. Sawada T, Shite J, Garcia-Garcia HM, et al. Feasibility of combined use of intravascular ultrasound radiofrequency data analysis and optical coherence tomography for detecting thin-cap fibroatheroma. Eur Heart J 2008;29:1136-46.
10. Rodriguez-Granillo GA, Garcia-Garcia HM, Mc Fadden EP, et al. In vivo intravascular ultrasound-derived thin-cap fibroatheroma detection using ultrasound radiofrequency data analysis. J Am Coll Cardiol 2005;46:2038-42.
11. Kume T, Akasaka T, Kawamoto T, et al. Measurement of the thickness of the fibrous cap by optical coherence tomography. Am Heart J 2006;152:755 e1-4.
12. Barlis P GN, Di Mario C, Prati F, Buellesfeld L, Rieber J, Dalby MC, Ferrante G, Cera M, Grube E, Serruys P. W, Regar E. A Multi-Centre Evaluation of the Safety of Intra-Coronary Optical Coherence Tomography. Eurointervention 2008;In press.
13. Bruining N, Verheye S, Knaapen M, et al. Three-dimensional and quantitative analysis of atherosclerotic plaque composition by automated differential echogenicity. Catheter Cardiovasc Interv 2007;70:968-78.
14. Diethrich EB PMM, Reid DB, Burke A, Ramaiah V, Rodriguez-Lopez JA, Wheatley G, Olsen D, Virmani R. Virtual Histology Intravascular Ultrasound Assessment of Carotid Artery Disease: The Carotid Artery Plaque Virtual Histology Evaluation (CAPITAL) Study. J Endovasc Ther 2007;14:676-86.
15. Garcia-Garcia H. M GN, Barlis P, Serruys P.W. Novel Intravascular Imaging Technologies: Jones and Bartlett Publishers, Inc., 2008.
16. Stary HC, Chandler AB, Dinsmore RE, et al. A definition of advanced types of atherosclerotic lesions and a histological classification of atherosclerosis. A report from the Committee on Vascular Lesions of the Council on Arteriosclerosis, American Heart Association. Arterioscler Thromb Vasc Biol 1995;15:1512-31.
17. Garcia-Garcia HM, Gonzalo N, Granada JF, Regar E, Serruys PW. Diagnosis and treatment of coronary vulnerable plaques. Expert Rev Cardiovasc Ther 2008;6:209-22.
18. Manfrini O, Mont E, Leone O, et al. Sources of error and interpretation of plaque morphology by optical coherence tomography. Am J Cardiol 2006;98:156-9.
19. Scanlon PJ, Faxon DP, Audet AM, et al. ACC/AHA guidelines for coronary angiography. A report of the American College of Cardiology/American Heart Association Task Force on practice guidelines (Committee on Coronary Angiography). Developed in collaboration with the Society for Cardiac Angiography and Interventions. J Am Coll Cardiol 1999;33:1756-824.
20. Shah PK, Falk E, Badimon JJ, et al. Human monocyte-derived macrophages induce collagen breakdown in fibrous caps of atherosclerotic plaques. Potential role of matrix-degrading metalloproteinases and implications for plaque rupture. Circulation 1995;92:1565-9.
21. Dirksen MT, van der Wal AC, van den Berg FM, van der Loos CM, Becker AE. Distribution of inflammatory cells in atherosclerotic plaques relates to the direction of flow. Circulation 1998;98:2000-3.
22. Cunningham KS, Gotlieb AI. The role of shear stress in the pathogenesis of atherosclerosis. Lab Invest 2005;85:9-23.

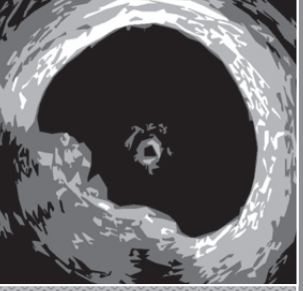

Part 5

Future developments in OCT imaging

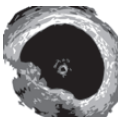

Chapter 26

Current and future developments in intra-coronary optical coherence tomography imaging

Peter Barlis, Joseph M. Schmitt

Optical coherence tomography (OCT) has become a key intra-coronary imaging modality able to traverse some of the limitations of angiography and intravascular ultrasound. In-vivo imaging with high resolution (around 15 micrometres) has given unique insights into not only atherosclerotic plaque, but also to the understanding of tissue responses underlying stent implantation. Novel developments with faster OCT pullback speeds will further simplify the procedural requirements and eventually eliminate the need for proximal vessel balloon occlusion during image acquisition. This report explores the current and future developments in OCT technology that will see this unique imaging modality become a key player in both the clinical and research arena for the interventional cardiologist.

The application of optical coherence tomography (OCT) to the coronary arteries has offered new insights into atherosclerosis and tissue responses following stent implantation. The clear and detailed images have generated an intense interest in adopting this technique for both clinical and research purposes. The first OCT system for coronary imaging was approved for clinical use in the European Union in 2004 and, up to now, more than 100 systems have been installed in catheterisation laboratories world-wide. OCT has been used for the detailed assessment of atherosclerotic plaque, in particular the quantification of thin-cap fibroatheroma (TCFA) and the distribution of macrophages (foam cells) surrounding vulnerable plaques. (1-6) In addition, OCT can precisely assess tissue coverage following stent implantation, (7-12) and in this regard, may provide greater insights into the potential link between stent endothelialisation and late thrombosis. This chapter details current and future developments in OCT imaging, which include exciting technological advancements that will consolidate the position of OCT as a key diagnostic tool to complement the armamentarium of the cardiologist well into the future.

Current OCT technology

At present, two commercial OCT systems, the M2 and M3 OCT Imaging Systems (LightLab Imaging, Inc., Westford, MA, USA), are available for clinical use. Both employ a dedicated fibre-optic imaging wire (ImageWire™, LightLab Imaging Inc., Westford, MA, USA) connected to a patient interface unit (PIU) which, in turn, connects to the system console. The imaging wire has a maximum outer diameter of 0.019″ (with a standard 0.014" radiopaque coiled tip) and contains a single-mode fibre-optic core that rotates within a transparent sheath. Figure 1 illustrates the M2 system console with the cart containing the optical imaging engine and the computer. The mouse, keyboard, two monitors, and the PIU are all mounted on top of the cart. Although both the M2 and M3 systems use the identical console and PC-based operating system, the latter permits imaging at a higher frame rate (20/sec for the M3 vs. 15.6/sec for the M2) with a faster maximum pullback speed (3.0mm/sec vs. 2.0mm/sec).

Figure 1. The LightLab M2 System console

OCT physics

Current OCT systems incorporate advanced near-infrared light sources and optical components that operate in a wavelength band centred on 1310 nm. Like intravascular ultrasound (IVUS), OCT measures the depth of reflections from tissue according to the round-trip propagation time of reflected energy. However, as the speed of light is much faster than that of sound, an interferometer is required to measure the backscattered light. The interferometer splits the light from the source into two paths – a reference path that directs the light to a reference moving mirror and a sample path that directs light through the fibre-optic imaging wire into the tissue and collects the backscattered light. The light that returns from both paths is recombined at a detector, generating the so-called interferogram from the sum of the reference and sample fields (Figure 2a). The maximum imaging depth of current OCT systems is 1.0-2.0 mm, depending on tissue type, with axial and lateral resolutions of 15 and 25 μm, respectively.

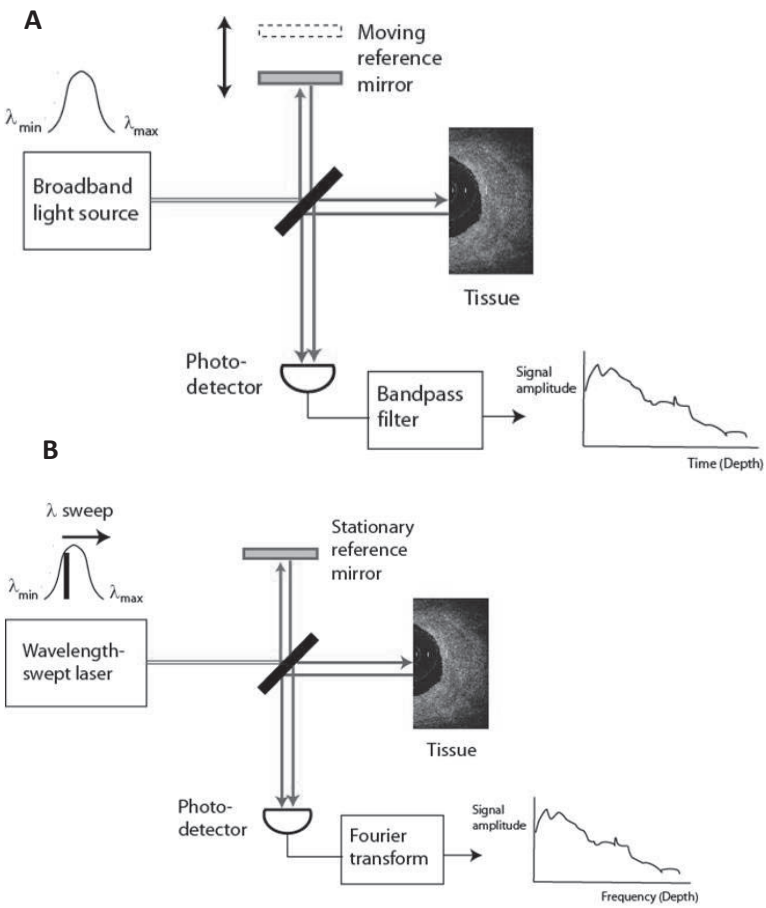

Figure 2. Main components of (A) time-domain and (B) Fourier-domain OCT systems. The red and blue lines depict the sample and reference beams, respectively, that generate the interference signal at the photodetector.

The time-domain OCT imaging method on which the M2 and M3 systems are based relies on a moving mirror to scan each depth position in the image pixel by pixel. This mechanical scanning process limits the rate at which images can be acquired. The latest generation of OCT systems employ Fourier-domain OCT acquisition methods, described in a later section of this report, that enable much faster image acquisition rates and pullback speeds.

Procedural requirements for OCT imaging

As near-infrared light penetrates only a short distance through blood, temporary blood clearance is required for OCT imaging. To clear blood according to the instructions for use of the LightLab M2 system, a proximal occlusion balloon (Helios, Goodman Co. Ltd., Nagoya, Japan) is inflated to between 0.5-0.7 atm, while simultaneously flushing physiological saline or Ringer's lactate solution through the distal lumen of the balloon catheter at a rate of 0.5 – 1 ml/s. Refinements in OCT technology have led to faster acquisition speeds and have encouraged a gradual shift from the cumbersome occlusive technique to a simpler, non-occlusive approach with flushing of viscous contrast through the guiding catheter. Even though initial reports have shown this to be feasible, (13) this technique is still regarded as "off-label" although, intrinsically, it has a number of advantages and eliminates the risk of balloon-related vessel injury.

Fourier-domain OCT

Principles

The development of a new generation of OCT systems with faster image acquisition speeds and greater scan depths, without loss of vital detail and resolution, is a major advancement in intravascular OCT imaging. Rather than using a broadband light source as in conventional time-domain OCT systems, Fourier-domain OCT (FD-OCT) imaging systems employ a novel wavelength-swept laser as a light source. (Figure 2b) The laser has a narrow spectral output that can be tuned electronically over a wide band of wavelengths (typically 1250 – 1350 nm, the same spectral band in which time-domain systems operate). As the wavelength of the laser sweeps, reflections from refractive-index discontinuities at different depths are encoded in the frequencies of the interference signals that they generate. An entire depth scan is reconstructed by Fourier transformation of the interference signals recorded during a single sweep of the laser. The bandwidth of the laser and width of its wavelength sweep determine the scan depth and axial resolution, respectively. FD-OCT systems can acquire images at line rates at least 10 times faster than time-domain systems without loss of image quality. This speed advantage results from the elimination of mechanical scanning of the reference mirror and the signal-to-noise advantages of Fourier-domain signal processing.

Fourier-domain OCT has been used for real-time, volumetric imaging of the eye, (14) gastrointestinal tract, (15) and coronary arteries (16). The principal advantage of Fourier-domain OCT in intra-coronary imaging applications is that it permits the acquisition of longitudinal sequences of cross-sectional images with significantly faster pullback speeds than conventional time-domain OCT. Fast pullback speeds are essential for imaging long segments of arteries with

minimal ischaemia, eliminating the need for proximal vessel balloon occlusion during image acquisition.

Technical specifications

Prototypes of FD-OCT systems are now undergoing evaluation in preparation for regulatory clearance for commercial sale. Table 1 compares the key specifications of conventional (time-domain) OCT systems with those of a representative first-generation Fourier-domain OCT system (LightLab Imaging, Inc, Westford, MA). The main performance advantages of the Fourier-domain OCT system are its faster frame rate, higher image line density, and faster maximum pullback speed. To enable imaging of coronary arteries with large lumens (> 4 mm), the FD-OCT system also has a wider scan diameter. The penetration depth and resolution of the first generation of Fourier-domain OCT systems do not differ significantly from those of commercial time-domain OCT systems.

Parameter	M2/M3 OCT	Fourier-domain OCT (LightLab prototype)
Source Wavelength	1250-1350 nm	1250-1350 nm
Axial resolution	15 – 20 μm	15 – 20 μm
Lateral resolution	25 – 30 μm	25 – 30 μm
Scan diameter (in saline)	6.8 mm	8.3 mm
Frame rate	M2: 15.6 f/sec M3: 20 f/sec	100 f/sec
Number of lines/frame	M2: 200 M3: 240	450
Maximum pullback speed	M2: 2.0 mm/sec M3: 3.0 mm/sec	20 mm/sec

Table 1: Comparison of the commercial time-domain OCT system and a first-generation Fourier-domain OCT system

Designed for rapid-exchange delivery, the first generation of FD-OCT imaging catheters can be delivered over a 0.014-inch guidewire through a 6F or larger guide catheter and have 2.5- 2.8 F crossing profiles. These catheters consist of a fibre-optic imaging core threaded through a hollow torque cable that rotates and pulls back within a transparent plastic sheath. To maintain high longitudinal resolution at fast pullback speeds, the torque cable rotates faster than a conventional IVUS catheter (100 rotations/sec versus 30 rotations/sec).

Preliminary experience with Fourier-domain OCT

Studies have been conducted to evaluate the safety and performance of prototype versions of the FD-OCT systems in both pre-clinical and clinical settings. The results of initial bench tests verify the improvements in image acquisition speed, lateral resolution, scan range, and other basic imaging specifications listed in Table 1. A key objective of early preclinical studies in an acute porcine model was to develop a reliable flush method that can be applied safely and effectively in the catheterisation laboratory. These experiments demonstrated that effective clearing of blood from the imaging field can be achieved by injecting saline, angiographic contrast media, or a mixture of contrast and saline, through the guide catheter. In preliminary studies, injection of 14 ml volume of contrast at a rate less than 4 ml/s was found to be sufficient to achieve an imaging period of 2-3 seconds consistently in all of the major coronary branches. At a pullback rate of 20 mm/s, an imaging period of 2 seconds is long enough to scan a 4-cm vessel segment. As saline and saline-contrast mixtures have lower viscosities, larger volumes and higher flow rates are required to achieve equivalent clear imaging times, especially in distal segments of highly branched arteries. The required flush volume depends on the proximity of side branches and the location of the imaging probe relative to the tip of the guide catheter. Therefore, fast rotation and pullback rates, combined with tight synchronisation of the movement of the pullback mechanism, are essential for imaging segments of arterial segments longer than a few centimetres.

The most extensive series of clinical studies of Fourier-domain OCT imaging to date began in October, 2007, at the Helios Heart Centre, Siegburg, Germany, in collaboration with LightLab Imaging. Over a period of 6 months, Dr. Eberhard Grube, who serves as principal investigator, and other senior cardiologists at the Centre (Drs. Buellesfeld, Mueller, and Gerkens) recorded pullback OCT images from 25 patients during coronary interventions, with an average of 2 pullback sequences acquired per patient. Figure 3 shows an example of an FD-OCT image extracted from a pullback image sequence recorded from one of the patients. The corresponding longitudinal (L)-mode image in the figure shows a profile of the vessel along its length. In this case, a 4.9-cm segment of the artery was imaged in 3.3 sec while contrast was injected through the guide catheter. The high resolution of the image is evident from the ability to distinguish the thin intimal, medial, and adventitial layers of the artery, with thicknesses less than 0.4, 0.15, and 0.2 mm, respectively.

The high line density of Fourier-domain OCT images is especially valuable for visualisation of stented arteries. Figure 4 shows examples of OCT images of stents that were obtained immediately after implantation and at long-term follow-up. In addition to visual assessment of the apposition of individual stents struts (Figure 4a), neointimal growth as thin as 20 μm (Figure 4b) and as thick as a 1 mm (Figure 4c) can be measured precisely along the length of the stent.

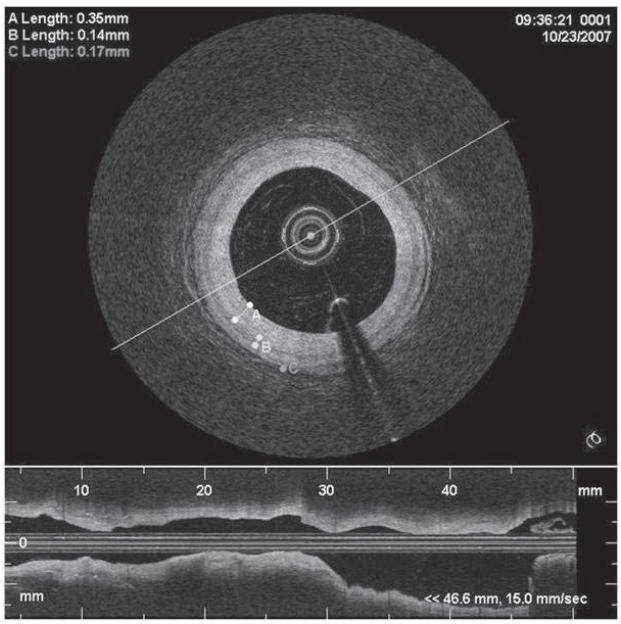

Figure 3. An example of an OCT image acquired with a prototype OCT system (LightLab Imaging, Westford, MA, USA) from the coronary artery of a patient undergoing percutaneous coronary intervention. The lengths listed in the upper left corner correspond to measurements of the thicknesses of the intima, media, and adventitia, denoted by the letters 'A', 'B' and 'C', respectively. The L-mode image (lower quarter of figure) shows a longitudinal image of the artery acquired during a 20 mm/s pullback. [Images courtesy of Dr. E. Grube, Siegburg Heart Center, Siegburg, Germany].

see colour section

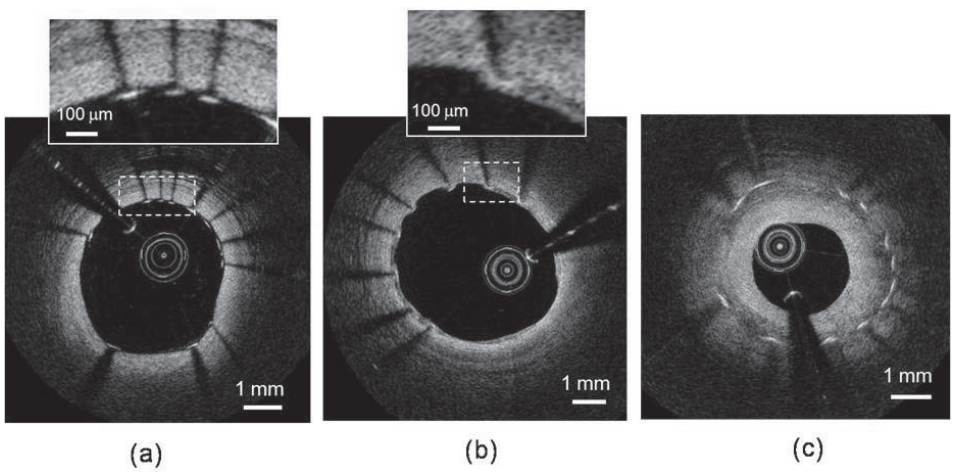

Figure 4. Examples of OCT images of stents acquired with a prototype FD-OCT system (LightLab Imaging, Westford, MA, USA). (a) Bare-metal stent imaged immediately after implantation. Stent imaged at long-term follow-up with (b) thin and (c) thick neointimal coverage. [Images courtesy of Dr. E. Grube, Siegburg Heart Center, Siegburg, Germany]

see colour section

Figure 5 shows examples of Fourier-domain images of fibrous, calcified, and lipid-rich lesions acquired from target arteries of patients undergoing interventional coronary procedures. Fourier-domain images of the main classes of atherosclerotic lesions exhibit the same defining characteristics as those of time-domain OCT images described in earlier publications (2). The reduced spacing between angular samples in the Fourier-domain images improves the sharpness of plaque boundaries, which may facilitate the detection of thin-capped lesions and lesions containing small clusters of foam cells.

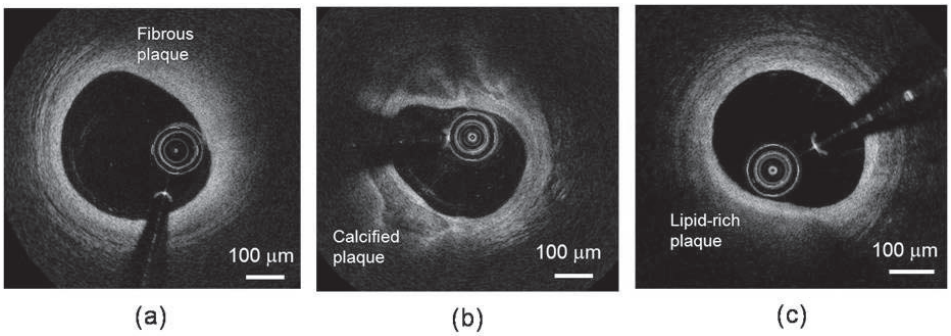

Figure 5. Fourier-domain OCT images of (a) fibrous, (b) calcified, and (c) lipid-rich lesions acquired with a prototype FD-OCT system (LightLab Imaging, Westford, MA, USA) [Images courtesy of Dr. E. Grube, Siegburg Heart Center, Siegburg, Germany].

Future developments

Continued advances in the technology of Fourier-domain OCT promise to improve the ease of use and to broaden the applications of OCT imaging in clinical practice and medical research. Quantitative plaque characterisation methods aimed at rapid identification of plaque types are under development. Computer-assisted detection of stent malapposition and denudation of endothelial coverage with OCT is also being explored. These future diagnostic tools, when combined with novel three-dimensional, colour-mapped displays, may enable cardiologists to detect therapeutic targets in real-time during percutaneous interventions.

Furthermore, novel stents including bioabsorbable magnesium stents or those made with poly-lactic acid offer an exciting era into the management of coronary artery disease with the potential to eliminate some of the problems related to permanent metallic stents. The development of such technologies, however, remains time consuming and expensive, often necessitating the sacrifice of animals to retrieve the stents. (17) The high-resolution imaging capabilities of OCT gives the potential for rapid in-vivo assessment of tissue response to various stent designs, thereby limiting the dependency on statistical comparisons in large numbers of animals. (17) The serial use of OCT is also an attractive concept, giving unique insights into the time course of stent endothelialisation following implantation. This application has been greeted with strong enthusiasm and OCT is now being incorporated into large multi-centre randomised stent trials aimed at complementing angiographic and clinical endpoints.

Conclusions

The ability to provide high-resolution imaging in-vivo is one of the most significant advances attributable to OCT. With even faster pullback speeds and simplification of the procedural requirements (e.g. by eliminating the need for proximal balloon occlusion), OCT will become more accessible to a greater number of centres and operators world-wide. Such advances will also see OCT consistently applied as a multi-vessel diagnostic modality, able to provide a truly representative assessment of the entire coronary tree.

References

1. Jang IK, Bouma BE, Kang DH, et al. Visualization of coronary atherosclerotic plaques in patients using optical coherence tomography: comparison with intravascular ultrasound. J Am Coll Cardiol 2002;39:604-9.
2. Jang IK, Tearney GJ, MacNeill B, et al. In vivo characterization of coronary atherosclerotic plaque by use of optical coherence tomography. Circulation 2005;111:1551-5.
3. Tearney GJ, Yabushita H, Houser SL, et al. Quantification of macrophage content in atherosclerotic plaques by optical coherence tomography. Circulation 2003;107:113-9.
4. Barlis P, Serruys PW, Gonzalo N, van der Giessen WJ, de Jaegere PJ, Regar E. Assessment of culprit and remote coronary narrowings using optical coherence tomography with long-term outcomes. Am J Cardiol 2008;102:391-5.
5. Barlis P, Ferrante G, Del Furia F, Di Mario C. In-vivo characterisation of coronary atherosclerosis with optical coherence tomography. Med J Aust 2008;188:728.
6. Barlis P, Serruys PW, Devries A, Regar E. Optical coherence tomography assessment of vulnerable plaque rupture: predilection for the plaque 'shoulder'. Eur Heart J 2008;29:2023.
7. Matsumoto D, Shite J, Shinke T, et al. Neointimal coverage of sirolimus-eluting stents at 6-month follow-up: evaluated by optical coherence tomography. Eur Heart J 2007;28:961-7.
8. Takano M, Inami S, Jang IK, et al. Evaluation by optical coherence tomography of neointimal coverage of sirolimus-eluting stent three months after implantation. Am J Cardiol 2007;99:1033-8.
9. Tanimoto S, Rodriguez-Granillo G, Barlis P, et al. A novel approach for quantitative analysis of intracoronary optical coherence tomography: high inter-observer agreement with computer-assisted contour detection. Catheter Cardiovasc Interv 2008:DOI: 10.1002/ccd.21482.
10. Tanigawa J, Barlis P, Di Mario C. Intravascular Optical Coherence Tomography: Optimisation of image acquisition and quantitative assessment of stent strut apposition. EuroIntervention 2007;3:128-136.
11. Tanigawa J, Barlis P, Di Mario C. Do unapposed stent struts endothelialise? In vivo demonstration with optical coherence tomography. Heart 2007;93:378.
12. Barlis P, Tanigawa J, Di Mario C. Coronary bioabsorbable magnesium stent: 15-month intravascular ultrasound and optical coherence tomography findings. Eur Heart J 2007;28:2319.
13. Prati F, Cera M, Ramazzotti V, Imola F, Giudice R, Albertucci M. Safety and feasibility of a new non-occlusive technique for facilitated intracoronary optical coherence tomography (OCT) acquisition in various clinical and anatomical scenarios. EuroIntervention 2007;3:365-70.
14. Lim H, Mujat M, Kerbage C, et al. High-speed imaging of human retina in vivo with swept-source optical coherence tomography. Optics Express 2006;14:12902-08.
15. Chen Y, Aguirre AD, Hsiung PL, et al. Ultrahigh resolution optical coherence tomography of Barrett's esophagus: preliminary descriptive clinical study correlating images with histology. Endoscopy 2007;39:599-605.
16. Yun SH, Tearney GJ, Vakoc BJ, et al. Comprehensive volumetric optical microscopy in vivo. Nat Med 2006;12:1429-33.
17. Bonnema GT, Cardinal KO, McNally JB, Williams SK, Barton JK. Assessment of blood vessel mimics with optical coherence tomography. J Biomed Opt 2007;12:024018.

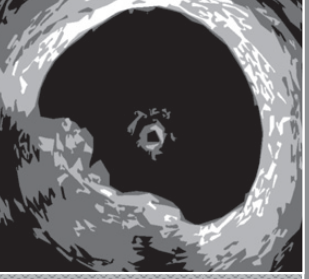

Part 6

Summary & Conclusions

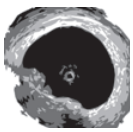

Chapter 27

Summary and Conclusions
Samenvatting en Conclusies
Peter Barlis

This thesis provides important data regarding the application of intracoronary OCT to the clinical and research fields while addressing the important issues of procedural safety and validity of OCT-derived data. The technique, with its sophisticated and elegant optics, are appropriately reviewed (***chapter 2***) with insights given into where OCT is placed amongst existing intravascular imaging technologies, namely IVUS (***chapter 3***). More specifically, the thesis embraces two key targets for OCT, namely the detailed assessment of coronary stents (***chapters 9-20***) and atherosclerotic plaque (***chapters 21-24***).

Safety of OCT

With the increased diffusion of OCT, surprisingly little has been documented in terms of its safety profile apart from isolated cases and small series. As with all aspects of interventional cardiology, a number of risks are inherent and, for the first time, ***chapter 4*** recalls the experience of 6 European centres with the implementation and use of the technique. In a total of 468 consecutive patients who underwent OCT, this chapter reviews the clinical indications of OCT imaging and explores in detail the safety profile of the technique. The need for a blood-free environment to image, often elicits transient chest pain and ECG changes which almost always resolve immediately following imaging. The chapter describes a risk of 1% of ventricular fibrillation which is inherent with occlusion balloon, contrast flushing and/or deep guide catheter intubation. In all cases, coronary spasm was not found to be problematic and this is in contrast to prior studies of IVUS.

Feasibility of OCT

First generation OCT systems demanded the use of an occlusion balloon situated in the proximal segment of the vessel inflated during simultaneous injection of Ringer's lactate via an injector (***chapter 5***). Refinements in OCT technology, with faster acquisition speeds have seen a gradual shift from the cumbersome occlusive technique to a simpler non-occlusive technique with flushing of viscous contrast through the guiding catheter. This currently remains "off-label" however has definite advantages, namely a shorter OCT procedure time and a larger amount of information with a longer pullback distance achieved compared to the use of the occlusion balloon (***chapter 8***). The non-occlusive technique is also applicable to most ostial and proximal coronary segments with significantly less patient discomfort (***chapter 8***).

When first confronted with OCT of a coronary artery, one cannot help be impressed by the clarity of the images. The understanding of OCT imaging however lies deep beyond this cursory assessment and requires appropriate interpretation of the material acquired. This remains one of the most painstaking aspects of offline image interpretation yet is one of the most important and rewarding once mastered. ***Chapters 6 and 7*** provide compelling evidence of a low intra and inter- observer variability expected when analysing OCT data and gives further validity of OCT as both a clinical and research tool. Further, OCT has now become integral to a number of multi-centre trials of the next generation drug-eluting stents (DES) looking at potentially using tissue coverage as a surrogate for long-term healing and, therefore, stent safety (***chapter 10 and 11***).

Clinical applications – Coronary stents

Much of what is currently known regarding stent safety has arisen based on studies using angiographic follow-up or IVUS in addition to invaluable information gained during the unfortunate post-mortem setting. In the latter, lack of endothelial coverage however has been shown to be a powerful predictor of stent thrombosis. Coronary angiography and IVUS lack the resolution to assess thin layers of coverage.

In the LEADERS trial OCT sub-study, 46 patients were randomized to receive either biolimus-eluting (BES) or sirolimus-eluting stents (SES) in an 'all-comer' patient population with very few exclusion criteria. Twenty patients were included in the analysis in the BES group (29 lesions with 4592 struts) and 26 patients in the SES group (35 lesions with 6476 struts). A total of 83 struts were uncovered in the BES group and 407 out of 6476 struts were uncovered in the SES group (weighted difference -1.4%, 95% CI -3.7 to 0.0%, p=0.04) at 9 months follow-up. There were 3 lesions in the BES and 15 lesions in the SES group that had ≥5% of all struts uncovered (difference -33.1% 95% CI -61.7 to -10.3%, p<0.01) indicating more complete tissue coverage in patients allocated to BES as compared with SES (***chapter 10***). The impact of this difference on clinical outcome and, in particular, on the risk of late stent thrombosis, is yet to be determined however further studies with even longer angiographic and OCT follow-up will help give useful insights.

In another DES randomised trial, ***chapter 11*** explores 2 different rapamycin-eluting stents (one with and one without a polymer coating). At 3-months post implantation, OCT identified a mean neointimal thickness of 77.1μm (95% CI 57.7-83.9) and 193.5μm (95% CI 122.7-206.9) p=0.016 for the polymer-coated rapamycin-eluting (Cypher) and non-polymer rapamycin-eluting (Yukon) stent respectively with no clinical adverse events in both groups. Binary stent strut coverage was 89.0% (CI 87.8-90.3) versus 97.2% (95% CI 96.6-97.8) p=0.023 for the Cypher and Yukon stents respectively. Such mechanistic trials using super high-resolution imaging with OCT may have important implications for the risk of stent thrombosis and therefore future stent design.

OCT can be used to guide optimal stent expansion at time of implantation. Indeed, stent expansion, apposition and symmetry were the three criteria of IVUS guided optimal stent deployment in the bare metal stent era, with at least the criterion of stent expansion maintaining its clinical relevance in the DES era. Since infra-red light is unable to penetrate through metal struts, OCT visualises only the endo-luminal surface of the strut. Hence, when assessing apposition, the strut and polymer thickness should be considered for each type of DES design. ***Chapter 5*** provides a classification of strut apposition into one of three categories: Struts buried in the intima for more than half of their thickness are defined as *'embedded'*, those apposed to the intima but not embedded are defined as '*protruding*' and those with no contact to the intima are *'malapposed'*. Using this classification, ***chapter 14*** compared the immediate OCT findings of 4 different DES implanted to complex coronary lesions. Further, in a separate study of 20 overlapping DES (10 patients, 661 struts) immediately after implantation, OCT identified 42% of struts were malapposed in the overlapping segment, despite aggressive stent optimisation (***chapter 12***). This may be a central factor in the reported delay in endothelialisation occurring in overlapping segments.

In addition to stent tissue coverage and apposition, OCT can be a complimentary imaging modality when examining stent fracture (***chapter 15***), absorption of biodegradable magnesium stents (***chapter 18***) and in cases of very late stent thrombosis (***chapter 19***), thereby yielding unique, ante-mortem findings.

Clinical applications – atherosclerotic plaque assessment

Acute coronary syndromes including myocardial infarction are leading causes of death, often caused by rupture of vulnerable plaque (VP). The detection of VP in the early phase of coronary artery disease therefore remains essential to limit morbidity and mortality while helping to target specific therapeutic interventions. Through retrospective, post-mortem studies, several characteristics of plaques that are prone to rupture have been identified including: the presence of a thin fibrous cap (<65 microns in thickness); a large lipid core and activated macrophages

near the cap. The limitation of such studies however remains their inability to provide crucial detail regarding the natural history and progression of VP, and, therefore prognosis. Several imaging modalities have been used to assess and identify VP including coronary angioscopy, IVUS and magnetic resonance imaging. Recently, there has been significant interest in the field of VP detection using OCT as it permits high-resolution imaging, principally suited to detect and quantify the thickness of a thin cap fibroatheroma (TCFA) and to estimate macrophage distribution (***chapter 2***).

In ***chapter 21***, OCT was used to assess culprit and remote coronary lesions and to investigate whether intra-coronary OCT in living patients, was able to visualise morphologic features associated with VP in post-mortem studies. Twenty-three patients successfully underwent OCT prior to percutaneous coronary intervention. The culprit lesion and mild-moderate coronary lesions remote from the target stenosis were investigated. The majority of plaques at remote segments were proximal to the culprit lesion (73.9%) and predominantly fibrous and lipid-rich. At 24-months clinical follow-up, the only event occurred in a patient with in-stent restenosis who underwent repeat percutaneous revascularisation. The detection of TCFA, particularly in stable patients is desirable and may principally allow for early intervention and prevention of adverse events long-term.

In ***chapter 22***, OCT was used in addition to other intra-coronary diagnostic techniques [IVUS Greyscale (IVUS-GS), IVUS Radiofrequency Data (IVUS-RFD) Analysis and Intravascular Magnetic Resonance Spectroscopy (IVMR)] in a unique pilot study to compare the capability for atherosclerotic plaque detection. These four imaging modalities have in common, the ability to give a detailed assessment of the composition of atherosclerotic plaques but do differ in the means of achieving this. Atherosclerotic plaques classified as soft by IVUS GS were mainly composed by fibro-fatty (80%) or necrotic core (20%) by IVUS RFD. These soft plaques were classified as "lipid rich" by OCT in the majority of cases (80%). IVMR confirmed the presence of lipid with a lipid fraction index ranging between 36 and 79 in these soft plaques. Besides this good agreement for soft plaques, IVUS GS, IVUS RFD and OCT had 100% agreement in the identification of calcified plaques.

In a study of 103 coronary bifurcations from 30 patients, OCT and IVUS-VH were used and found that there was a propensity of TCFA occurring in the proximal segments of the bifurcation compared to distal segments (***chapter 24***). Further, patients with acute coronary syndromes had a significant higher proportion of lesions with high-risk morphology plaques than stable patients [17/23 (73.9%) vs 28/80 (35%) p=0.002] highlighting the proximal rim of the ostium of the side-branch as a region more likely to contain thin fibrous cap and a greater proportion of necrotic core.

Future directions

The development of a new generation of OCT systems with faster image acquisition speeds and greater scan depths, without loss of vital detail and resolution, is a major advancement in intravascular OCT imaging. Rather than using a broadband light source as in conventional time-domain OCT systems, Fourier-domain OCT (FD-OCT) imaging systems employ a novel wavelength-swept laser as a light source (***chapter 25***). At a pullback rate of 20 mm/s, an imaging period of 2 seconds is long enough to scan a 4-cm vessel segment. Such advances will see OCT become more accessible to a greater number of centres and operators world-wide. It will also expand the utility of OCT with it applied as a multi-vessel diagnostic modality, able to provide a truly representative assessment of the entire coronary tree.

Conclusions

The present thesis has encompassed work undertaken during a very exciting period for interventional cardiology as a discipline. The demand for a greater understanding of the atherosclerotic process, the treatment of more and more complex lesions, and the steady introduction of new stents into clinical practice necessitate ongoing scrutiny and study to ensure our patients receive the best possible care. OCT has caused intense interest in interventional cardiology. Its application to the assessment of coronary stents has been greeted with strong enthusiasm. Such applications are currently unique to OCT and, despite the recent progress of non-invasive techniques such as 64 multi-slice computed tomography, conventional stents still represent a challenge to distinguish lumen and intimal hyperplasia within the stent. The ability of OCT to provide high-resolution imaging in-vivo is the most significant concept circumventing the limitations of other imaging modalities such as IVUS or the need for multiple animal experiments. Refinements in acquisition speeds with FD-OCT will also make the technique less procedurally demanding and thus able to be applied to many more centres, thereby remaining a key tool in the armamentarium of researchers and interventional cardiologists alike.

Deze thesis verstrekt belangrijke gegevens betreffende de toepassing van intracoronairen optisch coherentie tomografie (OCT) op de klinische en onderzoekgebieden terwijl het behandelen van de belangrijke kwesties van procedureveiligheid en geldigheid van OCT. Optisch coherentie tomografie is herzien (***hoofdstuk 2***) met inzicht wordt gegeven dat in waar OCT onder bestaande intravasculair technologieën wordt geplaatst, namelijk intravasculair ultrasone (IVUS) (***hoofdstuk 3***). Specifieker, omhelst de thesis twee zeer belangrijke doelstellingen voor OCT, namelijk de gedetailleerde beoordeling van coronaire stents (***hoofdstukken 9-20***) en atherosclerose (***hoofdstukken 21-24***).

Veiligheid van OCT

Zoals met alle aspecten van interventie cardiologie, een aantal risico's zijn inherent en, voor het eerst, ***hoofdstuk 4*** herinnert aan de ervaring van 6 Europese centra met de implementatie van OCT. In een totaal van 468 opeenvolgende patiënten ondergingen OCT, herziet dit hoofdstuk de klinische aanwijzingen van OCT en onderzoekt in het veiligheidsprofiel van de techniek.

Haalbaarheid van OCT

De eerste generatie OCT eisten het gebruik van een occlusieballon (***hoofdstuk 5***). De verbeteringen in OCT technologie, met snellere aanwinstensnelheden hebben een geleidelijke verschuiving aan de hinderlijke occlusieve techniek naar een eenvoudigere nietocclusieve techniek met het spoelen van contrast. Dit blijft momenteel 'van-etiket' nochtans welomlijnde voordelen heeft, namelijk een kortere OCT procedure tijd en een grotere hoeveelheid informatie met een langere bereikte pullback afstand in vergelijking met het gebruik van de occlusieballon (***hoofdstuk 8***).

Hoofdstukken 6 en 7 lever dwingend bewijs van een lage intra en inter verwachte waarnemersveranderlijkheid wanneer het analyseren van OCT gegevens en geeft verder geldigheid van OCT als zowel klinisch als onderzoekhulpmiddel. Verder, is OCT nu integraal aan een aantal berechtingen van volgende generatie drug-uitwassende stents (DES) (***hoofdstuk 10 en 11***).

Klinische toepassingen - Coronaire stents

Veel van wat momenteel gekend betreffende stent veiligheid is heeft zich gebaseerd op studies gebruikend angiografische of IVUS in toevoeging aan informatie die tijdens het postmortale. In de laatstgenoemden, is het gebrek aan endothelial dekking nochtans getoond om een krachtige voorspeller van stent trombose te zijn.

In de LEADERS OCT vsub-studie, 46 patiënten willekeurig verdeeld om of biolimus-A9 (BES) of sirolimus stents (SES) in een `alle-bezoeker' te ontvangen geduldige bevolking met zeer weinig uitsluitings criteria met volledigere weefseldekking in patiënten die aan BES wordt toegewezen zoals die met SES wordt vergeleken (***hoofdstuk 10***). Het effect van dit verschil op klinisch resultaat en, in het bijzonder, op het risico van recente stent trombose, moet nog worden bepaald nochtans verder zullen de studies met nog langere angiografische en OCT follow-up helpen nuttig inzicht geven.

Hoofdstuk 14 vergeleek de directe OCT bevindingen van 4 verschillende DES bij complexe coronaire letsels. Verder, in een afzonderlijke studie van 20 het overlappen DES (10 patiënten, 661 struts) onmiddellijk na inplanting, geïdentificeerda OCT 42% struts waren malapposed in het

overlappende gebied (***hoofdstuk 12***). In toevoeging OCT een vleiende weergave modaliteit zijn wanneer het onderzoeken van stent breuk (***hoofdstuk 15***), absorptie van biologisch afbreekbaar magnesium stents (***hoofdstuk 18***) en in gevallen van zeer recente stent trombose (***hoofdstuk 19***).

Klinische toepassingen - atherosclerotic plaquebeoordeling

De scherpe coronaire syndromen met inbegrip van myocardiaal infarct leiden doodsoorzaken, die vaak door breuk van 'vulnerable plaque' (VP). In ***hoofdstuk 21***, OCT gebruikt om beklaagde en verre coronaire letsels te beoordelen en te onderzoeken of intra-coronaire OCT in levende patiënten, konden visualiseren eigenschappen verbonden aan VP in postmortale studies. In ***hoofdstuk 22***, OCT werden naast andere intra-coronaire kenmerkende technieken in een uniek proefonderzoek gebruikt om het vermogen voor atherosclerotic plaqueopsporing te vergelijken.
In een studie van 103 coronaire vertakkingen van 30 patiënten, OCT en IVUS-VH werden gebruikt en werden gevonden dat er een tendens die van TCFA in de proximale segmenten van de vertakking in vergelijking met distale segmenten voorkomt (***hoofdstuk 24***).

Toekomstige richtingen

De ontwikkeling van een nieuwe generatie van OCT systemen met de snellere snelheden van de beeldaanwinst en grotere aftastendiepten, zonder verlies van essentiële detail en resolutie, is een belangrijke vordering in intravasculair OCT. Eerder dan het gebruiken van een breedband lichtbron zoals in conventionele tijd-domein OCT systemen, Fourier-Domein OCT (FD-OCT) wenden de weergavesystemen een nieuwe golflengte-geveegde laser aan als lichtbron (***hoofdstuk 25***).

Conclusies

De huidige thesis heeft het werk omvat dat tijdens een zeer opwindende periode voor interventionalcardiologie als discipline wordt ondernomen. OCT heeft intense rente in interventie cardiologie. Zijn toepassing op de beoordeling van coronaire stents is begroet met sterk enthousiasme. De verbeteringen in aanwinstensnelheden met zullen FD-OCT ook de techniek minder procedureel eisend als zo bekwaam om op veel meer centra zijn van toepassing geweest maken, daardoor blijvend zowel een zeer belangrijk hulpmiddel in onderzoeker en interventie cardiologie.

Acknowledgments

The choice to embark on a career in interventional cardiology was not an easy one. Many factors played their part to eventually guide along the road. Having completed my medical and cardiology training in Melbourne, overseas post-graduate experience was desirable yet so competitive to achieve. It was one gorgeous day in Melbourne (August 2004) that as a Cardiology Registrar at the Austin Hospital, Melbourne, I was preparing the computer projector for an invited speaker who had come to Australia for the recent Cardiac Society Conference. It was Professor Carlo Di Mario who was giving our Department a talk on the optimal treatment of bifurcation lesions. Wow, I thought, Carlo Di Mario here in our humble hospital.

I was introduced to Carlo by the then Director of Cardiac Surgery, Professor Brian Buxton who asked me to accompany Carlo for a tour of our hospital. It was at this stage where I brazenly asked: "Any chance of undertaking an interventional fellowship with you Professor"? With so many similar requests from fellows world-wide, Carlo gave a very polite answer expressing how competitive the process was but of course to email him a CV.

Well, the 6 month period that followed consisted of numerous emails back and forth, with Carlo seeing some merit in this 'Australian' Fellow to help start the interventional fellowship program with him at the Royal Brompton Hospital. A visit to London cemented my position, which began in earnest in January 2005.

This was indeed an exciting period. My wife and I were relishing in the joys of parenthood with our first baby, Anthony born just 3 months before. Here we were as a family of three, travelling to London, away from the comfort and safety of home with a newborn. Carlo made it all that much easier. He had arranged our accommodation in a lovely flat in Battersea; only a stones throw away from the Royal Brompton, with the beautiful Battersea Park right opposite. He made our stay so welcoming.

The training was truly amazing. Here, I was exposed to the most complex procedures while being mentored by one of the most gifted interventionalists ever. During my fellowship I also had the privilege of making a true life-long friend, Jun Tanigawa. He too, had moved with his young family from Japan, driven by the passion to further his research career and was Carlo's 'right-hand man' when it came to intravascular imaging. It was at this time that I was fortunate to dabble with optical coherence tomography and see the ups and downs of the initial experience trying to obtain satisfactory images. This indeed was the first system to be used in the UK and of course, it was in Carlo's lab.

Days and nights were spent either in the cath lab or in the fellow's office at the Brompton. Weekends spent writing papers in front of the computer with young Anthony in my arms.

With Carlo's support and encouragement, an opportunity arose to join the team at the Thoraxcenter, Rotterdam. This indeed was an experience. Meeting Professor Patrick Serruys for the first time was an honour. He set out what we wanted to achieve in terms of furthering my work with OCT and introduced me to Dr Evelyn Regar who was instrumental at consolidating my interests and in-depth analysis of OCT and has been a strong foundation throughout the thesis as co-promoter. An enormous thank you must also go out to the committee members for their presence at this thesis, it is indeed an honour for me – Prof van der Giessen, Prof de Feyter, Prof Boersma, Prof Pattynama, Dr Balk, Prof Wijns, and of course, my promoters, Professors Serruys and Di Mario.

The course of my fellowship has also been enriched by the numerous friends I have made along the way. Co-fellows at the Royal Brompton – Jun Tanigawa, Kostas Dimopoulos, Giuseppe Ferrante, Francesca Del Furia, Pablo Aguiar-Souto, Carl Schultz, Didier Locca and at the Thoraxcenter – Nieves Gonzalo, Hector Garcia-Garcia, Emanuele Meliga, Steve Ramcharitar, Yoshi Onuma and Neville Kukreja, just to name a few. The opportunity to also become involved in the functions of Cardialysis as a Core Lab was extremely valuable and I am grateful for the guidance of Gerrit van Es', Koen Commissaris and Marie-angèle Morel.

How can I also forget the wonderful Jurgen Ligthart, ever so passionate and devoted to his art of imaging. I am pleased I was also able to impart my enthusiasm for OCT onto you and I wait for the invitation to return for your OCT course! Another mate, Paul Cummins!. Well, I wait for you to come and visit Down Under for a Coldie! Along with the Prof, you have been the force behind EuroIntervention and I have no doubt that the journal will grow from strength to strength.

A big thank you must go out to Annet Louw and Willeke van der Bent who have been ever so supportive, especially once I returned back to Melbourne and had last minute requests for revised forms from the University. You both clearly spelt out the PhD requirements and guided me through each and every phase of the long (but rewarding) process.

Lastly, one cannot achieve and develop as an individual without the steadfast support and commitment of those close to them. My parents have worked tirelessly to devote themselves to giving me opportunities in life that they never had and for this, I am ever so grateful. My wife Kathy has been a tower of strength both to me and to our two lovely children Anthony and Zoe. Kathy, you encouraged me to embark on this 'often crazy' career and you sacrificed so much of yourself for our family. You are a true soul mate and companion in life. To Anthony, well, at time of writing, you are approaching the age of 4 and you are probably bored of daddy asking you to quieten down as I am '*writing my thesis*'. You too made a great sacrifice at such a young age of 3 months when mummy and daddy took you in the aeroplane, away from our loved ones in Melbourne. I hope what I have managed to achieve thus far will make you proud. Zoe, my beautiful little princess, you are now nearly 6 months and it is never more true than to say that all that we strive to achieve in life as parents is for our children.

Curriculum Vitae

Peter Barlis, MBBS, MPH, FESC, FCSANZ, FRACP

Date of birth: 28/02/1974
Place of Birth: Melbourne, Australia
Email: peter.barlis@gmail.com

Education & Appointments

1986-1991: Victorian Certificate of education (VCE) Northcote High School, Victoria, Australia

1992-1997: M.B.BS. University of Melbourne, Victoria, Australia

1999-2001: FRACP Trainee Internal Medicine & Cardiology, Austin Hospital, Australia

2002-2004: FRACP: Cardiology, Royal Australasian College of Physicians

2005: Australian Certificate of Civil Aviation Medicine (ACCAM), Monash University

2005-2006: Master of Public Health (MPH), Clinical Epidemiology, Biostatistics & Trial Design, Monash University, Department of Epidemiology & Preventive Medicine, Australia

2006-2008: Interventional Cardiology Fellowship, Royal Brompton Hospital, London, United Kingdom (Supervisor: Prof Carlo Di Mario)

2006-2009: Doctoral (PhD) Candidate, Erasmus University, Rotterdam, The Netherlands (Supervisors Prof P.W.J. Serruys & Prof C. Di Mario)

2008-present: Consultant Interventional Cardiologist, 185 Cooper St, Epping, 3076, Victoria, Australia

2008-present: RACP Regional Examiner, The Northern Hospital, 185 Cooper St, Epping, 3076, Victoria, Australia

2008-present: Fellow, The University of Melbourne, Faculty of Medicine, Dentistry and Health Sciences, Melbourne, 185 Cooper St, Epping, 3076, Victoria, Australia

Medical Licensure

Jan 1999 – Medical Practitioners Board of Victoria (MPBV), Australia – Full Registration Number: MPG300951

Jan 2006 – General Medical Council (GMC), United Kingdom – Full Registration Number: 6131732

Society Memberships

2008 Fellow of the Cardiac Society of Australia and New Zealand (FCSANZ)

2007 Fellow of the European Society of Cardiology (FESC)

2007 Member, European Association of Percutaneous Coronary Interventions (EAPCI)

2007 Member, British Cardiovascular Society (BCS)

2006 Member, British Cardiovascular Intervention Society (BCIS)

2006 Member, Medical Protection Society (MPS), United Kingdom

2005 Fellow, Royal Australasian College of Physicians (FRACP)

2004 Member, International Society for Adult Congenital Cardiac Disease

2003 Member, Internal Medicine Society of Australia (IMSA)

2003 Member, Australian Society for Medical Research (ASMR)

2002 Member, Australian Medical Association (AMA)

1998 Member, University of Melbourne Medical Society

Professional Background

Feb 1998 – Jan 1999: Internship, Austin Hospital, Victoria, Australia

Feb 1999 – Jan 2001: Resident, Departments of Cardiology, Nephrology, Intensive Care, Gastroenterology and Liver Transplantation, Oncology & Infectious Diseases, Austin Hospital, Victoria, Australia

Feb 2001 – Nov 2001: Internal Medicine & Cardiology Registrar, Department of Medicine, Austin Hospital & The Northern Hospital, Victoria, Australia

Nov 2001 – Jan 2002: Stroke & Vascular Registrar, Stroke Unit, The Northern Hospital, Victoria, Australia

Feb 2002 – Jan 2003: Elizabeth Austin Professorial Registrar, Advanced FRACP Trainee, Department of Medicine & Cardiology, Austin Hospital, Victoria, Australia

Feb 2003 – Jan 2005: Advanced Cardiology Registrar & Fellow, Department of Cardiology, Austin Hospital and The Northern Hospital, Victoria, Australia

Jan 2005 – Dec 2005: Consultant Physician, The Northern Hospital and Warringal Private Hospital, Victoria, Australia

Jan 2006 – March 2008: Honorary Clinical and Research Fellow, Department of Invasive Cardiology, Royal Brompton & Harefield NHS Trust, London, UK

April 2008-present: Consultant & Interventional Cardiologist, The Northern Hospital, Epping Victoria, Warringal Private Hospital, Heidelberg, Victoria, St Vincent's Private Hospital, Fitzroy, Victoria

List of Publications

Key Abstract Presentations

1. Locca D, Ferrante G, Bucciarelli-Ducci C, La Manna A, Grasso A, Prasad A, **Barlis P**, Pennell D, Kaski, J.C, Di Mario C. Abstract 6013: Troponin I, High sensitive C-reactive protein and Neopterin in Percutaneous Coronary Interventions: insight from Cardiac Magnetic Resonance Imaging. Circulation, Oct 2008; 118**:** S_1046. AHA Scientific Sessions, Nov 2008

1. **Barlis P**, Regar E, Dimopoulos K, van Geuns R, van de Giessen W, Ferrante G, Davies S, Gonzalo N, Serruys, P, Di Mario C. A randomized optical coherence tomography study of a biodegradable versus permanent polymer drug-eluting stent: A LEADERS Trial Sub-Study. Transcatheter Cardiovascular Therapeutics (TCT) Washington, October 2008.

2. **Barlis P**, Ramcharitar S, Redwood S, Tan, H.C, Dimopoulos K, O'Kane P, Sianos G, Kaplan S, Ferrante G, Regar E, Serruys P.W, Di Mario C. Long-term outcomes of bifurcation stenting using the culotte technique with drug-eluting stents. European Society of Cardiology (ESC) Congress, Munich, Germany, 2008

3. **Barlis P**, Del Furia F, Dimopoulos K, Tanigawa J, Ferrante G, Aguir-Souto P, Di Mario C. Comparison of an occlusive versus non-occlusive flush technique for imaging coronary arteries with optical coherence tomography. European Society of Cardiology (ESC) Congress, Munich, Germany, 2008

4. **Barlis P**, Dimopoulos K, Tanigawa J, Dzielicka E, Del Furia F, Ferrante G, Di Mario C. Reproducibility of intra-coronary optical coherence tomography derived measurements for stent strut apposition and tissue coverage. European Society of Cardiology (ESC) Congress, Munich, Germany, 2008

5. Gonzalo Lopez M.N, Serruys P.W, **Barlis P**, Ligthart J, Garcia-Garcia H.M, Regar E. Intra-coronary characterisation of atherosclerotic plaques using IVUS greyscale, IVUS radiofrequency data analysis, optical coherence tomography and intravascular magnetic resonance. European Society of Cardiology (ESC) Congress, Munich, Germany, 2008

6. **Barlis P**, Kaplan S, Dimopoulos K, La Manna A, Goktekin O, Tanigawa J, Di Mario C. Culotte versus T-stenting in bifurcation lesions: Immediate clinical and angiographic results and mid-term clinical follow-up. i2 Summit/ACC New Orleans 2007.

7. Kaplan S Kiris A, **Barlis P**, Gektekin O, Di Mario C. Management of coronary bifurcation lesions with drug eluting stents: single versus double stent techniques. European Society of Cardiology, 2007 - European Heart Journal (2007) 28 (Abstract Supplement), 326

8. Tanigawa J, **Barlis P**, Dimopoulos K, Dalby M, Moore P, Di Mario C. Strut malapposition in overlapping drug-eluting stents by optical coherence tomography. European Society of Cardiology (ESC) 2007

9. La Manna AG, Locca D, Goktekin O, **Barlis P**, Bucciarelli-Ducci C, Keenan N, Grasso A, Prasad SK, Pennell DJ, Di Mario C. Distal embolisation after percutaneous coronary intervention in stable and unstable angina: a prospective cardiovascular magnetic resonance and biomarkers study. European Society of Cardiology (ESC) 2007

10. Locca D, La Manna AG, Goktekin O, **Barlis P**, Bucciarelli-Ducci C, Prasad SK, Pennell DJ, Di Mario C. Myocardial injury following percutaneous coronary intervention in complex lesion: a Cardiovascular Magnetic Resonance imaging and cardiac marker study. European Society of Cardiology (ESC) 2007

11. Tanigawa, **Barlis P**, Di Mario C. Preliminary in-vivo experience of assessing stent strut apposition in complex lesions using Optical Coherence Tomography. TCT2006 Washington

12. Tanigawa J, **Barlis P,** Kaplan S, D Mario C. Drug eluting stent apposition in complex coronary lesions. CCT 2006 Kobe Japan

13. **Barlis P**, Horrigan MCG, Elis S, Chan RK, Wong MCG, Faroqoue O, Proimos G, Clark DJ. Treatment of unprotected left main coronary artery disease with drug eluting stents in patients at high risk for coronary artery bypass grafting. CSANZ Canberra 2006

14. van Gaal WJ, **Barlis P**, Lim C, Johns J, Horrigan M. Results of percutaneous coronary intervention in a consecutive group of patients with acute myocardial infarction. CSANZ Brisbane 2004

15. W.J. van Gaal, **Barlis P**, C. Lim, J. Johns, M. Horrigan. Use of aspirin prophylaxis in patients at risk of myocardial infarction. CSANZ Brisbane 2004

16. W.J. van Gaal, **Barlis P**, C. Lim, J. Johns, M. Horrigan. Rescue angioplasty following thrombolysis for acute ST elevation myocardial infarction. CSANZ Brisbane 2004

17. D.O Donnell, V. Nadurata, W .van Gaal, Chan B, **Barlis P**, H. Lim, A. Hamer, W. Mohammed, M. Horrigan. Local impact of MADIT II. CSANZ Brisbane 2004

18. **Barlis P**, MacIsaac R, Burrell LM. Optimising heart failure management in a metropolitan teaching hospital. National Congress for Medical Research, Melbourne 2003.

Book Editor

"Interventional Cardiology: Principles and Practice", Wiley-Blackwell publishing
Editors: Carlo Di Mario, George D. Dangas, Peter Barlis

Book chapters

1. Principles of intra-coronary optical coherence tomography
Peter Barlis, Jun Tanigawa, Patrick W. Serruys, Evelyn Regar
Chapter in "*Interventional Cardiology: Principles and Practice", Wiley-Blackwell* publishing
Editors: Carlo Di Mario, George D. Dangas, Peter Barlis

2. Novel intravascular imaging technologies
Hector M. Garcia-Garcia, Nieves Gonzalo, Peter Barlis, Patrick W. Serruys
Book chapter in: "*Imaging in Clinical Management*" Jones and Bartlett Publishers, Inc
Editors: Stephen J. Nicholls and Stephen Worthley.

3. Percutaneous coronary interventions for complex lesions (ostial and bifurcation lesions, left main lesions)
Savio D'Souza, Peter Barlis, Giuseppe Ferrante, Carlo Di Mario
Book chapter in: "Cardiovascular Interventions in Clinical Practice" Blackwell
Editors: Jürgen Haase, Hans-Joachim Schäfers, Horst Sievert and Ron Waksman.

Peer reviewed journals

1. **Barlis P**, Del Furia F, Ferrante G, Dimopoulos K, Aguiar-Souto P, D' Souza S, Di Mario C. Comparison of an occlusive versus non-occlusive technique in the acquisition of intra-coronary optical coherence tomography imaging. *EuroIntervention, In Press, 2009*

2. **Barlis P,** Di Mario C, Prati F, Buellesfeld L, Rieber J, Dalby M, Gonzalo N, Ferrante G, Cera M, Grube E, Serruys P.W, Evelyn Regar. A multi-centre evaluation of the safety of intracoronary optical coherence tomography. *EuroInterv.* In Press 2009.

3. **Barlis P**, Regar E, Serruys P.W, Dimopoulos K, van der Giessen W.J, van Geuns R.J, Ferrante G, Wandel S, Windecker S, van Es G.A, Eerdmans P, Jüni P, Di Mario C. An Optical Coherence Tomography Study of a Biodegradable versus Durable Polymer-Coated Limus-Eluting Stent: A LEADERS Trial Sub-Study. *European Heart Journal, in Press, 2009*

4. Moore P, **Barlis P**, Spiro J, Roughton M, Isley C, Di Mario C, Kharbanda R, Dalby M. A Randomised Optical Coherence Tomography Study of Coronary Stent Strut Coverage and Luminal Protrusion with Rapamycin-Eluting Stents. *JACC Cardiovascular Interventions, In Press, 2009*

5. **Barlis P**, Ramcharitar S, Redwood S, Tan H.C., Dimopoulos K, Kaplan S, O'Kane P, Sianos G, Ferrante G, Regar E, Serruys P.W., Di Mario C. Long-term outcomes of bifurcation stenting using the culotte technique with drug-eluting stents. *EuroInterv. In press 2009*.

6. **Barlis P**, Dimopoulos K, Tanigawa J, Dzielicka E, Ferrante G, Del Furia F, Di Mario C. Quantitative analysis of intracoronary optical coherence tomography measurements of stent strut apposition and tissue coverage. *Int J Cardiol* 2009.

7. Gonzalo N, Garcia-Garcia HM, Regar E, **Barlis P**, Wentzel J, Onuma Y, Ligthart J, Serruys PW. In Vivo Assessment of High-Risk Coronary Plaques at Bifurcations With Combined Intravascular Ultrasound and Optical Coherence Tomography. *J Am Coll Cardiol Img* 2009;2:473-482

8. **Barlis P**, van Soest G, Serruys PW, Regar E. Intracoronary optical coherence tomography and the evaluation of stents. *Expert Rev Med Devices* 2009;6:157-167

9. **Barlis P**, Schmitt JM. Current and future developments in intracoronary optical coherence tomography imaging. *EuroIntervention* 2009;4:529-533

10. Ghimire G, Spiro J, Kharbanda R, Roughton M, **Barlis P**, Mason M, Ilsley C, Di Mario C, Erbel R, Waksman R, Dalby M. Initial evidence for the return of coronary vasoreactivity following the absorption of bioabsorbable magnesium alloy coronary stents. *EuroIntervention* 2009;4:481-484

11. Lee W, Profitis K, **Barlis P**, Van Gaal WJ. Stroke and Takotsubo cardiomyopathy: Is there more than just cause and effect? *Int J Cardiol* 2009

12. Aguiar-Souto P, Ferrante G, Del Furia F, **Barlis P**, Khurana R, Di Mario C. Frequency and predictors of contrast-induced nephropathy after angioplasty for chronic total occlusions. *Int J Cardiol* 2008.

13. **Barlis P**, Di Mario C, van Beusekom H, Gonzalo N, Regar E. Novelties in cardiac imaging- optical coherence tomography (OCT). *EuroIntervention* 2008;4:C22-6

14. **Barlis P**, Dimopoulos K, Di Mario C. Letter by Barlis et al regarding article, "Two-year clinical outcomes with drug-eluting stents for diabetic patients with de novo coronary lesions. Results from a real-world multicenter registry. *Circulation*, 2008;118(18):e679

15. **Barlis P**, Serruys P.W. Gonzalo N, van de Giessen W, de Jaegere P, Regar E. Assessment of Culprit and Remote Coronary Narrowings Using Optical Coherence Tomography with Long-Term Outcomes. *Am Journal Cardiol.* 2008;102:391-5.

16. Ferrante G, Locca D, **Barlis P**. Effectiveness of drugs for contrast induced nephropathy. *Ann Intern Med.* 2008;149:214-5.

17. **Barlis P**, Serruys P.W, Devries A, Regar E. Optical coherence tomography assessment of vulnerable plaque rupture: predilection for the plaque 'shoulder'. *Eur Heart J* 2008;29:2023.

18. **Barlis P**, Ferrante G, Del Furia F, De' Souza S, Di Mario C. In-vivo characterisation of coronary atherosclerosis with optical coherence tomography. *Med J Aust.* 2008;188:728

19. Tanigawa J, **Barlis P**, Dimopoulos K, Dalby M, Moore P, Di Mario C. The influence of strut thickness and cell design on immediate apposition of drug-eluting stents assessed by optical coherence tomography. *Int J Cardiol* 2008.

20. Ferrante G, Cosentino N, **Barlis P**, Niccoli G. Association of adiponectin with adverse outcome in coronary artery disease patients: results from the AtheroGene study. *Eur Heart J* 2008;29:1922-3

21. Gonzalo N, Serruys PW, **Barlis P**, Ligthart J, Garcia-Garcia HM, Regar E. Multi-modality intra-coronary plaque characterization: A pilot study. *Int J Cardiol* 2008.

22. **Barlis P**, Sianos G, Ferrante G, Del Furia F, D'Souza S, Di Mario C. The use of intra-coronary optical coherence tomography for the assessment of sirolimus-eluting stent fracture. *Int J Cardiol* 2008.

23. Sianos, **Barlis P**, Di Mario C, Papafaklis M, Büttner J, Galassi A.R, Schofer J, Werner G, Lefevre T, Louvard Y, Serruys P.W, Reifart N. European experience with the retrograde approach for the recanalisation of coronary artery chronic total occlusions. A report on behalf of the EuroCTO club. *EuroIntery.*2008;4:84-92

24. **Barlis P**, Kaplan S, Dimopoulos K, Tanigawa J, Schultz C, Di Mario C. An indeterminate occlusion duration predicts procedural failure in the recanalization of coronary chronic total occlusions. . *Catheter Cardiovasc Interv.* 2008;71:621-628.

25. **Barlis P**, Di Mario C. Retrograde approach to recanalising coronary chronic total occlusions immediately following a failed conventional attempt. *Int J Cardiol.* 2008.

26. **Barlis P**, Kaplan S, Dimopoulos K, Ferrante G, Di Mario C. Comparison of Bare Metal and Sirolimus or Paclitaxel-Eluting Stents for Aorto-Ostial Coronary Disease. *Cardiology*; 2008: 111:270-276.

27. Di Mario C, **Barlis P**. Optical Coherence Tomography: A new Tool to Detect Tissue Coverage in Drug Eluting Stents. *J Am Coll Cardiol Intv.* 2008; 1: 174-175

28. Tanimoto S. Granillo R.G, **Barlis P**, de Winter S, Bruining N, Hamers R, Knappen M**,** Verheye S, Serruys P.W, Regar E. A Novel Approach for Quantitative Analysis of Intracoronary Optical Coherence Tomography. High inter-observer agreement with computer-assisted contour detection. *Catheter Cardiovasc Interv.* 2008;72:228-35.

29. Kaplan S, **Barlis P**, Kiris A, Dimopoulos K, Celik S, Di Mario C. Immediate procedural and long-term clinical outcomes following drug-eluting stent implantation to ostial saphenous vein graft lesions. *Acute Card Care* 2008;10:88-92.

30. Tanigawa J, **Barlis P**, Dimopoulos K, Di Mario C. Optical Coherence Tomography to Assess Malapposition in Overlapping Drug-Eluting Stents. *EuroInterv.*2008;3:580-583.

31. Tanigawa J, **Barlis P**, Di Mario C. Heavily Calcified Coronary Lesions Preclude Strut Apposition despite High Pressure Balloon Dilatation and Rotational Atherectomy: In-vivo Demonstration with Optical Coherence Tomography. *Circ J. 2008; 72: 157-60.*

32. Kaplan S, **Barlis P**, Tanigawa J, Goktekin O, Di Mario C. Unconventional treatment of aorto-ostial instent restenosis with marked protrusion into the aorta. *J Cardiovasc Med (Hagerstown).* 2008; 9:184-6.

33. **Barlis P**, Virmani R, Sheppard M, Tanigawa J, Di Mario C. Angiographic and histological assessment of successfully treated late acute stent thrombosis secondary to a sirolimus-eluting stent. *Eur Heart J.* 2007;28:1675

34. **Barlis P**, Wong MCG, Clark DJ. Stenting of unprotected left main coronary artery stenosis. *Heart Lung Circ* 2007; 16 Suppl 3:S34-8.

35. Di Mario C, **Barlis P**, Tanigawa J, Locca D, Bucciarelli-Ducci C, Kaplan S, Katoh O. Retrograde approach to coronary chronic total occlusions: Preliminary single European centre experience. *EuroInterv.* 2007. 3:181-187.

36. Kaplan S, **Barlis P**, Dimopoulos K, Tanigawa J, La Manna A, Di Mario C. Culotte versus T-stenting in bifurcation lesions: Immediate clinical and angiographic results and mid-term clinical follow-up. *Am Heart J* 2007;154:336-43.

37. **Barlis P**, Tanigawa J, Di Mario C. Coronary Bioabsorbable Magnesium Stent: 15 Month Intravascular Ultrasound and Optical Coherence Tomography Findings. *Eur Heart J.* 2007; 28:2319.

38. **Barlis P**, Horrigan, MCG, Elis, S, Chan, RK, Wong, MCG, Farouque, OM, Proimos, G, Clark, DJ. Treatment of unprotected left main disease with drug-eluting stents in patients at high risk for coronary artery bypass grafting. *Cardiovasc Revasc Med.* 2007; 8:84-9.

39. Tanigawa J, **Barlis P,** Dimopoulos K, Di Mario C. Stent strut apposition of cypher select and Taxus Liberte: A prospective optical coherence tomography study. *J Am Coll Cardiol.* 49:35B-35B.

40. **Barlis P**, Di Mario C. Still a future for the bare metal stent? *Int J Cardiol.* 2007; 121: 1- 3.

41. van Gaal, W, Clark DJ, **Barlis P**, Lim C, Johns J, Horrigan MCG. Results of Primary Percutaneous Coronary Intervention in a Consecutive Group of Patients with Acute ST Elevation Myocardial Infarction at a Tertiary Australian Centre. *Int Med J*. 2007;37:464-71

42. **Barlis P,** Lim E, Gow P, Seevanayagam S, Calafiore P, Chan RK. Giant Cardiac Myxoma. *Heart Lung Circ.* 2007;16:389-91.

43. **Barlis P**, Tanigawa J, Di Mario C. The use of drug eluting stents for coronary artery disease. *Controversies and Consensus in Imaging and Intervention.* 2007; Feb 20.

44. Tanigawa J, **Barlis P**, Di Mario C. Do unapposed stent struts endothelialise? In-vivo demonstration with Optical Coherence Tomography. *Heart* 2007; 93:378.

45. **Barlis P**, Tanigawa J, Di Mario C. Successful crossing of an angulated lesion using a new deflectable tip guidewire (Steer-IT™). *J Invasiv Cardiol.* 2007; 19:E154-5.

46. Tanigawa J, **Barlis P**, Di Mario C. Intravascular optical coherence tomography: optimisation of image acquisition and quantitative assessment of stent strut apposition. *EuroIntery.* 2007;3:128-136.

47. Dimopoulos K, Di Mario C, **Barlis P,** Pennell D, Goktekin O, Kaddoura S, Gatzoulis M. Haemodynamic Significance of an Anomalous Right Coronary with Inter-arterial Course Assessed with Intracoronary Pressure Measurements during Dobutamine Challenge. *Int J Cardiol* 2008;126:e32-5

48. Goktekin O, Kaplan S, Dimopoulos K, **Barlis P**, Tanigawa J, Akif Vatankulu M, Koning G, Tuinenburg J, Di Mario C. A New Quantitative Analysis System for Evaluation of Coronary Bifurcation Lesions: Comparison with Current Conventional Methods. *Catheter Cardiovasc Interv.* 2007; 69:172-80.

49. Denholm, J. T, **Barlis, P**. Blood donation and myocardial infarction. *Int J Cardiol.* Jan 19; 2007.

50. Locca DA, La Manna AG, Goktekin O, Tanigawa J, Keenan N, Wage R, **Barlis P**, Bucciarelli C, Pennell DJ, DiMario C. Distal embolization after percutaneous coronary intervention in stable and unstable coronary syndromes. *Am J Cardiol.* 2007; 99:32F

51. **Barlis P**, Tanigawa J, Kaplan S, Di Mario C. Complex coronary interventions: unprotected left main and bifurcation lesions. *J Interv Cardiol.* 2006; 19(6):510-524

52. **Barlis P**, Brooks M, Hare DL, Chan RK. Subclavian artery occlusion causing acute myocardial infarction in a patient with a left internal mammary artery graft. *Catheter Cardiovasc Interv*. 2006; 68: 326-331.

53. Tanigawa J, **Barlis P**, Di Mario C. Stenting of the left main ostium. Importance of choosing an optimal angiographic view. *EuroInterv*. 2006; 6: e3-5.

54. **Barlis P**, Calafiore P, O'Donnell D. Angina from a right coronary artery to right atrial fistula. *Heart*. 2006 92: 342.

55. Denholm JT, **Barlis P.** Blood donation: the new cardiovascular risk factor? *Int J Cardiol.* 2006;106:410

56. **Barlis P**, Horrigan MC, Chan RK, Ajani AE, Proimos G, Schumer W, van Gaal WJ, Rowe M, Eccleston D, Yan BB, Mun Cheong Y, Oliver LE, Clark DJ. What is the best contemporary treatment for in-stent restenosis? *Cardiovasc Revasc Med.* 2005;6:179-81.

57. **Barlis P**, Macisaac R, Hare DL, Burrell LM. Optimizing heart failure management: An Australian experience. *Int J Cardiol.* 2005; 112:256.

58. **Barlis P**, James P, Sundaravingam AB, Coombs PR, Lim K. Internal carotid artery dissection: never too old. *Intern Med J*. 2004; 34:69-70.

59. **Barlis P**. Utility of the jugular venous pressure and a third heart sound in quantifying prognosis in heart failure. *J Intern Med Soc Aust & New Zealand*, Vol 1, 2; 19, 2002

60. **Barlis P**, Horrigan MCG, Elis S, Chan RK, Wong MCG, Faroqoue O, Proimos G, Clark DJ. Treatment of unprotected left main coronary artery disease with drug eluting stents in patients at high risk for coronary artery bypass grafting. *Heart Lung Circulation*. 2006; 15S1: S142-43

61. **Barlis P**, MacIsaac R, Burrell LM. Optimising heart failure management in a metropolitan teaching hospital. *Clinical and Experimental Pharmacology and Physiology*. 2003. 30: A31

Chapter 2 Colour Section

Figure 1: the mobile OCT cart incorporating the system console, monitor, and patient interface unit

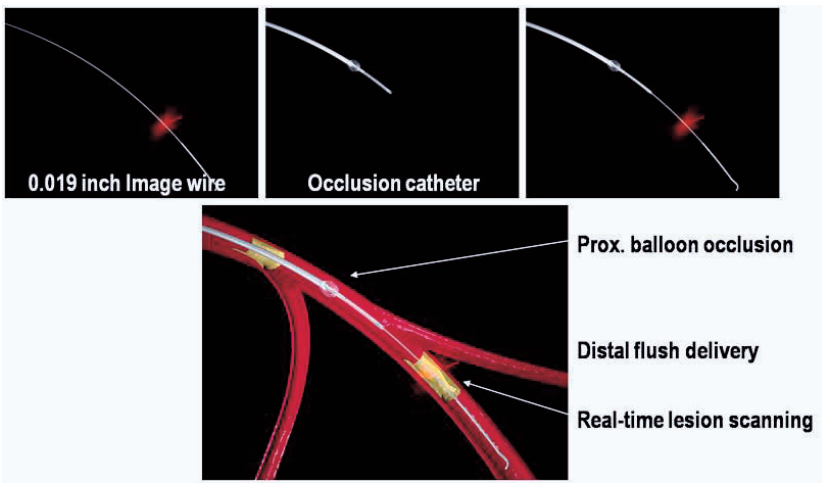

Figure 2: The OCT catheter and dedicated optical imaging wire (LightLab Imaging Inc., Westford, MA, USA) in current commercial use. The occlusion balloon is positioned proximal to the region of interest and the imaging wire is then inserted with real-time image acquisition performed at a rate up to 3 mm/sec

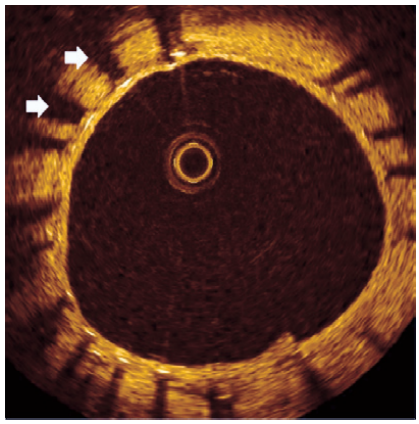

Figure 3 – This OCT cross-section shows a thin layer of tissue covering the stent struts. As infrared light is unable to penetrate the metal struts, shadowing results (arrows)

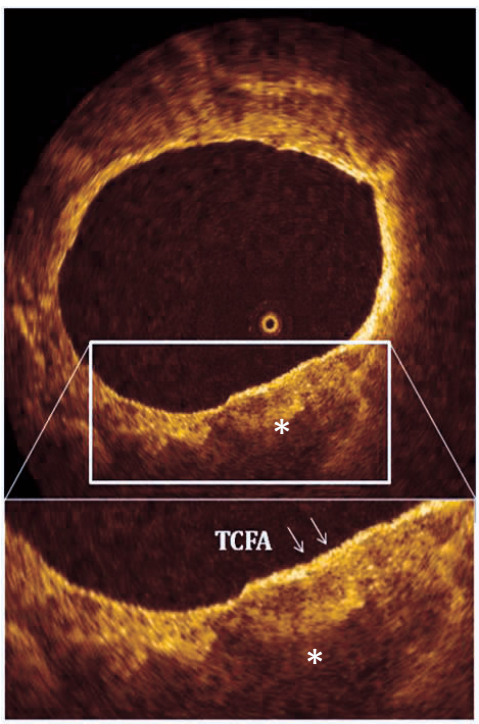

Figure 4: The OCT appearance of lipid-rich plaque and TCFA. This plaque has the typical characteristics of being poorly reflective with diffuse borders (*). The overlying thin fibrous cap is bright and highly reflective. The mean cap thickness was 44 microns.

Chapter 3

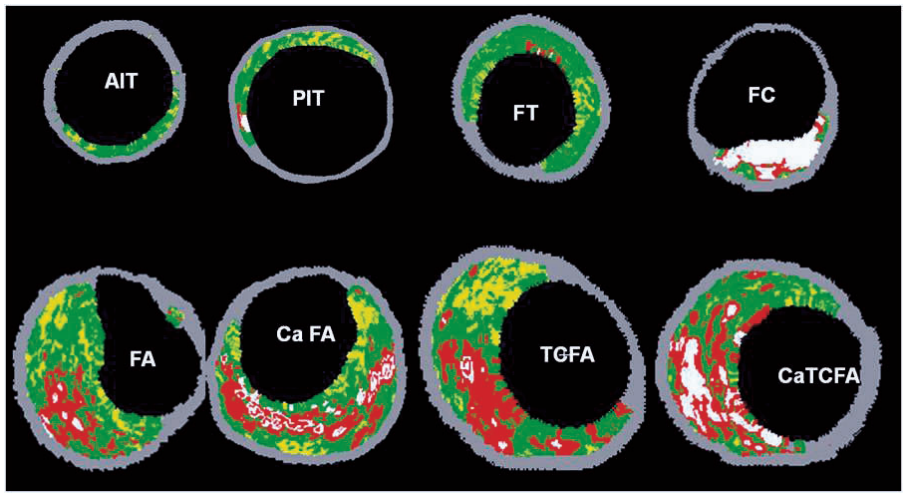

Figure 1. IVUS-Virtual histology proposed lesion types. AIT, adaptative intimal thickening; PIT, pathological intimal thickening; FT, fibrotic plaque; FC, fibrocalcific; FA, fibroatheroma;CaFA, calcified fibroatheroma; TCFA, thin-capped fibroatheroma.

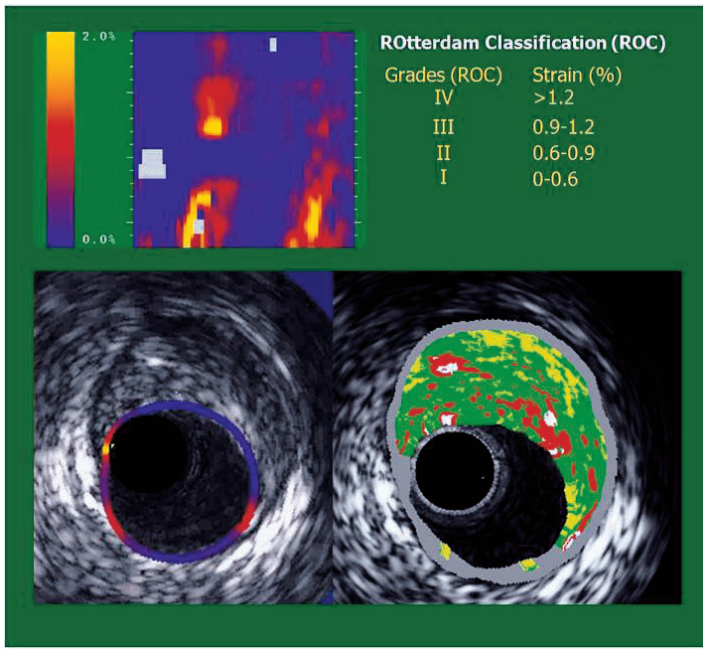

Figure 2. IVUS-palpography. In the upper left side the palpography strain map is opened up. The local strain is calculated from the gated radiofrequency traces using cross-correlation analysis and displayed, color-coded, from blue (for 0% strain) to red to yellow (for 2% strain). Plaque strain values are assigned a Rotterdam Classification (ROC) score ranging from 1 to 4 (ROC I= 0-<0.6 %; ROC II= 0.6- <0.9 %; ROC III= 0.9-<1.2 %; ROC IV= >1.2 %). At the bottom, in the same cross-sectional area a high-strain spot (ROC III) is shown (left); in the virtual histology (VH) image (right) a confluent necrotic core area in contact with the lumen is seen, suggesting an IVUS-derived thin capped fibroatheroma. The IVUS-VH color-code is fibrous tissue (green), fibro-fatty tissue (light green), necrotic core (red) and dense calcium (white).

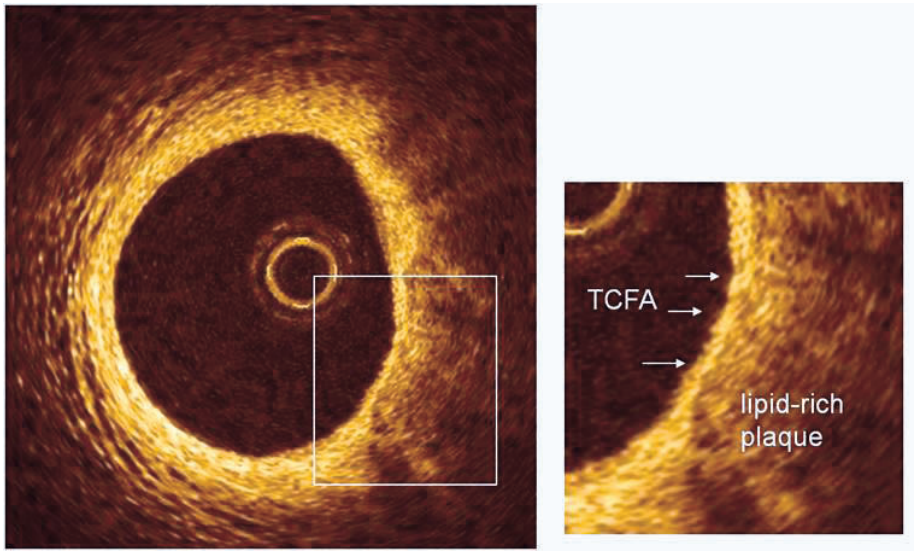

Figure 3: thin cap fibroatheroma visualised with OCT as a highly reflective thin band (arrows)

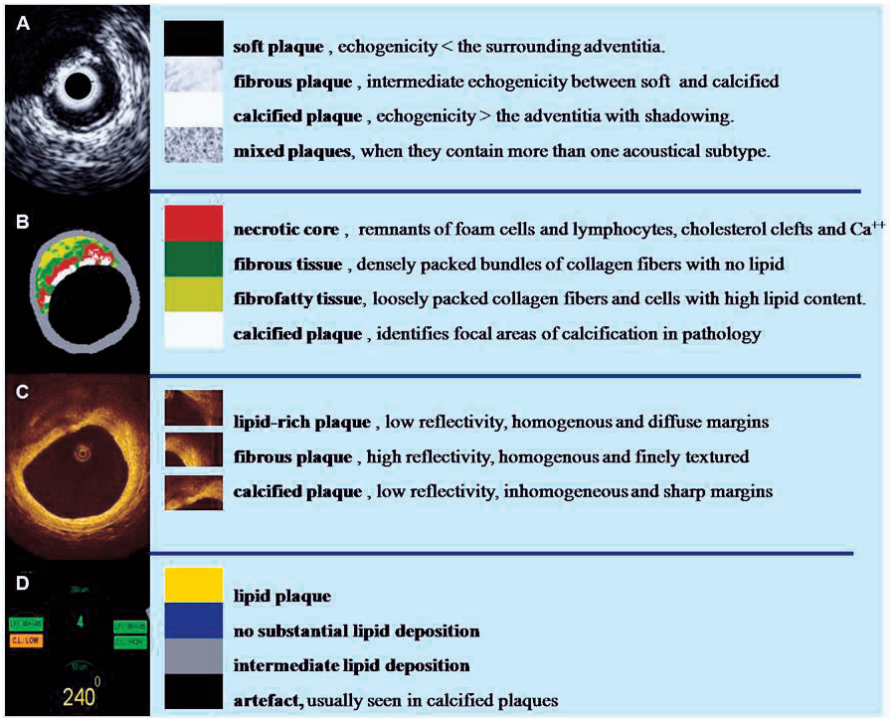

Figure 4. Multi-modality imaging in the coronary arteries. The same coronary segment (represented by one frame) has been imaged by 4 different imaging techniques. In the grey-scale IVUS (panel A), IVUS-virtual histology (panel B), optical coherence tomography (panel C) and intravascular magnetic resonance spectroscopy (IVMR) the results of the same frame across different techniques are shown. Of note, in the upper left quadrant of the plaque a calcified area is seen in three imaging modalities, but in IVMR where an artifact is observed. On the right hand side, the different plaque and tissues types across the coronary imaging techniques is shown.

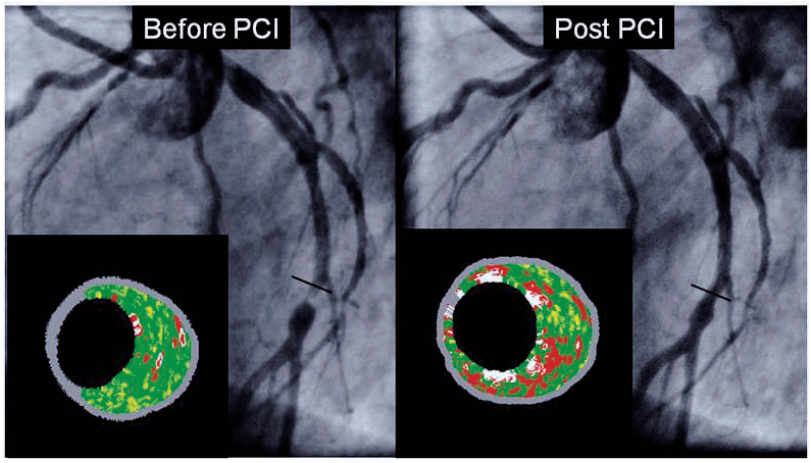

Figure 5. IVUS-virtual histology in stented segments. In the left hand side, a coronary angiogram of the left coronary system shows on the distal segment of the left circumflex artery an eccentric lesion. A pre-stenting virtual histology (VH) frame showed a fibrotic type of plaque (location of VH frame is indicated by a black line). On the right hand side, the post-stenting VH frame is depicted. Of note, at the lumen and surrounding areas an increase in the amount of "dense calcium" and "necrotic core" is observed. This is due to the presence of stent struts that are misclassified by VH. (percutaneous coronary intervention – PCI).

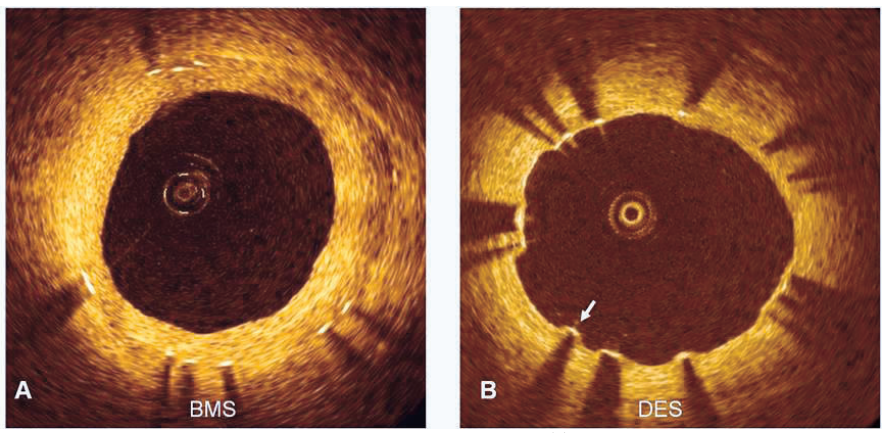

Figure 6: A: Demonstrates the optical coherence tomography (OCT) imaging of a bare metal stent 4 months following implantation. The circumferential tissue struts are visible with shadowing induced by the metal. The neointimal tissue measured between 140 and 220 microns in thickness
B: OCT imaging of a drug-eluting stent (DES) at 4 months follow-up showing the circumferential struts with a very thin neointimal layer (10-40 microns thick). The arrow indicates a strut with no visible tissue coverage

Chapter 7

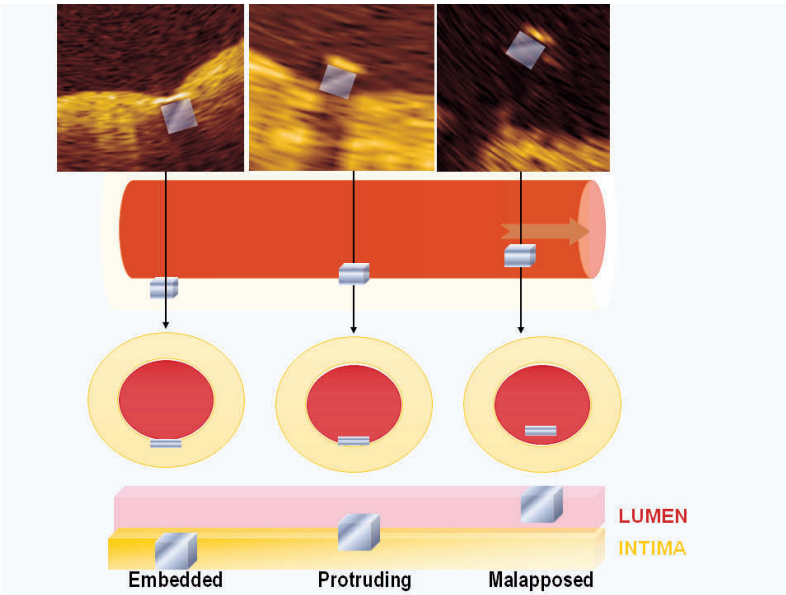

Figure 1 Optical coherence tomography classification of stent apposition into embedded, protruding or malapposed.

Chapter 9

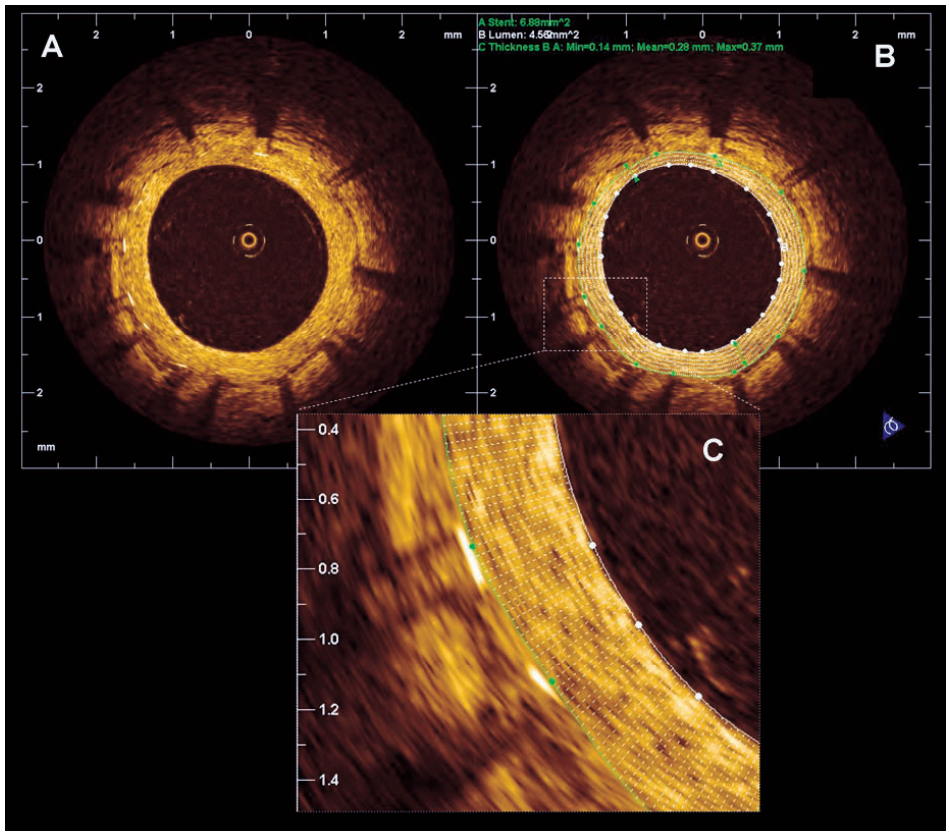

Figure 1: Tissue coverage measurement. A. Sirolimus eluting stent 9 months after stent implantation. B. The figure shows the lumen contour (white) and the stent contour (green). The tissue coverage area was calculated as stent area minus lumen area. The tissue coverage thickness was measured in 360 points (represented by the white chords). C. Magnification of 2 struts showing all the measurements (white chords) of the tissue coverage in front of every strut. For every strut the minimum, maximum and mean strut coverage was calculated.

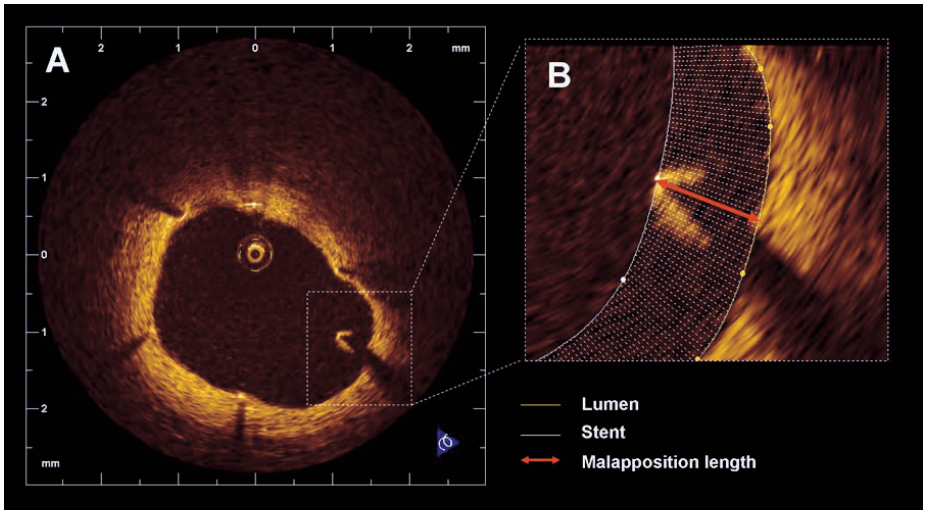

Figure 2: Malapposition. A. Example of a malapposed strut in a sirolimus eluting stent at 9 months follow up. **B**. Magnification of the malapposed strut. The yellow line represents the lumen contour and the white line corresponds to the stent contour. The distance from the endoluminal surface of the strut to the vessel wall (red arrow) was 440 μm (higher than the sum of the metal and polymer thickness for this type of stent).

Chapter 10

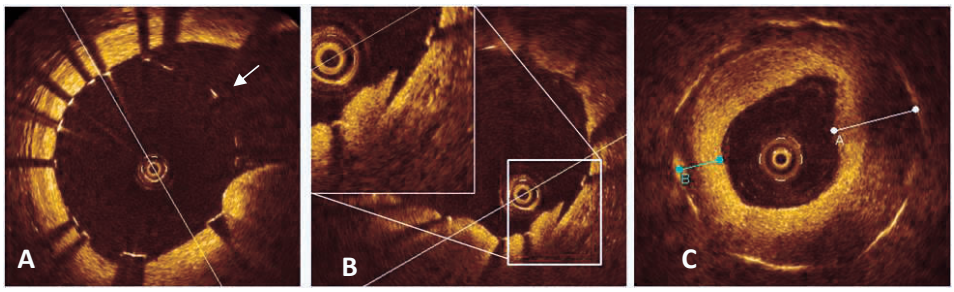

Figure 1 The application of optical coherence tomography (OCT) post-stenting. **A:** shows a stent immediately following implantation across a bifurcation. The struts at the carina are clearly seen to be malapposed (arrow) **B:** OCT cross section with magnification (insert, top left) showing a dissection flap immediately following *implantation of a stent* ***C:*** *Demonstrates significant intimal hyperplasia occurring 8 months following* stent implantation. The intimal tissue is seen to have a layered pattern with the endo-luminal aspect showing a bright, reflective and homogenous appearance in contrast to the layer abutting the stent struts which is seen to be poorly reflective. The thickness measured at the 2 points indicated was A-0.82mm and B-0.40mm

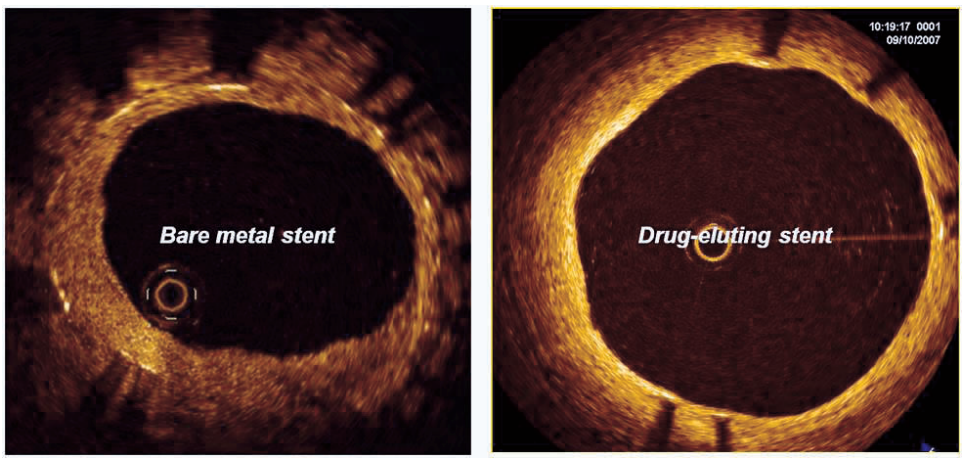

Figure 2 – Shows the contrasting amount of tissue covering struts in a bare metal (BMS) and drug-eluting stent (DES). The tissue thickness overlying the BMS measured between 0.14 and 0.42mm. In contrast, the DES was covered by a thin, concentric layer of tissue measuring 0.09mm.

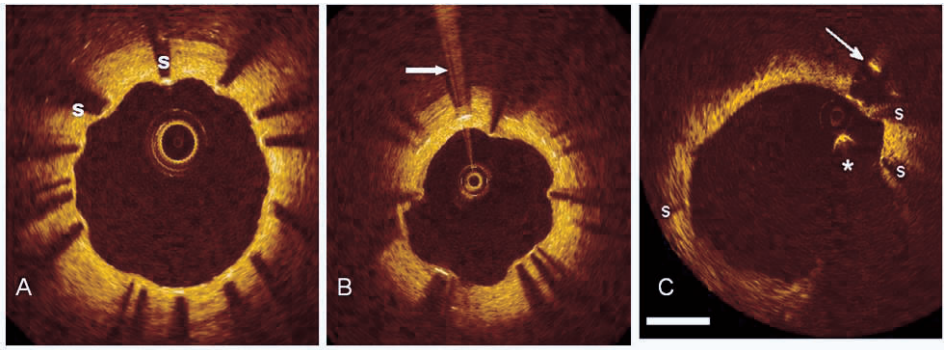

Figure 5 – A: Circumferential stent struts are shown covered by a thin layer of tissue. Dorsal shadowing is evident behind the stent struts (S) with only the luminal surface of the strut visible with OCT. **B:** demonstrates circumferential stent struts with shadowing and bright reflections caused by saturation of the detector registering the inferogram (arrow) **C:** Arrow indicates a double reflection between stent and catheter. This can occur if a stent strut is imaged face-on, and reflects the OCT beam specularly. Shadows of other stent struts are marked by s; stent struts that do not show up as the typical bright dot, but do cast a shadow, are imaged under an oblique angle. * is a guide wire artefact. White bar is 1 mm.

Chapter 11

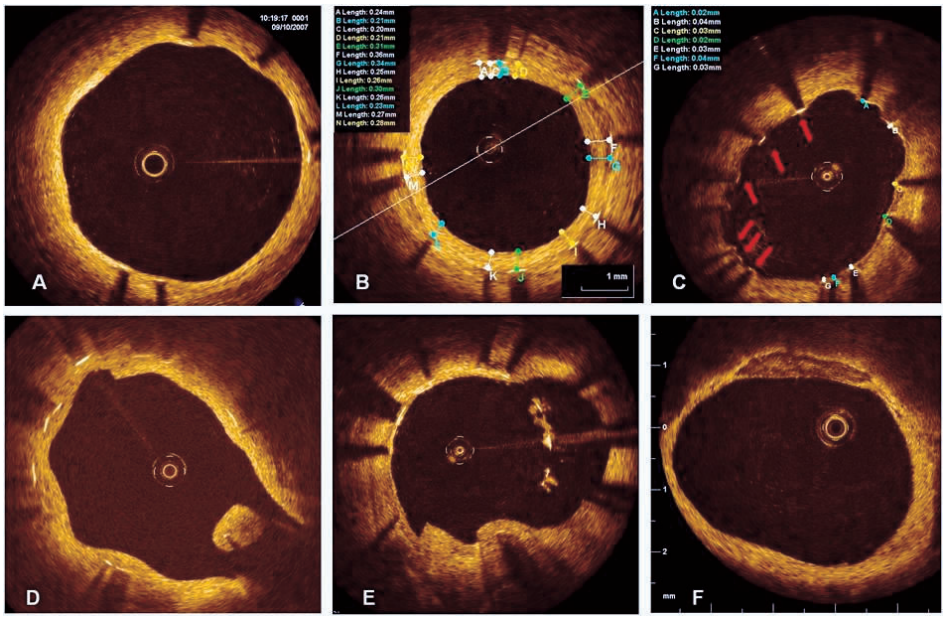

Figure 2: Examples of OCT findings

A. This 73 year old male received a biolimus-eluting stent (BES) 9 months prior to the right coronary artery. The stent is seen covered by a thin, uniform layer of tissue overlying all stent struts that are well apposed to the vessel wall.

B. Offline OCT analysis. A total of 14 stent struts are visible in this cross section with the observer having measured the thickness of tissue overlying each of the struts, expressed in the colored panel (top left) in mm. The mean neointimal thickness in this frame was 0.27mm (270μm).

C. Sirolimus-eluting stent (SES) struts are observed circumferentially. Struts between 7 and 11 o'clock are apposed but uncovered by tissue. Struts from 1 – 5 o'clock are observed covered with a very thin layer of tissue (mean thickness 0.03mm or 30μm). The stent was implanted in a patient who received 2 SES to the mid left anterior descending artery (LAD) 9 months prior following a presentation with a non-ST elevation myocardial infarction. He was asymptomatic at 9 month follow-up.

D. Nine month follow-up of a BES implanted in the LAD across the diagonal bifurcation. A solitary strut is observed (arrow) malapposed at the level of the carina. The strut was seen covered by a thick, uniform and homogenous tissue.

E. This OCT pullback frame from a 78 year-old male with prior stenting to the LAD/diagonal bifurcation with a SES. Struts are observed (1-3 o'clock) to be malapposed to the vessel wall with a heterogeneous tissue with different signal attenuations that may represent thrombotic material. The patient was asymptomatic at 9 month follow-up and on dual anti-platelet therapy.

F. Left main coronary artery OCT. This patient had a proximal LAD stent implanted 9 months prior. We extended the pullback beyond the stent into the left main coronary artery which demonstrates a well demarcated, non-flow limiting, low attenuation plaque (12 o'clock) consistent with calcium. Our sub-study exclusively used a non-occlusive technique for OCT imaging which requires pullback of the image wire during simultaneous flush of contrast via the guiding catheter. This is a significant advance over the traditional method of OCT imaging in which a proximally positioned balloon is inflated during image acquisition. Hence, ostial and proximal segments of coronary arteries were all able to be imaged thereby supporting the 'all comer' design of the LEADERS trial without any OCT anatomical exclusions.

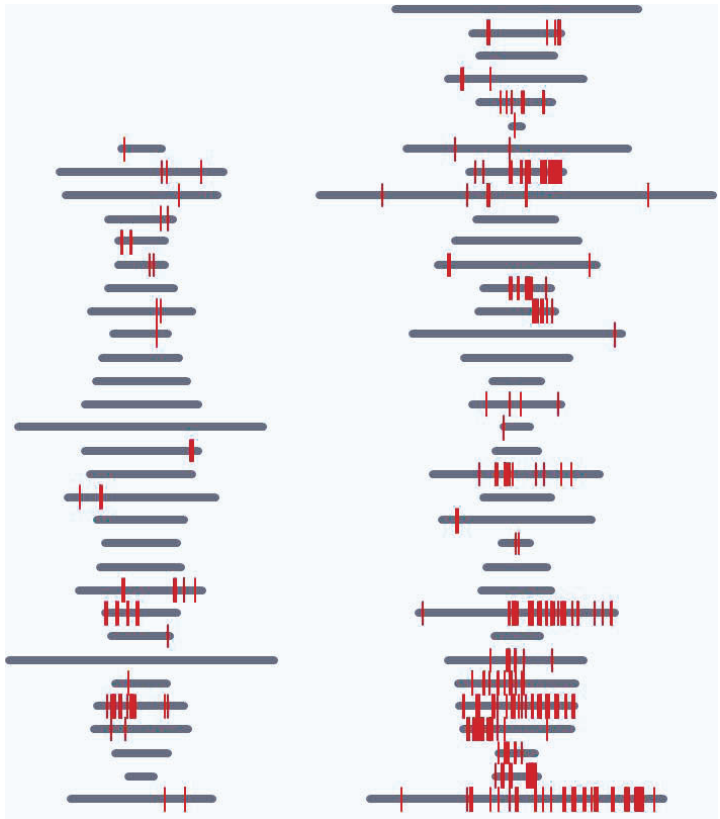

Figure 3: Graphical representation of stent coverage in lesions.

Grey horizontal bars represent lesions. Each uncovered strut is represented by a red line.

Chapter 12

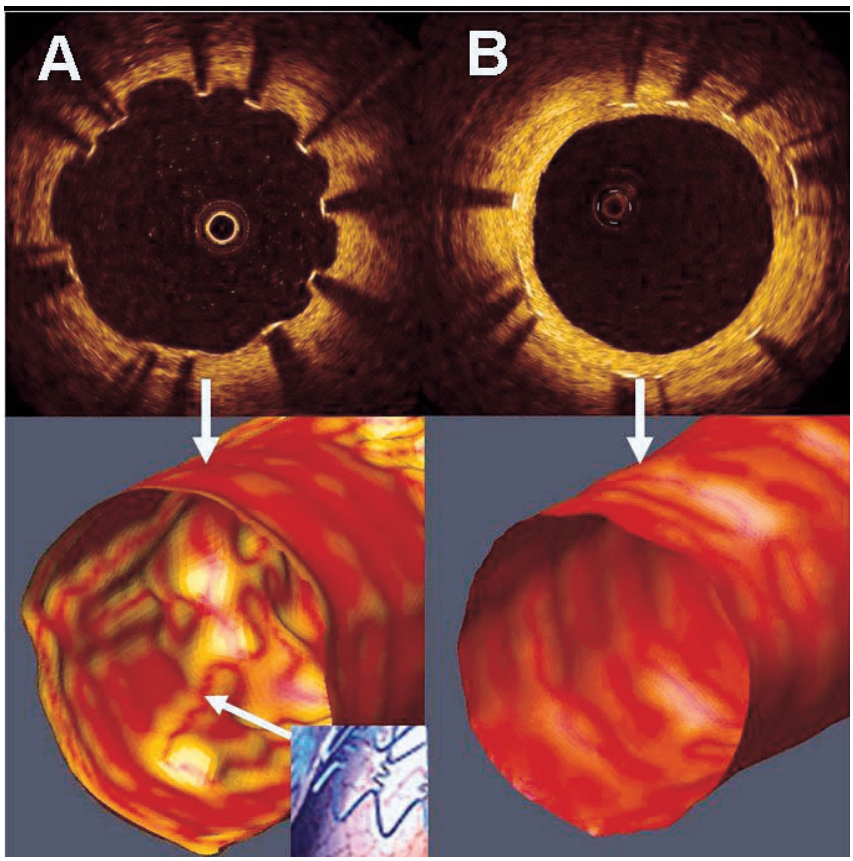

Figure 5: Representative 2-dimensional optical coherence tomography image of stent strut sections of an uncovered polymer rapamycin-eluting stent and a covered non-polymer rapamycin-eluting stent with paired 3-dimensional reconstructions and reference photograph of a polymer-coated rapamycin-eluting stent.

Chapter 16

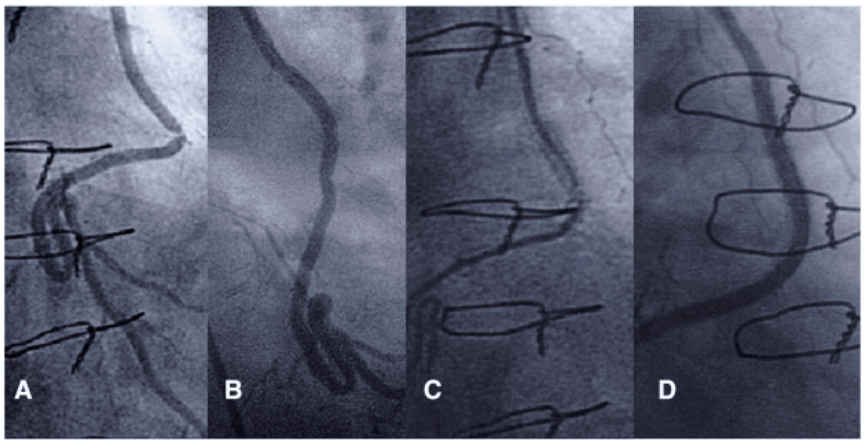

Figure 1 A: Illustrates the left internal mammary artery (LIMA) graft with a critical stenosis in the highly angulated mid-segment. B: Immediate angiographic appearance following pre-dilatation and implantation of two 3.5 mm bare metal Driver (Medtronic Inc., Minneapolis, US) stents. C: Angiography 12 months following initial stent implantation demonstrating critical in-stent-restenosis. D: Final angiographic result following treatment with a 3.5 × 33 mm sirolimus-eluting stent (SES).

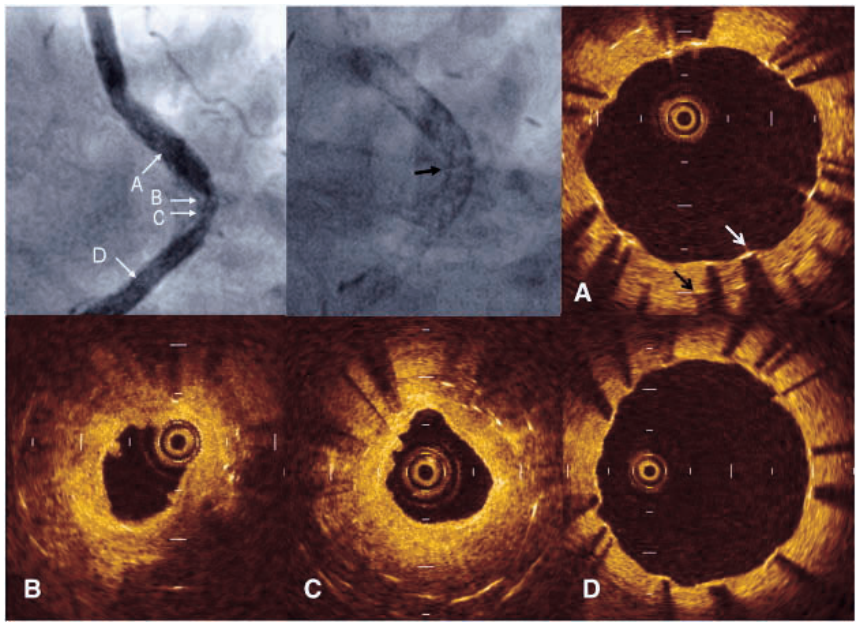

Figure 2 Two years following stenting, angiography confirmed a significant stenosis at the hinge point within the previously stented segment (black arrow). A: Optical coherence tomography (LightLab Imaging Inc., Westford, MA, USA) was acquired during simultaneous contrast flush through the guiding catheter at a pullback speed of 1 mm/s. This proximal cross-section shows 2 layers of stent struts coinciding with the previously deployed bare metal stent (black arrow) and the SES (white arrow). B–C: Imaging at the level of the stenosis reveals gross hyperplasia and almost complete obliteration of the lumen (minimal lumen area 0.71 mm^2) with absence of circumferential struts. D. OCT distal to the stenosis showed the struts of the SES were widely patent with thin coverage of neointimal tissue (10–30 μm).

Chapter 18

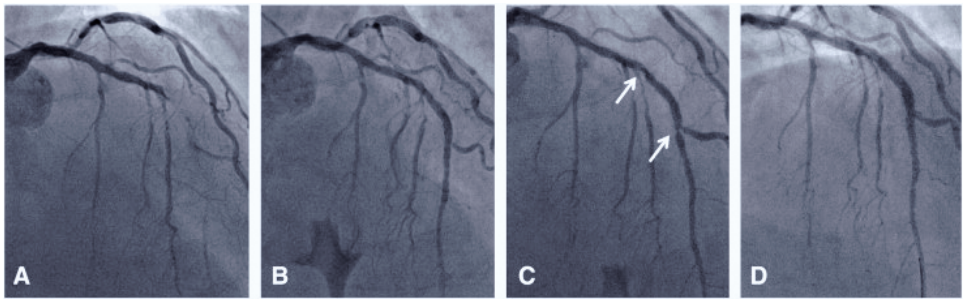

Figure 4. Antero-posterior cranial view showing the left anterior descending artery with significant stenosis in the mid-segment and diagonal branch. Immediately following implantation of 2 sirolimus-eluting stents. Nine-month follow-up angiography showed 2 sites of restenosis but no obvious fracture. Following high-pressure balloon dilatation and further stent implantation.

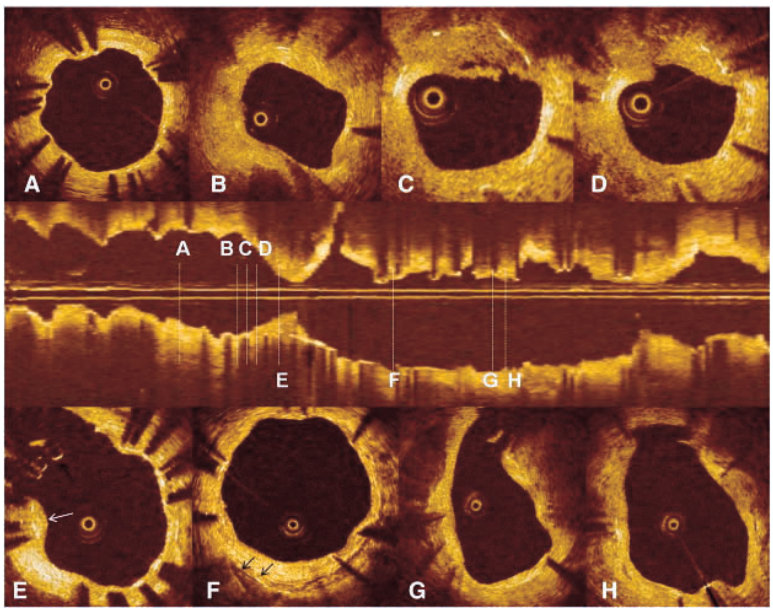

Figure 5. OCT demonstrating a widely patent stent with a thin layer of neointimal tissue. B–D: Shows the more distal lesion with significant luminal narrowing as a result of intimal hyperplasia. The cross-sections demonstrate the lack of circumferential stent struts and altered stent and vessel lumen geometry. E: Shows the OCT appearance at the level of the side branch. 3 stent struts are shown at the carina with no visible tissue coverage (black arrow) while the surround stent struts show an exaggerated intimal tissue response (white arrow). F: Demonstrates circumferential stent struts covered by a thin tissue layer. Also evident is a fibro-calcific plaque (black arrows) with its low reflective appearance and sharp margins. G–H: Shows the lack of circumferential stent struts resulting in considerable disruption of vessel and lumen geometry.

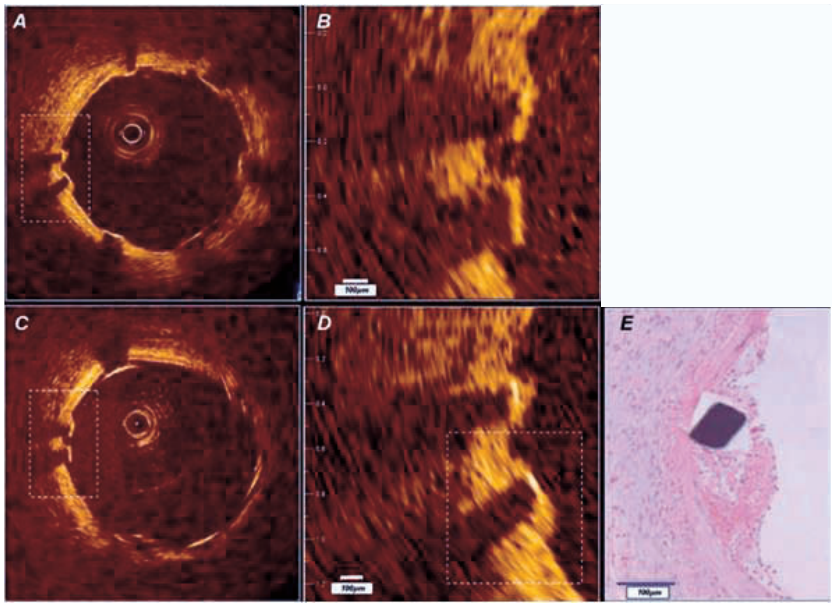

Figure 1. In vivo OCT (LightLab Imaging Boston, MA, USA) in a porcine coronary artery. A) Baseline OCT immediately after stent implantation shows adequate stent expansion and apposition of the struts against the normal coronary wall. B) Magnification demonstrating the stent strut vessel wall interface. C) Follow-up investigation at five days. The stent struts are clearly visible and show thin, bright reflective tissue coverage in the magnification D) Histology E) confirms the presence of a thin neointimal layer.

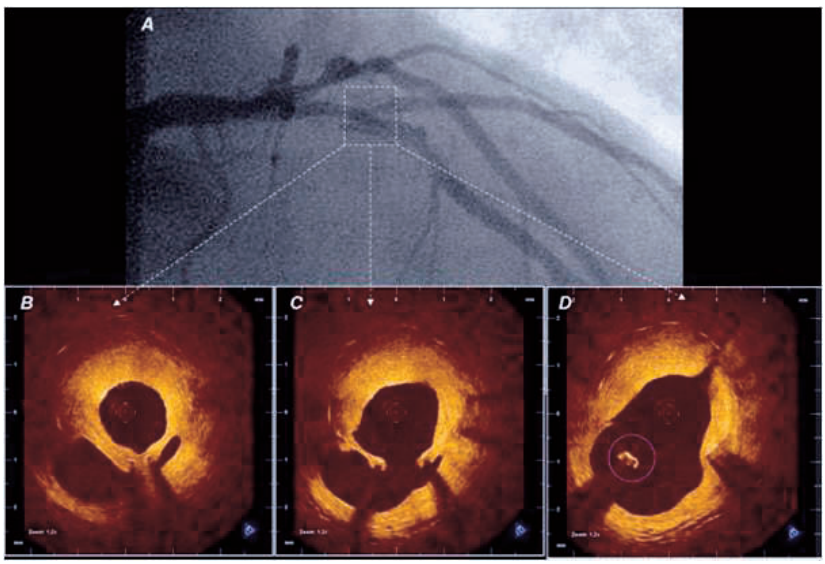

Figure 2. In vivo OCT (LightLabImaging™, Boston, MA, USA) in the LAD in a patient presenting with in-stent restenosis. A) The coronary angiogram shows a lumen narrowing within the stent that is covering the second diagonal branch. OCT visualises the complex coronary anatomy in great detail. The stent is covered by a thick neointima that shows a layered appearance with a bright, highly reflective luminal layer, an intermediate layer and a dark, signal poor layer surrounding the struts (B). The diagonal take off can be clearly seen (C) as well as a stent strut that is "floating" in the carina (D).

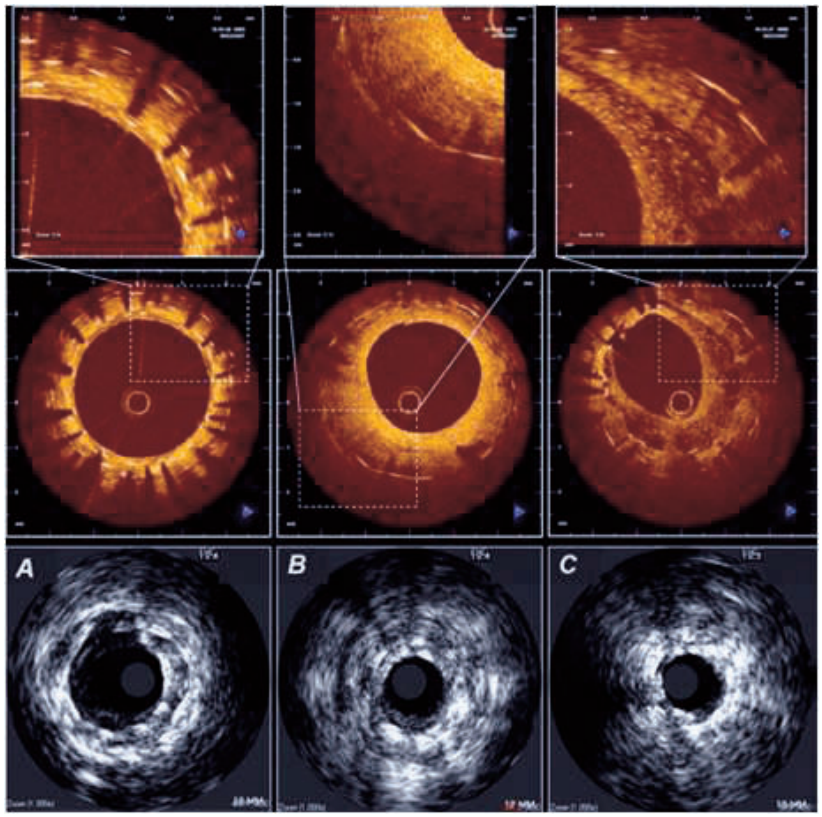

Figure 3. Demonstrates the information that can be gathered from IVUS (20Mhz, lower panels) and from OCT imaging (mid and upper panels, LightLabImaging™, Boston, MA, USA) in patients at follow-up after stent implantation. These are corresponding cross sections within a stent, imaged by both, OCT in the upper panels and by IVUS in the lower panels. The images represent the same spots within a coronary artery (A, B, C), and illustrates the different quality of information that can be obtained by OCT as compared to conventional grey scale IVUS. A) Three layers of stents can be seen. OCT is able to clearly visualise the individual stent struts, the neointimal layers separating the different stents and the very thin coverage of the most inner, luminal stent struts. B) a bright, eccentric and relatively thick neointimal layer can be seen C) an eccentric thick neointimal layer is visible, however, the structure of this neointima differs considerably from the example B) with a low-reflective and speckled appearance.

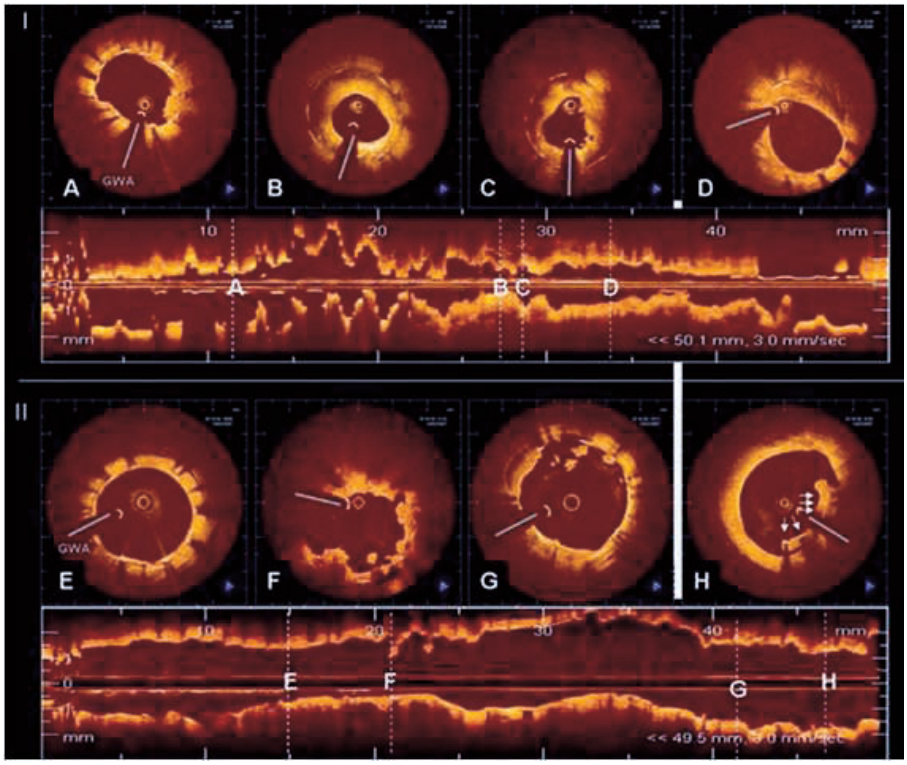

Figure 4. OCT (LightLab Imaging Boston, MA, USA) findings in two patients presenting with late drug-eluting stent (DES) thrombosis. OCT was performed in both cases immediately after thrombus aspiration and reveals completely different morphologic findings, possible suggesting two different mechanisms for late stent thrombosis, focal restenosis and incomplete strut coverage. I) Patient with late stent thrombosis three months after DES implantation in the left circumflex artery. OCT reveals an adequately expanded stent, all struts are well apposed against the vessel wall. All struts show tissue coverage, which is more pronounced in the proximal portion of the stent (D) as compared to the distal stent portion (A). There is focal in-stent restenosis (B, C) with severe lumen narrowing (MLA 1.63 mm2). The neointima shows a layered appearance with a luminal bright, highly reflective layer, an intermediate layer and a dark, signal poor layer surrounding the struts. Remnants of the thrombus are focally seen focally as irregular mural structures, protruding into the lumen (A, C). II) Patient with very late stent thrombosis four years after DES implantation in the left anterior descending artery. OCT reveals an adequately expanded stent, however, there is incomplete stent strut apposition at the proximal stent edge with incomplete tissue coverage in 21% of struts. (E) The distal stent portion, shows a well expanded and apposed stent with thin tissue coverage by OCT. F) irregular lumen borders with intraluminal remnants of the thrombus. G) proximal stent portion showing a strut without visible tissue coverage in 12 o'clock position and thrombus fragments in the lumen. H) proximal stent edge with incomplete apposition of five stent struts (arrows) against the vessel wall. The distance to the vessel wall is 200 micron. OCT shows tissue around the stent struts (DD thrombus, neointima). GWA: guidewire artefact.

Chapter 20

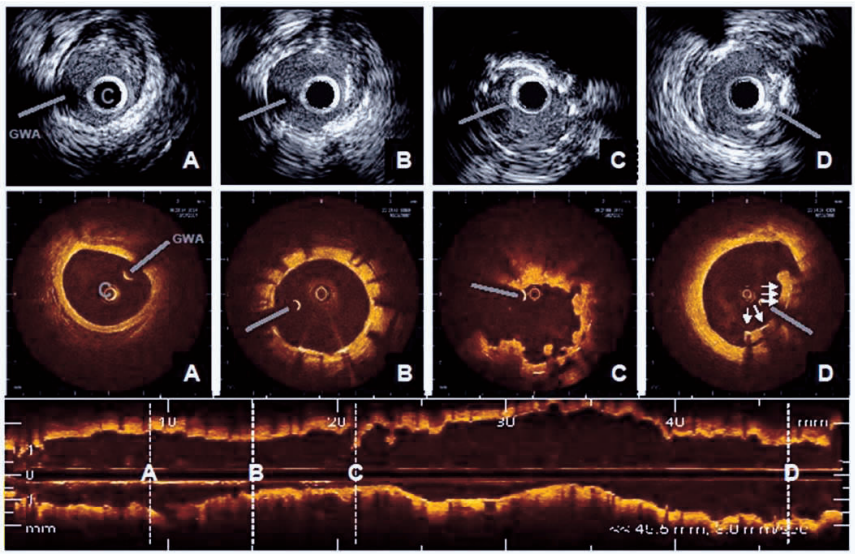

Figure 2: Intracoronary imaging after thrombus aspiration. Upper panels: IVUS (Atlantis, Boston Scientific, Natick, MA), lower panels: OCT (LightLab Imaging™, Boston, MA; cross sectional and longitudinal view) A) distal reference showing eccentric plaque in 11-4 o'clock position. B) distal stent portion, showing a well expanded and apposed stent with thin tissue coverage by OCT that is missed by IVUS. C) irregular lumen borders with intraluminal remnants of the thrombus D) proximal stent edge with incomplete apposition of 5 stent struts (arrows) against the vessel wall. The distance to the vessel wall is 200µm. OCT shows tissue around the stent struts (DD thrombus, neointima). Incomplete stent apposition may be caused initial malapposition or acquired malapposition caused by a vascular response to the stent. GWA= guide wire artefact; C= catheter artefact.

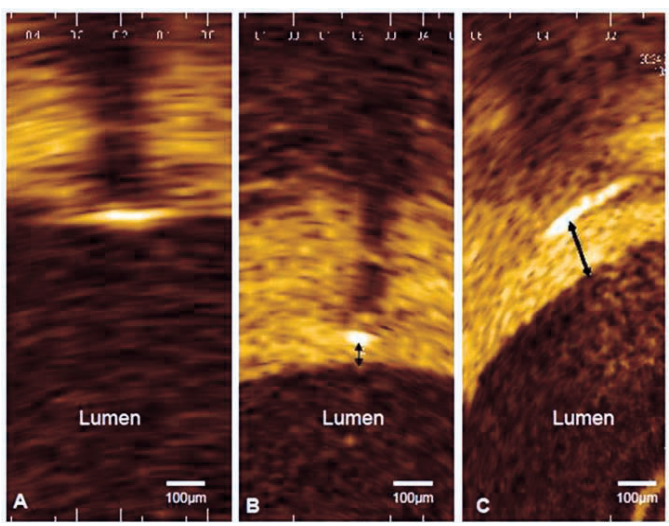

Figure 3: Spectrum of tissue coverage as seen by OCT in this stented segment. Tissue coverage was not visible in 21% (n=110) of the struts, while 79% (n=411 of 521) of the struts showed tissue coverage of various thickness. A) no visible coverage B) very thin coverage (40µm) C) maximal coverage (140 µm).

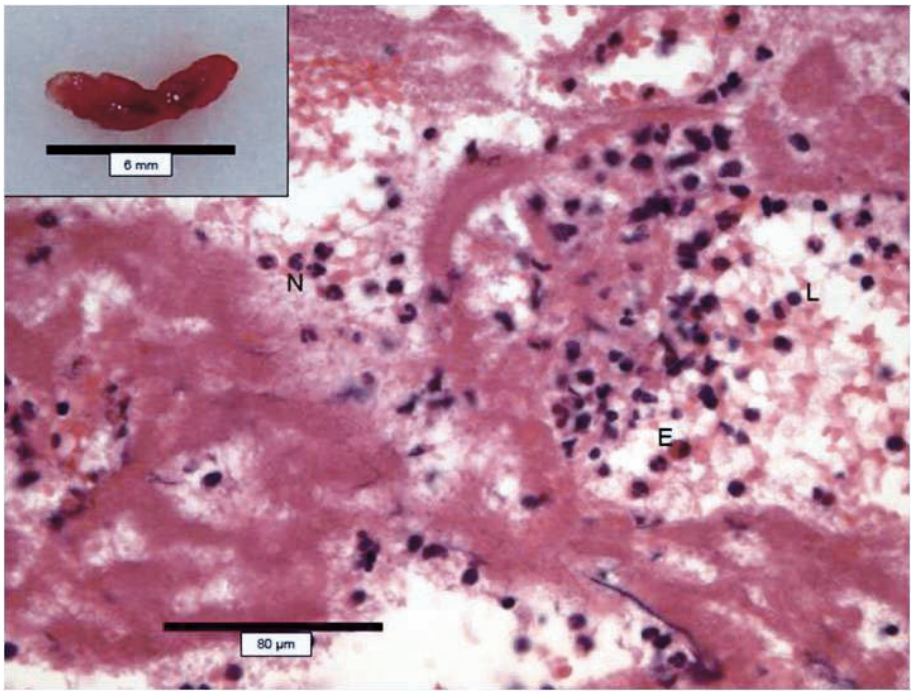

Figure 4: Histology of the aspirated thrombus: recent multilayered thrombus showing Zahn lines and containing abundant leukocytes consisting of eosinophils (E), neutrophils (N) and lymphocytes (L).

Chapter 22

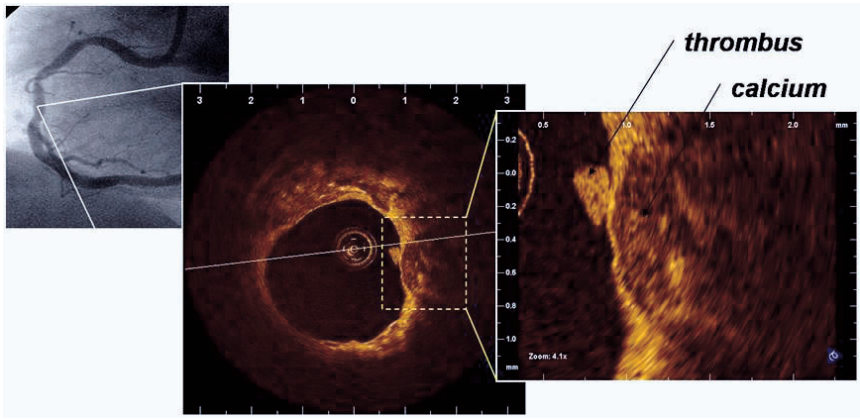

Figure 1: Angiography demonstrating a calcific mid-vessel lesion. A further calcific plaque with sharp and well-delineated margins was also observed by OCT remote and distal to the culprit lesion with attached mural thrombus

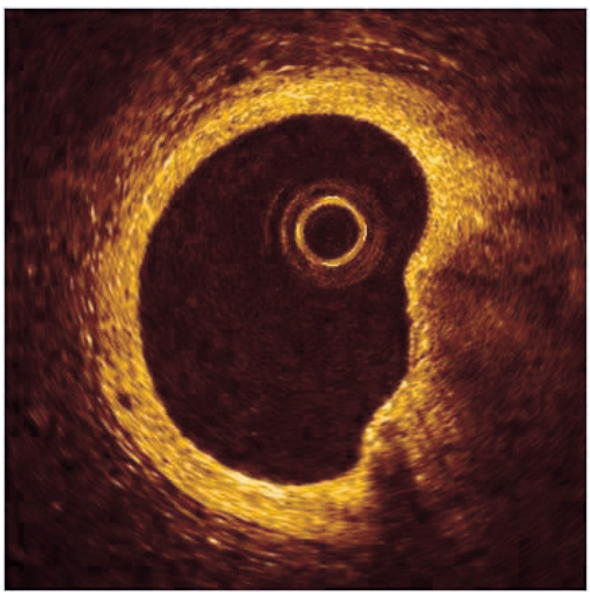

Figure 2: Thin-cap fibroatheroma (TCFA) assessed by OCT overlying a large lipid-rich plaque (2-5 o'clock position). The bright, highly reflective fibrous cap measured between 30-80 microns

Chapter 23

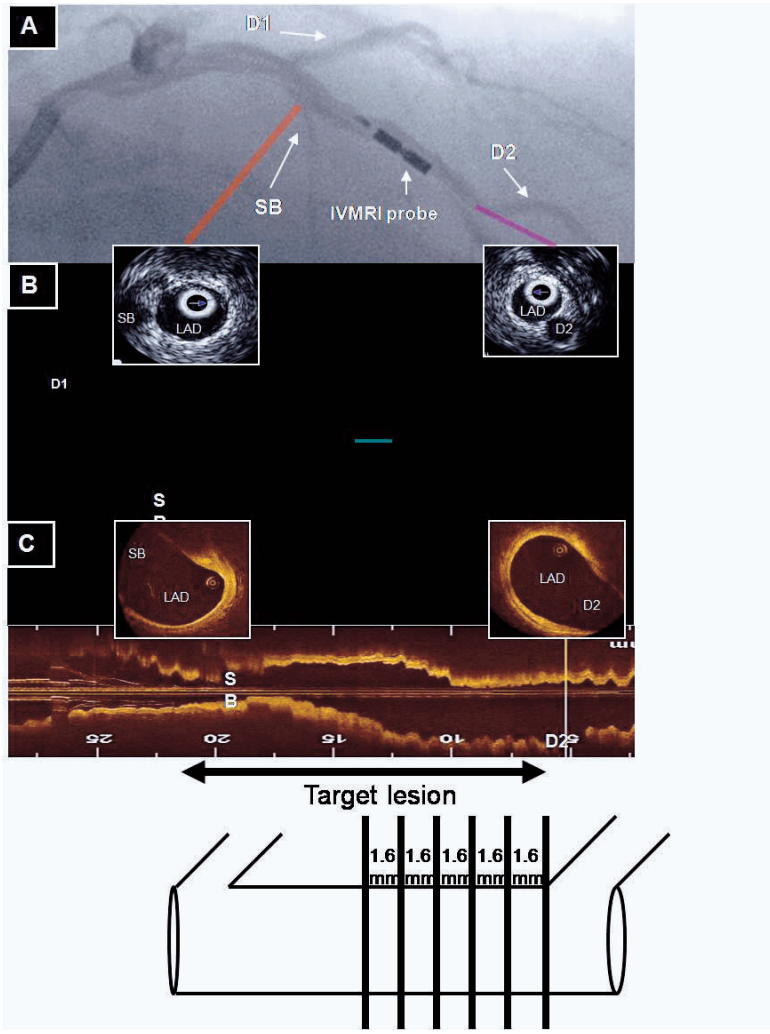

Figure 1. Matching of the OCT and IVUS pullbacks. The position of the IVUS, Optical Coherence Tomography (OCT) and Intravascular Magnetic Resonance Spectroscopy (IVMR) probe along the vessel was filmed before and after each acquisition (A). The "matching" of the region of interest in the IVUS (B) and OCT (C) pullback was based on the presence of anatomical landmarks (e.g. side branches visible in the longitudinal and cross-sectional views). To determine the longitudinal position of the IVMR probe in the vessel, a side branch was used as a marker. From the landmark to the proximal part of the vessel one frame every 1.6 mm was selected. D1: first diagonal, D2: second diagonal, SB: septal branch, LAD: left anterior descendent coronary artery. CS: cross section.

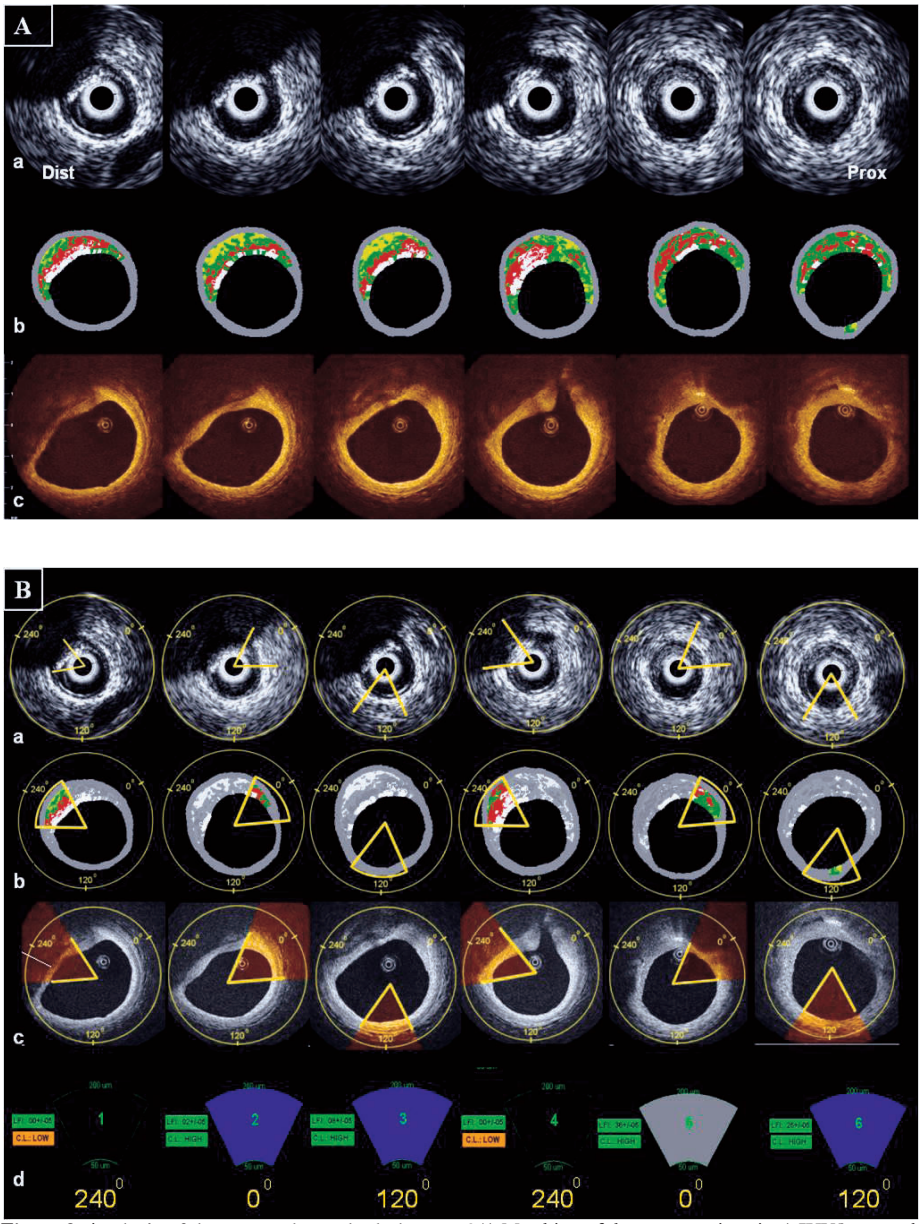

Figure 2. Analysis of the targeted matched plaques. 2A) Matching of the cross sections in a) IVUS greyscale b) IVUS Radiofrequency Data Analysis and c) Optical Coherence Tomography pullbacks. 2B) Analysis screen. After matching corresponding cross sections based on their longitudinal orientation, the region of interest is defined according to the orientation of the Intravascular Magnetic Resonance probe towards the vessel wall. The figure illustrates the results of the six target matched plaques (60 degrees sector) analyzed in one patient. Prox: proximal Dist: distal.

Chapter 24

Panel Legend A. Angiography in the right cranial view demonstrated stenosis in the mid left anterior descending artery (LAD) involving both small diagonal branches. The previously implanted LAD stent proximally was widely patent. The region corresponding to the optical coherence tomography (OCT) images is shown with the black arrow. **B-C**. Intravascular OCT (LightLab Imaging, Westford, Massachusetts, US) was acquired using a non-occlusive technique with a 3.0mm/sec pullback. OCT clearly demonstrated the presence of a lipid-rich plaque in the 6 to 9 o/clock position characterized by low reflectivity, speckled appearance with diffuse margins. This was covered with a bright rim of fibrous tissue corresponding to thin-cap fibroatheroma (TCFA). Mural thrombus was evident in all OCT cross-sections. The TCFA measured 20 microns thick and was found to be ruptured at each of the two shoulders of the plaque (arrows).

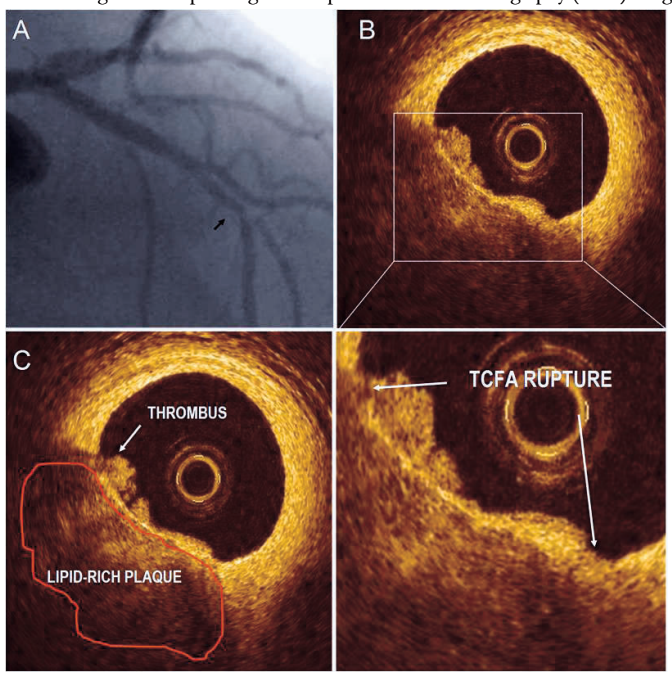

Chapter 25

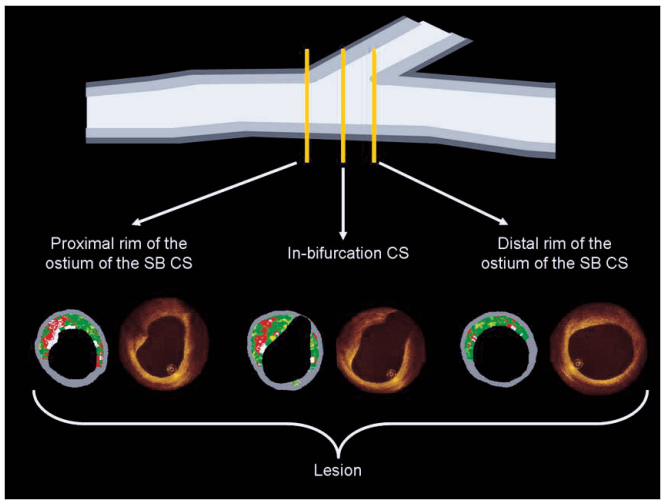

Figure 1: Bifurcation selection and analysis
Bifurcations that could be identified in both IVUS-VH and OCT pullbacks were included. A strict selection of the analyzed cross sections was followed to ensure correct matching between the two techniques. Plaques were analyzed only in the main branch. The lesion analysis included: i. proximal rim of the ostium of the side-branch cross section (first frame proximal to the take-off of the side-branch); ii. in-bifurcation cross section (frame with the larger ostial diameter of the side-branch) and iii. distal rim of the ostium of the side-branch cross section (first frame distal to the take off of the side-branch) SB: side-branch CS: cross section.

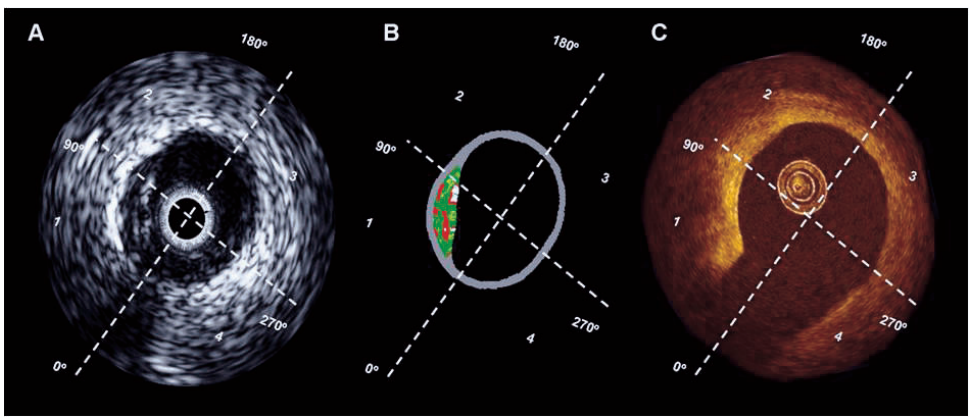

Figure 2: Location of the plaque in relation to the flow divider. To describe the plaque location in relation to the flow divider, the vessel cross section was divided in 4 quadrants according to the position of the side-branch. Quadrants 1 and 4 correspond to the ostium of the side-branch while quadrants 2 and 3 correspond to the part of the vessel wall located in front of the ostium of the side-branch. A: greyscale IVUS, B: virtual histology, C: optical coherence tomography.

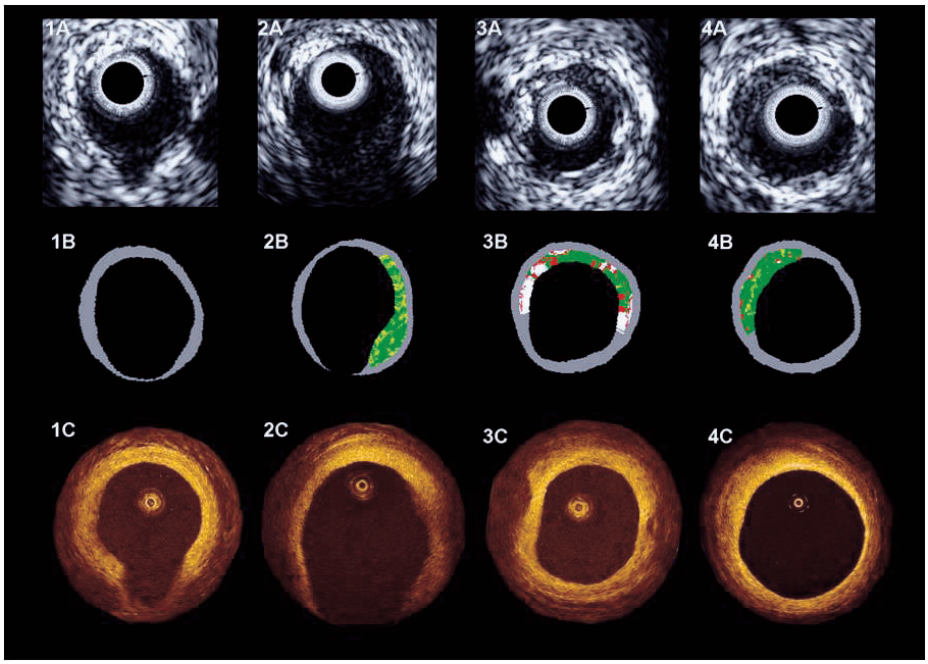

Figure 4: Low-risk plaques. Matched images of greyscale IVUS (A), virtual histology (B) and optical coherence tomography (C) for the 4 types of plaques considered of low-risk. 1: adaptive intimal thickening, 2: pathological intimal thickening, 3: fibrocalcific plaque 4: fibrotic plaque.

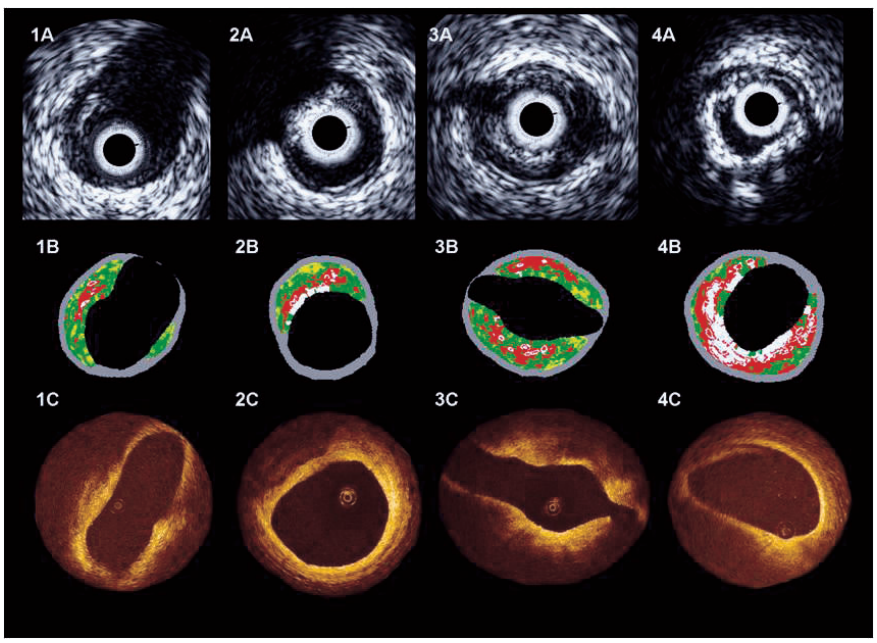

Figure 5: High-risk plaques. Matched images of greyscale IVUS (A), virtual histology (B) and optical coherence tomography (C) for the 4 types of plaques considered at high-risk of rupture. 1: fibroatheroma, 2: calcified fibroatheroma 3: thin-cap fibroatheroma 4: calcified thin-cap fibroatheroma.

Chapter 26

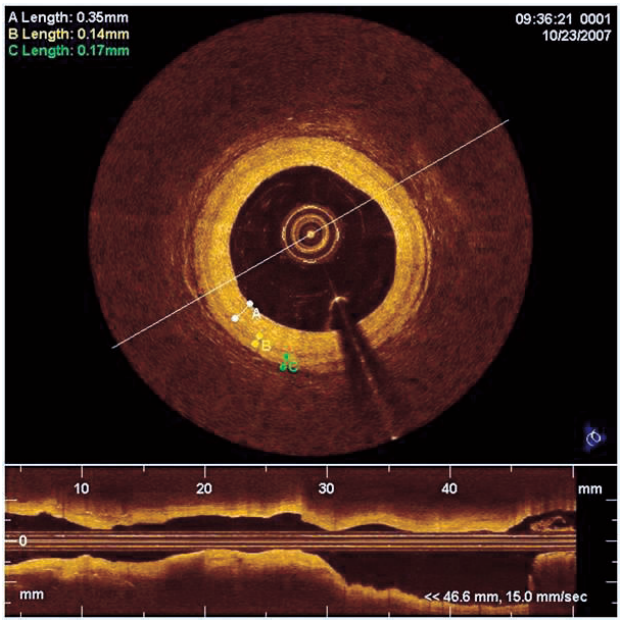

Figure 3. An example of an OCT image acquired with a prototype OCT system (LightLab Imaging, Westford, MA, USA) from the coronary artery of a patient undergoing percutaneous coronary intervention. The lengths listed in the upper left corner correspond to measurements of the thicknesses of the intima, media, and adventitia, denoted by the letters 'A', 'B' and 'C', respectively. The L-mode image (lower quarter of figure) shows a longitudinal image of the artery acquired during a 20 mm/s pullback. [Images courtesy of Dr. E. Grube, Siegburg Heart Center, Siegburg, Germany].

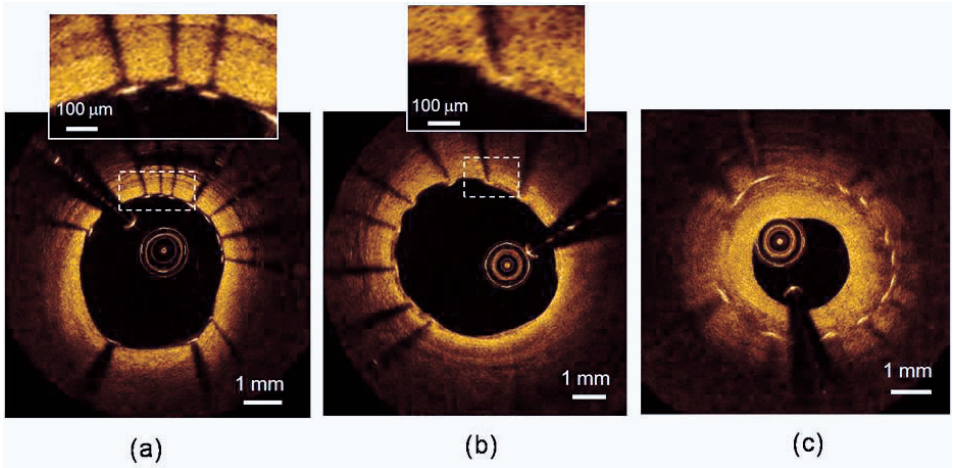

Figure 4. Examples of OCT images of stents acquired with a prototype FD-OCT system (LightLab Imaging, Westford, MA, USA). (a) Bare-metal stent imaged immediately after implantation. Stent imaged at long-term follow-up with (b) thin and (c) thick neointimal coverage. [Images courtesy of Dr. E. Grube, Siegburg Heart Center, Siegburg, Germany]

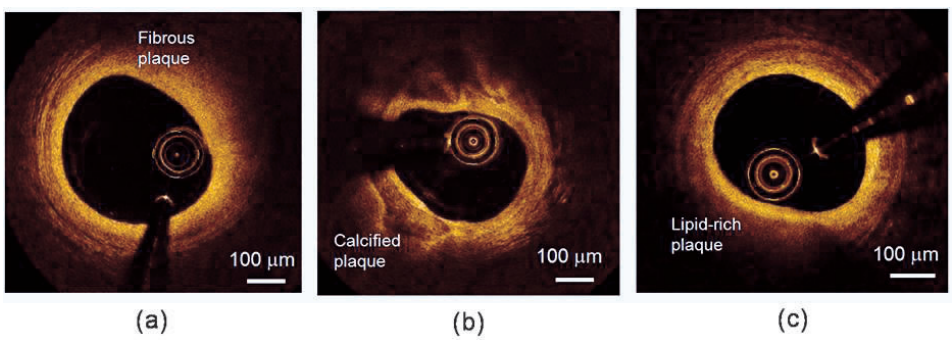

Figure 5. Fourier-domain OCT images of (a) fibrous, (b) calcified, and (c) lipid-rich lesions acquired with a prototype FD-OCT system (LightLab Imaging, Westford, MA, USA) [Images courtesy of Dr. E. Grube, Siegburg Heart Center, Siegburg, Germany].